NBS SPECIAL PUBLICATION 400-10

U.S. DEPARTMENT OF COMMERCE / National Bureau of Standards

Semiconductor Measurement Technology:

Spreading Resistance Symposium

ASTM
STP 572

NATIONAL BUREAU OF STANDARDS

The National Bureau of Standards[1] was established by an act of Congress March 3, 1901. The Bureau's overall goal is to strengthen and advance the Nation's science and technology and facilitate their effective application for public benefit. To this end, the Bureau conducts research and provides: (1) a basis for the Nation's physical measurement system, (2) scientific and technological services for industry and government, (3) a technical basis for equity in trade, and (4) technical services to promote public safety. The Bureau consists of the Institute for Basic Standards, the Institute for Materials Research, the Institute for Applied Technology, the Institute for Computer Sciences and Technology, and the Office for Information Programs.

THE INSTITUTE FOR BASIC STANDARDS provides the central basis within the United States of a complete and consistent system of physical measurement; coordinates that system with measurement systems of other nations; and furnishes essential services leading to accurate and uniform physical measurements throughout the Nation's scientific community, industry, and commerce. The Institute consists of a Center for Radiation Research, an Office of Measurement Services and the following divisions:

Applied Mathematics — Electricity — Mechanics — Heat — Optical Physics — Nuclear Sciences[2] — Applied Radiation[2] — Quantum Electronics[3] — Electromagnetics[3] — Time and Frequency[3] — Laboratory Astrophysics[3] — Cryogenics[3].

THE INSTITUTE FOR MATERIALS RESEARCH conducts materials research leading to improved methods of measurement, standards, and data on the properties of well-characterized materials needed by industry, commerce, educational institutions, and Government; provides advisory and research services to other Government agencies; and develops, produces, and distributes standard reference materials. The Institute consists of the Office of Standard Reference Materials and the following divisions:

Analytical Chemistry — Polymers — Metallurgy — Inorganic Materials — Reactor Radiation — Physical Chemistry.

THE INSTITUTE FOR APPLIED TECHNOLOGY provides technical services to promote the use of available technology and to facilitate technological innovation in industry and Government; cooperates with public and private organizations leading to the development of technological standards (including mandatory safety standards), codes and methods of test; and provides technical advice and services to Government agencies upon request. The Institute consists of a Center for Building Technology and the following divisions and offices:

Engineering and Product Standards — Weights and Measures — Invention and Innovation — Product Evaluation Technology — Electronic Technology — Technical Analysis — Measurement Engineering — Structures, Materials, and Life Safety[4] — Building Environment[4] — Technical Evaluation and Application[4] — Fire Technology.

THE INSTITUTE FOR COMPUTER SCIENCES AND TECHNOLOGY conducts research and provides technical services designed to aid Government agencies in improving cost effectiveness in the conduct of their programs through the selection, acquisition, and effective utilization of automatic data processing equipment; and serves as the principal focus within the executive branch for the development of Federal standards for automatic data processing equipment, techniques, and computer languages. The Institute consists of the following divisions:

Computer Services — Systems and Software — Computer Systems Engineering — Information Technology.

THE OFFICE FOR INFORMATION PROGRAMS promotes optimum dissemination and accessibility of scientific information generated within NBS and other agencies of the Federal Government; promotes the development of the National Standard Reference Data System and a system of information analysis centers dealing with the broader aspects of the National Measurement System; provides appropriate services to ensure that the NBS staff has optimum accessibility to the scientific information of the world. The Office consists of the following organizational units:

Office of Standard Reference Data — Office of Information Activities — Office of Technical Publications — Library — Office of International Relations.

---

[1] Headquarters and Laboratories at Gaithersburg, Maryland, unless otherwise noted; mailing address Washington, D.C. 20234.
[2] Part of the Center for Radiation Research.
[3] Located at Boulder, Colorado 80302.
[4] Part of the Center for Building Technology.

Semiconductor Measurement Technology:

Spreading Resistance Symposium

Proceedings of a Symposium
Held at the National Bureau of Standards
Gaithersburg, Maryland
June 13-14, 1974

James R. Ehrstein, Editor

Electronic Technology Division
Institute for Applied Technology
National Bureau of Standards
Washington, D.C. 20234

Under the Sponsorship of
Committee F-1 of the
American Society for Testing and Materials

and

The National Bureau of Standards

U.S. DEPARTMENT OF COMMERCE, Frederick B. Dent, *Secretary*
NATIONAL BUREAU OF STANDARDS, Richard W. Roberts, *Director*

Issued December 1974

National Bureau of Standards Special Publication 400-10

Nat. Bur. Stand. (U.S.), Spec. Publ. 400-10, 293 pages (Dec. 1974)

CODEN: XNBSAV

U.S. GOVERNMENT PRINTING OFFICE
WASHINGTON: 1974

For sale by the Superintendent of Documents, U.S. Government Printing Office, Washington, D.C. 20402
(Order by SD Catalog No. C13.10:400-10). Price $3.55.
Stock Number 0303-01358

PREFACE

This Symposium on Spreading Resistance measurements was held on June 13-14, 1974 at the National Bureau of Standards under the cosponsorship of this Bureau and Committee F-1 of the American Society for Testing and Materials. It consisted of three sessions as detailed in the Contents on pp. vi to viii.

The objective of the Symposium was to expose the state of the art with respect to the theory, practice and applications of the electrical spreading resistance measurement technique. This technique which has seen rapidly increasing interest and use over the last 10 or more years, has noteworthy versatility for profiling dopant concentrations over many orders of magnitude in multiple layer semiconductor structures. Nevertheless, the ever increasing demand on all measurement methods, caused by device fabrication utilizing active regions often less than 1 μm in thickness, taxes the theory, practice and successful application of all techniques, including the electrical spreading resistance.

It is hoped that this symposium, by illustrating the successful applications which have been made of the technique, and by indicating some of the areas where limitations have been found to exist, will encourage further effort by interested parties, to find solutions to those limitations.

Finally, by compiling a store of well documented measurement practice in one volume, it is hoped that the beginner in this technique will find rapid solutions to possible basic problems, so that he too may make rapid and successful use of this technique.

James R. Ehrstein
Editor

ABSTRACT

This Proceedings contains the information presented at the Spreading Resistance Symposium held at the National Bureau of Standards on June 13-14, 1974.

This Symposium covered the state of the art of the theory, practice and applications of the electrical spreading resistance measurement technique as applied to characterization of dopant density in semiconductor starting materials and semiconductor device structures. In addition to the presented papers, the transcripts of the discussion sessions which were held directly after the Theory, Practice and Applications sessions are also included. These transcripts, which were reviewed by the respective respondents for clarity, are essentially as presented at the symposium.

Key words: Dopant concentration, dopant profiles, metal-semiconductor contacts, resistivity, semiconductor surface preparation, silicon, spreading resistance.

SYMPOSIUM COMMITTEE

P. LANGER, Symposium Chairman
Bell Telephone Laboratories
Allentown, Pennsylvania

K. E. BENSON, Cochairman - Theory Session
Bell Telephone Laboratories
Allentown, Pennsylvania

F. VIEWEG-GUTBERLET, Cochairman - Theory Session
Wacker Chemitronic
Burghausen, West Germany

B. MORRIS, Cochairman - Practice Session
Bell Telephone Laboratories
Allentown, Pennsylvania

P. LANGER, Cochairman - Practice Session
Bell Telephone Laboratories
Allentown, Pennsylvania

A. MAYER, Cochairman - Application Session
RCA Corporation
Somerville, New Jersey

F. PADOVANI, Cochairman - Application Session
Texas Instruments, Inc.
Dallas, Texas

J. R. EHRSTEIN, Chairman - Publicity, Arrangements, Publication
National Bureau of Standards
Washington, D. C. 20234

CONTENTS

Certain commercial materials and equipment are identified in this paper in order to adequately specify the experimental procedure. In no case does such identification imply recommendation or endorsement by the National Bureau of Standards, nor does it imply that the material or equipment identified is necessarily the best available for the purpose.

AUTHOR INDEX

WELCOMING REMARKS
AT THE
ASTM/NBS SYMPOSIUM ON SPREADING RESISTANCE MEASUREMENTS
GAITHERSBURG, MARYLAND
JUNE 13, 1974
BY JUDSON C. FRENCH, CHIEF
ELECTRONIC TECHNOLOGY DIVISION
NATIONAL BUREAU OF STANDARDS

Good morning. It is a real pleasure for me to bid you welcome to the ASTM/NBS Symposium on Spreading Resistance Measurements on behalf of the National Bureau of Standards and, in particular, on behalf of the Bureau's Electronic Technology Division. I welcome also your co-host Bob Scace, Chairman of Committee F-1 on Electronics of the American Society for Testing and Materials.

Sharing this period of welcome with Bob is, I believe, representative of the long continuing cooperation between NBS and ASTM in many fields, always with the common interests of improvements in technology, in methods of measurement and specifications, and in the promotion of sound and effective voluntary standards.

Many of you are old friends of NBS and our Division but some are becoming acquainted with us for the first time at this Symposium. I would like to address my first few remarks to these new visitors. I am sure you are aware of the NBS role in maintaining and disseminating the primary standards of measurement for this Nation. But the Bureau carries on an amazingly wide variety of activities in other fields as diverse as pollution control and building research, dental materials and cryogenics, standard reference data and computer research, all stemming from the broad charter established by Congress nearly three quarters of a century ago. Here again in its breadth and subject matter the Bureau's interests parallel those of ASTM to a surprising degree.

Closest to the interests of this audience and of much of ASTM's Committee on Electronics is the work of our Electronic Technology Division. This Division focuses its resources on solving critical measurement and standardization problems associated with the manufacture, procurement, and application of essential electronic components.

Most of the work of this Division is devoted to semiconductor electronics. This comes as a surprise to many who ask: Why does the Bureau need to work in a field which so sophisticated, so technologically advanced, and so innovative? The answer is that the sophistication and innovative abilities of the semiconductor industry have led to the development of new processes and new devices much faster than the measurement techniques for their control and characterization have been developed.

In the fifteen years or more that our staff has worked with the semiconductor industry and its customers we have seen increasing need for improvements in practical methods of measurement for analysis, control, and specifications in this field. And we have learned that the Bureau can be especially helpful in this field because of its neutrality in evaluating measurement methods, and associated technology, and because its charter encourages it to work in the area of generic measurement for industry-wide use and market-place application. This is an area where individual companies understandably find less incentive for extensive research than in areas leading to new and proprietary processes and designs.

As a result, the NBS Semiconductor Technology Program has been established, having as its goal the development and standardization of improved methods of measurement for use in specifying materials and devices and in control of device fabrication processes: methods that have been well documented and tested for technical adequacy, are of demonstrated precision of an industrially acceptable level, and are acceptable to both users and suppliers.

If such methods are used by the electronics industry, they are expected to provide a more consistent set of measured results and interpretations and, hence, lead to improved quality control and yield in the manufacturer's plant, and to improved reliability and economy in the customer's applications.

But even when NBS is successful in providing such methods how does it assure the industry will use them? Only by working closely with the industry and its customers in the first place to ascertain for what measurements improvements are needed, then to carry on interlaboratory, or round robin, evaluation of the improved methods to show their practical value and precision, and finally to inform the electronics community of the resulting methods and to encourage their adoption as voluntary standards. This last step is important because NBS has no enforcement or regulatory authority in this field.

And here again we find ourselves working closely with ASTM which can so effectively provide an avenue to accomplishing these NBS aims, aims which are, of course, common to those of ASTM's Committee on Electronics.

Our Program now encompasses work on selected measurements, ranging from those needed to characterize silicon and oxides and interface states, through those for photolithography, process control using test structures, bonding and die attachment, and hermeticity; on to thermal and electrical properties of finished devices. And we report our output not only through ASTM but through many other channels including a special series of NBS publications with which many of you are familiar.

But I would like to reminisce for a moment, back to 1960 when our program was not so extensive and when our first project in the semiconductor materials measurement field was undertaken.

It was undertaken at the request of ASTM's Committee F-1 and the subject was measurement of resistivity. I have a very personal interest in this subject because I learned of the need in my first day of attendance at an F-1 meeting. And ASTM and NBS have done a lot together on this subject in the intervening years. We developed an improved four-probe method, improved in precision by an order of magnitude as a matter of fact, and the method and its various correction factors and other aspects now play a part in five ASTM standards. Later a scanning photovoltaic technique for convenient, essentially non-contacting, radial profiling was developed. Most recently we have issued a Standard Reference Material, comprising two boron doped silicon wafers with certified resistivity values for checking measurements; and their stability is now being tested in a long term cooperative experiment with the industry. These are the first Standard Reference Materials issued for the semiconductor industry's use.

But sophistication in the industrial development of devices has raised new problems which can only be solved by new techniques for resistivity measurements yielding resolution far beyond the capability of the currently standard four-probe technique. Where the four-probe method is limited to resolution of the order of millimeters, resolution of the order of micrometers and better is needed now for determination of crystal uniformity and for control of junction profiles.

The spreading resistance measurement method you will be discussing today and tomorrow is a leading contender in this field. We are working, as are many of you, to develop this method to a level of repeatability and understanding, both in and between laboratories, to meet the industry's needs. We are anxious to learn of the new developments to be reported here today and tomorrow.

So I will say no more now, except that it is a pleasure to be able to provide the facilities of the Bureau for this Symposium and to join with ASTM in encouraging the exchange of information in this rather new and very important field.

WELCOMING REMARKS FROM ASTM

Robert I. Scace

General Electric Company
Syracuse, New York

Good morning. On behalf of ASTM Committee F-1, the other sponsor of this meeting, I want to welcome you all. Spreading resistance measurements are only one of many measurement techniques with which Committee F-1 is concerned. To give some perspective, let me describe a little of ASTM's background in electronics for you.

ASTM is a large association of professional people who are engaged in developing standards on subjects ranging from railroad rails to surgical implants, and electronics is just one of over 120 such topics. Committee F-1 was established in 1955, developing out of work on electron tube materials which had previously been in a committee on copper. One of our major efforts has been in the development of ways to measure the properties of semiconductor silicon.

As Judson French has mentioned, NBS and ASTM have collaborated closely in this work, especially in resistivity measurements. Fifteen years ago we were lucky if two different people could measure the resistivity of a piece of silicon to within a factor of two, but now with the use of ASTM methods it is possible to do this measurement to an accuracy of a couple of percent. Similar progress could be cited for many other measurements essential to good process control in our industry.

Achievements such as these are one of the professional satisfactions of work in ASTM. We can all do our jobs better with better measurement tools and techniques. Another more personal reward is in the relationships established over the years with the people in ASTM. Committee F-1 meets three times a year to do its work, and this frequent contact on common technical problems results in close friendships with fellow professionals.

For the next two days we will be discussing spreading resistance measurements on silicon. This is a very powerful technique for analysis of structures and control of processes which is now mature enough to discuss at length. I hope you all find these sessions valuable, and I also encourage you to come to future Committee F-1 meetings to participate and to contribute further to the development of spreading resistance techniques.

NATIONAL BUREAU OF STANDARDS SPECIAL PUBLICATION 400-10, Spreading Resistance Symposium, Proceedings of a Symposium Held at NBS, Gaithersburg, Md., June 13-14, 1974.

Keynote Address
Symposium on Spreading Resistance
Gaithersburg, Maryland
June 13-14, 1974

Robert G. Mazur
Solid State Measurements, Inc.
600 Seco Road
Monroeville, Pennsylvania 15146

1. Introduction

This is the first symposium ever to be held on the subject of spreading resistance measurements. As I see it, the purpose in having this meeting is to gather together those who are currently using the spreading resistance measurement technique in their work on semiconductor processing problems along with others who would like to be able to do something about the same or similar problems, in the hope that, by sharing our knowledge and experience, we may all be better able to use the spreading resistance technique to our own advantage. I hope and believe that we will achieve this particular goal and that therefore in the future this meeting will be referred to as "The First Symposium on Spreading Resistance Measurements."

In deciding what I should talk about in a keynote speech for such an occasion, two related subjects came to mind. First, a number of individuals who haven't worked in the semiconductor industry from its earliest days have expressed an interest in the questions of where the technique came from as well as why and how it came about. Therefore, in the first part of my talk today I would like to relate the background of the spreading resistance technique as I know it.

The second subject that came to mind is also in response to certain people that I've met over the years. These are the people who, when first exposed to the spreading resistance technique, rapidly developed a "hang-up" with respect to the mechanics of the contacts used. In an attempt to shed some light in this area, I will devote the second part of this morning's talk to what I know about the achievement of reproducible, known-geometry, metal-semiconductor, small-area pressure contacts. These contacts are what I have often referred to in past discussions as "conditioned" contacts.

2. The Spreading Resistance Technique: Who, What, Why, Where and When.

The Spreading Resistance Technique is a method used to obtain quantitative measurement of the local resistivity of certain semiconductor materials. Currently, the technique is used most extensively on silicon. An essential feature of the technique is the achievement of sufficiently high spatial resolution so as to allow detailed evaluation of those variations in dopant concentration which are important to the manufacture of semiconductor devices. The technique is based on measurement of the "spreading resistance" or "constriction resistance" of small-area metal-semiconductor pressure contacts. It is currently in wide use in mapping inhomogeneities in silicon crystals and in obtaining thickness profiles of many of the diffused, epitaxial and ion-implanted layers produced during semiconductor device processing.

Small area metal-semiconductor pressure contacts are historically somewhat loosely called "point" contacts. The spreading resistance effect associated with such contacts has a distinguished place in the history of semiconductor technology. Certainly one of the earliest practical applications of a semiconductor device was the use of a point-contact rectifier in "crystal" radios during the early days of the radio age (1)[1]. Later, the

[1] Figures in brackets refer to literature citations at the end of this paper.

desire to understand and thus to improve point-contact diode detectors used in early World War II radar equipment sparked the efforts of a number of research groups in work on germanium and silicon. This work eventually led to the discovery of the transistor effect in late 1947 by Bardeen, Brattain and Shockley at the Bell Telephone Laboratories in Murray Hill, New Jersey (2).

However, there is an even closer relationship between spreading resistance measurements and the invention of the transistor. From the beginning of my work with the spreading resistance technique, I have been impressed by the fact that a key step in the Bardeen, Brattain and Shockley transistor invention involved a spreading resistance measurement (3). The experiment is detailed in the Physical Review for 1948 immediately following the note describing the transistor effect. This crucial experiment established the existence of additional charge carriers produced by injection from a metal-germanium point-contact identical to the emitter used in the first point-contact transistor. Brattain and Bardeen showed that the potential associated with a current flow through a metal-semiconductor point contact did not fall off with increasing distance from the point in accordance with a standard spreading resistance calculation but rather exhibited an anomalous decrease in the rate-of-change of potential in the immediate vicinity of the contact. This behavior was explained as being due in part to the injection of additional charge carriers into the semiconductor with a consequent lowering of the resistivity near the contact.

At this time, I'd like to call your attention to an interesting aspect of this Brattain-Bardeen injecting point-contact experiment, specifically that, to the best of my knowledge, the experiment has never been repeated. Not that I am suggesting that their work needs corroboration but I consider it surprising that such an elegant experiment which so nicely illustrates a basic phenomenon in semiconductor physics should not have been repeated many times over if for no other reason than for its educational effect.

This situation stands out even more in contrast with the often-repeated Haynes-Shockley experiment (4) which provides a measurement of the drift mobility of charge carriers in a semiconductor by timing the arrival of a pulse of injected carriers at a point down the electric field relative to the original point of injection into the bar. Because of its fundamental nature and its simplicity, the Haynes-Shockley experiment has been repeated many times over in a number of university and industrial laboratories since the description of the experiment was first published. Now, the question is: why has the equally fundamental and simple Brattain-Bardeen spreading resistance experiment not been repeated as many times? I would like to suggest that the main reason is the experimental difficulty of the Brattain-Bardeen measurement; it is no easy job to do a potential probe within micrometers of a metal-semiconductor point contact. I believe that the significance to us of the familiarity of the Haynes-Shockley experiment and the relative obscurity of the Brattain-Bardeen experiment is that our experimental problems with spreading resistance contacts are not trivial ones.

Before leaving this subject, I'd also like to point out that Brattain and Bardeen credit W. L. Bond with construction of their micromanipulator. If we should ever need to produce a name for an award of the like in conjunction with spreading resistance measurements, I think that the name of Bond should be a front-runner.

Returning to the history of spreading resistance after Bardeen, Brattain and Shockley, I must admit that I have no firsthand knowledge of developments during the 1950's. However, the relationship between semiconductor resistivity and point-contact spreading resistance must have been used off and on in semiconductor materials evaluation, at least sufficiently so as to warrant inclusion in several publications, including volume 6, Part B of the book "Methods of Experimental Physics", edited by K. Lark-Horovitz and V. A. Johnson (5). The basic spreading resistance measurement method is described under the heading "Spreading Resistance Measurements" in the chapter entitled "Conductivity Measurements on Solids". The treatment, while brief, is complete in that it indicates both the high spatial resolution of the technique as well as its primary problem—that of determining true contact dimensions.

My personal experience with the spreading resistance technique dates to the first job I was assigned on beginning work at the Westinghouse R & D Center in June of 1959. At that time, Westinghouse was in the middle of an extensive program to make use of germanium and

silicon dendrites, produced by growth from a supercooled melt. The end product of the dendritic growth process was a ribbon or strip of semiconductor single crystal, having a width of about 1 mm and a thickness of about 0.1 mm. The dendritic ribbon could be grown at a rate of several feet per minute and produced in lengths of up to several hundred feet with the dendrite being rolled up on a reel located above the crystal puller for storage and later use. The plan was to make use of the nearly perfect surfaces of this material for automatic device fabrication with no lapping, etching or other surface treatment of chips needed. My job was to measure the resistivity of as-grown dendrites using a traveling one-point potential probe.

Very soon after I began work (or perhaps even before that time) someone began to suspect that the dendrite material being grown was too inhomogeneous in resistivity to be of use in practical device manufacture. This later turned out to be the case and, unfortunately for the dendrite program, the inhomogeneities turned out to be inescapably associated with the fundamental growth habit of dendrites.

However, before the demise of the dendrite program became certain, I was given the additional task of developing some way of quantitatively evaluating dendrite cross-sectional resistivity variations. I began with the point-contact voltage breakdown technique which had already come into use for evaluating N on N^+ epitaxial silicon (6). Figure 1 shows some raw data obtained on a dendrite cross-section which was grown from a melt containing both P-type and N-type impurities. The conductivity type and the point-contact breakdown voltages measured at various points on the cross-section are shown. The data show that the central part of the dendrite (which grows first) is P-type of relatively lower resistivity as compared to the "arms" of the H-structure pattern in which such dendrites grow. The material between the "arms" of the H-structure solidifies last and is N-type. Although the point-contact breakdown technique did work more or less, I eventually abandoned it because of inadequate reproducibility as well as the fact that it was difficult to obtain absolute resistivity values over the wide range of both P- and N-type resistivities found in the dendritic material.

I next tried to use free-carrier infrared absorption with a small diameter lightbeam but soon found that, at least for me, this approach yielded a better thickness gauge than it did a dopant-level monitor.

Meanwhile, the reproducibility of I-V characteristics observed during point-contact breakdown voltage measurements as well as during low voltage point-contact rectification type testing was so good that I was led to consider the possibility of making spreading resistance measurements as described in the Lark-Horovitz book (5). I tried the technique, using the same traveling one-point probe apparatus that I had inherited on coming to Westinghouse, along with a Keithley 610A Electrometer. The 610A had an ohmmeter function built in via a constant current generator and an electrometer measurement of the total voltage across the current output terminals. The key feature for me was that this instrument had a useful sensitivity extending down to below one millivolt so that I was able to use low enough currents for a given resistivity sample such that the spreading resistance measurement could always be done with a total applied voltage in the vicinity of 10 millivolts. With such a low bias level, significant change in sample resistivity due to injection of excess carriers was avoided along with several other undesirable effects normally associated with voltages much greater than kT/q (e.g., high-field mobility modification and contact heating).

Figure 2 shows the probe and the 610A Electrometer as well as the stack of brass washers used to load the probe to 25 grams. This loading was used for germanium — I later used 45 grams for silicon measurements. These load values were dictated by the desire to have the load large with respect to frictional force in the distorted ball bearings used to pivot the probe arm and yet not so large as to crack samples during probing. The probes used were standard (at the time) phonograph needles.

Early results were encouraging. The spreading resistance values measured on a given sample were reproducible to within a few percent and furthermore, the size of the microcracked region left on the sample after a spreading resistance measurement agreed rather well with the circular contact size expected on the basis of a Hertz formula calculation for the case of a spherical surface having the radius of curvature of the phonograph needle

565-448 O - 75 - 2

mating with a plane surface (7). For the case of a silicon to osmium contact with a loading of 45 grams, I calculated just under 4 micrometers for the value of "a" where "a" is the radius of the contact spot.

The fact that the Hertz formula used in calculating contact size is based on the assumption of elastic stress in the materials involved while the micro-cracking in itself clearly indicated the existence of an inelastic situation didn't bother me much. A lot of physical situations behave even when the underlying assumptions are violated somewhat.

What did cause me to pause for a long while in the early development of the technique was the inability to fit a single value of "a" into the classical spreading resistance formula for both P-type and N-type material. According to my understanding of the situation, the simple formula $R_s = \rho/4a$ should have applied (7). Thus, the calculated and observed value for "a" should have been verified by a spreading resistance measurement on a single sample of known resistivity. However, and unfortunately, things were not so simple. Measurements on samples of different resistivities or of opposite conductivity types with the same resistivity led to inconsistent results when compared to the values expected from the simple $R_s = \rho/4a$ relationship. At first, it appeared that the calculated value for "a" would fit the experimental data if a proportionality constant "k" = about 3 were to be inserted for N-type material; i.e.

$$\text{for P-type, } R_s = \frac{\rho}{4a}$$

$$\text{and for N-type, } R_s = \frac{k\rho}{4a} \approx \frac{3\rho}{4a}$$

However, with more careful measurements over a wider range of P- and N-type resistivities, I found that, in fact, k was not a constant at all but rather a complicated function of ρ and that, furthermore, the $k(\rho)$ function for P-type material differed from the $k(\rho)$ for N-type samples.

This situation led others then and later involved in spreading resistance measurements to talk in terms of an "effective contact radius". I rejected the effective radius concept from the beginning for two reasons: 1) it didn't make sense physically--I just couldn't believe that impurity levels of one part per million or less could radically alter the hardness of silicon and germanium; 2) a much simpler explanation was available in that osmium has a larger work-function than silicon and should therefore make a rectifying contact on N-type silicon and an ohmic contact on P-type. Thus, even at zero bias, an additional resistance should be observed for the osmium, N-type contact as compared to the osmium, P-type contact. The measured resistances for N-type and P-type samples were in the right direction--with the measured spreading resistance on 1 ohm-cm N-type silicon, for instance, being about a factor of three larger than that measured on P-type 1 ohm-cm silicon. Furthermore, a work-function barrier effect would cause a variation in measured spreading resistance with change in sample resistivity in qualitative agreement with the shape of the $k(\rho)$ function.

The work function-determined zero-bias barrier model even fitted the fact that I subsequently found that "k" was not only a function of semiconductor material, conductivity type and resistivity but that it also depended on the mechanical finish of a sample surface and even the time elapsed between surface preparation and measurement. This behavior would be consistent with a model based on a property such as the work function which would be expected to have some dependence on the physical and chemical nature of the surface.

Despite the magnitude of the problem involved in understanding the contacts used in these early spreading resistance measurements, the high degree of reproducibility which was experimentally observed suggested that I could get on with the job that needed doing by generating a calibration curve of spreading resistance vs. resistivity through making measurements on known resistivity samples. With this approach, the complications posed by the complex dependence of the k-function on conductivity type and surface finish could be handled by generating separate calibration curves for P- and N-silicon with a particular surface finishing procedure that could be kept constant for both known-resistivity samples and the unknown test samples.

With calibration curves so generated, measurement results were at least good enough to successfully establish that germanium and silicon dendrites were extremely inhomogeneous in dopant concentrations.

Another result of generating the calibration curves was the fact that I became convinced that nothing other than a strongly empirical approach would suffice for further measurements with the spreading resistance technique. This conviction grew out of the discovery that the calibration curves for lapped and polished N-type silicon samples crossed each other in the vicinity of 1 ohm-cm. This result (and the surface "aging" effects) clearly indicated that spreading resistance measurements were affected by the electrical properties of the silicon surface and that therefore, a satisfactory theoretical understanding was beyond reach for some time to come.

Thus, my development work on the technique subsequent to this time was concentrated on making the contacts as reproducibly as possible and on achieving the highest degree of reproducibility possible in sample surface preparation.

Development work on the spreading resistance technique continued despite the close-out of the dendrite programs because new programs arose in which high spatial resolution measurements were needed, especially in research and development into the growth of multilayer homo-epitaxial silicon structures for use in high-power devices. This work was primarily under the direction of T. L. Chu who then headed the epitaxial growth work at the Westinghouse R & D Center. Without his early support, the spreading resistance work at Westinghouse might easily have ended in its infancy.

The state of development achieved during this part of the work at Westinghouse is illustrated by the data and remarks presented as oral papers by myself and by Dave Dickey at the ECS Meeting in Pittsburgh in 1963 (8).

The 1963 "state-of-the-art" is also well illustrated by the 1966 paper, co-authored by Dave Dickey and me (9). This is so because this paper was my first and it took a couple of years to actually get into print.

As is made clear in the 1966 paper, by the middle of the 1960's we had a useful and practical technique. We knew that it involved three basic requirements:

1) Reproducible contacts: these had to be mechanically generated in such a way that they were reproducible over periods of months or longer. They had to be produced without even microscopic sliding or other motion during contact-make and had to be capable of positioning within ±1 micrometer of a given standard placement.

2) Low applied voltage: the voltage across spreading resistance contacts had to be small enough so as to avoid significant amounts of carrier injection, contact heating or the like.

3) Calibration: the spreading resistance technique is a comparison technique. Unknown resistivity samples must be evaluated through the use of calibration curves produced by making spreading resistance measurements on samples of known resistivity (these calibration samples are generally measured with a 4-point probe and are prepared so as to have the same surface finish as the unknown resistivity material to be measured).

   N.B. Because of this dependence on calibration, the results obtainable with the spreading resistance technique are limited in accuracy only by the quality and the quantity of the calibration work done.

While the technique practiced up until 1966 was a manual one, it was useful and practical. This is illustrated by Figure 3 which is a resistivity profile produced by the manual spreading resistance technique as of about 1962. Figures 4 and 5 illustrate early use of the automatic spreading resistance probe at Westinghouse in profiling thick epitaxial structures then under development for power device use. A typical process-control problem

which illustrates the need for spreading resistance data is shown by the defective profile of Figure 5. Figure 6 illustrates a typical N on P^+ epitaxial structure.

The main drawback to our measurements at the time involved the need to correct the raw data in order to obtain true resistivity/impurity concentration values in thin layers of interest. This need arose because of the existence of two basic assumptions in the derivation of the equation $R_S = \rho/4a$, i.e.:

1) all sample boundaries are at "infinity", i.e., far away from the contact as compared to the size of the contact (see Holm (7)).

2) the resistivity in the semiconductor sample is uniform throughout.

The paper by Dickey (8) gives a theoretical solution to the boundary condition imposed by the presence of an (insulating) *p-n* junction within several contact diameters or less of the probe. The results and limitations of this and several other correction schemes will be the subject of several papers to be presented here in the next two days. Suffice it to say that the correction factors are probably the greatest problem in the use of spreading resistance measurements today.

3. The Nature of the "Conditioned" Probe

Rather than getting into any discussion at all of correction factors, I'd like to use my remaining time to get into the second part of this talk. This involves abandoning the historical approach in order to present a contact model and some remarks which will reflect my best current understanding of the mechanical and physical aspects of what I call "conditioned" probes.

I believe that this aspect of the spreading resistance technique is worth taking the time for now for three reasons:

1) "conditioned" contacts are the primary requirement for a practical spreading resistance measurement technique;

2) the mechanical aspects of spreading resistance contacts have not been discussed in detail in the published literature;

3) I believe that a realistic picture of the contacts used for spreading resistance measurements is fundamental to proper understanding and use of measurement results.

In my early attempts to get around the problem posed by not being certain of the true dimensions of the spreading resistance contacts, I elected to proceed by first assuming that the Hertzian value for "a" as calculated was correct. This then suggested that 1 Ω·cm P-type silicon involved a barrier free contact and led to the selection of 1 Ω·cm P-type samples for use in checking probes. On such samples, measurements should depend only on geometrical spreading resistance. These standard samples eventually became our "QTA" samples, with "QTA" being an abbreviation for "Qualification, Test and Alignment".

During subsequent checking of probes on these samples, I found that, despite the fact that new probes would have a variable and relatively high measured spreading resistance when first run, they would subsequently show a lower and quite uniform value after being used in making spreading resistance measurements on lapped (bevelled) samples. Typically, new probes would give values of up to three or four thousand ohms on the QTA sample, but, after running on lapped samples for one or two thousand measurement points, the probes would consistently show a decrease of measured QTA resistance to about 600 Ω.

This behavior, when viewed in the light of the known inability of simple cleaning processes to remove all residual abrasive from lapped silicon samples, led me to begin thinking of the probes as undergoing some kind of "conditioning" process. This process was not at all well understood but the results were so reproducible from one probe to another that I felt justified in using probes so "conditioned" for routine measurements--depending, of course, on calibration curves for absolute results.

My understanding of the conditioning process has increased only slowly over the years--mostly as a result of using hundreds of probes on many individual pieces of spreading resistance apparatus over a long period of time. While I still cannot claim complete understanding of the process, the attainment of stabilized measured spreading resistance values on a standard (QTA) sample for many different probe tips strongly suggests the achievement of a mechanically reproducible contact situation subsequently involving only elastic deformation of the metal probe.

Furthermore, while it is well known that the true electrical contact area between contact members is small as compared to the size of the apparent contact region (7), experimental evidence shows that even the apparent area of the spreading resistance contacts being used for measurements is very small — for the 45 gm probes used in my early work, the overall contact area was 5×10^{-7} cm^2. It seemed obvious that there had to be some limit to the "normal" orders-of-magnitude difference between apparent contact size and the actual electrically-conducting contact size; i.e., given a conducting region small enough and with sufficiently high pressures, the electrically-conducting contact size should approximate the apparent contact size. This idea eventually became embodied in a definition of a useable and practical "conditioned" spreading resistance contact.

Basically, by a "conditioned" probe, I mean one which is so contoured and chemically treated that, despite the fact that the surface of the probe is rough on a micro-scale, the micro-contacts made by it when it is set down on a silicon surface are sufficient in number and grouped closely enough so that the overall effect is as if there is a single circular contact of specific, reproducible radius "a". A corollary idea is that, under these conditions, "a" is large enough relative to the load applied that the pressure at the metal semiconductor interface will be within the elastic range of the metal involved and the contact will therefore be mechanically reproducible.

A rather complete treatment of the geometrical concept behind this definition of a "conditioned" contact is contained in the work of J. A. Greenwood (10).

I can also offer a few further remarks relative to the details of spreading resistance contacts and probes which may aid you in becoming comfortable with the idea of a "conditioned" probe.

The probes used for spreading resistance measurements are initially imperfectly contoured--they are nominally of a one mil (25 μm) radius of curvature at the tip and are otherwise contoured as shown in Figure 7. The probe tips are rough on the micro-scale, having a surface roughness of approximately 1 μm. Thus, when set down on a smooth silicon surface, they initially contact the silicon at several randomly-scattered points corresponding to high-spots in the tip-contact region. As the load on the probe increases, the contact area increases, both by enlargement of the first contact spots and contact-make at new spots.

The initial contact points are the regions under which the applied pressure first exceeds the fracture stress of the silicon material and are therefore the points from which micro-cracks will radiate upon lifting the probe. Note that it may be possible for the stress at some of the later contact points to be large enough to crack and displace the brittle silicon oxide layer while not becoming great enough to cause cracking in the silicon. This would result in no micro-cracks radiating from these points and hence no way to visually tell afterwards that electrical contact was made at such a point.

Furthermore, current density is quite non-uniform in a flat circular contact--very little current flows through the center of the contact. Therefore, lack of true electrical contact in the central region of a contact pattern will in general not appreciably affect the measured spreading resistance. One way of looking at this is to observe that in using contacts for spreading resistance measurements, we are primarily concerned with the perimeter of the contact.

The model as described here also suggests that the individualized patterns of micro-cracks observed for a particular probe are primarily indicative of the detailed micro-topography of that probe tip and are not necessarily directly related to the electrical

properties of the final contact. Therefore, detailed study of contact-spot micro-crack patterns may well turn out to be a study of the micro-metallurgy of osmium-tungsten (or whatever other material the probe is fabricated from) rather than anything else.

Thus, I now see the "conditioning" process as one wherein the probe tip is so contoured and roughened (on a micro-scale) that, when properly placed on a silicon surface, it produces a contact which may well be a cluster of micro-contacts but, if so, the cluster is so grouped that the result is the same as if the electrically-conducting area was a single spot with the radius "a" given by the Hertz relationship for the probe radius of curvature and the load and materials involved.

Given acceptance of this "conditioned" probe concept and definition and the equipment capable of producing such contacts without sliding or other mechanical problems, the practical problem becomes one of knowing when the "conditioned" contact situation is reached.

I believe that the primary criterion for assessing contact quality must be a reproducibility check on a standard sample. In line with this approach, we use slices taken from a common batch of 1 ohm-cm, p-type silicon wafers which were "chem-mechanically" polished years ago. Through direct experience, we have been able to establish practical limits for spreading resistance values obtained on these standard samples for conditioned probes under normal conditions.

The criteria and limits that we now suggest are the following:

Table 1

a) Probe Load	45 gms	20 gms
b) Measured resistance per probe on UNREFINISHED QTA sample	300-700 ohm	600-1000 ohm
c) Diameter of Circumscribed Circle around contact spot pattern	8-9 μm	5-6 μm

In addition to these criteria there are several other "characteristics" of conditioned probes that may be useful in your evaluation of the suitability of particular probes for spreading resistance measurements. These are:

1) conditioned probes make contacts whose measured spreading resistance on QTA samples is relatively stable in time. Where vibration is not unusually severe, measurement values on QTA samples will remain stable within several percent or less after a typical initial increase of approximately 5%.

2) conditioned probes yield measured values on QTA samples which are much more uniform from one point to the next than are the values obtained with unconditioned probes.

3) conditioned probes are more easily seen in the microscope than are unconditioned probes, probably because of a larger number of micro-contacts with a resultant increase in light scattered from the (111) plane facets produced by fracture.

The remarks that I offer here are based on my own attempts to rationalize the behavior of spreading resistance probe contacts during measurements over a period of some 13-14 years. I hope that these comments will assist others in increasing their understanding of the physics and mechanics of the "point" contact used in the spreading resistance measurement technique.

1. H. C. Torrey and C. A. Whitmer "Crystal Rectifiers", 1st ed., McGraw-Hill Book Co., New York (1948).

2. J. Bardeen and W. H. Brattain, Phys. Rev. 74, 230 (1948).

3. W. H. Brattain and J. Bardeen, Phys. Rev. 74, 231 (1948).

4. J. R. Haynes and W. Shockley, Phys. Rev. 75, 691 (1949).

5. "Methods of Experimental Physics" V. 6, Part B, Solid State Physics, ed. by K. Lark-Horovitz and V. A. Johnson, Academic Press (1959).

6. J. Brownson, J. Electrochem. Soc. 111, 919 (1964).

7. R. Holm, "Electric Contacts Handbook", 3rd ed. Springer, Berlin (1958).

8. R. G. Mazur, Abs. No. 56 and D. H. Dickey, Abs. No. 57, Papers presented at the Pittsburgh Meeting of the Electrochemical Society, Spring, 1963. See Extended Abstracts of the Electronics Div. Vol. 12, No. 1.

9. R. G. Mazur and D. H. Dickey, J. Electrochem. Soc. 113, No. 3 (255-259) March 1966.

10. J. A. Greenwood, Brit. J. Appl. Phys., 17, 1621-1631 (1966).

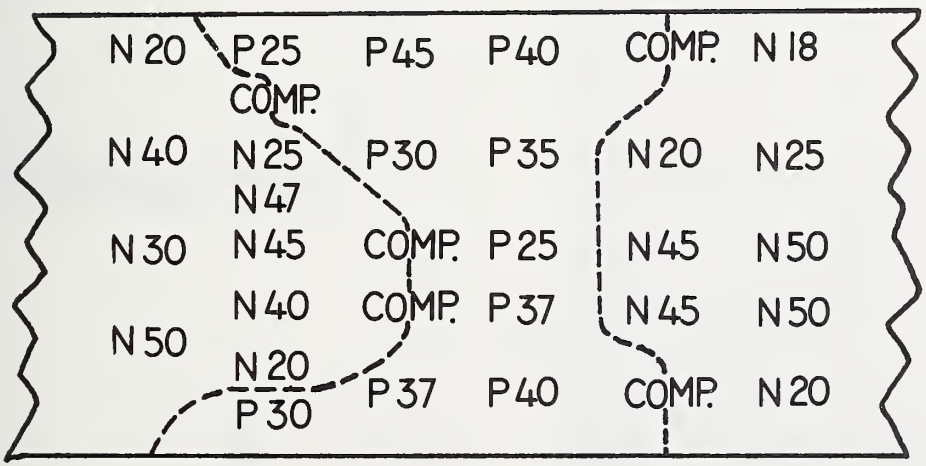

Figure 1 - Map of a three-zone dendrite cross-section, showing the experimentally-determined conductivity type and point contact breakdown voltage as a function of position on the cross-sectional surface. Vertical: approximately 0.25 mm; Horizontal: approximately 0.9 mm.

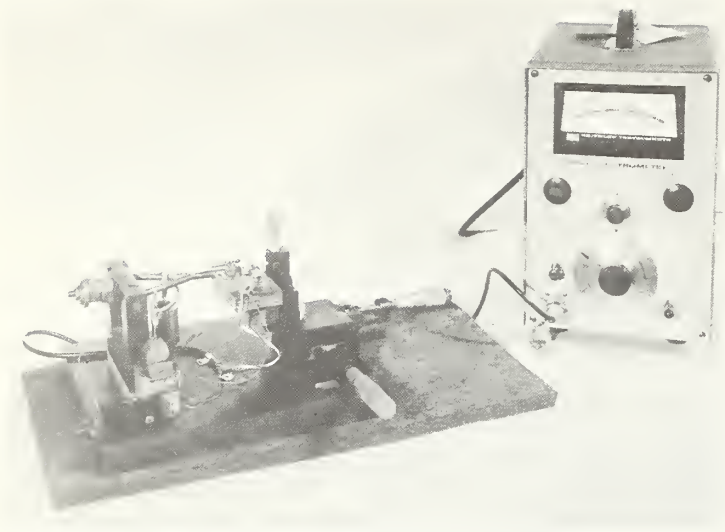

Figure 2. The first Westinghouse spreading resistance probe apparatus.

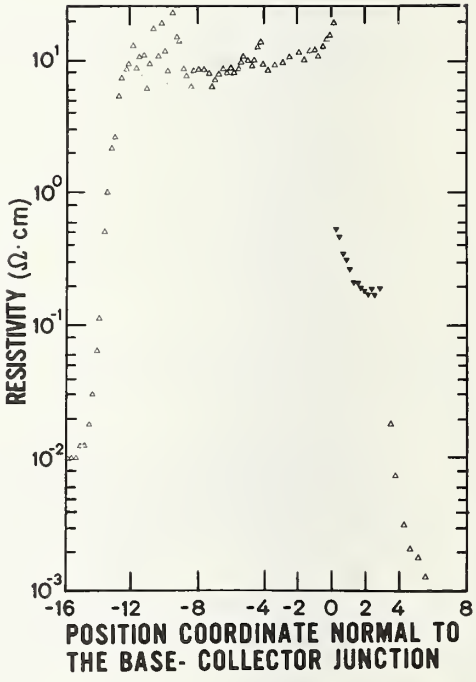

Figure 3. Spreading resistance - derived resistivity profile of a defective epitaxial thyristor structure: manual probe data, circa 1962.

Figure 4. Early automatic spreading resistance profile of a P^+ NN^+ epitaxial power device structure.

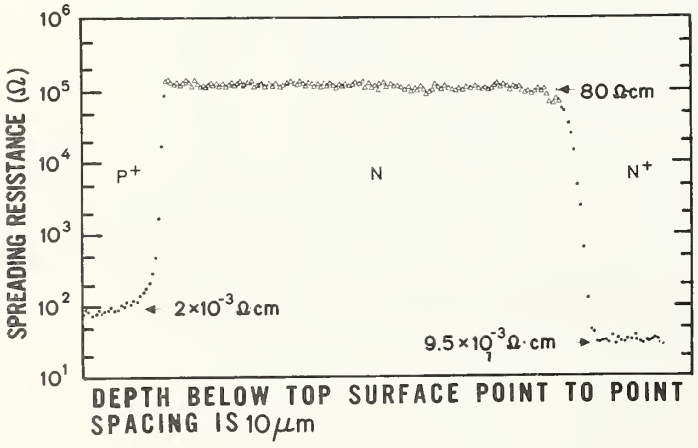

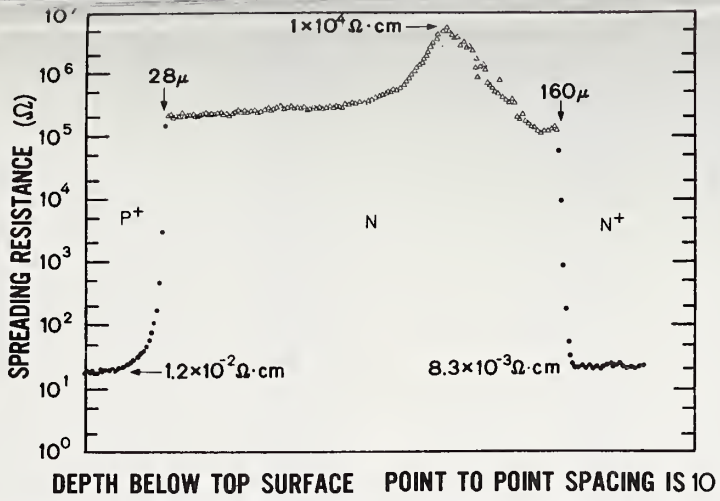

Figure 5 - Early automatic spreading resistance profile of a P^+ NN^+ epitaxial structure with an anomalous profile due to lack of epi-dopant control during the early stages of growth.

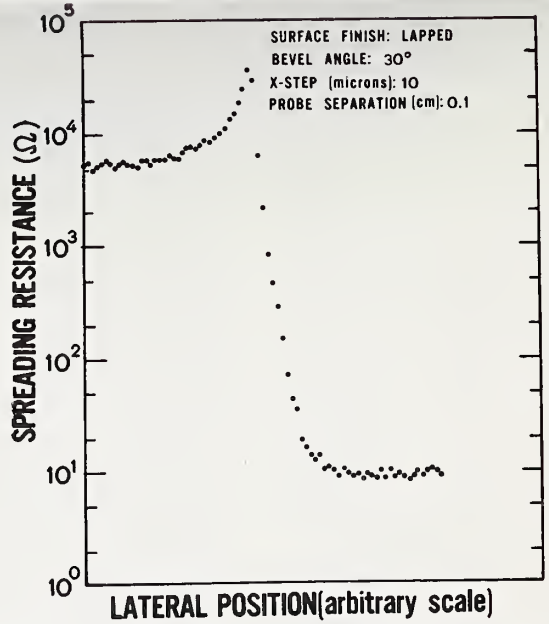

Figure 6. A typical N on P^+ epitaxial structure as profiled with the automatic spreading resistance probe.

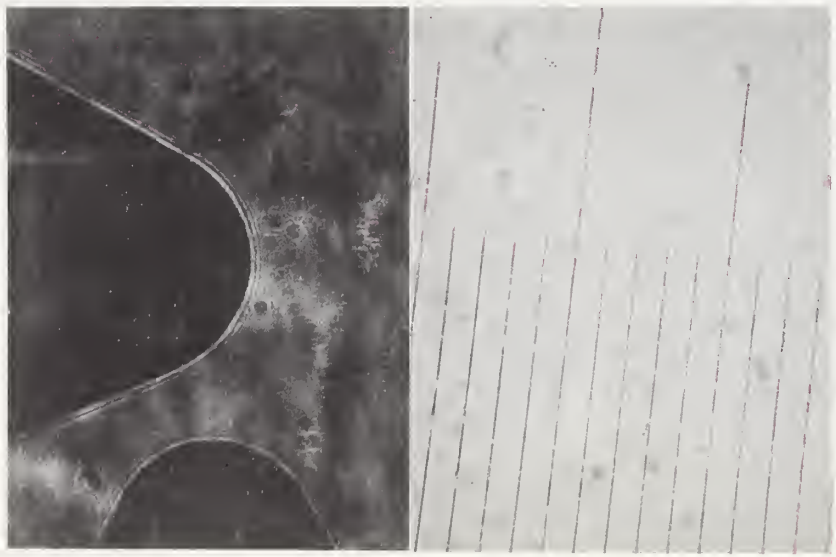

Figure 7. Shadow graph of two spreading resistance probe tips with a 10 μm stage micrometer scale.

NATIONAL BUREAU OF STANDARDS SPECIAL PUBLICATION 400-10, Spreading Resistance Symposium, Proceedings of a Symposium Held at NBS, Gaithersburg, Md., June 13-14, 1974.

The Physics of Spreading Resistance Measurements

Stephen J. Fonash

Engineering Science Department
Pennsylvania State University, University Park, Pennsylvania 16802

The spreading resistance method is uniquely suitable for the determination of electrical resistivities in a number of situations. However the technique does not simply measure the resistivity beneath the contacts. Considering the two probe configuration, what is actually measured is the ratio $\Delta V/I$. Here ΔV is the difference between the Fermi levels of the probes necessary to maintain the sampling current I. This difference in the Fermi levels of the probes depends on the zero bias resistance of the probe - semiconductor contacts, the effective resistivity of the layers in a multilayer structure, and the configuration of the structure. The zero bias resistance depends on temperature and details of the metal-semiconductor contact including surface history. Effective resistivities enter into the measurement - and not the actual resistivities - because of the fact that the use of pressure probes creates a stress field under the contacts. This field falls off with a characteristic length of the order of the contact radius. Thus piezoresistivity effects - well known for Si - can be operative under the contacts. As a consequence of these various effects the interpretation of what $\Delta V/I$ is actually measuring is not straightforward. Practical application of the spreading resistance technique necessitates making certain simplifying assumptions. In light of the various phenomena involved in a spreading resistance measurement it is imperative that the implications of these assumptions to the accuracy of the measurement be understood.

Key words: Correction factor; crystallographic orientations; effective contact radius; interfaces; metal-semiconductor contacts; multilayered structure; piezoresistivity; resistivity; spreading resistance; stress; zero bias resistance.

1. Introduction

The use of the spreading resistance technique [1-5][1] for resistivity measurements in homogeneous and inhomogeneous semiconductor materials is finding increasing popularity. Ostensibly this method is quite simple and straightforward. However, due to geometrical

[1] Figures in brackets indicate the literature references at the end of this paper

effects, the presence of material interfaces, the presence of space charge regions, and the presence of stress fields, there are a number of physical phenomena which come into play when this measurement is made. An understanding and appreciation of these various phenomena involved in a spreading resistance measurement is necessary for a meaningful application of this technique.

To determine what physical phenomena are playing a role in spreading resistance measurements and to determine how they influence the measurement a simple two probe configuration [2] will be assumed for this discussion. (See figure 1) Obviously the conclusions that will be reached can be applied to other configurations used in spreading resistance measurements. As is shown in this figure, it is also assumed that this measurement is being made on a layered structure for generality.

In the configuration depicted, a current I is flowing into probe contact one and flowing out of probe contact two. These metal probe-semiconductor contacts are, ideally, flat circular areas whose radii are determined by the force on the probe and the Young's moduli of the metal and the semiconductor [3,6]. The electrostatic potential ψ which is set up by this current flow must be such that

$$\left.\frac{\partial \psi}{\partial Z}\right|_{Z = h_4} = 0 \qquad \text{(all r)} \tag{1}$$

and

$$\left.\frac{\partial \psi}{\partial Z}\right|_{Z = 0} = 0 \qquad \text{(all r not under the contacts)} \tag{2}$$

Under the contacts, since there is a current flowing,

$$\left.\frac{\partial \psi}{\partial Z}\right|_{Z = 0} \neq 0 \tag{3}$$

In addition, since no current flows out the sides of the structure,

$$\left.\frac{\partial \psi}{\partial X_n}\right|_{\text{lateral surfaces}} = 0 \tag{4}$$

where X_n is a coordinate normal to any lateral surface under consideration.

These four statements constitute very general constraints on ψ, the electrostatic potential. However ψ as a function of position in the structure must actually be found since the potential difference ΔV between the probes, necessary to drive I, is to be computed. Really it is the ratio $\Delta V/I$ which is to be found since this is the quantity measured by the spreading resistance technique

2. The Physical Phenomena Involved

To be more specific, the quantity to be measured $\Delta V/I$ can be written as

$$\Delta V/I = \frac{-\Delta V}{\int_0^a \int_0^{2\Pi} \frac{1}{\rho_{eff}} \frac{\partial \psi}{\partial Z}\Big|_{Z=0} r_1 dr_1 d\theta_1} \qquad (5)$$

where the subscripts refer to a polar (r,θ) coordinate system situated, for convenience in discussing this integral, at the center of circular contact one. This expression assumes that, just beneath the metal probe-semiconductor contact, the current is carried by drift in the semiconductor. The need for an effective resistivity - instead of the actual resistivity ρ - will become apparent; ρ_{eff} reduces to ρ in the absence of a mechanical stress field. The fundamental question, what does $\Delta V/I$ measure, can be answered by a study of eq. (5)

It is clear that eq. (5) underscores the necessity of finding the electrostatic potential $\psi = \psi(r,\theta,Z)$ in the semiconductor. At first glance this is straightforward since ψ should satisfy Laplace's equation in the semiconductor and it is known to be subject to the boundary conditions given by eq. (1) - (4). However, the potential difference measured between probe one and probe two, the quantity ΔV, is the difference between the Fermi levels (electrochemical potentials) of the two metal probes. Thus, if ψ is to be written in terms of ΔV as it must be to obtain an answer from eq. (5) which depends only on the structure, it is necessary to relate the Fermi level in metal one to ψ in the semiconductor beneath contact one. Correspondingly it is necessary to relate the Fermi level in metal two to ψ in the semiconductor beneath contact two.

With a layered structure such as that shown in figure 1, a second problem becomes apparent: ψ does not satisfy Laplace's equation in the interface regions. In these interface regions (1 - between layers I and II, 2 - between layers II and III, and 3 - between III and IV) there is an assumed abrupt change in resistivity. That is, in the interface regions, a transition occurs from one value of doping density to another. Figure 2 shows, in cross-section, some region of interface 1, for example; figure 3 shows the band diagram for this cross-section. In general these transition layers are of width w_j where $j = 1,2,3$. From figure 3 it is seen that a charge density σ_j exists in these interface regions. Consequently

$$\nabla^2 \psi = 0 \qquad (6)$$

may be assumed valid for layers I, II, III, and IV; it can not be assumed valid for the interface regions.

Considering the first problem, it is apparent that a boundary condition at the contacts relating the Fermi levels of the metals and ψ is needed [7]. If the electrostatic potential[2] in the semiconductor is measured (see figure 4) henceforth with respect to the Fermi level

[2] The electrostatic potential in the semiconductor is measured positively down, from the Fermi level of probe two, to the position of the Fermi level in the semiconductor in this analysis. See figure 4.

of metal probe two, then it follows that the current density normal to the contact at some point (r_2,θ_2) in the metal-semiconductor boundary two is continuous at the boundary and that [7,8]

$$\left[\frac{1}{\rho_{eff}} \quad \frac{\partial\psi}{\partial Z}\right]_{Z=0} = C\psi_2 \tag{7}$$

Here ψ_2 is the value of ψ under this contact (ie, Z = 0) at some general (r_2,θ_2); this polar coordinate system at contact two is defined analogously to (r_1,θ_1). A similar condition may be developed for contact one; ie, [7,8]

$$\left[\frac{1}{\rho_{eff}} \quad \frac{\partial\psi}{\partial Z}\right]_{Z=0} = C(\psi_1 - \Delta V) \tag{8}$$

where ψ_1 is the value of ψ under contact one (ie, Z = 0) at some general (r_1,θ_1). Of course ΔV is the difference between the Fermi levels of the probes, as stated previously.

The quantity C is the reciprocal of the zero bias resistance of the contacts per unit area. They have been assumed to be identical. Equations (7) and (8) - as well as the remaining analysis - assume that the bias ΔV is small compared to kT so that the J-V characteristics of the metal-semiconductor contacts may be linearized.[3] Equations (7) and (8) may be written in integral form as

$$I = \int_0^a \int_0^{2\Pi} C\psi_2 r_2 dr_2 d\theta_2 \tag{9}$$

and

$$I = \int_0^a \int_0^{2\Pi} C\,(\Delta V - \psi_1)\; r_1 dr_1 d\theta_1 \tag{10}$$

These constraints are placed on the solution to eq. (6).

Having related ψ to the metal Fermi levels through eq (7) and (8) - a necessity since it is the difference between these Fermi levels which is actually measured - it is now possible to turn to the problem posed by the interfacial regions between layers. Rather than finding the electrostatic potential in these space charge regions [9], an alternative approach is to relate the solutions for ψ in two adjacent layers. If these interfaces are sufficiently thin, the current normal to these transitions regions is constant through the regions (9,10). Thus it follows that (see fig. 2 and 3)

$$\left[\frac{1}{\rho_{eff}} \quad \frac{\partial\psi}{\partial Z}\right]_{h_j} = \left[\frac{1}{\rho_{eff}} \quad \frac{\partial\psi}{\partial Z}\right]_{h_j+w_j} \tag{11}$$

[3] As is discussed in ref. [8], the current density depends on the difference in the Fermi levels between the metal and the semiconductor. If the general expression for this current density given in ref. [8] is linearized about zero bias, (7) and (8) result. That is, the right hand sides of (7) and (8) are just Taylor series expansions of the J-V characteristics.

is one such relation joining solutions in adjacent layers. Since eq. (6) is second order, another joining relation is needed [9,10]. Following reasoning similar to that which led to eq. (7) and (8), it is seen that this relation is provided by

$$\frac{1}{\rho_{eff}} \frac{\partial \psi}{\partial Z}\bigg|_{h_j} = C_j \left[\psi\big|_{h_j} - \psi\big|_{h_j + w_j} \right] \tag{12}$$

where all of these quantities in eq. (12) can depend on position in the boundary planes $Z = h_j$ and $Z = h_j + w_j$ of interface region j.

Of course, rather than using eq. (11) and (12), one could determine the electrostatic potential in the interface regions by solving Poisson's equation [9]. Boundary conditions would then be imposed on the electrostatic potential and its normal derivative (the electric field) at h_j and $h_j + w_j$, if this approach were selected. Such an approach is, of course, an exact one as opposed to the approximations (eq. (11) and (12)) involved in the alternative. From a practical point of view, one is forced to select eq. (11) and (12) in dealing with these interface regions [9].

With either approach ψ is completely specified in the semiconductor. Further, it must obey eq. (1)-(4) as well as conditions (9) and (10). Thus in principle ψ can be completely determined and the resistance measured experimentally (ie, eq. (5)) can be evaluated in terms of the material parameters of the semiconductor structure. That is, it is possible to establish what is being measured by the ratio $\Delta V/I$. Unfortunately, examination of the conditions on ψ as developed above demonstrates that the ratio $\Delta V/I$ can not just depend on the resistivity beneath the contacts since ψ does not. From this development presented it is clear that $\Delta V/I$ will depend on C, the parameter characterizing the probe-semiconductor contacts, on the geometry, the interfacial regions and the effective resistivity ρ_{eff}.

At this point it is necessary to establish why it is an effective resistivity that enters into ψ and, therefore, into $\Delta V/I$. This effective resistivity that appears in the conditions imposed on ψ (see eq. (7),(8),(11) and (12)) arises from the presence of stress fields in the material. As is well known, in the presence of a stress field the resistivity must be expressed as a second rank tensor $\underline{\underline{\rho}}$ [11,12]; thus

$$\underline{\underline{\rho}} = \rho \begin{bmatrix} 1 + \Delta_{11} & \Delta_{12} & \Delta_{13} \\ \Delta_{21} & 1 + \Delta_{22} & \Delta_{23} \\ \Delta_{31} & \Delta_{32} & 1 + \Delta_{33} \end{bmatrix} \tag{13}$$

where ρ is the scalar resistivity (in the absence of any stress). The second rank tensor $\underline{\underline{\Delta}}$ is related to the stress tensor $\underline{\underline{X}}$ by the fourth rank piezoresistance tensor $\underline{\underline{\underline{\underline{\Pi}}}}$ [11,12] Of course $\underline{\underline{\Delta}}$ vanishes if there is no stress field. Obviously there is a stress field under the probes [3,13]. This could even extend down (see figure 1) to at least the first interfacial region.

So it is an effective resistivity - determined from eq. (13) - which enters into ψ. If the probe has a pressure p applied to it, then for a {100} plane on Si (n or p type) ρ_{eff} under the contacts is given, after some manipulation, by

$$\rho_{eff} = \rho \, (1 - p\Pi_{11}) \tag{14}$$

For contacts on a {111} plane, the corresponding expression is

$$\rho_{eff} = \rho \frac{\left[\left\{1-\frac{p}{3}(\pi_{11}+2\pi_{12})\right\}^3 - 2\left\{\frac{p}{3}\pi_{44}\right\}^3 - 3\left\{\frac{p}{3}\pi_{44}\right\}^2\left\{1-\frac{p}{3}(\pi_{11}+2\pi_{12})\right\}\right]}{\left[\left\{1-\frac{p}{3}(\pi_{11}+2\pi_{12})\right\}^2 + \left\{\frac{p}{3}\pi_{44}\right\}^2 + 2\left\{\frac{p}{3}\pi_{44}\right\}\left\{1-\frac{p}{3}(\pi_{11}+2\pi_{12})\right\}\right]} \quad (15)$$

for n or p type Si. Here the Π_{ij} are components of a collapsed $\underline{\underline{\Pi}}$. [11]

Using data for the Π_{ij} in the literature [11,12] and $p = 10^{10}$ dynes/cm^2 results in the determination that, for {100} planes, under the contacts

$$\rho_{eff} \approx 2\rho \quad \text{for n-type Si} \quad (16)$$

and

$$\rho_{eff} \approx .94\rho \quad \text{for p - type Si} \quad (17)$$

For {111} planes, under the contacts

$$\rho_{eff} \approx \rho \quad \text{for n - type Si} \quad (18)$$

and

$$\rho_{eff} \approx .10\rho \quad \text{for p - type Si} \quad (19)$$

Unfortunately these are just estimates since data at high stress levels are not available for the Π_{ij} and the Π_{ij} depend on doping. However, the point has been made that an effective resistivity - due to stress - enters into ψ. Whether or not ρ_{eff} differs significantly from ρ depends on the stress and the crystallographic orientation. On the basis of eq. (18) and (19) alone one would estimate that the measured resistance $\Delta V/I$, for a given resistivity, would be lower for p-type material than for n-type if both had a {111} orientation and identical contacts and geometry. This piezoresistance effect may also be at least partially responsible for correction factors of less than unity which are seen on p-type Si. [14].

The zero bias resistance per area of the probe - semiconductor contacts, which enters into ψ and, therefore, into $\Delta V/I$, also depends on stress. In fact C is a function of the stress, temperature, doping, and crystallographic orientation [14-16]. The quantity C depends, in addition, on surface history. [14,16] Thus, in a spreading resistance measurement, $\Delta V/I$ depends on considerably more than just the resistivity of the material beneath the contact, as this above development has indicated.

3. Practical Considerations

The measured quantity $\Delta V/I$ depends on the contacts, mechanical stress, temperature, and the geometrical configuration of the layers as well as their resistivity and transition regions. Therefore, it is not surprising that, to employ the spreading resistance technique, it is necessary to assume that the resistivity of layer I (see figure 1) is related to the

measured $\Delta V/I$ by

$$\frac{\Delta V}{I} = K\left[\frac{\rho_I}{2a_{eff}}\right] \tag{20}$$

where K is a correction factor and the remaining terms are the ideal spreading resistance for a semi-infinite slab using the two probe configuration [17]. The quantity a_{eff} should be the radius of the contacts - a quantity depending only on the mechanical properties of the probe - semiconductor system. In actual fact, if K is used to correct for structure (that is, used in some manner to account for eq. (11) and (12) as is done in ref. [17]), it is found that a_{eff} is an effective radius not a geometrical radius. It can vary by a factor of more than 2 with resistivity [17] and in practical applications is determined from a calibration curve obtained from a body of uniform resistivity. Obviously the effective radius is attempting to account for the various other phenomena involved in a spreading resistance measurement which were discussed in section 2.

It is interesting to establish how eq. (2) may be obtained from eq. (5), a statement which is fundamentally correct. If eq. (5), (7), and (8) are manipulated, it follows from some straightforward algebra that eq. (5) can be written as

$$\frac{\Delta V}{I} = \frac{2}{\int_0^a \int_0^{2\Pi} C r_1 dr_1 d\theta_1} + \frac{1}{I} \frac{\int_0^a \int_0^{2\Pi} C(\psi_1 - \psi_2)\, r_1 dr_1 d\theta_1}{\int_0^a \int_0^{2\Pi} C\, r_1 dr_1 d\theta_1} \tag{21}$$

where the probes have been assumed identical. In the term involving ψ_1 and ψ_2, it is necessary to evaluate these quantities at equivalent points under the contacts in integrating. Obviously the first term on the right may be interpreted as a resistance arising from the contacts only. The second term involves (through the conditions on ψ) the contacts, the geometry of the layered configuration, the interfacial regions, and the piezoresistivity effects.

If C is assumed constant and very large (ie, ohmic contacts between the probes and the semiconductor) the metal Fermi levels line up with the Fermi level of the semiconductor just beneath the contact. Thus in this case, $\psi_2 = 0$ and $\psi_1 = \Delta V$ replace eq. (7) and (8) and eq. (21) reduces to

$$\frac{\Delta V}{I} \simeq \frac{1}{I\Pi a^2} \int_0^a \int_0^{2\Pi} (\psi_1 - \psi_2)\, r_1\, dr_1\, d\theta_1 \tag{22}$$

Using an approximation in eq. (22) for ψ proposed by Schumann and Gardner [9] allows eq. (21) to be finally reduced to

$$\frac{\Delta V}{I} = K \left.\frac{\rho_{eff}}{2a}\right|_{z=0} \tag{23}$$

where K is a function of the various layer resistivities (which may actually depend on stress at least for the first layer), the radius a, and the geometry [9]. Of course, here a is the radius of the contacts.

565-448 O - 75 - 3

The approximation for ψ used to obtain eq. (23) assumes the C_j of eq. (12) are infinite. Further it does not obey the conditions $\psi_1 = \Delta V$ and $\psi_2 = 0$ applicable in the assumed case of ohmic contacts but rather fits a postulated current distribution under the contacts - an expediency used to avoid mixed boundary conditions [9]. Thus if the K of Schumann and Gardner is used in eq. (2), a_{eff} is attempting to account for piezoresistivity and the zero bias resistance of the contacts. It can not account for the C_j quantities of the interface layers since it is usually obtained from a calibration curve for uniform material.

Thus using eq. (21) and a K developed as indicated is beset with assumptions and simplifications. This fact has led Hu [17], in commenting on the limits of accuracy one could expect from eq. (21), to note that this "mathematical model of the multilayer spreading resistance rests on a number of simplifying assumptions, most of which are not accurate."

4. Conclusions

From eq. (21), it can be seen that the quantity being measured for the structure shown in fig. 1 is

$$\frac{\Delta V}{I} = 2R_c + R \tag{24}$$

where R_c is a measure of the contact resistance only and R depends on the contacts, the resistivities, and the geometry of the structure. If eq. (20) is used for R, the accuracy of the measurement is limited obviously by the choice of K and a_{eff}; that is, the accuracy is limited by the approximation used for ψ in the term

$$\frac{1}{I}\,\frac{\int_0^a \int_0^{2\pi} C\,(\psi_1 - \psi_2)\, r_1 dr_1 d\theta}{\int_0^a \int_0^{2\pi} C\, r_1 dr_1 d\theta_1}$$

In practice the term involving R_c in eq. (24) is frequently neglected.

5. References

(1) Holm, R., Electric Contacts Handbook, Springer, Berlin (1967).

(2) Gardner, E.E., Hallenback, J.F., and Schumann, P.A., Solid-St. Electron, 6, 311 (1963).

(3) Mazur, R.G. and Dickey, D.H., J. Electrochem. Soc. 113, 255(1966).

(4) Gupta, D.C. and Chan, J.Y., Rev. Sci. Instr. 41, 176 (1970).

(5) Schumann, P.A., Gorey, E.F., and Schneider, C.P., Solid St. Tech. 15, 50 (1972).

(6) Kramer, P. and Van Ruyven, L., Solid St. Electron, 15, 757 (1972).

(7) Foxhall, G.F. and Lewis, J.A., Bell System Tech. Journal. 43, 1609 (1964).

(8) Fonash, S.J., Solid St. Electron, 15, 783 (1972).

(9) Schumann, P.A. and Gardner, E.E., J. Electrochem. Soc: Solid St. Sci. 116, 87 (1969).

(10) Brook, P. and Smith, J.G., Electronics Lett., 9, 253 (1973).

(11) Smith, C.S., Phys. Rev. 94, 42 (1954).

(12) Smith, C.S., Solid St. Physics (F. Seitz and D. Turnbull, Eds.) 6, 175. Academic Press, Inc. N.Y. (1958).

(13) Severin, P.J., Solid St. Electron. 14, 247 (1971).

(14) Kramer, P. and Van Ruyven, L.J., Solid St. Electron. 15, 757 (1972).

(15) Kramer, P. and Van Ruyven, L.J., Appl. Phys. Lett. 20, 420 (1972)

(16) Fonash, S.J., J. Appl. Phys., 45, 496 (1974).

(17) Hu, S.M., Solid-St. Electron. 15, 809 (1972).

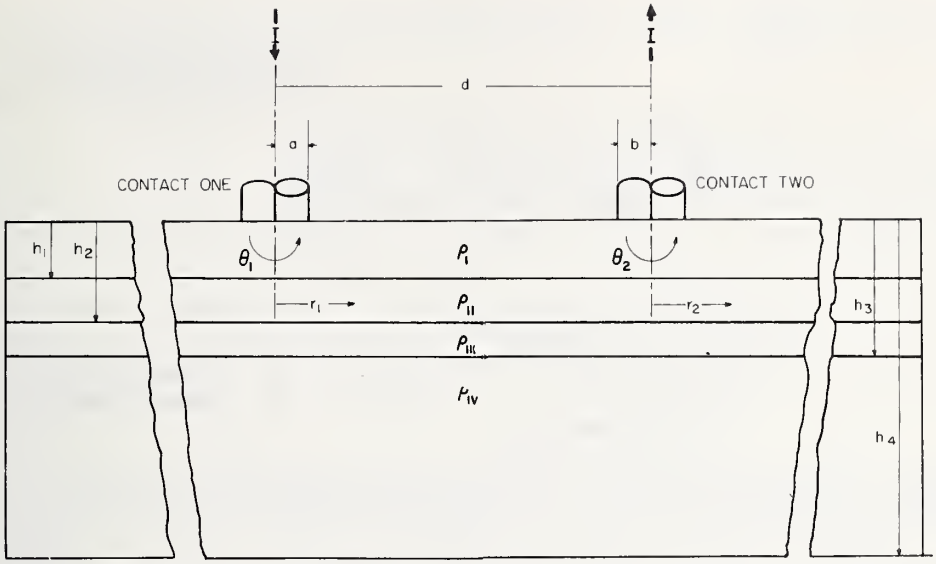

Figure 1. Configuration for Spreading Resistance Measurements on a Layered Structure. The Two-probe setup is shown.

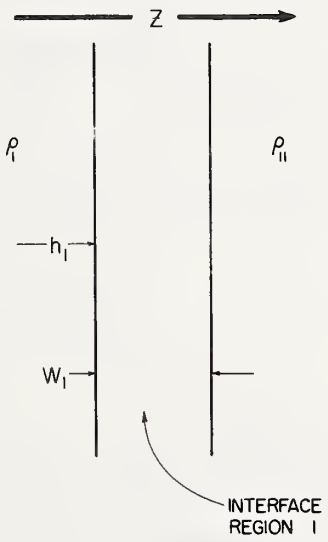

Figure 2. The Transition -or Interface- Region Between Two Ideally Uniform Layers.

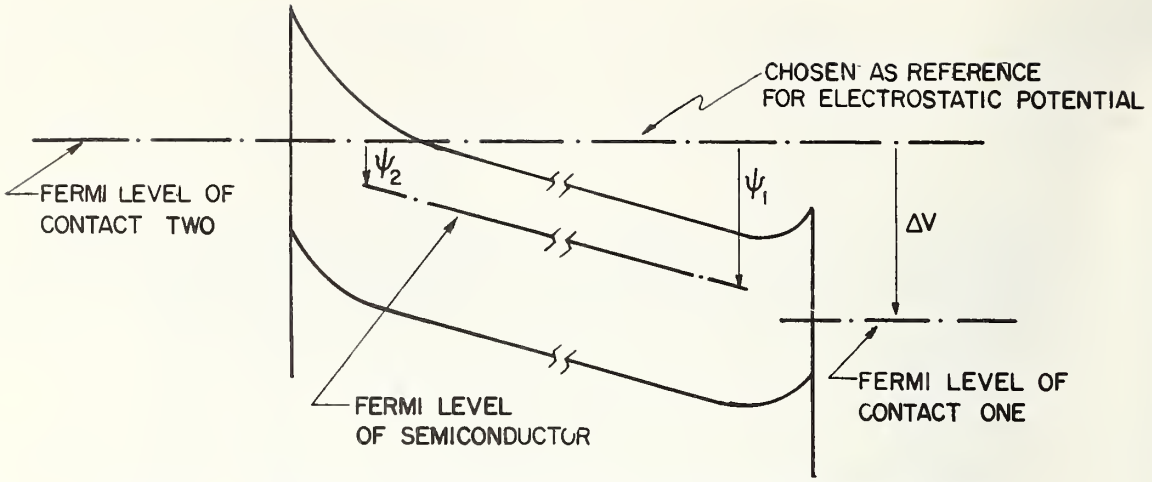

Figure 3. An Energy Band Diagram Through an Interface Region Such as That Shown in Figure 2. Bias Drop Across this Region is Indicated.

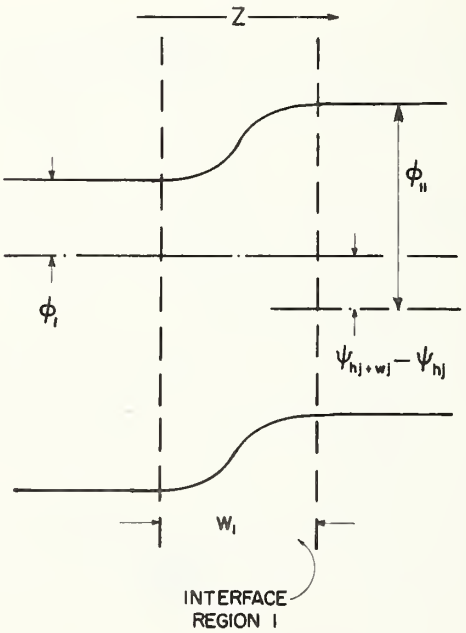

Figure 4. Diagram Showing the Energy Band Bending Under the Contacts. Also indicated is the reference electrostatic Potential.

NATIONAL BUREAU OF STANDARDS SPECIAL PUBLICATION 400-10, Spreading Resistance Symposium, Proceedings of a Symposium Held at NBS, Gaithersburg, Md., June 13-14, 1974.

FORMAL COMPARISON OF CORRECTION FORMULAE FOR SPREADING RESISTANCE MEASUREMENTS ON LAYERED STRUCTURES

P.J. Severin

Philips Research Laboratories
Eindhoven, The Netherlands

The spreading resistance of a metal contact on a semiconductor sample is analysed for infinite geometry, with three different boundary conditions: a specified potential of the contact, a uniform contact current density and a current density dependent on contact resistance. The cases of a thin layer on a perfectly conducting substrate and on a non-conducting substrate are analysed each for the boundary conditions of uniform current density and of the current density distribution valid for the infinite geometry. With a perfectly conducting substrate the two boundary conditions yield about 10% difference. With a non-conducting substrate calculations based on both current density distributions produce in the thin layer approximation the same ln r dependence required. The constant terms in both approaches are different by 5% and the constant current density result in addition agrees with the result obtained with a totally different transmission-line approach. The actual three-point-probe measurement situation is discussed. The danger of correcting the precise spreading resistance measurement results with an error of 1%, with formulae derived on the basis of a formal model which is sensitive to the choice of the boundary conditions by up to 10%, is stressed. The effects of undefined thickness, bevel edge and transition layer curving upwards are mentioned as further complications.

Key words: Contact resistance, correction formulae, sheet resistance, silicon, spreading resistance.

1. Introduction

Spreading resistance measured on a structure of infinite lateral extent, but finite layer thickness d is different from the spreading resistance measured on an infinite geometry. Their ratio is generally referred to as a correction formula for a finite thickness measurement result. Such formulae have been derived by Schumann and Gardner [1], initially for a two-layer system and extended later [2] to a graded structure. This theory has been used in computer solutions by Yeh [3], Kokhani [4], Hu [5] Some preliminary studies are available in the form of reports [6, 7].

In the standard solution for infinite geometry a constant potential V_o of the contact of radius A is specified and the potential $V(r,z)$ and the current density distribution $J_z(r,o)$ over the contact are calculated. In the approach followed by Schumann et al. [1] to solve the potential for finite layer thickness d the same current density distribution $J_z(r,o)$ is

[1] Figures in brackets indicate the literature references at the end of this paper.

used to calculate $V(r,o)$. The potential V_o of the probe is obtained by averaging $V(r,o)$ over the contact area. This problem is solved for any ratio of the resistivities ρ_1 of the layer and ρ_2 of the substrate. In order to check the validity of this approach we have studied the sensitivity of the solutions for the two limiting cases $\rho_2 = 0$ and $\rho_2 = \infty$ to the choice of the boundary conditions. In particular we studied the cases $d/A \ll 1$ and $d/A \gg 1$, which have well known solutions.

In the next section the case of infinite geometry is investigated using the conventional approach (2.1) and assuming a uniform current density over the contact (2.3). The effect of the boundary condition resulting from contact resistance which modifies the current density distribution over the contact, is also examined (2.2). In the third section, devoted to the case $\rho_2 = 0$, the approach of Brooks and Mattes [8] is shown to be incorrect (3.1) and the approach with uniform current density over the contact (3.2) is compared to the results obtained by Schumann et al. [1] (3.3). In the fourth section, devoted to the case $\rho_2 = \infty$, the same two approached are again compared, (4.1) and (4.2), and both approximations are found to yield divergent integrals for $V(r,z)$. When the difference between the potential V_o of the contact and the potential $V(r,o)$ is introduced the malignant terms cancel. With both approaches in the thin layer approximation the satisfying result is found that the potential depends on r as $\ln r$, (4.1) and (4.2). This is also the experimentally verified result of an elementary consideration (4.3). A transmission-line approach, valid for thin layers with a contact resistance which influences the current distribution at the contact, described earlier [9], is compared with the present results (4.3). In the approximation of dominant contact resistance this transmission-line approach produces exactly the same expression as did the uniform currrent density approach (4.1). Schumann's approach yields a slightly different result. Spreading resistance measurements are essentially three-point-probe measurements. Two different probe configurations are currently in use with different but related formulae. The difference in particular for thin layers is discussed in the fifth section.

The experimental results of spreading resistance measurements are extremely precise [10], about 1%. The conversion to the local resistivity, let alone to the local dope atom concentration, is hindered by the uncertainties originating from the choice of a not sufficiently realistic model for a thin layer structure. In addition to this, the effective contact resistance due to micro-contacts, deeper damage or barrier-resistance, should be taken into account. Furthermore, the effects of the bevel edge, of the finite transition layer at the interface and of the modification of the transition layer due to the exposure at the bevel are mentioned in the summary.

2. Infinite geometry

The potential distribution due to a circular metal disk of radius A at potential V_o on a semi-infinite medium of resistivity ρ has been discussed by various authors. Formulated in this way or as the problem of a charged disk on top of an isolating medium it is a classical text book example of the application of mixed boundary conditions [11, 12]

2.1. Mixed boundary conditions solution

In cylindrical coordinates, shown in figure 1, the potential $V(r,z)$ is a solution of Laplace's equation, which reads for circular symmetry

$$\frac{1}{r}\frac{\partial}{\partial r}\left(r\frac{\partial V}{\partial r}\right) + \frac{\partial^2 V}{\partial z^2} = 0 \quad . \tag{1}$$

The solution can be easily obtained with separation of variables to be given in terms of a Bessel function $J_o(kr)$

$$V(r,z) = \int_0^\infty dk \; f(k) \; J_o(kr) \; e^{-kz} \; . \tag{2}$$

In this solution as a first boundary condition has been used $V(r, \infty) = 0$, and the second boundary condition at z = 0 is of mixed nature [12], for the potential of the contact (3)

$$V_o = \int_0^\infty dk \; f(k) \; J_o(kr) \qquad \text{for} \quad 0 < r < A \; , \tag{4a}$$

and for the electric field strength

$$E_z(r,0) = \int_0^\infty dk \; f(k) \, k \; J_o(kr) = 0 \qquad \text{for} \quad r > A \; . \tag{4b}$$

To this set of dual integral equations

$$f(k) = \frac{2V_o}{\pi} \; \frac{\sin Ak}{k} \tag{5}$$

is known to be the solution because

$$\int_0^\infty dk \; \frac{\sin Ak}{k} \; J_o(kr) = \begin{cases} \frac{\pi}{2} & \text{for} \quad 0 < r < A \\ \arcsin \frac{A}{r} & \text{for} \quad r > A \end{cases} \tag{5a}$$

and

$$\int_0^\infty dk \; \sin Ak \; J_o(kr) = \begin{cases} (A^2 - r^2)^{-1/2} & \text{for} \quad 0 < r < A \\ 0 & \text{for} \quad r > A \; , \end{cases} \tag{5b}$$

so that the potential becomes

$$V(r,z) = \frac{2V_o}{\pi} \int_0^\infty dk \; \frac{\sin Ak}{k} \; J_o(kr) \; e^{-kz} \; . \tag{6}$$

The current i_o flowing into the metal contact is given by

$$i_o = \frac{2\pi}{\rho} \int_0^\infty dr \; r \; E_z(r,0) \; , \tag{7}$$

which with eqs (6) and (5b) becomes

$$i_o = \frac{4A}{\rho} \; V_o \tag{8}$$

or

$$R_s = \frac{\rho}{4A} \; , \tag{8a}$$

the well known spreading resistance formula for infinite geometry. It is interesting to note that the electric field has infinite strength at r = A, which is physically unrealistic.

2.2. The influence of contact resistance on the current density distribution.

In practice the ideal spreading resistance as given by eq. (8a) is seldom or never measured. The contact to the semi-conductor is not as perfect as it is supposed to be in formulating the problem: usually an extra voltage drop is noted due to zero-bias-barrier resistance [13,14], a multitipped [10,15,16] or otherwise incomplete contact. This effect is usually taken into account by calibrating the probe so that the effective spreading resistance

$$R_e = k(\varsigma)\,\frac{\varsigma}{4A}\,, \tag{9}$$

or introducing a series contact resistance R_c to $\varsigma/4A$

$$R_c = (k(\varsigma)-1)\,\frac{\varsigma}{4A}\,. \tag{9a}$$

However, it is not self evident that the extra voltage drop can be considered as being due to a series resistance which does not influence the current density distribution over the contact area. This problem can be analysed as follows. The boundary condition which incorporates the specific contact resistance R_c' (Ω cm^2), is

$$V(r,0) = V_0 - R_c' J_z(r,0)\,, \tag{10a}$$

which with $\Lambda = R_c'/\varsigma$ and

$$J_z(r,0) = -\frac{1}{\varsigma}\left(\frac{\partial V}{\partial z}\right)_{z=0}$$

gives

$$V(r,0) = V_0 + \Lambda\left(\frac{\partial V}{\partial z}\right)_{z=0}\,. \tag{10b}$$

The contact resistance makes the mixed boundary conditions quite complicated, but by choosing an oblate spheroidal coordinate system the same boundary conditions can be formulated conventionally [17]. With the coordinates shown in figure 2,

$$z = \xi\eta$$
$$r^2 = (1-\xi^2)(1+\eta^2) \tag{11}$$

Laplace's equation can be separated by putting

$$V(\xi,\eta) = X(\xi)\cdot Y(\eta) \tag{12a}$$

into

$$\frac{d}{d\xi}\left(1-\xi^2\right)\frac{dX}{d\xi} + X = 0\,, \tag{12b}$$

$$\frac{d}{d\eta}\left(1+\eta^2\right)\frac{dY}{d\eta} + Y = 0\,. \tag{12c}$$

The solution to eqs (12b) and (12c) in terms of Legendre polynomials $P_n(x)$ and $Q_n(x)$ reads

$$X(\xi) = a_n P_n(\xi) + b_n Q_n(\xi)$$

$$Y(\eta) = c_n P_n(j\eta) + d_n Q_n(j\eta). \qquad (13)$$

From the boundary conditions it follows that some coefficients are zero, because with r, z $\to \infty$ likewise $\eta \to \infty$, and $P_n(z) \to \infty$ as z^n, the coefficients $c_n = 0$ to satisfy V $\to$ 0, for r, z $\to \infty$. Because at $\xi = 0$ the electric field;

$$\frac{1}{\xi}\frac{\partial V}{\partial \xi} = \frac{1}{\eta}\frac{\partial V}{\partial \eta} = 0$$

the solution should be even in ξ. Finally $Q_n(\xi)$ has a singular point at $\xi = 1$ so that the coefficient b_n must be zero. Hence the solution is

$$V(\xi, \eta) = \sum_{n=0}^{\infty} a_{2n} P_{2n}(\xi) \cdot Q_{2n}(j\eta). \qquad (14)$$

When this solution is subjected to the newly formulated boundary condition, eq. (10b), the condition to be satisfied reads

$$\sum_{n=0}^{\infty} a_{2n} P_{2n}(\xi) \left[Q_{2n}(0) + \frac{j\Lambda}{|\xi|} \left(\frac{\partial Q_{2n}(j\eta)}{\partial j\eta} \right)_{\eta=0} \right] = 1. \qquad (15)$$

This condition can be converted into an infinite system of linear equations for the unknowns a_{2n}, which upon proper truncation can be numerically solved to the required precision. The total current i_o can then be easily calculated from

$$i_o = \frac{2\pi}{\rho} \int_0^1 d\xi \sum_{n=0}^{\infty} P_{2n}(\xi) \cdot \left(\frac{\partial Q_{2n}(j\eta)}{\partial j\eta} \right)_{\eta=0} a_{2n}$$

$$= \frac{2\pi}{\rho} j a_o. \qquad (16)$$

The calculation of a_o has been done and the surprising result is that for the parameter Λ/A assuming the values 0, 0.1, 1 and 10 the resistance is, by at most a few percent larger than the resistance obtained by simply adding $R_c'/\pi A^2$ and $\rho/4A$ in series. The parameter Λ/A, apart from a factor $\pi/4$, is equal to the ratio of these two resistances and the range investigated covers any practical situation. Hence in the infinite geometry the separation implied in eqs (9) and (9a) turns out to be allowed. However, the effect of contact resistance R_c on spreading resistance is more complicated in a finite geometry. An example is treated in sec. 4.4

2.3. Solution with uniform contact current density distribution

An alternative way to avoid the mixed boundary conditions and the infinite field strength at r = A is to specify the electric field, instead of the potential at the contact. The electric field corresponding to a uniform current density distribution at the contact is given by

$$E_z = \frac{i_o \rho}{\pi A^2} \qquad \text{for } 0 < r < A \qquad (17a)$$

and, as before,

$$E_z = 0 \qquad \text{for } r > A. \tag{17b}$$

The potential of eq. (2) then yields

$$\int_0^\infty dk\ f(k)\ k\ J_0(kr) = \begin{cases} \frac{i_0 \rho}{\pi A^2} & \text{for} \quad 0 < r < A \quad (17c) \\ 0 & \text{for} \quad r > A \quad (17d) \end{cases}$$

and f(k) follows from comparison with

$$\int_0^\infty dk\ J_1(kA)\ J_0(kr) = \begin{cases} \frac{1}{A} & \text{for} \quad 0 < r < A \\ 0 & \text{for} \quad r > A \end{cases}, \tag{18}$$

so that the potential reads

$$V(r,z) = \frac{i_0 \rho}{\pi A} \int_0^\infty dk\ \frac{1}{k}\ J_1(kA)\ J_0(kr)\ e^{-kz}. \tag{19}$$

According to this equation the potential at z=0 of the contact depends on r. This is a direct consequence of the choice of the uniform current density boundary condition. By averaging the potential V(r,o) over the contact area V_o, expressed in $R_s = V_o/i_o$, is found to be

$$R_s = \frac{8}{\pi}\frac{\rho}{4A} \int_0^\infty dx\ \frac{1}{x^2}\ J_1^2(x) = \frac{32}{3\pi^2}\frac{\rho}{4A}. \tag{20}$$

It is to be concluded that at least for the infinite geometry this approximation of an uniform current density at the contact is a fairly good one, differing by only 8% from the result in eq. (8a).

It is worth noting here that R_s has never yet been verified with sufficient precision to be able to decide unequivocally between eqs (8a) and (20). Generally, spreading resistance measurements are hampered by a large contact resistance, which has not been determined separately with sufficient precision and accuracy. An experimental determination of R_s/ρ, within a few percent error, was done recently with a mercury probe [18]. Because the mercury probe has a much larger contact diameter 2A=1 mm than any conventional probe and should be applied on a carefully prepared surface, the contact resistance does not play a role. The spreading resistance on bulk material has been found to satisfy eq. (8a) or (20) over a range of four decades of resistivity on N-type Si, as shown in figure 3.

3. Thin layer on infinitely conducting substrate

3.1. The Brooks and Mattes approach

A structure to which a spreading resistance measurement is frequently applied, consists of a thin layer of thickness $d \lesssim A$ on a much better conducting substrate. Considering the substrate as a perfect conductor this problem has been treated by Brooks and Mattes [8]. Unfortunately, they made an error and the problem should be formulated as follows.

The potential again is a solution of Laplace's equation

$$V(r,z) = \int_0^\infty dk \; C_1(k) \left(e^{kz} + C_2(k)\, e^{-kz} \right) J_0(kr) \,, \tag{21}$$

which, because V(r,d)=0 and hence

$$C_2(k) = - e^{2kd} \,, \tag{22}$$

can be simplified to

$$V(r,z) = \int_0^\infty dk \; C_1(k) \left(e^{kz} - e^{k(2d-z)} \right) J_0(kr) \,. \tag{23}$$

The mixed boundary conditions corresponding to eqs (4a) and (4b) now read as

$$V_0 = \int_0^\infty dk \; C_1(k) \left(1 - e^{2kd} \right) J_0(kr) \qquad \text{for} \quad 0 < r < A \tag{24a}$$

and

$$E_z(r,0) = - \int_0^\infty dk \; C_1(k)\, k \left(1 + e^{2kd} \right) J_0(kr) = 0, \quad \text{for } r > A. \tag{24b}$$

There is no known analytical solution to these dual integral equations and this line of reasoning cannot be pursued.

Brookes and Mattes arrive at the mixed boundary conditions on the surface in the form

$$V_0 = \int_0^\infty dk \; c_1 \; f(k) \; J_0(kr) \qquad \text{for} \quad 0 < r < A \tag{25a}$$

and, with the correction of an obvious misprint,

$$\int_0^\infty dk \; k \; c_2 \; f(k) \; J_0(kr) = 0 \qquad \text{for } r > A \,, \tag{25b}$$

to which

$$f(k) = \frac{2V_0}{\pi} \; \frac{A}{c_1} \; \frac{\sin Ak}{Ak} \tag{25c}$$

would be a solution were it not that C_1 and C_2 are functions of k, which they derive later, and not constants as they appear to suggest. Their final result, which has been computed and is plotted in figure 4, is however remarkably close to the results obtained otherwise.

3.2. Solution with uniform contact current density distribution

As discussed in sec. 3.1, the potential cannot be solved analytically assuming a constant potential of the contact V_0. However, an analytic solution can be obtained if it is assumed that the electric field is

uniform over the contact area, as done for the infinite geometry in sec. 2.3.

Application of the boundary condition eq. (17) and the relation eq. (18) to the non-zero field strength of eq. (24b) yields

$$C_1(k) = J_1(kA) \cdot A \; \frac{1}{k(1+e^{2k\alpha})} \; \frac{\rho i_o}{\pi A^2} \tag{26}$$

and hence

$$V(r,z) = A \frac{\rho i_o}{\pi A^2} \int_0^\infty \alpha k \; \frac{J_1(kA)}{k} \; J_0(kr) \; \frac{e^{-k(z-\alpha)} - e^{k(z-\alpha)}}{e^{-k\alpha} + e^{k\alpha}} . \tag{27}$$

Now the average value of V(r,o) over the contact area, the applied potential V_o, with $y = \alpha/A$ and $x = kA$, expressed in $R_s = V_o/i_o$, is

$$R_s = \frac{8}{\pi} \frac{\rho}{4A} \int_0^\infty dx \; \frac{J_1^2(x)}{x^2} \; \frac{e^{xy} - e^{-xy}}{e^{xy} + e^{-xy}} . \tag{28}$$

The validity of this equation can be checked by considering the two extreme cases of a very thick and a very thin layer. With a very thick layer, $y \to \infty$, and R_s approximates the expression for infinite geometry eq.(20). For a very thin layer the integral eq. (28) yields as expected

$$R_s = \frac{8}{\pi} \frac{\rho}{4A} \int_0^\infty dx \; \frac{J_1^2(x)}{x^2} \; xy = \frac{\rho \alpha}{\pi A^2} . \tag{29}$$

Eq. (28) has been computed and is presented as a plot of $R_s(\alpha/A)/R_s(\infty)$ vs d/A in figure 4.

3.3. Solution with infinite geometry contact current density distribution

The choice of a uniform electric field is one of several possibilities to avoid the mixed boundary conditions by specifying the electric field at the top side of the structure. Schumann et. al.[1] have based their analysis on the choice of the field strength at the contact that exists with an infinite geometry

$$E_z(r,o) = \frac{i_o \rho}{2\pi A (A^2 - r^2)^{1/2}} \qquad \text{for } 0 < r < A \tag{30a}$$

and, as before,

$$E_z(r,o) = 0 \qquad \text{for } r > A. \tag{30b}$$

The potential, subjected to the boundary condition V(r,d)=0, as before, is given by eq. (23). Now applying to the non-zero field strength of eq.(24b) the boundary conditions eq. (30), it can be seen from eq. (5b) that

$$C_1(k) = \frac{i_o \rho}{2\pi A} \; \frac{\sin kA}{k} \; \frac{1}{1+e^{2k\alpha}} . \tag{31}$$

Hence the potential reads

$$V(r,z) = \frac{i_o \rho}{2\pi A} \int_0^\infty dk \, \frac{\sin kA}{k} J_o(kr) \frac{e^{-k(z-d)} - e^{k(z-d)}}{e^{-kd} + e^{kd}} . \tag{32}$$

The average value of V(r,o) over the contact area, V_o, expressed in $R_s = V_o/i_o$, yields

$$R_s = \frac{4}{\pi} \frac{\rho}{4A} \int_0^\infty dx \, \frac{\sin x}{x^2} J_1(x) \frac{e^{xy} - e^{-xy}}{e^{xy} + e^{-xy}} . \tag{33}$$

Making the approximation for a thick layer directly from the potential eq. (32) at the surface $z = 0$, it is found that the potential equals the potential for the infinite geometry eq. (6). The spreading resistance eq. (33), in the same approximation correctly yields R_s as in eq. (8a). For a thin layer the spreading resistance is found to be given as expected by eq. (29). Eq. (33) has also been computed and plotted in figure 4.

3.4. An experimental approach

An experimental approach has been followed by Cox and Strack [19] who studied the resistance in the case in point as a function of contact radius A. They assumed that the resistance is composed of the contributions due to contact resistance, spreading resistance corrected for finite thickness and residual resistance:

$$R = \frac{R_c'}{\pi A^2} + \frac{\rho}{4A} f\left(\frac{d}{A}\right) + R_o . \tag{34}$$

By plotting the total resistance R vs 1/A the three different components can be separated. From electrolytic tank experiments they concluded that the function f obeys the empirical relation

$$f\left(\frac{d}{A}\right) = \frac{2}{\pi} \arctan \frac{2d}{A} , \tag{35}$$

which has the correct value in the extremes d → o and d → ∞ . Eq. (35) has also been plotted in figure 4.

4. Thin layer on zero-conductivity substrate

4.1. Solution with uniform contact current density distribution

Another structure for which it is of interest to know the spreading resistance as a function of the thickness $d \lessapprox A$ is a thin layer on a non-conducting substrate or separated from a conducting substrate by an isolating layer.

The potential is again given by eq. (21) and the electric field at z=d equals

$$E_z(r,d) = -\int_0^\infty dk \, k \, c_1(k) \left(e^{kd} - c_2(k) e^{-kd} \right) J_o(kr) . \tag{36}$$

Because $E_z(r,d) = 0$ should be valid for all r

$$C_2(k) = e^{2kd} \tag{37}$$

and hence the electric field at z=0 is

$$E_z(r,0) = -\int_0^\infty dk\ k\, C_1(k) \left(1 - e^{2kd}\right) J_0(kr) . \tag{38}$$

Applying the boundary condition eq. (17) and eq. (18), eq. (38) yields

$$V(r,z) = \frac{\rho i_0}{4A} \frac{4}{\pi} \int_0^\infty dk \frac{J_1(kA)}{k} J_0(kr) \frac{e^{k(z-d)} + e^{-k(z-d)}}{e^{kd} - e^{-kd}} . \tag{39}$$

The average value of V(r,o) over the contact area, V_o, with y = d/A and x = kA is found to be

$$V_o = \frac{i_o \rho}{4A} \frac{8}{\pi} \int_0^\infty dx \frac{J_1^2(x)}{x^2} \frac{e^{xy} + e^{-xy}}{e^{xy} - e^{-xy}} . \tag{40}$$

For a very thick layer the potential and the spreading resistance approximate the expressions for infinite geometry eqs (19) and (20). For any other layer, and mathematically for any layer, the integral eqs. (39) and (40) do not exist. However, when the potential at the distance r at the surface z=0 is referred to the averaged potential V_o of the contact, a non-divergent integral is found because the malignant terms cancel

$$V_o - V(r,0) = \frac{\rho i_0}{\pi A} \int_0^\infty dx \frac{J_1(x)}{x} \frac{e^{xy} + e^{-xy}}{e^{xy} - e^{-xy}} \left\{ \frac{2J_1(x)}{x} - J_0\left(x \frac{r}{A}\right) \right\} . \tag{41}$$

For a very thin layer, y $\rightarrow$ o, the integral in eq. (41) can be solved exactly. Then for z=0 eq. (39) can be approximated as

$$V(r) = \frac{\rho i_0}{\pi d} \int_0^\infty dx \frac{1}{x^2} J_1(x) J_0\left(x \frac{r}{A}\right) \tag{42}$$

and invoking the expression [20]

$$\int_0^\infty dx \frac{J_1(bx)}{x^2} \left(J_0(ax) - 1\right) = \frac{-b}{4} \left(1 + 2 \ln \frac{a}{b}\right) , \tag{43}$$

it follows that

$$V(r) = \frac{\rho i_0}{\pi d} \left[-\frac{1}{4} \left(1 + 2 \ln \frac{r}{A}\right) + \int_0^\infty dx \frac{J_1(x)}{x^2} \right] . \tag{44}$$

This is a satisfying result because this dependence on r is exactly the dependence which follows from an irrefutable elementary consideration, eqs (49) and (50), which, moreover, has been verified experimentally with high precision by us. Using eq.(44) the non-divergent integral eq. (41) can be written as

$$V_o - V(r) = \frac{\rho i_o}{\pi d}\left[-\int_0^\infty dx\, \frac{J_1(x)}{x^2}\left(1 - \frac{2J_1(x)}{x}\right) + \left(\frac{1}{4} + \frac{1}{2}\ln\frac{r}{A}\right)\right] \tag{45}$$

Because the integral equals 1/8, eq. (45) can be written as

$$V_o - V(r) = \frac{\rho i_o}{8\pi d} + \frac{\rho i_o}{2\pi d}\ln\frac{r}{A} . \tag{45a}$$

In this way it has been shown that by considering the potential difference the divergency of the integral is removed, that the correct dependence of the thin layer resistance on the distance r is obtained and that the resistance between the contact and r=A equals $\rho/8\pi$ d. In sec. 4.3 it will be recapitulated that this value has also been obtained earlier [9] from a very different transmission-line model. In the absence of a zero-voltage reference at infinity, R_s should be defined from a three point-probe system to be discussed in sec. 5.

4.2. Solution with infinite geometry contact current density distribution

Applying the Schumann et al. [1] approximation to this structure, by imposing the boundary condition eq. (30) and the relation eq. (5a) to eq. (38) it is found that

$$V(r,z) = \frac{i_o \rho}{2\pi A}\int_0^\infty dk\, \frac{\sin Ak}{k}\, J_0(kr)\, \frac{e^{k(z-d)} + e^{-k(z-d)}}{e^{kd} - e^{-kd}} . \tag{46}$$

Hence the average value of V(r,o) over the contact area, V_o, yields

$$V_o = \frac{i_o \rho}{4A}\,\frac{4}{\pi}\int_0^\infty dx\, \frac{\sin x}{x^2}\, J_1(x)\, \frac{e^{xy} + e^{-xy}}{e^{xy} - e^{-xy}} . \tag{47}$$

For a very thick layer this expression approximates the expression for infinite geometry eq. (6). For any other, and mathematically for any layer, the integrals eqs (46) and (47) are divergent. Again referring the potential at the distance r at the surface z=0 to the averaged potential V_o, a non-divergent integral is found

$$V_o - V(r) = \frac{\rho i_o}{2\pi A}\int_0^\infty dx\, \frac{\sin x}{x}\, \frac{e^{xy} + e^{-xy}}{e^{xy} - e^{-xy}}\left\{\frac{2J_1(x)}{x} - J_0\left(x\frac{r}{A}\right)\right\} . \tag{48}$$

For a very thin layer, y $\rightarrow$ o, eq. (48) reads

$$V_o - V(r) = \frac{\rho i_o}{2\pi d}\int_0^\infty dx\, \frac{\sin x}{x^2}\left\{\frac{2J_1(x)}{x} - J_0\left(x\frac{r}{A}\right)\right\} . \tag{48a}$$

which can be solved exactly to yield

$$V_o - V(r) = \frac{\rho i_o}{6\sqrt{2}\,\pi d} - \frac{\rho i_o}{2\pi d} \ln \frac{r}{A} . \qquad (48b)$$

This result cannot experimentally be distinguished from eq. (45a) obtained with the constant current density approach.

4.3. Solution with transmission-line approach

From elementary considerations it is clear, that at a distance r from the centre $E_z(r,z)=0$, that the total current i_o is related to $E_r(r,z)$ as

$$E_r(r,z) = \frac{i_o \rho}{2\pi d r} , \qquad (49)$$

and that hence for a thin layer the potential difference between points at r=A and r equals

$$V(A) - V(r) = \frac{i_o \rho}{2\pi d} \ln \frac{r}{A} . \qquad (50)$$

The difference between the potential V_o of the contact and the potential at r=A should be added to the potential eq. (50). However, this potential is only independent of z when the layer is very thin with respect to the probe radius. For this geometry a transmission-line model has been worked out [9], where the current is assumed to flow in the z-direction only through the contact resistance R_c at the metal-silicon interface and radially anywhere else. The resistance R_m between the contact and the cylinder wall at r=A has been calculated to be

$$R_m = \frac{\rho}{2\pi d} F(u) , \qquad (51)$$

with $u^2 = A^2 \rho / R_c' d$. The function $F(u) = I_o(u)/uI_1(u)$, where I_o and I_1 are modified Bessel functions of the first kind, is plotted in figure 5. An essentially similar approach with a linear geometry has been followed for many years to derive the contact potential based on an expression [9] given by Shockley. Eq. (51) can be used for the same purpose.

This approach can be compared to that followed in sec. 4.1 only when R_c is dominant, so that the contact resistance can be considered as a series resistance which does not affect the current density distribution. Under these conditions

$$R_m = \frac{R_c'}{\pi A^2} + \frac{\rho}{8\pi d} , \qquad (52)$$

exactly and almost the same result as obtained in eqs (45a) and (48b), respectively, along totally different lines.

5. Three-point-probe configurations

For spreading resistance measurements two different three-point-probe configurations are currently in use each with different, but related correction formulae. They are presented in figure 6, as parts of an in-line four-point-probe arrangement with three equal probe distances s, because the two configurations can be easily related in this way.

It will be shown that the two configurations yield very different measurement results with thin layers in particular. The three probes are referred to as voltage, current and common probe. The spreading resistance is measured below the common probe.

From superposition of the potentials due to the input and output currents the potential differences measured in configurations A and B can easily be shown to be

$$V_{23}^{(A)} = 2\,V(s) - V(2s) - V_o \tag{53}$$

and

$$V_{23}^{(B)} = V(2s) - V_o \,, \tag{54}$$

where V_o is the potential drop of the common probe due to spreading resistance. Reversing the current in B and superimposing this configuration onto A the normal four-point-probe arrangement is obtained, that is

$$V_{23}^{(AB)} = 2\,V(s) - 2\,V(2s) \,. \tag{55}$$

The four-point-probe measured potential for a thin layer on an isolating substrate is given by

$$V_{23}^{(AB)} = \frac{i_o \rho}{\pi d} \ln 2 \tag{56}$$

and for bulk material by

$$V_{23}^{(AB)} = \frac{i_o \rho}{\pi s} \,. \tag{57}$$

Comparing the voltage drop due to the spreading resistance $i_o \rho / 4A$ to $V_{23}^{(AB)}$, it is evident that the contribution $V_{23}^{(AB)}$ is negligible for bulk material ($s \gg A$). For a thin layer the sheet resistance generally seriously reduces the precision of the desired information which is in the spreading resistance term.

The next problem to be treated is whether the voltage or the current probes can be replaced by a bottom contact.

When the structure to be investigated is such that the support is thick or highly doped so that it can be considered as an equipotential surface, a voltage or current contact can be connected to it. Calling the bottom potential V_b the potential difference reads in configuration A_1 of figure 6 as

$$V_{23}^{(A_1)} = V(s) - V_o \tag{58}$$

565-448 O - 75 - 4

and in configuration B_1 as

$$V_{26}^{(B_1)} = V(2s) - V_o \,, \tag{59}$$

which is identical to eq. (54) of configuration B. The difference between eqs (53) and (58) amounts to half the four-point-probe value. When in configurations A_1 and B_1 the voltage probe is displaced towards infinity, the measurement result is evidently the same as with a bottom voltage contact.

In figure 6D the configurations A and B are presented with bottom current contacts. When the configurations C and -C are superimposed on D the voltages read

$$V_{23}^{(D)} + V_{23}^{(C)} = V_{23}^{(A)} \tag{60}$$

and

$$V_{23}^{(D)} - V_{23}^{(C)} = V_{23}^{(B)} \,. \tag{61}$$

Hence in configuration D

$$V_{23}^{(D)} = \frac{1}{2}\left(V_{23}^{(A)} + V_{23}^{(B)}\right) = V(s) - V_o, \tag{62}$$

which is equal to $V_{23}^{(A)}$, and in configuration C

$$V_{23}^{(C)} = \frac{1}{2}\left(V_{23}^{(A)} - V_{23}^{(B)}\right) = V(s) - V(2s) \,, \tag{63}$$

which is half the four-point-probe value. Upon applying a bottom current contact the potential is reduced in configuration A and is increased in configuration B by half the normal four-point-probe value.

6. Summary and conclusions

The resistance between a metal contact of radius A at uniform potential and an electrode at infinity to material of resistivity ρ of infinite extent is the spreading resistance $\rho/4A$. An extremely thin top layer representing a contact resistance is generally considered as a series resistance. It turns out to influence the potential distribution itself and to increase the resistance by 4% over the series combination. Imposing the boundary condition of a uniform current density distribution over the contact area instead of a uniform potential yields a spreading resistance higher by at most 8% over the series combination.

The potential problem for a layer of finite thickness d is solved for a perfectly conducting and a non-conducting substrate. For both problems the boundary conditions of uniform current density and of the current density distribution found with infinite thickness are tried.

For the first problem a difference of about 10% is found with both

oundary conditions. Another published solution is found to be athematically incorrect. For the second problem both boundary conditions ield divergent integrals for the potential. However, the difference etween the potential of the contact and the potential at some point r ields a finite integral. With the boundary condition of uniform current ensity at the contact the ln r-dependence of the voltage is found which ollows from elementary considerations and which has been verified expe- imentally. Moreover, the other voltage term representing the geometrical- y constrained spreading resistance for a thin layer turns out to be qual to the value obtained from a completely different approach based on transmission-line model. The other boundary condition of the same ensity distribution as found for infinite geometry also yields the ln r- ependence and a constant term smaller by 5%.

The latter approach has been followed by Schumann et al.[1] in their alculation of the spreading resistance not only as a function of d/A, as one here, but also as a function of the ratio of layer to substrate esistivity ρ_1/ρ_2 , of which only the two extremes have been studied ere. It is evident that all results are only valid as far as the model s valid and it is the pertinent conclusion of this contribution that qually reasonable boundary conditions yield results which are different y about 10%. Agreement with experimental results of this precision xists only for the ln r-dependence, which is found with both approaches. he infinite geometry expression $\rho/4A$ has been verified with about this recision with a Hg probe[18] and experiments in which probes with small ontact area are used, are troubled by contact resistance. Schumann's hoice of the boundary conditions is a logical one because the infinite eometry with $\rho_1/\rho_2 = 1$ can be used as a reference in this way. evertheless, in view of the results obtained above it appears worth epeating Schumann's computer exercise with various conditions. It is robably safe to say that in interpreting thin layer spreading resistance easurements, which may be precise with in 1%, the precision drops to bout 10%.

It would, moreover, also be better to include from the very beginning he influence of the contact resistance, which influences the current ensity distribution at the contact, particularly for a thin layer on a ess conducting substrate. When all this preliminary mathematical work or spreading resistance on a non-bevelled structure has been done orrectly, the influence of the edge on a bevelled surface should be ncluded, as with four-point-probe correction formulae for finite geometry.

Furthermore, it should be realized that on any layered structure the ransition is not abrupt but extends over a finite length, due to dope tom gradient, space charge or both. Therefore in spreading resistance orrection formulae the thickness obtained with the infrared multiple nterference method should be used with caution [21 , 22] .

Finally on a bevelled structure the complication arises that the harge carrier distribution is perturbed by the exposure of the transi- ion on the bevel. In a PN-junction the zero-bias depletion layer xtends so far to both sides of the junction that the net charge anishes. In a bevelled PN-junction therefore the lower-side boundary of he depletion layer curves upwards where the top-side boundary would ntersect the bevel surface. The top-side boundary then must also curve pwards and a modified space charge pattern results suggesting a smaller epth of the interface. These effects are well known to give rise to ower surface break-down voltages, as discussed by Davies and Gentry [23]. imilar effects occur, on a smaller scale, with an NN^+ junction where harge spills over a few Debye lengths into the lowly doped layer, but ay show a different space charge distribution near the bevelled surface.

It is the author's opinion that sufficiently reproducible and precise preading resistance measurements can be done, but that for the interpre- ation of the data to extract explicit and accurate information on the esistivity of layered or bevelled structures theory is seriously deficient.

Acknowledgement

The assistance of Prof.Dr. C.J. Bouwkamp in some analytical problems, of Ir. W. Fontein in some numerical problems and of Dr. J.D. Wasscher in carefully reveiwing the manuscript is gratefully acknowledged.

References

1 P.A. Schumann and E.E. Gardner, J.Electrochem.Soc. 116 (1969) 87.
2 P.A. Schumann and E.E. Gardner, SolSt.Electr.12 (1969) 371.
3 T.H. Yeh, Silicon Device Processing, NBS Spec.Publ. 337 (1970) 111.
4 T.H. Yeh and K.H. Kokhani, J. Electrochem.Soc.116 (1969) 1461.
5 S.M. Hu, Sol.St.Electr. 15 (1972) 809.
6 E.E. Gardner and P.A. Schumann IBMTR 22191, July 1965.
7 E.E. Gardner, P.A. Schumann and E.F. Gorey, IBMTR 22394, May 1967.
8 R.D. Brooks and H.G. Mattes, BSTJ 50 (1971) 775.
9 P.J. Severin, Philips Res. Repts 26 (1971) 359.
10 P.J. Severin, Symposium on spreading resistance measurements, NBS (1974).
11 R. Holm, Electrical contacts handbook, Springer Verlag, Berlin, 1958.
12 J.N. Sneddon, Mixed boundary value problems in potential theory, North-Holland Publ. Co. Amsterdam ,1966.
13 R.G. Mazur and D.H. Dickey, J.Electrochem.Soc. 113 (1966) 255.
14 W.A. Keenan, P.A. Schumann, R.P.Phillips and A.H. Tong, Ohmic contacts to semiconductors, ed. B. Schwartz, Electrochem.Soc. (1969) 263.
15 P.J. Severin, Silicon Device Processing, NBS Spec.Publ. 337 (1970) 224.
16 P.J. Severin, Sol.St.Electr, 14 (1971) 247.
17 C.J. Bouwkamp, IEEE Transact. Antennas and Propagation, AP-18 (1970) 152.
18 P.J. Severin, Paper 75 presented at the Chicago, Illinois, Meeting of the Electrochemical Society, May 13-18, 1973.
19 R.H. Cox and H. Strack,Sol. St.Electr. 10 (1969) 1213.
20 I.S. Gradshteyn and I.M. Ryzhik, Table of integrals, series and products, Acad.Press, 1965, 6. 533.
21 P.J. Severin, Appl.Opt. 9 (1970) 2381; 11 (1972) 691.
22 P.J. Severin, J.Electrochem.Soc. 121 (1974) 150.
23 R.L. Davies and F.E. Gentry, IEEE Transact. Electron Devices ED 11 (1964) 313.

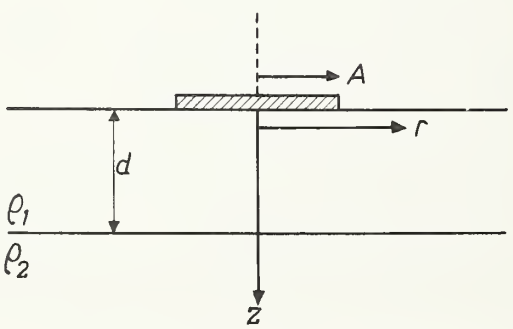

Figure 1. The geometry of the contact and the two-layer structure.

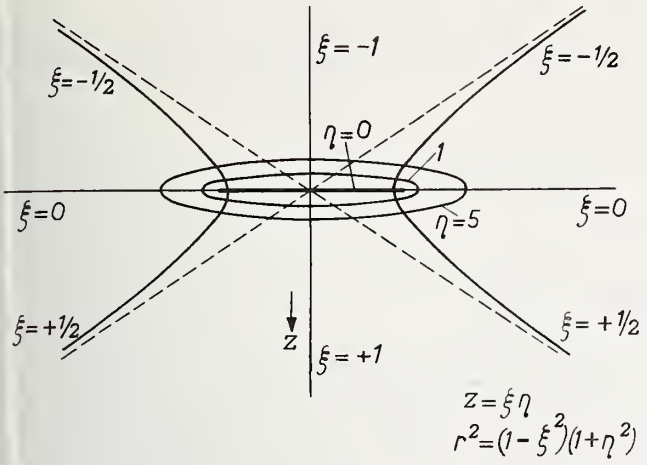

Figure 2. The oblate spheroidal coordinate system schematically drawn.

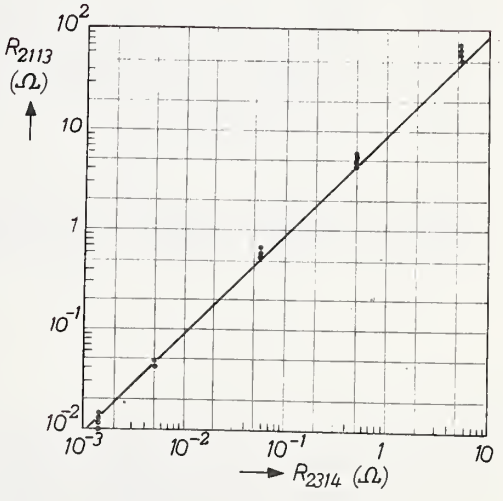

Figure 3. The spreading resistance $R_{2113} = V_{21}/i_{13}$ (fig. 6B) plotted vs the four-point-probe resistance R_{2314}, both measured with mercury probes, on bulk samples. The solid line represents $R_s = \rho/4A$, where 1 Ω corresponds to ρ = 0.2 Ωcm.

Figure 4. The spreading resistance R, normalized by the spreading resistance on infinite geometry $R_\infty = \rho/4A$, plotted vs the normalized thickness d/A, as calculated by Brooks and Mattes (sec. 3.1), by Schumann (sec. 3.3), by Severin (sec. 3.2) and measured by Cox and Strack (sec. 3.4). The two ranges are noted on the horizontal axis.

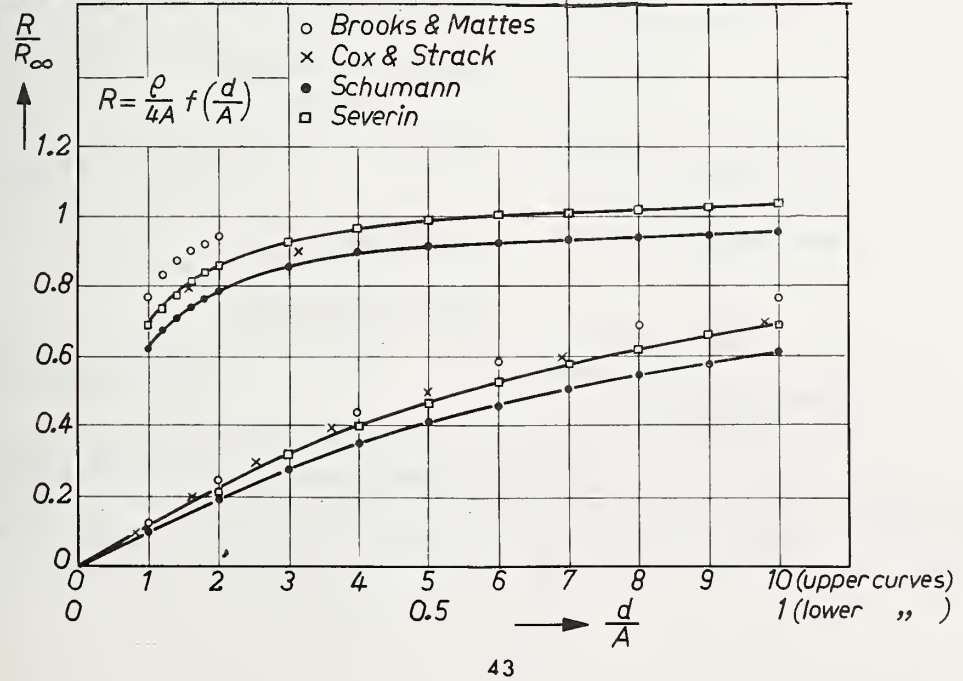

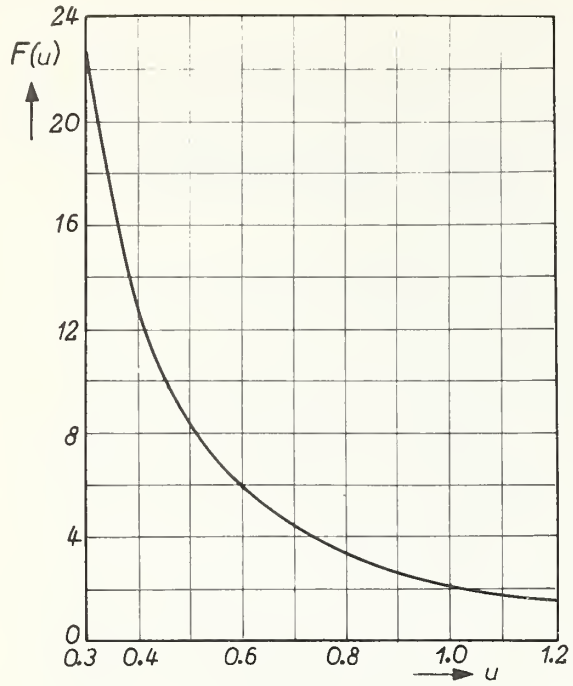

Figure 5. The function F(u) with $u^2 = A^2 \rho / R'_c d$.

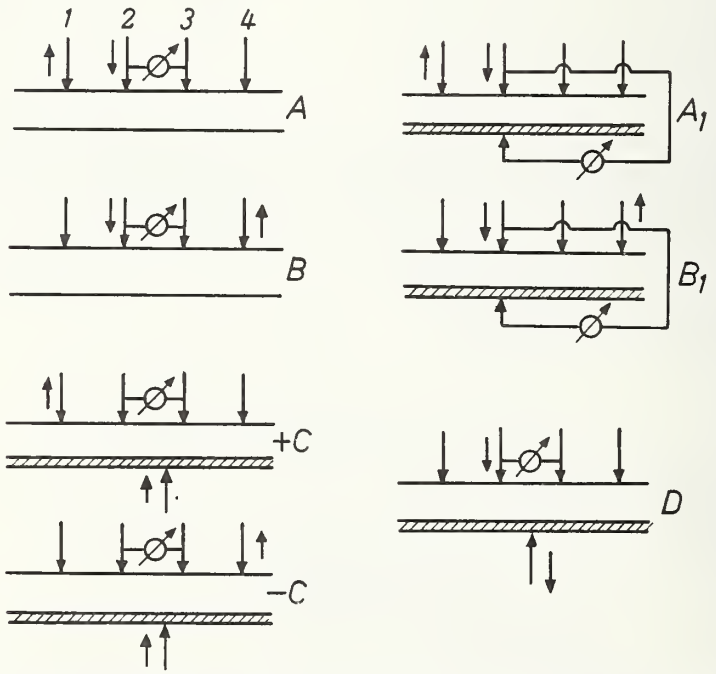

Figure 6. The two alternative three-point-probe arrangements for spreading resistance measurements (A and B), modified with bottom voltage probe (A_1 and B_1), and modified for bottom current probe (D), with two arrangements used in the text (C and -C).

NATIONAL BUREAU OF STANDARDS SPECIAL PUBLICATION 400-10, Spreading Resistance Symposium, Proceedings of a Symposium Held at NBS, Gaithersburg, Md., June 13-14, 1974.

Two-Point Probe Correction Factors

D. H. Dickey

Bell and Howell Research Laboratory
Pasadena, California

The effects of sample boundaries on resistivity measurements made with a two-point spreading resistance probe are calculated for various boundary conditions. The results are presented in the form of dimensionless correction factors. The problem of depth-dependent resistivity in a thin layer is considered, and a method for correcting measurements on such layers is described.

Key words: Boundary correction; calculations; electrostatic analogue; resistivity; semiconductor; spreading resistance.

1. Introduction

The two-point spreading resistance probe as originally developed [1][1] was characterized by a sampling volume substantially smaller than then-current resistivity probes. The accuracy available with the technique did not justify correction for sample boundaries when it was used for bulk samples of even moderately small size. Improvements in the accuracy of the technique in recent years, coupled with the desire for probing smaller and smaller samples has made correction for sample boundaries a necessity. The purpose of this paper is to present correction factors for a variety of boundary conditions, including conducting and non-conducting edge, end and subsurface boundaries. A simplified approach to the problem of a depth-dependent variation in resistivity in a thin layer will also be presented.

2. Method of Calculation

The resistivity of a sample is assumed to be related to the resistance measured between the two probes according to

$$\rho = 2aR/F \text{ ohm-cm} \qquad (1)$$

where a is the contact radius and F is a dimensionless factor that contains the correction for sample boundaries.

The following development is similar in many respects to that used by Uhlir [2] for the conventional four-point resistivity probe, and makes use of his results for those cases

[1] Figures in brackets indicate the literature references at the end of this paper.

involving image sources. The basic approach is to invoke the electrostatic analogue of the current flow problem, in which equipotential contacts are replaced by capacitor plates and current sources are replaced by electrostatic charges.

A point charge in free space establishes the same potential distribution as that of a current I flowing from a point into an infinite medium of homogeneous resistivity if the charge has magnitude

$$q = I\rho/4\pi \text{ esu} \tag{2}$$

In practicality, current flows from a surface contact into a half-space of resistive medium, so the current required to establish a certain potential distribution is one-half that implied by equation 2. Rewriting equation 1 for F in terms of the potential difference between the two probes, we find

$$F = 2a\ \Delta V/I\rho \tag{3}$$

Combining equations 2 and 3, the correction factor we seek for two probes on the surface of a half-space can be written in terms of the electrostatic analogue as

$$F = (a/\pi)\Delta V/q \tag{4}$$

where q is the charge on one contact, -q is on the other and ΔV is the potential difference between them.

To illustrate, we take the simple case of a semi-infinite solid with the probes separated by a distance s. We replace the contacts with two capacitor plates having charges +q and -q and calculate the potential difference between them. The potential on the first plate is

$$V_1 = q\pi/2a - q/s \tag{5}$$

where the first term is owing to the charge on the first plate (the capacitance of a disc is $2a/\pi$ esu) and the second term is the contribution from the negative charge on the other plate; assumed to be concentrated in a point. The potential on the second plate is equal to that on the first, but opposite in sign, so the potential difference is

$$\Delta V = q(\pi/a - 2/s) \tag{6}$$

and the correction factor, from equation 4, is

$$F = 1 - 2a/\pi s \tag{7}$$

This expression represents a negligible correction for very large values of s/a, and should be valid for any practically attainable smaller probe separations.

3. Calculations for Abrupt Boundaries

3.1. The Infinite Slab

The method of images may be used to calculate the correction factor for the case in which the probes are on one surface of a thin slab. The arrangement of the image plates in the electrostatic analogue is illustrated in figure 1. Each plate has associated with it an infinite array of images, which ensure that the normal derivative of the potential will vanish in the planes corresponding to the upper and lower boundaries of the slab. As before, we write the potential on the first plate as a sum of contributions from each of the real and image charges. Fortunately, the contribution from exactly such an array of image charges has been conveniently summed by Uhlir. Using his result, we find

$$V_1 = q\pi/2a - q/s + (q/2t)M(s/2t) \tag{8}$$

where the first two terms are the potentials owing to the charges on the two real plates, t is the slab thickness and $M(\lambda)$ is a function tabulated by Uhlir. The M-function has the limiting form for large s/t:

$$M(\lambda) = 1/\lambda + 2\ell n\lambda - 0.2318 \qquad (\lambda > 1.5) \tag{9}$$

The potential on the second plate is again equal but opposite in sign to that on the first, so from equation 4 we obtain

$$F = 1 - 2a/\pi s + (a/\pi t)M(s/2t) \tag{10}$$

This result is valid for slab thickness greater than the contact radius, but breaks down somewhat for smaller thicknesses because the image charges can no longer be assumed to be concentrated in a point.

For very small sample thicknesses, the resistance model is equivalent to one in which the equipotential contacts extend through the entire thickness of the sample. The problem therefore becomes two-dimensional and can be solved in many ways. An electrostatic analogue is the two-parallel-wire transmission line, for which the capacitance per length t is

$$C = t/4\ell n(2s/a) \text{ esu} \tag{11}$$

The capacitance is just $q/\Delta V$, and since this problem is not confined to a half-space the correction factor is one-half that given by equation 4. The result is

$$F = 2a\ell n(2s/a)/\pi t \tag{12}$$

Equations 10 and 12, valid for large and small sample thicknesses, respectively, are graphed versus t/a for s/a = 100 in figure 2. The two formulas are in excellent agreement for t = a.

In the case where the lower surface of the slab is a conducting boundary, the electrostatic analogue consists of the same array of images as shown in figure 1 but with different signs. The lower set of signs indicated in figure 1 apply in this case. These images can be considered to be made up of two superimposed sets: those about P_1 being a set with charge -q and spacing 2t superimposed on a set with charge +2q and spacing 4t. This arrangement satisfies the requirement that the tangential component of the field must vanish in the plane corresponding to the lower boundary. Again using the results of Uhlir

for the potential owing to the image charges, assuming they can be represented by point sources, the potential on P_1 is

$$V_1 = q\pi/2a - q/s + (q/2t)M(s/4t) - (q/2t)M(s/2t) \tag{13}$$

V_2 is the same, but with opposite sign, so

$$F = 1 - 2a/\pi s + (a/\pi t)[M(s/4t) - M(s/2t)] \tag{14}$$

This formula is useful for sample thickness greater than the contact radius.

For very thin layers on a conducting substrate the measured spreading resistance should be independent of probe separation s. The electrostatic analogue is the parallel disc capacitor with plate separation 2t. The capacitance in electrostatic units, including the effects of fringing, is

$$C = (1/8t)[a + (2t/\pi)\ell n2]^2 \text{ esu} \tag{15}$$

Again, this model is not confined to a half-space, so the correction factor is one-half that given by equation 4:

$$F = (4t/\pi a)/[1 + (2t/\pi a)\ell n2]^2 \tag{16}$$

Equations 14 and 16 are graphed as a function of t/a in figure 3. The agreement at $t = a$ is not exact, but close enough that we can assume the validity of equation 16 for $t < a$, and equation 14 for $t > a$.

3.2. The Quarter-Infinite Solid

The case in which the probes are near and parallel to the edge of a thick sample requires only two image contacts instead of the infinite arrays encountered with a thin sample. The potential on each plate is therefore the sum of four terms, and the potential difference is

$$\Delta V = 2q[\pi/2a - 1/s \pm 1/2w \mp 1/\sqrt{4w^2 + s^2}\,] \tag{17}$$

where w is the distance from the line between the probes and the sample edge. The upper set of signs apply when the edge is insulated, and the lower set applies when the edge is a conducting boundary. The correction factor is:

$$F = 1 - 2a/\pi s \pm a/\pi w \mp 2a/\pi\sqrt{4w^2 + s^2} \tag{18}$$

If the line between the probes is perpendicular to a sample boundary, the potentials on the two contacts are not equal and opposite since there is no longer a symmetry plane midway between them. The potentials can however be immediately written, and the resulting correction factor is

$$F = 1 - 2a/\pi s \pm a/2\pi\ell \mp (2a/\pi)/(2\ell + s) \pm (a/2\pi)/(\ell + s) \tag{19}$$

where ℓ is the distance from the boundary to the nearest probe. Again, the upper set of signs apply if the edge is insulated, and the lower set applies for a conducting boundary.

3.3. The Semi-Infinite Slab

For the case in which the probes are parallel to the edge of a thin slice, four infinite arrays of images are required. The potential on one of the contacts can be obtained from the superposition of three pairs of arrays of the type shown in figure 1. If the probes are parallel to the edge, the potential on the positive contact is

$$V_1 = q\pi/2a - q/s + (q/2t)M(s/2t) \pm q/2w \mp (q/2t)M(2w/2t)$$

$$\mp q/\sqrt{4w^2 + s^2} \pm (q/2t)M(\sqrt{4w^2 + s^2}/2t) \qquad (20)$$

where w is the distance from the edge and the upper signs are used if the edge is insulated. The potential on the negative contact has the same magnitude so the correction factor is

$$F = 1 - (a/\pi)[2/s \mp 1/w \pm 2/\sqrt{4w^2 + s^2}]$$

$$+ (a/\pi t)[M(s/2t) \mp M(w/t) \pm M(\sqrt{4w^2 + s^2}/2t)] \qquad (21)$$

This result is valid only for sample thickness greater than the contact radius. For thinner samples, a model similar to that used to obtain equation 12 is useful. Other correction factors for more complicated boundary conditions can be obtained by using the process outlined in the preceding cases.

4. Inhomogeneous Resistivity

The final case to be considered is the one in which resistivity varies with distance from the surface of an infinite slab. If the resistivity is a monotonically increasing function of depth, the profile can be approximated by dividing the sample into a number of superimposed electrically parallel bodies, each with a different thickness. For illustration, consider the rectilinear resistivity profile shown in figure 4. This profile is the result of superimposing three bodies of thickness t_0, t_1 and t_2, each having uniform resistivity 3ρ. The relation between ρ, the surface resistivity, and the spreading resistance measured at the surface is in this example:

$$\rho = 2a\ R(1/F_0 + 1/F_1 + 1/F_2)/3 \qquad (22)$$

where F_n is the correction factor calculated from the thickness t_n. In practice, one must estimate the thicknesses t_1 and t_2, these being the depth at which the resistivity is 3ρ and $3\rho/2$, respectively. If measurements are made at various depths on an angle-lapped sample, the t_n's can be estimated with increasing accuracy by considering first the deepest measurements and working out to the original surface.

In general, the surface resistivity obtained by this method from a division of the sample into N superimposed parts each with resistivity $N\rho$ is

$$\rho = 2a\ R \sum_{n=0}^{N-1} 1/NF_n \qquad (23)$$

where F_0 is calculated from the total sample thickness, F_n from the depth at which the resistivity is approximately $N\rho/n$, and R is the spreading resistance measured at the surface.

5.References

[1] R.G. Mazur and D.H. Dickey, Electro-Chem. Soc. Abstracts, 12, N. 148 (1963)

[2] A. Uhlir, Bell Syst. Tech. J., 34, 105 (1955)

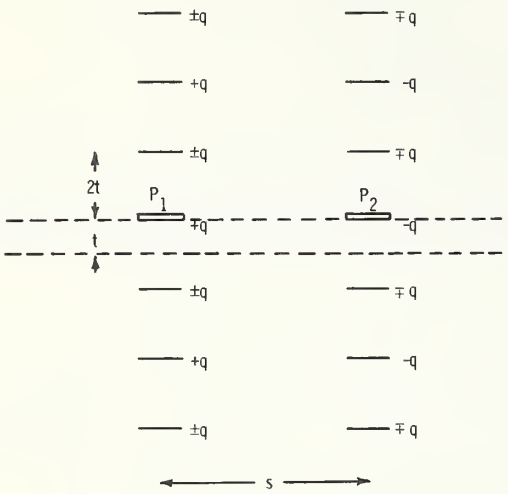

Figure 1. Arrangement of image contacts for an infinite slab. Upper and lower signs are for insulated and conducting lower boundary, respectively.

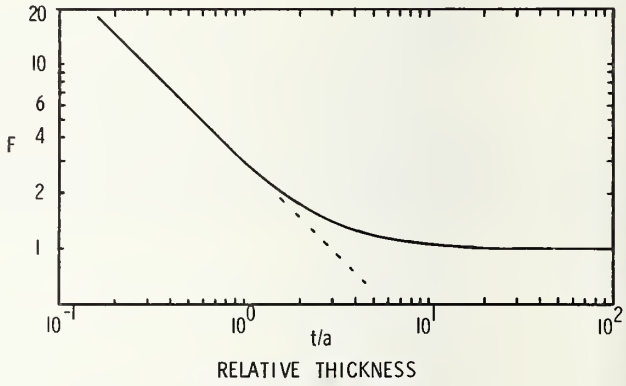

Figure 2. Correction factor, F, versus the ratio of sample thickness to contact radius for insulated boundaries and probe separation s = 100 a.

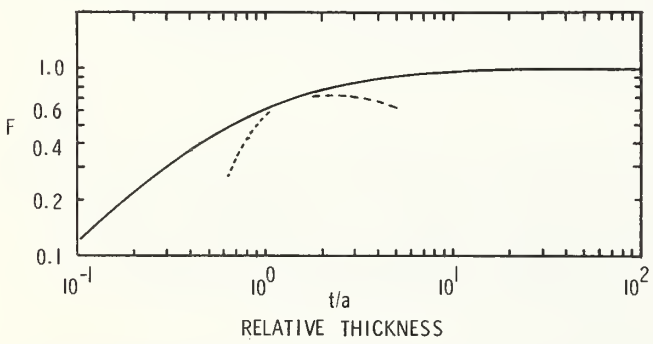

Figure 3. Correction factor, F, (formed by splicing equations 14 and 16) versus the ratio of sample thickness to contact radius for a slab with conducting lower boundary. Probe separation s = 100 a. The dotted lines are the continuation of the individual equations beyond the point of joining.

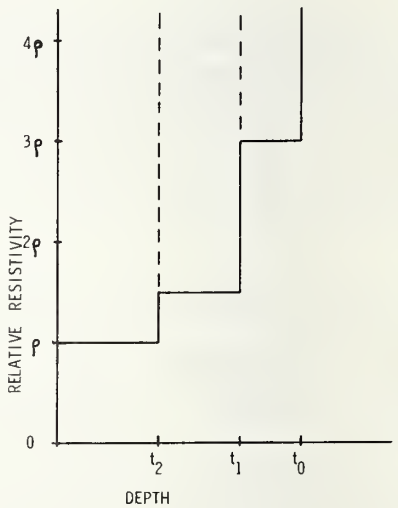

Figure 4. Resistivity profile resulting from the superposition of three layers of different thickness but uniform resistivity 3ρ.

NATIONAL BUREAU OF STANDARDS SPECIAL PUBLICATION 400-10, Spreading Resistance Symposium, Proceedings of a Symposium Held at NBS, Gaithersburg, Md., June 13-14, 1974.

On the Validity of Correction Factors applied to Spreading Resistance Measurements on Bevelled Structures

P. M. PINCHON

R.T.C La Radiotechnique Compelec
Route de la Délivrande
B.P. 6025 - 14 Caen France

The correction factors in spreading resistance measurements are generally determined by using a plan-parallel model of a single or multi-layer structure. This paper will discuss the applicability of these factors to the profiling measurements on a bevel, and call attention to possible systematic errors which can appear in the case of an insulated layer or a low/high type of structure.

After a short discussion on the spacial resolution of the spreading resistance probe, the case of a homogeneous isolated layer is examined in more detail. A simplified expression for the value of spreading resistance was calibrated against published data using fitting coefficients.

It is then easy to show that the use of a correction derived for parallel structures is not correct for the case of a thin, isolated layer, when the measurement is made on a bevel.

Indications are also given on the parameters which could minimise the problem

The experimental part of this paper shows a series of profiles made with P-type epitaxial layers.

After the application of the usual corrections, the various electrical boundaries or geometrical conditions are seen to affect the results in accordance with the discussion. An edge effect which is significant even at great distance from the edge, is also described.

In the absence of a three dimensional theory for correction, the use of small spacing is recommended in conjunction with a small radius of contact and a shallow bevelling angle.

Key words: Accuracy; bevelled structures; correction application; correction factors; edge effect; profiles; resistivity profiling; small spacing; spreading resistance.

1. Introduction

According to Mazur [1], the spreading resistance technique has been increasingly popular in the last years for resistivity measurements mainly due to its high spacial resolution compared to other methods. But in the case of measurements on thin layers, the measurement values must be corrected to give the actual resistivity depending on geometrical factors and on the nature of the layer boundary.

Theoretical models have been used to derive these correction factors in the simple case of a two-layer system [2,3] and later, extended to a graded structure, [4] using a multilayered approach. Up to now these calculations of corrections have always been based on a plan-parallel structure having infinitely wide lateral dimensions.

The aim of the present paper is to examine in which conditions these correction factors can be applied to measurements made on bevelled structures where the lateral homogeneity is evidently not maintained at large scale (compared to the contact radius) and what kind of errors are involved in doing so.

2. Qualitative background

We shall assume that the probe has a plain, circular contact with the material, of no contact resistance.

The figure 1 shows qualitatively what shape of current streams and equipotential lines are involved in three distinct cases, under a spreading resistance probe : a) thin layer on shorting substrate, b) infinitely thick sample, c) thin layer on insulating substrate. In all cases the current sink is considered located at infinity, and the layers or the bulk supposed to be homogeneous in resistivity.

In the case of thick samples, figure 1b the equipotential surfaces tend rapidly to be hemispherical as the distance increases from the probe. Using this approximation it can easily be shown that 95% of the voltage drop is obtained at a distance x related to the radius of contact, r_o by :

$$x/r_o \approx 40/\pi \qquad (1)$$

In the case of a highly conducting boundary, figure 1a, it is evident that the voltage drop is confined in a very small space, smaller than that of the thick sample. On the contrary, the case of the insulating boundary, figure 1c, indicates that the voltage drop is practically in the lateral direction, and closely related to the sheet resistance of the layer. It will be seen later how this lateral voltage drop can still be of importance at distances greater than 20 r_o.

Let us take as reference, the spacial resolution of the thick homogeneous sample. Thus, the fact of the non homogeneity at large scale in the lateral direction in the case of a bevelled layer becomes important in structures of the low/high type and very pronounced for an insulated layer.

3. Semiquantitative model

Let us restrict our discussion to the case of homogeneous thin layer, of thickness : t, resistivity : ρ , limited by an insulating boundary.

Elementary theory shows that the lateral resistance of a disc, having an inner contact of radius : r_b , an outer contact of raidus : r_x , figure 2, is given by

$$R_{bx} = \left(\rho/2\pi t\right) \cdot Ln\left(\frac{r_x}{r_b}\right) \qquad (2)$$

[1] Figures in brackets indicate the literature references at the end of this paper.

With an arbitrary geometry of 3 point contacts, as shown in figure 3, the circumference of the contact of radius : r_b being the common electrode, it is easy to obtain the voltage drop between the circumferential contact and the voltage probe : (V-Vo), assuming that the distances : a, b and c are large compared to r_b :

$$V - V_o = \frac{\rho i}{2\pi t} \cdot Ln \left(\frac{ab}{c} \cdot \frac{1}{r_b} \right)$$

For thin layers, the graph in figure 1 suggests that the spreading resistance is dominated by the lateral sheet resistance. Thus, by comparison with the spreading resistance of the infinitely thick material it becomes :

$$\frac{V - V_o}{i} = R_{SR} = \left(\frac{\rho}{4r_o} \right) \cdot \frac{2r_o}{\pi t} \cdot Ln \left(\frac{ab}{c} \cdot \frac{1}{r_b} \right) \qquad (3)$$

If we relate r_b to r_o, introducing a fitting parameter such as $r_b = \alpha r_o$, a linear relation of the correction factor (C.F) is found versus $(t/r_o)^{-1}$ this being confirmed by the published data of Gardner [3] obtained by more accurate derivation, for the range of $t/r_o < 1$.

Using the in-line geometry, with a spacing : s, the common electrode on one side, the fitting parameter is obtained by comparison with Gardner's curve and found : $\alpha \approx 0.8$. The value of the spreading resistance for thin layer is then approximated, for $t/r_o < 1$ by :

$$R_{SR} \approx \left(\frac{\rho}{4r_o} \right) \frac{2r_o}{\pi t} \cdot Ln \left(\frac{2s}{0.8 r_o} \right) \qquad (4)$$

This indicates that the spreading resistance is mainly equivalent to the resistance of a sheet having a side injection contact of $0.8\ r_o$ radius.

For thicker layers, using again approximate models including fitting parameters we may decompose the spreading resistance into

$$R_{SR} = R_1 + R_2 \qquad (5)$$

where R_{SR} = total spreading resistance
R_1 = "local" resistance
R_2 = "lateral" resistance

and,
$$R_1 = \frac{\rho}{4r_o} \cdot \left(1 - \frac{2r_o}{\pi \beta t} \right) \qquad (6)$$

$$R_2 = \frac{\rho}{4r_o} \left\{ \frac{2r_o}{\pi t} \cdot Ln \left(\frac{2s}{\gamma t} \right) \right\} \qquad (7)$$

where β and γ are fitting parameters;

βt represents the radius of a hemisphere in which the "local"resistance is expressed, and

γt represents the radius of a ring from which the "lateral" sheet resistance starts to become of importance.

By fitting with Gardner's curve, an agreement of $< \pm 10\%$ is obtained for $t/r_o > 0.5$, making :

$$\beta = 0.7 \quad \text{and} \quad \gamma = 0.8$$

Using these semi-empirical relations the correction factor (C.F.), for a variety of $2s/r_o$ and t/r_o values can be derived.

Table 1 gives a set of (C.F.) values ranging from large spacing ($2s/r_o = 2000$) to relatively small spacing ($2s/r_o = 20$) and for three relative thicknesses: $t/r_o = 0.5$, 2 and 5.

The values in table 1 agree reasonably well with those reported by Schumann, Gorey and Schneider [5] taking into account of the appropriate probe geometry.

These values are rewritten in the form $\frac{CF - CF_{(20)}}{CF_{(20)}}$ in table 2, in order to illustrate the relative importance of the lateral resistance outside a radius of $20r_o$, where $CF_{(20)}$ is the correction factor for $\frac{2s}{r_o} = 20$.

Table 1. Evaluated correction factors in the case of an insulated, homogeneous layer : $2s/r_o$ relative probe spacing ; t/r_o = relative thickness ; probe geometry : 3 pt. in-line, common probe on one side

		$(2s/r_o)$ 2000	500	100	20
(t/r_o)	0.5	9.9	8.2	6.1	4.1
	2	2.8	2.4	1.9	1.35
	5	1.6	1.4	1.2	1.024

Table 2. Ratio of the resistance outside a distance of 20 r_o to the resistance at $20r_o$: $\frac{CF - CF_{(20)}}{CF_{(20)}}$

		$(2s/r_o)$ 2000	500	100
(t/r_o)	0.5	1.4	1.0	0.5
	2	1.1	0.8	0.4
	5	0.55	0.37	0.17

From table 2 it is obvious that it is not correct to apply the standard correction factors as determined for laterally homogeneous models in the case of a bevelled layer.

Let us take a numerical example, as may be found in practice :

$r_o = 4\mu m$
$s = 1000\mu m \quad (2s/r_o = 500)$
$t = 10\mu m$
tangent of the bevel angle : 1/50

The length of the bevelled part of the layer is only 500μm, length over which the sheet resistance varies from nominal to infinity. But from table 2 it is seen that a very significant part of the spreading resistance comes from the lateral part included from 80μm ($=20r_o$) to 1000μm (=s) outside the measuring probe.

Thus in general, a three dimensional model is needed for correction factor calculation in the case of an insulating limit or more generally in the case of low/high resistivity structures. In view of the complexity of this task it seems more practical to look at the conditions for which the error involved in the application of classical correction would be minimised.

Obviously a small spacing arrangement is favourable in conjunction with a low bevel angle in such a way that the sheet resistance variation in the direction of the slope may be small compared to the probe spacing distance.

However the very last portion of the bevel can never fulfill the right conditions even with a small probe spacing . Of course the error is confined to a thinner portion of the layer in this case.

4. Experimental procedure

Experiments have been done using an automatic S.R prober of our construction which prints on a semi-log paper, the uncorrected resistance values versus distance. The system works in the constant voltage mode (10mV) with a dual polarity print at each point ; it has a 3 pt. in-line probe made with tungsten carbide needles , having a tip radius of $\approx 20\mu m$. The applied contact force is 20 - 25 grams.

For the experimental part shown hereafter, P type silicon layers have been selected. We found, as others have, that the contact resistance is lower for P-type material. Thus the measurements are more sensitive to bulk properties (i.e. proximity of an interface).

When measuring a bevel, we always apply a metallic shorting strip on which the two accessory probes make contact directly. This shorting is made of indium-gallium paint applied together with a mechanical scratching. Only the common probe is working outside the strip at a distance : d which is recorded after the measurement. This arrangement is depicted in figure 4.

The correction procedure has been done as follows : r_o is deduced in each series of experiments from the measurement itself on a thick part of known resistivity (substrate or average resistivity of a thick layer) according to :

$$Rm = Rc + R_{SR} = \frac{K\rho}{4r_o} \qquad (8)$$

where : Rm is the measured resistance in opposition to R_{SR}, the theoretical one and where Rc is the contact resistance supposed to be independent of the layer thickness.

A value of K = 1.2 has been used for all corrections on P type material.

Thus the applied correction : M, is related to the calculated correction : (C.F.), corresponding to the simple one-layer system and a plan-parallel structure as mentioned in the previous section, by :

$$M = \frac{K - 1 + (C.F.)}{K} \qquad (9)$$

Trials with K = 1.0 or K = 1.4 instead of 1.2 gave very minorchanges in the corrected results and hardly any for the part of the layer thicker than 2 microns.

5. Results

5.1. Edge effect

In order to illustrate a boundary effect which may be observed at large geometrical scales, in accordance with the discussion given in section 3, an edge effect has been tentatively looked for in the case of an insulating boundary. An experimental result of this nature has been already given by Severin [6] at the edge of a heterotype epitaxial slice . Here, we used a P layer : 8μm thick, resistivity : 4Ωcm, on an N-type substrate. We first recorded the surface measurements over a length of 1 cm at the center of the slice, and found it essentially flat. Then the slice was cleaved in two parts and

565-448 O - 75 - 5

re-measured on one half, in the same region as before and in the direction perpendicular to the broken edge, the probes being parallel to it. The probe spacing was s = 3mm.

The result is shown in figure 5 which illustrates clearly the expected edge effect. It amounts to a 20% increase at a distance as large as $\frac{1}{2}$ mm. Also on figure 5 is plotted, for comparison, the calculated effect using an image method and the approximate relations given in section 3. (The calculated curve has been drawn arbitrarily at a level of 10KΩ).

5.2 Comparison of Corrected Profiles Having Different Boundary Conditions

In these series of measurements, the depth profiles of resistivity are compared as a function of the boundary nature. In the same epitaxial run three different substrates have been coated with a P type layer, in order to compare the effects of boundaries in the case of : P/N, P/P and P/P+ configurations.

In the P/P case the choice of the substrate was such that its resistivity would approach the one expected for the layer, thus allowing a profile which does not require a correction (substrate resistivity : 3.95Ωcm).

The uncorrected measurements are given in figure 6. The corrected P/N and P/P+ profiles are compared to the P/P, uncorrected, in figure 7. It can been seen that the agreement with the P/P profile is better for the P/P+ corrected profile than for the P/N profile.

In any case the slope of the P layer on the N substrate is wrong according to the two others and the possible autodoping contribution which would have led to the reverse tendency. This is attributed to the use of a correction factor which does not fulfil the conditions of bevel measurements.

5.3 Experiments Using Thickness and Probe Spacing Variations

Here, a rather thick (26.5μm) P type layer on N substrate has been profiled using three distinct values of the distance d, between the probe track and the shorting strip (see fig 4) The layer has an average resistivity of 5.8Ωcm as measured by the 4 pt probe method.

The actual measurements are shown on figure 8 and the corrected profiles, figure 9. Now the measurements are taken at a short distance from each other, on the same bevel, and thus the differences in profiles are likely to be due to the correction errors. They are smaller for the smaller spacing (d = 120μm). Then, on the other half of the same slice the layer has been thinned down to 8μm by etching, bevelled and measured in the same manner as the previous portion, again using three different spacings d.

The corrected profiles are shown on figure 10. It can be observed that the profile slopes differ markedly, and the one obtained with the smaller spacing (d = 120μm) is considered to be more accurate than the others.

If we admit that there must be an agreement between the profiles of figures 9 and 10, and that this would be optimum for the smaller spacing, then a downward shift of 20% is necessary for the last experiment. This is attributed to a small change in the experimental conditions between the two experiments (which were not done in the same day). By doing so, we obtained figure 11, which shows the comparison of the six corrected profiles.

6. Discussion

The errors involved by using the common correction factors in the case of an insulated layer can be sketched as in figure 12 where the practical situation is represented in dark lines and the situation for which the usual C.F has been calculated is in dotted lines. The discussion is also restricted to homogeneous layers, for simplicity.

At the starting point (fig 12a) the measurement is higher than it would be for a continuous layer because an edge effect occurs, this being roughly equivalent to that of a vertically cut layer at half the level length. Then the corrected value is too high.

At a point near to the middle of the bevel (fig 12b) the higher conductance (two times higher) of the left hand part compensates for the absence of layer at the right. Then the usual C.F. is nearly correct for all probe spacings.

At the last position close to the junction (fig 12c), the very high conductance of the left hand side overcompensates for the absence of the layer at the right. Then the measurement is too low after correction.

This qualitative behaviour is clearly observed in figures 7, 9, 10 and 11.

7. Conclusion

The errors involved by the application of correction factors determined for plan parallel models in the case of bevel measurements have been discussed in a semi quantitative manner and the behaviour verified by a few experiments.

A three dimentional model is in principle required to derive the correction factors in the case of low/high configuration. Using the common C.F., the errors after correction can be minimized using a contact radius, a probe spacing and a bevel angle as small as possible. The general benefit in using a small probe spacing has already been reported [5].

The present work leads to the same conclusion explaining by simple models the physical nature of the benefit in layer profiling.

8. References

[1] Mazur, R. G., Dickey, D.H. J.Electrochem. Soc. 113 255 (1966)

[2] Dickey, D. H., Electrochem. Soc. Conf. Pittsburg, Abstr. No 57, April (1963)

[3] Gardner, E. E., Symposium on Manufacturing In-Process Control and Measuring Techniques for Semiconductors, Vol II, p 19. Manufacturing Technology Division, A.F. Materials Lab. (1966)

[4] Schumann, P. A., Gardner, E. E. Solid-State Electron. 12 371 (1969)

[5] Schumann, P. A., Gorey, E. F., Schneider, C. P., Solid-State Technology 50 (March 1972)

[6] Severin, P. J. Philips Res. Repts. 26 359 (1971)

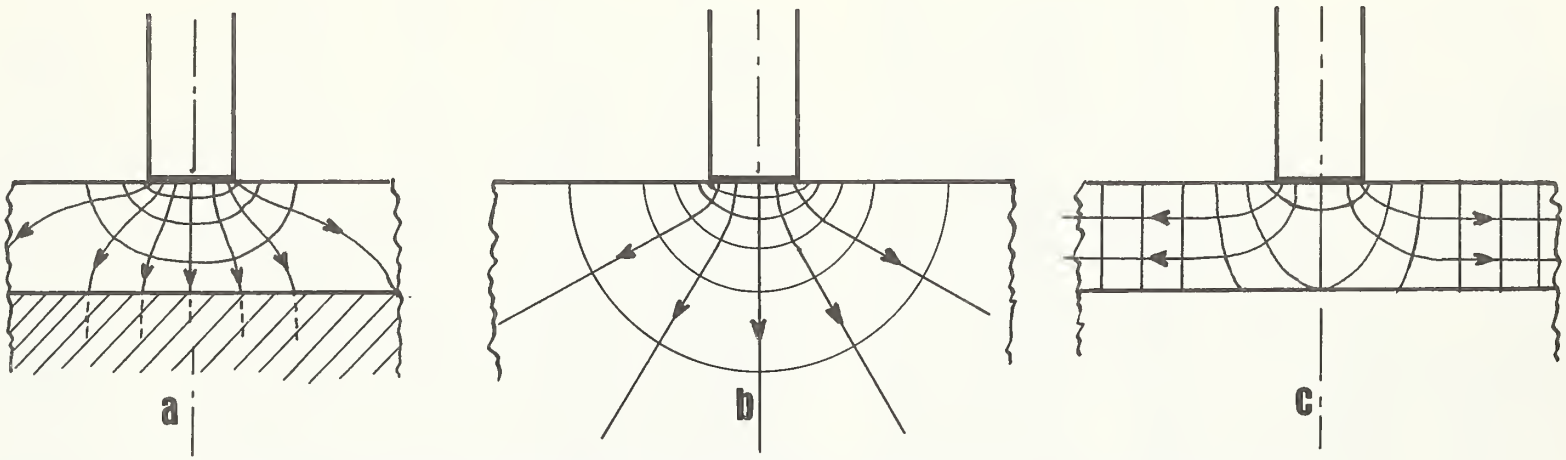

Figure 1. Qualitative shape of current flows and equipotential lines. a) short-circuiting boundary; b) thick homogeneous sample; c) insulating boundary.

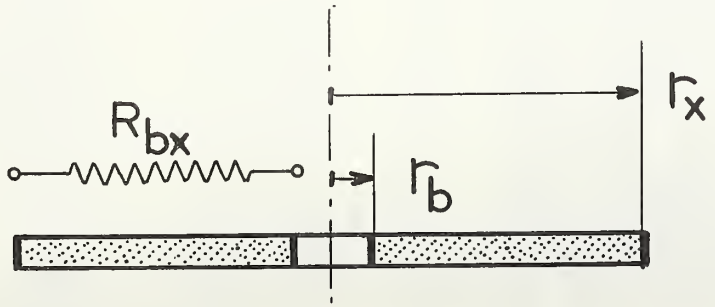

Figure 2. Lateral resistance of a disc.

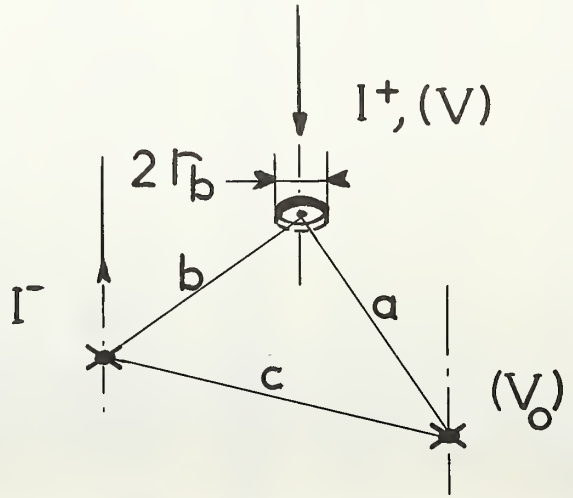

Figure 3. Resistance of a disc measured with three contacts of arbitrary location. The ring of radius r_b is the common contact.

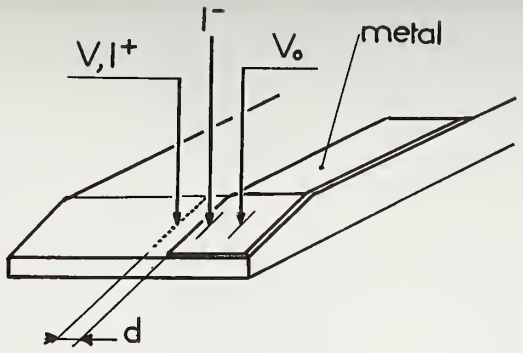

Figure 4. Contacting set-up used in our measurements on bevels.

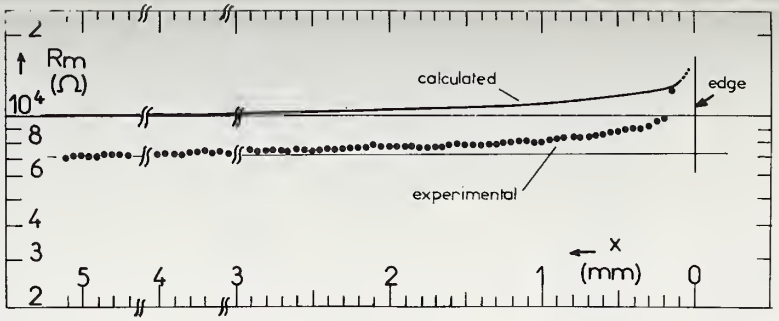

Figure 5. Measurements at the surface of a P layer on N substrate, in a direction X, perpendicular to a cleaved edge.
Layer thickness = 8μm
Layer resistivity = 4Ωcm
Interprobe distance = 3mm

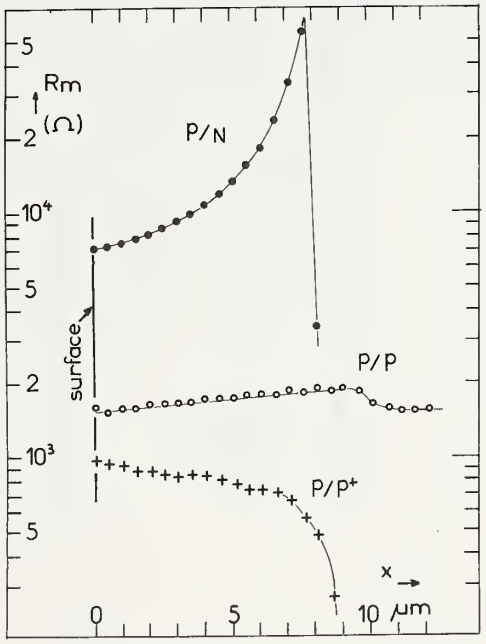

Figure 6. Uncorrected profiles of three P-type layers coming out of the same epitaxial run, (resistivity of the P-type substrate = 3.95Ωcm).

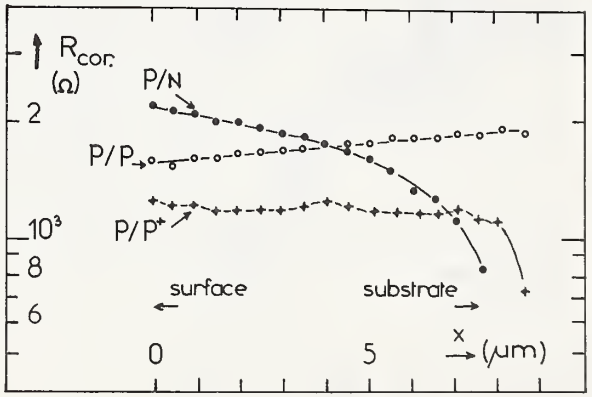

Figure 7. Profiles of figure 6, after correction, using k = 1.2, and r_o deduced from the measurements on the P-type substrate.

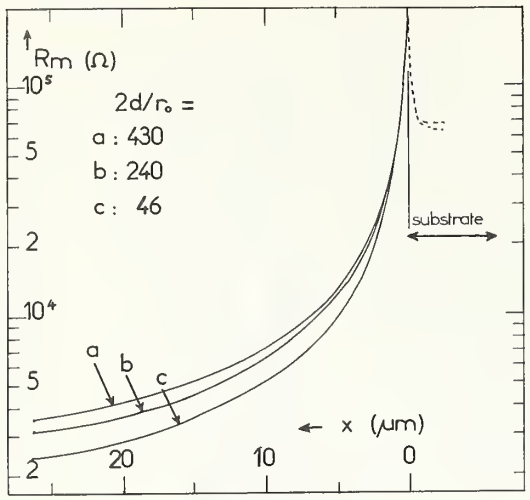

Figure 8. Uncorrected profiles of one P-layer on N-substrate. The distance, d, from the probe to the strip is the parameter.

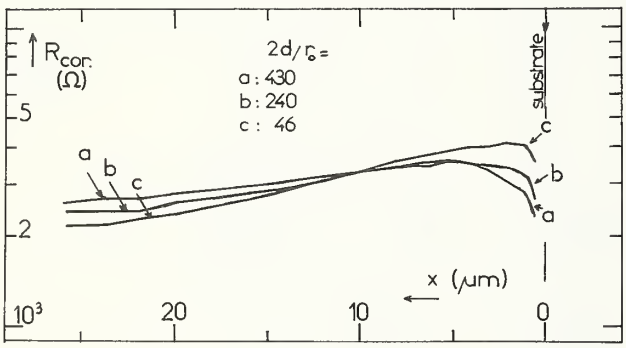

Figure 9. Same profiles as in figure 8, after correction, using k = 1.2, r_o = 5.2μm and d as indicated for $2d/r_o$.

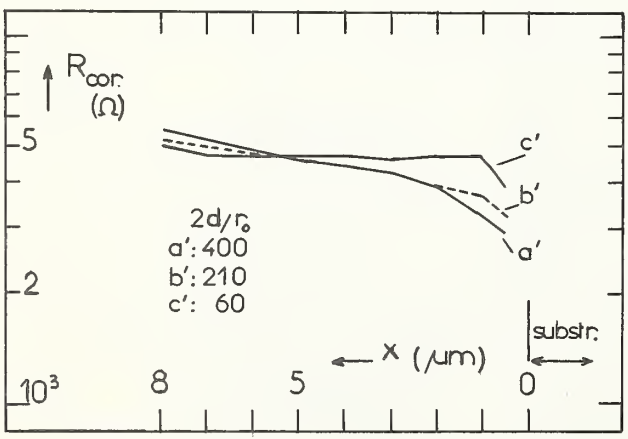

Figure 10. Corrected profiles for a portion of the same slice as figure 9, but after thickness reduction of the layer to 8μm prior to measurements.

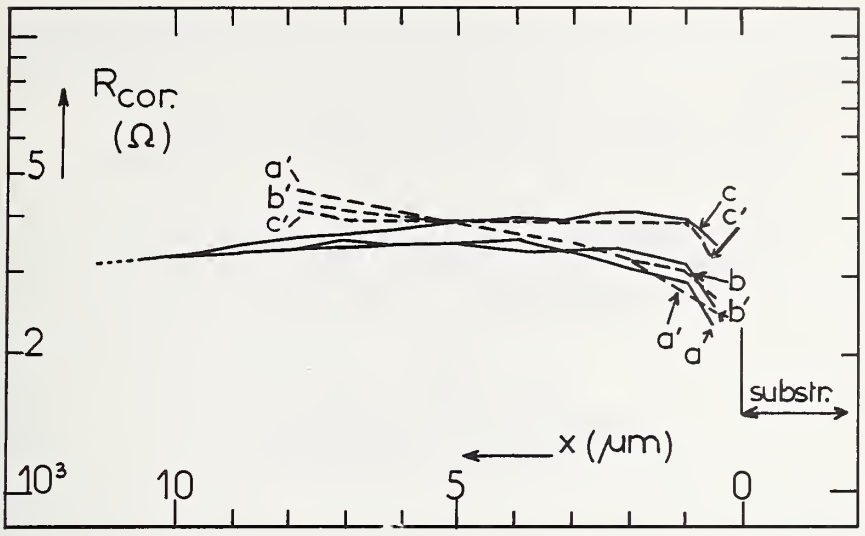

Figure 11. Comparison between the profiles of figures 9 and 10 (the data of figure 10: curves a', b' and c' have been shifted downwards by 20% for better agreement).

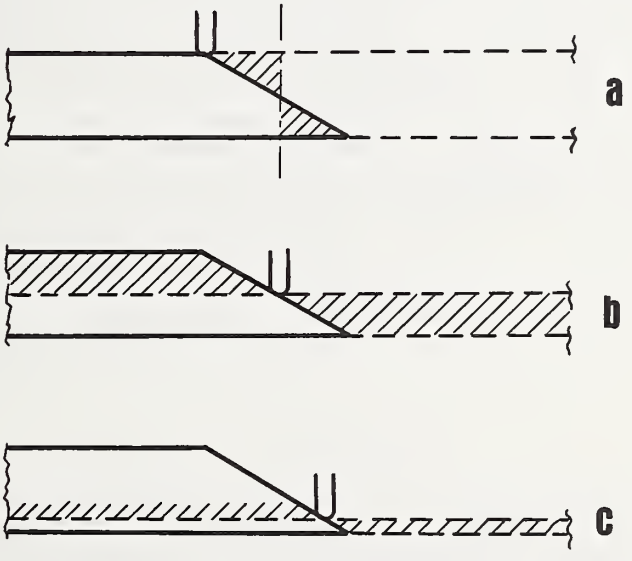

Figure 12. Qualitative effect of the bevel geometry: the usual correction factor is: too small in a) (edge effect) nearly adequate in b) too large in c)

NATIONAL BUREAU OF STANDARDS SPECIAL PUBLICATION 400-10, Spreading Resistance Symposium, Proceedings of a Symposium Held at NBS, Gaithersburg, Md., June 13-14, 1974.

SRPROF, A Fast and Simple Program for Analyzing Spreading Resistance Profile Data

B. L. Morris and P. H. Langer
Bell Telephone Laboratories, Incorporated
Allentown, Pennsylvania

and

J. C. White, Jr.
Western Electric Company
Allentown, Pennsylvania

The spreading resistance technique is an excellent method of measuring epitaxial resistivity profiles. In many cases it is the only method by which the complete profile may be measured. However, thin film correction factors must be used to convert the spreading resistance into a corrected resistivity. Previous calculations of these correction factors have emphasized a mathematically complex solution which necessitates the use of a large computer. The correction factors used here are calculated from a relatively simple algorithm which allows the use of a minicomputer. A documented program is presented which uses these algorithms. This program, written in FOCAL for use on the PDP8 series of minicomputers, is fast, accurate, easy to use, and provides a complete data reduction system. Examples of corrected spreading resistance profiles are presented, and compared with independent results such as diode C-V and four point probe measurements.

Key words: Resistivity profiles; spreading resistance; thin film correction factors.

1. Introduction

If a flat circular probe of radius a is brought into contact with a semi-infinite material of resistivity ρ, and a current I is passed through this structure, practically all of the potential drop will occur within 1.5 x a of the point of contact.[1][1] This is shown schematically in Figure 1. For a contact in which the surface barrier resistance (Schottky resistance) can be neglected, the resistance of the structure is

$$R_s = \rho/4a \quad . \tag{1}$$

This is known as the spreading resistance. Since real metal-semiconductor

[1]Figures in brackets indicate the literature references at the end of this paper.

contacts can have appreciable barrier resistance, an empirical calibration of R_s vs. ρ is necessary. These calibration curves are constructed for silicon by measuring R_s and ρ on a large number of samples, both N and P type, <100> and <111> orientations, with resistivities from 0.001 ohm-cm to 100 ohm-cm.

The spreading resistance set used in this work is the model ASR-100 built by Solid State Measurements, Inc.[2] This unit measures the total contact resistance between two probes, each of which have a radius of contact of approximately 3 microns. For the two-probe case, eq (1) is modified to read

$$R_s = \rho/2a \tag{2a}$$

or

$$\rho = 2a\ R_s \quad . \tag{2b}$$

The assumption that the material is infinitely thick, i.e., that $t/a >> 1$, is not true for most of the structures used in semiconductor devices. In particular, epitaxial films, which are grown on substrates of different resistivity, usually have thicknesses which are of the same order of magnitude as the probe radius. For these thin films, the equipotential lines shown in figure 1 will be distorted, and the relation between R_s and ρ will be subject to a thin film correction factor (CF):

$$\rho = 2a\ R_s/CF \quad . \tag{3}$$

The CF depends upon the relative resistivities of the film (ρ_1) and substrate (ρ_2), as well as the film thickness. If $\rho_2 > \rho_1$, the potential lines will tend to be pushed out of the substrate. In the limit where $\rho_1/\rho_2 = 0$, which is the effective ratio when the film-substrate boundary is an insulating one (i.e., a p-n junction), the potential lines are unable to penetrate the boundary. In this case the measured value of R_s for a given ρ will be higher than predicted by eq (2a), and the CF in eq (3) should be greater than unity. If the boundary is a conducting one, potential lines will be drawn into the substrate, making the value of R_s too low. In this case the CF will be less than unity.

2. Previous Work

A great deal of effort has gone into the problem of calculating the exact solution of the potential distribution for a real (i.e., multilayer) semiconductor material under a charged circular disc.[3-5] For the simple case of a two probe measurement on a two layer system, with a layer of resistivity ρ_1 and thickness t, and an infinitely thick substrate of resistivity ρ_2, the spreading resistance is [3]

$$R_s = \frac{V}{I} = \frac{\rho_1}{2a}\left[\frac{4}{\pi}\int_0^\infty \left(\frac{1 + Ke^{-2Hx}}{1 - Ke^{-2Hx}}\right) \sin(X)\ \left(\frac{J_1(x)}{x^2} - \frac{J_o(Sx)}{2x}\right) dx\right] \tag{4}$$

where R_s is the spreading resistance, $H = t/a$, $K = (\rho_2 - \rho_1)/(\rho_2 + \rho_1)$,

S = 2s/a (s is the spacing between the two probes), x is an integration parameter, and J_0 and J_1 are Bessel functions. The term within the square bracket is the CF. These CFs are shown schematically in figure 2.

Unfortunately, the relatively simple calculation of eq (4) is not always a proper representation of the complex structure of a real epitaxial profile, a more realistic approach is the multilayer concept.[3-4] This method involves a numerical solution, in which the determinant of a (2N + 2) x (2N + 2) matrix must be calculated in order to compute the correction factors of a profile with N points.[4] This calculation takes approximately 10 minutes of CPU time on an IBM Model 360/85 to correct a profile of 25 points,[4-5] although a recent paper by Hu[5] states that it is possible to reduce this time by a factor of about 30.

3. Calculation of CF Algorithms

If spreading resistance profiles are to be used to evaluate epitaxial material on a routine basis, the data reduction scheme, which includes calculation of the thin film CF, should have the following properties; accuracy, ease of utilization, and low cost. In the final analysis, the accuracy of the calculated CF can only be determined by comparing the corrected spreading resistance profile with a profile determined by an independent measurement technique. While this comparison includes all of the other possible sources of error inherent in a spreading resistance profile measurement, and of course in the "other" technique, it is the ultimate test of the entire system, which is really what is important. The ease of utilization includes total effort needed to reduce the "raw" data produced by the apparatus into a final profile. Since our ASR-100 is equipped with a data acquisition system which reproduces the data on punched paper tape, it was advantageous to use a system which could read this tape as a primary input. This factor, combined with the need for an easily accessed low cost system, led us to consider writing a program which could be used on a PDP8 minicomputer currently in our laboratory.

A minicomputer using an interactive language such as FOCAL runs at a much slower speed than a large computer using FORTRAN, therefore it was felt that the only method by which a reasonable calculating speed could be obtained would be to fit the results of eq (4) to a simple mathematical expression, and then modify this function until the results agreed with independent profile measurements.

Initial attempts to fit a simple polynomial function were not successful due to the extreme non-linear behavior of the CF, as seen in figure 2. For the insulating boundary condition (K = +1), a function of the type $CF = A + Be^x$ was then tried. The limits of this CF, as t/a approaches zero and infinity, are respectively infinity and unity, suggesting a function of the form

$$CF_{ins} = 1 + B \exp (m \cdot t/a) \quad , \tag{5}$$

where m = m (t/a). The best fit of this CF to the values of eq (4) was found for the case where B = 1.4 and m (t/a) is shown in Table 1.

Equation (5) assumes that the p-n junction is a perfectly insulating boundary. As the junction is approached, and the resistivity of the layer rises toward that at the junction, this assumption is no longer true, and results in over-correction of these last points.[5] Experimental data obtained from profiling heavily doped ($\approx 10^{17}$ cm^{-3}) p-type epi on an n-type substrate were used to derive an empirical correction eq (5). The best solution, one that did not produce over correction was found to be:

$$CF_{ins} = 1 + 1.4 \exp [m \cdot (t/a) \cdot K^{0.2}] \quad (6)$$

where $K = (\rho_2 - \rho_1)/(\rho_2 + \rho_1)$ as in eq (4).

Table 1.

t/a	Insulating boundary "m"	Conducting boundary "n"
0.1	34.32	-0.0637
0.2	13.55	-0.1174
0.3	7.587	-0.1622
0.4	4.905	-0.1995
0.5	3.426	-0.2303
0.6	2.511	-0.2558
0.7	1.899	-0.2767
0.8	1.466	-0.2943
0.9	1.149	-0.3091
1	0.9087	-0.3216
2	0.0248	-0.3830
3	-0.1599	-0.4041
4	-0.2169	-0.4142
5	-0.2355	-0.4199
6	-0.2399	-0.4239
7	-0.2372	-0.4277
8	-0.2330	-0.4306
9	-0.2267	-0.4331
10	-0.2207	-0.4354
20	-0.1706	-0.4431
50	-0.1381	-0.4430
100	-0.1842	-0.4789

All of the corrections discussed so far have applied to one-dimensional, semi-infinite material. In fact there is a two-dimensional effect in the CF, analogous to that of the four point probe. In this latter measurement, the sheet resistance of a large wafer is $R_s = (\pi/\ell n2) \cdot V/I$, but if the probes are on the edge of the wafer, the relation is $R_s = 1/2\ (\pi/\ell n2) \cdot V/I$. In spreading resistance measurements, this limit is arrived at as the p-n junction on the beveled wafer is approached by the probes. This 2-dimension factor, CF_{2D}, must be multiplied by the one-dimensional CF_{ins} to get the proper resultant. CF_{2D} depends upon the spacing between the two probes, and the lateral distance of the probes from the junction. This factor was experimentally determined for our probe spacing of 0.6 mm, and is shown in Table 2.

The conducting boundary condition has a CF_{CD} with the following properties:

1. $CF_{CD} \leq 1$ in all cases
2. $CF_{CD} \to 1$ as $t/a \to \infty$
3. $CF_{CD} \to 1$ as $K \to 0$.

As in the case of the insulating boundary, a simple polynomial could not be found to fit. Equation (4) was used to generate values of CF_{CD} as a function of t/a and K. The best fit was found to be

$$CF_{CD} = 2 - \exp [n \cdot K/(t/a)] \quad (7)$$

where n = n (t/a) is given in Table 1.

Table 2.

Two-Dimensional Correction Factor for Finite Sheet Size

X (μm) (Lateral distance from edge)	$CF_{2D} = R(x)/R(\infty)$
0	2.00
10	1.72
20	1.60
30	1.46
40	1.39
50	1.33
60	1.29
80	1.22
100	1.17
120	1.14
140	1.10
160	1.08
180	1.06
200	1.04
1,000	1.00

Equation (7) is strictly valid only for the single layer approximation. Schumann and Gardner[3] have shown that the multilayer approach is quite important for $N/N^+/P$ structures, where the insulating N^+/P boundary can have a large effect on the N/N^+ CF. This effect becomes more pronounced as: 1. the N^+ layer becomes thin, 2. the resistivity of the point on the N layer approaches that of the N^+ layer. An empirical correction for this double layer case has been incorporated into our conducting CF, this is:

$$CF'_{CD} = CF_{CD} \cdot [1 + 1.4 \exp (m \cdot TP \cdot UR/RJ] \quad (8)$$

where RJ = resistivity of last point in N layer
UR = uncorrected resistivity of the point to be corrected
TP = $(X + TK(N^+))/a$
X = depth of point to be corrected
$TK(N^+)$ = thickness of N^+ layer

and $m = m [TP^{\sqrt{UR/RJ}}]$.

At the N/N^+ boundary where UR = RJ and X =0, this factor reduces to the insulating boundary CF. For points on the N layer having relatively high resistivity ($UR \gtrsim 100 \times RJ$), or for the very thick N^+ layers ($TK(N^+) \gtrsim 10 \times a$), this factor approaches unity.

4. Programming of SRPROF (Spreading Resistance PROFile)

The complete program utilizing the correction factor algorithms discussed in the previous section is shown in Appendix I. Comment "cards" and a

variable list are shown in Appendix II. The programming language is 8K FOCAL, an interactive language developed by Digital Equipment Corporation for use on the PDP8 series of minicomputers. It is quite similar to BASIC, which, in various forms, is used on many large and small computers. A flow chart of the program is shown in figure 3.

The initial parameters entered on the keyboard are wafer identification, scale factor, orientation, points on oxide (i.e., not on the beveled surface), thickness and conductivity type of J layers. This data is terminated by entering a thickness of zero.

The data tape generated by the data acquisition system of the ASR-100 is then entered into the tape reader, a 9999 entered from the keyboard terminates the data. Any "bad" points can be edited at this step by manually entering the point number and the "correct" resistance of that point.

Starting with the first layer (J = 1) the program calculates the number of points in this layer, the uncorrected resistivity of the last point in this layer, calculates the relevant CF, and prints out all data for this point. A typical output is shown in Appendix III. The Resistivity is the corrected value, the Doping is calculated from Irvin's work,[7] SR is the actual spreading resistance, UR is the uncorrected resistivity, and RC is the radius of contact, RC = UR (2 x SR). Layers are separated by a blank line. The output speed is limited by the Teletype printout rate of 10 characters/sec. The computer has sufficient core storage for approximately 100 data points, in addition to the program itself.

5. Results and Summary

The accuracy of the corrected spreading resistance profile, and thus of the CF calculations, can only be verified by comparing the results to those of an independent measurement technique. For the conducting substrate boundary condition, diode C-V profiling is an ideal method of directly measuring the carrier concentration profile, however, it is limited in depth by breakdown voltage. Two examples of this comparison are shown in figure 4. Wafer A988-7 is relatively thin epi with a sharp interface. Wafer RL5-1 has been heated at 1,200°C for 8 hours to produce a large amount of outdiffusion. In both cases the two methods match well over the limited range of the C-V profile.

For epitaxial layers grown on opposite type substrates, sheet resistance may be easily measured by a four point probe. This sheet resistance can also be calculated by SRPROF using a point by point summation of the calculated resistivity. In most cases that we measured this calculated sheet resistance matches the measured value within $\pm$ 10%, and in all cases within $\pm$ 20%.

In conclusion, SRPROF is shown to be a fast, convenient, and accurate method of reducing spreading resistance profile data, which is applicable to epitaxial layers with either conducting or insulating substrates.

References

[1] R. Holm, "Electric Contacts Handbook", Springer, Berlin (1967).

[2] Solid State Measurements, Inc., Monroeville, Pennsylvania.

[3] P. A. Schumann and E. E. Gardner, Jr., Solid St. Elec. 12, 371 (1969).

[4] T. H. Yeh and K. H. Khokhani, J. Electrochem. Soc. 116, 1461 (1969).

[5] S. M. Hu, Solid St. Elec. 15, 809 (1972).

[6] F. M. Smits, Bell System Tech. J. 37, 711 (1958).

[7] J. C. Irvin, Bell System Tech. J. 41, 387 (1962).

Appendix I

```
2Ø.1Ø C SRPROF
2Ø.11 E
2Ø.12 T !!!;A "SLICE"P,"SF"SF,"ORNT"OR," POINTS ON OXIDE"Z
2Ø.14 T !!;S J=1;S LT=FLOG(1Ø);D 27
2Ø.16 A "  THK"TK(J);I (TK(J))2Ø.24,2Ø.24;A "TYPE"T(J)
2Ø.17 S J=J+1;G 2Ø.16
2Ø.24 T !!,"ENTER TAPE",!;S I=1
2Ø.25 A R(I);I (9ØØØ-R(I))2Ø.3;I (R(I)-.1)2Ø.28
2Ø.26 S I=I+1
2Ø.28 G 2Ø.25
2Ø.3Ø S P=-1;S SP=-2
2Ø.33 S P=P+1;S SP=SP+1;I (6ØØØ-R(P))2Ø.42
2Ø.34 I (FITR<R(P)/1ØØØ>-2)2Ø.36,2Ø.37
2Ø.35 I (FITR<R(P)/1ØØØ>-4)2Ø.37,2Ø.38
2Ø.36 S R(P)=FEXP<LT*(R(P)/5ØØ+2)>;G 2Ø.33
2Ø.37 S R(P)=FEXP<LT*(3ØØØ=R(P))/5ØØ>;G 2Ø.33
2Ø.38 S R(P)=FEXP<LT*(R(P)-1ØØØ)/5ØØ>;G 2Ø.33
2Ø.42 S SP=SP-Z;F I=1,SP;S R(I)=R(I+Z)
2Ø.44 A !!,"HOW MANY BAD POINTS?"P,!
2Ø.45 S K=Ø;I (P-1)2Ø.49
2Ø.46 T !,"LIST I (FROM TRUE EDGE) AND R(I)",!
2Ø.47 A "I"I,"R(I)"R(I),!
2Ø.48 S K=K+1;I (K-P)2Ø.47
2Ø.49 D 24.5
2Ø.52 S J=1;S NP(J)=FITR(TK(J)/SF)+1;S S=NP(J);S SH(J)=Ø
2Ø.54 S I=S;D 21;S RJ(J)=UR
2Ø.56 F I=1,NP(J);D 21;D 22;D 23;D 24
2Ø.62 S J=J+1;T !;S SH(J)=Ø;I (TK(J)-.1)25.8
2Ø.63 S NP(J)=FITR<(TK(J)-TK(J-1))/SF>
2Ø.64 S M1=S+1;S M2=M1+NP(J)-1;S S=S+NP(J)
2Ø.65 I (TK(J+1)-.1)2Ø.69;D 2Ø.54
2Ø.67 F I=M1,M2;D 21;D 22;D 23;D 24
2Ø.68 G 2Ø.62
2Ø.69 S RJ(J)=1E2Ø;G 2Ø.67

21.11 S D=SF*(I-1);I (SP-I)25.8;S K=FLOG(R(I)/1ØØØ)
21.13 I (T(J)-14)21.16,21.14,21.16
21.14 I (OR-111)21.22,21.32,21.22
21.16 I (OR-111)21.42,21.51.21.42
21.22 S UR=-.56655+1.Ø596*K+.Ø18Ø5*K↑2-.33462E-Ø2*K↑3
21.23 S UR=UR-.84Ø64E-Ø4*K↑4;G 21.6
21.32 S UR=-.79246+.9936*K+.Ø24673*K↑2+.65968E-Ø3*K↑3
21.33 S UR=UR-.1731E-Ø3*K↑4-.39394E-Ø4*K↑5;G 21.6
21.42 S UR=-.18876+1.Ø387*K+.Ø59796*K↑2+.27823E-Ø2*K↑3
21.43 S UR=UR-.1Ø481E-Ø2*K↑4-.14122E-Ø3*K↑5;G 21.6
21.51 I (R(I)-85Ø)21.54
21.52 S UR=-.33364+2.2216*K-.7Ø895*K↑2+.12841*K↑3
21.53 S UR=UR+.91Ø35E-Ø4*K↑4-.13896E-Ø2*K↑5;G 21.6
21.54 S UR=-.57755+.71456*K-.Ø37836*K↑2-.33Ø79E-Ø2*K↑3
21.6Ø S UR=FEXP(UR)

22.12 S RC+UR*1EØ4/(2*R(I));S X=TK(J)-D;S TR=X/RC
22.14 S XK=<RJ(J)+1E-Ø7-UR>/<RJ(J)+UR>
22.16 I (TK(J+1)-.1)22.22
```

```
22.18 I (T(J)-T(J+1))22.22,22.42
22.22 S K=1;I (TR-.1)22.92; I (TR-99)22.23;S XM=-.184;G 22.32
22.23 I (TR-TO(K))22.26,22.26;I (TO(K+1)-TR)22.26
22.24 S XM=IN(K+1)-(IN(K+1)-IN(K))*(TO(K+1)-TR)/(TO(K+1)-TO(K))
22.25 G 22.32
22.26 S K=K+1;G 22.23
22.32 S XX=TR*XM*FEXP<.2*FLOG(FABS(XK))>;S P=1Ø*X/SF;S Z=1
22.33 I (23Ø-P)22.35;S Z=1.8923-.Ø1528*P+1.Ø364E-Ø4*P↑2
22.34 S Z=Z-2.7879E-Ø7*P↑3+1.895E-1Ø*P↑4
22.35 S CF=Z*(1+1.4*FEXP(XX));G 22.94
22.42 S K=1;I (TR-.1)22.46;I (TR-99)22.43;S XM=.48;G 22.48
22.43 I (TR-TO(K))22.46,22.46;I (TO(K+1)-TR)22.46
22.44 S XM=CD(K+1)-(CD(K+1)-CD(K))*(TO(K+1)-TR)/(TO(K+1)-TO(K))
22.45 G 22.48
22.46 S K=K+1;G 22.43
22.47 S XM=CD(1)
22.48 S CF=2-FEXP(-XM*XK/TR);I (CF-.Ø1)22.92
22.52 S TP=(X+TK(J+1))/RC;I (TP-99)22.54;S TP=99
22.54 S TR=FSQT(UR/RJ(J))*FLOG(TP);I (4.6-TR)22.62;S TR=FEXP(TR);S K=1
22.56 I (TR-TO(K))22.58,22.58;I (TO(K+1)-TR)22.58
22.57 D 22.24;G 22.65
22.58 S K=K+1;G 22.56
22.62 S XM=-.18
22.65 S XX=XM*TP*UR/RJ(J);I (-XX-1ØØ)22.68;S XX=-1ØØ
22.68 S CF=CF*(1+1.4*FEXP(XX));I (.1-CF)22.94
22.92 S CF=.Ø9
22.94 S CR=UR/CF;I (1.5-I)22.96;S LR=CR;R
22.96 S AV=(CR+LR)/2;S LR=CR;D 25

23.12 I (T(J)-14)23.2,23.3
23.20 I (CR-.926)23.22;S P=7.2E-17;S K=1;G 23.4
23.22 I (CR-.Ø324)23.23;S P=3.3E-11;S K=.65;G 23.4
23.23 I (CR-.ØØ755)23.24;S P=1.47E-14;S K=.832;G 23.4
23.24 S P=4E-17;S K=.966;G 23.4
23.30 I (CR-1.43)23.32;S P=2E-16;S K=1;G 23.4
23.32 I (CR-.Ø847)23.33;S P=6.97E-14;S K=.837;G 23.4
23.33 I (CR-.ØØ715)23.34;S P=6.93E-Ø9;S K=.543;G 23.4
23.34 I (CR-.ØØ128)23.35;S P=2E-16;S K=.94;G 23.4
23.35 S P=1.43E-12;S K=.744
23.4Ø S NN=FEXP<FLOG(1/(P*CR))/K>

24.12 I (CF-.1)24.2
24.14 T %4.Ø2,D,%11.Ø4,CR,"  "%3.Ø3,NN,%7.Ø4,CF,%9.Ø3,R(i),%8.Ø4,UR
24.15 T %6.Ø3,RC,!;R
24.2Ø T %4.Ø2,D,"      T/R TOO SMALL TO GET CF",%14.Ø3,R(I),%8.Ø4,UR
24.22 G 24.15
24.50 T !!!," DEPTH    RESISTIVITY   DOPING     CF          SR";G 24.52
24.52 T "        UR        RC",!,"(MICR)     (OHM-CM)";G 24.54
24.54 T "      (CM-3)              (OHMS)    (OHM-CM)   (MICR)",!!;R

25.1Ø I (.1-CF)25.15;R
25.15 S SH(J)=SH(J)+SF*1E-Ø4/AV;R
25.2Ø T !!;S Z=J-1;F P=1,Z;D 25.5
25.4Ø G 25.8
25.5Ø T "SHEET RES OF LAYER",%2,P," =",%7.Ø2,1/SH(P)," OHM/SQ",!;R
25.8Ø T!,"END",!!;Q

27.12 F K=1,9;S TO(K)=K/1Ø
27.14 F K=1Ø,19;S TO(K)=K-9
27.16 S TO(2Ø)=2Ø;S TO(21)=5Ø;S TO(22)=1ØØ
27.2Ø S CD(1)=.Ø63716;S CD(2)=.11739;S CD(3)=.162256;S CD(4)=.19951
27.22 S CD(5)=.23Ø29;S CD(6)=.255749;S CD(7)=.27679;S CD(8)=.294377
27.24 S CD(9)=.3Ø91Ø3;S CD(1Ø)=.321649;S CD(11)=.383Ø58
```

```
.26 S CD(12)=.4Ø4117;S CD(13)=.414196;S CD(14)=.419867
.27 S CD(15)=.42397Ø;S CD(16)=.427666;S CD(17)=.43Ø6Ø1
.28 S CD(18)=.4331Ø9;S CD(19)=.435383;S CD(2Ø)=.443Ø56
.29 S CD(21)=.443Ø31;S CD(22)=.478852
.4Ø S IN(1)=34.32Ø5;S IN(2)=13.5469;S IN(3)=7.5875;S IN(4)=4.9Ø45
.42 S IN(5)=3.42615;S IN(6)=2.51Ø9;S IN(7)=1.8989;S IN(8)=1.46676
.44 S IN(9)=1.146676;S IN(1Ø)=.9Ø866l;S IN(11)=.Ø24871
.46 S IN(12)=-.159883;S IN(13)=-.216875;S IN(14)=-.23553
.47 S IN(15)=-.23995;S IN(16)=-.237247;S IN(17)=-.233Ø4
.48 S IN(18)=-.2267;S IN(19)=-.22Ø73;S IN(2Ø)=-.17Ø56
.49 S IN(21)=-.138155;S IN(22)=-.18421
```

Appendix II

Variable List

```
          SCALE FACTOR (MICRONS/POINT)
          ORIENTATION (lll OR 1ØØ)
 (J)      THICKNESS OF JTH LAYER
(J)       TYPE (N OR P) of JTH LAYER
(I)       SPREADING RES (OHMS) OF ITH POINT
          POINT INDEX
          LAYER INDEX
          TOTAL NUMBER OF POINTS
 (J)      NUMBER OF POINTS IN JTH LAYER
          UNCORRECTED RESISTIVITY (OHM-CM)
          CORRECTED RESISTIVITY
          CORRECTION FACTOR
          DEPTH (MICRONS)
          RADIUS OF CONTACT (MICRONS)
```

Comment Cards

```
.20       Read Tape
.29       Calculate true R (I)
.40       Correct to bevel edge
.43       Edit bad points
50        Do first layer
60        Do remaining layers
10        Calculate UR
20        N <100>
30        N <111>
40        P <100>
50        P <111>
10        Calculate CF
20        Insulating boundary
40        Conducting boundary
50        Correct for insulating boundary below cond layer
10        Calculate doping
05        Calculate sheet resistance
10        CF data matrix
```


5-448 O - 75 - 6

SLICE:H4Ø488 SF:.11 ORNT:1ØØ POINTS ON OXIDE:4

  THK:3.25 TYPE:N   THK:25Ø TYPE:N   THK:Ø

ENTER TAPE
::9999

HOW MANY BAD POINTS?:Ø

DEPTH (MICR)	RESISTIVITY (OHM-CM)	DOPING (CM-3)	CF	SR (OHMS)	UR (OHM-CM)	RC (MICR)
Ø.ØØ	Ø.4695	Ø.129E+17	Ø.6968	591.56Ø	Ø.3271	2.765
Ø.11	Ø.4573	Ø.133E+17	Ø.6886	57Ø.162	Ø.3149	2.761
Ø.22	Ø.4712	Ø.129E+17	Ø.6779	578.Ø94	Ø.3194	2.763
Ø.33	Ø.4766	Ø.127E+17	Ø.667Ø	575.438	Ø.3179	2.762
Ø.44	Ø.4781	Ø.126E+17	Ø.6555	567.542	Ø.3134	2.761
Ø.55	Ø.4889	Ø.123E+17	Ø.644Ø	57Ø.162	Ø.3149	2.761
Ø.66	Ø.4800	Ø.126E+17	Ø.6344	552.Ø75	Ø.3Ø45	2.758
Ø.77	Ø.4793	Ø.126E+17	Ø.6234	541.999	Ø.2988	2.756
Ø.88	Ø.4787	Ø.126E+17	Ø.6125	532.1Ø6	Ø.2932	2.755
Ø.99	Ø.4915	Ø.122E+17	Ø.5993	534.562	Ø.2946	2.755
1.1Ø	Ø.49Ø1	Ø.123E+17	Ø.5869	522.395	Ø.2876	2.753
1.21	Ø.4843	Ø.124E+17	Ø.5745	5Ø5.824	Ø.2782	2.75Ø
1.32	Ø.4827	Ø.125E+17	Ø.65Ø2	492.Ø38	Ø.27Ø4	2.748
1.43	Ø.4884	Ø.123E+17	Ø.5459	485.288	Ø.2666	2.747
1.54	Ø.486Ø	Ø.124E+17	Ø.53Ø7	469.893	Ø.2579	2.744
1.65	Ø.4897	Ø.123E+17	Ø.5144	459.197	Ø.2519	2.743
1.76	Ø.4941	Ø.122E+17	Ø.4979	448.744	Ø.246Ø	2.741
1.87	Ø.5Ø22	Ø.119E+17	Ø.4785	438.529	Ø.24Ø3	2.74Ø
1.98	Ø.4696	Ø.129E+17	Ø.4658	399.944	Ø.2187	2.734
2.Ø9	Ø.4564	Ø.134E+17	Ø.4488	374.972	Ø.2Ø49	2.732
2.2Ø	Ø.3983	Ø.157E+17	Ø.439Ø	32Ø.626	Ø.1749	2.727
2.31	Ø.3474	Ø.185E+17	Ø.4323	275.422	Ø.15Ø2	2.726
2.42	Ø.3Ø56	Ø.216E+17	Ø.4226	236.591	Ø.1292	2.73Ø
2.53	Ø.2243	Ø.312E+17	Ø.4394	179.473	Ø.Ø986	2.746
2.64	Ø.1349	Ø.573E+17	Ø.4876	117.489	Ø.Ø658	2.799
2.75	Ø.Ø744	Ø.127E+18	Ø.5733	73.451	Ø.Ø427	2.9Ø4
2.86	Ø.Ø469	Ø.297E+18	Ø.6554	5Ø.816	Ø.Ø3Ø8	3.Ø27
2.97	Ø.Ø224	Ø.116E+19	Ø.7931	26.546	Ø.Ø178	3.352
3.Ø8	Ø.Ø14Ø	Ø.275E+19	Ø.8911	16.982	Ø.Ø125	3.681
3.19	Ø.Ø1Ø8	Ø.448E+19	1.ØØØ1	13.932	Ø.Ø1Ø8	3.861
3.3Ø	Ø.Ø1Ø6	Ø.462E+19	1.ØØØ1	13.614	Ø.Ø1Ø6	3.884
3.41	Ø.Ø1Ø6	Ø.459E+19	1.ØØØ1	13.677	Ø.Ø1Ø6	3.879
3.52	Ø.Ø1Ø6	Ø.462E+19	1.ØØØ1	13.614	Ø.Ø1Ø6	3.884
3.63	Ø.Ø1Ø5	Ø.468E+19	1.ØØØ1	13.49Ø	Ø.Ø1Ø5	3.893
3.74	Ø.Ø1Ø6	Ø.462E+19	1.ØØØ1	13.614	Ø.Ø1Ø6	3.884
3.85	Ø.Ø1Ø6	Ø.459E+19	1.ØØØ1	13.677	Ø.Ø1Ø6	3.879

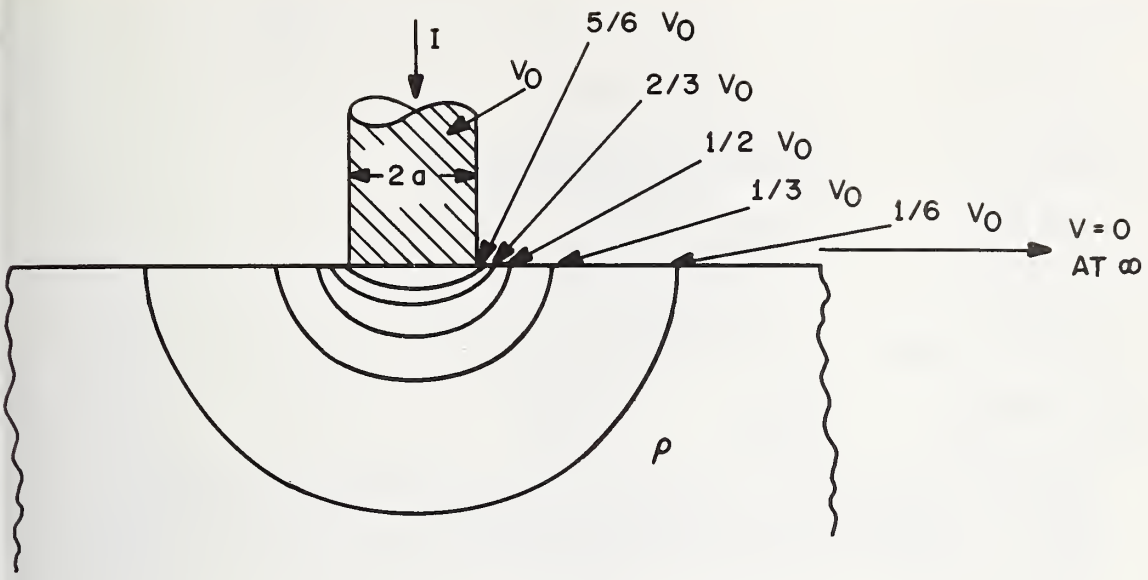

Figure 1. Potential distribution due to equipotential probe on semi-infinite solid of homogenous resistivity, ρ.

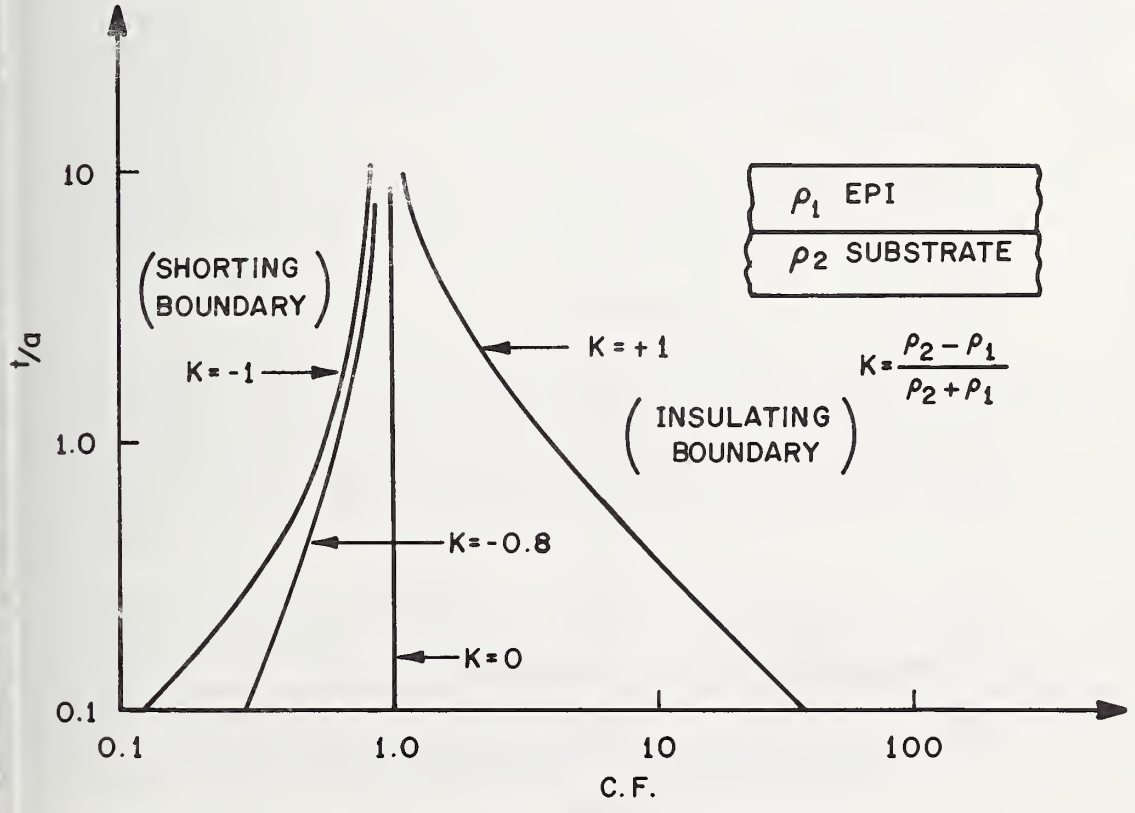

Figure 2. Spreading Resistance Correction Factors.

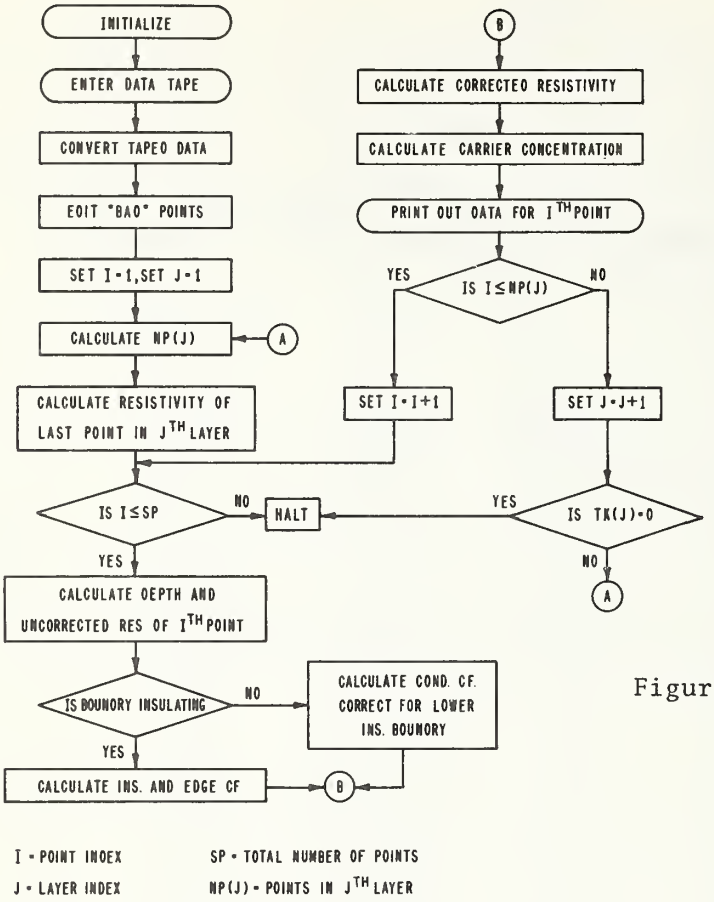

Figure 3. Flow Diagram of SRPROF.

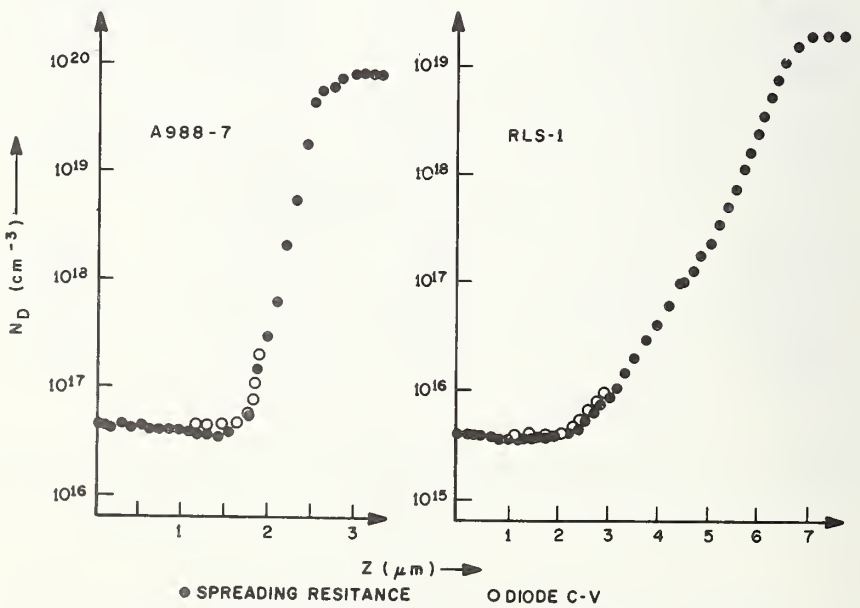

Figure 4. Comparison of Spreading Resistance and Diode C-V profiles.

NATIONAL BUREAU OF STANDARDS SPECIAL PUBLICATION 400-10, Spreading Resistance Symposium, Proceedings of a Symposium Held at NBS, Gaithersburg, Md., June 13-14, 1974.

Multilayer Analysis of Spreading Resistance Measurements

Gregg A. Lee

Texas Instruments Incorporated
Dallas, Texas 75222

Spreading resistance measurements provide a highly flexible technique for the determination of dopant profiles in semiconductors. However, because each measurement samples a greater depth into the sample than the depth difference between successive measurements, the direct conversion of resistivity readings to dopant concentration values will not yield a correct profile.

The technique discussed in this report analyzes direct spreading resistance readings to deduce a "true" dopant profile. The model used is that of circular contacts to a laterally infinite medium which is partitioned vertically into layers of homogeneous resistivity, each layer corresponding to one spreading resistance measurement point. The analysis is performed by a computer program. Some detail in the development of the program is discussed.

The results of this analysis technique compare favorably to profile results of other profiling techniques such as capacitance voltage and incremental sheet resistance on profile types to which they can be applied. The program execution time is usually fast enough that the computer charge is less than the direct charge billed for making the spreading resistance measurements.

Key Words: Correction factors, computer modeling, dopant profiles, multilayer spreading resistance model, resistivity, semiconductor dopant concentration, spreading resistance.

1. Introduction

Spreading resistance measurements provide a potentially powerful method for determining dopant concentration rofiles in semiconductor materials, because continuous profiles can be obtained over several orders of magnitude of oncentration change and across p-n junctions. The profiles are obtained by stepping the probe points down a bevel pped at a small angle to the original surface (fig. 1). Each measurement point is assumed to approximate a easurement on a flat surface formed by removing all material from the sample above the depth of that point on the evel. By using small angles (17′ to 5°) it is possible to obtain profiles in which consecutive points differ in depth by ss than 200 Å [1][1].

Unfortunately, the precision of the geometry is negated by the comparatively large volume in the material being rofiled which is sampled by the electrical measurement. This volume may extend one to several microns into the aterial (which in shallow devices may involve orders of magnitude of resistivity change). As a result, the haracteristics at a given depth in the material being profiled affect not one, but several of the measurement points on he bevel. Thus, the direct result of spreading resistance measurements is somewhat like a profile of local averages, ther than of discrete point values. Figure 2 shows a hypothetical example of this effect. Concentration rather than sistivity is plotted since this is the value of interest in process modeling and design.

The method described here, which is performed by a computer program, alleviates this problem by deducing the rue" profile from spreading resistance data as originally recorded.

Figures in brackets indicate the literature references at the end of this paper.

2. Theoretical Model

The theoretical model employed is similar to that utilized by several other authors[2,3,4]. The continuou resistivity profile is approximated by a stack of layers, each of homogeneous resistivity, with thicknesses equal to th spacing of the spreading resistance data. The potential distribution in this structure can be solved numerically an employed to derive the actual profile from the originally measured values.

2a. One Probe Potential Distribution

The general solution of Laplace's equation in cylindrical coordinates (r, θ, z) for a circularly symmetric potenti such as that resulting from a single probe is:

$$V(r,z) = \int_0^\infty [A(\lambda)J_0(\lambda r)e^{\lambda z} + B(\lambda)J_0(\lambda r)e^{-\lambda z}]\, d\lambda$$

where V is voltage and A and B are arbitrary functions of the integration variable λ. This can be rewritten as:

$$V(r,z) = K \int_0^\infty e^{-\lambda z} \frac{\sin(\lambda r_0)}{\lambda} J_0(\lambda r)d\lambda + K \int_0^\infty \theta(\lambda)e^{-\lambda z} \frac{\sin(\lambda r_0)}{\lambda} J_0(\lambda r)d\lambda$$

$$+ K \int_0^\infty \psi(\lambda)e^{\lambda z} \frac{\sin(\lambda r_0)}{\lambda} J_0(\lambda r)d\lambda$$

where

$$A(\lambda) \equiv K\,[1 + \theta(\lambda)]\, \frac{\sin \lambda r_0}{\lambda}$$

$$B(\lambda) \equiv K\psi(\lambda)\, \frac{\sin \lambda r_0}{\lambda}$$

and r_0 is the effective radius of contact of the probe, which is assumed to be circular. In the case of a layer structure, a separate voltage function, V_i, is defined for each layer, such that:

$$V_i(r,z) = K \left[\int_0^\infty e^{-\lambda z} \frac{\sin(\lambda r_0)}{\lambda} J_0(\lambda r)d\lambda + \int_0^\infty \theta_i(\lambda)e^{-\lambda z} \frac{\sin(\lambda r_0)}{\lambda} J_0(\lambda r)d\lambda \right.$$

$$\left. + \int_0^\infty \psi_i(\lambda)e^{\lambda z} \frac{\sin(\lambda r_0)}{\lambda} J_0(\lambda r)d\lambda \right] \qquad (2.0)$$

At this point boundary conditions are imposed which assume that current is flowing, which may be inconsiste with Laplace's equation if charge accumulation exists. However, the expected error introduced is not large[5], *a the results of the method do agree with other profiling techniques.*

The boundary conditions are these: (refer to fig. 3)

I. No current flows through the surface of the structure beyond the radius of the probe contact:

$$\left.\frac{1}{\rho_1}\ \frac{\partial V_1}{\partial z}\right|_{\substack{z=0\\ r=r_o}} = 0$$

II. At each layer interface

a. V is continuous:

$$V_i\,(r,h_i) = V_{i+1}\,(r,h_i)$$

b. The current component perpendicular to the interface is continuous:

$$\left.\frac{1}{\rho_i}\ \frac{\partial V_i(r,z)}{\partial z}\right|_{z=h_i} = \left.\frac{1}{\rho_{i+1}}\ \frac{\partial V_{i+1}(r,z)}{\partial z}\right|_{z=h_i}$$

III. Two possible appropriate boundary conditions exist for the bottom layer. One assumes that the last layer is semi-infinite and of homogeneous resistivity. The other assumes that a junction exists beneath the last layer.

In the first case, the boundary condition is that

$$\lim_{z\to\infty} V_N(r,z) = 0$$

In the second case, no current crosses the junction:

$$\left.\frac{1}{\rho_N}\ \frac{\partial V_N(r,z)}{\partial z}\right|_{z=h_N} = 0$$

When the expression for $V_i(r,z)$ is substituted into these equations, they reduce to the following set of equations. ote that θ_i and ψ_i are functions of λ only, as previously defined.

$$\theta_1 - \psi_1 = 0 \qquad (2.1)$$

$$(\theta_i - \theta_{i+1})\,e^{-2\lambda h_i} + (\psi_i - \psi_{i+1}) = 0 \qquad (2.2)$$

$$(-\theta_i + \beta_i\theta_{i+1})\,e^{-2\lambda h_i} + (\psi_i - \beta_i\psi_{i+1}) = e^{-2\lambda h_i}\,(1 - \beta_i) \qquad (2.3)$$

or the first case:

$$\psi_N = 0 \qquad (2.4a)$$

or the second case:

$$-\theta_N\,e^{-2\lambda h_N} + \psi_N = e^{-2\lambda h_N} \qquad (2.4b)$$

Where

$$\beta_i \equiv \frac{\rho_i}{\rho_{i+1}}$$

This gives 2N equations, which are sufficient for the solution of the N θ's and N ψ's. An additional bound condition involving the current distribution under the probe contact has been used by some authors to resolve I equation 2.0[6]. However, because the final form of the current distribution will be affected by the second probe apparatus, in this treatment its resolution is deferred until after the potential distribution of the two probes combination is determined.

The solution of the system of equations derived above will be treated in detail in a later section. At this p just note that only the solution of V_1, and thus θ_1 (since equation 2.1 shows that $\psi_1 = \theta_1$) is necessary, since surface potential is the only potential encountered by the probe.

2b. Two Probe Potential Difference Measurement

The voltage measured by the spreading resistance apparatus is the potential drop between the two probe poi This is derived from a superposition of the one probe solution for each of the two probes. For this solution p contacts are assumed. This is not too unreasonable since the ratio of the probe spacing to the physical con diameter is 600 to 10, and that of the probe spacing to the effective electrical contact diameter 600 to 3.

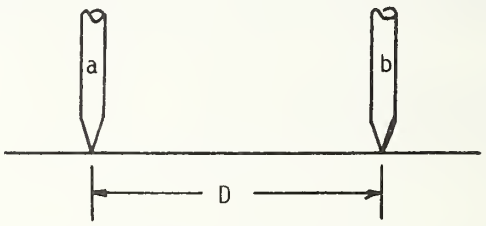

The measured potential difference between the probes Vm, is

$$V_m = V_a - V_b$$

where V_a and V_b are the potentials at probe a and probe b.

Each potential consists of two components: the potential due to probe a and that due to probe b. Note tha one probe solution coordinates of b relative to a and a relative to b are both (r = D, z = 0), where D is the p spacing. Their coordinates relative to themselves are of course (0,0). That is:

$$Va = V_1(0,0) - V_1(D,0)$$

$$Vb = V_1(D,0) - V_1(0,0)$$

So

$$\begin{aligned} Vm &= Va - Vb \\ &= V_1(0,0) - V_1(D,0) - V_1(D,0) + V_1(0,0) \\ &= 2\,[V_1(0,0) - V_1(D,0)] \end{aligned}$$

Noting from equation 2.1 that $\theta_1 = \psi_1$, expressing V_1 in the form derived in equation 2.0 yields:

$$V_m = 2K \int_0^\infty (1 + 2\theta_1)\, J_o(\lambda \cdot 0) \frac{\sin(\lambda r_o)d\lambda}{\lambda} - 2K \int_0^\infty (1 + 2\theta_1)\, J_o(\lambda D) \frac{\sin(\lambda r_o)d\lambda}{\lambda}$$

$$V_m = K \int_0^\infty (1 + 2\theta_1)\, [1 - J_o(\lambda D)] \frac{\sin(\lambda r_o)d\lambda}{\lambda}$$

where the 2 has been absorbed into K.

The method of performing this integration is discussed in Section 5.

2c. Resolution of the Proportionately Constant K.

The boundary condition imposed in order to resolve K is that the measured voltage on a semi-inifinite substrate of homogeneous resistivity should equal the voltage measured on that same substrate covered by a finite layer of equal resistivity. That is, a two layer problem:

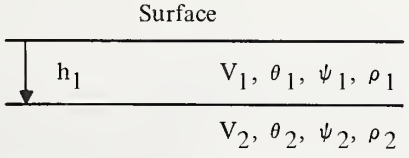

$\rho_1 = \rho_2$

Two layer problem on semi-infinite medium.

In this case the boundary equations, in matrix form, are:

$$\begin{matrix} (2.1) \\ (2.2) \\ (2.3) \\ (2.4a) \end{matrix} \begin{bmatrix} 1 & 1 & 0 & 0 \\ e^{-2\lambda h_1} & 1 & -e^{-2\lambda h_1} & -1 \\ -e^{-2\lambda h_1} & 1 & 1e^{-2\lambda h_1} & -1 \\ 0 & 0 & 0 & 1 \end{bmatrix} \times \begin{bmatrix} \theta_1 \\ \psi_1 \\ \theta_2 \\ \psi_2 \end{bmatrix} = \begin{bmatrix} 0 \\ 0 \\ e^{-2\lambda h_1}(1 - \beta_1) \\ 0 \end{bmatrix}$$

which solves to:

$$\theta_1 = \psi_1 = \frac{(\beta_1 - 1)\, e^{-2\lambda h_1}}{(\beta_1 + 1) - e^{-2\lambda h_1}(\beta_1 - 1)}$$

Since $\rho_1 = \rho_2, \beta_1 = 1$. So $\theta_1 = \psi_1 = 0$ and

$$V_{m2} = K \int_0^\infty \frac{\sin(\lambda r_o)}{\lambda} [1 - J_o(\lambda D)]\, d\lambda$$

$$= K \int_0^\infty \frac{\sin(\lambda r_o)}{\lambda} \, d\lambda - K \int_0^\infty \frac{\sin(\lambda r_o)}{\lambda} J_o(\lambda D) \, d\lambda$$

$$= K \int_0^\infty \left[\frac{\pi}{2} - \sin^{-1} \left(\frac{r_o}{D} \right) \right] .$$

On a semi-infinite substrate the measured spreading resistance voltage would be:

$$V_{m1} = I \frac{\rho_1}{2r_o}$$

The defined boundary condition is that $V_{m1} = V_{m2}$, so

$$K \left[\frac{\pi}{2} - \sin^{-1} \left(\frac{r_o}{D} \right) \right] = \frac{I\rho_1}{2r_o}$$

and

$$K = \frac{I\rho_1}{2r_o} \left[\frac{\pi}{2} - \sin^{-1} \left(\frac{r_o}{D} \right) \right]^{-1}$$

This expression could have been developed directly from the model of two discs on a semi-infinite medium. The direct result of this development is:

$$\frac{V}{1} = \frac{\rho}{\pi r_o} \left(\frac{\pi}{2} - \sin^{-1} \frac{r_o}{D} \right)$$

However, it has been traditional to neglect the second term and write

$$\frac{V}{1} = R = \frac{\rho}{2r_o}$$

The approach just shown was used primarily to employ standard formulations as much as possible for familiarity.

It is necessary to keep the $\sin^{-1}(r_o/D)$ term because the iterative technique (Section 3a) employed in the solution tends to reinforce this small error on successive iterations resulting in an error several times as large as that in the initial approximation.

3. Solution Technique

Replacement of K in the expression for V_m yields:

$$V_m = \frac{I\rho_1}{2r_o} \left[\frac{\pi}{2} - \sin^{-1} \left(\frac{r_o}{D} \right) \right]^{-1} \int_0^\infty [1 + 2\theta_1(\lambda)] \frac{\sin(\lambda r_o)}{\lambda} [1 - J_o(\lambda D)] \, d\lambda .$$

Previous authors[2,3,4] have chosen to reorder this equation to:

$$2r_o \frac{V_m}{I} = \rho_1 \left[\frac{\pi}{2} - \sin^{-1}\left(\frac{r_o}{D}\right)\right]^{-1} \int_o^\infty (1 + 2\theta_1) \frac{\sin(\lambda r_o)}{\lambda} [1-J_o(\lambda D)]\, d\lambda$$

and to define

$$\rho_o = 2r_o \frac{V_m}{I}$$

Since ρ_o would be the correct resistivity if the measurement of Vm and I were taken on a semi-infinite sample of homogeneous resistivity. (This is the usual calibration procedure for a spreading resistance probe.) In addition, the bracketed factor is defined as a "correction factor", so that

$$C = \left\{\frac{\pi}{2} - \sin^{-1}\left(\frac{r_o}{D}\right)\right\}^{-1} \int_o^\infty (1 + 2\theta)\, [1-J_o(\lambda D)] \frac{\sin(\lambda r_o)}{\lambda}\, d\lambda, \qquad (3.1)$$

and thus

$$\rho_o = \rho_1 \cdot C \qquad (3.2)$$

As Hu has pointed out[4], this is not an entirely appropriate terminology since "correction factor" implies an arbitrary adjustment on "fudge factor" rather than a logical data reduction scheme. However, in spite of the name, the format is a convenient one and is used here.

3a. Iterative Technique

The last equation can be reordered to

$$\rho_1 = \rho_o / C \qquad (3.3)$$

where C is a function of r_o, d, and θ_1. θ_1 is itself a function of $h_1\ h_2 \ldots h_N$ and $p_1\ p_2 \ldots P_N$. In other words, the equation for the "corrected" value of ρ_1 is not explicit in that C is a function of ρ_1. In general the integral factor of C has no analytical solution, and thus the equation cannot be solved explicitly for ρ_1.

The approach to solving for ρ_1 taken here is to define ρ_o as an approximation of ρ_1 and to obtain successfully better approximations of ρ_1 from an iterative solution of 3.3. Since the calibrations obtained with the Texas Instruments apparatus allow r_o to be assumed constant, $\rho_2 \ldots \rho_N$ and $h_1 \ldots h_N$ do not vary throughout the solution. Thus C may be treated as a function of ρ_1 only.

Simple Relaxation:

$$\rho_{1,i+1} = \frac{\rho_o}{C(\rho_{1,i})}$$

always converges, but often very slowly in terms of the number of repetitions required. In addition, the only available convergence criterion is comparison of successive values of ρ_1. The iteration is terminated when $\Delta\rho/\rho$ falls below a predefined limit. However, in some cases the convergence is so slow that $\Delta\rho/\rho$ may reach .001 when ρ_1 is still 10% aways from the correct value.

A Newton-Raphson technique, which uses both the last value of ρ_1 and its derivative to compute a new ρ_1, converges 3 to 5 times as fast as relaxation, but suffers the same weakness of convergence criteria and may oscillate in some cases, especially if the input data is not smooth, rather than converge. The relations used for iteration is:

$$\rho_{1,i+1} = \rho_{1,i} - \frac{\left(\rho_{1,i} - \frac{\rho_o}{C(\rho_{1,i})}\right)}{\left(1 + \frac{\rho_o}{C^2(\rho_{1,i})} \cdot C'(\rho_{1,i})\right)}$$

where $C_1 \equiv \Delta C/\Delta\rho_1$ from the previous iteration or from an extra $(\rho_1, C(\rho_1))$ pair generated if $\Delta\rho_1$ would be too large.

Both relaxation and the Newton-Raphson method can be characterized as analytic techniques. Another technique which can be employed is a pragmatic hunting method which converges about one-half as quickly as the Newton-Raphson technique, but converges absolutely and to a known absolute accuracy. The technique is a familiar one, and best described as "bracketing". If a criterion can be found to determine if the correct value of ρ_1 lies between two other values of ρ_1, a search along the ρ_1 axis can be conducted using an arbitrary step size $\Delta\rho$ until the criterion is met. Once this has occurred, the correct value of ρ_1 is bracketed to a known accuracy. By splitting the bracket and retesting either of the two new brackets created for the presence of the correct value the bracket size can be reduced by one-half. Repeating the process results in a one digit accuracy improvement each 3.322 (=$(\log 2)^{-1}$) iterations.

The correct value of ρ_1 will have the following characteristics:

$$\rho_1 = \frac{\rho_o}{C(\rho_1)} = \rho_o \left\{ \left[\frac{\pi}{2} - \sin^{-1}\left(\frac{r_o}{D}\right) \right]^{-1} \int_o^\infty (1 + 2\theta)\,[1 - J_o(\lambda D)] \frac{\sin(\lambda r_o)}{\lambda} d\lambda \right\}^{-1}$$

In other words, two relationships must be simultaneously satisfied:

$$\text{A:} \quad \frac{1}{C(\rho_1)} = \left\{ \left[\frac{\pi}{2} - \sin^{-1}\left(\frac{r_o}{D}\right) \right]^{-1} \int_o^\infty (1 + 2\theta)\,[1 - J_o(\lambda D)] \frac{\sin(\lambda r_o)}{\lambda} d\lambda \right\}^{-1}$$

$$\text{B:} \quad \rho_1 = \frac{\rho_o}{C}$$

The relationship of these two equations is depicted qualitatively in figure 4. Curve B is clearly a straight line. The shape of curve A has been determined from numerical solutions of $C(\rho_1)$ and, except for local curvature reversals associated with noisy data, the shape has been qualitatively the same for every case tested. Since the two curves cross at the correct solution of ρ_1, C_A-C_B will change sign at this point. This is the bracketing criterion discussed previously. The initial search is always conducted upward to avoid the trivial solution at $\rho_1 = 0$. Figure 4 also illustrates a hypothetical series of approximations toward the correct value of ρ_1.

The program normally uses a combination of Newton-Raphson and relaxation techniques to achieve short running time. However, bracketing is selected for use on profiles which are ill-suited to the Newton-Raphson analysis.

3b. Bootstrap Solution

An iterative solution is applied to only one layer at a time. The method for correcting the entire structure is a bootstrap process proceeding from the deepest to shallowest layer. In other words, the deepest layer is corrected on the basis of the semi-infinite substrate or a junction boundary condition. Then the next is corrected on the basis of the corrected value of the bottom layer and boundary conditions, the next on the basis of these two corrected values, etc. The shallower layers, of course, do not affect the layer being corrected since they were not present at the point on the bevel at which the measurement was made.

3c. Summary

The sections which follow represent the greatest practical difficulties in performing the solution. However, they are in fact sub-procedures to the scheme just discussed. So before proceeding a more concise summary of the overall method is in order:

Resistivity layers are corrected one at a time, proceeding from the bottom to the top of the layer structure using the previously corrected layers in the solution of later ones. The corrected resistivity value is obtained from the iterative solution of the implicit equation:

$$\rho_1 = \rho_o / C(\rho_1)$$

In this equation, $C(\rho_1)$ represents the following numerical integration:

$$C(\rho_1) = \left(\frac{\pi}{2} - \sin^{-1}\left(\frac{r_o}{D}\right)\right)^{-1} \int_o^\infty (1 + 2\theta)\,[1\text{-}J_o(\lambda D)]\,\frac{\sin(\lambda r_o)}{\lambda}\,d\lambda$$

The values of $\theta_1(\lambda)$ in this integral are obtained from the numerical solution of 2N simultaneous equations where N is the number of layers in the structure.

4. Numerical Integration of C

In Section 3 it was found that

$$C(\rho_1) = \left(\frac{\pi}{2} - \sin^{-1}\left(\frac{r_o}{D}\right)\right)^{-1} \int_o^\infty (1 + 2\theta)\,[1\text{-}J_o(\lambda D)]\,\frac{\sin(\lambda r_o)}{\lambda}\,d\lambda.$$

This integration is performed numerically using Simpson's Rule, which can be applied successfully since all functions in the integrand are quite smooth. Two problems in performing the integration exist, however. First, the upper integration limit is not finite; some way of approximating the upper limit with some finite limit must be found. And second, the integrand is a product of three factors whose characteristics, or at least those pertinent to numerical integration, are quite different.

The first problem is solved by breaking the integral into two parts and evaluating them separately:

$$\int_o^\infty (1 + 2\theta)\,[1\text{-}J_o(\lambda D)]\,\frac{\sin(\lambda r_o)}{\lambda}\,d\lambda =$$

$$\int_o^L (1 + 2\theta)\,[1\text{-}J_o(\lambda D)]\,\frac{\sin(\lambda r_o)}{\lambda}\,d\lambda + \int_L^\infty (1 + 2\theta)\,[1\text{-}J_o(\lambda D)]\,\frac{\sin(\lambda r_o)}{\lambda}\,d\lambda$$

The first integral can be evaluated by usual numerical techniques, but the second integral still has an infinite upper limit. If L is chosen large enough, however, θ_1 can be made arbitrarily close to zero. (See Section 6, fig. 6 and fig. 8). In this situation, the second integral becomes

$$\int_L^\infty [1\text{-}J_o(\lambda D)]\,\frac{\sin(\lambda r_o)}{\lambda}\,d\lambda$$

which, in a reversal of the process used above, can be rewritten as

$$\int_{L}^{\infty} [1-J_0(\lambda D)] \frac{\sin(\lambda r_0)}{\lambda} d\lambda =$$

$$\int_{0}^{\infty} [1-J_0(\lambda D)] \frac{\sin(\lambda r_0)}{\lambda} d\lambda - \int_{0}^{L} [1-J_0(\lambda D)] \frac{\sin(\lambda r_0)}{\lambda} d\lambda.$$

The first of these two integrals can be solved analytically. The second can be evaluated numerically to an arbitrary accuracy. Because the integral from L to ∞ has been approximated by an integral which does not involve θ_1, its value will be independent of the layer structure. Thus it can be stored as a constant, so long as r_0 and D do not change.

When all physical dimensions (h, r_0, and D) are measured in multiples of r_0, a value of L = 50 is adequate to justify the approximation just discussed. (r_0 and D in this case are on the order of 1 to 3 microns and 600 microns.)

The second problem mentioned manifests itself chiefly as a conflict between the maximum value of λ required to drive θ_1 to 0 and the small value of $\Delta\lambda$ required to adequately approximate the Bessel function. D in units of r_0 is approximately 400. This means that a zero of J_0 occurs for every change in λ of approximately .008. Even the questionable allowance of 5 points per zero would require 31,250 integration points to reach $\lambda = 50$. Fortunately, J_0 decreases in magnitude with increasing argument value. As λ increases, the value of $(1-J_0(\lambda DJ))$ becomes dominated by the 1 allowing the size of the integration increment, $\Delta\lambda$, to be increased. However, near $\lambda = 0$ the size of $\Delta\lambda$ must be greatly reduced to prevent truncation errors caused by the subtraction of $J_0(\lambda D)$ from 1, inasmuch as $J_0(\lambda D)$ approaches 1 as λ approaches 0. This rapidly diminishing number cannot simply be ignored (i.e. assumed to be zero) because in some cases $(1 + 2\theta)$ rises as fast as $(1-J_0(\lambda D))$ falls. In the case of the first layer above a junction, $(1 + 2\theta)$ may rise nine orders of magnitude as λ decreases from 10^{-2} to 10^{-11}, while the value of the entire integrand rises 1 order and then falls eight.

The solution to these problems lies in careful selection of integration increments and some adjustment during execution. The necessary number of integration increments is between twenty-two and twenty-three thousand.

5. Solution of θ_1

Each layer requires 3 to 20 iterations for the solution of equation 3.3 to converge. Each iteration requires that the integral in equation 3.1 be evaluated once. Finally, each evaluation of the integral requires that a value for $\theta_1(\lambda)$ be determined at nearly 23,000 values of λ. Thus it is quite important that a fast method of solution for the system of equations 2.1 and 2.4 be used. The next sections describe this method.

5a. Reduction from 2N to 2N-2 Equations

The set of simultaneous equations is solved numerically, but before the solution is performed, it is possible to analytically reduce the size of the coefficient matrix by two in each direction by eliminating two equations and two variables. Equations 2.1-2.4a, restated in matrix form, are:

$$
\begin{bmatrix}
1 & 1 & & & & & & & & & & \\
E_1 & 1 & -E_1 & -1 & & & & & & & & \\
-E_1 & 1 & \beta_1 E_1 & -\beta_1 & & & & & & & & \\
 & & E_2 & 1 & -E_2 & -1 & & & & & & \\
 & & -E_2 & 1 & \beta_2 E_2 & -\beta_2 & & & & & & \\
 & & \cdot & \cdot & \cdot & \cdot & & & & & & \\
 & & & \cdot & \cdot & \cdot & \cdot & & & & & \\
 & & & & \cdot & \cdot & \cdot & \cdot & & & & \\
 & & & & E_{N-2} & 1 & -E_{N-2} & 1 & & & & \\
 & & & & -E_{N-2} & 1 & \beta_{N-2}E_{N-2} & -\beta_{N-2} & & & & \\
 & & & & & & E_{N-1} & 1 & -E_{N-1} & 1 & & \\
 & & & & & & -E_{N-1} & 1 & \beta_{N-1}E_{N-1} & -\beta_{N-1} & & \\
 & & & & & & & & & 1 &
\end{bmatrix}
\times
\begin{bmatrix}
\theta_1 \\ \phi_1 \\ \theta_2 \\ \psi_2 \\ \cdot \\ \cdot \\ \\ \\ \\ \\ \theta_{N-1} \\ \psi_{N-1} \\ \theta_N \\ \psi_N
\end{bmatrix}
=
\begin{bmatrix}
0 \\ 0 \\ E_1(1-\beta_1) \\ 0 \\ E_2(1-\beta_2) \\ \cdot \\ \cdot \\ \\ \\ \\ \\ 0 \\ E_{N-1}(1-\beta_{N-1}) \\ 0
\end{bmatrix}
$$

where $E_j \equiv e^{-2h_j\lambda}$. The geometry is as in figure 3 with $h_N \to \infty$. The areas of the matrix not shown are entirely zeros.

The case shown is for the infinite substrate boundary condition (2.4a). For the junction boundary condition (2.4b) the last row of the matrix would become:

$$
\begin{bmatrix} -E_N & 1 \end{bmatrix}
\begin{bmatrix} \psi_N \end{bmatrix}
=
\begin{bmatrix} E_N \end{bmatrix}
$$

with the junction at h_N in figure 3.

In both cases ψ_1 and ψ_N, and the outside rows and columns of the coefficient matrix can be eliminated. Since the first equation is $\theta_1 = \psi_1$, the first two columns represent the same variable and so can be added and the top row eliminated. For the infinite substrate case, ψ_N is zero and so can simply be removed, along with its coefficients, the right most column. The junction case for ψ_N is similar to that for ψ_1. Since the last equation expresses ψ_N as a function of θ_N only, this expression can be substituted into the previous two equations and the last row and column eliminated. The result for a semi-infinite substrate is

$$
\begin{bmatrix}
E_1+1 & -E_1 & -1 & & & & & & \\
-E_1+1 & {}_1E_1 & -\beta_1 & & & & & & \\
 & E_2 & 1 & -E_2 & 1 & & & & \\
 & -E_2 & 1 & \beta_2 E_2 & -\beta_2 & & & & \\
 & \cdot & \cdot & \cdot & \cdot & & & & \\
 & & \cdot & \cdot & \cdot & \cdot & & & \\
 & & & \cdot & \cdot & \cdot & \cdot & & \\
 & & & E_{N-2} & 1 & -E_{N-2} & -1 & & \\
 & & & -E_{N-2} & 1 & \beta_{N-2}E_{N-2} & -\beta_{N-2} & & \\
 & & & & & E_{N-1} & 1 & -E_{N-1} & \\
 & & & & & -E_{N-1} & 1 & \beta_{N-1}E_{N-1} &
\end{bmatrix}
\times
\begin{bmatrix}
\theta_1 \\ \theta_2 \\ \psi_1 \\ \cdot \\ \cdot \\ \cdot \\ \\ \\ \theta_{N-1} \\ \psi_{N-1} \\ \theta_N
\end{bmatrix}
=
\begin{bmatrix}
0 \\ E_1(1-\beta_1) \\ 0 \\ E_2(1-\beta_2) \\ \\ \\ \\ 0 \\ E_{N-2}(1-\beta_{N-2}) \\ 0 \\ E_{N-1}(1-\beta_{N-1})
\end{bmatrix}
$$

For the junction case the last 2 rows become

$$\begin{bmatrix} E_{N-1} & 1 & -(E_{N-1}+E_N) \\ -E_{N-1} & 1 & \beta_{N-1}(E_{N-1}-E_N) \end{bmatrix} \begin{bmatrix} \psi_{N-1} \\ \theta_N \end{bmatrix} = \begin{bmatrix} E_N \\ E_{N-1}+\beta_{N-1}(E_N-E_{N-1}) \end{bmatrix}$$

The elimination of the two equations and variables just discussed does reduce the solution time somewhat, but especially for large, N, not significantly. It does, however, put the matrix into a better format on which to perform a diagonal solution algorithm.

5b. Matrix Solution

The high sparcity and regularity of the coefficient matrix make it possible to construct a "diagonal algorithm" which solves for θ, in onepass of an iterative calculation along the diagonal of the matrix. Its development is straightforward from consideration of a Gauss reduction in which steps for which the result is known because of zeros involved in the calculator are eliminated. The algorithm is constructed to end at θ, rather than θ_N, as would be conventional for the matrix as it has been presented.

The matrix need not be stored as a 2N X 2N away, but can be compressed to 2N X 4. This saves considerable storage and is convenient for programming the diagonal algorithm as well.

Finally, to repeat a point made earlier, no back substitution to solve $\theta_2, \psi_1, \ldots, \theta_N, \psi_N$ is necessary since only θ_1 appears in the expression for V_1.

5c. Intermediate Coefficient Storage

As mentioned previously, the only coefficients in the matrix which change between iterations are those which involve ρ_1. This fact, and the fact that the matrix can be solved in one pass, make it possible to save the values generated by the reduction at the last step before it enters the final two rows, and restart at this point on subsequent iterations. This reduces the number of operations required for the matrix solution to those required for the solution of a 3 X 3 matrix on all but the first iteration. Of course a different set of coefficient values must be stored for each value of λ at which θ_1 is evaluated. This is practical only if the number of λ's is relatively small. This is the case as explained in the next section.

5d. Approximation of θ_1 by Interpolation and Extrapolation

The greatest time savings in evaluating θ_1 is not in finding a fast way to solve for θ_1, but in avoiding the solution entirely. It is possible to compute values for θ_1 at a relatively small (typically about 50) number of values of λ and interpolate or extrapolate θ_1 at other values. The importance of this fact is made clear by the fact that the integration involves nearly 23,000 values of λ.

Figures 5, 6, 7, and 8 illustrate the behavior of $(1 + 2\theta_1)$ for two different situations. Figures 5 and 7 show original and corrected profiles for a steep gradient away from a junction, and for a steep epi interface. Figures 6 and 8 show the associated values of $(1 + 2\theta)$ vs λ at various values of N.

The boundary condition in figure 5 is that of a junction at the bottom layer. The $(2 + 2\theta_1)$ function for this type profile is fitted very well by a power law, at least in the region $0 < \lambda < 2$.

It can be demonstrated that for the junction boundary condition, as $\lambda \to 0, \theta_1 \to \infty$.

This would present a serious problem to numerical integration were it not for the fact that the entire integrand converges to 0 at $\lambda = 0$. If λ is taken near enough to 0, the contribution of the the integrand at that point becomes immaterial.

Values of $(1 + 2\theta_1)$ generated by a profile similar to figure 7 are best fitted by a parabola. The actual system used is a fitted parabola to *each* set of three consecutive points, with overlaps averaged. The overlapping is done to avoid problems at inflection points.

The criterion of "good fit" used in both cases is the agreement to .1% of the value of $(1 + 2\theta_1)$ computed exactly and interpolated at the midpoint of two successive values of λ to be used as a basis for interpolation. If adequate agreement does not exist, the midpoint is incorporated as an exactly calculated point in addition to the two original points, and the test performed again in each of the two new intervals.

For intermediate values of λ, a parabola fit is used with either boundary condition. For large values of λ, $1 + 2\theta$, approaches 1 asymptomatically. θ_1 can be approximated in this region by an extrapolation of an exponential fit to two selected values of θ_1 at relatively low values of λ. This extrapolation is used to calculate a few point values of θ_1 and the rest are linearly interpolated between them. The purpose of this exercise is to avoid excessive time consuming exponential calculations. (In no case, has the approximated value of θ_1 in the "tail" region differed from an exact value by an amount affecting the first three significant digits.)

6. Data Pre-Processing

When input data is not "smooth", the Multilayer Analysis may magnify input irregularities into the output profile. Figure 9, the original and analyzed profile of an epi-substrate interface, is an example of this effect. The output profile is quite irregular even though the input appears smooth to the eye. The effect occurs when layers beneath the layer being corrected make a major contribution to the measured voltage. When this is true, the program decides that minor variations in the measured voltage must be caused by major ones in the single surface layer since its contribution to the total measured voltage is relatively small. In figure 9 this is particularly true since the surface layer at the point where irregularity begins is underlain by layers of from one to three orders of magnitude higher conductivity than the surface layer.

The problem is not in the program per se, but in the fact that the theoretical physical model used does not consider the problem of noisy data and also in the fact that although the model is a reasonable approximation of a smooth profile, it is a poor one for the derivative of the profile. The problem, then, cannot be solved by any change to the analysis technique short of complete revision. It must be solved at the input data. This is reasonable anyway, since one normally believes that the profile is really smooth and that variations of the type discussed here are indeed noise.

Modifying the input data presents two problems. The first is to define criteria of "smoothness". The second is to smooth the data while avoiding both the loss of information originally contained in the data and the introduction of an arbitrary shape to the data profile from the smoothing technique.

The second problem may not be completely avoidable, and in any case cannot be measured quantitatively, so the best approach is to do as little as possible and accept some irregularity in the output profile if it is not severe.

Since the problem arises from the poor model of the derivative supplied by a step function profile, the basic criterion of smoothness is a locally monotonic set of first differences, which are the finite difference analog of the first derivative. The first difference between two data points is:

$$\Delta_1 V_i \equiv V_{i+1} - V_i$$

(Voltage, V, is normally smoothed since this is the form of the raw data, but R or ρ could be smoothed as well.) No consideration of Δ_h, the depth change, is necessary, since it is constant. The second difference is defined as:

$$\Delta_2 V_i \equiv \Delta_1 V_{i+1} - \Delta_1 V_i$$

Notice that if the set of first differences varies monotonically, then all second differences have the same sign.

Since the first differences must be smooth, it is these values on which the smoothing routine operates. However, data may be too noisy to allow this operation to be performed directly. The routine followed is this:

- The initial data values are smoothed.
- First differences are computed from the smoothed values.
- These first differences are smoothed.
- The final profile is recomputed based on the smoothed differences.

565-448 O - 75 - 7

The smoothing procedure referred to is as follows:

- A best fit parabola is generated for *each* set of five consecutive original points.
- The center point of the five is recomputed from the parabola.

This avoids imposing a functional shape because no two points are adjusted using the same parabola. It also avoids displacing the profile because only initial data is used to generate the smoothed result. That is, the parabolas are fitted only to initial values, not to the smoothed results for previously adjusted points.

Second order smoothing does occur, however, when the first differences computed from a smoothed data set are themselves smoothed. When a smoothed data profile is recomputed from the smoothed differences, displacement of the profile from its original envelope is avoided by allocating the change in the first difference equally to the positions of the data points at each end of the interval. Expressed algebraically for a non-end point:

$$V_{\text{smooth},i} = V_i + \frac{1}{2}\left(\Delta_1 V_{1\ \text{smooth},i-1} - \Delta_1 V_{1,i-1}\right) - \frac{1}{2}\left(\Delta_1 V_{1\ \text{smooth},i} - \Delta_1 V_{1,i}\right)$$

Thus, the resulting profile contains not the smoothed differences, but differences changed in the direction of the smoothed values, but limited by the original data envelope.

Two tests of this technique are particularly important. First, does the profile drift from its original position? And second, does originally smooth data remain smooth? Both can be tested by smoothing profiles generated from various polynomial and transcendental functions whose values and first derivatives are continuous. These profiles are by definition already smooth. It was found that after five iterations of smoothing previously smoothed output, the maximum deviation at any data points was .055% from the original. The results of the first smoothing operation deviated at most .049%. The deviations on subsequent iterations did trend further in the same direction as the first iteration deviations. This and the fact that the greatest parts of the deviations appear on the first iteration suggest that some arbitrary shaping occurs. However, it is small.

At this point, the smoothing program makes no judgment as to the adequacy of the smoothing. In fact, no firm criteria have been developed. The program simply performs the smoothing routine and supplies the initial and smoothed data along with first and second differences. Neither does it attempt to remove grossly erroneous data values from the initial data before smoothing. Occasionally it does change the shape of the profile, but only at very sharp peaks or bends. Obviously it is still necessary to screen the results of smoothing before using them.

As an example of the results of this data preprocessing, figure 6 was obtained from the data used in figure 9, but after smoothing. The smoothing routine cannot handle really noisy data at all. The best procedure in this case is very much as in the past. A best fit curve is drawn by eye and smooth data read from this curve for input to the analysis program.

7. Results

The effect of this analysis on different profile types has been illustrated in figures 5 and 7, but these only verify that the results are qualitative as expected. Some measure of quantitative accuracy can be obtained by comparison of dopant profiles obtained from analyzed spreading resistance data and other profiling techniques. The techniques used were junction and mercury probe capacitance-voltage measurements and incremental sheet resistance. While these techniques cannot be used on all types of profiles, they do have a known reliability for specific profile shapes.

The result of such comparisons is general agreement, but certain discrepancies exist. The first is illustrated in figure 10, a comparison of analyzed and unanalyzed spreading resistance profiles and capacitance-voltage profiles of an epi-substrate structure. The dip in the analyzed spreading resistance profile at the interface of the flat section of the profile and the steeply rising section is a program artifact. Fortunately, it is one which is easily recognized by an experienced user and thus need not be confusing. The absolute dimensions of the structure involved determined the importance of this defect; the feature is quite prominent in figure 10, but not nearly so in figures 5 and 7, whose absolute depth is greater.

The effect seems to arise from a discrepancy between the probe model and reality. Recall that the model used or the probe contact was a single circle of uniform potential. However, optical microscopy and SEM of the probe tips nd the probe "prints" left on a sample reveal that the contact is actually composed of a large number of smaller ontacts over a generally circular area. Furthermore, when a calibration of spreading resistance versus resistivity is ttempted using the equation $R = \rho/2r_o$, the value of r_o obtained is significantly less than the radius of the probe rint[1]. Unfortunately, an analytical solution for a model more resembling the probe geometry has not been possible ecause of the complex boundary conditions involved in a tight array of contacts, either in a density distribution or ome arbitrary pattern.

A simple "non-real" model can explain the value of r_o obtained by the calibration. If the contact is viewed as aving a constant voltage, but a limited number of conducting areas in a uniform distribution so that the probability hat a contact touches a given point within the limits of the array is δ, then the development of the two probe quation is nearly identical to that of the conducting disc model. The final form is

$$R = \frac{\rho}{2\delta r_D} - \frac{\rho}{\pi\delta r_D} \sin^{-1} \frac{r_D}{D} \frac{\rho}{2\delta r_D},$$

here r_D is the radius of the damaged area of the probe point, or the limit of the contact array. Since δ is the robability of contact to an arbitrary point, $\delta = A_C/A_D$, where A_C is the total area of contact and A_D is the area of he region of the array of contacts, or the damaged area. Thus the r_o measured in calibration is

$$r_o = r_D \frac{A_C}{A_D}$$

This allows a solution for A_C, but this is of little help since neither the density nor the size of the individual ontacts is revealed in the calibration procedure. Also, observation of probe point hardly suggests uniformity. This odel does help to confirm the conjecture that A_C is less than A_D, however.

The value of r_o given by a R vs ρ calibration is usually called the "effective" radius, and is treated as though it ere the radius in a calibration for uniformly doped samples. This is reasonable since the lateral displacement between he points of contact is small compared to the probe to probe distance.

Multilayer analysis, however, is concerned with the potential distribution immediately beneath the probe, so the istribution near individual contacts is important. Figure 11 is a hypothetical representation of the real problem. In a istributed contact array with individual contacts small enough for the potential distribution near each contact to semble that of an isolated small circular contact, the previously developed contact model indicates that the voltage ear the small contact will fall off more quickly than that near a large one.

The single contact probe model then may look too deep in calculating C, and for certain geometries it overcorrects"; thus, the dip. But the problem is more than one of depth alone; the shape of the potential under the robe is also important. Simply reducing the value of r_o does indeed remove the dip, but it also moves the rest of the nalyzed profile away from the capacitance-voltage data. Figure 12 repeats the C-V curve of figure 10, but with the -V data reduced to a smooth curve. The two analyzed spreading resistance curves are for $r_o = 1.556\,\mu m$, the value ven by calibration, and for $r_o = .5\,\mu m$, the largest value which removes the dip. Intermediate values produce profiles etween the two shown.

A typical comparison of an incremental sheet resistance profile to an analyzed spreading resistance profile of a allow phosphorus diffusion is shown in figure 13. The results are in good agreement on the steeply inclined portion the profile, but they differ near the surface. It is not completely clear whether this is a program artifact or whether arises in the measurement technique since unexpected deviations of the original profile near the surface may occur all shapes of profile, as in figure 7. Reducing the value of r_o for this type of profile produces no better correlation nd no improvement in the analyzed profile shape near the surface. Removing the coating used to enhance the quality the surface-to-bevel corner on the sample reduces the effect, but does not eliminate it.

Since the multilayer analysis is performed by a computer program, an important consideration is speed of execution, which will significantly affect the practicality of the measurement by affecting cost. Figure 14 is a plot of run time vs points in the profile. These are typical; noisy data and abrupt corners will increase the run time.

The analysis program cost is usually about one-half or less of the cost of the original data acquisition.

Conclusions

The multilayer analysis of spreading resistance data provides a significant improvement over directly calibrated data when exact profile shape is of interest.

However, the analysis makes certain mistakes related to deficiencies in the probe contact model now used. These errors are easily recognized, but require that the analysis results be screened by someone familiar with the problem.

An improved contact model will be necessary to correct the problem. This is a logical next step to consider.

The cost of the analysis is reasonable for routine use.

Acknowledgements

The author wishes to thank Gordon Cumming for considerable discussion both on modeling and on programming techniques, and Francois Padovani and Fred Voltmer for providing spreading resistance measurements.

References

[1] F. Voltmer, personal communication.

[2] P. A. Schumann, Jr., and E. E. Gardner, "Spreading Resistance Correction Factors," *Solid-State Electronics*, Vol. 12, pp. 371-375 (1969).

[3] T. H. Yeh and K. H. Khokhani, "Multilayer Theory of Correction Factors for Spreading Resistance Measurements," *J. Electrochem. Soc. Electrochem. Tech.*, Vol. 116, No. 10 (1969).

[4] S. M. Hu, "Calculation of Spreading Resistance Correction Factors", *Solid-State Electronics*, Vol. 15, No. 7F, pp. 809-817 (1972).

[5] See also: P. A. Schumann, Jr. and E. E. Gardner, "Multilayer Potential Distribution," Technical Report 22,404, IBM Components Div., East Fishkill.

[6] E. E. Gardner and P. A. Schumann, Jr., "Potential Distribution in Multi-Layered Structures," IBM Technical Report 22, 191.

[7] H. Ruiz, "On the Calibration and Performance of a Spreading Resistance Probe," this publication.

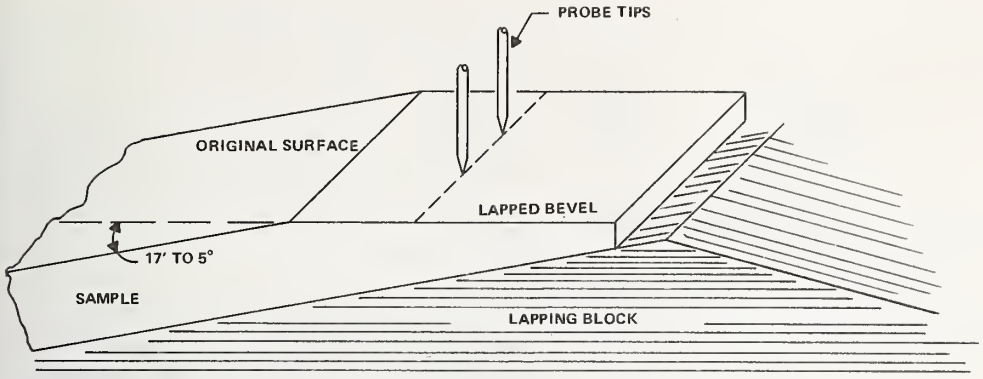

Figure 1. Spreading Resistance Probe Geometry (Scale Distorted).

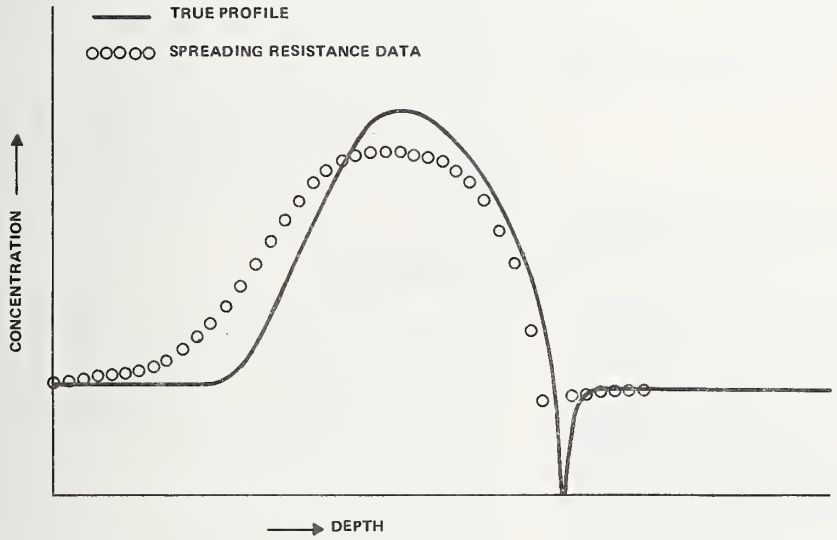

gure 2. Hypothetical Concentration Profile and Resulting Spreading Resistance Readings if the Left is Nearer the Top of the Bevel.

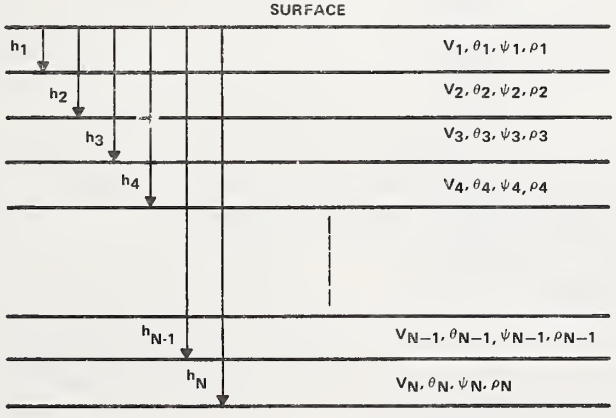

Figure 3. Multilayer Structure.

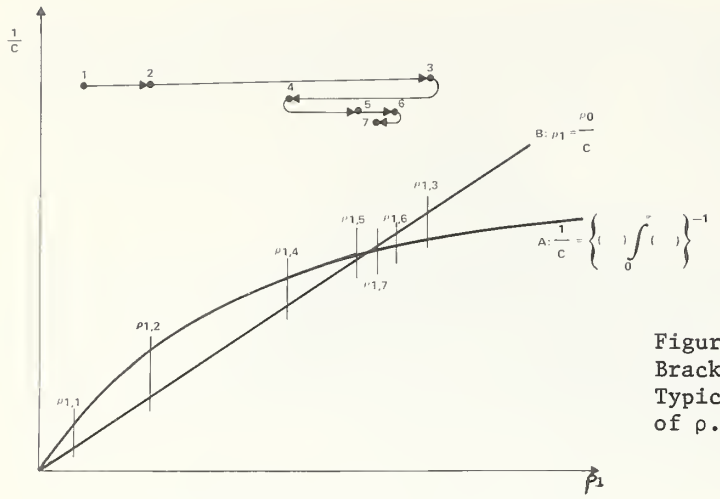

Figure 4. Qualitative Representation of Bracketing Convergence Technique and a Typical Set of Consecutive Approximations of ρ.

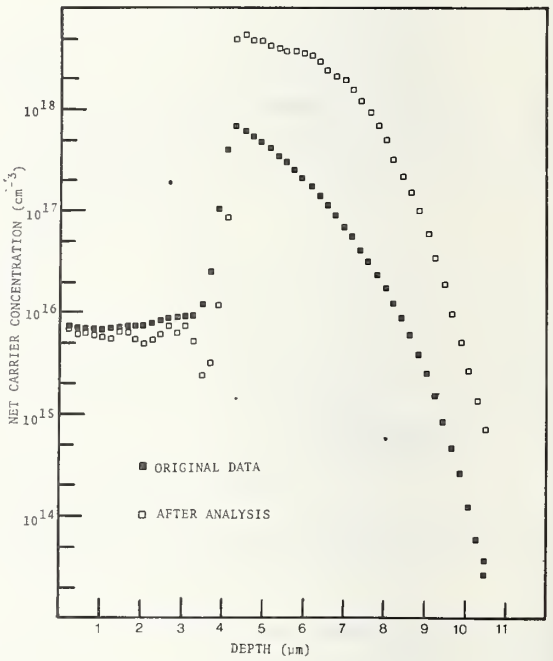

Figure 5. Original Data and Result of Multilayer Analysis for Epi-DUF-Junction Structure.

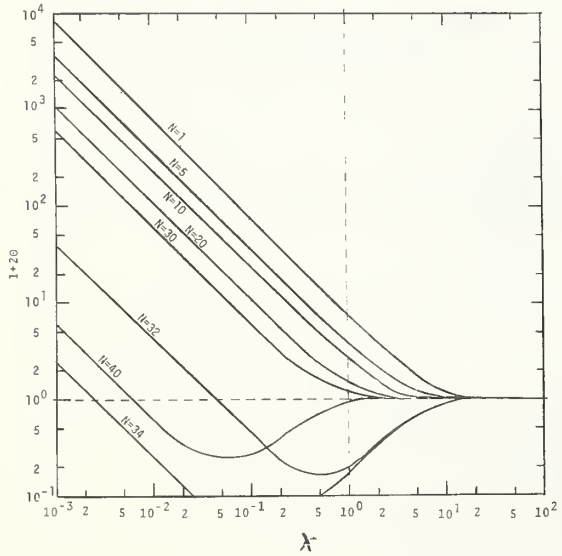

Figure 6. 1 + 2θ versus λ for Profile Shown in Figure 5.

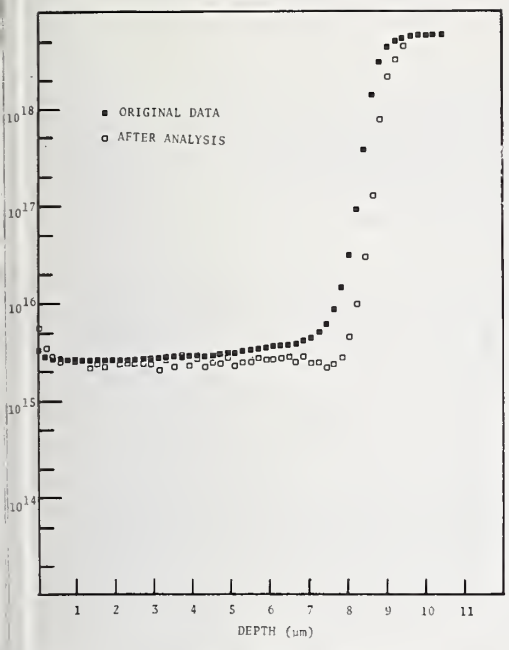

gure 7. Original Data and Multilayer alysis Results for an Epi Layer on finite Substrate Structure.

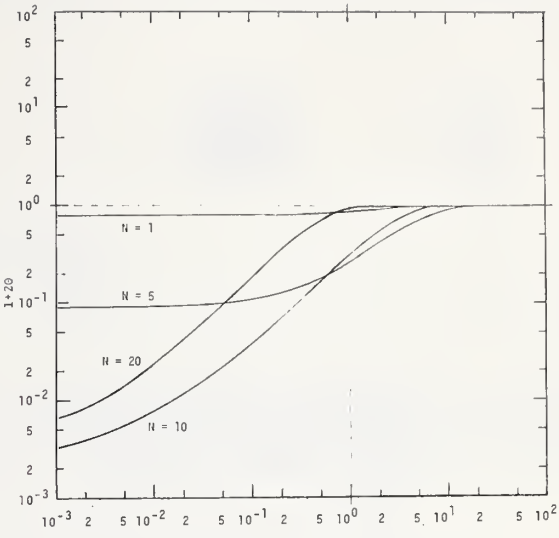

Figure 8. $1 + 2\theta$ versus λ for Profile Shown in Figure 7.

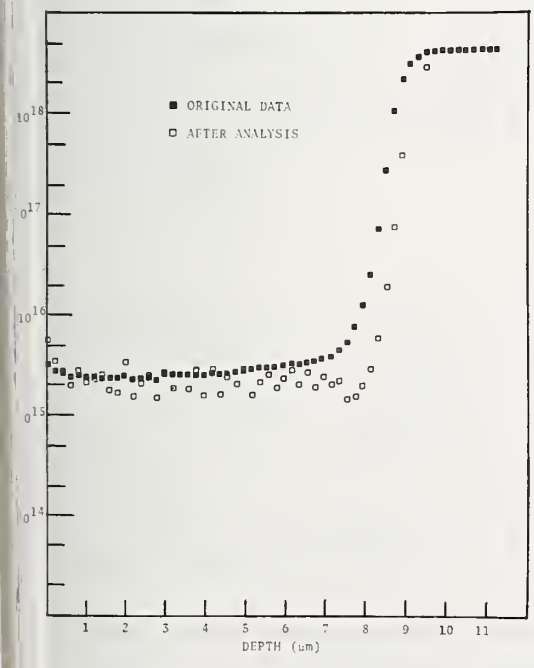

igure 9. Result of Analysis of Data ithout Preprocessing.

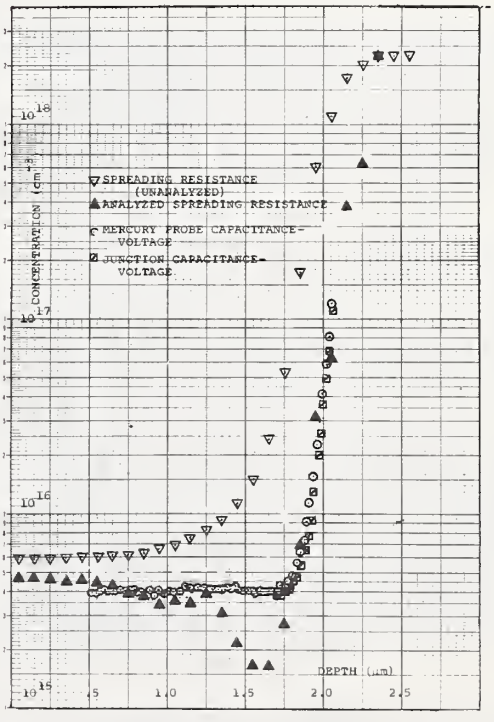

Figure 10. Comparison of Spreading Resistance and Capacitance-Voltage Profiles.

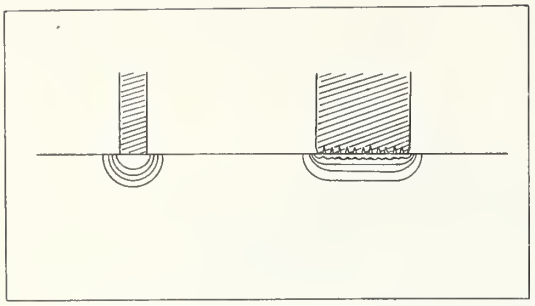

Figure 11. Hypothetical Comparison of Single and Multiple Contact Probe Voltage Equipotentials Showing Deeper Penetration of Single Probe Field Near the Surface.

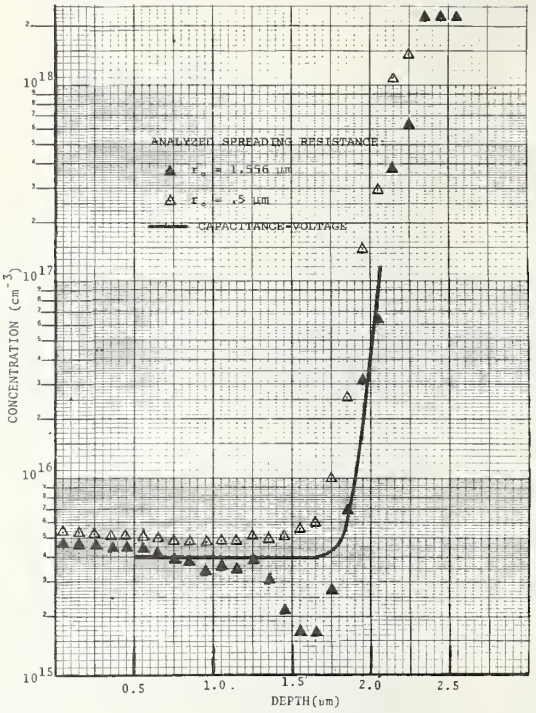

Figure 12. Effect of Changing Effective Radius of Contact, r_o, on the Analyzed Spreading Resistance Profile.

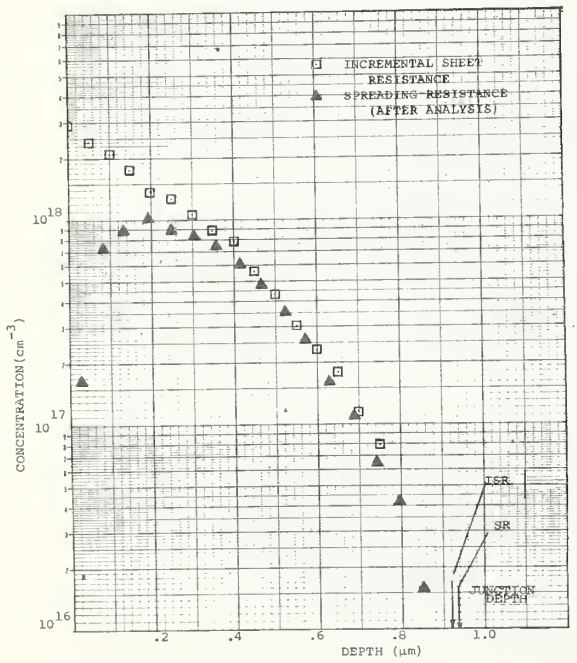

Figure 13. Comparison of Analyzed Spreading Resistance and Incremental Sheet Resistance Profiles.

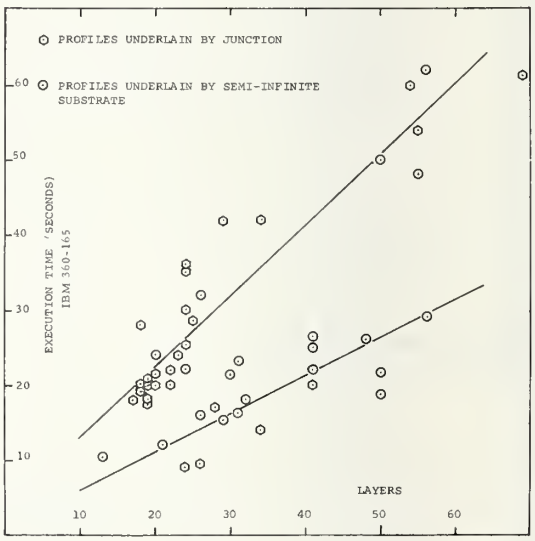

Figure 14. Execution Time versus Number of Layers in the Profile for Two General Types of Profiles. Times Vary Considerably Due to Noise and Shape of Individual Profiles.

NATIONAL BUREAU OF STANDARDS SPECIAL PUBLICATION 400-10, Spreading Resistance Symposium, Proceedings of a Symposium Held at NBS, Gaithersburg, Md., June 13-14, 1974.

An Automated Spreading Resistance Test Facility

James C. White, Jr.
Western Electric Co., Inc.
555 Union Blvd.
Allentown, Pa. 18103

An automated spreading resistance test facility has been designed and constructed at the Allentown Works of the Western Electric Co. This system has been shown to provide a rapid, semi-nondestructive, and reproducible measurement of epitaxial layer resistivity which can be used in a production environment. The system has the advantages of operator independence, well protected probes, and four-inch capability. Surface or in-depth measurements can be performed with on-line calculations of resistivity and impurity concentration. Cycle time is less than five seconds per measurement and system reproducibility is ± 1.3% (1S).

Key Words: Automated testing; epitaxial silicon; impurity concentration; resistivity; semiconductor materials; silicon; spreading resistance.

1. Introduction

Probably the first question that comes to mind when the automation of a test facility is proposed is "Why Automate?". The motives for automation range from a desire to remove operator variability from a measurement to a need for rapid reproducible measurements. At Western Electric - Allentown, the spreading resistance technique was investigated as a tool to satisfy the need for a rapid, nondestructive method for measuring epitaxial layer resistivity. A rapid technique was desirable for use for epitaxial reactor control. A nondestructive technique was attractive for a measurement directly on product with minimal damage to the wafer.

2. Alternative Measurement Techniques

The most widely used measurement technique for determining epitaxial layer resistivity is the four-point probe or control wafer technique (1)[1]. While this technique is rapid, it is not directly applicable to a majority of the epitaxial material being processed today. An isolating junction must exist between the epitaxial layer and the substrate. Therefore, n/n+ and p/p+ structures are not directly measurable nor is the technique easily applied to wafers with subdiffused patterns. For these structures, substrates of opposite conductivity type from the layer to be deposited are placed in the reactor and layers deposited on these wafers are evaluated using a four-point probe. The assumption is made that the growth conditions on these control wafers do not differ significantly from those on the product wafers.

Other techniques such as diode voltage-capacitance and MOS voltage-capacitance (2) are destructive and/or require extensive sample preparation prior to measurement.

Because the spreading resistance technique appeared to satisfy the requirements for both a rapid and a semi-nondestructive measure of epitaxial layer resistivity directly on any type of structure, it was investigated as a possible tool for use in a production environment.

Figures in parentheses indicate literature references at the end of this paper.

3. Why Automate?

A manual system was first constructed to determine the precision and to gain a working knowledge of the technique. The experience gained from use of this manual system demonstrated that the technique had the resolution and precision required for an epitaxial layer resistivity measurement. However, many of the advantages of the technique were lost in the manual system.

To satisfy the requirement of rapid feedback for epitaxial reactor control, it was felt necessary to provide for on-line calculation of resistivity and/or impurity concentration incorporating the relevant calibration and correction factors. Because of the importance of reproducible contacts between the probes and the wafer surface, it was deemed imperative that lowering and loading of the probes, application of current, and measurement of voltage all be done in a controlled manner with no operation interaction if possible. Moreover, because of the ability of the spreading resistance technique to detect small fluctuations in resistivity, several measurements on a wafer were desirable to obtain an average resistivity. Based on these criteria, the decision was made to automate the spreading resistance facility (Fig. 1).

4. Automated Facility Description

A block diagram of the automated test system is shown in Figure 2. The heart of the system is a Hewlett-Packard 2116C digital computer with 16K words of memory and a 16 bit word. Control and timing of all measurement functions are handled via this computer. The computer is programmed in BASIC. A conversational language was chosen in lieu of machine language because of the versatility and programming ease offered by conversational languages. Calibration curves, correction factors, sequencing, and other variables are easily changed by anyone with a minimum of programming experience. The constant current supply is marketed by COSAR and is continuously programmable over the range of one nanoampere to one ampere with a compliance voltage of 50 volts.

The wafer stage is positioned by two 500 steps/revolution stepping motors driving an X-Y movement with a twenty pitch lead screw. This provides 0.0001 inch resolution and a total travel of four inches in both the X- and Y-directions.

The remainder of the electronics consists of a high impedance digital voltmeter, a digital thermometer for temperature corrections if desired, and an X-Y recorder and a Teletype for output of resistivity and/or impurity concentration.

The probing arrangement selected is manufactured by Jandel Engineering Limited (Figure 3). This probe consists of three tungsten carbide needles individually loaded by gram gauges. These gauges are readily adjustable in the range of 0-100 grams. A kinematic needle guidance system employing precision ruby ball guides and polished tungsten carbide rods eliminates any sideplay of the needles and keeps friction to a minimum. Because of the subsequent availability and industry acceptance of the Mazur two-probe spreading resistance test system, the decision was made to convert the Western Electric system for a two-probe measurement. The three probes have been maintained, however, providing the versatility of performing a one-, two-, or three-probe measurement at will.

5. Measurement Sequence

The testing sequence begins with a series of questions to be answered by the system operator. The conductivity types of the layer and the substrate, crystallographic orientation, and thickness of the epitaxial layer are input via the Teletype. The wafer is then automatically positioned under the probes and the measurement sequence begins.

To insure a reproducible contact between the probes and the wafer surface and to keep wafer damage to a minimum, the probes are lowered to the wafer surface under their own weight. The loading is then applied at a controlled rate through an air dashpot. No current is forced until the probes are at rest on the wafer surface and are fully loaded. This precaution is taken to protect the integrity of the probes and to further reduce wafer damage.

The constant current supply is automatically ranged to produce a voltage at the probes of between five and fifty millivolts. At each measurement location, voltage measurements are taken with current flowing in both the forward and reverse directions to minimize erroneous measurements due to injection and electrical noise. For most samples, measurements can then be performed with normal incident light. An added benefit of the forward-reverse current pair is the capability of detecting the presence of p-n junctions from large forward-reverse voltage differences.

From each resistance measurement, an uncorrected resistivity is calculated using calibration curves developed from four-probe measurements on bulk polished wafers. This result is then corrected for finite layer thickness using a routine similar to that described by Dr. Bernard Morris (3) and the impurity concentration is calculated from a piecewise-linear fit to Irvin's curves (4). If desired, on-line plotting of resistivity or impurity concentration vs. wafer position is available.

For surface measurements, a series of measurements are taken in an X-pattern as shown in Figure 4. When all measurements on the wafer are complete, the wafer is returned to its home position, well away from the probes. Radial resistivity gradient, average resistivity, and standard deviation for the wafer are output on the Teletype.

While the chief use of the automated spreading resistance system is for measuring average surface resistivity, in-depth capability has also been provided. The surface preparation for this method involves a rotary grooving technique which produces a cylindrical groove in the wafer surface. This technique was chosen over angle-lapping because of the sharp angle produced by the groover at the wafer surface and the subsequent ease with which this edge can be aligned. An interference-contrast microscope mounted at a known fixed distance from the probes is used for the alignment.

An initial dialogue similar to that for surface measurements is answered with the additional input of groove width. The edge of the bevel is automatically aligned with the probes and a series of measurements is taken. If small steps, less than 0.0005 inch, are to be taken, a zig-zag motion is incorporated to prevent overlapping of damaged areas. At each measurement location, the depth of the measurement is calculated, based on the width of the groove and the lateral distance moved, and the resistivity is corrected for this depth. As for surface measurements, output can be selected on the Teletype and/or the on-line plotter.

6. Summary

The decision was made to develop an automated spreading resistance test system to provide versatility not available in any other system. A system was developed which has the reliability, versatility, and reproducibility necessary for daily use in a production environment. The system has the advantages of operator independence, well protected probes, and four-inch capability. Surface or in-depth measurements can be performed with programmable cycle times, on-line calculations and corrections of resistivity and impurity concentration, and on-line plotting of these corrected results. The system is able to accomplish this with a total cycle time of only five seconds per measurement and has been found to be reproducible to $\pm$ 1.3% (1S).

7. References

(1) W. J. Patrick, Solid State Electronics 9, 203 (1966).

(2) W. C. Niehaus, W. VanGelder, T. D. Jones, P. H. Langer, Silicon Device Processing (National Bureau of Standards Special Publication 337), 256-72 (1970).

(3) B. E. Morris, Symposium on Spreading Resistance Measurements (1974).

(4) J. C. Irvin, Bell System Tech. J. 41, No. 2, 387-410 (March 1962).

FIGURE 1 AUTOMATED SPREADING RESISTANCE TEST FACILITY

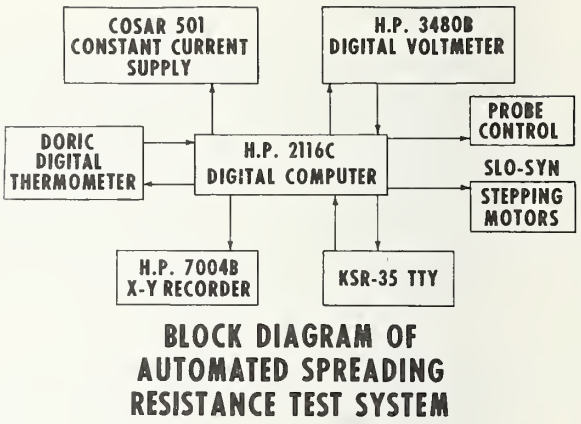

FIGURE 2 BLOCK DIAGRAM OF AUTOMATED SYSTEM

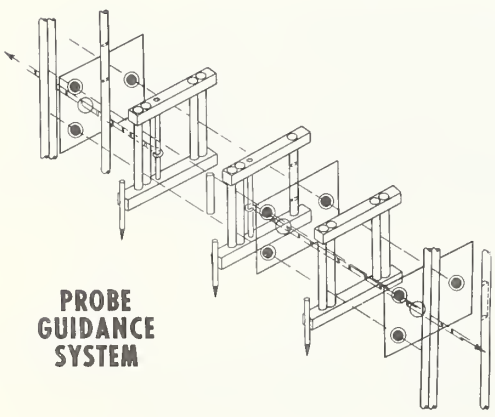

FIGURE 3 PROBE GUIDANCE SYSTEM

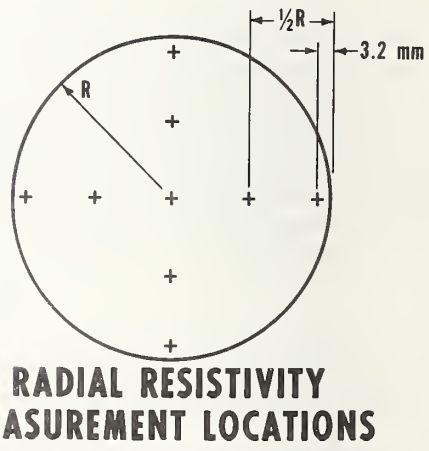

FIGURE 4 RADIAL RESISTIVITY MEASUREMENT LOCATIONS

NATIONAL BUREAU OF STANDARDS SPECIAL PUBLICATION 400-10, Spreading Resistance Symposium, Proceedings of a Symposium Held at NBS, Gaithersburg, Md., June 13-14, 1974.

Angle-Bevelling Silicon Epitaxial Layers, Technique and Evaluation

P.J. Severin

Philips Research Laboratories
Eindhoven, Netherlands

The properties of a steel probe for a spreading-resistance system are discussed stressing the effect of micro- and macrocontacts. The need is explained for producing small-angle bevels and a lapping jig for making such bevels is described. With small-angle bevels the slice topography cannot be neglected and a simple instrument is described by which the surface topography of the whole slice can be recorded. By recording the slice topography before and after bevelling the local reduction of thickness by the bevelling process is determined. This method can be used for angles between 1/500 and 1/2000. It is indispensable for the proper interpretation of spreading resistance measurements on bevelled N on N^+ junctions.

Keywords: bevel, interferometer, jig, microcontacts, silicon, spreading resistance, steel probe, topography.

1. Introduction

For advanced applications of epitaxially grown structures the dope concentration profile and the extent of the concentration gradient between substrate and epitaxial layer are of paramount importance. This is of particular interest for thin layers, a few microns or less thick. The capacitance-voltage technique [1][1] is very well suited for study of the charge carrier distribution up to a level of about 10^{17} cm^{-3}, but for study of the full interface properties surface probing techniques should be used and therefore the interior should be exposed by bevelling the slice. The method for surface probing is the spreading resistance technique, which is accepted now as a very powerful tool for investigating epitaxially grown structures.

For obtaining a large resolving power with the bevel technique the probe averagingdepth should be as small as possible. With the spreading resistance probe used by us the horizontal averaging lengthis fairly large, about 25 μm. Therefore the bevel angle must be very small. This implies, however, that for precise correlation between horizontal position and depth below the original surface the departure from ideal flatness of the slice is taken into account. In the next section the spreading resistance probe used in our laboratory for several years is discussed and a number of details essential for understanding the mode of operation is presented. A polishing jig and a laser-operated interferometer are described in the third section. Their use in producing the bevel and for evaluating the local bevel angle, taking into account any departure from perfect flatness of the slice, is explained in the

[1]Figures in brackets indicate the literature references at the end of this paper.

fourth section. The method is illustrated with a fully worked-out example: an N on N^+ epitaxial layer is bevelled, evaluated and spreading-resistance measured. The formalism for deducing the resistivity profile is critically discussed in another contribution to this Symposium [2].

2. The steel spreading resistance probe

The spreading resistance probe system now in use in our laboratory [3,4,5] for several years is based on the use of a specially hardened steel probe taken from a conventional Dumas four-point-probe head. This probe is broken and sharpened until the untouched bottom of the tip is about 25 μm across, which yields a mechanical contact diameter of about 15 μm.

Microscopic evidence proved conclusively that the bottom surface of the probe is multi-tipped and that the mechanical contact to the silicon is made up of a number of microcontacts. With high-power dark-field illumination the most pronounced prints made by the microcontacts are visible and with a chromic etch these prints stand out more clearly. With an interference contrast microscope more details can be seen of the etched print, but the size and depth of the microcontacts cannot be assessed and must be less than 0.1 μm. With a scanning electron microscope the print could not be found, because the minute damage due to the microcontacts is more wide than it is deep. For a given probe the print pattern is completely reproducible, and shown in figure 1.

It is well-known that below a circular metal contact to a semiconductor of resistivity ρ the potential drops from the applied potential V_o to about 0.1 V_o at a depth of about twice the radius. This holds for each of the many microcontacts of radius a. At that level the equipotential lines are almost horizontal and the microcontacts cannot be distinguished individually any more. This occurs at a depth which is very shallow compared to the diameter 2A of the total contact area and therefore this new, deep, macrocontact is again subjected to the spreading resistance phenomenon.

In this model the micro- and macrocontact resistance R_{si} and R_{sa} can be considered acting in series. The currents through the microcontacts are supposed to be independent and the series combination of the macro- and microcontacts yields the equivalent circuit shown in figure 2 with

$$R_s = \frac{\rho}{4A} + \frac{\rho}{4na} \quad , \tag{1}$$

where n and a are the number and average radius of the microcontacts. For a steel probe total spreading resistance was found [3,4] to be proportional to ρ over four decades, both for N- and P-type Si

$$R_s = \frac{\rho}{4A^*} \quad , \tag{2}$$

where A^* represents the equivalent radius of the contact. A number of authors have reported that for their, harder, probes

$$A^* = \frac{A}{k(\rho)} \quad , \tag{3}$$

where $k(\rho)$ is a correction factor of order unity attributed to a variety of causes, generally ρ-dependent zero-bias-barrier resistance in series to the true spreading resistance.

Although it appears possible to experimentally separate the two contributions R_{sa} and R_{si} because they have widely different thermal time constants, and non-linearities can readily be generated in the microcontacts, we simply measure A^* and A and apply eqs (1) and (2).

The value of A is found from microscopic examination of the print

and the value of the equivalent radius A^* is found from calibration measurements. The latter depends weakly on the nature, surface texture and preparation of the semiconductor. It is slightly different for each probe and decreases slowly during a probe lifetime.

Normally a large contact resistance is undesired because it spoils the proportionality to ρ of the spreading resistance in series, as shown in eq. (3). The resistance of the microcontacts shows a spreading resistance controlled proportionality to ρ and their contribution is welcomed because of the ensuing small information collecting depth a. This will be discussed below in connection with the resolving power.

It is an essential property of this type of steel probe that the microcontact distribution after a short formation process shows hardly any alteration in many thousands of measurements on polished silicon. Evidently the probe is loaded elastically only. When the probe is applied to a lapped sample the distribution pattern of the microcontacts changes, but the value of na remains very nearly the same. It is well-known from mechanical and thermal contact studies and experiments in friction and wear that any metal surface has protrusions. These are referred to as asperities. The protrusions, often harder than the matrix material by an order of magnitude, have been the subject of many controversial experiments and speculative theories. Their nature and origin are problems beyond the scope of this paper. The reproducibility of this steel probe spreading resistance amounts to about 1%, as shown by some surface probing tracks, presented in figure 3.

Typical values of the various parameters for a load F = 150 gram on polished N-type silicon are A^*=2.2 μm, A = 12.5 μm, hence na = 2.7 μm, which with n ≈ 100 yields a ≈ 0.03 μm; also $R_{si}/R_{sa} \approx 5$. Generally a small contact radius is considered desirable for spreading resistance measurements. However, with a steel probe the load cannot be reduced without seriously degrading the performance of the spreading resistance probe.

The following experiments were done with the intention of shedding some light on the dependence of A and A^* on the load F. The probe is broken in order to expose a large number of asperities and sharpened until the contact area left untouched is only slightly smaller than the stable area found after plastic deformation with the lowest load used in the experiment. Then with successively increased loads the probe is applied on a lapped and subsequently on a polished surface. The values of A^*_1 and A^*_p on both types of surface and of A_p on the polished surface are determined. On a lapped surface no print is visible so that A_1 cannot be determined but at a given load must be between A_p at the same and the lower load. It turns out that A^*_1 increases linearly with F, as shown in figure 4, whereas the radius A_p is almost constant. Below a load of 100g a very erratic signal was produced. Apparently the spreading resistance on polished material can only be properly measured with a probe which is on the verge of yielding. Above 100 g the probe is again loaded up to the yield strength on polished material. The contact on lapped material at low loads is determined by na only, but at about 100 g the influence of A is dominant. On lapped material not only the probe asperities, but also, probably even more important, the roughness of the sample determines the microcontact contribution. Because the asperity pattern is completely rearranged by application of the probe to lapped material, the value of A^*_p determined by the asperities, does not show very systematic dependence on F.

In figure 5 the results of similar experiments with another probe and sample are presented, the only difference being that the starting probe radius A was about 10 μm. Here the signal on polished material at low loads was again very erratic, but A^*_1 again increases almost linearly. As mentioned above, the experiments on polished silicon are influenced by the measurements on lapped material in between. This procedure is necessary to keep an unfractured probe tip over so long a load range. Over a shorter range the probe reshaping on lapped material is not needed

and the curve labelled A_p^{**} is found. The slope, $A_p^{**} \sim F^{2/3}$, is more or less equal to the slope for A_p and for A_p^{*} above 100 g. It is also clear that the microcontact contribution plays an important role. It is interesting to note that in figures 4 and 5 the three values of the equivalent radius for polished slices are almost equal at 150 g. That is why this is chosen as the working load.

As mentioned above, the double-stage probe structure has a bearing on the resolving power of the spreading resistance probe. With surface probing both the micro- and macrocontact stage average horizontally over about 2A. A relatively large contribution R_{si} could be a drawback for surface probing. When the horizontal resistivity distribution in a silicon slice is the desired information, this could be shielded by the variations in a one micron thick top layer. However, it has been found that spreading resistance tracks with pronounced maxima and minima do not change when a one micron thick layer is removed. Hence although the microstage represents about three quarters of the total resistance, the microcontacts penetrate any surface layer which may be different due to circumstances beyond control. More important, surface probing of a thin epitaxial layer can be done advantageously with an shallow stage which contributes significantly to the total resistance. It ranks among the most favourable properties of the steel probe that for the microcontact stage which represents about three quarters of the spreading resistance, any isotype thin layer can be considered as a sample of infinite thickness. The thickness correction should be applied to the deep contribution only, if necessary. For a heterotype structure the thickness correction is a function of both the micro- and macrocontact contributions, as shown elsewhere [2,5]. In general the thickness corrections have been calculated for an abruptly layered structure and evidently some doubt exists of the value of d in a real structure. In case the shallow stage contribution is sufficiently large, the improvement obtained by applying the more or less accurate correction is good enough.

In summary, we use a probe which averages horizontally over a circle about $2A \approx 25\,\mu m$ across and in depth over a length of about $3a \approx 0.1\,\mu m$. For surface probing the small information sampling depth is a great asset. For profiling averaging horizontally over 25 μm is quite a nuisance for, with a desired resolving power of 0.05 μm in depth, the angle should be 1/500 or more. We shall describe in the next section how bevels up to 1/2000 can be produced and evaluated.

3. The bevelling jig and the interferometer

Conventional angle-lapping jigs have been used before for bevel and stain measurements at relatively large angles. The reliability of these instruments is limited by mechanical tolerances. Here we first describe a more stable and versatile tool, which matches well the interferometer to be described later.

As shown in figure 6, the slice S to be bevelled is mounted on a piston A. It can slide without play in the holder B and can be fixed at any height and position by screw C. This assembly rests on three balls on the support ring D and can be moved with respect to the support by two screws E. With one screw the assembly can be tilted about the axis between the other screw and the third ball. In this way the angle between the axes of B and D can be varied in a simple and precise way. The holder B and the support D are held in position by three resilient clamps F. The jig rests on a number of pieces of silicon G glued to the support D. Hence during lapping and polishing no foreign particles are produced and because their total surface area of about 10 cm^2 is much larger than the area to be bevelled the pressure and rates are constant during the process. The slice is mounted on the piston A in a thick layer of beeswax by heating. When it is allowed to cool slowly, the slice assumes its equilibrium position.

The lapping and polishing is done on a machine on which the slice is subjected to three different motions. For the lapping a slurry of water and Al_2O_3 is used. The subsequent polishing is done with diamond paste until the roughness is reduced sufficiently to make the surface mirror-like. At this stage the surface shows some pits and scratches due to deep lapping damage, but usually the polishing process is not continued. It has been found that there is about 20% difference in spreading resistance between touched and non-touched parts. Because profiles are measured generally on a logarithmic scale, this difference in calibration is unimportant. It can be reduced by chem-mechanical polishing.

A bevel of relatively steep slope and mirror surface quality can easily be evaluated with an interference microscope. In order to obtain a reliable value for the slope at least a dozen contour lines should be visible, and it has been found that for steep angles up to, say, 1/200 reliable results can be obtained. However, for small angles the slice turns out not to be flat enough to unambiguously define its slope with respect to the reference flat. Moreover, the method is time consuming and it is impossible to obtain an overall impression. In this section an instrument of greater field of view is described with which the untouched part of the surface of a bevelled slice can be seen and used as a horizontal reference in determining the slope of the bevel.

The optical layout of this interferometric instrument, which is not at all critical, is shown in figure 7. A HeNe laser (1) operating at 6328 Å at about 2 mW power level provides an extremely monochromatic, coherent, relatively intense and narrow light beam. The light is incident on a diffuser (3), which serves as an intense and monochromatic light source. Via a semi-reflecting mirror (5) the enlarged-diameter parallel beam is incident on the polished side of the silicon slice (7) which is positioned face to face with a semi-reflecting optical flat (8), about 1 cm thick. The fringe system arising from multiple interference at the positions of appropriate slice-flat distance is imaged by a lens (9) onto a screen, a television camera or a photographic camera (10). As the light turns out to be still so coherent that speckles can be seen, the diffuser (3) is mounted on a motor axis which revolves sufficiently fast that they disappear. With the instrument shown in figure 7 the complete topography of slice (7) with a diameter up to the diameter of the parallel light beam is obtained in a single picture. Examples of such a picture are given in figures 8 and 10 below. In these pictures the distance between two contour lines corresponds to a height difference equal to $\lambda/2 = 0.316$ μm and the resolving power is about 0.06 μm.

4. Evaluation of bevel angle

In general a slice is not flat and, although the bevel as produced may be flat, local thickness of a bevelled epitaxial layer plotted vs horizontal position may not be a straight line. Typical surface topographs of silicon slices can be seen in figure 8. Usually the contour lines show a maximum or a minimum, manifested by closed lines, and sometimes saddle points■ . The radius of curvature of an extremum is roughly between 2 and 20m for 250μm thick slices. Hence the slope may change over 5 mm by an angle 1/500. However, with the procedure to be described such variations in slope do not present a real problem because the profiles of both the original surface and the polished bevelled surface can be measured accurately. To produce a bevel the slice is mounted on the jig of

■) This implies that concavity measured as a standard routine [6] and commonly called bowing or dishing, does not adequately describe the topography of silicon slices.

565-448 O - 75 - 8

figure 6 and the mirror (8) of figure 7 is placed on top of the silicon pieces G of the jig. Using the screws E the piston A is adjusted such that on the television monitor a pattern arises with easily recognizable features. This pattern is photographed. Then the desired angle is adjusted with screws E and the piston is lowered until the slice touches the optical flat and is fixed again with screw C. After lapping and polishing the slice is positioned again such that the pattern on the non-touched part of the slice compares well to the photograph made earlier and photographed again.

In practice the procedure runs as follows. A mark, labelled A in the inset of figure 9, is scratched on the slice. In order to see this mark on the photograph a small rectangular patch of paper, noted B in figure 9, is glued to the slice. The slice is adjusted to such an angle with the optical flat that a number of closely spaced interference fringes perpendicular to the patch is visible, and photographed (figure 10a). The slope of the part to be bevelled may correspond to the desired angle, otherwise the desired angle is adjusted, the patch of paper is removed and the slice is bevelled. As before, a patch of paper is glued on the slice and the slice is adjusted as well as possible in the same position as before bevelling and photographed (figure 10b). Then, from the photographs the profiles along the spreading resistance track to be made, are measured and plotted. Of course it will not be possible to reproduce precisely the pattern on the non-touched part. This is shown clearly in figure 9, where curve A represents the profile as measured on the original photograph. After bevelling, the profile labelled B is measured, which is different from the original one, though the left-hand side non-touched parts should be identical. This arises from the fact that the angles with respect to the optical flat in the two cases were slightly different. This can be corrected by pivoting curve B around the origin so that A and B are coincident. The difference between curve A and the first part of curve B turns out to be, as expected, a straight line, labelled C. Extrapolating this correction, due to slightly different tilt of the slice, over the range where the slice has been bevelled, the true surface profile curve A_2 is obtained from the measured curve B. The difference between curve A_1 and A_2, plotted as a curve labelled D, is the true depth below the original surface. Due to the surface topography and the nature of the polishing process, there is no linear relation between depth and horizontal position. Therefore some method to obtain a curve like curve D of figure 9 is definitely indispensable for precise and accurate work on spreading resistance profiles.

5. Discussion and conclusions

With a specially hardened steel probe spreading resistance measurements can be done on chem-mechanically polished and epitaxially grown surfaces with a precision of about 1%. Because of the large contact area, about 25 μm across, which cannot be made smaller, the slope of a bevel should be 1/500 for a resolving power of about 0.05 μm in depth. For such slopes a procedure has been developed which takes into account the original surface topography. In this way the horizontal and vertical scales are correctly correlated. When the bevel is chem-mechanically polished the spreading resistance can be measured with a precision also of about 1%.

The inference of the dopant atom distribution from the measured spreading resistance profile is obstructed by a number of serious difficulties, which are itemized below.

1. The correction formulae which should be applied to the spreading resistance measured on a layer of finite thickness have been critically discussed elsewhere [2] and the sensitivity of the solution to the boundary conditions chosen makes the validity of these expressions dubious within about 10%.

2. The transition of the layered structure is not abrupt so that the thickness, particularly of thin layers or near the bevel edge, is not well defined.
3. The measured data should be corrected for the proximity of the bevelled layer edge, particularly in the case of steep bevels.
4. The charge carrier density n can be deduced from the resistivity ρ only with the well-known curves, which are valid, however, only in uniform and neutral material; neither condition is satisfied, because mobile charge carriers generate a space charge in any steep atom profile. Moreover the spreading resistance correction formulae have been derived using Laplace's equation, implying the absence of space charge.
5. The space charge is perturbed due to the exposure on the bevel [2].
The micro- and macrocontact contributions should be distinguished carefully. A dominant macrocontact resistance, which is more common for small than for large contact area probes, is more sensitive to corrections. A large probe with dominant microcontact contribution hardly needs any correction for finite thickness. Therefore the items 1 to 3 do not apply to our probe system. The problem of the necessary small-angle bevel where the original surface topography is important for the correlation between depth and horizontal scale, has been solved.

Acknowledgement

The assistance of Mr.G.Poodt and Mr.H. Bulle in the experimental work and of Dr. J.D. Wasscher in carefully reviewing the manuscript is gratefully acknowledged.

References

1. P.J. Severin and P. Poodt, J.Electrochem. Soc. 119 (1972) 1384.
2. P.J. Severin, Proc. Symp. Spreading Resistance Measurements, NBS, Gaithersburg, 1974.
3. P.J. Severin, Sol. St. Electr. 14 (1971) 247.
4. P.J. Severin, Silicon Device Processing, NBS Special Publ. 337 (1970) 224.
5. P.J. Severin, Philips Res. Repts. 26 (1971) 359.
6. Monsanto Evaluation Standards, Monsanto Electronic Materials, St. Peters, Missouri, 1973, no 16-ME-005-0472.

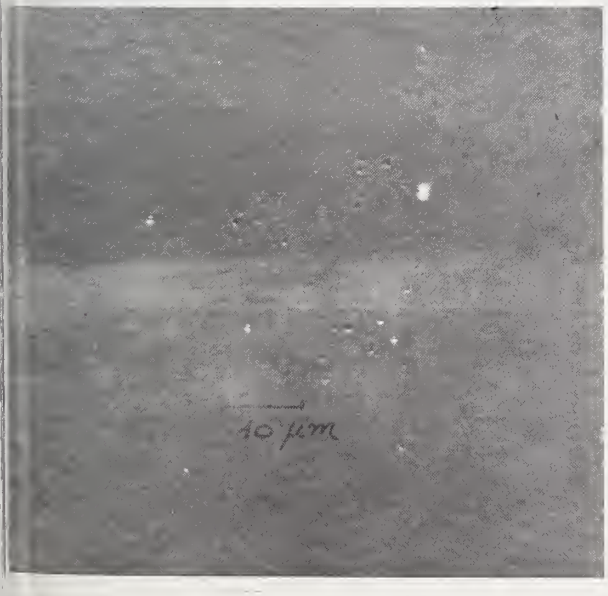

Figure 1. The print of a steel probe as seen with an interference contrast microscope.

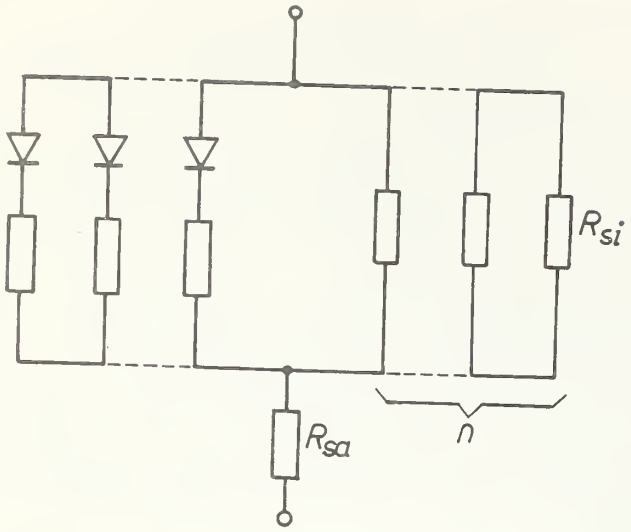

Figure 2. The equivalent circuit of the spreading resistance probe contact as measured with a specially hardened steel probe. R_{si} is the microcontact contribution of ohmic, low-resistance, high-pressure contacts and diodic, high-resistance, low-pressure contacts which can be neglected. R_{sa} is the microcontact contribution acting in series.

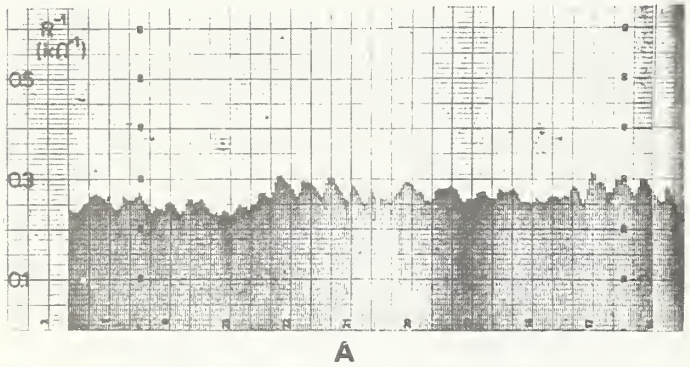

A

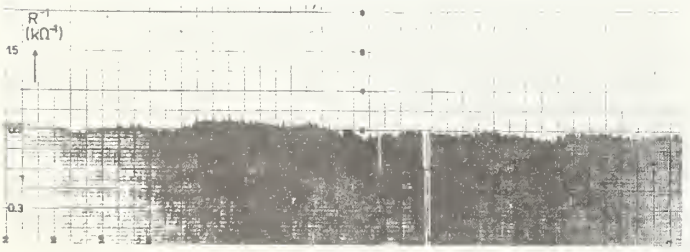

B

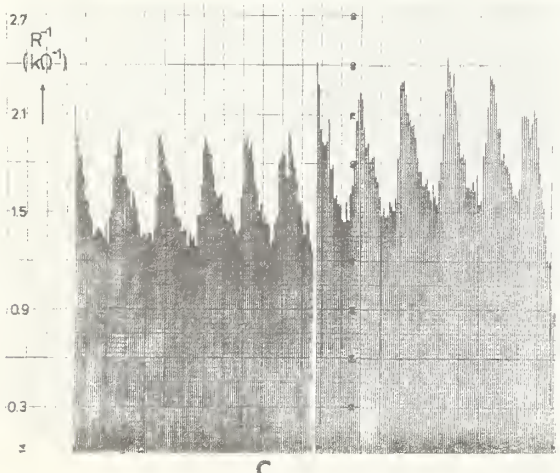

C

Figure 3. The reproducibility of the steel probe system is demonstrated by some tracks on an epitaxial layer (a), an N substrate (b) and a longitudinal section (c).

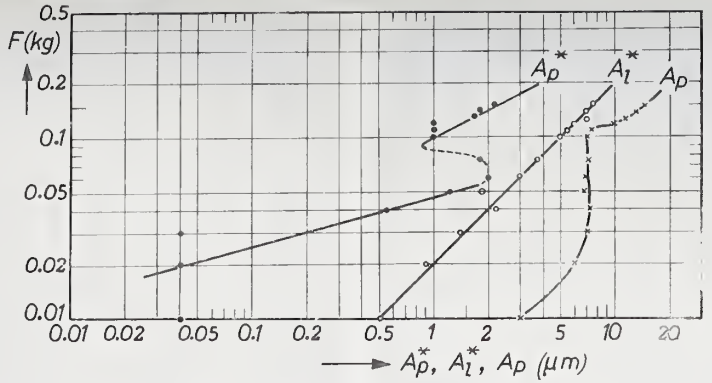

Figure 4. The effective radius on lapped A_l^* and on polished A_p^* material, the real radius A_p measured on polished material as functions of the load F. The probe is applied to lapped and polished material alternately.

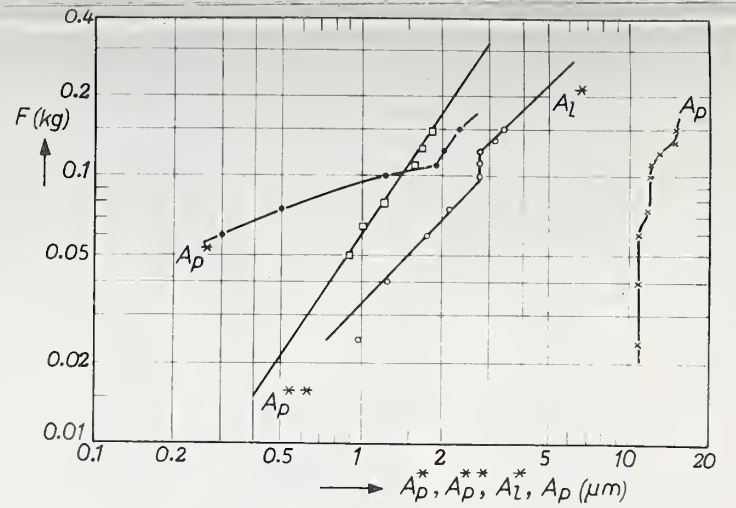

Figure 5. The same parameters as presented in figure 4, but with a larger starting real radius A_p. The effective radius A_p^{**} is measured on polished material without interjacent lapped material probing.

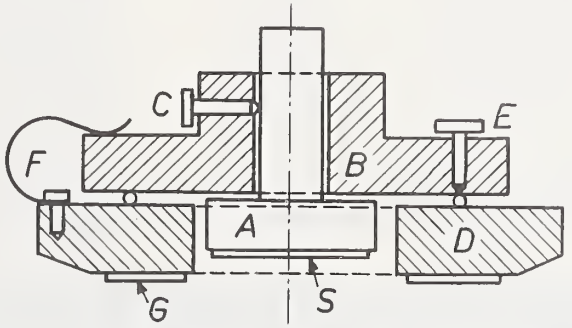

Figure 6. Schematic view of the angle-polishing jig. The slice S is waxed to the piston A, which fits tightly into holder B and can be clamped with screw C. With the screws E the slice can be tilted with respect to the support D, which rests on pieces of silicon G.

Figure 7. The layout of the interferometer with the slice placed polished side up: laser (1), mirror (5), diffuser (3), lenses (2, 4, 9), optical flat (8), slice (7), (television) camera (10).

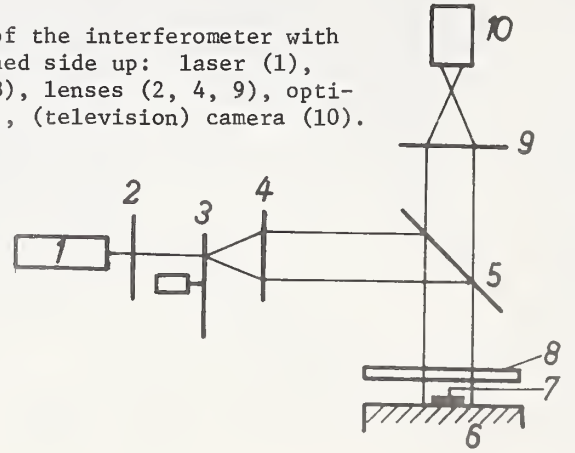

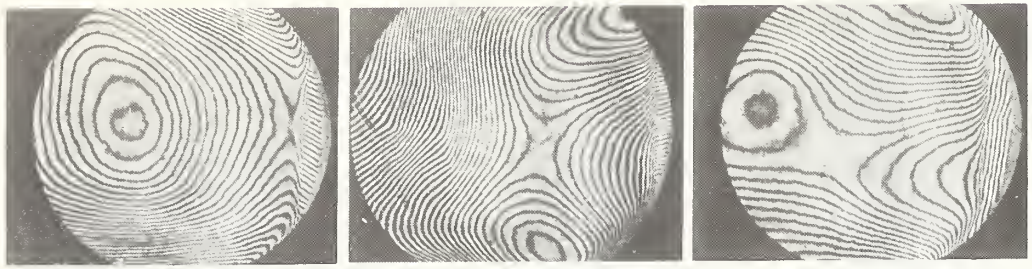

Figure 8. Typical topographs of silicon slices. On the right-hand side of the reference flat the aluminum support is visible, which also reflects.

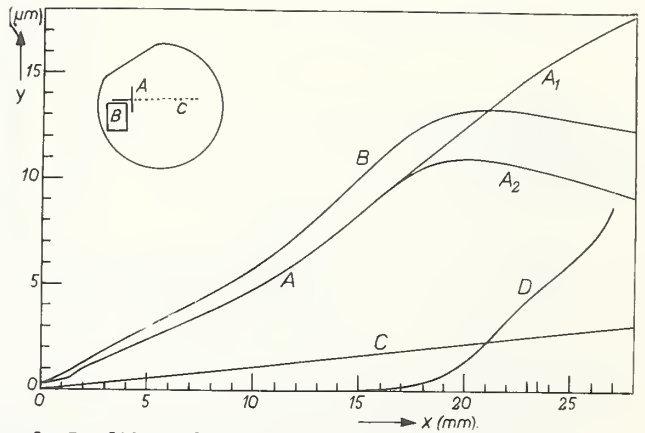

Figure 9. Profiles of the original surface (A), of the bevelled surface (B) and the depth below the surface (D). The auxiliary line (C) is the difference between the left-hand sides of A and B. When the right-hand side of B, is corrected by the difference C, the line A_2 is found. The difference between A_1 and A_2 yields curve D which represents the true depth below the original surface. In the inset the scratch mark A, the patch of paper B and the spreading resistance track C are shown.

Figure 10. Topograph of a slice adjusted before bevelling (a) and after bevelling (b). A small rectangular patch of paper glued on the slice serves as a starting point for the photographic analysis and spreading resistance measurements.

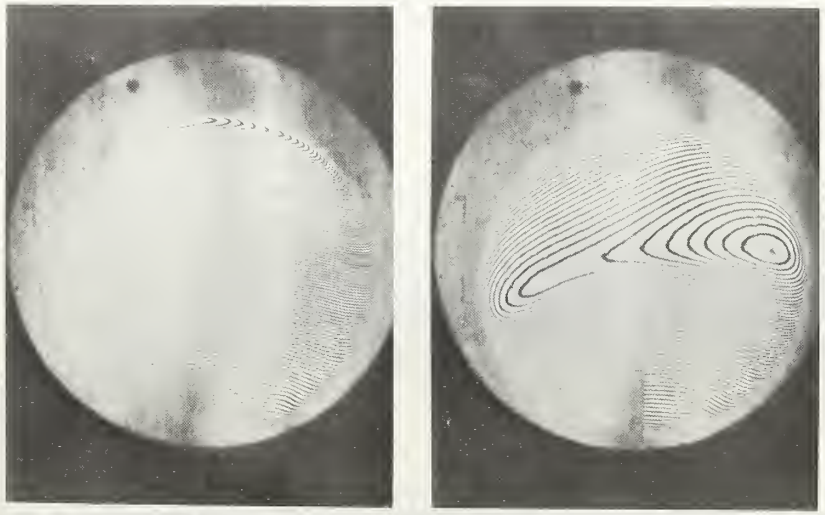

Figure 11. A spreading resistance track on an N on N^+ bevelled epitaxial layer, probed at 25 μm intervals. The slope at the center of the profile can be evaluated from fig. 10 to be 1/720.

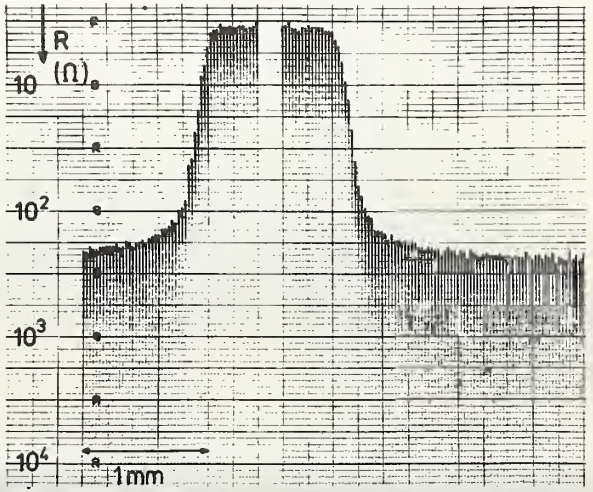

NATIONAL BUREAU OF STANDARDS SPECIAL PUBLICATION 400-10, Spreading Resistance Symposium, Proceedings of a Symposium Held at NBS, Gaithersburg, Md., June 13-14, 1974.

Spreading Resistance Measurements on Silicon with Non-blocking Aluminum-Silicon Contacts

J. Krausse

Siemens AG, UB B GE 1
8 München 46, Frankfurter Ring 152
F.R. Germany

The paper concerns the measurement of resistivity fluctuations in n-type silicon starting material in the resistivity range from 1 to 1000 Ω cm. The microscopic resistivity fluctuations that are associated with the well-known striations require a measurement technique of high accuracy and high local resolution. We chose the spreading resistance method. However, in contrast to the conventional method, in which the metal probe is pressed directly onto the silicon surface, we supply the silicon slice with non-blocking aluminum-silicon contacts. The radius of the contact area is exactly defined. Any contact radius can be realized according to the resolution desired in lateral direction and in depth. When the metal probe is applied to the aluminum-silicon contact, the contact is not destroyed. Thus it is possible to perform spreading resistance measurements and four-point probe measurements along one and the same measuring track and in this manner at the same time to vary the local resolution. A comparison of both measurement results will in particular yield information on the conditions of the resistivity in axial direction of the slice. Essential prerequisites for an absolute measurement are fulfilled with the aluminum-silicon contact. However, the investigations made up to now show that the resistivity calculated from the spreading resistance is smaller than the one obtained with the four-point probe measurement by approximately a factor of 0.8.

Key words: Absolute measurements; aluminum-silicon contact; four-point probe measurements; local resolution; n-type silicon; resistivity inhomogeneities; spreading resistance; striations.

1. Introduction

The lateral and the axial distribution of the resistivity in starting silicon is e.g. in several respects of importance for the electrical properties of power devices. Since resistivity variations as low as 5 to 20% can be distinctly effective, it has to be the aim to measure such variations as exactly as possible. The microscopic resistivity fluctuations associated with the well-known striations are of the order of $\Delta\varrho \approx \pm$ 10 to 20% (see [1]-[4]) and therefore require a measurement method with high accuracy and high local resolution.

---

[1] Figures in brackets indicate the literature references at the end of this paper.

Our interest is concentrated mainly on n-doped silicon material with a resistivity in the range of 10 to 1000 Ω cm, as it is used for manufacturing power devices. For the manufacture of devices silicon slices are processed that are cut perpendicularly from rods grown in ⟨111⟩ -direction. We perform measurements of the resistivity fluctuations on such slices.

2. The Conventional Spreading Resistance Method

The well-known method of MAZUR and DICKEY [5] presented itself as a suitable measuring procedure. This procedure at present is an important method to determine the doping distribution of diffusion profiles and multilayer structures. However, as yet it is not clear if it is suitable for an exact quantitative measurement of the relatively small resistivity variations in starting silicon. The reason lies in the fact that the physical properties of the contact between metal probe and silicon surface are hard to define. This manifests itself in the calibration factor k which is rather obscure. For the spreading resistance R_s of a circular, two-dimensional contact of radius a

$$R_s = \frac{\varrho}{4a} \tag{1}$$

holds. However, the conventional spreading resistance method yields a resistance R_c for which one can write

$$R_c = k \cdot R_s = k \cdot \frac{\varrho}{4a} . \tag{2}$$

The factor k contains the whole problematic nature of the conventional spreading resistance method. It depends on several details of the handling of the metal point as well as on the properties of the bulk and the surface both of the silicon to be measured and of the metal point. KRAMER and VAN RUYVEN [6] published a compilation of k-factors that were measured in different laboratories, figure 1. Note that the k-values scatter by approximately a factor of 10. In addition, in the range of high resistivity that is of interest to us, the k-factor always depends strongly on the resistivity of the silicon material. k decreases with increasing resistivity. According to eq (2) this means that R_c depends less than proportionally on ϱ . This in turn means an increase in the inaccuracy of the measurement for a $\Delta\varrho$ -determination.

3. The Non-blocking Aluminum-Silicon Contact

In contrast to the conventional spreading resistance method, in which the probe is pressed directly onto the silicon surface, we supply the surface with non-blocking aluminum-silicon contacts. In [4] and [10] we have already described the reasons that led us to take this step, as well as the structure and the preparation of the aluminum-silicon contact.

A cross-section of the structure of an aluminum-silicon contact as we use it presently is drawn in figure 2. Etching the polished cross-sections makes visible the phosphorus diffused n-region. The etch patterns obtained in this way confirm the well-known observation that the underdiffusion amounts to about 2/3 of the penetration depth b of the phosphorus. The radius of the contact is thus given by

$$a = \frac{\Phi}{2} + \frac{2}{3} b . \tag{3}$$

In order to measure the spreading resistance, a metal probe is applied onto the aluminum of the contact. The resistance R_c of the contact is obtained from a current-voltage measurement between the probe and the back surface of the slice which is diffused and contacted across the entire area. Normally we operate with a constant dc-current of 10 μA. The polarity is always "probe plus". The thickness d of the silicon slices is normally approximately 500 μm. As the penetration depth b of the phosphorus diffusion we choose for routine measurements $b \approx 6$ to 12 μm, in contrast to our first investigations [4,10] . By this means an ohmic behavior of the current-voltage characteristic could be obtained over a wide voltage range. Figure 3a gives two typical examples of characteristics that were measured on silicon of very different resistivity. (This result and all the following ones were obtained for a temperature of 23°C). Here, as in the following, ϱ_S indicates the resistivity that was calculated according to eq (5) from the contact resistance of the aluminum-silicon contact (see section 5). Even for the case of the high-resistivity silicon the characteristic shows ohmic behavior in the wide voltage range between approximately 30 mV ($\approx$ 1kT/e) to 1V ($\approx$ 40kT/e). For the polarity "probe plus", the ohmic behavior continues even up to voltages of approximately 20V, while for the polarity "probe minus", an overproportional increase of the current is observed with rising voltage.

It should be mentioned here already that four-point probe measurements, for which four probes are lowered onto four adjacent aluminum-silicon contacts, show a purely ohmic behavior independent of the current direction (see figure 3b; ϱ_4 indicates the resistivity measured by the four-point probe measurement). Here again we would like to emphasize the wide voltage range in which Ohm's law holds even for the case of the high-resistivity silicon. In contrast to a conventional four-point probe measurement, the characteristic shows ohmic behavior into the range of 1V.

We see two essential advantages in the aluminum-silicon contact:

a) The possibility to vary the local resolution (by a variation of the radius a; by a combination of spreading resistance measurement and four-point probe measurement).

b) The aluminum-silicon contact constitutes a spreading resistance contact with clearly defined reproducible properties that are homogeneous across the contact area and across the area of the wafer. Essential conditions for an absolute measurement of the spreading resistance are fulfilled.

In the following two sections we will discuss these two topics in detail.

4. Local Resolution

The volume in the silicon that is covered by the spreading resistance measurement is approximately a hemisphere with a radius 3a (approximately 80% of the spreading resistance is concentrated in this volume). In contrast to the conventional spreading resistance method, the radius a of an aluminum-silicon contact is clearly defined. Since any contact radius larger than 2 μm can be realized technically, the local resolution in axial and lateral direction can be varied in the desired way by a proper adjustment of the contact radius.

A typical example for an experimental realization is shown in figure 4. Results of spreading resistance measurements are plotted here that were measured along two parallel tracks of aluminum-silicon contacts. The distance between tracks was 180 μm, the distance between aluminum-silicon contacts 60 μm. The tracks ran from wafer rim to wafer rim through the center of the wafer. The measurement curves are interrupted every 2 mm over a distance of 200 μm. This representation should indicate that the sequence of aluminum-silicon contacts had gaps every 2 mm of 200 μm length, for technical reasons during the preparation of the structure. In the figures the resistivity $\varrho_S(x)$ at the location x is plotted, normalized to the mean value of all measurement points along the track. The way the value of $\varrho_S(x)$ is calculated from the spreading resistance will be treated in detail in section 5 (see eq (5)).

The two contact tracks differ only in the radius a of the aluminum-silicon contacts. By means of a very shallow phosphorus diffusion (b = 0.7 µm), it was possible to obtain aluminum-silicon contacts with a very small radius. The measuring track of figure 4a consisted of such contacts with a radius a = 3.0 µm. In contrast, the aluminum-silicon contacts of the track of figure 4b had a radius of 16.5 µm. Thus, while in figure 4a a depth of about 9 µm was resolved, in figure 4b the wafer was covered to a depth of approximately 50 µm.

Qualitatively, one can recognize the same macroscopic resistivity profile for both tracks. However, quantitatively, in the case of figure 4b the decrease of the resistivity in the center is larger by about 50% than in figure 4a. This comparison shows the inhomogeneous resistivity distribution in axial direction. This is in accord with observations made by VOSS of the infrared breakdown radiation from diodes which were prepared from silicon wafers cut from the silicon rod parallel to the pulling direction [11] .

While in figure 4a microscopic resistivity variations were observed in the center of the wafer, figure 4b shows a quite undisturbed, continous resistivity profile in this area. Obviously, the resistivity variations in figure 4a are very inhomogeneous in axial direction and were therefore averaged out in figure 4b.

In contrast to this, the quite strong microscopic resistivity variations outside the center of the wafer change only slightly in the transition from figure 4a to figure 4b. This is demonstrated further in the section figure 4c where both measurement curves are plotted together. (The separation of the two curves on the left side of the figure is caused by the different macroscopic resistivity profile which is superimposed over the microscopic variations. This also reflects the different depth resolution of the two measurements). The investigations in [10] suggest that here we are dealing with resistivity variations associated with the well-known striations.

The example chosen in figure 4 demonstrates that no essential information is lost for the manufacturer of power devices with the relatively large contact radius. This statement could be verified for various rods and led us to normally use contact radii of a$\approx$10 to 20 µm for routine measurements. The advantages are:

a) We can diffuse phosphorus with deep penetration (b$\approx$6 to 12 µm). Thereby the current-voltage characteristic obtains an ohmic behavior over a wide range (see figure 3a).
b) An exact determination of the radius a is necessary for an absolute measurement of the spreading resistance (see section 5). The accuracy of the measurement becomes better with increasing radius.

In order to save measuring time and in order to ensure a proper handling of the measurement apparatus for routine measurements, we furthermore normally use structures in which the aluminum-silicon contacts have a distance of 200 µm.

For a routine measurement of a silicon slice we provide the entire surface of the slice with aluminum-silicon contacts in a square grid arrangement. The distance between contacts is 200 µm in x-direction as well as in y-direction. The arrangement permits a measurement along two tracks that are perpendicular to each other and run through the center of the slice, see figure 5. The flat is already ground into the rod to indicate the position of the wafers in the rod.

Since the aluminum-silicon contact is not destroyed by the application of the metal probe, one and the same contact can be measured several times. Hence, it is possible to start out with a spreading resistance measurement along a track, then remove the counter electrode of the wafer and repeat the measurement along the same track using four probes as a four-point probe measurement. Here the probes are arranged in the direction of the track[2] . Since the distance between probes is 200 µm

[2]Investigations of this aspect showed that in this arrangement the lateral resolution is better than when the probes are applied perpendicular to the track.

now the resolution in lateral and axial direction is distinctly reduced. The silicon wafer is certainly covered into a depth of at least 200 µm. In the following two examples (figures 6 and 7[3]) we will show that by a comparison between spreading resistance measurement and four-point probe measurement valuable information on the axial resistivity distribution can likewise be gained. In the upper part of the figures in each case spreading resistance results are depicted, in the lower part the four-point probe results.

In figure 6 a high-resistivity silicon wafer was measured. As an unusual feature it can be seen that for the spreading resistance measurement in y-direction the resistance increases from rim to rim by about a factor of three. In the case of the four-point probe measurement the increase of the resistivity is significantly less. The comparison shows that the resistivity increase measured with the spreading resistance method cannot be homogeneous in axial direction, since it would have to be noticeable to the same quantitative degree with the four-point probe measurement.

Figure 7 depicts results taken from a silicon wafer in which the resistivity variations associated with striations are very distinct. The figure can be considered as a typical example for a strong resistivity dip outside the center of the wafer. The corresponding four-point probe measurement, in comparison, yields only a very slight indication of the dip. The comparison of both results leads to the conclusion that the resistivity dip is highly localized in axial direction even more than in lateral direction.

5. Absolute Measurement

For the calculation of the spreading resistance of an aluminum-silicon contact, we approximate the geometrical shape of the s_n-n junction in figure 2 by a semi-ellipsoid with radius a of the circular base and height b. Then the spreading resistance is given by

$$R_s = \frac{\varrho}{4a} \cdot \frac{\arccos \frac{b}{a}}{\frac{\pi}{2} \cdot \sqrt{1 - \frac{b^2}{a^2}}} \quad . \tag{4}$$

According to eq (3) the radius a can be calculated from the diameter Φ of the SiO_2-window and the penetration depth of the phosphorus diffusion.

From experience with the conventional spreading resistance method, we know that we cannot equate the contact resistance R_c of an aluminum-silicon contact and the spreading resistance R_s from the start. We therefore write in formal analogy to eq (4)

$$R_c = \frac{\varrho_s}{4a} \cdot \frac{\arccos \frac{b}{a}}{\frac{\pi}{2} \cdot \sqrt{1 - \frac{b^2}{a^2}}} \quad . \tag{5}$$

Here ϱ_s is the resistivity as calculated from the measurement of the contact resistance. This measured value is plotted in figures 4, 6, 7 and 8. Only in the case that the resistance R_c of an aluminum-silicon contact is determined solely by the spreading resistance, i.e., if

$$R_c = R_s \tag{6}$$

As to the calculation of ϱ_s see section 5, especially eq (5).

For the calculation of eq (4) based on eq (53b) and (54) of [12] the author wishes to thank E. Spenke. For the limit of b = 0 one obtains the well-known relation of eq (1) for a circular two-dimensional contact, for b = a the relation $R_s = \varrho / 2\pi a$ of a semispherical contact.

holds, the calculated ϱ_S -value equals the actual resistivity ϱ of the material.

In order to check if the assumption in eq (6) holds true, a second method is required that also permits an absolute measurement of the resistivity. For this purpose the four-point probe measurement with aluminum-silicon contacts presented itself, as was treated already in section 4.

The exact theory of the four-point probe measurement requires that the contact radius a of the aluminum-silicon contacts and the phosphorus penetration depth b be small as compared to the probe distance s of 200 µm. This was not fulfilled. Thus, we first of all had to make sure that the finite dimensions of the aluminum-silicon contact do not distort the four-point probe measurement. For this check one takes advantage of the fact, that the distance between the probes, s, can be varied very easily, e.g., by just using every second (s = 400 µm) or every third (s = 600 µm) aluminum-silicon contact for the four-point probe measurement. In this fashion, four-point probe measurements could be performed with greatly varying distances between probes. The probe distance s and the thickness d of the investigated wafers[5] were varied in the range

s = 200 to 3000 µm
d = 150 to 2000 µm
d/s = 0.2 to 10.

Here, a was never larger than 20 µm. The ϱ_4 -values were calculated according to SMITS [14] for $d/s < 1.4$ and according to VALDES [15] for $d/s > 1.4$. Within the measuring accuracy of ± 2% no influence was noticed of the distance between probes on the $\overline{\varrho}_4$ -value. In addition, in deviation from the normal case by feeding the current into the two inner probes and measuring the voltage at the two outer ones, we were able to verify that the ϱ_4 -value is independent of such exchange of probes.

Similar results had already been obtained by SEVERIN [16] when investigating his unconventional four-point probe method, in which mercury is used as a contact. In this case, too, the diameter of the mercury contact was already of the order of the probe distance.

In order to check the assumption in eq (6), spreading resistance measurements and four-point probe measurements (s = 200 µm) were performed in x- and y-direction (figure 5), the latter measurements after the bottom diffused layer was removed. The spreading resistance measurements were evaluated according to eq (5). For both tracks (i.e. for approximately 2 · 150 measurement points) the average values $\overline{\varrho}_S$ and $\overline{\varrho}_4$ were calculated and compared with each other.

Typical results that so far were confirmed quantitatively by all our measurements are shown in figure 9. Plotted are the results obtained from 33 silicon slices. The slices were taken from three different silicon rods that differed as far as their average resistivity and their microscopic resistivity variations were concerned:

group 1: 11 wafers in the range $\overline{\varrho}_4$ = 207 Ωcm ± 16%.
"Short wave-length" microscopic resistivity variations with small "amplitude". Figure 6 shows the measured resistivity distribution of one of these slices. (The slant of the curve measured in y-direction is not typical, though).

---

[5] Included in these investigations was neutron activated silicon with very homogeneous resistivity [13] which will be treated in connection with figures 8 and 9.

group 2: 12 wafers in the range $\bar{\varrho}_4 = 39.1\ \Omega\text{cm} \pm 4\%$.
"Long wave-length" microscopic resistivity variations of large "amplitude". Figure 7 shows the measured resistivity distribution of one of these slices. (The resistivity dip in x-direction is not typical, though).

group 3: 10 wafers in the range $\bar{\varrho}_4 = 3.19\ \Omega\text{cm} \pm 2.5\%$.
Neutron activated silicon [13], no microscopic resistivity variations. Figure 8 shows the measured resistivity distribution of one of these slices[6].

Since the spreading resistance measurement reaches into a much lower depth of the silicon wafer than the four-point probe measurement, the values $\bar{\varrho}_S$ and $\bar{\varrho}_4$ do not correspond to the same volume in the specimen. Hence, it is not surprising that values $\bar{\varrho}_S/\bar{\varrho}_4$ smaller than one are measured. However, it has to be noted that the relation $\bar{\varrho}_S/\bar{\varrho}_4$ is <u>always</u> smaller than one. On the average it is approximately 0.8. This result cannot be explained by the differing local resolution of the two methods, especially since it was also obtained with the homogeneous silicon of group 3.

Analogous to the conventional spreading resistance method we are forced to introduce a calibration factor

$$k = \frac{\bar{\varrho}_S}{\bar{\varrho}_4} \tag{7}$$

for the aluminum-silicon contact in eq (5):

$$R_C = k \cdot R_S = k \cdot \frac{\varrho}{4a} \cdot \frac{\arccos \frac{b}{a}}{\frac{\pi}{2} \cdot \sqrt{1 - \frac{b^2}{a^2}}} \tag{8}$$

Naturally, this step rests on the assumption that principally $\bar{\varrho} = \bar{\varrho}_4$ holds true and that there can be no doubt as to the accuracy of the four-point probe measurement.

The k-values of figure 9 were plotted in figure 1. It should be noted that MAZUR and DICKEY [5] and KRAMER and VAN RUYVEN [6] also measure k-values smaller than one, although only in the high resistivity part of their measurements range. If one takes into account that the k-value is determined by many factors (description of the s_n-n junction by a semi-ellipsoid, which holds only approximately; the approximation: underdiffusion = 2/3 . b; the measurement of the penetration depth of the phosphorus, b, and the diameter Φ ; current-voltage measurement etc.), a deviation of the k-values from the theoretical value of k = 1 by 20% is basically not surprising. However, it is disturbing that k is always smaller than one by approximately 20%. This points to a systematical error.

We could not determine unequivocally whether the two ϱ_S -dips measured with the spreading resistance method in y-direction had to be considered as properties of the material or whether they rather were pure measurement errors.

For this reason we varied drastically the experimental conditions:

a) a from 2.5 to 50 µm } where the distance between two contacts and the
b) d from 150 to 2000 µm } thickness of the wafer were always larger than 10a. (figure 9 also comprises two different values of a and in the case of the homogeneous silicon also different values of d).

c) b from 0.7 to 12 µm

d) measurements of $\overline{\varrho}_S$ and $\overline{\varrho}_4$ on wafers that were cut along the ⟨111⟩ -direction from a rod pulled in that direction[7].

e) measurements of $\overline{\varrho}_S$ and $\overline{\varrho}_4$ on contacts without metallization. The metal point was applied directly onto the phosphorus diffused silicon.

f) ac-measurements of $\overline{\varrho}_S$. The frequency was approximately 150 Hz.

In none of these cases was there a noteworthy influence on the k-values. The k-values were always scattered statistically around $k \approx 0.8$.

The term "statistically" applies here only with restrictions. Unfortunately, at the time of these investigations silicon with homogeneous resistivity was not yet available to us. Since the local resolution of the two measurement methods was different, we would have had to investigate a large number of wafers in order to arrive at a statistical interpretation. It would have been too time-consuming. Therefore, in some cases only four silicon slices were measured with one experimental condition varied. We can thus not claim true "statistics". It is only recently that in the neutron activated silicon we have a material with homogeneous resistivity. The investigations are to be repeated with this material. Surely, results with still higher certainty will be obtained with respect to the k-value.

6. Final Remarks

A disadvantage of the aluminum-silicon contact consists in the time-consuming and costly processing steps needed for the preparation of the contacts. As far as simplicity is concerned, the conventional spreading resistance method in many cases would be better suited, since it requires only a simple surface treatment of the silicon slice. Therefore, it is now our aim to help answer the technically interesting question whether the conventional spreading resistance method permits measurement of relatively small resistivity variations in starting silicon with satisfactory accuracy. We intend to perform measurements of comparison between the conventional spreading resistance method and our method of measurements with aluminum-silicon contacts. The measurements are to be performed on the same wafer on adjacent tracks. In order to arrive at a result as general as possible, we have sent silicon wafers of groups 1, 2 and 3 in figure 9 after they were measured by us to a number of laboratories. These laboratories are concerned with the conventional spreading resistance method and will use it to measure our silicon wafers.

7. Acknowledgements

The author would like to thank J. Burtscher for helpful discussions. He also would like to thank G. Schuh for supplying the wafers with aluminum-silicon contacts and H. Windisch for taking the measurements.

---

[7] In contrast to the investigations of GARDNER et al. [7] (see figure 1) and MURRMANN, SEDLAK [17], with aluminum-silicon contacts there is no indication of a dependence of the k-factor on crystal orientation.

8. References

[1] Mühlbauer, A., Kappelmeyer, R., and Keiner, F., Widerstandsfeinstreifung in tiegelgezogenen Si-Kristallen, Z. Naturforsch. 20a 1089 (1965).

[2] Mazur, R.G., Resistivity inhomogeneities in silicon crystals, J. Electrochem. Soc. 114 255 (1967).

[3] Krausse, J., Widerstandsschwankungen in Siliziumkristallen, paper presented at the 2. DFG-Kolloquium in Burghausen (1970).

[4] Burtscher, J., Dorendorf, H.W., and Krausse, J., Electrical measurement of resistivity fluctuations associated with striations in silicon crystals, IEEE Trans. Electron. Dev. ED-20 702 (1973).

[5] Mazur, R.G., and Dickey, D.H., A spreading resistance technique for resistivity measurements on silicon, J. Electrochem. Soc. 113 255 (1966).

[6] Kramer, P., and van Ruyven, L.J., The influence of temperature on spreading resistance measurement, Solid-St. Electron. 15 757 (1972).

[7] Gardner, E.E., Schumann, P.A., and Gorey, E.F., Measurement techniques for thin films, p.258, Electrochem. Soc. (1967).

[8] Pinchon, P., private communication to P. Kramer and L.J. van Ruyven, ref. [6].

[9] Keenan, W.A., Schumann, P.A.Jr., Tong, A.H., and Phillips, R.P., Ohmic contacts to semiconductors, p. 263, Electrochem. Soc. (1969).

[10] Burtscher, J., Krausse, J., and Voss, P., Inhomogeneities of the resistivity in silicon: two diagnostic techniques, Semiconductor Silicon (Ed. by H.R. Huff and R.R. Burgess), p. 581, The Electrochem. Soc. (1973).

[11] Voss, P., private communication

[12] Ollendorff, F., Grundlagen der Erdschluß- und Erdungsfragen, Berlin, Verlag von J. Springer (1928).

[13] Schnöller, M., Breakdown behavior of rectifiers and thyristors made from striation-free silicon, IEEE Trans. Electron. Dev., to be published.

[14] Smits, F.M., Measurement of sheet resistivities with the four-point probe, Bell Syst. Techn. J. 711 (1958).

[15] Valdes, L., Resistivity Measurements on germanium for transistors, Proc. IRE 42 420 (1954).

[16] Severin, P.J., private communication, to be published.

[17] Murrmann, H., and Sedlak, F., Spreading resistance correction factors for {111} and {100} surfaces, published in this volume.

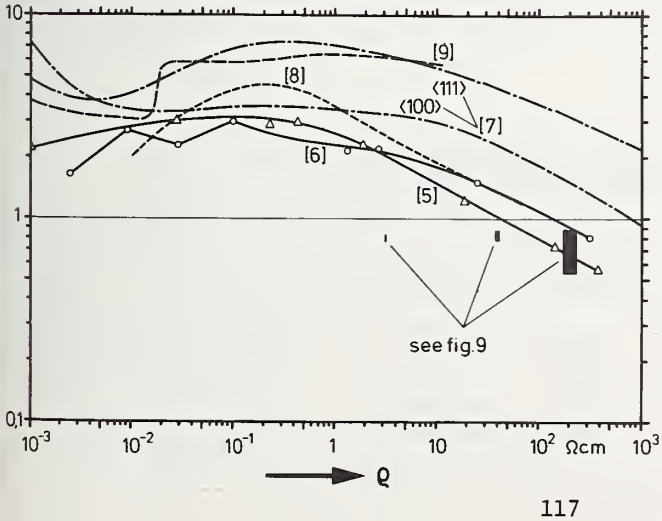

Figure 1. The factor k as a function of the resistivity for *n*-doped silicon (see figure 2 in [6]). The bars correspond to measurements on aluminum-silicon contacts, figure 9.

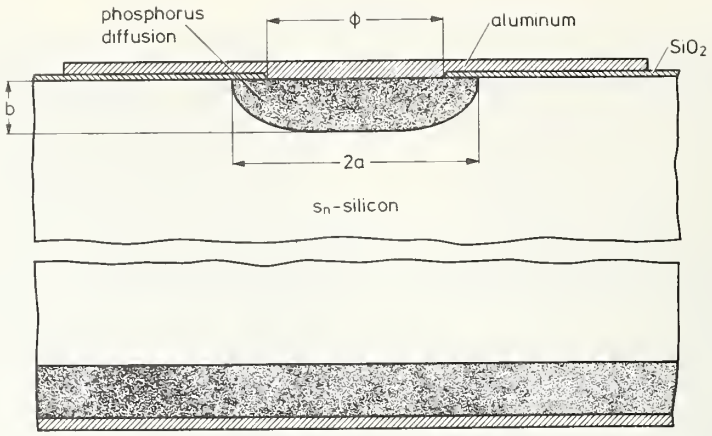

Figure 2. Cross-section through a non-blocking aluminum-silicon contact.

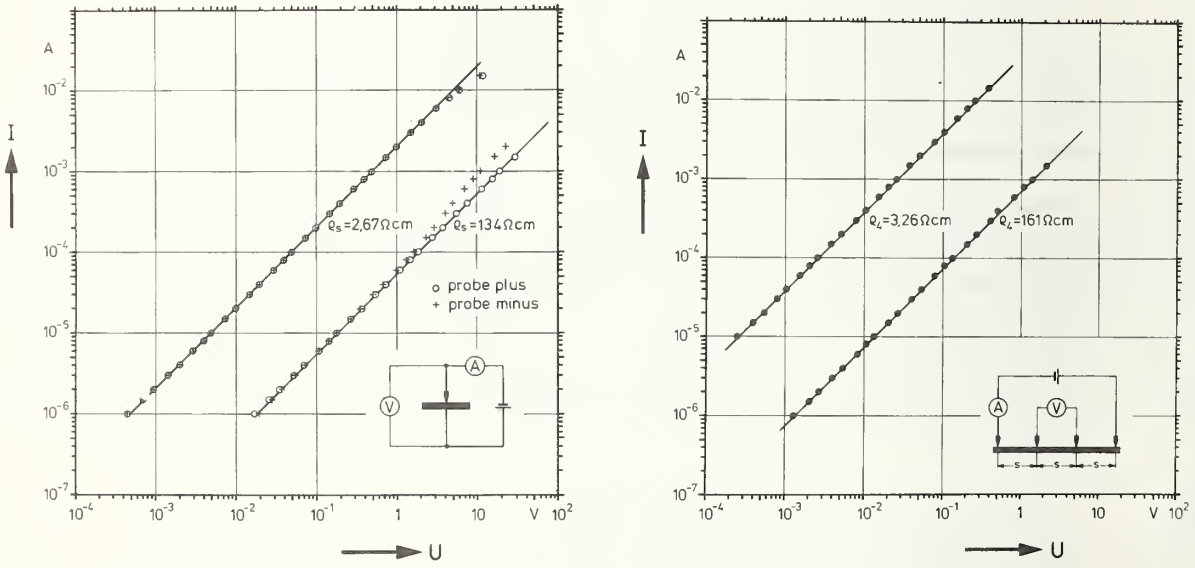

Figure 3. U-I characteristic: a) spreading resistance measurement, a = 10 µm (2.67Ωcm) or 12.5 µm (134Ωcm); b) four-point probe measurement, s = 200 µm.

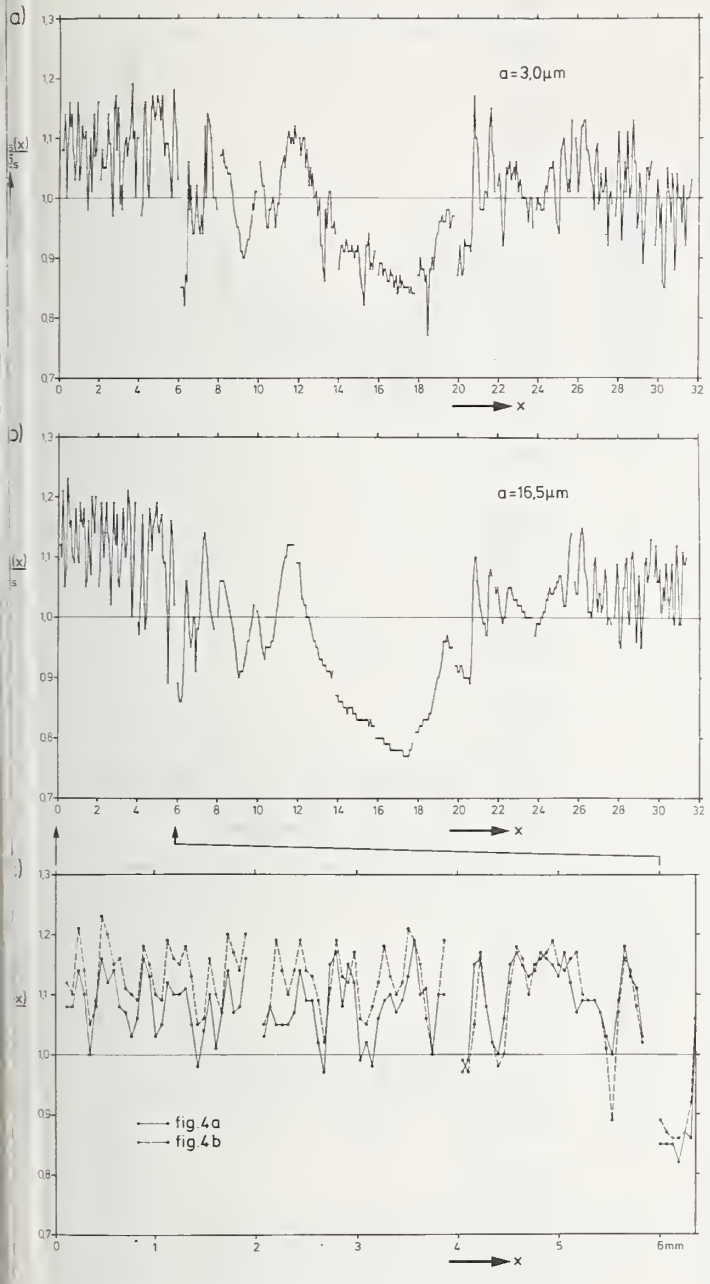

Figure 4. Lateral resistivity fluctuations along a diameter of a silicon slice (average resistivity 55 Ωcm)

a) a = 3.0µm (ϕ = 5µm; b = 0.7µm)
b) a = 16.5µm (ϕ =32µm; b = 0.7µm)
c) comparison of the two results in a) and b) for the 0-6 mm positions

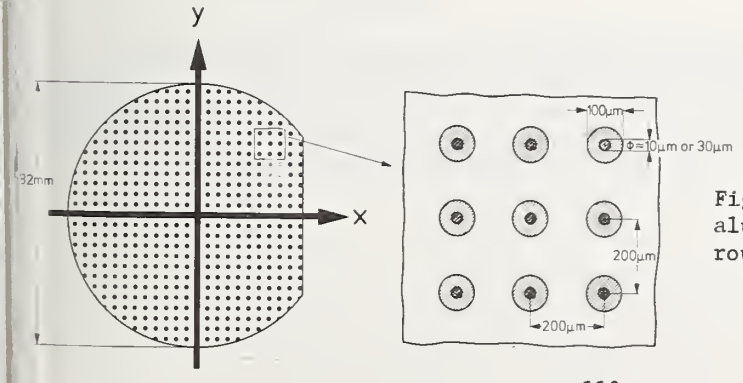

Figure 5. Arrangement of the aluminum aluminum-silicon contacts for a routine measurement.

565-448 O - 75 - 9

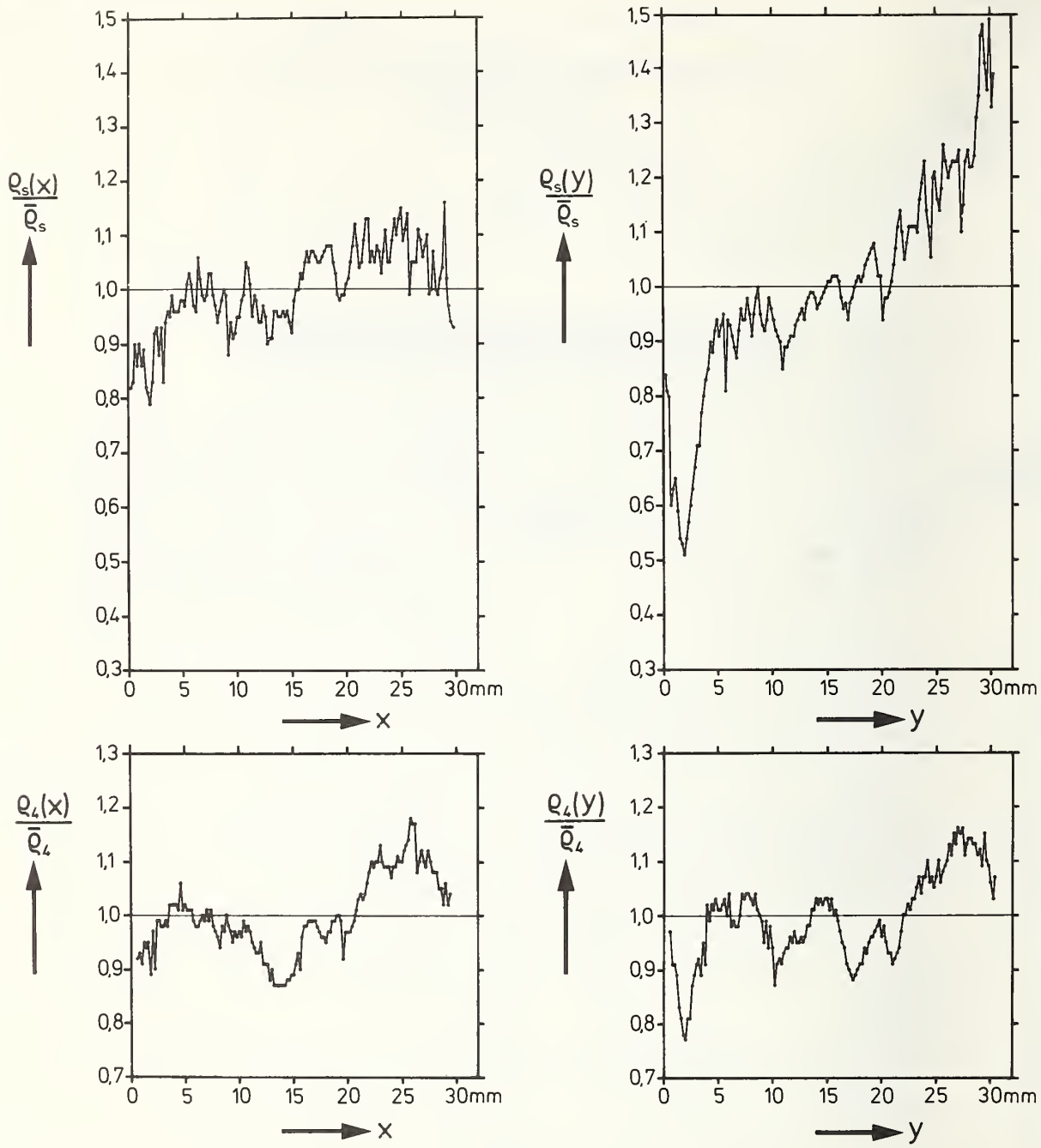

Figure 6. Lateral resistivity fluctuations along two diameters of a silicon slice (average resistivity 207 Ωcm)
ρ_s: spreading resistance measurement, a = 12.5 µm
ρ_4: four-point probe measurement, s = 200 µm.

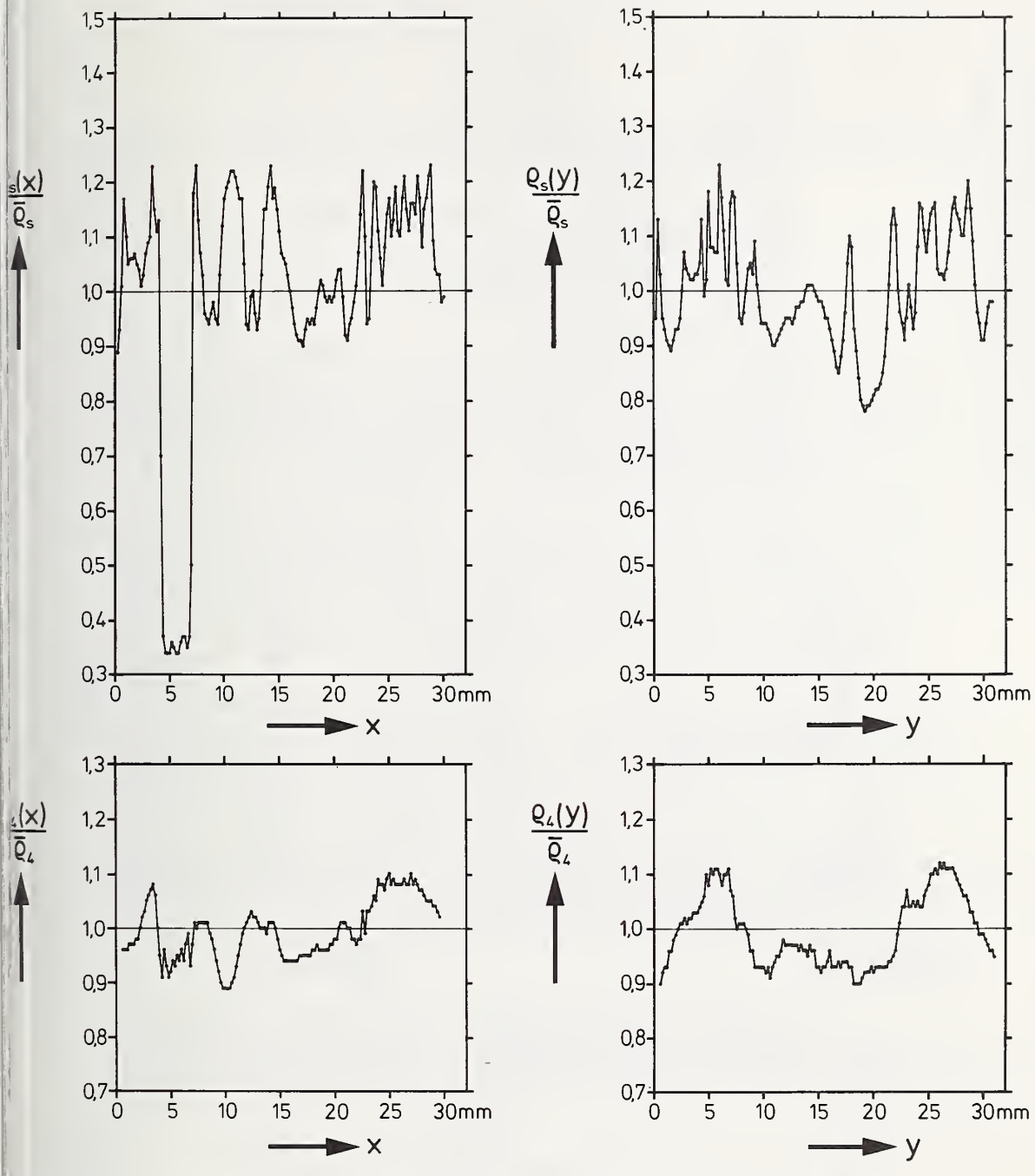

Figure 7. Lateral resistivity fluctuations along two diameters of a silicon slice (average resistivity 38.7 Ωcm)
ρ_4: four-point probe measurement, s = 200 µm
ρ_s: spreading resistance measurement, a = 10 µm

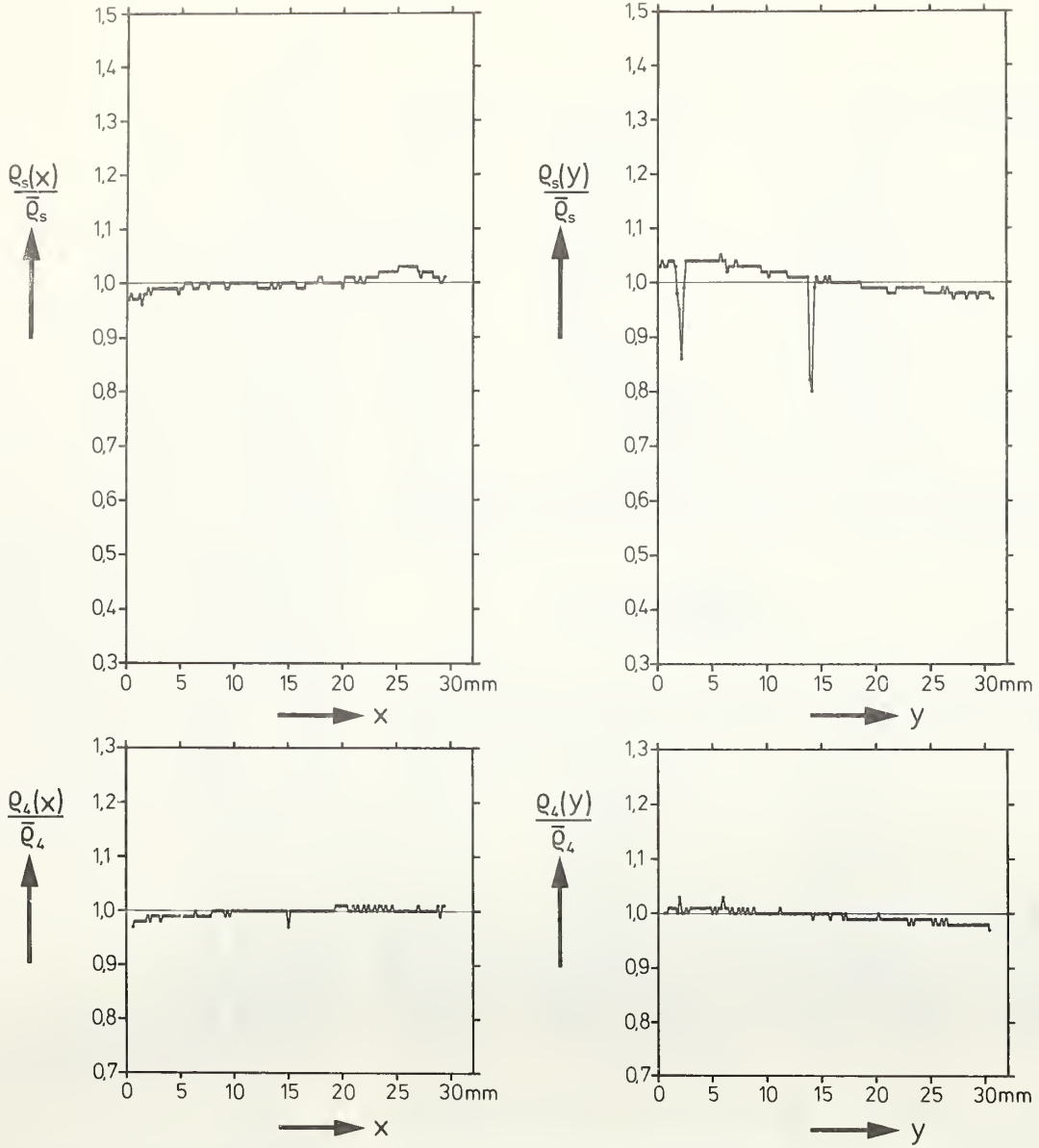

Figure 8 Lateral resistivity fluctuations along two diameters of a neutron activated silicon slice (average resistivity 3.17 Ωcm)
ρ_s: Spreading resistance measurement, a =10μm.
ρ_4: Four-point probe measurement, s = 200μm.

Figure 9. The factor $k = \bar{\rho}_s / \bar{\rho}_4$ of aluminum-silicon contacts. Comparison of the absolute values of $\bar{\rho}_s$ (spreading resistance measurement) and of $\bar{\rho}_4$ (four point probe measurement)

group 1: a = 12.5 μm or 22.5 μm; ϕ= 11.5 μm
or 32μm; b = 10μm; d ≃ 500μm.
group 2: a = 10μm or 20μm; ϕ= 10.5μm
or 31μm; b = 7μm; d≃ 500μm.
group 3: a = 10 m or 20 m; = 12 m
or 32 m; b = 6 m; d 200 m,100

group 3: a = 10μm or 20μm; ϕ= 12μm or 32μm;
b = 6μm; d ≃200μm, 1000μm, 2000μm

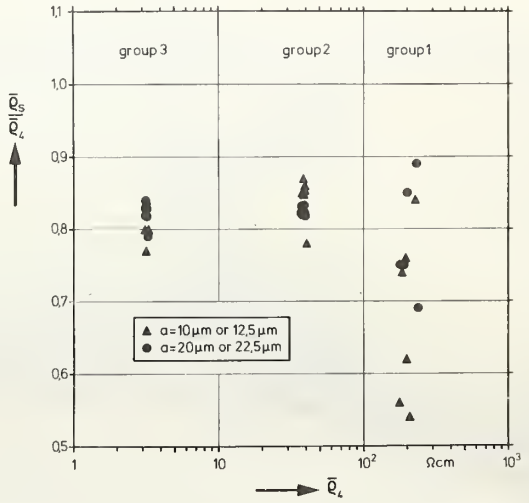

NATIONAL BUREAU OF STANDARDS SPECIAL PUBLICATION 400-10, Spreading Resistance Symposium, Proceedings of a Symposium Held at NBS, Gaithersburg, Md., June 13-14, 1974.

The Preparation of Bevelled Surfaces for Spreading Resistance Probing by Diamond Grinding and Laser Measurement of Bevel Angles

A. Mayer and S. Shwartzman

RCA Solid State Division
Somerville, N.J.

A rapid and reproducible method for preparing bevelled surfaces on silicon has been developed as a preliminary to spreading resistance probe measurement of doping profiles or junction depth determination by staining. Several chips can be bevelled simultaneously. The sample is mounted on a carrier which is clamped on the tilting table of a microtome. The tilt is adjusted until a laser beam reflected from the surface to a calibrated wall chart is deflected to the desired angle. The bevel is then ground with a high-speed diamond wheel mounted on the microtome, taking cuts of several micrometers at a time. The bevel edge is clearly defined even for very shallow angles. The angle is accurately measured with the same laser.

Because the ground surface is highly reflective, in contrast to a lapped surface, a good reading of very small angles of less than 30 minutes can be obtained. Up to a 6 meter base line is used with a 1mw He-Ne laser and the reflection is visible in normal room light.

Factors entering into spreading resistance are discussed, such as mechanical damage incurred in bevelling, probe impact damage, and surface cleanliness. Judged by spreading resistance, the amount of damage incurred during grinding is small and reproducible, provided care is taken to maintain the spindle so that it runs without vibrating.

Key Words: Bevelling, diamond grinding, laser bevel angle measurement, layer thickness determination, materials, resistivity measurement, silicon doping profiles, spreading resistance measurement, surface damage.

1. Introduction

Solid state device properties depend on the distribution of carriers round p-n junctions. The bevel-and-stain method [1,2] in conjunction with our point probe resistivity has been the most widely used procedure for this urpose, but the spreading resistance probe (SRP) is gradually supplanting it.

The major reasons for the slowness of the introduction of SRP into design engineering and process control are (a) the slowness of sample preparation, (b) the slowness of obtaining the SRP readings, (c) the lack of information about the effect of sample preparation on the precision of the resistance readings, (d) the lack of standard samples of sufficient uniformity to nsure that the choice of the area was not the main reason for an observed hange in the calibration graph and, by implication, the stability of the robe including the contact points and internal electrical circuits. Only

recently has sufficient work been done in commercial SRP* design and in the study of sample uniformity by Subcommittee 6 of the ASTM Committee F-1 to show that calibration graphs are reasonably stable and approximate straight lines. The speed and reproducibility of sample preparation present a bottleneck inhibiting the use of the SRP as a production control tool.

The work reported here was undertaken to improve the rate of sample preparation (bevelling) to provide a basis for mechanizing the procedure. High-speed grinding offered a chance to achieve this goal and it also provided a shiny bevelled surface which permitted the angle to be measured by optical reflection; the normal method consists of lapping, (which leaves a matte surface) and measuring the angle by depth of focus of a toolmakers microscope.

Precision equipment was developed which led to the establishment of grinding at any desired angle as a routine method for bevelling samples and a novel high-precision method for measuring bevel angles with a laser as part of the total mechanical package.

It is known that the measured spreading resistance is the sum of series resistance terms and the spreading resistance [3,4]. It has also been observed that surface preparation contributes to the observed value and its stability on storage. In order to make the bevelling procedure useful for production control it became necessary to provide some insight into the contributing factors, such as the degree of mechanical damage of bevelling in relation to that added by the impact of the probe points; the contribution due to the multiple contact points on each probe and the reason for the increased contact resistance when probes were used to measure only smooth surfaces. This report describes the development of the novel bevelling and measuring system which resulted from these enquiries.

2. Surface Grinding Development

2.1 Consideration of Surface Damage

A survey of the literature on spreading resistance measurement indicates that the method of surface preparation plays a major part in the reproducibility of SRP readings.

Severin [5] observed that the contact to silicon is multipoint. Gorey et al., [6] deliberately prepared multipoint tips by sandblasting. The makers of the SRP suggest that apparent high spreading resistance, R_S, readings obtained on a standard sample can be brought back to normal by allowing the points to impact on a roughly lapped silicon surface, a procedure which is called reconditioning. We agree with these observations and have also found that continued operation of the probe tips on only chemically polished surfaces gradually leads to high R_S readings and that these can then be made to read the normal, lower value after reconditioning.

The high readings probably result from the multiple contact points gradually wearing away on the smooth sample surface giving a smaller effective contact area and reconditioning then roughens the probe points again. The rough appearance of a normal imprint of a probe point is shown in the scanning electron micrograph, figure 1. This effect is different from the observation that the R_S of a lapped surface is greater than that of the polished surface of the same wafer. The reason for the latter effect is the degree and depth of damage incurred during sample preparation. That uncontrolled (impact) damage causes variable change in measured R_S can also be inferred from the observation that the drop rate of the probe tip on the silicon surface has to be well controlled. This is illustrated in figure 2; here the probe tip was allowed to impact repeatedly on the same area of a polished wafer and this led to a rapid increase of the measured R_S with each extra impact. It is similar to the observation that insufficient damping of the probe descent leads to high R_S readings. The effect of damage is most pronounced on highly doped silicon and disappears in the 10-100 ohm-cm range and

*We use a Model ASR-100 made by Solids State Measurements, Inc. Murrayville, Pa.

nay even reverse at higher resistivities. This effect is discussed in more detail and quantitatively later on.

Similar conclusions about damage were reached by Gupta et al.[7] who measured the R_S of lapped samples after progressive removal of damage by etching with hydrogen chloride, and also by Chu and Ray [8] who worked on germanium.

2.2 Grinding Machine

The importance of the above observations in the choice of a grinding machine for preparing bevels becomes clear when it is considered that vibration of the spindle is likely to cause uncontrolled damage. The best machines tried so far are an air-driven, pressure-mist lubricated spindle* which has been in operation on a daily basis for a year and a similar, but belt-driven one for 4 months. Most of the data reported here were obtained with the former. It is being operated on 25 and 40 psi air pressure at speeds of 30,000-60,000 rpm. The main problems in the installation were mounting the spindle rigidly on a level platform and the balancing and dressing of the ½" O.D. diamond cup wheel** to reduce vibration. Periodic redressing with an alumina or carbide stone is necessary to maintain reproducibility. Cutting is performed with air or oil cooling and an "elephant trunk" is used to exhaust the small amount of dust and mist generated. As can be seen from the photograph, figure 3a and the schematic, figure 3b the spindle is mounted on a microtome bed***; this has a ratchet feed capable of lifting the specimen in 1 to 25μm increments per stroke. The specimen is mounted rigidly with wax**** on a steel block which is indexed so that it can be lined up in the microtome clamp by means of a .5mm wide steel key.

2.3 Bevelling by Grinding

The microtome is supplied with a tilting table which can be set so that the waxed specimen is level with the sliding plane. It is then a simple matter to tilt the specimen to subtend the desired angle to the sliding plane and to measure this angle by means of a Helium-Neon laser mounted parallel with the spindle. After setting the tilt the grinder is started and allowed to take a 3-5μm cut per stroke. Each stroke takes less than 4 seconds so that even a 100μm thick layer can be sectioned in less than 2 minutes. Finishing strokes of 1-2μm at a time help to produce a finish with minimal damage on the bevelled surface. For examining very thin layers we routinely bevel at a 34 minute angle to obtain a tangent of about 0.01 or a magnification factor of 100, while a 0.2 tangent (∿11 degrees) is used to obtain complete cross-sections of wafers or for thick epitaxial layers. Table I can be used as a guide for selecting bevel angles and step length in relation to layer thickness.

Table I. Guide to Bevel Angles & Step Length in Relation to Layer Thickness. To obtain the true thickness multiply the SRP step by the tangent.

	Layer Thickness			
m	up to 3	2-15	10-60	50-150
il	up to .12	.1-.6	.4-2.5	2-6
RP step,μm	5	10	10	10
an α	.008-.012	.018-.025	.08-.12	.2-.4
pprox. α	½°	1°	6°	11°

H.P.Smith, Assoc., Cheshire, Conn; AVON spindle

* Sample Marshall Labs.,Lyndhurst,N.J.; 100 concentration,9μm diamond, plastic bonded cup wheel.

** Reichert Sliding "Om E" microtome.

*** Sticky wax, Corning Rubber Co., N.Y.

2.4 Surface Cleaning

When a suitable bevel has been ground, the block is transferred to the SRP, the surface is wiped with a Q-tip moistened with solvent* and air dried before measuring the R_S. This treatment removes oil mist and debris from the surface. In contrast to surfaces which have been prepared by lapping or chemical-mechanical polishing which is usually carried out with water based slurries, we have found that the surfaces prepared by dry grinding and solvent cleaning are stable. They show no significant drift upon standing in laboratory air, and give reproducible R_S when a fresh surface is prepared by grinding as shown by the following example: The surface of a test wafer having n- and p- type epitaxial layers was measured regularly each morning, then reground, cleaned and its R_S re-read each day for about a month. The longest time between regrinding was 68 hours, the shortest 30 minutes. The mean resistivity recorded was 17.57Ω-cm on the p-type layer, with a standard deviation, SD,of 4%. The n-type layer measured 13.3Ω-cm with a 6% SD. It should be noted that these figures include errors due to the true differences in resistivity of the sample as more of the sample was ground away.

The probable reason for this stability of the surface is that the freshly exposed silicon sees only the relatively dry room air. It is believed that surface charge effects are often due to charge separation and migration of impurities ionized in the presence of the highly hydrated silicon oxide film that forms when silicon is abraded under water. Similar stability could be achieved on surfaces prepared with aqueous media by baking them at 150°C for about 15 minutes. The suggested new method of surface preparation is simple and provides the basis for routine process control because of its relative insensitivity to what would normally be regarded as a very crude surface treatment. An illustration of the effect of impurities when samples are prepared by wet-lapping with silicon carbide is given in figure 4. Here, the surface was just rinsed in water after lapping, air dried and the R_S measured, then the sample was cleaned with hot ammonia-hydrogen peroxide (SC-1) solution and dried at 150°C for 15 minutes before remeasuring. Note that the apparent noise as well as the average level of the R_S value has changed significantly. When this series of experiments was repeated with the above sample the freon-solvent cleaning and drying step consistently produced less noisy readings than the aqueous treatments. The absolute level of the R_S varied by more than 10%.

2.5 Standard Sample Preparation

It became clear in the course of this work that the reproducibility of R_S on lapped surfaces, and later also on mechanical-chemically prepared surfaces required standardization of the cleaning and drying procedure. It was noted when this was done that the day-to-day reproducibility of the R_S still showed variations which were traced to the fixturing used in the lapping or polishing process; the pressure applied during the operation could vary considerably and give rise to various degrees of surface damage. Bevelling with an aqueous silica gel slurry on a glass or Lucite plate was also found to be a process difficult to control routinely so as to guarantee the same level of residual damage. This may have been the main reason for the changes in the slope of the calibration graphs prepared daily when the SRP was first introduced into service. Kim, et al.[9] also found that surfaces prepared with 0.03 to 10μm alumina gave R_S readings which were too noisy to resolve resistivity striations.

When the grinding procedure was introduced as a routine process the calibration graphs remained constant over long periods (months) and also became straight lines when plotted as logarithms of R_S against resistivity, as shown in figure 5. This graph was constructed from 18 samples of (111) and 7 samples of (100) oriented silicon, which had been selected for being reasonably homogeneous, a very difficult task for the high resistivity range. There is no significant difference statistically, when both the (111) and (100) or only the (111) samples are plotted. This is in contrast to private

*51% Freon-TF with 49% methanol was a satisfactory solvent.

information indicating that some workers find that the n-type and some that the p-type curves for (111) and (100) are significantly different. Much of this sort of discrepancy is probably due to bulk resistivity measurement problems. The next point of interest is the marked difference between chemically polished and ground surfaces: note that the surface damage due to grinding affects the n- and p-type highly doped samples in a similar manner and very markedly and that the effect almost disappears at high resistivities. We have no reliable samples for a good comparison in the greater than 100Ω-cm range. Perhaps this effect is due to the introduction of crystal defects which change the effective carrier mobility, i.e., the trapping cross-section for large carrier densities is greater than for the low carrier densities.

2.6 Factors Affecting Reproducibility

The confidence placed in any measurement procedure rests on the ability to calibrate the instrument so that this calibration can be reproduced over long periods of time. Our data suggest that the following factors enter into this: grinding and impact damage, condition of the SRP points, and standard sample uniformity.

The grinding process appears to introduce somewhat less damage than lapping, and is more reproducible on a routine, long term basis. The major problems are vibration in the spindle due to bearing wear, a loose clamp or support block, or a grinding wheel which requires dressing. A good maintenance schedule is essential. A daily check is easily made with a low resistivity sample by observing the height of the step in the R_s readings between the chemically polished and the ground surface as indicated in figure 6. In the range 10^{20} to 10^{14} carriers per cc a chemically polished surface gives the lowest spreading resistance. Even with the greatest care in adjusting the descent rate on our probe the surface is damaged. As can be seen in figure 2, repeated impact on the same point causes drastic changes in the apparent resistivity. Slight changes in the descent rate can change the degree of damage and the observed R_s. This is most obvious with low resistivity samples, for example a 0.011Ω-cm n-type polished sample which was measured repeatedly over a 6 week period, often two and three times a day gave a R_s between 14 and 24 ohm, the average was 19.8 ohm and the SD was 12.4%; the maximum fluctuation during a day was 9%. To evaluate the variation in R_s due to variation in grinding these figures were compared with R_s readings of the same sample after bevelling. The calibration graph covering the range 10^{20} to 10^{14} carriers per cc shown in figure 5 is based on the statistical average of samples read at least 10 times. It indicates a difference of 14 ohm between polished and ground surfaces of the test sample while the average difference observed was 12 ohm with a SD of 11.8%. No difference was observed between samples which had been freshly ground and ones which had been held for 16 hours after bevelling. The SD in a similar test for a 1Ω-cm n-type sample ($R_s \approx 10^3$ ohm) was 5.4% and for a p-type, 20Ω-cm sample ($R_s \approx 10^4$ ohm) it was 10.8%.

The data suggest that the variation in grinding damage contributes slightly less to the total noise than the variation in impact damage. The main practical benefit of this test is that it provides a ready means of monitoring the impact damage, by routinely checking the R_s of a low resistivity standard sample having a damage-free, preferably an epitaxial, surface. We can then set a limit to the value that is acceptable, and take appropriate action if it is too high - adjust the impact height or recondition the points on a lapped surface.

If we read the R_s on a freshly bevelled portion of the same sample we can again set a limit to the step height we wish to tolerate. If the observed value is greater, re-balancing the grinder will usually obviate the fault. It has already been noted that silicon reference samples prepared from bulk crystal more often than not exhibit considerable resistivity variation across the diameter. These gradients or striations are known to reflect the crystallization phenomena of the solid-liquid interface, variations of an order of magnitude over less than millimeter distances are not uncommon. We have regularly prepared material by epitaxial deposition of 50

to 100μm thick layers on high resistivity opposite type substrates. Spreading resistance measurements made on these epi layers show less than a 10% variation in R_S values over the surface of a 50mm diameter wafer and suggest that this is probably the best method for the preparation of standard samples for the calibration of the spreading resistance probe. These layers can be measured by the four-point probe technique in conjunction with a thickness measurement and the only uncertainty then lies in the calculation oftthe integrated resistivity over the thickness and the p-n junction correction for the built-in field when the two kinds of measurements,-four-point probe and spreading resistance- are compared. Subcommittee 6 of the ASTM Committee F-1 on Electronic Materials is working on this approach to standardization.

The work mentioned above on the evaluation of impact and mechanical damage required a large number of repetitive readings to be made by several operators. It became apparent that once the initial shyness of a new operator faced with a complex looking apparatus had worn off, no problems arose in the rapid acquisition of the necessary skill for bevelling, determination of the bevel angle and SRP readings.

In normal day-to-day practice we find grinding to give us satisfactory R_S data in terms of process control. In addition it is rapid and lends itself to the preparation of multiple samples and to mechanization.

3. Angle Measurement by Laser Reflection

3.1 Choice of Method

Process control requires the routine measurement of the width of subsurface layers. In order to convert the track marks of the SRP to width measurement it is necessary to know the bevel angle precisely. The suggested procedure for the ASR-100 probe is to use the calibrated toolmaker's microscope as a depth gage; the precision of the tangent measurement depends on the ease of focusing at the start of the bevel and at some known distance along the bevel; this procedure is time consuming and requires well trained personnel for reliable output. A somewhat improved measurement of the angle, in common use at RCA, depends on reflection of a collimated light beam from the top surface and from the bevel, followed by measurement of the displacement of the two rays at a distance of about 50cm. This method cannot be applied to lapped samples because the surface is not sufficiently reflective but ground bevels do give reasonable reflections. However, to measure small angles accurately a much longer pathlength is necessary and then the light intensity is insufficient.

3.2 Use of Laser

We have successfully substituted a He-Ne laser for the collimated light beam. A 1mw He-Ne laser* is mounted on the microtome used for grinding the bevels and serves in the first instance to adjust the tilt of the stage to obtain any desired bevel angle, and after the bevel has been ground it is used to measure the tangent of the angle precisely, without having to handle the sample further. It obviates the need for lapping blocks with different, precisely machined angles, it has great flexibility in permitting angles from 20 degrees to less than 30 minutes i.e. angles with tangents of 0.2 to 0.01 to be selected and measured accurately, giving a range of multiplication factors from 3 to 100. The arrangement for measuring the tilt of the sample before grinding and the finished angle after grinding are shown in the photographs figure 8a and b. The laser beam which has a diameter of 0.8mm is allowed to impinge on the top surface of a sample waxed to the prealigned and levelled carrier block. The tilting stage is then adjusted so that the reflected beam is deflected to the desired angle, α, or rather

* RCA Model L15404 and Exciter Model L15427A.

to the desired tangent of α. This is determined by the distance between the initial reflection of the level sample, and the new position Y (after tilting) divided by twice the optical pathlength $\overline{ABC}$ between the sample and the scale: $\tan \alpha = \overline{XY}/2\ \overline{ABC}$

It is essential to ensure that the laser beam is at near normal incidence to minimize errors in calculating the tangent of the angle. After grinding the bevel, its angle is measured precisely using the same laser and the same optics. This time two reflected beams are visible one from the sample surface and one from the bevel. The sequence of operations is shown in figure 8a,b,c,d.

The longer the baseline $\overline{ABC}$ between sample and scale, the more precise is the reading of the beam separation. We have used a 6m baseline to measure angles smaller than 20 minutes. In the existing permanent apparatus a 1.8m baseline is used which gives a 36mm separation of the reflected beams from a 34 minute angle with a tangent of 0.01 (corresponding to a magnification of 100). The laser beam we use has a nominal diameter of 0.8mm and a divergence of 1 mrad. Surface scattering causes the reflected spot to widen to about 5mm in practice, as compared to a calculated 2.6mm. With silica gel polished bevels the reflection tends to be more diffuse or elongated, especially with small angles, due to some edge rounding. Excessive periodic vibration in the spindle can produce deep ridges which cause a diffraction pattern to form and this makes it difficult to detect the center of the reflection. Figure 9 shows photomicrographs of bevels obtained with a well balanced wheel.

4. Comparison and Reproducibility of Bevel Angle Measurements

The reproducibility of the laser measurement was determined by 10 repeat tests by each of two operators who measured the bevel angle on one piece of silicon over a 5mm bevel length over a period of days. The average was a tangent of .0533 with a SD of 1.25%. The measurements were also compared with the depth of focus technique suggested by the SRP manufacturer and with tracing the profile of the angle using a calibrated surface profilometer* as shown in Table II.

Table II. Comparison of tangent measurements of the bevel angle. Each figure consisted of 6 readings taken by two operators over a one month period.

	Laser	Profilometer	Depth of Focus
verage	.0073	.0075	.0087
pread ±	.0008	.0059	.002
verage	.0143	.0153	.0155
pread ±	.0009	.0014	.0010
verage	.104	.105	.100
pread	.001	.002	.004

The depth of focus is not only the most tedious but also gives the least reproducible results, and the laser method is the most convenient and agrees well with the profilometer procedure.

In conclusion we can say that the combination of laser angle measurement and SRP track distance measurement produced values for the thickness of epitaxial layers which were in excellent agreement with infrared interferometric methods, and that the procedure is well suited for routine process control and engineering design work.

Summary

High speed grinding has been shown to be a useful method for the preparation of bevels prior to spreading resistance profiling of silicon samples.

*Talysurf 4, Engis Equipment Corp.

The main advantages of the new procedure are its speed, convenience, cleanliness and accuracy. Multiple samples can be bevelled and their angles determined rapidly on one block which is designed to fit directly onto the SRP. Simply wiping the surface with solvent is sufficient to get reproducible surface conditions. This method reduces the variability of R_s readings by suppressing surface hydration and charge separation from impurity ions. By combining the grinder with a laser it is easy to select the desired angle and to measure it precisely without removing the samples from the apparatus. Also a wide range of angles can be selected so that full cross-sections of 150μm thick wafers are as readily made as very shallow bevels of less than 30 minutes to measure thin layers with equal ease. In addition, the bevel edge is readily visible and sharp. It should be noted that the bevel preparation by grinding is a useful technique on its own because the ground surface is shiny and can be stained by the methods used on polished samples.

An examination of the factors which contribute to the total resistance measured by the spreading resistance probe indicate that damage due to the method of surface preparation can be separated from damage caused by the impact of the probe points provided homogeneous standard samples are available. The SR difference between the damage-free and the bevelled surface is a good guide to set up procedures which ensure that the grinder and the probe are kept in good operation condition in routine use. Lastly, we have found that the operation is readily learned and is relatively insensitive to operator experience.

6. Acknowledgements

We are happy to record that Paul Delpriore's and Eric Cave's help, ideas and encouragement, and Bernice Upton's devoted detailed work have contributed greatly to the success of this project.

7. References

[1] "Test for Thickness of Epitaxial or Diffused Layers in Silicon by Angle Lapping and Staining Technique", ASTM Method F 110-72, 1972 Annual Book of ASTM Standards, Part 8, p American Society for Testing Material Philadelphia.

[2] Bond, W.L. and Smits, F.M., Bell System Technical Journal, 35 1209, 1956.

[3] Mazur, R.G. and Dickey, F.J., J. Electrochem, So., 113, 255, 1966.

[4] Gupta, D.C. ibid., 116, 670, 1970.

[5] Severin, P.J., Solid State Electronics, 14, 247, 1971.

[6] Gorey, E.F., Schneider, C.P. and Poponiak, M.R., J. Electrochem Soc., 117, 721, 1970.

[7] Gupta, D.C., Chan, J.Y. and Wang, P., Rev. Sci. Instr., 41, 1681, 1970.

[8] Chu, T.L. and Ray, R.L., Solid State Tech., 14, 37, 1971.

[9] Kim, K.M., Kumagawa, M. Lichtensteiger, M., Mugai, A. and Martin, E., Annual Reports 1972-7: Research in Materials, Massachusetts Institute of Technology, p. 299.

Figure 1. Scanning electron micrograph of a spreading resistance probe impact area on silicon. Magnification 10,000 X; 70° specimen tilt.

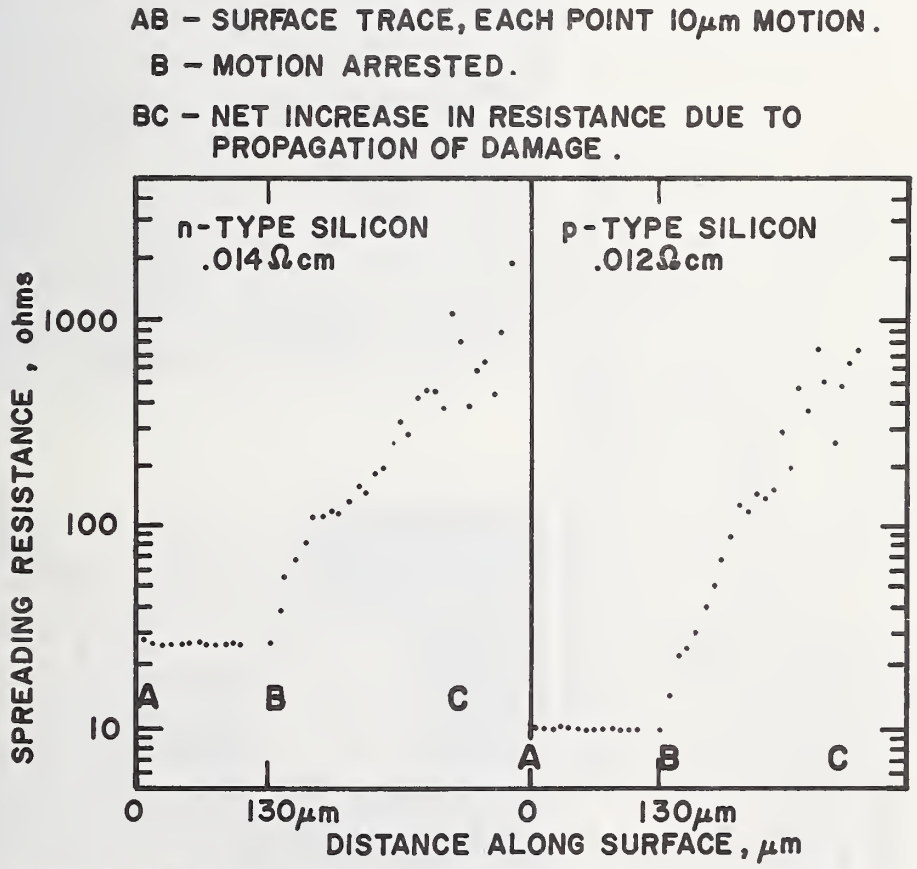

gure 2. Change in resistance from repeated impact of spreading resistance probe points on e same place on the surface of a silicon wafer.

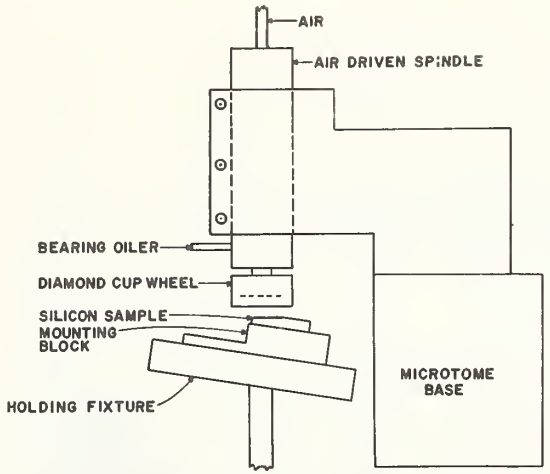

Figure 3a. Grinding spindle positioned over silicon sample.

Figure 3b. Photograph of grinding assembly consisting of a microtome (x), a high speed grinding spindle (y) and a mounting block and hold fixture (z).

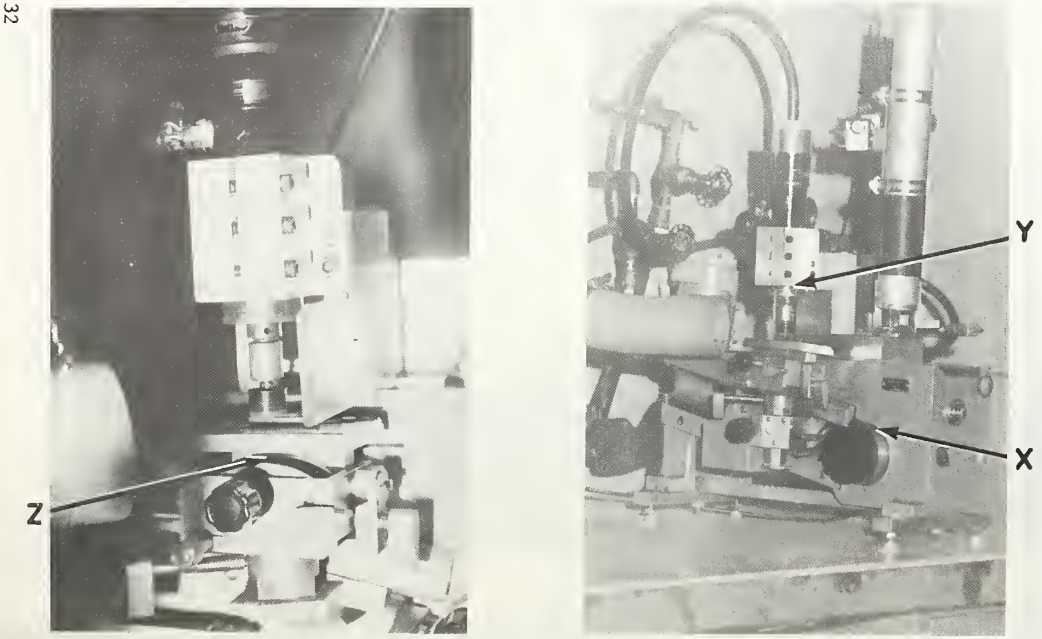

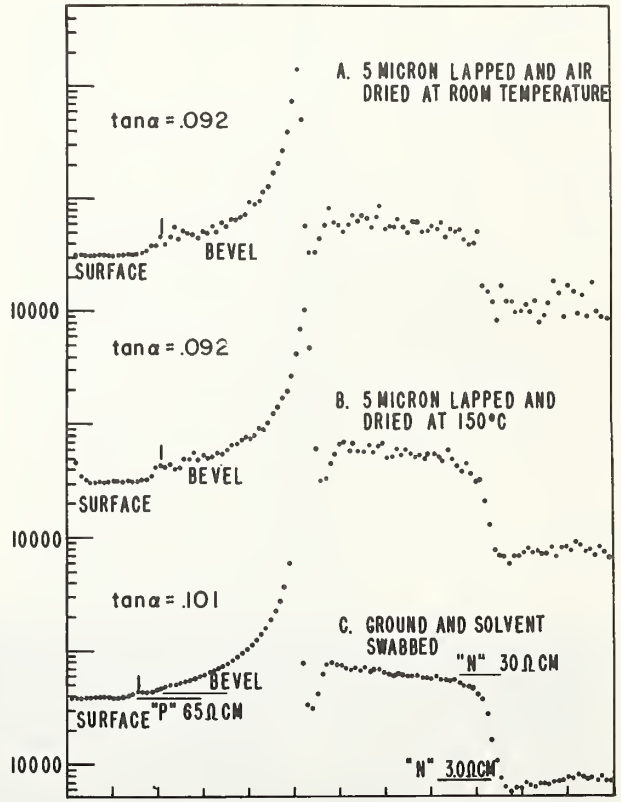

Figure 4. The Effect of Surface Preparation on Spreading Resistance Profiles.

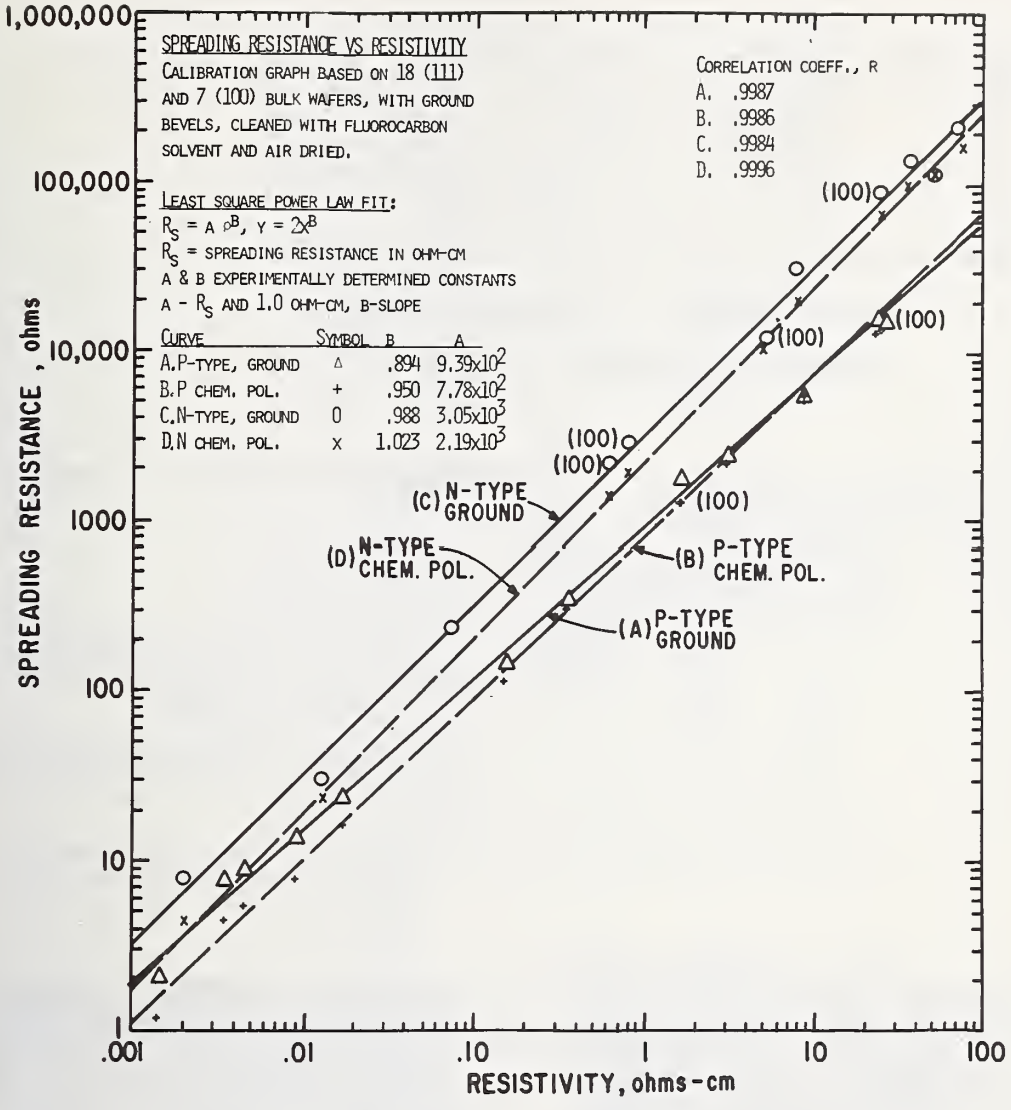

Figure 5. Spreading Resistance vs. Resistivity.

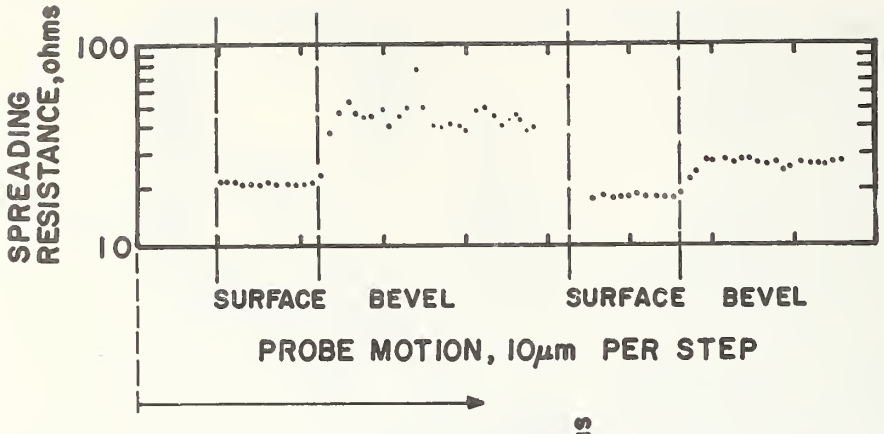

Figure 6a. Spreading resistance profiles of polished surface and ground bevel of 0.11 ohm-cm n-type silicon. Left, before dressing the grinding wheel. Right, after dressing the wheel.

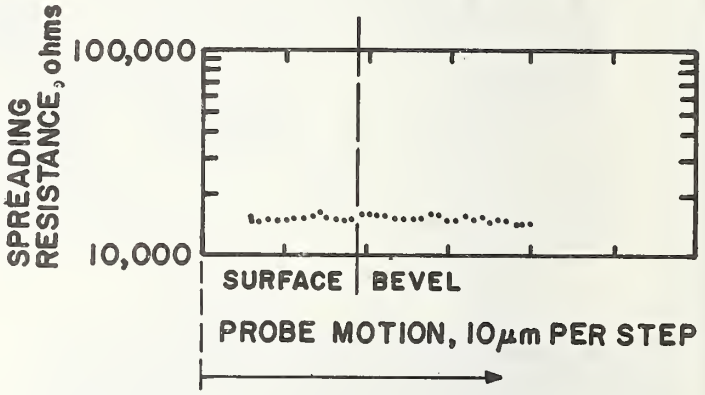

Figure 6b. Spreading resistance profile of polished surface and ground bevel of 23 ohm-cm p-type silicon.

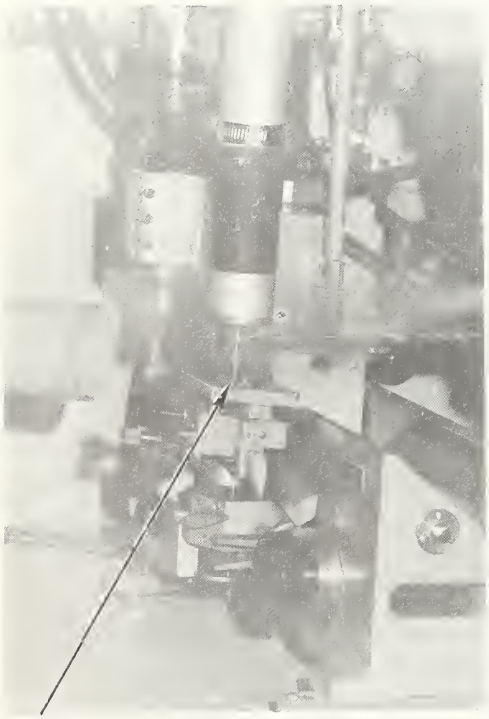

Figure 7a. Laser Beam Impinging on The Silicon Chip.

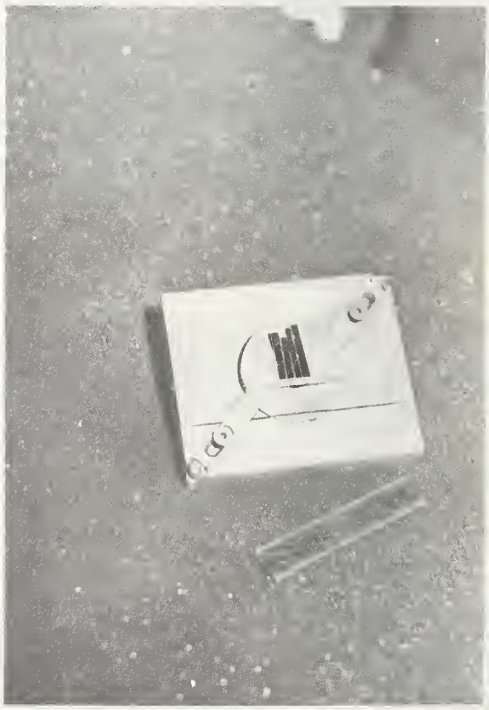

Figure 7b. Holding Fixture with Alignment Blade.

565-448 O - 75 - 10

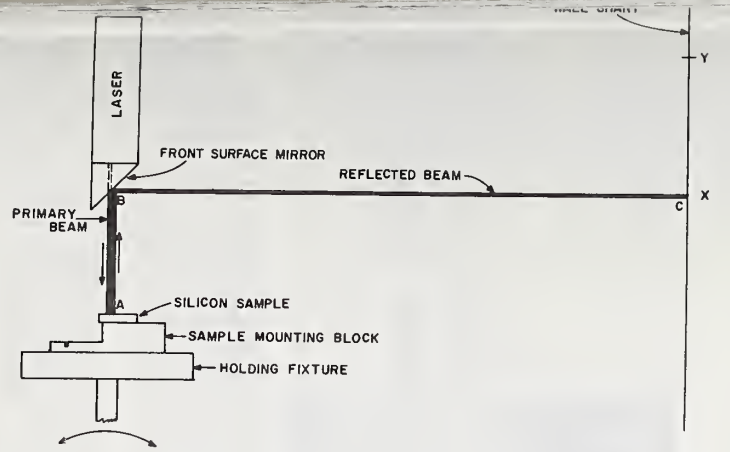

Figure 8a. Adjust the holding fixture so that the reflected laser beam ABC coincides with point x on the wall chart.

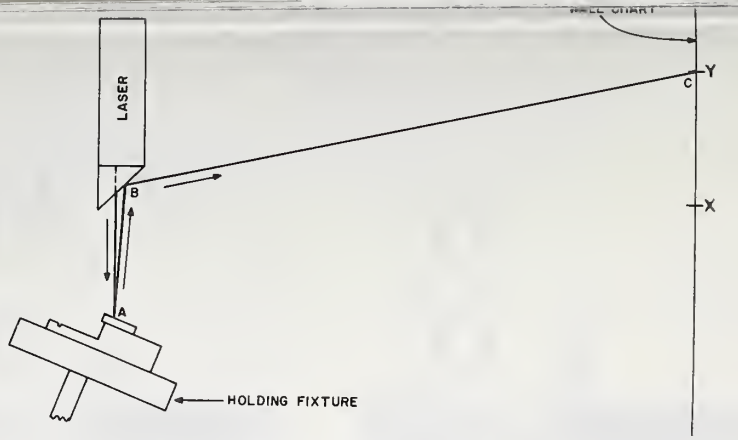

Figure 8b. Select the desired tangent & adjust beam ABC, by tilting the holding fixture, to point y on the wall chart. The distance XY=2•(ABX)•(tan X). Lock the holding fixture and grind the bevel. Example: If the actual distance from the sample is 150cm and the angle desired is approximately 5°, then XY=2 (150cm) (.1) XY=30cm; .1= tan of 5° 43'.

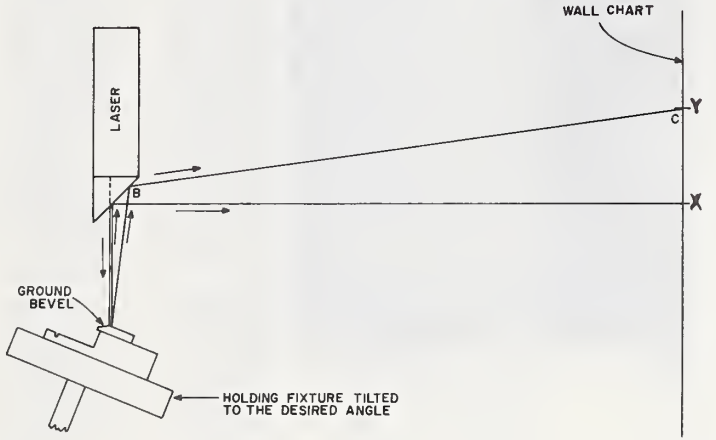

Figure 8c. Readjust the holding fixture so that ABC is moved back to point X on the wall chart.

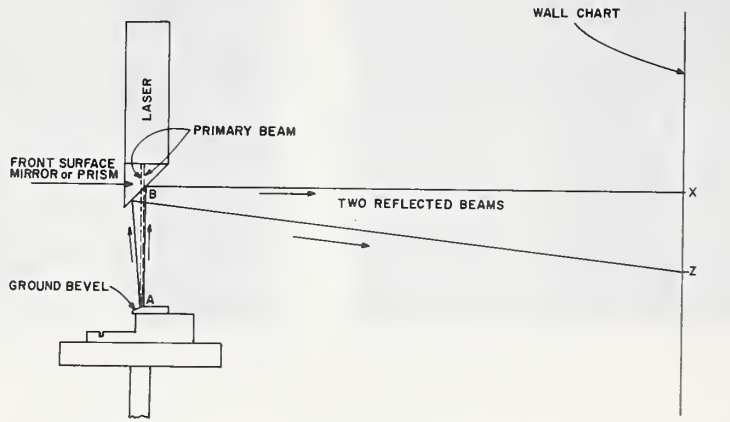

Figure 8d. Read the distance between the two spots (X and Z) on the wall chart and calculate the exact tangent. Example: tan α=XY/2ABC tan α=30cm/300cm=0.1.

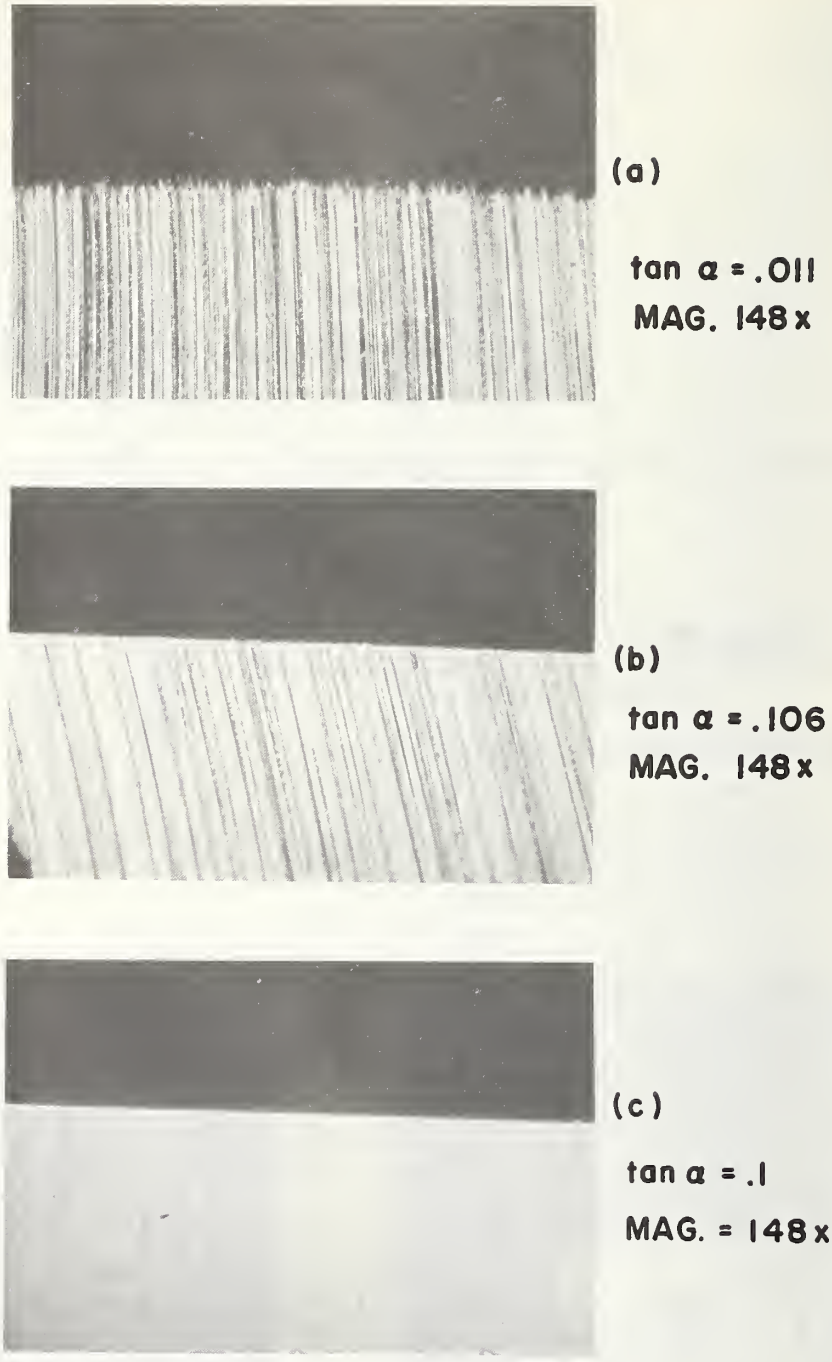

Figure 9. Photomicrographs of 38' and 6°, ground bevels.

NATIONAL BUREAU OF STANDARDS SPECIAL PUBLICATION 400-10, Spreading Resistance Symposium, Proceedings of a Symposium Held at NBS, Gaithersburg, Md., June 13-14, 1974.

Spreading Resistance Correction Factors for (111) and (100) Surfaces

H. Murrmann and F. Sedlak

Siemens AG, Werk Halbleiter
Munich, Germany

The effective contact radius for spreading resistance measurements on Si has been evaluated by comparision of S.R. for epitaxial layers limited by a pn-junction or by a well conducting buried layer for different crystal orientation. The contact radius on (100) surfaces showed to be greater by a factor of 1,26 than for a (111) plane. Furthermore measurements were made on samples for both (100) and (111) orientation in the resistivity range of 0,01 to 80 Ωcm with n and p-type doping. Data for spreading resistance and resulting from the predetermined contact radius for the resistivity dependent correction factor are given.

Key words: Contact radius, correction factors, silicon, spreading resistance, surface orientation.

1. Introduction

The spreading resistance underneath a flat circular contact (radius a) n a semiconductor (resistivity ϱ) can be expressed in the form

$$R_{SR} = \frac{\varrho}{4a} \cdot k(\varrho) \cdot k(\mathcal{E}) \qquad (1)$$

In this formula the first term $\varrho/4a$ represents the spreading resi- tance (S. R.) of an ohmic contact on top of a semi-infinite medium of etal with resistivity ϱ (figure 1). If energy barriers have to be consi- ered between the contact and the medium (as is the case for most contacts etween metal and semiconductor) a generally ϱ-dependent factor $k(\varrho)$ des- ribes this effect. If furthermore the resistivity of the sample is non- niform, the distribution of the electric field $\mathcal{E}$ will be influenced, iving rise to a correction term $k(\mathcal{E})$ dependent on the ϱ-distribution n the vicinity of the contact.

When applying the spreading resistance technique to quantitative easurements on semiconductors, both these corrections have to be taken nto account. This generally includes a calibration of the specific quipment with samples of known uniform resistivity, in which case the $(\mathcal{E})$-correction can be neglected.

Curves of measured spreading resistance vs. resistivity for n- and -type silicon have been published for different probe tip material and ontact radius [1], [2], [3], [4].[1] From these graphs the ϱ-dependent orrection can be derived provided the contact radius is sufficiently ell known.

[1] Figures in brackets indicate the literature references at the end of this paper.

Only very limited data exist for the influence of crystal orientation on the correction factor [2]. On the other hand there is strong experimental evidence, that differences exist between SR-measurements on (111) and (100) surfaces.

Figure 2 shows plots of $R_{S.R.}$ for (111) and (100) samples. In this case p-type Si-substrates (8 cm) were used with a buried layer diffusion (As, x_j = 4,5 µm, R = 25 Ω/□) and a n-type epitaxial layer (As, d_{epi} = 2,5 µm, ϱ = 0,8 Ωcm). Though the thickness and resistivity in both samples are the same, the SR-values show considerable differences. As the resistivity distribution in the first approximation can be assumed to be identical, the reason for such discrepancies can only arise from differences in $k(\varrho)$ or in the contact radius for the two surface orientation. In the following investigations we tried to distinguish between these two effects.

2. Determination of contact radius

2.1 Theoretical consideration

The question of what the effective contact radius will be, when a probe with a spherical tip is pressed onto a flat surface is very difficult to answer. Several investigators have dealt with this problem considering more or less idealized contact areas [1], [4] resulting from application of the Hertz formulas [6] as well as arrangements of multipoint contacts [5]. Optical evaluation of the surface depression after removal of the tip in general only gives on approximate figure for the contact area. We have decided to try an evaluation by S.R. measurements making use of equation (1):
As stated above the S.R.-value for a given ϱ at the surface is dependent on the field distribution . The potential and hence the factor $k(\varrho)$ has been calculated for the special arrangement of a layer 1 with resistivity ϱ_1 on top of a layer 2 with ϱ_2 respectively (figure 3).
Two configurations are of specific interest:

a) $\varrho_2 = \infty$: This implies that an insulating boundary limits the region of layer 1. Technologically this is realized by a pn-junction.

b) $\varrho_2 = 0$: Here the conductivity of layer 2 is assumed to be much greater than in layer 1. This case can be approximated by an highly doped underlay of the same conduction type.

In both cases the field correction factor is only dependent on the ratio of d/a [1]. In figure 3 the results of a calculation following Schumann and Gardner [7] are plotted as a function of d/a. If we furthermore compare two configurations with $\varrho_2 = \infty$ and $\varrho_2 = 0$ respectively but otherwise identical ϱ_1 and d, the ratio of the corresponding spreading resistances is merely given by $k(\infty)/k(0)$ independent of ϱ and barrier effects but only dependent on the ratio of d/a (figure 4).

$$\frac{R_{SR}\ (\varrho_2 = \infty)}{R_{SR}\ (\varrho_2 = 0)} = \frac{k(\infty)}{k(0)} = f\left(\frac{d}{a}\right) \qquad (2)$$

So we may derive from the S.R.-ratio a certain value of d/a from figure 4 and, when the thickness of layer 1 is known, the effective contact radius of our spreading resistance equipment can be found.

---

1) There exists a slight dependence on the spacing between the probes used for measurement, but this effect is neglible for our considerations.

2.2 Experimental

For the experiments Si-wafers (1,25" diam.) with (111) and (100) orientation and both p-type material (8 Ωcm) were used. After a thermal oxidation (1 µm SiO_2) the oxide was removed from a half of each wafer and a buried layer diffusion was carried out (Sb, 25 Ω/□, x_j = 4,5 µm) while the other half of each slice was masked by the oxide. Following complete oxide-stripping, As-doped epilayers were deposited (1150°C, $SiCl_4$) in four different runs with projected thickness of 2, 3, 5 and 8 µm. The epithickness was evaluated by both IR-reflection and stacking faults above the buried layer diffused halves. S.R. measurements were made with a Mazur Automatic Spreading Resistance Probe (ASR-100) with two probes loaded with a force F of either 20 g or 45 g each. The measurements were taken on the unprepared Si-surface after epitaxy on the half above the buried layer (denoted as R_{SR} (0)) and on the other half, where the n-epilayer is isolated from the adjacent substrate by a pn-junction (R_{SR} (∞)). Table 1 shows data of some of the slices examined.

Wafer Nr.	F = 20 g		F = 45 g		d_{epi} by IR	
	R(∞) [kΩ]	R(0) [kΩ]	R(∞) [kΩ]	R(0) [kΩ]	[µm]	
2	12,0	1,55	8,7	0,98	2,10	(111)
4	11,3	1,50	7,5	0,83	2,02	
6	5,95	1,26	5,4	0,88	2,95	
7	6,40	1,75	5,6	1,03	3,02	
12	5,80	2,40	5,0	1,6	5,36	
14	2,55	1,53	2,08	1,07	7,85	
15	3,35	1,97	2,70	1,35	8,16	
01	10,5	0,84	-	-	1,94	(100)
03	10,2	0,82	-	-	2,02	
07	5,2	0,98	4,72	0,58	3,12	
08	5,8	0,92	5,3	0,54	2,98	
09	3,75	1,41	3,28	0,97	5,92	
012	3,40	1,26	2,97	0,84	5,68	
016	2,52	1,35	2,12	0,94	8,72	

Table 1: S.R. above a pn-junction (R(∞)) and buried layer (R(0)) for different probe loading F (ASR-100, 2 tungsten probes with spacing of 600 µm, measurement voltage 10 mV, resistivity of the epilayer 0,6 - 1,3 cm).

2.3 Results

From the ratio $R(\infty)/R(0)$ using figure 4 and the determined epithickness, an effective contact radius (a) was evaluated with the results shown in table 2.

Table 2. Contact radius for different probe loadings and two orientations

	F = 20 g	F = 45 g	$\frac{a\ (45\ g)}{a\ (20\ g)}$
a (111) [um]	2,20	2,82	1,26
a (100) [um]	2,90	3,45	1,25

Within an experimental error of ± 8 % the values of (a) showed no dependence on the epithickness within the range examined, indicating that the thickness effective for S.R. and the thickness deduced from IR-reflection is approximately the same [1].

According to an early study of Hertz [6], the radius of the contact area resulting from a spherical probe (radius A, modul of elasticity E_1) elastically pressed onto a flat medium (elasticity modul E_2) by a force F is given by

$$a = 1{,}1 \left[\frac{F.A}{2} \left(\frac{1}{E_1} + \frac{1}{E_2} \right) \right]^{\frac{1}{3}} \qquad (3)$$

If the S.R.-contact mainly follows the laws of elasticity, the ratio of the effective radius for two loadings F_1 and F_2 is given (independently on orientation) by

$$\frac{a\ (F_1)}{a\ (F_2)} = \sqrt[3]{\frac{F_1}{F_2}} = 1{,}31 \qquad (4)$$

The result derived from the measurements show a very good agreement with this simple theoretical model (table 2).

3. Measurement on (111) and (100)

3.1 Experimental

In order to compare different crystal planes of otherwise identical material the following procedure for sample preparation was chosen: The resistivity of a number of n and p-doped Si-slices (orientation (111), thickness 200 um) with homogenous doping was measured by conventional 4 point probing. From the middle part of each slice we subsequently cut two samples of 4 x 4 mm^2. Taking one sample of each slice we stacked them together and mounted them on a fixture under a certain orientation (figure 5).

---

1) The only difficulty showed up for d_{epi} less than 2 um at (100) orientation with 45 g loading, where obviously the pn-junction got leaky giving rise to $R(\infty)$-values lower than expected. The data for this special case have not been considered in the evaluation for table 2.

Then the sample block was polished[1] in order to expose the desired crystal plane as predetermined by the sample orientation and the angle on the mounting fixture. By repeating this procedure we finally got two calibration blocks, one with (111) and one with (100)-surfaces, each consisting of 8 samples covering a range of 0,010 to 20 cm for n-type and 0,013 to 78 cm for p-type material[2]. Then S.R.-measurements were made with the two-probe arrangement of the ASR 100. The polishing procedure and measurement was repeated a total of five times within three months.

3.2 Results

The S.R.-data as received from the calibration blocks is given in figure 6. Each point is a mean value of the five different measurements. From this we finally plotted in figure 7 the ϱ-dependent correction factor as a function of resistivity using the different contact radii for (111) and (100) as determined in section 2 for 1 Ωcm n-material and assuming these values to be valid for the whole resistivity range and p-type as well.

4. Conclusions

From the data given in section 1 and from additional analysis of the measured values we finally can summarize the following conclusions of our examinations:

a) The effective contact radius of our probes is a factor of 1,26 greater on a (100) than on a (111) surface (n-material).

b) The spreading resistance on a (111) surface is always greater than for a (100) surface within the resistivity range of 0,01 to 20 cm. This holds for n- as well as for p-type material. The difference is greatest in the region of 1 Ωcm, where we find a factor of 2,1 (n) and 1,8 (p) respectively.

c) This behaviour can partially be attributed to the difference in the effective contact radius.

d) There remains at least in the 1 Ωcm region a clear difference in the resistivity dependent correction factor between (100) and (111).

e) The spread of the values from repeated measurements is much smaller for (100) orientation than for (111)

We hope that these experimental investigation are of some use for others dealing with S.R.-measurements and their theoretical explanation.

---

1) Polishing was done first with Linde A abrasive and a final finish with Syton polish.

2) It was checked by X-ray measurement, that each sample surface had the desired orientation within $\pm$ 2,5°.

5. References

[1] Mazur, R. G. and Dickey, D. H., A Spreading Resistance Technique for Resistivity Measurements on Silicon, J. Electrochem. Soc. 113, 255 (1966).

[2] Gardner, E. E., Schumann, P. A. and Gorey, E. F., Measurement techniques for thin films, p. 258, Electrochem. Soc. (1967).

[3] Keenan, W. A., Schumann, P. A., Tong, A. H. and Philips, R. P., Ohmic contacts to semiconductors, p. 263, Electrochem. Soc. (1969).

[4] Kramer, P. and van Ruyven,L.J., The Influence of Temperature on Spreading Resistance Measurements, Sol. State Electr. 15, 757 (1972).

[5] Severin, P.J. Measurement of Resistivity of Si by the Spreading Resistance Method, Solid-State Electron. 14, 247 (1971).

[6] Hertz, H., Über die Berührung fester elastischer Körper und über die Härte. Ges. Werke, Bd. 1 (Leipzig 1895).

[7] Schumann, P. A. and Gardner, E. E., Application of Multilayer Potential Distribution to Spreading Resistance Correction Factors, J. Electroch. Soc. 116, 87 (1969).

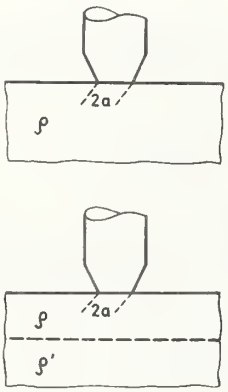

a) $R_{S.R.} = \frac{\rho}{4a}$ (metal)

b) $R_{S.R.} = \frac{\rho}{4a} \cdot k(\rho) \cdot k(\xi)$ (semiconductor)

Figure 1. Schematic for S.R. of a circular contact area (radius a) on a semi-infinite metal and a semiconductor with inhomogenous resistivity.

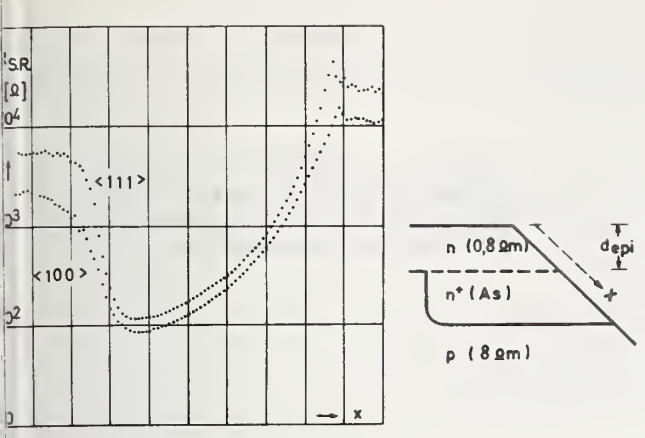

Figure 2. SRM on $n\ n^+p$ structures with (111) and (100) orientation but with identical dopings.

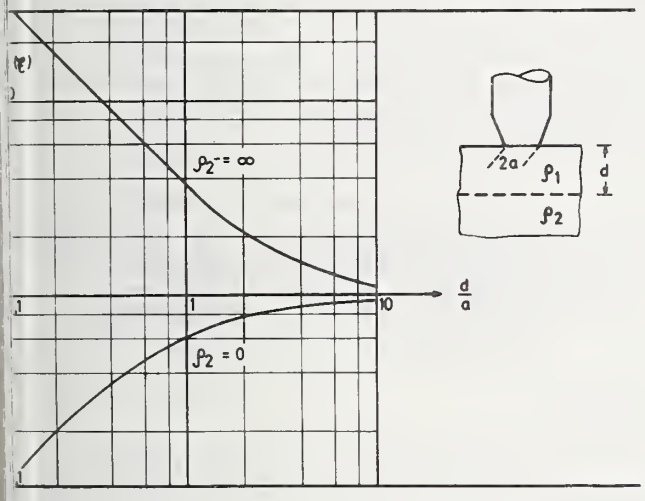

Figure 3. Correction factor due to distortion of the electric field ℓ by a two layer configuration. (Two probe arrangement with a spacing of 0,6 mm).

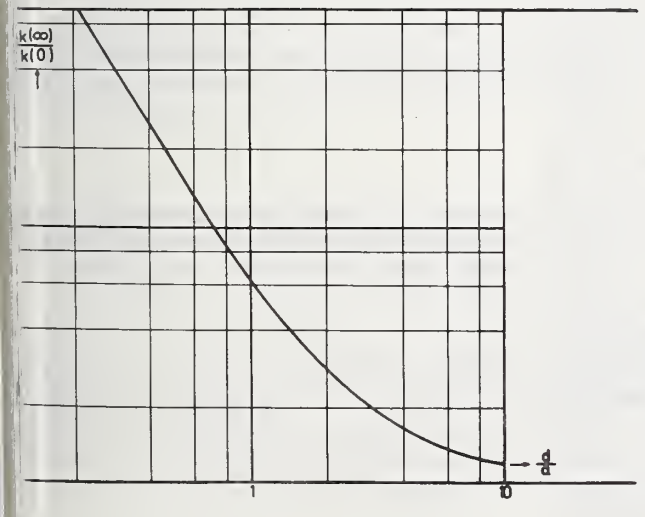

Figure 4. Ratio of the field correction factor for a two layer arrangement with $\rho_2 = \infty$ and $\rho_2 = 0$ respectively (two probes with 0,6 mm spacing).

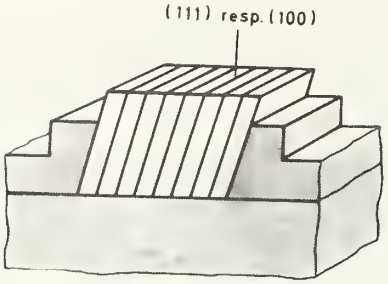

Figure 5. Calibration block consisting of several samples with different resistivities and (111) or (100) surface orientation.

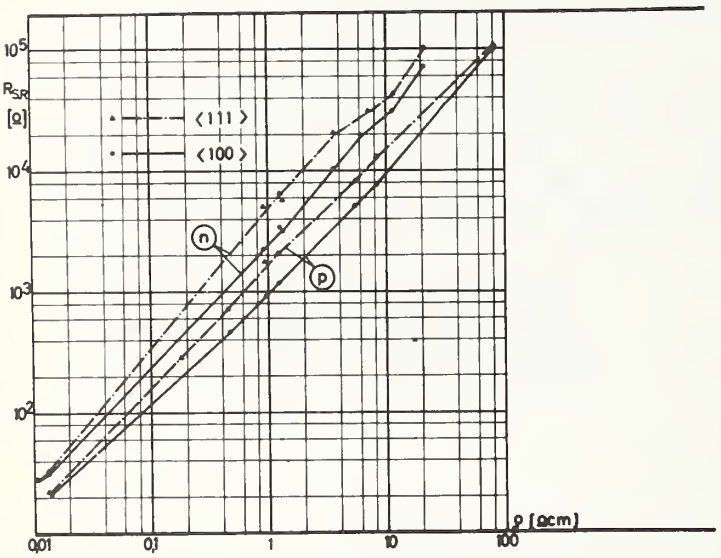

Figure 6. Spreading resistance for n and p-type material and for (111) and (100) surface orientation. (ASR-100, probe spacing 0,6 mm, two tungsten probes (tip radius 25 µm) with a load of 20 g each).

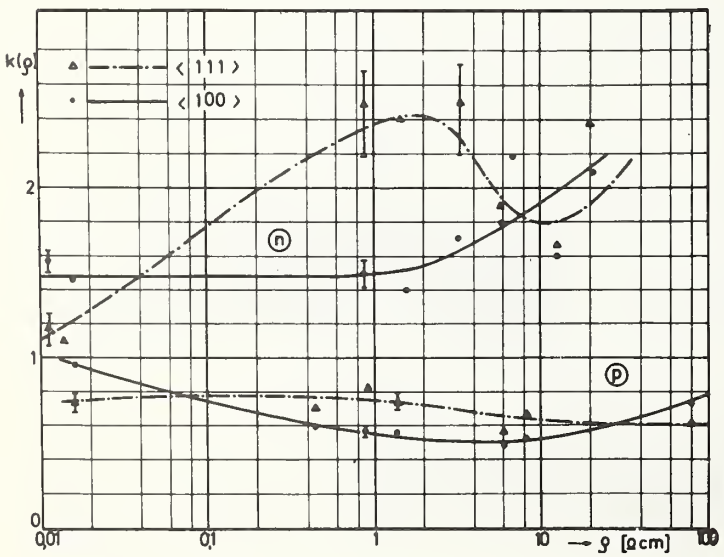

Figure 7. Resistivity dependent correction factor derived from figure 6 with values of contact radius from table 2.

NATIONAL BUREAU OF STANDARDS SPECIAL PUBLICATION 400-10, Spreading Resistance Symposium, Proceedings of a Symposium Held at NBS, Gaithersburg, Md., June 13-14, 1974.

On the Calibration and Performance of a Spreading Resistance Probe

H. J. Ruiz and F. W. Voltmer

Texas Instruments Incorporated
Dallas, Texas 75222

In this paper, techniques are presented for material standards selection for calibration purposes, materials and calibration block preparation, and techniques for data collection and processing for the spreading resistance probe. A description of the variation with time of the calibration of a spreading resistance probe is presented. Problems encountered with characterization of high resistivity p-type silicon are discussed, and examples of the probe performance in the characterization of germanium are also presented.

Key words: Automated resistivity measurements, calibration, germanium characterization, sample preparation, silicon characterization, spreading resistance, surface effects.

1. Introduction

Spreading resistance measurements [1][1] are currently being used throughout the semiconductor industry to characterize semiconductor materials in the bulk [2,3], in epitaxial, diffused, and buried layers [1], and in some cases in finished devices [4]. The method consists in measuring the total resistance of a metal-semiconductor point contact and relating it through empirical calibrations of the bulk resistivity of the material.

Spreading resistance measurements today provide the most practical tool for characterizing semiconductor materials, especially those involving n/n^+ and p/p^+ structures. The spreading resistance, R_s, of a circular contact [5] of radius a on a material with resistivity ρ is given by

$$R_s = \rho/4a \tag{1}$$

However, it has been shown [1] that the exact relationship between spreading resistance and material resistivity must be modified by an empirical factor K such that

$$R_c = KR_s \tag{2}$$

where R_c is the total electrical resistance between the metal probe and the silicon. Depending on the probe material used and the experimental conditions, several authors [6] have shown marked variations in the behavior of K as a function of resistivity. Nevertheless, all previous work seems to agree that the effective contact radius of the probe increases towards low and high resistivity values for both n- and p-type silicon. In obtaining accurate calibration data, the parameters of importance in achieving good accuracy and

[1] Figures in brackets indicate the literature references at the end of this paper.

reproducibility are sample surface preparation, temperature control of the samples, a good set of bulk material standards whose resistivity has been determined by a different method such as the four-point probe, and properly conditioned probes. Careful selection of material standards cannot be over-emphasized.

2. Equipment Description

2.1. Probes

Two different apparatuses were used in obtaining the data presented in this report. One of the apparatuses was an in-house design with electrically activated mechanisms for all moving parts. The probe tip material was an osmium-ruthenium alloy which has a 6 μm tip radius and operated under a 20 gm load. The other spreading resistance probe had air-accuated relays for all moving parts, an osmium-tungsten alloy probe tip with a 25 μm radius, and operated under 40 gm loading. The probe assembly and the stepping motor were obtained from Solid State Measurements, Incorporated.[2]

2.2. Electronics

Two probes make contact with the material surface to be characterized. The probe spacing is 600 μm. The sample to be measured is generally electrically floating and the probes are biased at +10 mV and -10 mV. By measuring the current flowing between the probes, one calculates electronically the value of R_C, and a logarithmic amplifier provides a signal proportional to the value of the spreading resistance. By adjusting the value of R_O, the bias resistance for zero current flow, one can cover values of spreading resistance from 1 Ω to 100 MΩ. The electronics are calibrated by shunting the probes with a 1% resistor of the appropriate value, and adjusting the electronics so that the appropriate reading is obtained. Shunting resistors from 1 Ω to 100 MΩ are available in the instrument. To avoid the erratic behavior of rotary switches in the calibrate mode, push-button switches are used to activate mercury-wetted relays. Thus, in the calibrate mode, one can for example change the shunting resistor from 1 Ω to 10 KΩ without having to go through the decades in between.

2.3. Data Processing

The signal in millivolts which is proportional to the value of the spreading resistance is digitized through a millivoltmeter, passed through an interface card, and fed into an HP9810 minicomputer. The data can be on line converted to spreading resistance, resistivity, carrier concentration, and plotted simultaneously on either a linear or logarithmic scale. A program is also available for providing on line single layer correction factors when characterizing single layer epitaxial or diffused films. The data obtained from the minicomputer can be stored in magnetic tape, punched tape, or IBM cards for further processing, as is the case when one performs multilayer analysis of the data.

3. Calibration Block Preparation

3.1. Material Standards Selection

Silicon wafers in the range .01 to 100 Ω-cm were selected as potential material standards for calibration blocks. Using a 4-point probe for resistivity measurements, approximately 100 wafers were found in the desired resistivity range for both n- and p-type material. Out of these wafers, ∿20 were selected for each type as material standards for calibration. The wafer selection was achieved through the following procedure:

(a) Each wafer was measured 10 consecutive times on 10 different occasions (a total of 100 measurements) near the center of the wafer. For example, see table 1.

---

[2] Solid State Measurements, Inc., 600 Seco Rd., Monroeville, Pa. 15146.

(b) The measurements were corrected for temperature and thickness variations.

(c) Near the center of the slice, resistivity readings were made .5 mm apart, and slices which exhibited more than 10% variation in the readings were rejected as material standards. Spreading resistance measurements were also used to determine which wafers had less than 10% microsegregation of dopant.

(d) The resistivity value of the wafers chosen was the average of the 100 readings described in (a), and an attempt was made at obtaining a minimum of 4 different material standards per decade in resistivity.

3.2. Materials Preparation

The wafers chosen were individually waxed down on microscope glass slides. Using a diamond wafering saw, .5 mm × 1.0 mm × 20 mm bars were cut out from each wafer as indicated in figure 1. One bar from each of the wafers selected as material standards was waxed down on a 0° stainless steel block which was threaded for mounting under the spreading resistance probe. All of the bars were waxes down adjacent to each other and in order according to resistivity to facilitate measurements to be made. Using a silicon carbide 1200 grit, the samples were ground to the same thickness. Lustrox[3] 1000 was then used to chemically-mechanically polish the samples until a scratch-free mirror-like surface was obtained.

Table 1. Example of Four Point Probe Readings Taken for Material Standard Evaluation for Calibration Purposes

		1	2	3	4	5	6	7	8	9	10
Sample	1	1.040	1.057	1.051	1.056	1.042	1.043	1.060	1.045	1.043	1.035
No.	2	1.030	1.053	1.055	1.054	1.053	1.034	1.052	1.051	1.042	1.035
11	3	1.040	1.059	1.059	1.062	1.051	1.044	1.051	1.054	1.052	1.036
	4	1.040	1.053	1.055	1.068	1.050	1.037	1.052	1.042	1.054	1.043
N-Type	5	1.050	1.060	1.051	1.065	1.051	1.037	1.056	1.051	1.040	1.040
⟨111⟩	6	1.050	1.060	1.058	1.058	1.060	1.040	1.048	1.048	1.035	1.034
	7	1.046	1.055	1.067	1.050	1.051	1.046	1.059	1.048	1.042	1.037
	8	1.050	1.056	1.057	1.060	1.054	1.042	1.045	1.050	1.045	1.043
	9	1.057	1.062	1.054	1.049	1.055	1.039	1.049	1.043	1.048	1.041
	10	1.055	1.068	1.058	1.053	1.063	1.045	1.058	1.051	1.050	1.047
Average		1.0458	1.0583	1.0565	1.0575	1.053	1.0407	1.0530	1.0483	1.0451	1.0391

Average = 1.0497; Standard Deviation = .00695

4. Probe Calibration

4.1. Technique

4.1.1. Data Collection

The calibration block containing the prepared bars is mounted under the probe apparatus for spreading resistance measurements. Twenty measurements, one every 20 μm, are made on each one of the bars. The measurements are made automatically, the data is electronically transferred on line to an HP9810 computer, and the computer computes the average value of spreading resistance of each bar, and stores it along with the standard deviation of each set of measurements. The process continues until all of the bars in the calibration block have been read. The computer has stored the resistivity value of each one of the bars.

---

[3] Trademark of Tizon Chemical Corporation, Flemington, New Jersey.

4.1.2. Data Processing

Once the measurements have been completed on the calibration bars, a linear least square fit is performed on the logarithm of the spreading resistance and the logarithm of the resistivity of each bar. A printout is obtained of the least square fit parameters of the data and the correlation of the data points in relation to a linear fit. At the same time, a plotter, on command from the HP9810 computer, plots the data points and the line representing the linear fit of the points on log-log graph paper. An example of the type of graphical display of the calibration data is shown in figures 2 and 3. Figure 2 corresponds to calibration data on n-type material, and figure 3 corresponds to calibration data on p-type material.

4.2. Calibration Parameters

The expression for spreading resistance is given by

$$R_S = \frac{K\rho}{4a} \tag{3}$$

Over the range of interest, let us neglect the dependence of the empirical factor K on the resistivity of the material ρ. We thus have

$$\rho = \gamma R_S \tag{4}$$

where γ is a constant. A linear fit through the calibration data points shown on figures 2 and 3 gives an equation of the form

$$\text{Log } \rho = A \text{ Log } R_S + B \tag{5}$$

where A is the slope of the line and B is its intercept (A and B will be called calibration coefficients). For figure 2, the values of A and B are 1.025 and -3.466 respectively. In figure 3, A and B are .989 and -2.99 respectively. From the calibration coefficients we can compute the resistivity of material of spreading resistance R_S through

$$\rho = 10^B R_S^A \tag{6}$$

4.2.1. Variation of Calibration Coefficients with Time

Weekly during the past two years, we have performed calibration runs of the spreading resistance probe using the same calibration block. Figure 4 shows the statistical distribution obtained from the measurements made on each one of the different samples on the calibration blocks. One should note that the standard deviation of the measurements becomes larger with increasing resistivity, specially in p-type material. Figure 5 shows a plot of A and B as a function of time for three sets of identical probes. The places where the value of coefficient A took a sudden deviation appeared to correlate very well with that point in time in which the probes became erratic with an increased amount of scatter. After the probes were replaced, the behavior of the calibration coefficients was back to "normal." The model proposed in equation (3) implies either a linear relationship between R_S and ρ or a functional dependence of K on ρ. In the range over which our calibrations are made, it is important to know whether or not the linear relationship holds. In equation (5), the value of A determined over 100 calibration runs is such that A = 1.000 is within the σ limits of the frequency distribution of A. This implies that the linear model described in equation (3) is valid. While we use the specific value of A as determined in the weekly calibration runs for determining sample resistivity, it would be equally valid from a statistical point of view to set A equal to unity. However, our data definitely establish that n- and p-type silicon behave differently. The difference in the value of B must be due to a dependence of K on the semiconductor material, its orientation, and type. Figure 6 shows a variation of the calibration coefficients for different probe materials. Figure 5 corresponds to data taken with 25 μm radius probes made of osmium-tungsten alloy at 40 gms loading. Figure 6 corresponds to 6 μm radius probes made of osmium-ruthenium alloy with 20 gms loading. Figure 7 corresponds to histograms showing the frequency distribution of

coefficients A and B for both n- and p-type calibrations. Each set of probes that exhibited a marked deviation in the calibration coefficients as shown in figure 5 was discarded. This occurred after about 250,000 measurements.

4.2.2. Comparison of Two Probes

The performance of the two probes has been similar, except that the osmium-ruthenium probe exhibits larger scatter in the high resistivity end, specially on p-type material. Typical calibration factors for both probes are summarized below for p-type material.

	6 μm Radius, 20 gms Load Osmium-Ruthenium Probe	25 μm Radius, 40 gms Load Osmium-Tungsten Probe
A	.992	.990
B	-3.25	-2.950
% scatter at 70 cm p-type	∿20%	<5%

The range over which A varied for the osmium-tungsten probe was from .91 to 1.08. For the osmium-ruthenium probe, the range of variation of A was from .90 to 1.07. The difference in B of the probes is indicative of the difference in the electrically active radius of each probe.

5. Probe Performance

5.1. Characterization of N- and P-Type Silicon

In the resistivity range of .01 to 100 Ω-cm, the performance of the probe was very satisfactory on n-type material. Measurements obtained in this range were within 10% of measurements obtained on the same material using other characterization technqiues [7], i.e., C-V measurements, 4-point probe measurements, etc. Characterization of p-type material had similar performance in the .01 to 10 Ω-cm range. For resistivities larger than 10 Ω-cm however, the measurements were not as reproducible and were very sensitive to the conditions of the sample surface. The empirical factor K in equation (2) has a different value for p-type material than it does for n-type material. As can be seen from the calibration plots of figures 2 and 3, the parameter K is more sensitive in the high resistivity region of both n- and p-type calibrations.

5.2. Problems with High Resistivity P-Type Silicon

We have observed that surface preparation of the samples can contribute considerably to error in the characterization of high resistivity p-type silicon. A mechanically polished p-type high resistivity sample (∿70 Ω-cm) was used in the measurements to determine the effect of surface preparation on spreading resistance measurements. The sample was first measured as received and the point is the first one on figure 8. The sample was then placed in boiling water for the amounts of time indicated in figure 8. At the end of each time cycle, the sample was allowed to dry in air and reach room temperature before measurements were made. The bars in figure 8 indicate the range over which the data scattered. It is important to note that neither an HF dip nor a boiling water bath affected the readings obtained on a sandblasted piece of silicon from the same slice. This clearly indicates that surface effects on a polished slice are a dominant factor in resistivity determination of high resistivity p-type material. In an effort to determine if surface conduction was a dominant factor in the phenomena, the following experiment was performed. A piece of the slice being used in this experiment was sandblasted everywhere except for two circular areas about 200 μm in diameter. The distance between the center of these areas was ∿600 μm, the probe separation. It was believed that microcracks introduced into the surface this way would impede carrier motion along the surface. However, this did not occur and the behavior of this specially prepared sample was identical to that shown in figure 8. We also had a slice cleaved in two pieces and placed on the sample holder such that each probe would fall on a different piece. The two pieces were far apart physically so that the only

current path was through the vacuum chuck. Again, the behavior was the same. In an attempt to gain understanding of this phenomenon, the following experiment was also performed. A high resistivity slice, p-type, was placed in an oxidizing ambient for various times. The resistivity of the slice as determined by the spreading resistance probe was measured as a function of oxide thickness and the results are shown in figure 9. The measurement accuracy of oxide thickness below 50 Å was questionable; however, the data point out an interesting surface phenomena. At this point, the only conclusive statement we can make about our observations is that we are not dealing with a problem of surface conduction, but rather a problem having to do with metal-semiconductor contacts which are markedly affected by surface treatment or condition of the material. Again we must point out that we do not observe this phenomena in n-type material up to ∿150 Ω-cm in resistivity. In performing our measurements and calibration on p-type material higher than 10 Ω-cm, we have had to re-polish the calibration block previous to any characterization of freshly polished material.

6. Summary

Techniques have been presented for the calibration of spreading resistance apparatus and the preparation of material standards for calibration purposes. It has been shown that with proper care in the material standards selection and preparation, one should be able to obtain an accuracy of 10% for measurements on both n- and p-type silicon in the range .01 to 100 Ω-cm. However, for resistivities higher than 10 Ω-cm, special attention must be paid to surface treatment and condition of the samples to be measured. The relative accuracy of the probe can be ∿1%, as has been shown by shunting the probes with a resistor of value between 10 and 10 KΩ, and observing that the variations in repeated measurements are ±.5%.

Potential problems have been outlined concerning the characterization of high resistivity p-type silicon. It has also been shown that the performance of the probe on germanium is comparable to its performance on silicon material.

7. References

[1] R. G. Mazur and D. H. Dickey, "A Spreading Resistance Technique for Resistivity Measurements," J. Electrochem. Soc. 113 (1966) 255.

[2] F. W. Voltmer and H. J. Ruiz, "Use of the Spreading Resistance Probe for the Characterization of Microsegregation in Silicon Crystals," 1974 Spreading Resistance Symposium, Gaithersburg, Maryland.

[3] A. F. Witt, M. Lichtensteiger, and H. C. Gatos, "Experimental Approach to the Quantitative Determination of Dopant Segregation During Crystal Growth on a Microscale," J. Electrochem. Soc. 120 (1973) 1119.

[4] H. J. Ruiz and F. W. Voltmer, to be published.

[5] R. H. Holm, Electric Contacts, pp. 11-19, Springer, Berlin (1969).

[6] P. Kramer and L. J. Van Ruyven, "The Influence of Temperature on Spreading Resistance Measurement," Solid State Electronics 15 (1972) 757.

[7] Gregg Lee, Walter Schroen, and F. W. Voltmer, "Comparison of the Spreading Resistance Probe with Other Silicon Characterization Techniques," Spreading Resistance Symposium, 1974, Gaithersburg, Maryland.

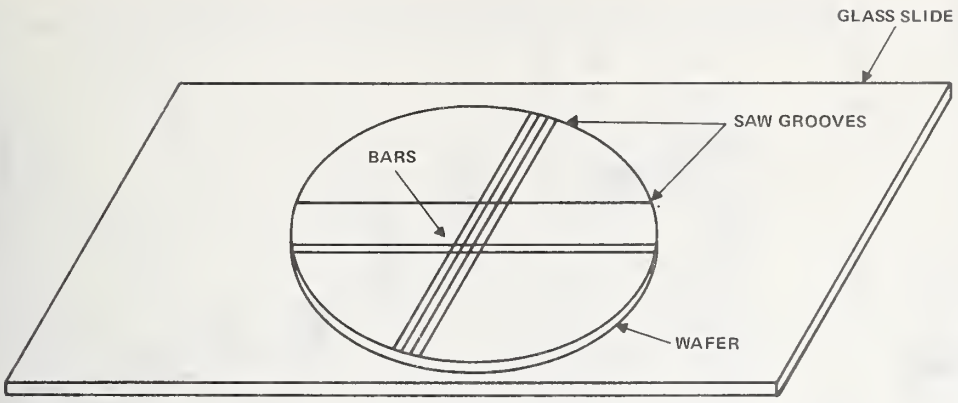

Figure 1. Technique for Obtaining Calibration Bars from Material Standards.

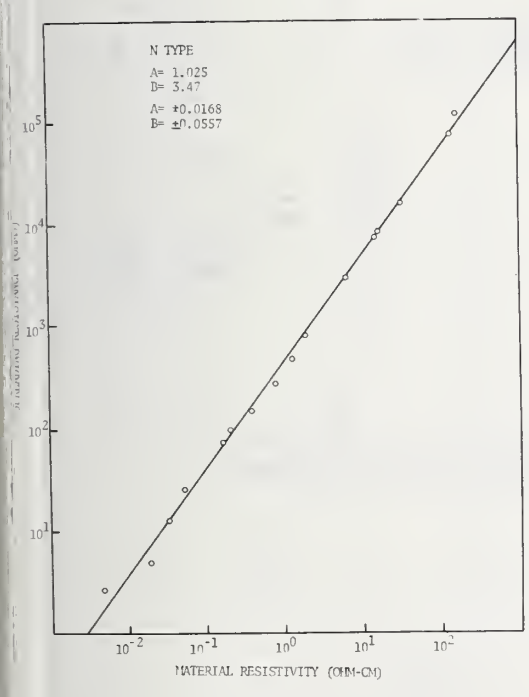

Figure 2. *N*-Type Calibration Curve - Spreading Resistance vs. Resistivity.

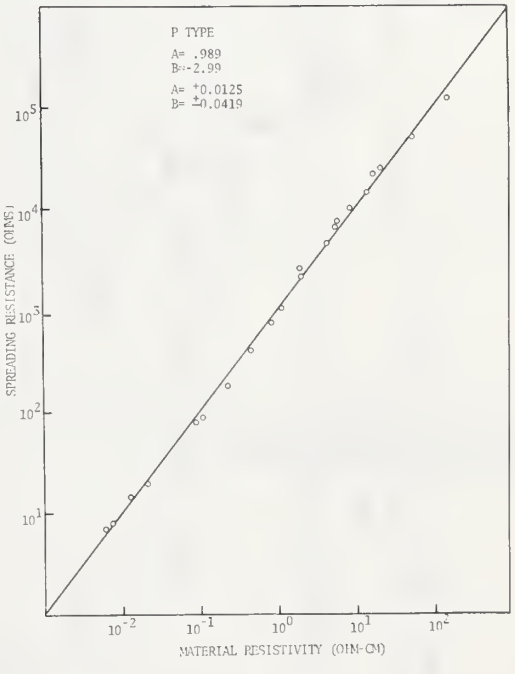

Figure 3. *P*-Type Calibration Curve - Spreading Resistance vs. Resistivity.

565-448 O - 75 - 11

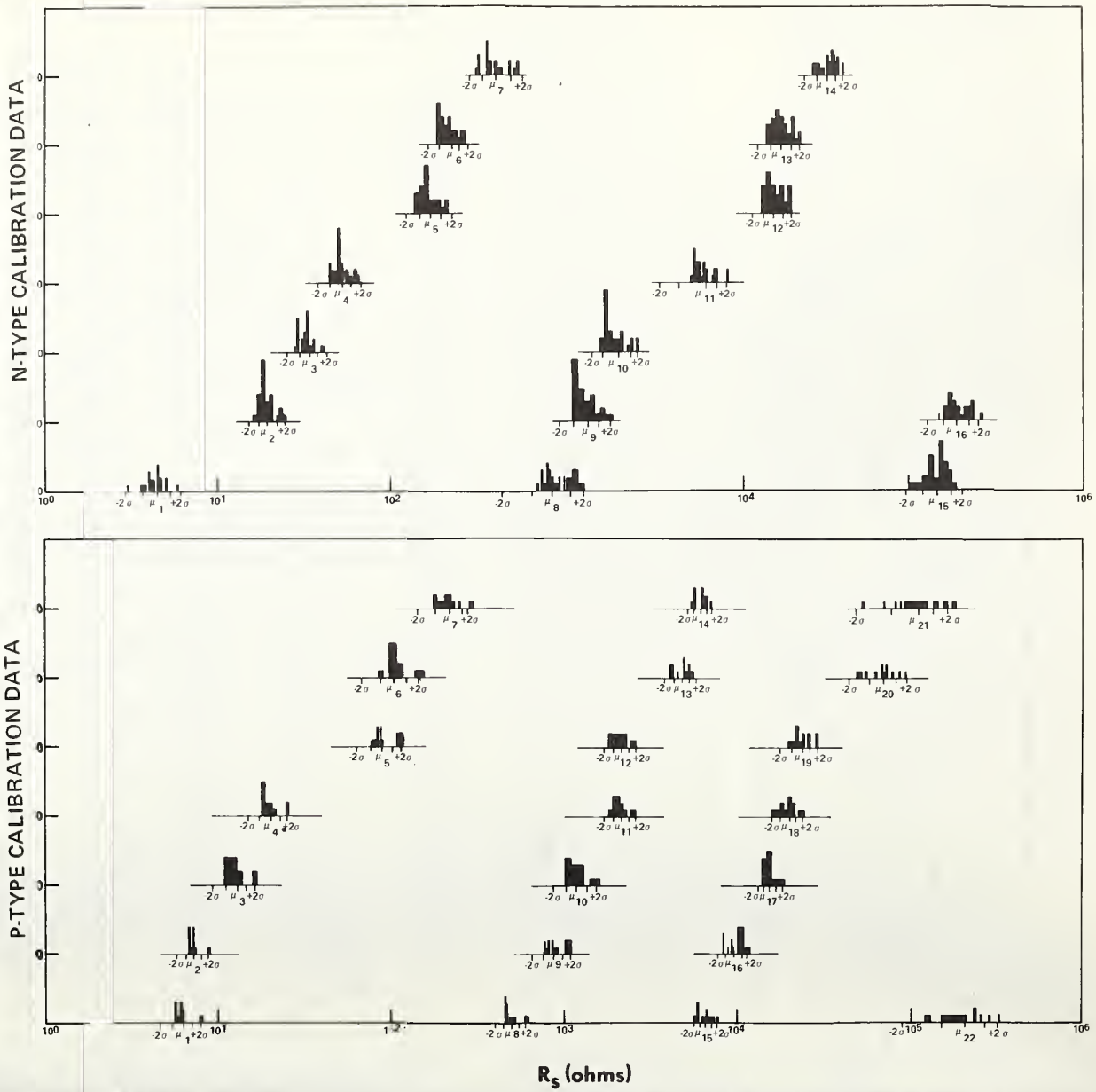

Figure 4. Statistical Distribution of Each Set of Calibration Measurements.

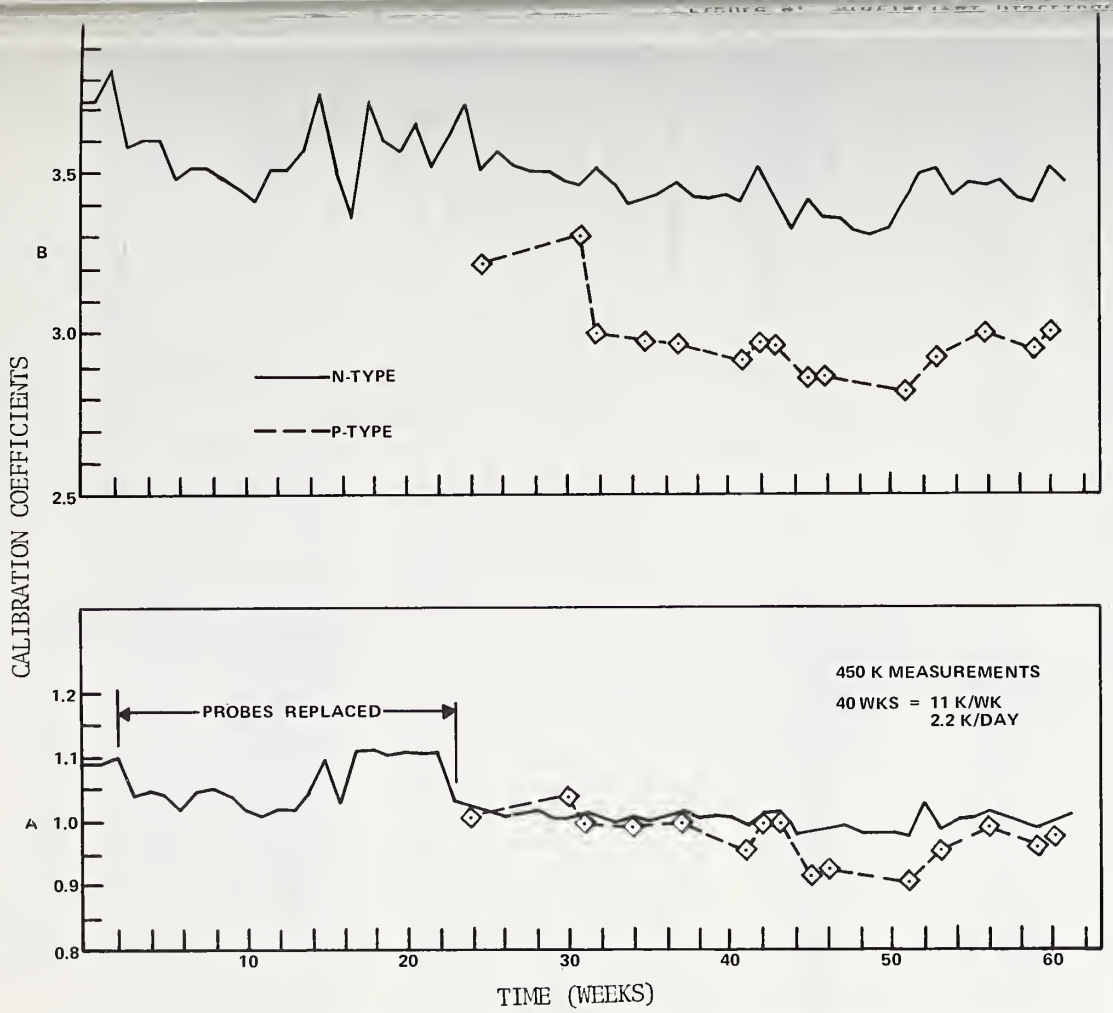

Figure 5. Variation with Time of Calibration Coefficients A and B. 25 μm Osmium-Tungsten Probe, 40 gms. Loading.

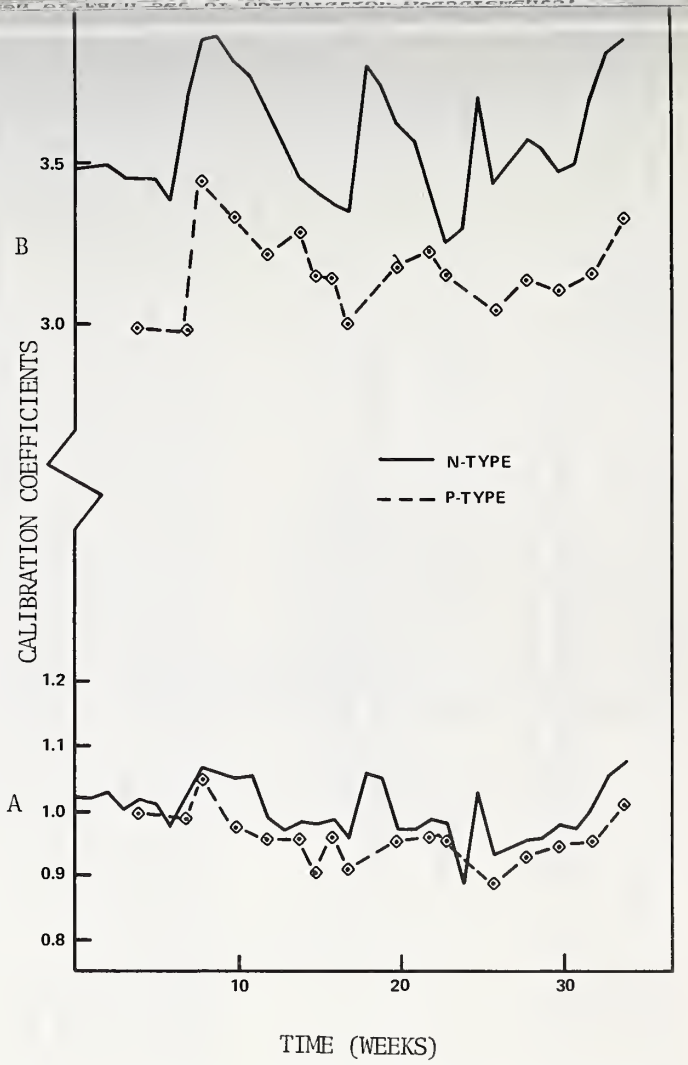

Figure 6. Variation with Time of Calibration Coefficients A and B. 6 μm Osmium-Ruthenium Probe, 20 gms. Loading.

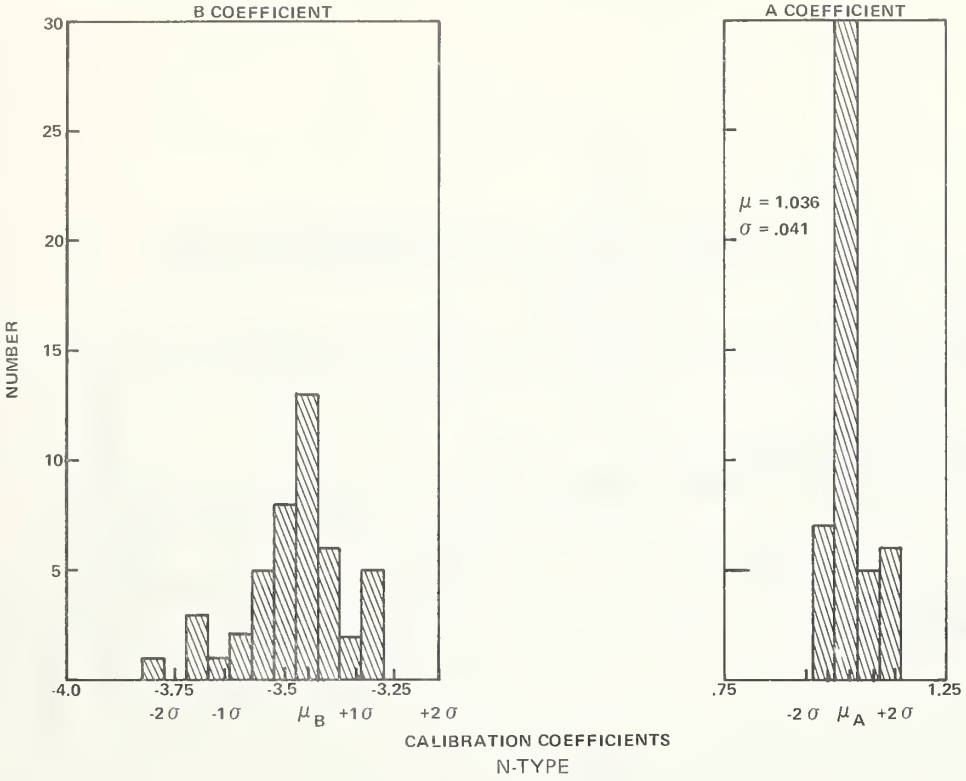

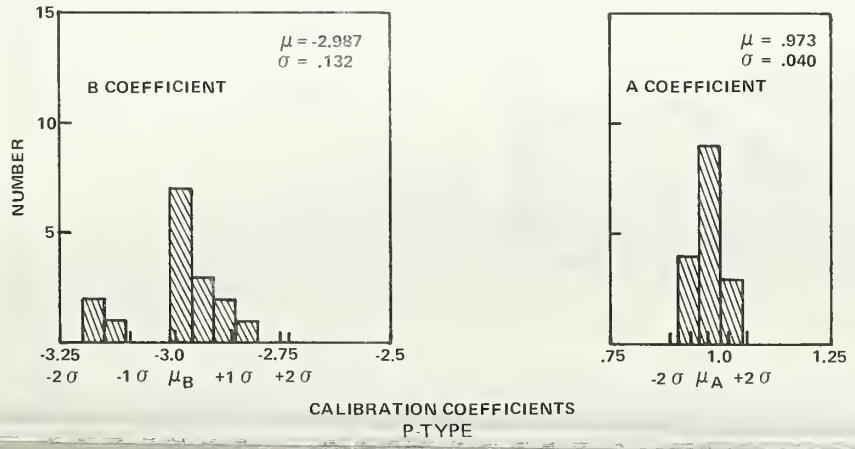

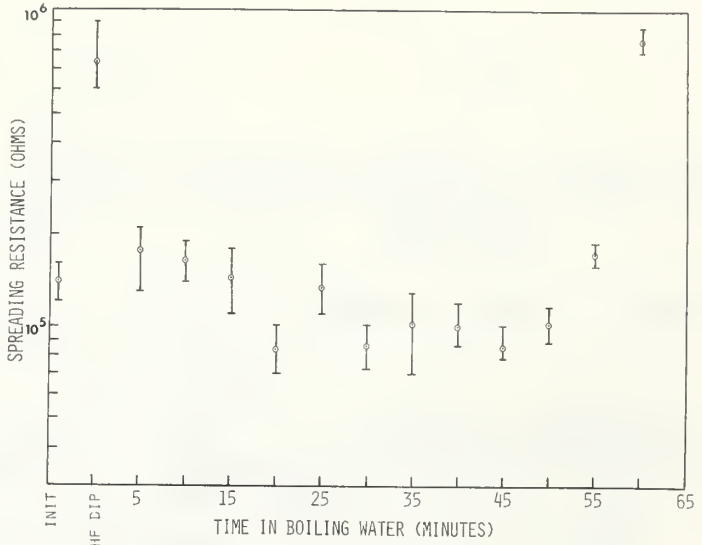

Figure 8. Effect of Surface Treatment on Spreading Resistance Measurements of a 70 Ω-cm *P*-Type Specimen.

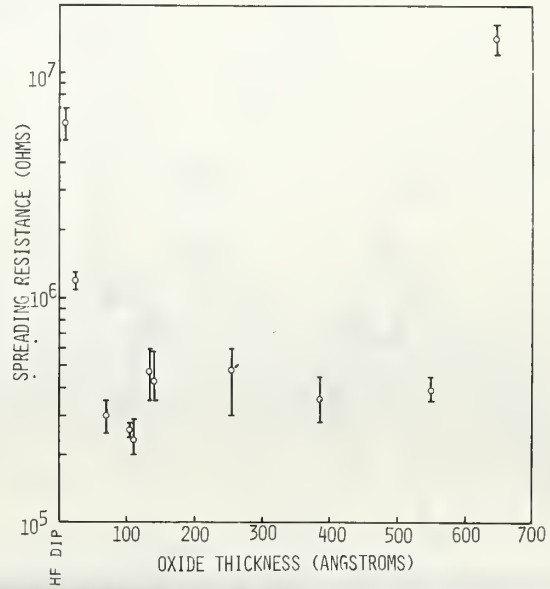

Figure 9. Effect of Oxide Build Up on Spreading Resistance

NATIONAL BUREAU OF STANDARDS SPECIAL PUBLICATION 400-10, Spreading Resistance Symposium,
Proceedings of a Symposium Held at NBS, Gaithersburg, Md., June 13-14, 1974.

Comparison of the Spreading Resistance Probe with other Silicon Characterization Techniques

Walter H. Schroen, Gregg A. Lee, and Fred W. Voltmer

Semiconductor Research and Development Laboratories
Texas Instruments Incorporated
Dallas, Texas 75222

Range and precision of doping concentration data in silicon materials gained by the spreading resistance technique are compared to values obtained by other characterization methods. They include junction and MOS capacitance-voltage techniques, mercury probe, four-point probe, incremental sheet resistance technique, ion microprobe, and optical methods. The comparison considers precision and resolution of each technique, range of silicon resistivities and layer thicknesses, experimental effort, analytical interpretation, and time and cost of data acquistion and evaluation. Examples are presented which demonstrate the range of applicability of each technique and how they can supplement each other so that they cover the total doping range of silicon devices.

Key Words: automation; bevelling; comparison; four-point probe; incremental MOS capacitance-voltage; incremental sheet resistance; infrared spectrometer; ion microprobe; junction capacitance-voltage; lap and stain; mercury probe; Schottky capacitance-voltage; scanning Michelson interferometer; spreading resistance.

1. Introduction

The spreading resistance probe has recently been widely applied as a means of determining semiconductor resistivity. Some uses to which it has been or may be put are shared with other measurement techniques. Thus it has become pertinent to review the general capabilities of the spreading resistance probe and its alternatives and, where possible, to make direct comparisons of the results of one or more techniques.

Spreading resistance is presently employed for three general purposes: production control, measurement of resistivity laterally across a silicon slice, and measurement of dopant concentration versus depth into a sample. The key advantage provided by spreading resistance for production control is its ability to probe small areas within an integrated circuit to measure a local resistivity value. In this application reproducibility is extremely important. For scanning across a silicon slice, the probe measurements must be not only reproducible but also of high precision and volume resolution in order to detect micro-segregation or local oxygen content in crystals. The spreading resistance probe is the only tool which has sufficient spatial resolution to perform this function. Other papers presented at this Symposium discuss the application to production control and scanning measurements of the spreading resistance technique [1 to 6] *, thus this paper is restricted to the comparison of techniques used to measure dopant concentration versus depth, commonly called the dopant profile.

This comparision is performed with two questions in mind. First, for a given measurement, which is the best technique to choose from a number of alternatives. Second, however, how may the capabilities of different techniques be employed to supplement each other to provide a more complete or accurate measurement. A number of points of comparison are pertinent; they are listed in figure 1. Precision and spatial resolution have already been mentioned above. For the present purpose, the range of silicon resistivity and the range of layer thickness which can be resolved are also important. Furthermore, it is useful to know whether or not the measurement process destroys the sample and to know the degree of effort required to obtain the experimental data and then to analyze it. Last and by no means least, is the cost of equipment required for the technique, the cost of making the measurement and of analyzing the data.

A point worth mentioning is that the spreading resistance probe and many other techniques discussed here measure electrically active dopants. For many investigations it is advantageous to supplement this capability with a technique able to measure the total concentration, or active plus neutral dopants. The comparison of this paper will first be concerned with techniques measuring only electrically active dopants; for the purpose of supplementing the spreading resistance probe, it will then list briefly the capability of total concentration techniques.

2. Capabilities and Limitation of the Spreading Resistance Probe

The local impurity concentration η is inferred from the local measured resistivity according to the expression

$$\eta = 1/\rho_1 q\mu(n),$$

where the mobility, μ, is inferred as a function of the carrier concentration n, and ρ_1 is the measured local resistivity. In the spreading resistance technique, the contact resistance of the small metal-semiconductor contact is determined and related to the resistivity by the fundamental relation

$$R_s = \frac{V}{I} = \frac{\rho_0}{2 r_o} = \frac{\rho_1 \times C}{2 r_o},$$

where r_o is the effective radius of the probe contact, determined by calibration with known resistivity standards. C is the "correction factor" [7] which reduces the measured resistivity ρ_1 to the true resistivity ρ_0.

The spreading resistance probe lends itself to automated operation, data acquisition and data evaluation. A sophisticated probe is capable of operating as either a "one-point" or two-point probe. The descent rates on static loading may be controlled independently for the two probes to ensure a constant and identical contact area for each probe. The probes have been calibrated for silicon, and the linear slope of unity, when spreading resistance is plotted versus resistivity, verifies a constant contact area. A highly developed mechanical system allows stepping in 2.5, 5, 10, 25, 50, 100, and 250 μm steps automatically, through a 1-inch translation. Smaller steps can be taken, but the mechanical damage to the silicon owing to probe impact would overlap, and it is still debated whether actual measurement can be taken under these conditions. The entire mechanical control system is pneumatic, ensuring that during electrical measurement of the resistivity, the system is otherwise in a quiescent state.

A constant 10 mV potential is applied to the probes after they contact the surface, and the current is measured using a log converter which is linear over 8 decades. Standard resistors are used to calibrate the spreading resistance. The calibration between spreading resistance and resistivity is obtained by measuring silicon samples of known resistivity and from the resistivity and spreading resistance determining the contact area. The resistivity can be determined using either a calibrated 4-point probe or by making Hall measurements. The precision of these calibrations depends on the homogeneity of the reference sample, which can be determined by qualitative spreading resistance measurements.

3. Comparison of Profiling Techniques in Reference to Sample Processing

Figure 2 lists five profiling techniques which are generally used for determining the concentration of electrically active dopants: spreading resistance, incremental sheet resistance, incremental MOS capacitance-voltage, junction capacitance-voltage, and MOS and Schottky contact capacitance-voltage. In addition to these techniques, the four-point probe and lap and stain techniques are listed for supplying reference points. Section 6 of this paper discusses supplementary techniques for determining active plus neutral dopants, namely the ion microprobe, several optical methods, and the nuclear activation analysis.

A comparison and overlay of the most appropriate and accurate profiling techniques is presented in figures 3, 4, and 5. (see also [8]). The sequence of transistor processing steps is illustrated for typical impurity concentrations and

depths. The superposition of the techniques is shown at decisive processing stages: in figure 3, after the diffusion of the buried layer, in figure 4, after epitaxial deposition, and in figure 5, after base and emitter diffusions. The symbols indicating the various techniques have not been selected as actual data points, but rather to indicate the qualitative capabilities of the techniques. The connecting line has been added for clarity, but does not represent an actual theoretical model.

The most versatile technique is the spreading resistance probe. It is shown qualitatively as "uncorrected data," this means the data as measured by the probe and translated into concentration values as though each measurement were made on a homogeneous sample. By applying a multilayer model analysis these data points can be brought into close agreement with theoretical predictions and also with other techniques such as the junction CV data [7,9]. The spreading resistance probe can cover the widest range of doping concentrations, it can be used to measure both very shallow layers and deep diffusions. It can probe close to pn-junctions and can measure both n- and p-type conducting material. It is the only convenient technique to monitor buried layers and deep diffusions.

3.1. Incremental Sheet Resistance Technique

The incremental sheet resistance technique for determining concentration profiles had been used extensively in the past several years [10] for the identification of control problems in the manufacture of shallow devices ($<1\,\mu$m). The method consists of measuring the sheet resistance after removing thin (about 200 Å) layers of silicon by anodic oxidation and stripping in HF. From the resistivity profile, a concentration profile is obtained by using suitable conversion data, such as that of Irvin [11]. The incremental sheet resistance is an absolute technique since it compares differences of resistivity data. It is the best technique known for measuring profiles in the high concentration regime and in extremely shallow layers. It fails, however, to measure concentrations lower than 1×10^{18} carriers/cm^3, so that it is difficult to probe close to junctions. The primary drawback of the technique is the long period of time necessary to perform the anodization and stripping experiments. An experienced technician may take at least one day to measure a profile. The evaluation of the data can be automated, but little automation can be applied to the experiment itself.

3.2. Incremental MOS Capacitance-Voltage Technique

The relatively new incremental MOS CV technique [12] is capable of acquiring precise data in extremely thin layers, such as ion implanted layers and bases of microwave transistors. The technique is best applicable at lower doping concentrations, in particular concentrations where the incremental sheet resistance technique can no longer acquire data (i.e., at concentrations lower than 10^{18} carriers/cm^3). The incremental MOS CV technique removes thin layers of silicon by the growth of anodic oxide. MOS CV measurements are made after each oxidation. The oxide is then removed, a new oxide is grown and another MOS CV measurement is made. The process is repeated enough times to acquire data for a complete profile. For each MOS CV curve the maximum width of the space charge layer W_m is determined and plotted versus X_s, the total thickness of silicon removed. The impurity profile is found by calculating the curve W_m (X_s) for a series of theoretical profiles. The profile whose W_m (X_s) curve matches the experimental curve, is taken as the correct profile. The difficulty with this technique is its very time consuming experimental procedure, which is even slower than the incremental sheet resistance technique, and the instability of the anodic oxide. It turns out that only for aluminum metallization is the anodic oxide stable enough for precise capacitance measurements. Processes have unfortunately not yet been developed to grow oxides stable enough for mercury probe contacts or gold ball bonds, either of which would accelerate the data acquistion. Another requirement of the incremental MOS CV technique is an extensive analytical computer program to convert the depletion region measurements for concentration data. This analytical technique is particularly demanding when very steep profiles are considered, such as a three order of magnitude change in concentration over a depth of $.2\,\mu$m [12].

3.3. Junction Capacitance-Voltage Technique

The junction CV technique is one of the most effective methods of determining the concentration profile in epitaxial material. An automated real-time system is shown in figure 6; it permits acquisition of CV data, transfer of the data into a computer, evaluation of the data for the plot of doping concentration vs. geometrical distance, and output of the data in printed form or by an x-y recorder. The expected profile as it relates to the cross sectional geometry of the sample-under-test, is shown in the upper left portion of figure 6.

In addition to automated data taking, computer programs have been developed [13] which take into account several corrections of the junction capacitance-voltage data. One correction is for the toroidal capacitance surrounding a circular capacitor dot; the smaller the dot area relative to diffusion depth, the more important the contribution of this toroidal capacitance. Another correction is the contribution of the capacitance caused by the space charge layer penetration into the heavily doped side of the diffused junction. In figure 7 the two corrections are seen to pull the profile in opposite directions and in this sense are compensating corrections. In the example shown, the importance of the corrections is that the resistivity of the epitaxial material varies from 3.1 to 3.7 ohm cm (18% variation) and the thickness of the epitaxial material varies from 5.0 to 6.1 μm at 10^{16} carriers/cm^{-3} concentration (20% variation).

For efficient process evaluation, electrical data acquisition and evaluation should be automated through the largest extent reasonable. Not only does automation save time, it also reduces the involvement of human operators and simplifies data retrieval. An example of an automated data reduction scheme is shown in the lower part of figure 6. Another more general example is given in figure 8. A coupler system connects standard laboratory instrumentation with a programmable calculator and allows data output on paper tape; an x-y recorder displays the evaluated measurements.

3.4. Mercury Probe and Schottky Capacitance-Voltage Technique

A modification of the junctions CV technique is the mercury probe or Schottky CV method. It employs a mercury dot of precisely determined and reproducible area to contact silicon surfaces directly without the need of fabricating a junction. Consequently, it lends itself for investigating unprocessed material (except for cleanups) with regard to doping concentration and layer thickness. The method is thus nondestructive except for some possible but reversible mercury contamination of the semiconductor surface. The relatively minor limitations of the mercury CV technique are: A back-side contact is required for the slice; the sample should be flat to the order of the mercury contact area; and the operation is limited to the breakdown voltage of the Schottky contact. The Schottky CV and the MOS CV technique are applicable only to thin or lightly doped epitaxial layers. When thick or heavily doped epitaxial layers have to be measured, one has to resort to the junction CV technique where part of the layer is used up by the diffusion. It should be stressed again that because of its nondestructive operation, the mercury contact or multiple mercury contacts lend themself for automated real-time on-line production control.

3.5. Examples for Comparison of Techniques

Figure 9 shows an overlay of actual data points for spreading resistance measurements, junction capacitance-voltage measurements, and mercury probe capacitance-voltage measurements. For the spreading resistance probe, both data "as taken" and after multilayer analysis are shown. It can be seen that there is very good agreement for the surface value of the concentration for all three techniques after the spreading resistance data has been analyzed. The profile then proceeds to show the epitaxial concentration and the interface of the epitaxial layer and the diffusion of the buried layer (see figure 7). There is also very good agreement between the three techniques for the definition of the epitaxial thickness and the slope of the buried layer. The dip of the concentration displayed by the analyzed spreading resistance data is an artifact of the multilayer analysis and is discussed in other papers at this Symposium [7,9]. In brief, the dip is caused by an overreaction of the multilayer analysis to this steep increase of concentration under the epitaxial layer. In addition, the multilayer analysis assumes that a circular contact is made between the probe and the silicon while in reality there are many microcontacts in an array. Since it is an artifact, this dip can be disregarded.

Figures 10 and 11 illustrate the outstanding capabilities of the incremental sheet resistance for determining profiles in very shallow layers. This technique has been used in the past few years as a tool for ion implantation investigations and the development of models for doping profiles. Figure 10 shows the capabilities of the incremental sheet resistance technique for ion implant boron modeling. A dense array of data points can be acquired in very shallow layers and at relatively high concentrations. The data points fit very well the model predictions developed by Prince and Schwettman [14]. The technique has successfully identified small discrepancies between theory and experiments, such as indicated in figure 10 for the conditions of 1000°C annealing temperature at 30 minutes steam oxidation and the choice of the segregation coefficient k = 10. On the other hand, figure 10 clearly exhibits the limitations of the incremental sheet resistance technique. Carrier concentrations smaller than about 2-10^{17} cm^{-3} cannot be resolved. The technique is therefore not able to probe close to p-n junctions.

Figure 11 demonstrates the capabilities and limitations of the incremtnal sheet resistance probe for implanted arsenic and comparison with As implant models. The probe is able to detect the arsenic tail observed in ion implanted arsenic layers and the relative immobility of this tail with annealing times and temperatures. As stated earlier, the incremental sheet resistance technique detects only the electrically active dopants. There is, therefore, a discrepancy between the theoretical model, which accounts for the total amount of dopants, and the electrically active part of it. Models are presently being developed [15,9] to account for the percentage of electrical activation in implanted arsenic.

It is important that the spreading resistance values are "corrected" by the multilayer analysis [7] before they are compared to incremental sheet resistance data. Figure 12 underlines dramatically the shift of the original data points (crosses) towards the corrected values (diamonds and squares). There is good agreement between incremental sheet resistance and spreading resistance values after multilayer analysis has been applied to the spreading resistance data. Right under the surface, however, the spreading resistance technique (diamonds in figure 12) seems to suggest a significant decrease in the phosphorus concentration. The probable origin of this drop is an effective reduction in carrier concentration caused by the formation of a depletion region under the surface generated by the deposition of the protective silicon nitride film. As figure 12 shows, the depletion region is partially reversed and eliminated (square-shaped data points), when the silicon nitride film is removed. Consequently, this doping dip can be disregarded as an artifact.

4. Small Angle Bevels for Spreading Resistance Probe

Figure 13 demonstrates the importance of the protective silicon nitride layer mentioned above. It is mandatory for the extremely shallow bevels of angles of 0.3 degrees or less to have a very well defined edge between the original silicon surface and the slope of the bevel. It has been found that unprotected silicon slices, or silicon oxide-covered slices, may give rounded interface edges. Silicon nitride covered samples, on the other hand, turned out to result in very well-defined sample slope edges when the films exhibited the correct hardness achieved by the right composition between silicon nitride and silicon. Only with this well defined edge is it possible to probe very close to the surface, and thus to measure the very high concentration parts of the doping layers.

5. Techniques for Acquisition for Singular Data Points

Figures 3 and 4 mention two techniques which can supply singular data points for material characterization: The four point probe and the lap-and-stain technique.

5.1. Four-Point Probe

The four-point probe measures the average resistivity or net impurity concentration of substrates or diffused layers. It has been employed as an indispensable material characterization tool for many years. Only recently have test equipment, specimen preparation, measurement procedure, evaluation, and precision been subject to detailed investigation with regard to reproducibility, and has a concise description of the standard method for measuring resistivity of silicon slices with a collinear 4-probe-array been published by the ASTM [16]. The four-point probe determines average resistivities from current and voltage measurements. The evaluation assumes layers whose lateral dimensions are large and whose thickness is small in comparison to the spacing of the probes. For typical probe spacings, this condition is amply met by diffused layers and also by 1 to 3 inch diameter wafers. If either the wafer thickness or the lateral dimension of the semiconductor sample is comparable to the probe spacing, correction factors must be applied [17].

5.2. Angle Lap and Stain Technique

It is the junction between opposite conductivity types where the angle and stain technique delivers an important data point on the concentration profile for material evaluation. Lap-and-stain is destructive. The semiconductor sample, whether large or small, is affixed to a rigid support, whose surface angle (i.e., perpendicular to its long axis) may lie in the range from 90 degrees to approximately 0.1 degree, and this support is held in alignment with a polishing plate by

use of a precision collar. Using the silicon nitride overcoat shown in figure 13, the integrity of the bevel-surface interfac can be preserved. After obtaining a fresh, scratch-free polished surface at some specified angle which will reve diffusion, ion implantation, epitaxial or even damaged layers, the sample is subjected to a combination of illuminatio and chemical (usually acidic) etchants which will sharply distinguish such subsurface qualities as junction depth, abrup concentration changes (in like-type material), shapes of penetration areas, and anomalous defects such as spikes, pipe or induced damage.

6. Techniques for Determination of Concentration of Active Plus Neutral Dopants

6.1. Ion Microprobe

The ion microprobe is able to determine the profiles of diffused or ion implanted layers even for two-componer interactive situations. Figure 14 gives an example of boron and arsenic implanted layers which show a significant effe on the boron distribution after the arsenic implant, the so-called base retardation. The ion microprobe is an importar analysis tool to acquire data for developing two-component interactive doping models [18], and for determining th factor of electrical activation of dopants during annealing or diffusion heat treatments. The ion microprobe destructive.

6.2. Optical Methods

Two nondestructive techniques to measure the thickness of silicon epitaxial material are the dispersive infrare spectrometer and the scanning Michelson interferometer. The IR interferometry, using the reflection inteferen spectrum obtained on an IR spectrometer, has been reviewed recently by Severin [19] and has been exploite extensively during the past decade. A standardized procedure based on IR interference has been adopted by ASTM.

Even though IR interferometer measurements have contributed considerably to simplify the measurement epitaxial films, in particular when based on a computerized system, the problem of mechanical wear resulting fro repeated cycling of the scanning mechanism in an IR spectrometer, remains. An automated scanning Michelso interferometer has been developed [20], based on computer handling of the required Fourier analysis. Since r restrictive slit mechanism is required and a reasonably wide angular aperture can be used without impairing performanc the radiation throughput of the system is quite large. All wavelengths are viewed simultaneously by the detector, and a detector noise-limited system, this multiplexing of the spectrum will especially improve the signal/noise ratio. Tl complete system for the measurement of epitaxial layer thickness utilizing the scanning Michelson interferometer is routine use for volume slice evaluation.

It should be kept in mind, however, that IR measurements are employed for epi films on buried layers of the sa conductivity type, and the value measured is somewhat within the high concentration side of the interface profile (s figure 4, arrow "Reflected IR") since it is there that the absorption and reflection take place. IR measurements cann read epitaxial layers on opposite conductivity type because there is no absorption in the depletion region.

7. Conclusions and Recommendations

When compared with other resistivity profiling techniques, the spreading resistance probe has been shown to be t most versatile. Its precision approaches that of incremental sheet resistance for shallow layers, yet can provide ent doping profiles. It is rapid, and is easily adapted to automation. No special processing is required, other than an lapping, and therefore does not suffer from profile changes owing to oxidation or junction formation as in the C techniques. Spreading resistance profiles can be obtained from finished devices as well.

There are, however, several areas where care must be taken in making spreading resistance measurements. Samp must be carefully and reproducibly prepared and the probe tips must be adequately conditioned. Adequate standa must be available for conversion of spreading resistance to resistivity.

Several explicit recommendations for further work include extremely shallow angle sample preparation, i.e. less han 15', definition of procedures for reproducible surface preparation, establishment of calibration procedures as being efined by ASTM to provide multi-laboratory precision development of on-line multi-layer correction factors for omplex profile evaluation, and reduction of probe spacing to 25 μm for probing smaller bars.

8. References

1] White, J., An automated spreading resistance test facility, NBS/ASTM Symp. on Spreading Resistance Measurements, Gaithersburg, Md., June 1974.

2] Ruiz, H., and Voltmer, F. W., On the calibration and performance of a spreading resistance probe, NBS/ASTM Symp. on Spreading Resistance Measurements, Gaithersburg, Md., June 1974.

3] Goldsmith, N., Experimental investigation of two probe spreading resistance correction factors for diffused layers, NBS/ASTM Symp. on Spreading Resistance Measurements, Gaithersburg, Md., June 1974.

4] Edwards, J., Spreading resistance and MOS C-V radial resistivity profiles of silicon wafers — a direct comparison, NBS/ASTM Symp. on Spreading Resistance Measurements, Gaithersburg, Md., June 1974.

] Voltmer, F., Bulk microsegregation in silicon, NBS/ASTM Symp. on Spreading Resistance Measurements, Gaithersburg, Md., June 1974.

] Vieweg-Gutberlet, F., Investigation of local oxygen distribution in silicon by means of spreading resistance, NBS/ASTM Symp. on Spreading Resistance Measurements, Gaithersburg, Md., June 1974.

] Lee, G. A., Rapid multilayer correction factors, NBS/ASTM Symp. on Spreading Resistance Measurements, Gaithersburg, Md., June 1974.

] Schroen, W., The impact of process control on parameter stability — a review, *Semiconductor Silicon* 1973, ed. by H. R. Huff and R. R. Burgess, (Electrochem. Soc., Princeton, New Jersey, 1973), pp. 738-758.

] Schroen, W., Application of the spreading resistance technique to silicon characterization for process and device modeling, NBS/ASTM Symp. on Spreading Resistance Measurements, Gaithersburg, Md., June 1974.

[10] Donovan, R. P., and Evans, R. A., Incremental sheet resistance technique for determining diffusion profiles, *Silicon Device Processing*, ed. by Ch. P. Marsden (NBS Spacial Publ. 337, Washington, D.C., 1970), 123-131.

[11] Irvin, J. C., Resistivity of bulk silicon and of diffused layers in silicon, Bell Syst. Techn. J. 41, 387-410 (1962).

[12] Kronquist, R. L., Soula, J. P., and Brilman, M. E., Diffusion profile measurements in the base of a microwave transistor, Solid-State El., **16**, 1159-1171 (1973).

[13] Buehler, M. G., Peripheral and diffused layer effects on doping profiles, IEEE Trans. Electron Devices, ED-19, 1171-1178 (1972).

[14] Prince, J. L., and Schwettman, F. N., Diffusion of boron from implanted sources under oxidizing conditions, J. Electrochem. Soc. **121**, 705-710 (1974).

[15] Shah, P. L., to be published.

[16] *1971 Annual Book of ASTM Standard*, (American Society for Testing and Materials; Philadelphia, 1971), Part 8, 697-711.

[17] Smith, F. M., Measurement of sheet resistivities with the four-point probe, Bell System Tech. J. **37**, 711-718 (1958).

[18] Fair, R. B., Quantitative theory of retarded base diffusion in silicon npn structures with arsenic emitters, J. Appl. Phys. 44, 283-291 (1973).

[19] Severin, P. J., On the infrared thickness measurements of epitaxially grown silicon layers, J. Appl. Optics 9, 2381-2387 (1970).

[20] Cox, P. F., and Stalder, A. F., A Fourier transform method for measurement of epitaxial layer thickness, J. Electrochem. Soc. **120**, 287-292 (1973).

COMPARISON OF TECHNIQUES FOR SILICON DOPANT PROFILING

- HOW DO THE CHARACTERIZATION TECHNIQUES COMPARE?
- HOW CAN THE TECHNIQUES SUPPLEMENT EACH OTHER?

PRECISION
RESOLUTION
RANGE OF SILICON RESISTIVITIES
RANGE OF LAYER THICKNESS
SAMPLE CONSERVATION
EXPERIMENTAL EFFORT
ANALYTICAL INTERPRETATION
EQUIPMENT COST
TIME AND COST OF DATA ACQUISITION AND EVALUATION

Figure 1. Comparison of Techniques for Silicon Dopant Profiling

SILICON CHARACTERIZATION TECHNIQUES

- CONCENTRATION OF ELECTRICALLY ACTIVE DOPANTS
  - SPREADING RESISTANCE
  - INCREMENTAL SHEET RESISTANCE
  - INCREMENTAL MOS CAPACITANCE/VOLTAGE
  - JUNCTION CAPACITANCE/VOLTAGE
  - MOS AND SCHOTTKY CONTACT CAPACITANCE/VOLTAGE
  - FOUR POINT PROBE
  - LAP AND STAIN
- CONCENTRATION OF ACTIVE PLUS NEUTRAL DOPANTS
  - ION MICROPROBE
  - OPTICAL METHODS
  - NUCLEAR ACTIVATION

Figure 2. Silicon Characterization Techniques

Figure 3. Profile in Techniques Processing Steps — DUF Through Emitter Diffusion

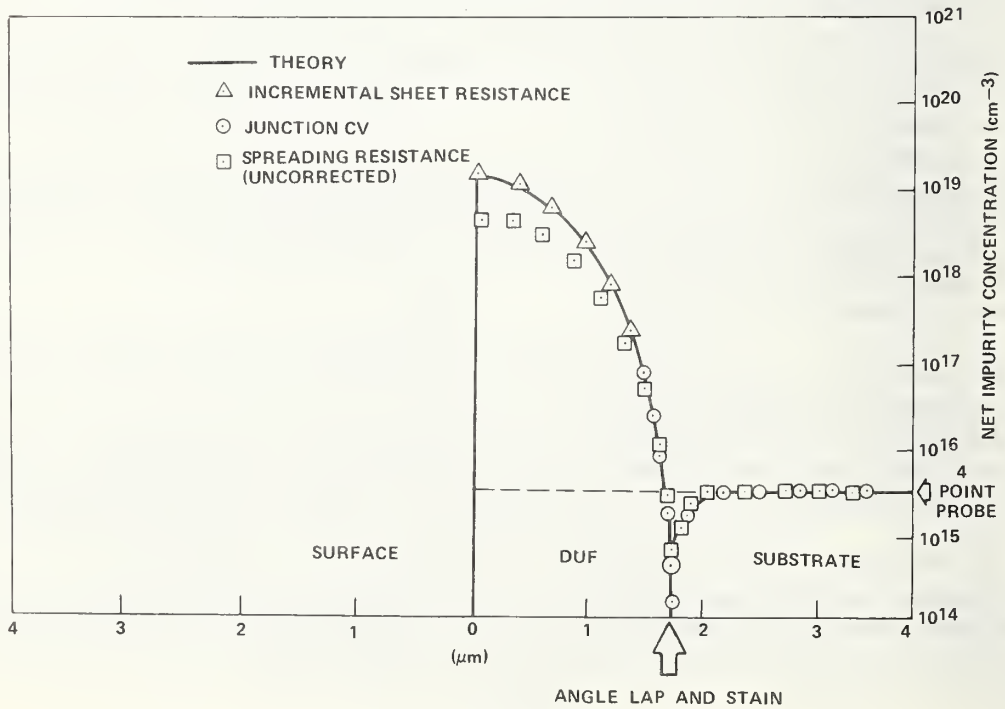

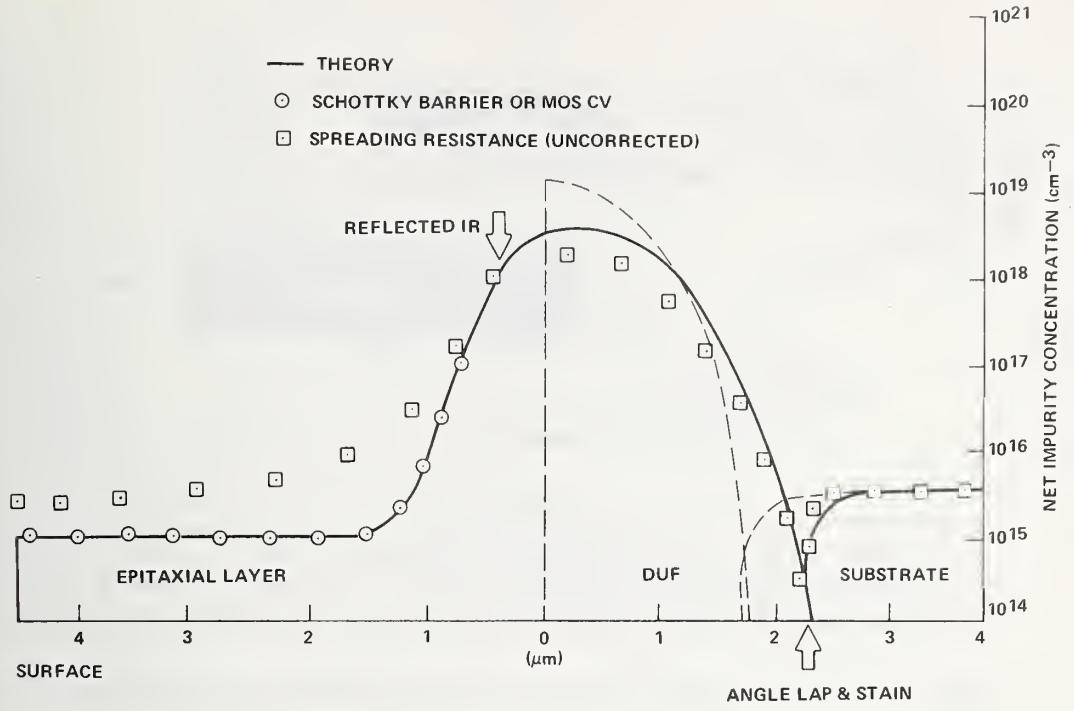

Figure 4. Profiling Techniques. Processing Steps – Dotted Line: After DUF, Solid Line: After Epitaxial Deposition

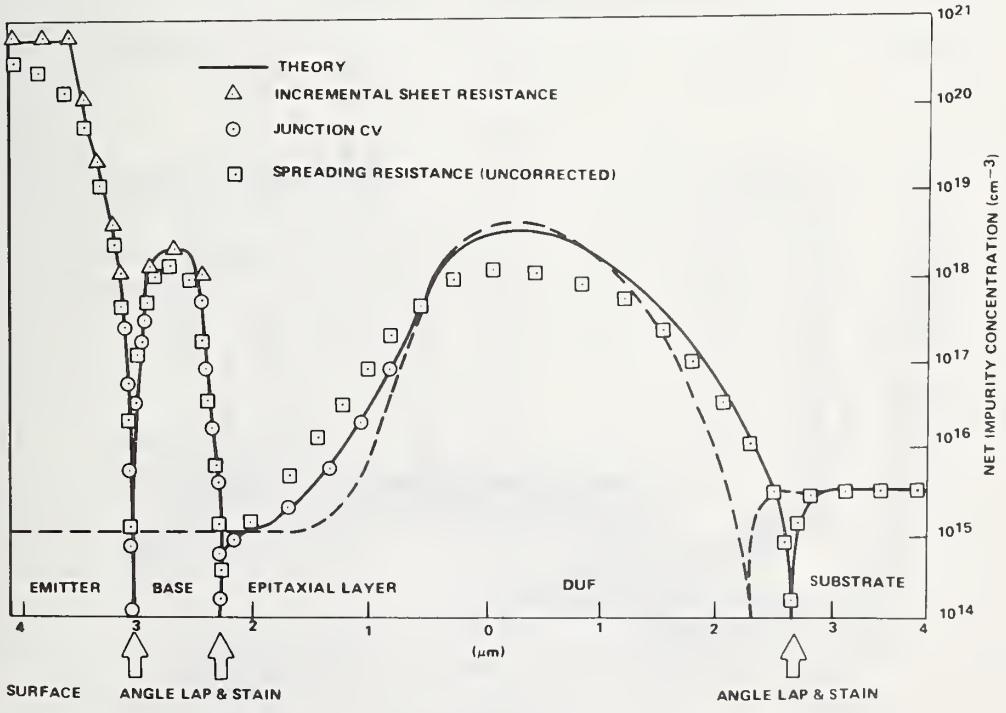

Figure 5. Profiling Techniques. Processing Steps – Dotted Line: After Epitaxial Deposition, Solid Line: After Base and Emitter Diffusion

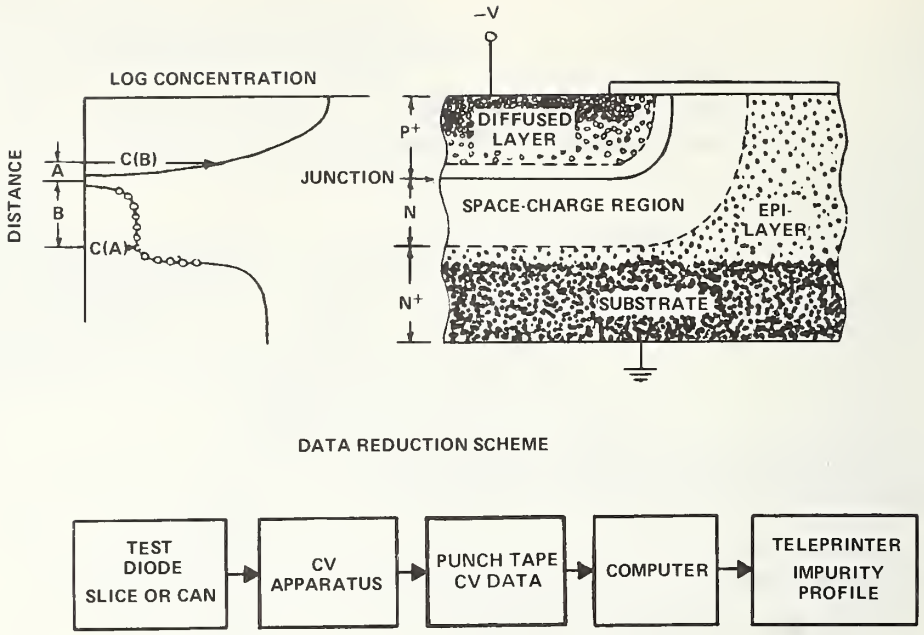

Figure 6. Epitaxial Layer Impurity Profiles Using the Diode Capacitance-Voltage (C-V) Method

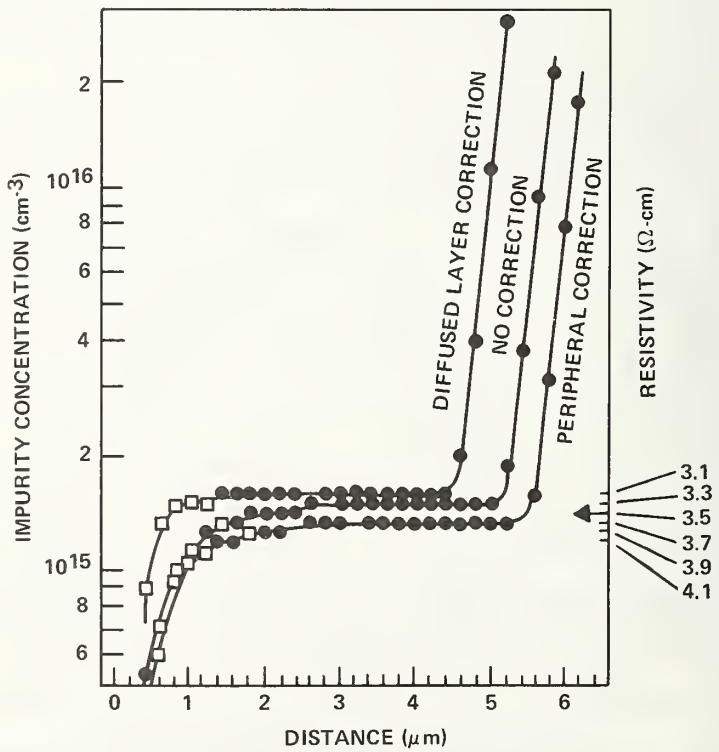

Figure 7. Capacitance-Voltage Technique for Various Corrections

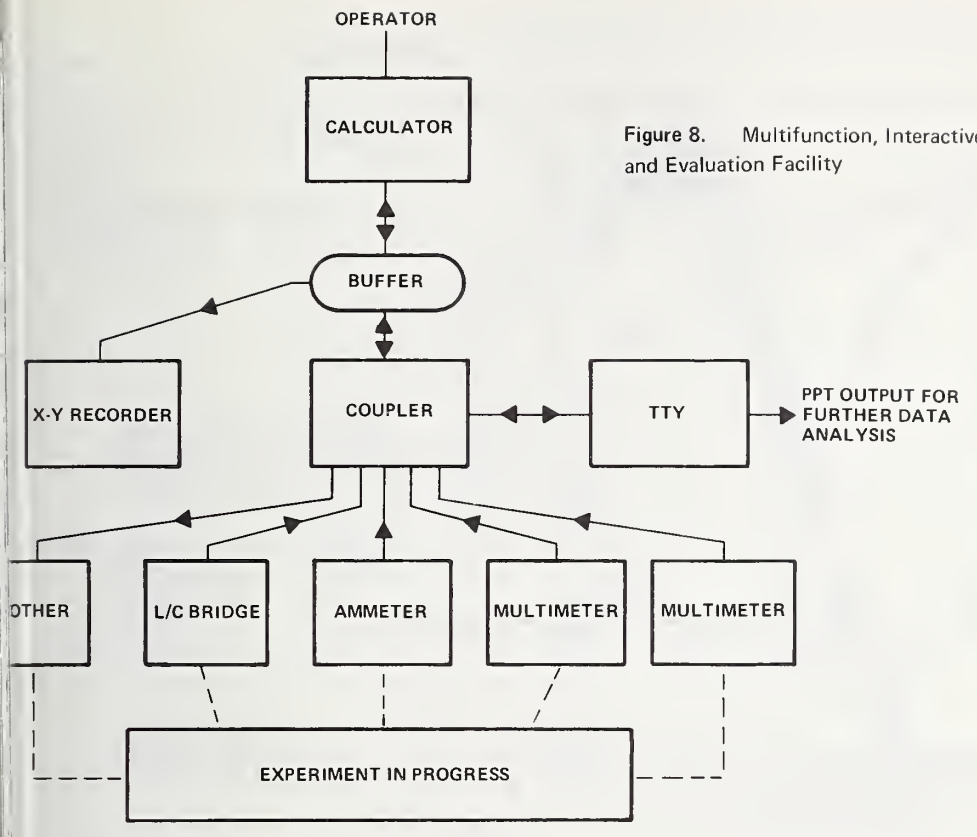

Figure 8. Multifunction, Interactive Data Aquisition and Evaluation Facility

Figure 9. Multilayer Analysis Verification

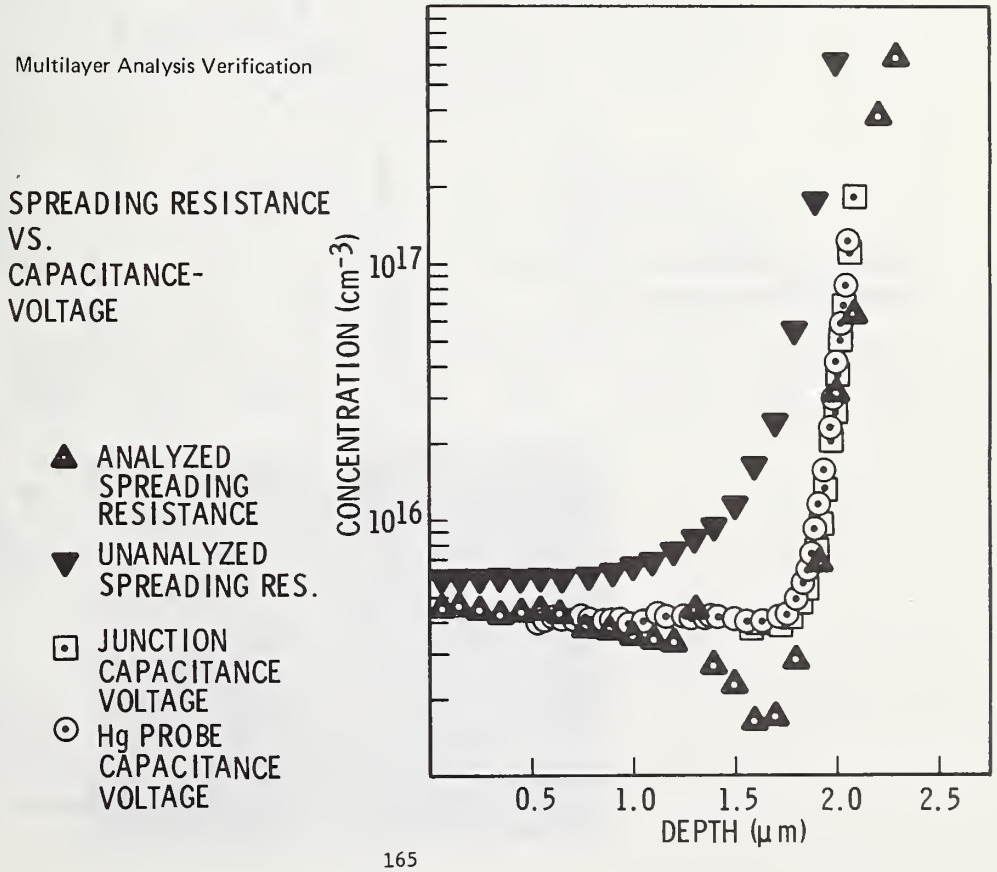

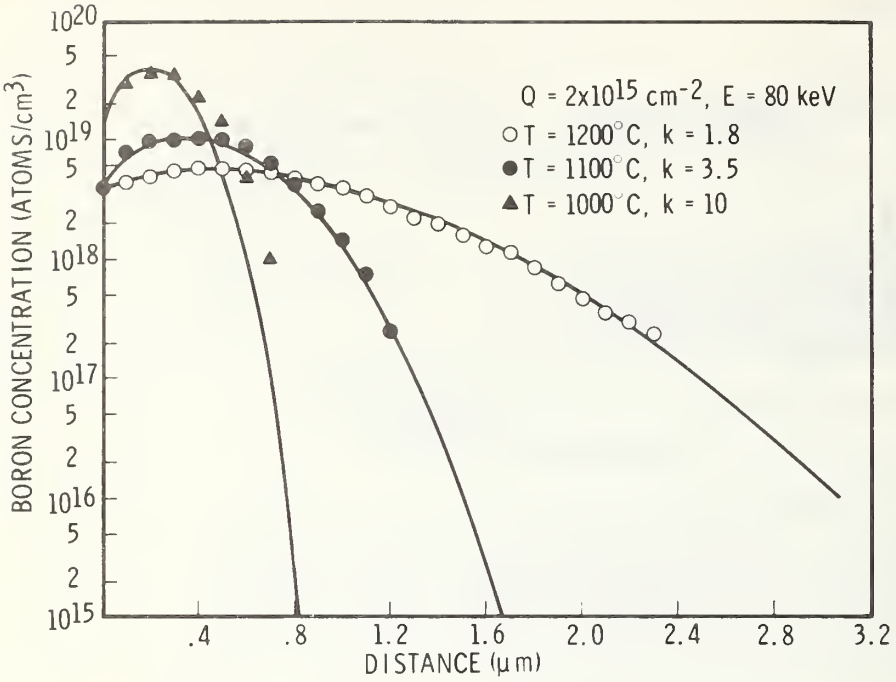

Figure 10. Predicted and Experimental Boron Profiles for 30 Min Steam Oxidation

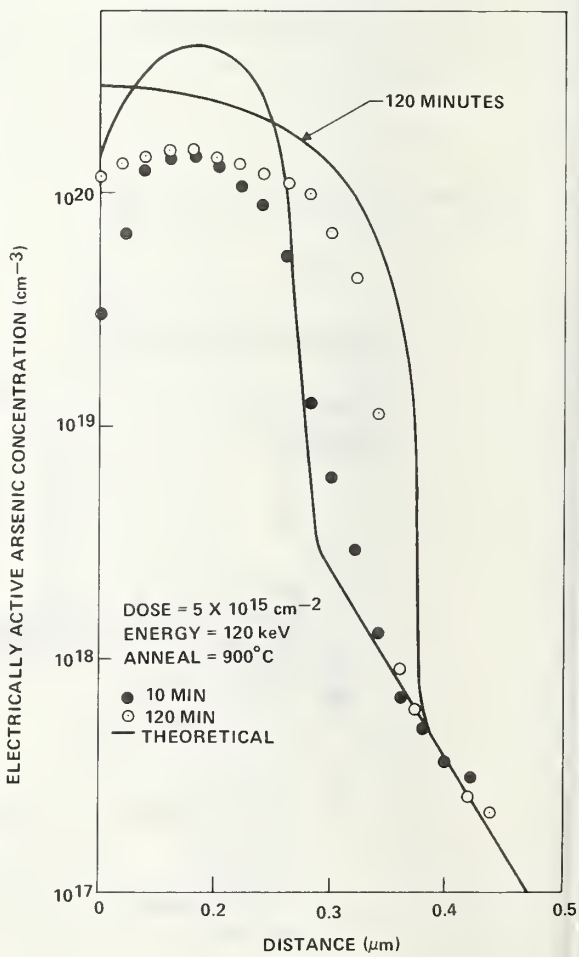

Figure 11. Ion-Implanted Arsenic Profile, Model and Experimental Data

Figure 12. Multilayer Analysis Verification

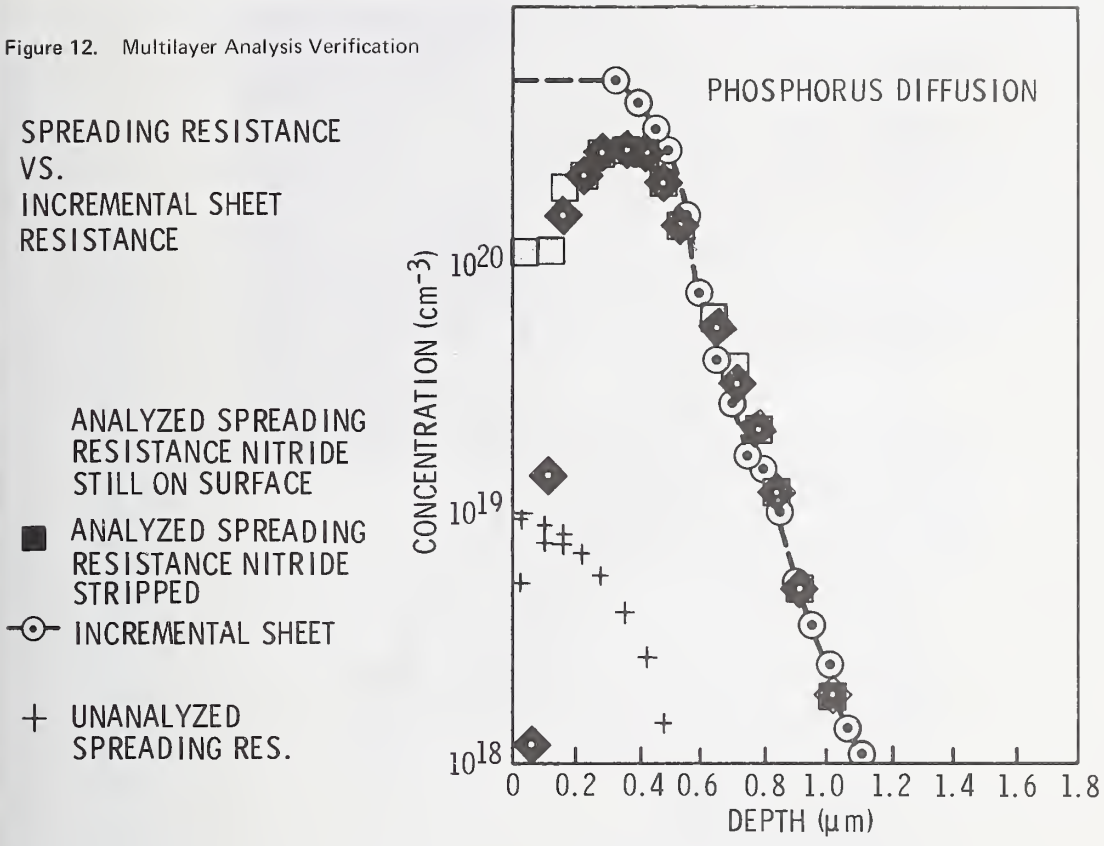

Figure 13. Well Defined Shallow Angle Lap

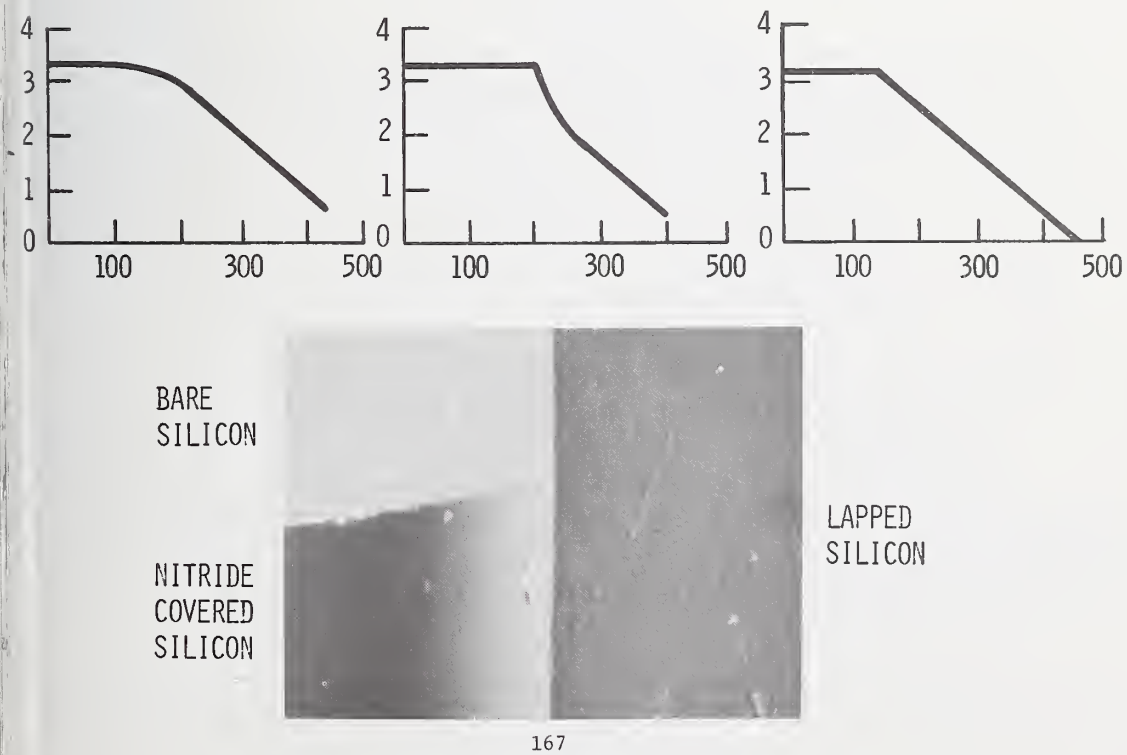

565-448 O - 75 - 12

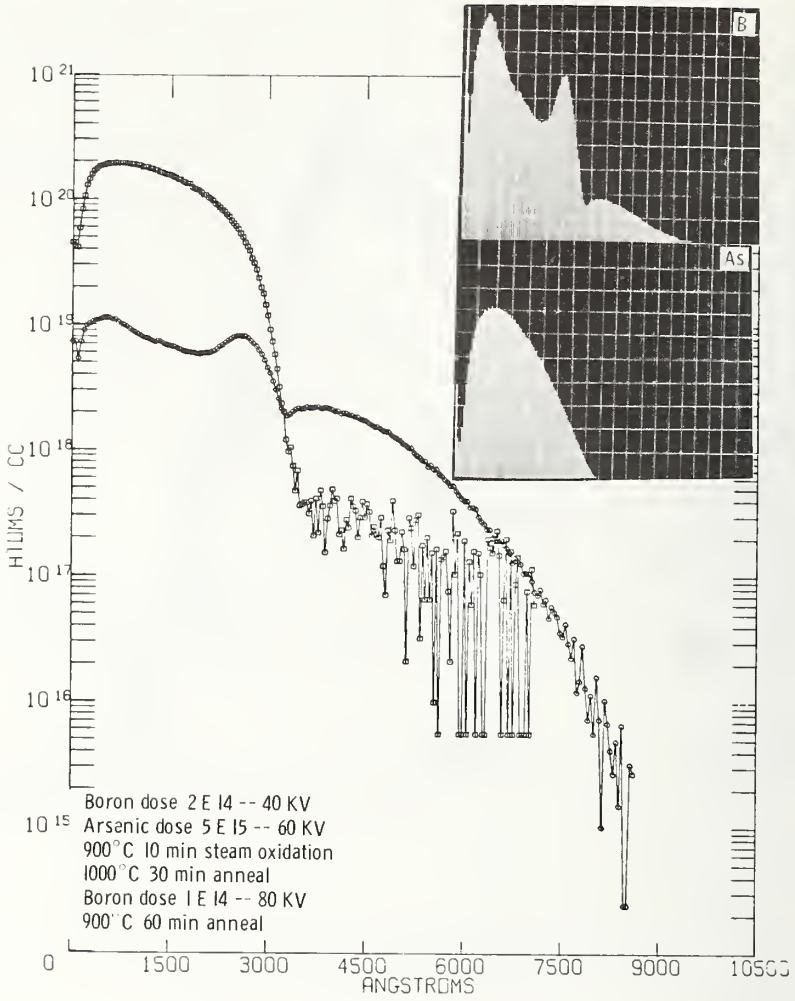

Figure 14. Ion Microprobe for Ion-Implanted Boron and Arsenic

NATIONAL BUREAU OF STANDARDS SPECIAL PUBLICATION 400-10, Spreading Resistance Symposium, Proceedings of a Symposium Held at NBS, Gaithersburg, Md., June 13-14, 1974.

Preparation of a Lightly Loaded, Close-Spaced Spreading Resistance Probe and its Application to the Measurement of Doping Profiles in Silicon

J.L. Deines, E.F. Gorey, A.E. Michel, and M.R. Poponiak

IBM System Products Division, East Fishkill Facility, Hopewell Junction, New York 12533

A commercially available spreading resistance probe, the ASR-100, was modified to operate with lighter probe loading and smaller probe spacing. The advantages of device structure profiling, increased resolution, and reduction in the "correction factor" in the converted impurity concentration profile are realizable with smaller probe spacing. The effect of the probe modifications on sample profiles and profile quality is discussed for thin epitaxial layers, bipolar transistor structures, and ion-implanted layers. Sample preparation, as influenced by the beveling technique, is also shown to have an effect on profile quality. A novel method for precise measurement of very small bevel angles is described.

Key words: Bevel angle measurement; correction factor; epitaxial layer; impurity concentration; ion-implanted layer; neutron activation; probe loading; probe spacing; spreading resistance

1. Introduction

The trend toward development of high density integrated circuits as heightened existing problems in device characterization. Thin pitaxial layers, ion-implanted layers and micron-size devices require ccurate and precise measurement of electrical and physical parameters. he spreading resistance technique has been shown to be an effective easurement tool [1-6].* The commercial availability of an automatic preading resistance probe, the ASR-100 [7], has made production control ealizable by decreasing the time required for a measurement and ecreasing operator measurement error. The existence of an automatic robe provides the potential for measurement standardization, which s highly desirable as the need for accuracy and precision increases.

This paper describes efforts to improve the spreading resistance easurement, determine optimum sample preparation procedures, and ptimize the capability of the commercial probe. Accordingly, a eveling procedure employing diamond paste and water was used to ignificantly decrease data scatter by yielding smooth, beveled urfaces and sharp bevel angles. Probe spacing was reduced to 25 μm, ermitting device profiling, greater profile resolution, and a reduction n correction factor used for computer correction of spreading resistance rofiles. Probe loading was decreased to minimize probe penetration,

*Figures in brackets indicate the literature references at the end of this paper.

adding a high degree of sensitivity. A technique for more accurate measurement of the very shallow bevel angles required for thin layer resolution is presented as an inexpensive addition to the spreading resistance probe. The effect of these probe modifications is shown in example profiles. Correlation of spreading resistance profiles of ion-implanted layers with neutron activation analysis demonstrates the accuracy and validity of the measurements. The correction program for spreading resistance profiles will not be discussed here except to say that it was an APL program developed by S.M. Hu [8] utilizing the multilayer approximation of Schumann and Gardner [9] for a circular contact to compute the resistivity profile and the Irvin's [10] curve to convert to concentration.

2. Probe Modification

2.1 Probe Spacing

The ASR-100 Automatic Spreading Resistance Probe provides the semiconductor industry with a machine capable of a high degree of reproducibility and accuracy in measurements. Installation of the ASR-100 was followed by a period of experimentation to determine the ability of the machine and to ascertain and implement modifications for improvement. Among the first points considered was a modification of the detachable probe mount to permit close probe spacing. Schumann, et.al., [11] described the benefits of using a close probe spacing of the order of 12 μm. Close probe spacing permits the profiling and measurement of very small regions on device wafers. In addition, the close spaced probe arrangement requires a smaller correction factor when converting the raw spreading resistance vs. depth profile to an impurity concentration vs. depth profile. The as-delivered ASR-100 permitted varied probe spacing down to 635 μm. Shorting due to the geometry of the probe mount prevented closer spacing. A simple redesign of the probe mount permitted probe spacing of 50 to 75 μm without shorting or probe tip modification. Grinding of the tungsten carbide probe tips to a chisel-like geometry permitted 10 μm spacing. The development of the close-spaced probe is illustrated in figure 1.

The effect of probe spacing on a sample with a thin (~.6 μm) ion-implant layer is shown in figure 2. In this case, probe spacing was varied from 20 to 606 μm. The large changes in the uncorrected profiles dramatize the effect of close-probe spacing. Note that the uncorrected profile at 20 μm spacing is closest to the corrected profiles and that the neutron activation profile compares reasonably well with the corrected profile at 20 μm spacing. The large probe spacing appears to accentuate deficiencies in the correction theory, resulting in inadequately corrected profiles.

Figure 3 shows the effect of probe spacing on raw spreading resistance profiles obtained in laboratory room light and shielded from room light. There is no observable difference between the close-spaced profiles. Although junction depth is not affected by probe spacing, the photovoltage at the junction is affected by probe spacing and lighting conditions. Significantly more photovoltage is developed for wide-spaced probes than for close-spaced probes. This effect can be used to advantage; wide spacing and room light can make junction determination easier.

The obvious advantage of close-spaced probes, the ability to profile very small areas, is shown in figure 4. Three corrected profiles of an epitaxial layer over arsenic and boron diffused areas and a non-diffused area are shown. The width of the diffused pattern was 5.0 mil. All three profiles were obtained on a single bevel in the key area between the devices measuring 20 mils. Probe spacing in this case was 30 μm.

2.2 Probe Loading

Loading on the probe tips can affect profile quality, machine integrity, nd profile reproducibility [12]. Light loading has an obvious advantage in inimizing probe penetration that can distort or result in inaccurate profiles. eyond this, excessive loading can change the probe calibration. This can be een if the condition of the probe tips is described. The probe tip is not a phere or single point of contact. Rather, it contains a number of sharp, mall tips which are necessary to penetrate native oxide and insure reasonable etal-silicon contact. Reduction in probe loading reduces the force with hich the probe impacts the silicon, decreasing the chance of changing this ulti-tip configuration and consequently the probe calibration. Light oading can reduce probe wear, offering longer probe tip life. It can be nferred that light probe loading and close probe spacing are features with a igh degree of interdependence. Probe loading was changed by adjusting the osition of the probe arm weights. The load was measured by counterbalancing gainst known weights.

The effect of probe loading on an N-type epitaxial layer over an N^+ ubstrate is shown in figure 5. The 40 gram load profile indicates a 0.25 μm hift in the apparent junction depth as compared to the 10 gram load profile. n addition, all the uncorrected data points indicate a higher impurity oncentration in the 40 gram profile than the 10 gram profile. This discrep- ncy in the uncorrected data and the junction depth is due to probe penetration r "punch-through." The probe tip in the heavier load case penetrates the ilicon and the measurement is influenced by the higher concentration layers elow the beveled surface. A larger correction factor compensates for the arger effective radius of contact seen by the probe tip yielding corrected rofiles at very nearly the same concentration level. The lightly loaded robe produces less penetration, requires less of a correction factor, and ntroduces minimal error in the junction depth determination. It is possible n certain simple structures, such as shown here, to compensate the oncentration levels for excessive probe loading and punch-through via the orrection scheme. The effect of punch-through on very thin layers, however, an result in gross error in the resolution of the junction depth and profile hape. The effect of a 0.25 μm shift in X_j for a 0.3 or 0.5 μm layer would e disastrous.

The effect of probe penetration on a complicated structure is shown in igure 6, where the sample was P-type epitaxy over a diffused P-type region n an N^+ substrate. The uncorrected and corrected reference profiles of the 0 gram load are given in figure 6a and for the 40 gram load in figure 6b. he surface intercept at 10 grams is 2.9×10^{13} At/cc and at 40 grams is $.3 \times 10^{14}$. Note also the trend of higher impurity concentration in the pitaxy and the lower peak height in the 40 gram profile. The 40 gram rofile shows higher epi concentration and lower peak height due to punch- hrough, its effect on the radius of contact, and influence by the buried ayers. For this case the correction program is unable to yield an dequately corrected profile.

Calibration curves are influenced by probe loading. The calibration nd sample profiles should be done at the identical probe load. Differences n calibration due to probe loading for P and N-type (100) are shown in igure 7. The 40 gram load calibration is shifted downwards from the 10 gram alibration by a factor of approximately two in both the N and P standards. igure 8 goes further in showing differences in calibration resulting from rystal orientation. The P-type (100) and (111) calibration curves were ound to be virtually identical for the different probe loadings. There were ifferences in the N (100) and N (111) calibration for both probe loadings. he 40 gram load appears to mask the differences below 0.4 ohm-cm. At 10 gram oading the differences in the curves are evident throughout the range easured.

3. Sample Preparation for Spreading Resistance

3.1 Beveling

a. Surface Preparation

Spreading resistance is an extremely useful and sensitive tool for determining impurity concentration profiles, junction depth, etc. Its sensitivity makes sample preparation an extremely important step in the measurement process. Rounded bevels make the determination of the bevel edge and zero depth measurement difficult. Excessively rough bevels can cause significant scatter in the data, which is amplified when corrected.

The abrasive beveling medium most used in spreading resistance measurements has probably been 0.3 μm Al_2O_3 in water. Care in the beveling procedure can result in fine, uniformly abraded surfaces. Scratches or other imperfections and irregularities in the beveled surface can cause appreciable scatter in obtained data, particularly on profiles requiring high resolution. Figure 9a gives the raw spreading resistance vs. depth profile of an N epitaxial layer over an N^+ substrate which was beveled by lapping with 0.3 μm Al_2O_3 in water on a frosted glass plate. The sample had been mounted with glycol-phalate on a bevel block for lapping and transferred to the special mandrel for mounting on the spreading resistance probe. Scatter in the data is evident in this high resolution profile of 2 log cycles. The sample was rebeveled with water on a frosted glass plate which had been prepared by working with a silicon slug and 0.25 μm diamond paste. The excess paste was removed and the imbedded grit with water was used for beveling. The resultant bevel edge was sharp, the bevel quite smooth, and scatter in the data was significantly reduced as shown in figure 9b.

b. Bevel Angle Measurement

Shallow bevel angles in the order of 30 minutes or less are necessary for satisfactory investigation of thin structures. Of critical importance to such shallow bevel profiles is the bevel angle measurement. The goniometer is not accurate enough to resolve these shallow angles. Tong, et.al.,[13] introduced the Small Angle Measurement (SAM) apparatus as a means of measuring shallow bevel angles with far greater precision than the goniometer. Beyond this, certain modifications in the SAM technique have been made to permit small angle measurements on any laboratory microscope [14 Use of the ASR-100 microscope and rotatable stage facilitates the MSAM (Microscope SAM) measurement and completely eliminates the need for the specially constructed SAM apparatus. Measurement of the bevel angle at the location where the profile was taken is now insured, thus increasing the accuracy of the depth measurement.

The MSAM apparatus is shown in figure 10. The ASR-100 rotatable stage and sample mounting block can substitute for the base plate and protractor assembly. A thin wire of diameter $\underline{s}$ is inserted within the barrel assembly of the 3X measuring objective or any long working distance lens. During normal microscope use, the wire and the wire image projected below are not visible because the lens has a short depth of field. In angle measurement use, the beveled sample actually yields two images of the wire, one reflected off each of the flat and beveled surfaces. An angle measurement is made by focusing on the images of the wire. Rotation of the sample causes a rotation of the images, each rotating about its own axis. The images are aligned by rotating the microscope stage until the side of one image barely touches the opposite side of the other image. At this point an angle reference reading, $\alpha 1$, is recorded as in figure 11. The stage is rotated until the images cross over each other as in figures 12 and 13 and are aligned edge to edge on the side opposite from that used for the reference reading, as shown in figure 14 A second angle reading, $\alpha 2$, is made here. The total angular rotation, α, is calculated, $\alpha = \frac{\alpha 1 - \alpha 2}{2}$. The rotation angle α is converted to the sample bevel angle $\emptyset$ by the relation:

$$\sin \phi = \frac{S}{2d \sin \alpha}$$, where d is

he distance from the wire to the sample bevel edge (0.805" in this case) and is the width of the wire, 0.0153".

MSAM data on several shallow angle beveled samples is compared with nterferometer and SAM data in table 1. The MSAM data is an average of ten easurements taken over a period of ten days.

Table 1. Comparison of Shallow Bevel Measurement Techniques

ample	Interferometer	SAM	MSAM* Ave Ø	MSAM Ave % Dev
1	16.2'	16.2'	16.3'	1.4%
2	22.7'	23.3'	23.1'	1.6%
3	52.0'	52.0'	51.6"	0.5%

* s = 0.0069 inches
d = 1.049 inches

The addition of a second wire parallel to, and a known distance from, he single wire gives an effective increase in s, enabling a wider range of ngles to be measured with a single objective lens attachment.

4. Summary

Modification of a commercial spreading resistance probe to operate with mall probe spacing and light probe loading has resulted in more accurate rofiles requiring less correction than wide, heavy probes. The sensitivity f the probe has been increased and beveling procedures improved to reduce ata scatter. Shallow bevel angle measurement has been shown to be accurate, uick, and inexpensive.

5. Acknowledgement

The authors would like to express their appreciation to Dr. S. M. Hu for is comments and suggestions on spreading resistance correction and Dr. R. H. astl for the neutron activation analysis.

6. References

1] R.G. Mazur and D.H. Dickey, J. Electrochem. Soc., 113, 255 (1966).

2] E.E. Gardner, P.A. Schumann, Jr., and E.F. Gorey, Electrochem. Soc. Symposia Proceedings "Measurement Techniques for Thin Films," April 1967.

3] D.C. Gupta, ibid, 116, 670 (1969).

4] C.K. Chu, ibid, 115, 192c (1968).

[5] R.G. Mazur, ibid, 114, 255 (1967).

[6] D.C. Gupta, J.Y. Chan, and P. Wang, ibid, 116, 301c (1969).

[7] Reference Manual and Operating Instructions for the ASR-100 Automatic Spreading Resistance Probe, Solid State Measurements, Inc., 1971.

[8] S.M. Hu, Solid State Electronics 15, 809 (1972).

[9] P.A. Schumann, Jr., and E.E. Gardner, J. Electrochem. Soc., 116, 87 (1969).

[10] J.C. Irvin, Bell Syst. Tech. J., 41, 387 (1962).

[11] P.A. Schumann, Jr., E.F. Gorey and C.P. Schneider, "Small Spaced Spreading Resistance Probe," Solid State Tech. (1972).

[12] P.A. Schumann, Jr., J.M. Adley, M.R. Poponiak, C.P. Schneider and A.H. Tong, J. Electrochem. Soc., 116, 150c (1969).

[13] A.H. Tong, E.F. Gorey and C.P. Schneider, Rev. of Sci. Instruments, 43, 320 (1972).

[14] J.L. Deines, E.F. Gorey and M.R. Poponiak, IBM Tech. Disclosure Bulletin, 15, #10, "Measurement of Small Angles with a Microscope, " (1973).

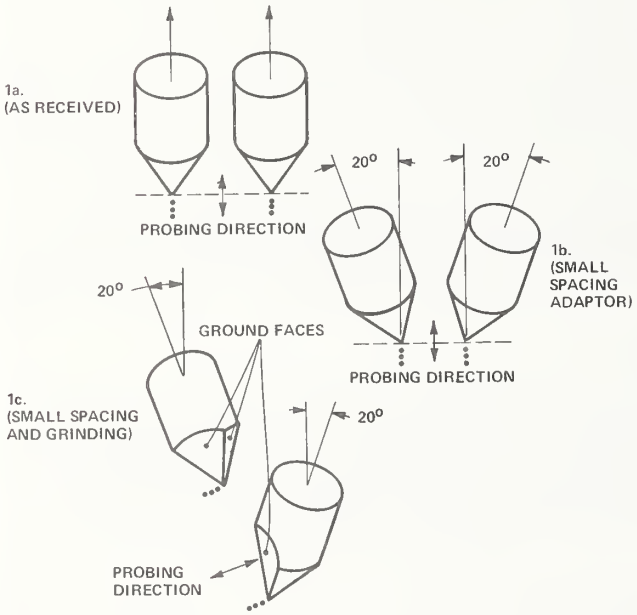

Figure 1 Close spacing probe tip modifications.

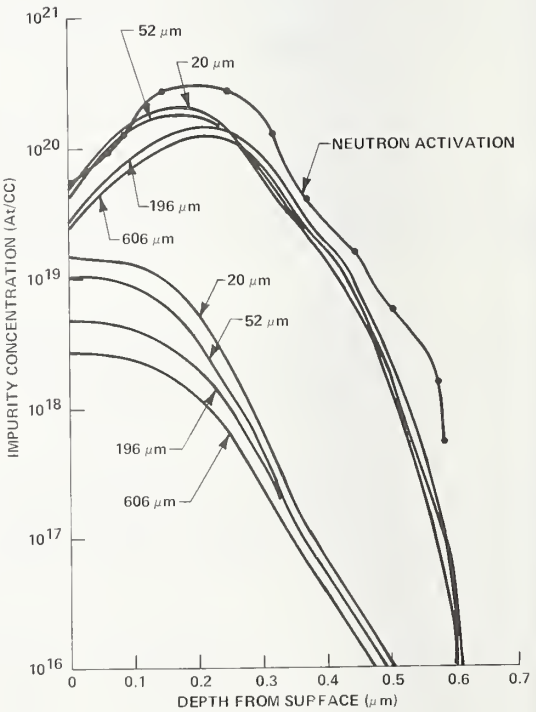

Figure 2 Effects of probe spacing on spreading resistance profiles of thin structures as compared with neutron activation analysis.

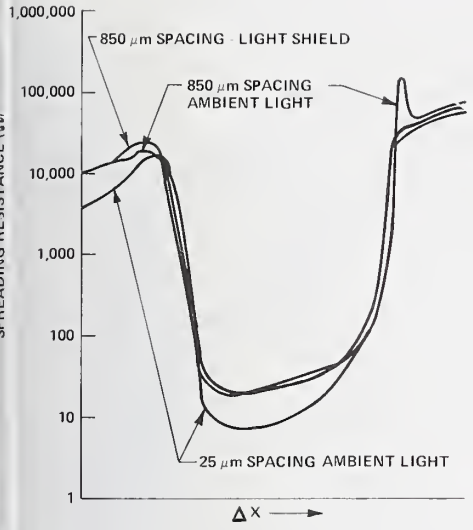

Figure 3 The effects of ambient light and probe spacing on spreading resistance profiles.

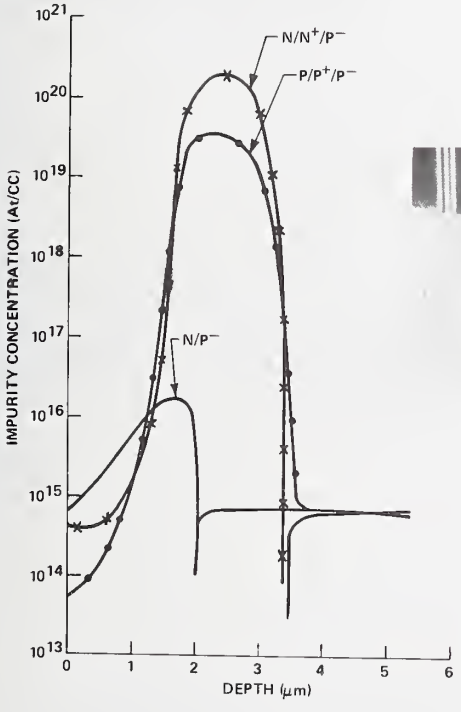

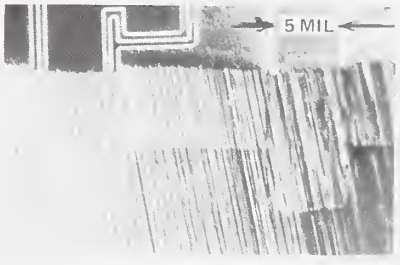

Figure 4 Corrected spreading resistance profiles of small device structures. Probe spacing 30 μm.

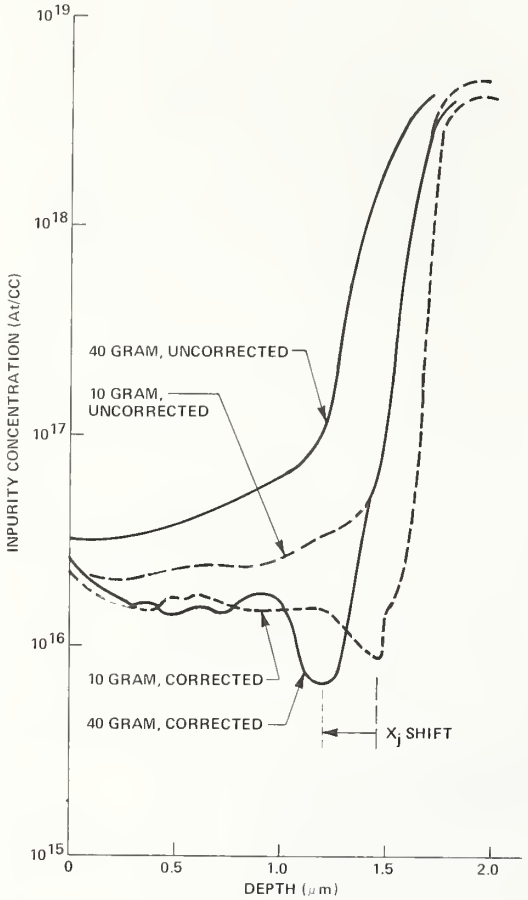

Figure 5 Probe penetration effects as a function of probe loading on a simple N/N+ structure.

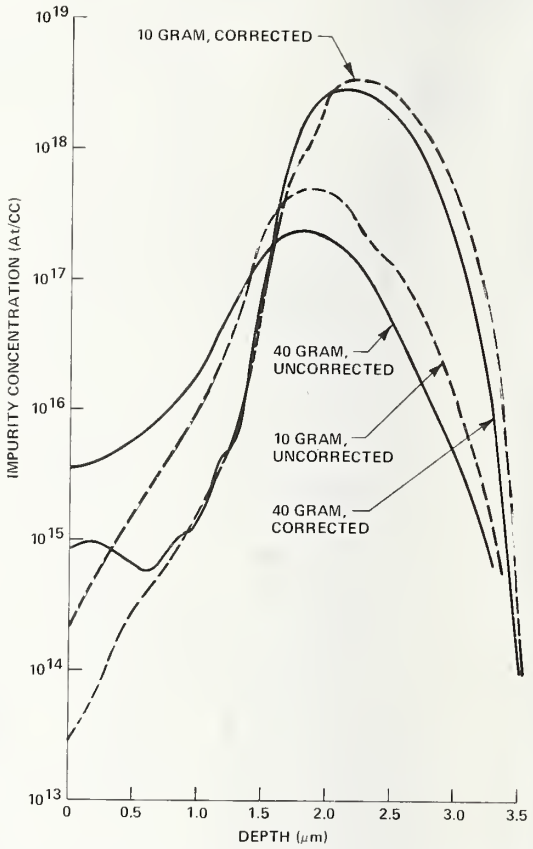

Figure 6 Probe penetration effects as a function of probeloading on a complicated P-/P+/N- structure.

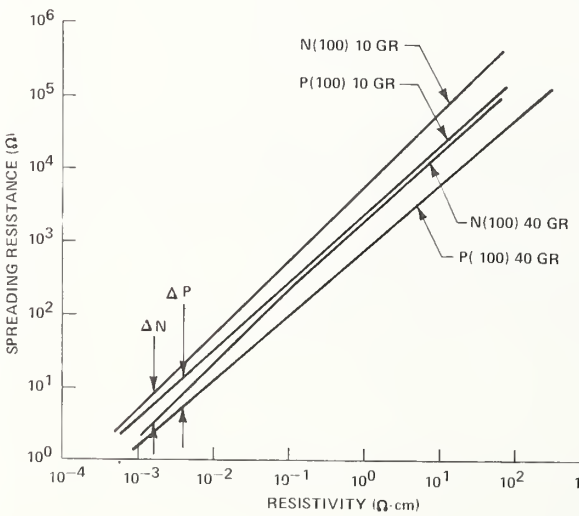

Figure 7 Calibration curves of (100) orientation P and N-type silicon at 10 and 40 grams loading.

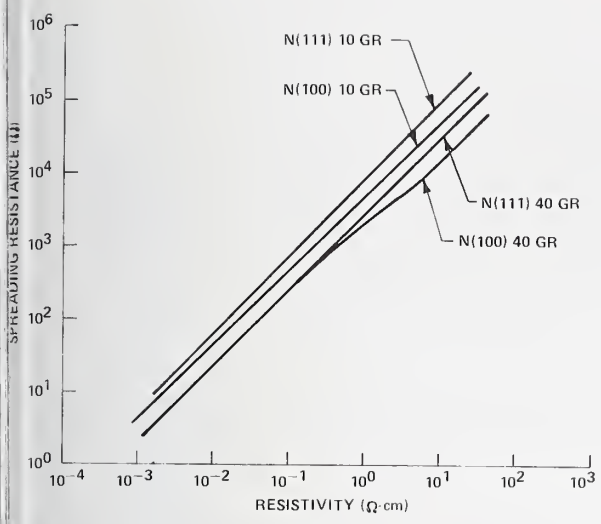

Figure 8 Effects of probe loading on (100) and (111) calibration curves.

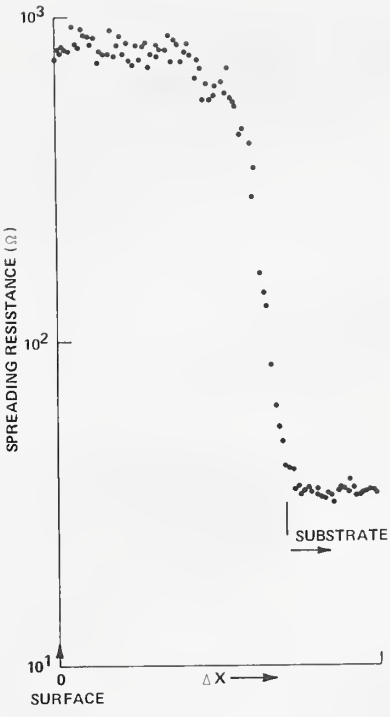

Figure 9a Spreading resistance profile utilizing 0.3 μm Al_2O_3 in water on a frosted glass.

Figure 9b Spreading resistance profile utilizing only water on a glass frosted with 0.25 μm diamond.

Figure 10 Microscope small angle measurement assembly (MSAM).

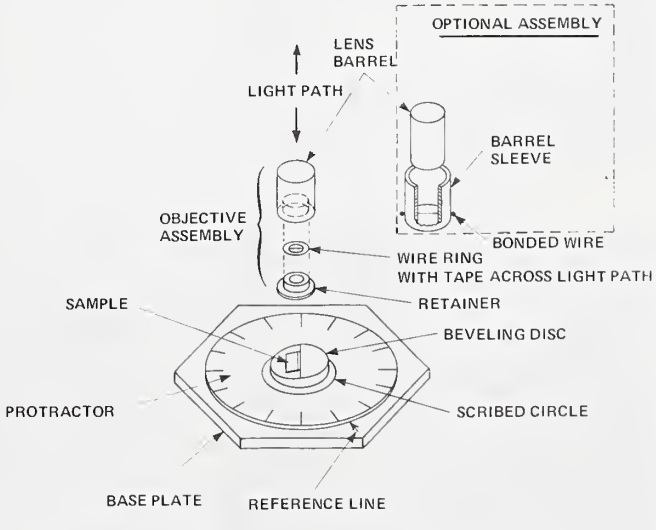

ROTATABLE STAGE OF ASR-100 REPLACES BASE PLATE AND PROTRACTOR.

Figure 11 Photograph taken with MSAM system showing double images (1 & 2) of wire. Images are positioned edge to edge at this orientation of sample stage: 91°. This is the starting point of specimen bevel angle measurement. By a second exposure, image (b-b') of sample's bevel surface is also shown. NOTE: microscope focal point must be changed between these exposures.

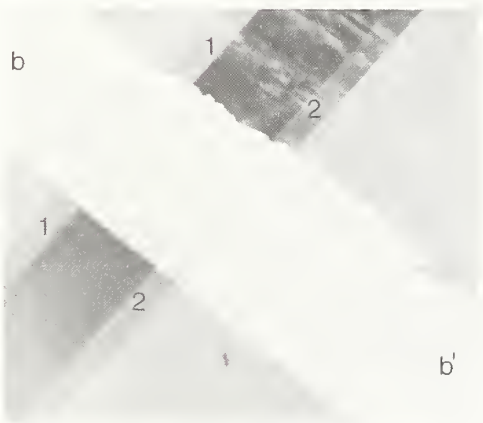

Figure 12 Double exposure photograph of wire images (1 & 2) and sample's bevel surface. Sample stage orientation is 72°. Dark band is overlap of wire images.

Figure 13 Double exposure photograph of wire images and sample's bevel surface. Sample stage orientation is 54.5°; wire images (dark band) have crossed over each other.

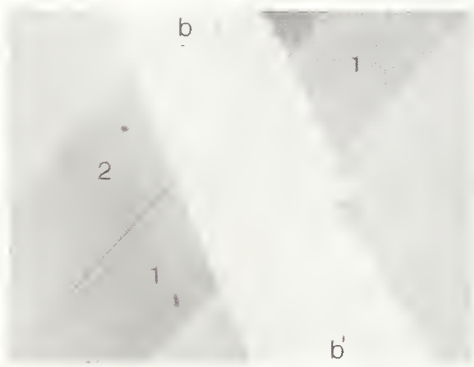

Figure 14 Double exposure photograph of wire images and sample's bevel surface. Images have completely crossed and are positioned edge to edge. This is the final step of measurement. Orientation is 44°. Total α = 1/2 x 47° =23.5°. Specimen bevel angle = 69.5' where s = 0.0153 in. and d = 0.0805 in.

NATIONAL BUREAU OF STANDARDS SPECIAL PUBLICATION 400-10, Spreading Resistance Symposium, Proceedings of a Symposium Held at NBS, Gaithersburg, Md., June 13-14, 1974.

A Direct Comparison of Spreading Resistance and MOS-CV Measurements of Radial Resistivity Inhomogeneities on PICTUREPHONE® Wafers

J. R. Edwards and H. E. Nigh

Bell Laboratories
555 Union Boulevard
Allentown, Pa. 18103

Small scale (~ 50 μm) radial impurity concentration inhomogeneities in silicon wafers have been measured using both the MOS-CV method and the spreading resistance technique. The MOS-CV measurements were made using photolithographically defined 50 μm square capacitors placed on 75 μm centers and the spreading resistance measurements were made using a model 100 ASR probe on the same wafers after removal of the MOS capacitors.

A direct comparison between these methods is presented for three specific types of ⟨111⟩ oriented silicon wafers with an impurity concentration range between 5 and 10 x $10^{14}/cm^3$. In addition, a photograph showing the direct effect of radial resistivity variations on the dark field coring of a PICTUREPHONE® target is included.

Key words: Dark field coring; MOS-CV techniques; PICTUREPHONE®; radial resistivity inhomogeneities; silicon resistivity; spreading resistance techniques.

1. Introduction

In this paper we report the direct measurement of small scale (~ 50 μm) adial resistivity inhomogeneities in silicon crystals using the MOS-CV ethod. In addition, spreading resistance measurements using the ASR-100 preading resistance probe were done on the same wafers which allows a irect comparison between MOS-CV and spreading resistance measurements. In he past, the spreading resistance probe technique has been used by several xperimentalists to measure small-scale radial resistivity inhomogeneities n silicon crystals [1,2][1]. Since this technique is empirical, reliable alibration is necessary. Most investigators use four point probe measure-nts for calibration, but the four point probe does not give adequate alibration for the small spatial resolution desired in studying the radial nhomogeneities in PICTUREPHONE® target material or in IC's. In particular, e will demonstrate that the video shading which occurs in the dark field isplay of silicon PICTUREPHONE® targets can be caused by substrate

igures in brackets indicate the literabure references at the end of this aper.

resistivity variations in the target material as small as 10% over a distance of 0.01 inches [3].

2. Experimental Procedure and Discussion of Methods Used

Although spreading resistance measurements can be made over a wide impurity concentration range ($10^{14}/cm^3$ to $10^{20}/cm^3$), precise measurements are more difficult for the low range. Fortunately this range is particularly well suited for the MOS-CV method [3,4] and is also the impurity concentration used for PICTUREPHONE® target material. As a consequence, the wafers used in this study were ⟨111⟩ oriented n-type silicon wafers with an impurity concentration 5 to 10 x $10^{14}/cm^3$ (10-5 Ω-cm resistivity). Both float-zone refined and Czochralski pulled wafers were used.

The silicon wafers were chemically etched to remove saw damage and one side was polished using Syton polishing compound. An 1100°C thermal oxide of 1500-1800Å was grown on the wafers after suitable chemical cleaning. The MOS capacitors were made by vacuum depositing aluminum and subsequently photolithographically defining 50 μm square pads on 75 μm centers. This choice of MOS pad size allows approximately 270 measurements on the diagonal of the 0.850 inch diameter wafer used for PICTUREPHONE® targets. After the MOS measurements were made, the aluminum and the SiO_2 were chemically removed to prepare the wafer for spreading resistance measurements. Thus, both types of measurements could be made without any heat treatment altering the radial resistivity profile.

The C-V measurements were made at 1 MHz using a Boonton Model 71-AR capacitance meter. The choice of thermal oxide resulted in capacitance values approximately 1/2 pfd or less which allows full use of the 1 pfd range. The analogue output from the capacitance meter was recorded to 3 significant digits using a DVM and the data reduction was done by computer. Since the MOS-CV method averages the impurity doping over a region about 1 μm below the surface, there are two different methods which can be used to evaluate the impurity concentration for absolute calibration of the spreading resistance probe. In the first method, only two measurements are necessary for the max-min high frequency technique [3]: oxide thickness, and the accumulation - inversion capacitance ratio. This means that absolute values of capacitance are not necessary, which in turn eliminates absolute capacitance calibration. Only the linearity of the analogue output of the capacitance meter is necessary. Because the thermal oxide is uniform to ± 30Å, only a single oxide measurement by a U-V Spectrophotometer is necessary to obtain the oxide thickness. Since the MOS-CV method uses only known constants and measured parameters, it is estimated that the precision with this method is ± 2% and the absolute value of the impurity concentration calculated is 10%. This precision clearly allows determination of impurity concentration inhomogeneities across a slice which vary ± 10% over a distance of 50 μm. The second method of MOS-CV evaluation uses the change of capacitance in the depletion region with respect to the applied voltage in order to calculate the doping as a function of the depth. For this measurement, the absolute value of the capacitance and the differential change of voltage are needed in addition to the oxide thickness. The precision of this method is estimated to be ± 5% with an accuracy of 15%. Since the MOS-CV measurement techniques complement each other, a high degree of precision with a spatial resolution of approximately 25 μ is assured.

When the spreading resistance probe is calibrated relative to the MOS-CV measurements, a precision of ± 3% is possible for the spreading resistance measurements using the ASR-100 spreading resistance probe on chem-etched, Syton polished silicon wafers. In comparison, we observed that the precision and reproducibility for the probe is only ± 20% to 30% on a mechanically lapped surface.

Using the wafers calibrated by the MOS-CV, it was found that additional yton polishing allowed the sample to be reused as a standard. This is mportant when considering day-to-day calibration of the spreading resistance robe. Several other factors were observed which affect the precision of the preading resistance technique, the primary one being the probe wear. It was ound that a 5% deviation from the control measurements indicated excessive robe wear. This usually occurred after about ten thousand measurements on Syton polished surface. The probes could be regenerated by using the probes n a mechanically lapped silicon wafer for a few hundred measurement cycles.

3. Experimental Comparison

The ASR-100 spreading resistance probe was operated in the two probe ode with the probes spaced about 40 mils apart. The actual values of esistivity measured at 100 μm increments are plotted in figures 1-3 for a ypical float zone refined wafer, a typical Czochralski pulled wafer and a pecially prepared Czochralski wafer. The next three figures show the re- istivity data converted to impurity concentration using the MOS measurements s calibration points. This change was done to enable a direct comparison to ne MOS-CV impurity concentration data shown in figures 7-9. Both typical afers show dark field coring and also clearly demonstrate variations of mpurity concentration greater than ± 10%. Routine four point probe measure- nts would not reveal these inhomogeneities, but both spreading resistance nd MOS-CV do allow a direct measurement. As a direct example of the effect resistivity inhomogeneities, figure 10 shows a silicon PICTUREPHONE® arget made from a wafer whose radial resistivity profile had been measured. ote the dark field coring corresponding to the resistivity variations of 10% for this Czochralski wafer.

In conclusion, it has been shown that the spreading resistance probe can easure the radial resistivity profile of a wafer to a precision of ± 3% for properly prepared wafer. This has been verified using MOS-CV measurements, nd the effect on dark field coring has been demonstrated by an actual target notograph.

4. References

] Mazur, R. G., J. Electrochem. Soc. Vol. 114, No. 3, March 1967, p. 255.

] Gupta, D. C., Chan, J. Y., and Wang, P., J. Electrochem. Soc., Vol. 117, No. 12, December 1970, p. 1611.

[3] Grove, A. S., Snow, E. H., Deal, B. E., and Sah, C. T., Jap. 3S, 2458 (1964).

[4] Kennedy, D. P., Murley, P. C., and Kleinfelder, W., IBM J. Res. Dev. (1968) p. 399.

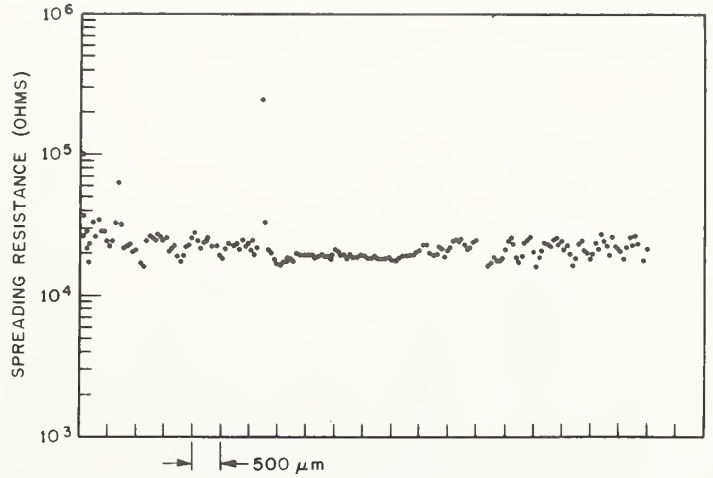

Figure 1. Spreading resistance measurements for the typical float zone refined wafer. Notice the large short-range fluctuations on both sides.

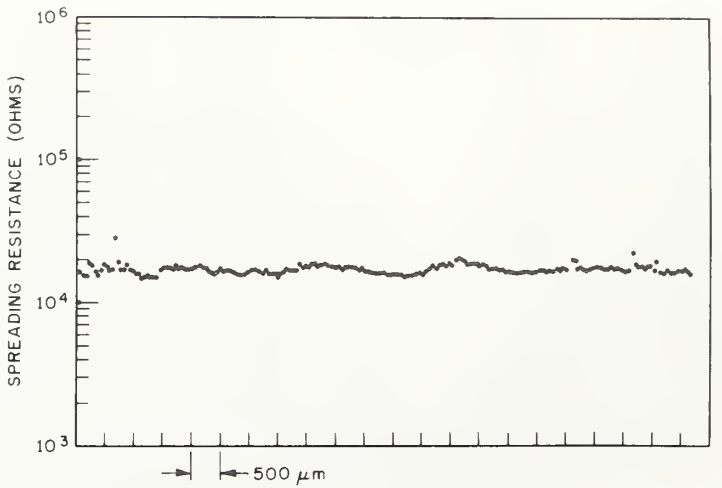

Figure 2. Spreading resistance measurements for typical Czochralski wafer. Notice the characteristic core in the center.

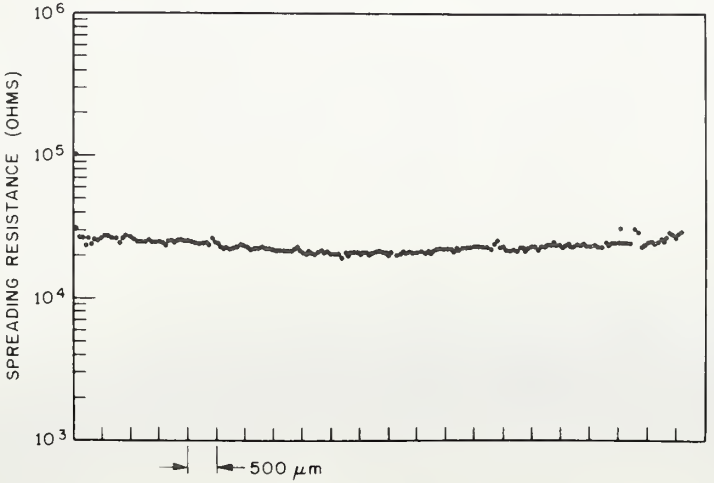

Figure 3. Spreading resistance measurements for special uniform wafer. Notice in particular the small fluctuations and the broad uniform center core.

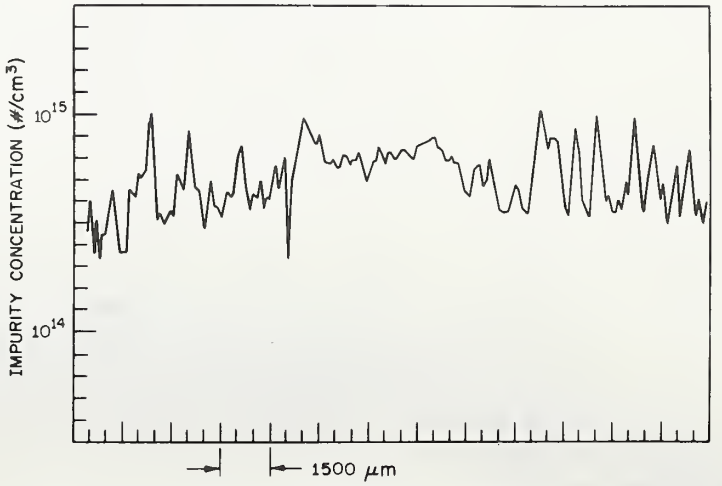

Figure 4. Spreading resistance impurity concentration profile for measurements of figure 1 using MOS-CV calibration. This profile can now be directly compared with figure 7.

565-443 O - 75 - 13

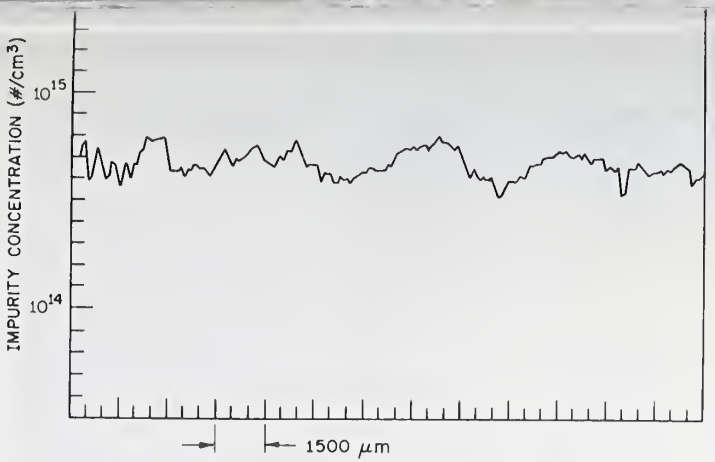

Figure 5. Spreading resistance impurity profile for measurements of figure 2. This profile can now be directly compared with figure 8.

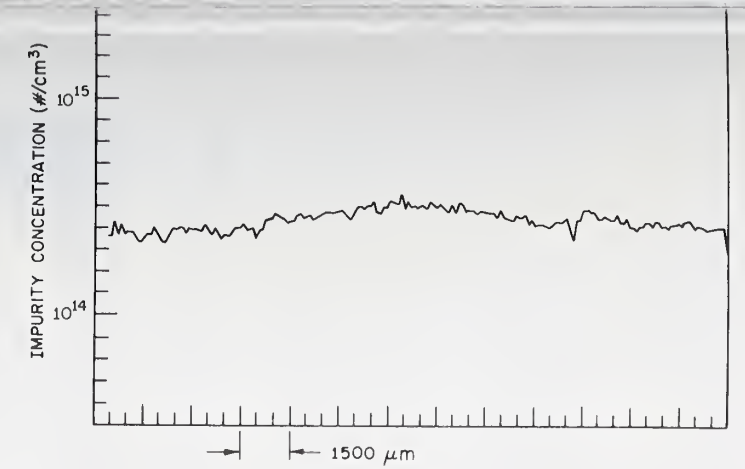

Figure 6. Spreading resistance impurity profile for uniform wafer whose resistance measurements are shown in figure 3.

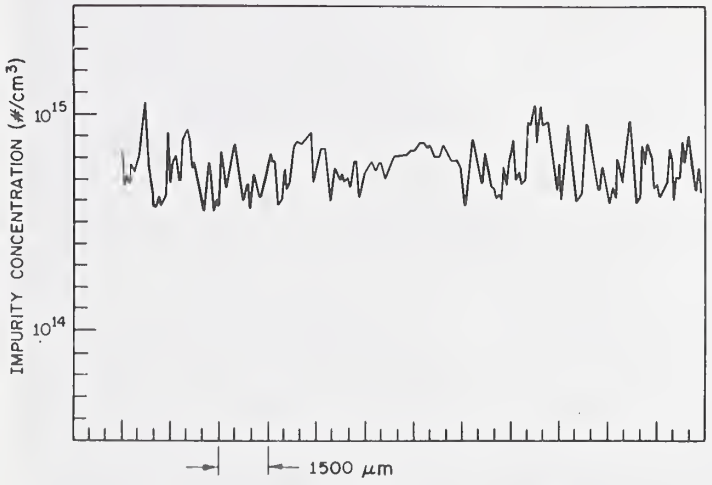

Figure 7. MOS-CV impurity concentration for the typical float zone refined wafer.

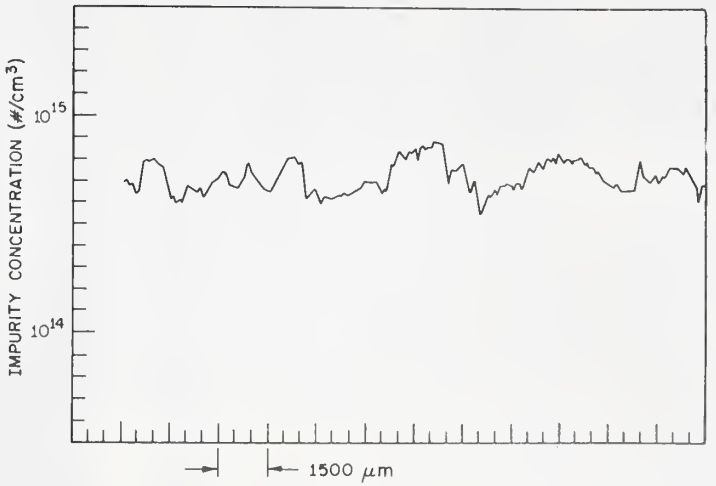

Figure 8. MOS-CV impurity concentration for the typical Czochralski pulled wafer.

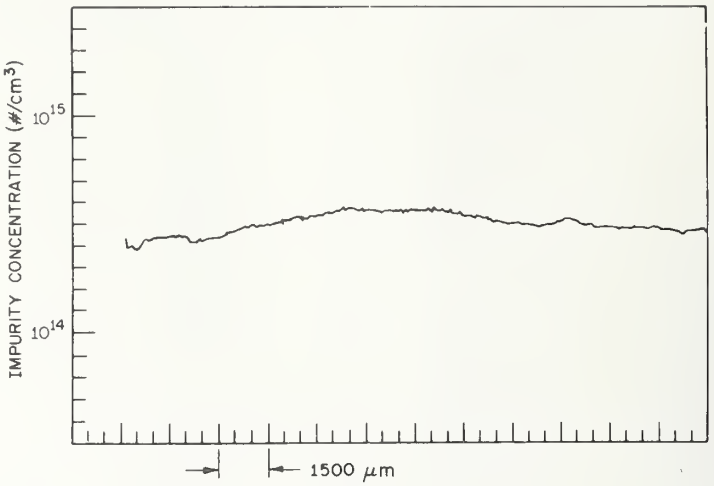

Figure 9. MOS-CV impurity concentration for the specially prepared Czochralski pulled wafer.

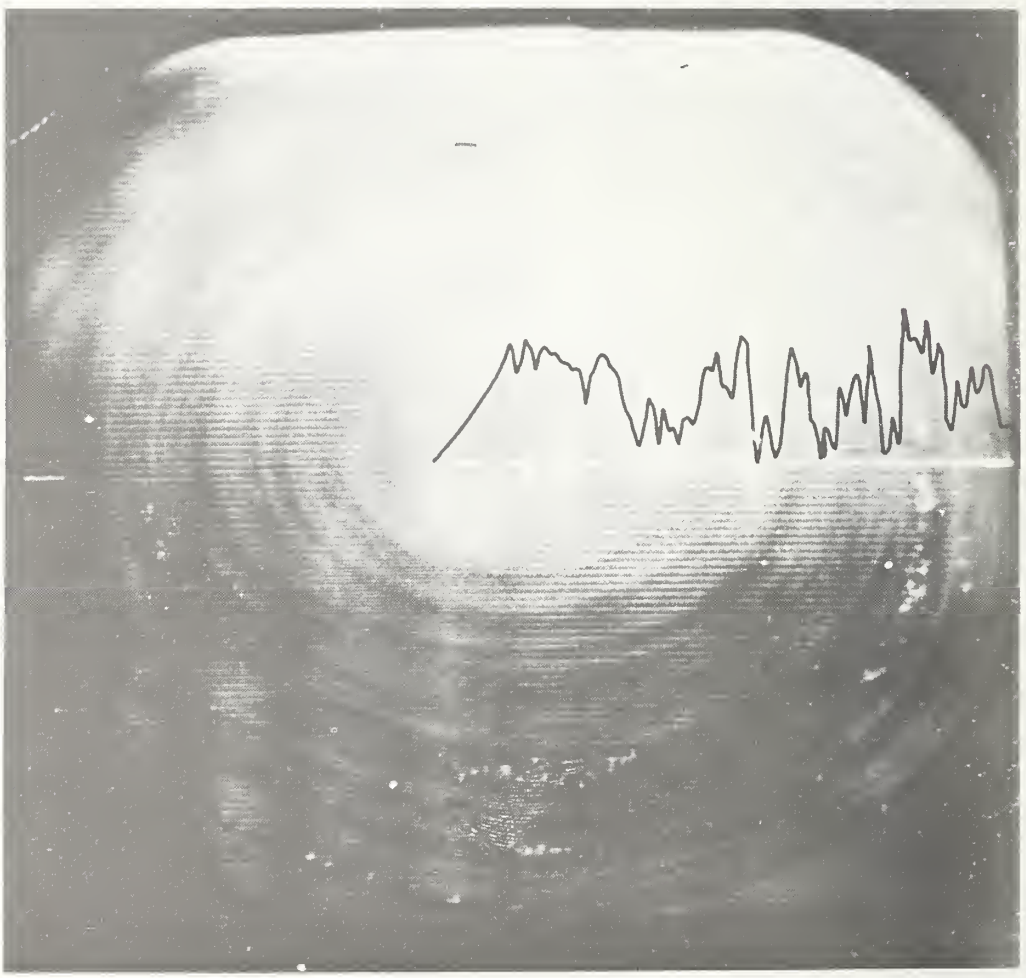

Figure 10. Picture showing dark field coring pattern for a PICTUREPHONE target wafer with the impurity profile superimposed.

NATIONAL BUREAU OF STANDARDS SPECIAL PUBLICATION 400-10, Spreading Resistance Symposium, Proceedings of a Symposium Held at NBS, Gaithersburg, Md., June 13-14, 1974.

Investigations on Local Oxygen Distribution in Silicon Single Crystals by Means of Spreading Resistance Technique

Fritz G. Vieweg-Gutberlet

Wacker-Chemitronic GmbH.
Physical Laboratory
D-8263 Burghausen, West Germany

By means of spreading resistance measurements subsequent to heat-treatments at approx. 450°C and 1100°C alternatively the local distribution of oxygen in the donor state in Silicon single crystals was examined. Oxygen striations have not been found which is in correspondence to a distribution coefficient of $k_o = 1.25 \pm 0.17$ for oxygen in Silicon. The radial distribution of oxygen in the donor state is more or less uniform except for an edge area of about 1.5 mm where the oxygen content seems to be considerably lower. A very strong relationship between electrically activated oxygen (donor state) and swirls was found: in regions containing swirls a smaller amount of oxygen was activated to the donor state. This result fits De Kock's model describing swirls as consisting of vacancy-OXYGEN-clusters.

Key words: Oxygen in Silicon, Silicon single crystals, spreading resistance measurements, swirls.

1. Introduction

More or less knowledge exists about the local oxygen distribution in Silicon ngle crystals. In connection with swirls the question arises if swirls may be lated to oxygen striations. The experiments carried out in the past either by frared transmission or by resistivity measurements have been handicapped by a very or local resolution. We selected the spreading resistance probe to continue the ectrical measurements from the past with the best resolution one can obtain up to w.

It is well known that oxygen in Silicon may be changed from the electrically utral (interstitial) into a donor state by a heat-treatment at 450°C. It is also ll known that oxygen may be removed from the donor state by a heat-treatment at gher temperatures and "crash cooling" of the sample. [1][1]

[1] Figures in brackets indicate the literature references at the end of this paper

The change between the electrically neutral and the donor state with respect to the heat-treatment is detectable by resistivity measurements. In our experiments we employed the spreading resistance probe for the resistivity measurements in order to get highest local resolution.

Under the assumption that oxygen in Silicon does not change its local position by diffusion during a heat-treatment at 1100°C for approx. 90 minutes and for very small differences in concentration, the local distribution of oxygen in form of striations must be detectable by a change of the magnitude of the striations with respect to the heat-treatment.

2. Procedure

A large number of samples of Silicon single crystals zone floated as well as crucible pulled was taken. The following procedure was applied to the samples:

The as grown sample was polished and measured by spreading resistance.

The sample was heat-treated at 1100°C (open air) for 90 minutes. Within a few minutes the sample was brought to room temperature ("crash cooling") to avoid any activation of the donor state of oxygen due to the 450°C temperature range. After relapping the surface the sample was polished and measured by spreading resistance.

The sample was then heat-treated at 1100°C (open air) for 90 minutes and very slowly cooled down to room temperature so that the sample was kept for approx. 1 hour in the temperature range of approx. 450°C. That means that oxygen will be activated from the neutral to the donor state. After relapping the sample was polished and measured by spreading resistance.

Relapping of the sample after the heat-treatment was found to be necessary due to the formation of a surface layer by the heat-treatment which is quite uniform in resistivity. After removing this layer by lapping off a few micrometers the bulk resistivity characteristic was found.

The spreading resistance measurements subsequent to the heat-treatment or on the as grown material were taken in the same trace as correctly as possible. The obtained spreading resistance profiles have been compared qualitatively by superimposing one over the other. A quantitative evaluation was done by converting the spreading resistance readings into values of carrier concentration and comparing the values obtained by crash cooling and 450°C treatment respectively.

The difference " Δ " (cm^{-3}) between the values obtained by heat-treating the sample for a long time at 450°C and the so called "crash cooling" is related to donors generated by converting oxygen from the neutral into the donor state.

3. Results

In all our experiments we could not find any indication for oxygen striations. The result is the same in cross section and longitudinal section for zone-floated as well as for crucible pulled Silicon. This can be explained by the results of Yatsurugi et al. who claim from their experiments that the distribution coefficient of oxygen is $k_o = 1.25 \pm 0.17$ [2] .

For crucible pulled Silicon the radial distribution of the activated oxygen was found to be more or less uniform except for an edge area of approx. 1.5 mm. This is in agreement with Graff's results obtained by IR absorption at 9 /um wavelength [3] .

The average change of carrier concentration due to the oxygen activation (donor state) at 450°C is quite different for zone floated and crucible pulled Silicon crystals. This is related to the different oxygen content in these crystals. In most of the zone floated crystals no change in carrier concentration was observable. For crucible pulled crystals having an oxygen content of about 10^{17}-10^{18} atoms cm^{-3} (IR absorption [4] [5]) the average change in carrier concentration was approx. 10^{15} cm^{-3} which corresponds to the results obtained by Fuller and Logan [1] for a heat-treatment at 450°C for approx. 1 hour. In this case the change in carrier concentration in the edge area (which is near to the skin of the as grown crystal) is approx. 10^{13} cm^{-3}.

Plotting the calculated values of donor generation (" Δ ", cm^{-3}) in radial and axial direction of the crystal sample under test some areas have been found where the donor generation was much lower with respect to the other parts of the crystal. The distance between those regions of lower donor generation gave us the impression that these areas might be related to swirls. Therefore the samples have been etched for swirls applying Chromium Acid etch [6] . A comparison between areas of a lower donor generation obtained by spreading resistance measurement with areas showing swirls after etching gave a 100% correlation for swirls and areas of lower donor generation. The correlation is of such a quality that substructures in the density of shallow etch pits in the swirl bands correspond to substructures in the spreading resistance curves.

4. Discussion of the Results

With respect to the literature there is no doubt that additional donors generated by a heat-treatment at 450°C are related to oxygen. Therefore the local distribution of the additional donors is related to the local distribution of activated oxygen atoms. Two effects obtained by our measurements must be discussed:

4.1. The Edge Area

In an area of approx. 1.5 mm from the skin of the crystal a much lower amount of activated oxygen exists. Therefore we assume that the oxygen content is lower than in the entire crystal which is in agreement with Graff's results [3] . This may be due to out-diffusion of oxygen or $Si\text{-}O_x$ -formation on the Silicon surface or evaporation of oxygen from the melt in the miniscus area near to the liquidus solidus interface. Indications are that all of these effects work together.

4.2. Swirls

In the swirl bands oxygen is bound to the swirl forming complexes in such a form that the single oxygen atom cannot be activated to the donor state. That means that in the swirls oxygen is still there but will not be activated by 450°C heat-treatment. This is in agreement with De Kock's model describing the swirl forming complexes as VACANCY-OXYGEN-CLUSTERS.

This also explains some of the difficulties in the comparison of the 9 /um IR absorption coefficient with chemically obtained oxygen contents because oxygen bound to the swirlforming complexes does not show the 9 /um -resonance.

On the other hand our results may explain what the reason for the swirl formation is: We found that oxygen is incorporated to the Silicon crystal in a uniform distribution. With respect to the rotation rate and the growth speed the crystal will be supersaturated by vacancies in form of spiral bands. This nonuniformity of vacancy supersaturation generates the nonuniform arrangement of vacancy oxygen clusters WHICH IS SWIRL.

A discussion of this mechanism will appear in a later publication.

Acknowledgement

I am greatly indebted to my coworkers P. Siegesleitner (spreading resistance measurements) and Mrs. A. Mayer (sample preparation and the heat-treatment experiments).

I also have to express my thanks to my colleagues at Wacker-Chemitronic for providing me with samples and for critical discussion of the results.

This work was supported by the German Federal Ministry of Research and Technology, contract Nos. NT 381 and NT 506.

5. References

[1] Fuller and Logan
J. Appl. Phys. 28 (1957)
p.1427

[2] Yatsurugi, Akiyama, Endo and Nozaki
J. Electrochem. Soc. 120 (1973)
p. 975

[3] Graff, Grallath, Ades, Goldbach and Tölg
Solid State Electr. 16 (1973)
p. 887

[4] ASTM, F 121-70 T
Annual Book of Standards, part 8 (1973).
The American Soc. for Testing and Materials

[5] Kaiser and Keck
J. Appl. Phys. 28 (1957)
p. 882

[6] Method of Test for the Detection of Swirls and Striations in Chemically Polished Silicon Wafers, ASTM Standard, to be published.

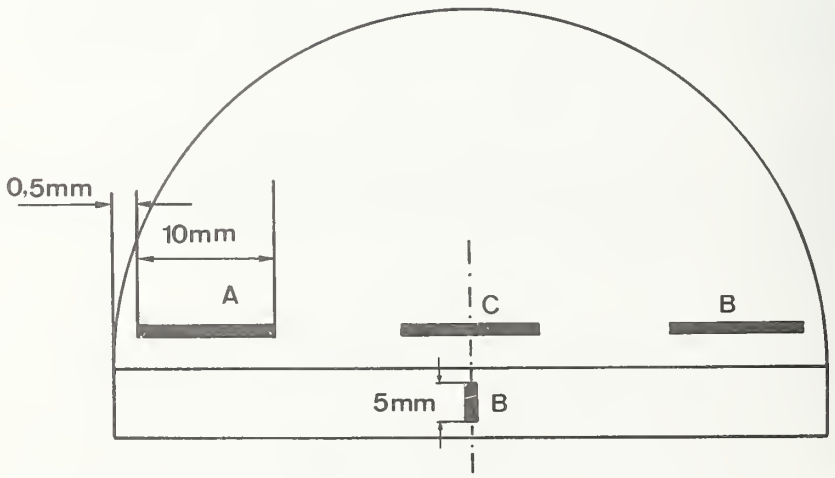

Fig.1 Location of the Spreading Resistance Trace (trace A) of the measurements reported in this paper.

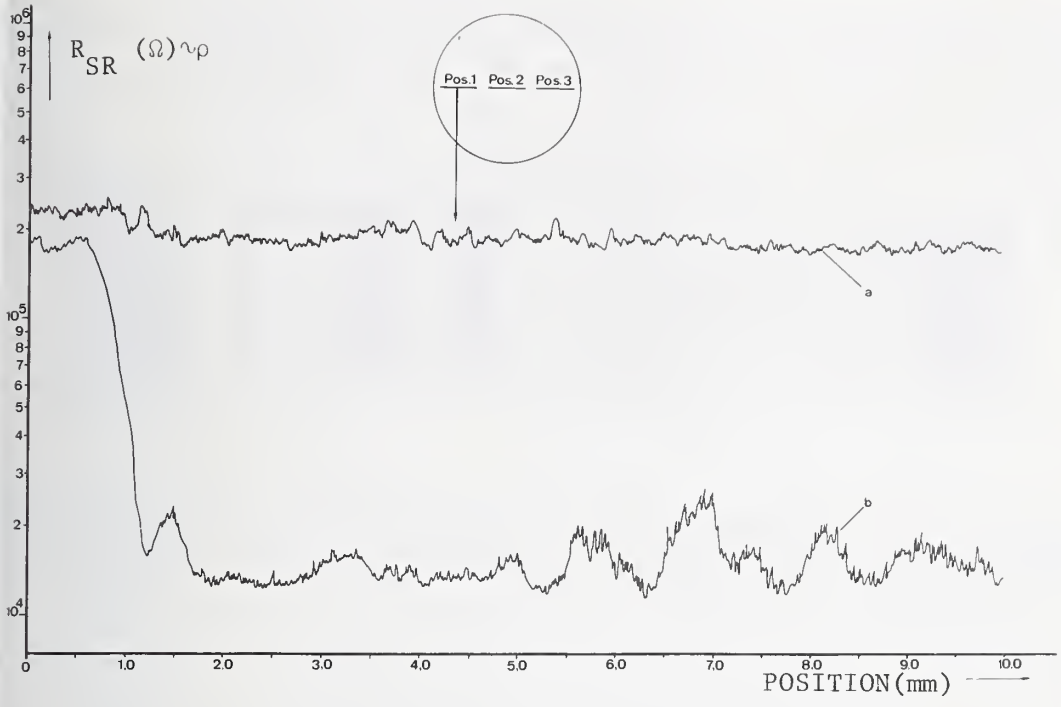

Fig. 2 Spreading Resistance Profiles of Trace A (fig. 1)
Profile "a": 1100°C, 90 minutes, "crash cooling"
Profile "b": 1100°C, 90 minutes, slow cooling (approx. 1 hr. for 450°C)

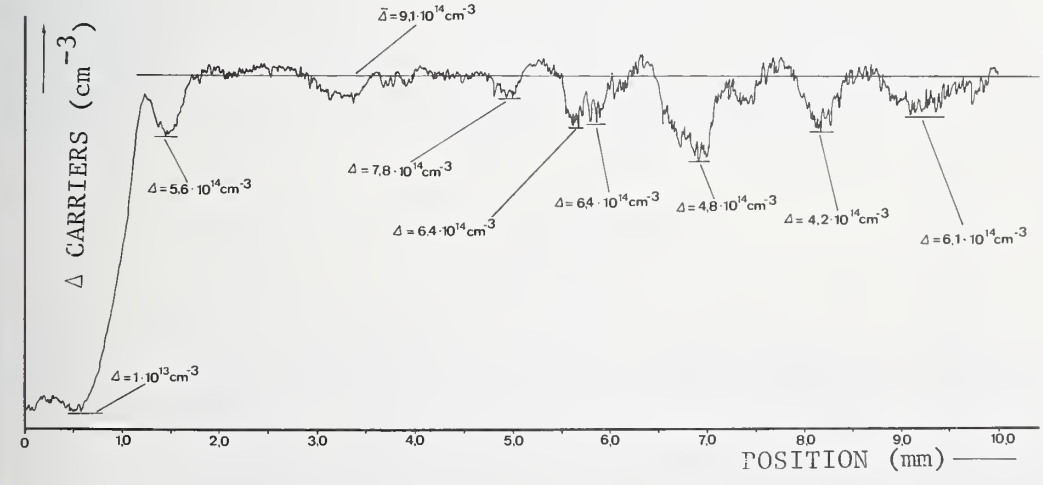

3 Difference "Δ" (donors cm^{-3}) calculated by deducting carrier concentration ned from profile "a" from carrier concentration of profile "b" of Fig. 2.

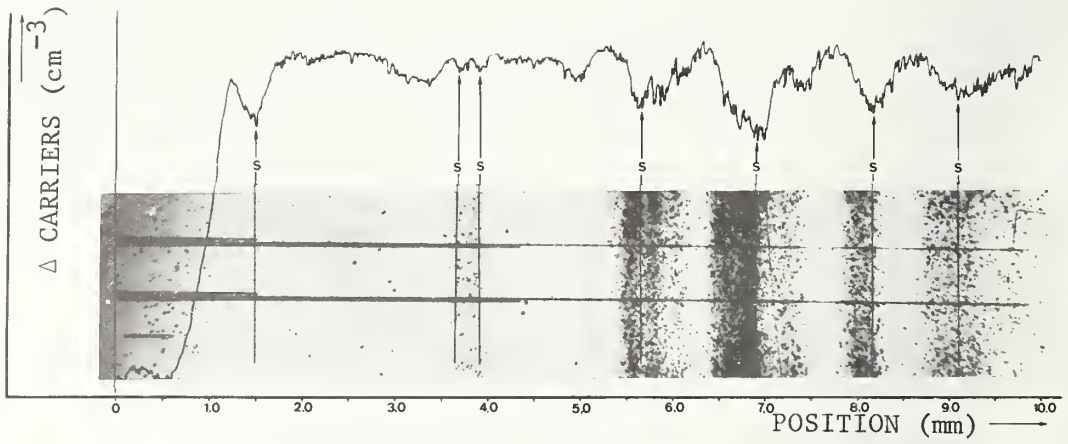

Fig. 4 Comparison of "Δ" (donors cm^{-3}) profile of figure 3 with the swirl-pat obtained by etching the sample. The two horizontal lines in the photograph ind the spreading resistance probe traces.

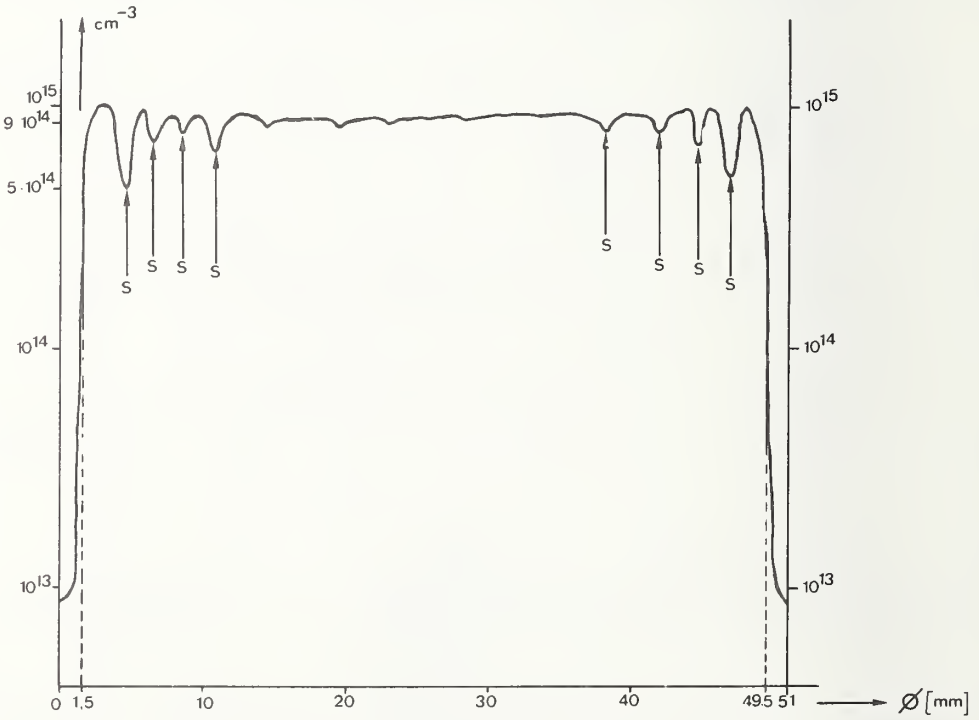

Fig.5 The Radial Profile of donors generated at 450°C equivalent to the oxyg distribution. Note the edge area of approx. 1.5 mm. and the swirl bands marke

NATIONAL BUREAU OF STANDARDS SPECIAL PUBLICATION 400-10, Spreading Resistance Symposium, Proceedings of a Symposium Held at NBS, Gaithersburg, Md., June 13-14, 1974.

Use of the Spreading Resistance Probe for the Characterization of Microsegregation in Silicon Crystals

F. W. Voltmer and H. J. Ruiz

Texas Instruments Incorporated
Dallas, Texas 75222

A technique for using the spreading resistance probe to quantitatively characterize microsegregation in single crystal silicon is presented. For the first time, the use of Fourier Transformations of the resistivity is developed to provide accurate quantitative information as to the periodicity and amplitude of the various components giving rise to the resistivity variations. It is demonstrated that the probe is reproducible and is capable of measuring fluctuations in resistivity to ±1 percent, which is well below the normally observed microsegregation. Examples of the use of the technique are given by characterizing microsegregation in two Czochralski grown crystals and one modified float zone crystal. The periodicity of the principle resistivity fluctuation of the Czochralski grown crystals is evaluated by Fourier transform analysis and agrees well with the anticipated fluctuations in impurity incorporation based on growth parameters.

Key words: crystal growth; Czochralski; Fourier transform; microsegregation; resistivity characterization; silicon; Spreading resistance.

1. Introduction

The growth of doped single silicon from the melt or by the floating zone technique results in periodic variations impurity incorporation, the magnitude and frequency being determined by the impurity species and growth nditions. Recently, the spreading resistance probe has been used to qualitatively characterize the fluctuations.[1][1] this paper, a technique is presented for the first time, to use the spreading resistance probe in conjunction with ourier transform analysis to quantitatively characterize the impurity microsegregation.

2. Experimental Technique

2.1. Crystal Growth

A number of 2000 gm, 2″ diameter phosphorus doped (nominally 0.8 ohm-cm) silicon crystals were grown by Czochralski technique under various growth conditions (viz. crucible and seed spin, pull rate and thermal vironment) for characterization of microsegregation of the dopant impurity. Material was pulled from melts heated radio frequency induction and by radiant heat from resistance heaters. The Czochralski crystals were principally own in the ⟨111⟩ direction, although crystals were also grown oriented along the ⟨100⟩ and ⟨115⟩ directions. osphorus was chosen as the dopant impurity because of its relatively low effective segregation coefficient (.45) mpared with boron and therefore its enhanced microsegregation. In addition, a crystal was grown by the modified ating zone technique for comparison. The growth conditions included variation in pull rate from 2.75 to 9 cm/hr and seed rotation rates from 1 rpm to 75 rpm. The crucible was counterotated at 10 rpm for the most of crystals.

[1] igures in brackets indicate the literature reference at the end of this paper.

2.2. Sample Preparation

The crystals as grown were approximately 12 inches long and 2 inches in diameter. Axial slabs 1/2 inch long were cut from the crystal at one inch intervals for axial microsegregation characterization of spreading resistance, and for interface delineation by etching. The configuration and location of the slabs are depicted in figure 1. Slabs were taken at intervals to determine the influence of fraction solidified on the microsegregation. In order to allow for single point spreading resistance measurements, the slabs were chemically-mechanically polished on one side and a gold ohmic contact formed on the other side. The backside gold contacts were flash evaporated directly on the cleaned back surface. The contact resistance of the gold-silicon interface was negligible when compared with the spreading resistance contact.

2.3. Spreading Resistance Measurements – The Apparatus

Single point spreading resistance measurements using a modified Solid State Measurements[2] mechanical probe station and TI control system and electronics (figure 2) were made on samples from various positions along each of the crystals.

The probe tips were Tungsten-Osmium with a probe radius of 25 μm and a loading of 40 gms. The value of spreading resistance measured is electronically fed to a minicomputer which is used for on line conversion of spreading resistance to either resistivity or carrier concentration.

The sample is mounted on a copper vacuum chuck which is electrically isolated from any equipment. This allows us to use the vacuum chuck as part of the current path when making single probe measurements.

2.4. Spreading Resistance Measurements – The Technique

The spreading resistance measurements were made on samples approximately 2" × 1/2" × 1/16" cut from the crystal as shown in figure 3 so that the axial resistivity could be profiled. The sample was placed on the spreading resistance probe chuck with the gold side down and held fast with a vacuum. The probe chuck was electrically isolated and allowed a return current path for the probe bias.

A diagram of the locations of the measurements on the sample are also shown in figure 3 along with the interface demarcation. Because the solid-liquid interface in crystal growth is usually curved, single point probe measurements were made to optimize the spatial resolution. Use of two probes would have resulted in measurements which gave the average resistivity of the regions being sampled by the two probes. Alignment of the probes collinear with the growth direction is critical to insure accurate determination of the spatial frequency. A misalignment would increase the apparent periodicity of the striations. Accuracy of the alignment is estimated to be better than 0.2 degrees.

The measurement sampling frequency was chosen a 10 μm/step. A sampling frequency of 5 μm/step was also tried, but did not provide any more information than the 10 μm/step frequency which was finally chosen. The distance over which measurements were taken ranged from 1.5 to 4.5 mm.

The measurements were done automatically at the rate of 10 measurements per minute. The data, either measured spreading resistance or computed resistivity values, were stored on either magnetic or punched paper tape. It was subsequently transcribed to data cards for processing on an IBM 360 using an FFT (Fast Fourier Transform) program. The data were also plotted such that any abnormal points (such as those caused by dust, scratches, etc.) could easily be corrected in the data card file before the FFT program was run.

2.5. Spreading Resistance Measurements – Reproducibility

In characterizing microsegregation using the spreading resistance probe, one is concerned with measuring small fluctuations in the resistivity over small dimensions. To determine the instrument's capability, three experiments were performed; the first to establish the variations inherent in the electronics of the apparatus; the second to establish the variations inherent in the mechanics of the apparatus; and the third, to establish reproducibility.

The first of the experiments consisted of connecting a 1000 ohm resistor across the probe input to the log detector and cycling through a series of pseudo-measurements. The results of this sequence of measurements are

[2] Solid State Measurements, Inc., 600 Seco Rd., Monroeville, Pa. 15146

plotted in figure 4 as resistivity as though one were measuring a sample of uniform spreading resistance such that $2R_S$ = 1000 ohms. Fluctuations in the converted resistance (i.e., resistivity) were thus due to instabilities in the electronics of the log converter and the A/D converter. As is apparent, the resistivity variation is less than ±0.5%. This is more than an order of magnitude better than the resistivity variations due to microsegregation which are typically measured.

The second experiment was to measure the resistivity variations on a uniform surface diffusion in order to determine if the resistivity variations measured in the virgin material were due to impurity variations or mechanical instability of the probes. It was assumed that the diffusion surface concentration was relatively constant. The diffusion was adjusted such that the resistivity after diffusion was approximately 0.1 ohm-cm on a 10.0 ohm-cm substrate. The results, again plotted as resistivity, are given in figure 5. The results are only slightly more than ±0.5% indicating the stability of the mechanical system. These measurements constitute a worst-case situation, and the probe stability is likely to be even better.

The third concern is the reproducibility of measurements of microsegregation where the resistivity fluctuations are on the order of 10%. Two sets of resistivity measurement were made adjacent to one another, and the resultant resistivity profiles are shown in figure 6. The reproducibility is apparent; only the absolute values are different owing to the slight lateral displacement of the probes for the two measurements.

The results of these three experiments indicate that the probe as configured is adequate to characterize microsegregation in bulk silicon in a reproducible manner.

3. Analytical Technique

Earlier attempts to describe the microsegregation of dopant impurities in semiconductors on solidification have been largely qualitative. Determining the frequency distribution has resulted from counting striations or resistivity variations in plotted data. For very periodic functions, with a single dominant frequency, this technique yields reasonable results. In crystal growth, however, there are often a number of parameters, both thermal and mechanical, which influence the impurity incorporation. Each of these parameters is likely to have a different frequency and hence the impurity distribution may be a composite of a number of frequencies. In order to grow crystal with uniform resistivity distribution, it is necessary to identify the source of the various resistivity fluctuations and this requires analysis of the composite resistivity profile. The technique presented in this paper for determining the relative strength and the periodicity of the various components of the resistivity fluctuations is Fourier Transform analysis.

The axial resistivity profile constitutes a complex spatially periodic function $\rho(x)$. The fundamental frequency components making up this function are derived from the temporally periodic conditions during growth. The temporal spectrum of the resistivity is thus obtained from

$$\rho(\omega) = \int_{-\infty}^{\infty} \rho'(x) e^{i\omega x} dx \qquad (1)$$

The function $\widetilde{\rho(\omega)}$ is complex and the spectrum is evaluated from

$$|\rho(\omega)| = \sqrt{\rho^*(\omega) \cdot \rho(\omega)} \qquad (2)$$

where $\rho^*(\omega)$ is the complex conjugate of $\rho(\omega)$.

The actual integration was performed numerically using FFT algorithm on an IBM 360 computer.

The non-zero average resistivity and the gradual change in the average resistivity owing to normal segregation give rise to a large spectral peak at zero frequency (i.e., the transform of a constant is a zero frequency component to the spectrum). This peak complicates the evaluation of the spectrum. In order to minimize the problem, a linear least square fit to the resistivity was obtained and subtracted on a point-wide basis to eliminate all ramp and square wave components of the function. Thus the actual resistivity function which is transformed is $\rho'(x) = \rho(x) - \overline{\rho(x)}$ where $\rho(x)$ is the actually measured resistivity profile and $\overline{\rho(x)}$ is the resistivity as determined by a least square fit to the actual data.

4. Results

In this section, representative results of measurements made on several single crystals of silicon are presented. The resistivity plots and transformed resistivity spectra are given for data taken on three crystals grown under varying conditions. Two of the crystals were grown by the Czochralski technique and the third by a modified float zone technique. In figure 7, the actual resistivity profile is shown for measurements made at the center and edge of one of the crystals. This crystal was pulled at 13.7 cm/hr, with the seed rotated at 35 rpm and the crucible counter-rotated at 10 rpm. The sample was taken at g = 0.6, where g is the molten fraction remaining at the time of solidification.[2] The transform of the edge resistivity modified by subtracting the average as derived from a linear least square fit is given in figure 8. The obvious spectral line at 58.8 μm agrees well with the observed frequency on the resistivity plot, while the resistivity fluctuations corresponding to the 2000 μm peak are not as readily apparent. In this case, the 58.8 μm periodicity can be accounted for by the growth of crystal during one revolution to within 10%. This value is arrived at by determining the length of crystal grown in one revolution, i.e., periodicity = (seed pull rate ± crucible lift rate) ÷ (seed spin ± crucible spin). The peak at 2000 μm corresponds to approximately one minute of growth which is very near the thermal time constant of the crystal puller.

The resistivity measurements made on the second crystal, pulled at 11.0 cm/hr and with a seed rotation of 1 rpm and a crucible counter-rotated at 1 rpm is presented in figure 9. The sample is taken at g = 0.6. The transform of this spectrum is shown in figure 10. Here again there is an obvious spectral line, however, at a wavelength of 875 μm, although the low frequency peak 2000 μm is not present. The peak at 875 μm agrees within experimental accuracy to the calculated growth of the crystal in one revolution, viz 914 μm.

The resistivity profile of a modified float-zone grown crystal, as distinct of the Czochralski grown crystals described above, is shown in figure 11. The growth conditions for this crystal were pull rate, 15 cm/hr; pull spin, 20 rpm. The transform of the resistivity spectrum is given in figure 12.

5. Conclusions

It has been shown that the spreading resistance probe can be used to quantify the resistivity microsegregation in silicon crystals. Instrument noise is shown to be less than ±0.5% and measurement reproducibility has been demonstrated. An analytical technique is described which allows calculation of the fundamental frequencies which contribute to the microsegregation. The results allow identification of those mechanisms which are dominant during crystal growth in determining impurity incorporation, and determination of the relative strengths of those mechanisms. A subsequent publication will discuss the results from a crystal growth point of view.

6. Acknowledgments

The authors wish to acknowledge the assistance of Roy O. Byrd in making the spreading resistance measurements.

7. References

[1] Witt, A. F., M. Lichtensteiger, and H. C. Gatos, "Experimental Approach to the Quantative Determination of Dopant Segregation During Crystal Growth on a Microscale: Ga Dope Ge, J. Electrochemical Society 120 1119 (1973).

[2] See for example Pfann, W. G., Zone Melting, John Wiley & Sons, Inc., New York 1958.

Figure 1. The configuration and location of slabs cut from the crystal for spreading resistance characterization.

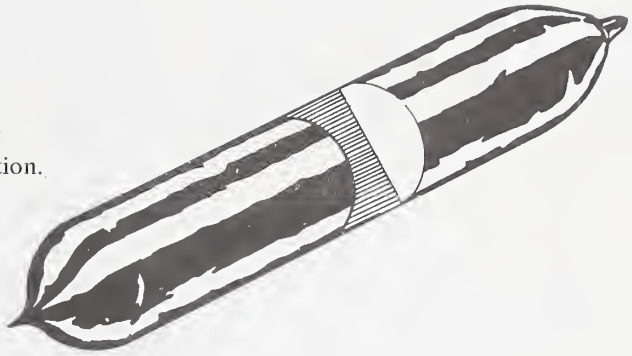

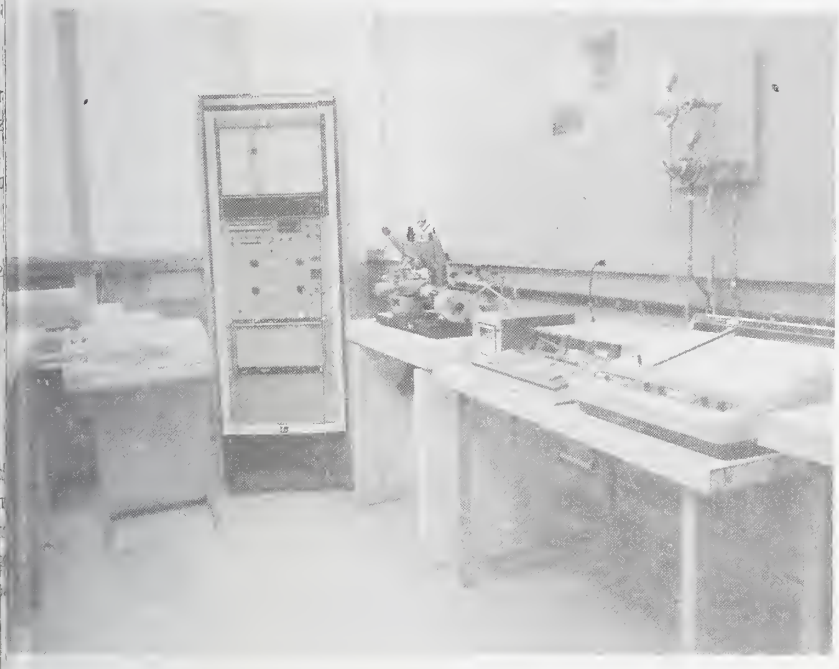

Figure 2. Photograph of spreading resistance apparatus.

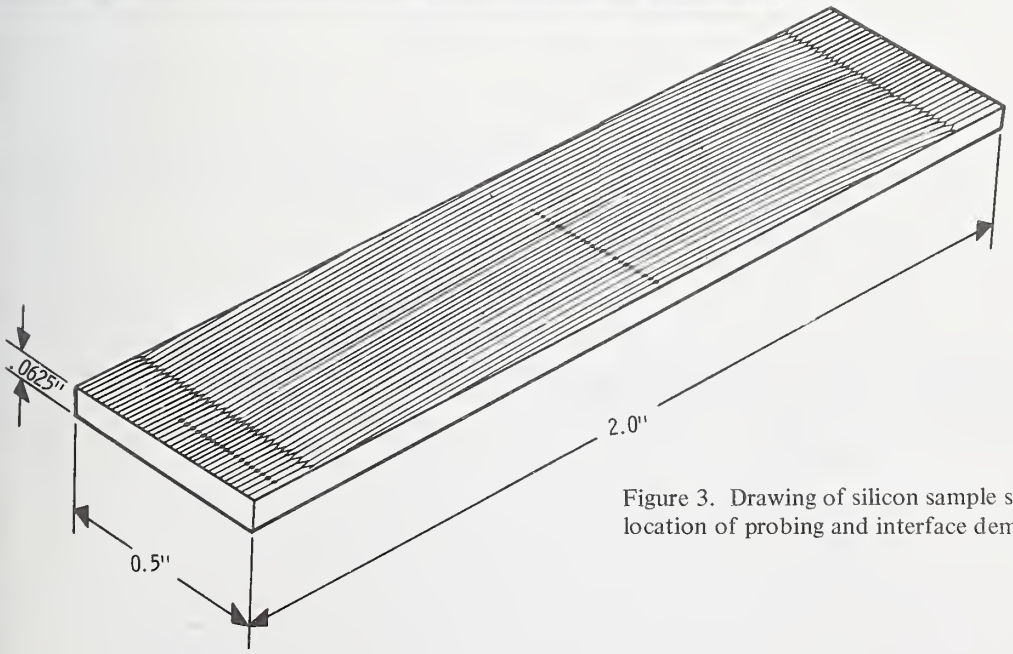

Figure 3. Drawing of silicon sample showing location of probing and interface demarcation.

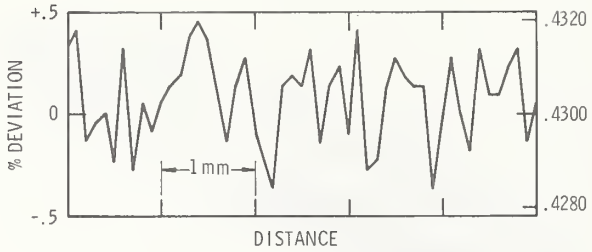

Figure 4. Variation in instrument output for 1000 ohm constant impedance across input to electronics. (See text)

Figure 5. Variations in surface resistivity of a uniform diffusion.

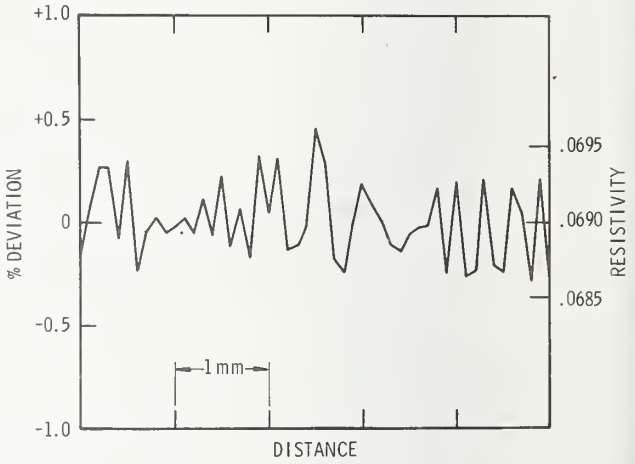

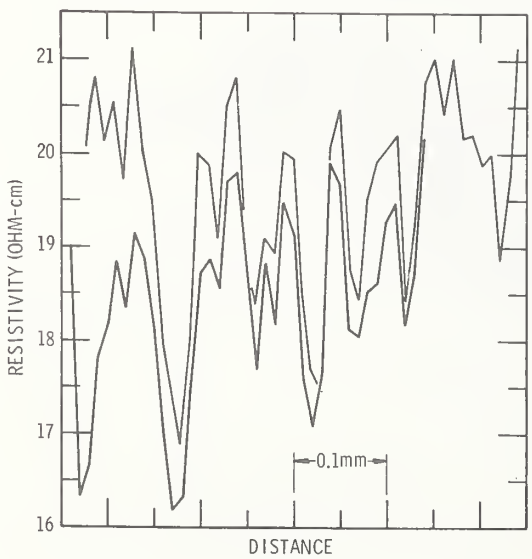

Figure 6. Reproducibility of microsegregation measurements determined by measuring resistivity in two adjacent regions.

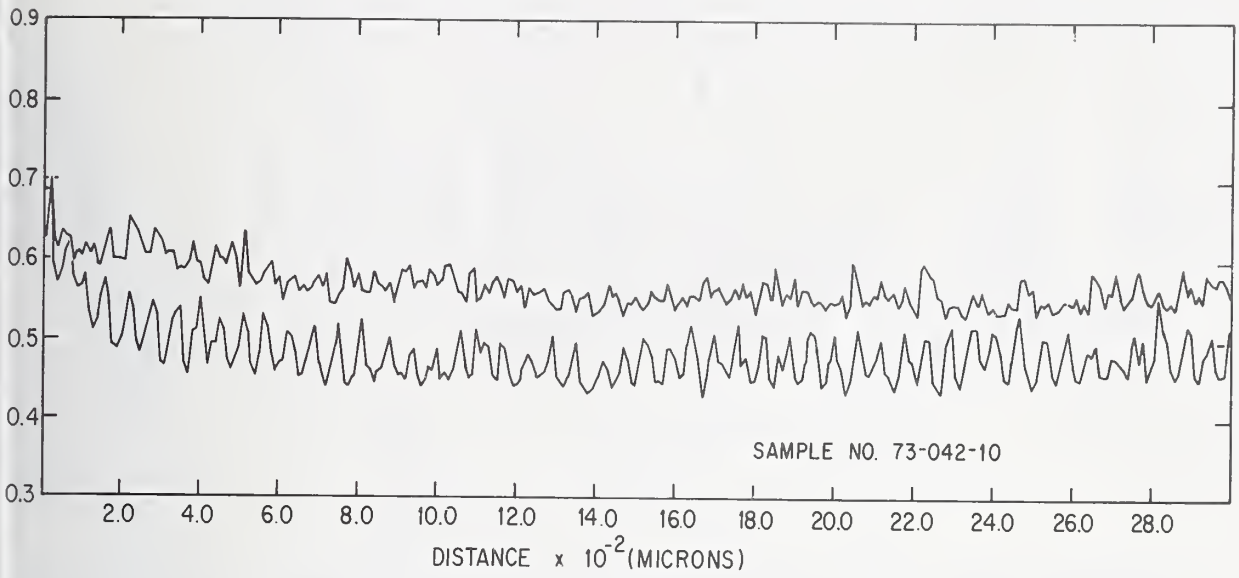

Figure 7. Axial resistivity of sample 73-042-10 measured at edge and center. (See text for growth conditions)

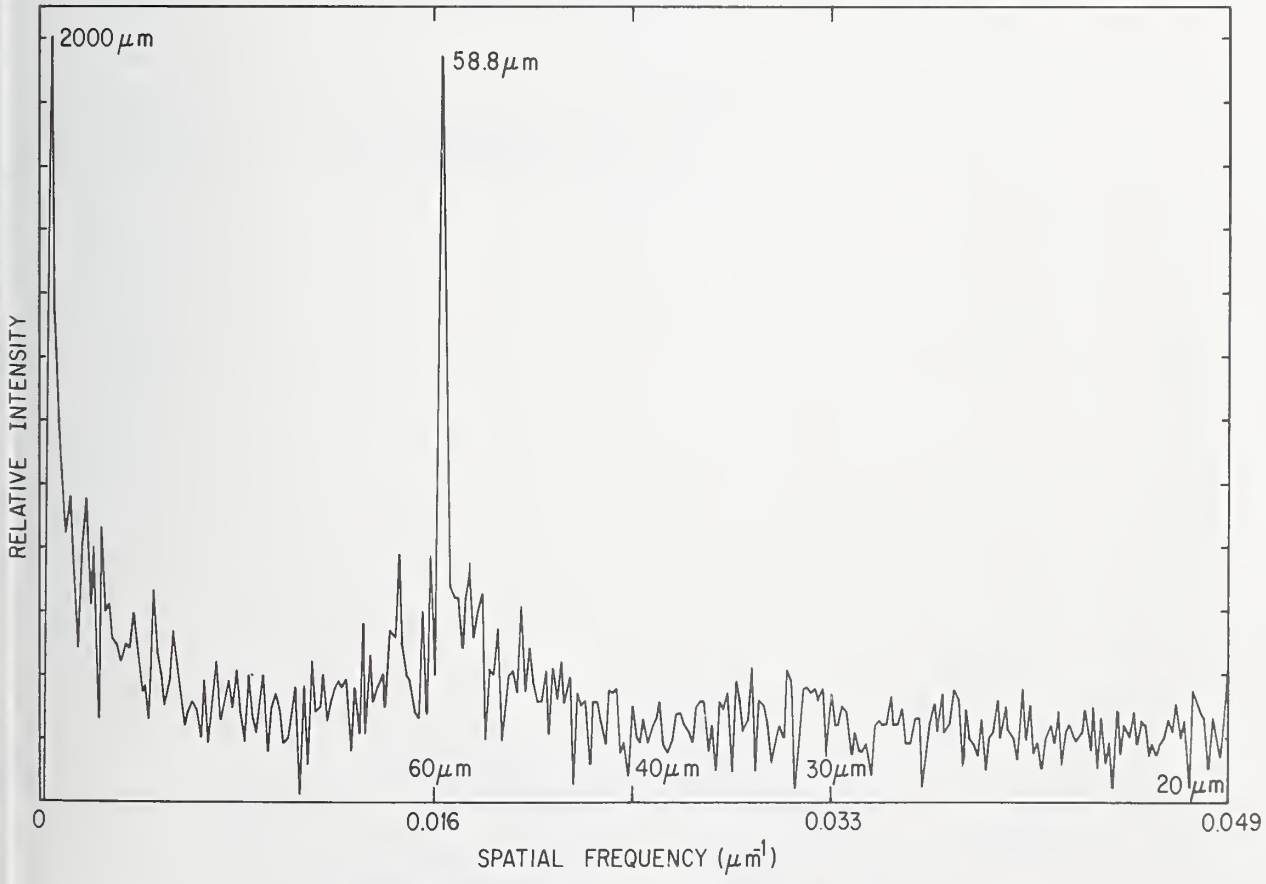

Figure 8. Transform of edge resistivity shown in Figure 7.

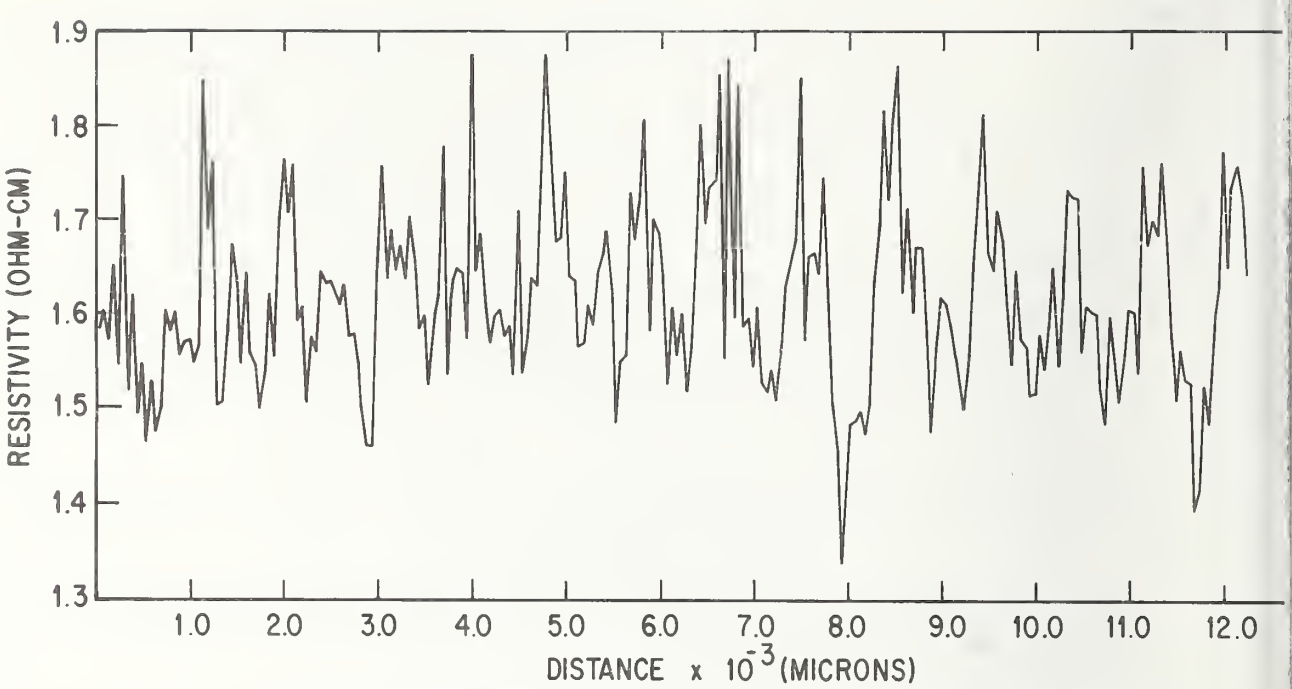

Figure 9. Axial resistivity of sample 73-049-6 measured at center. (See text for growth conditions)

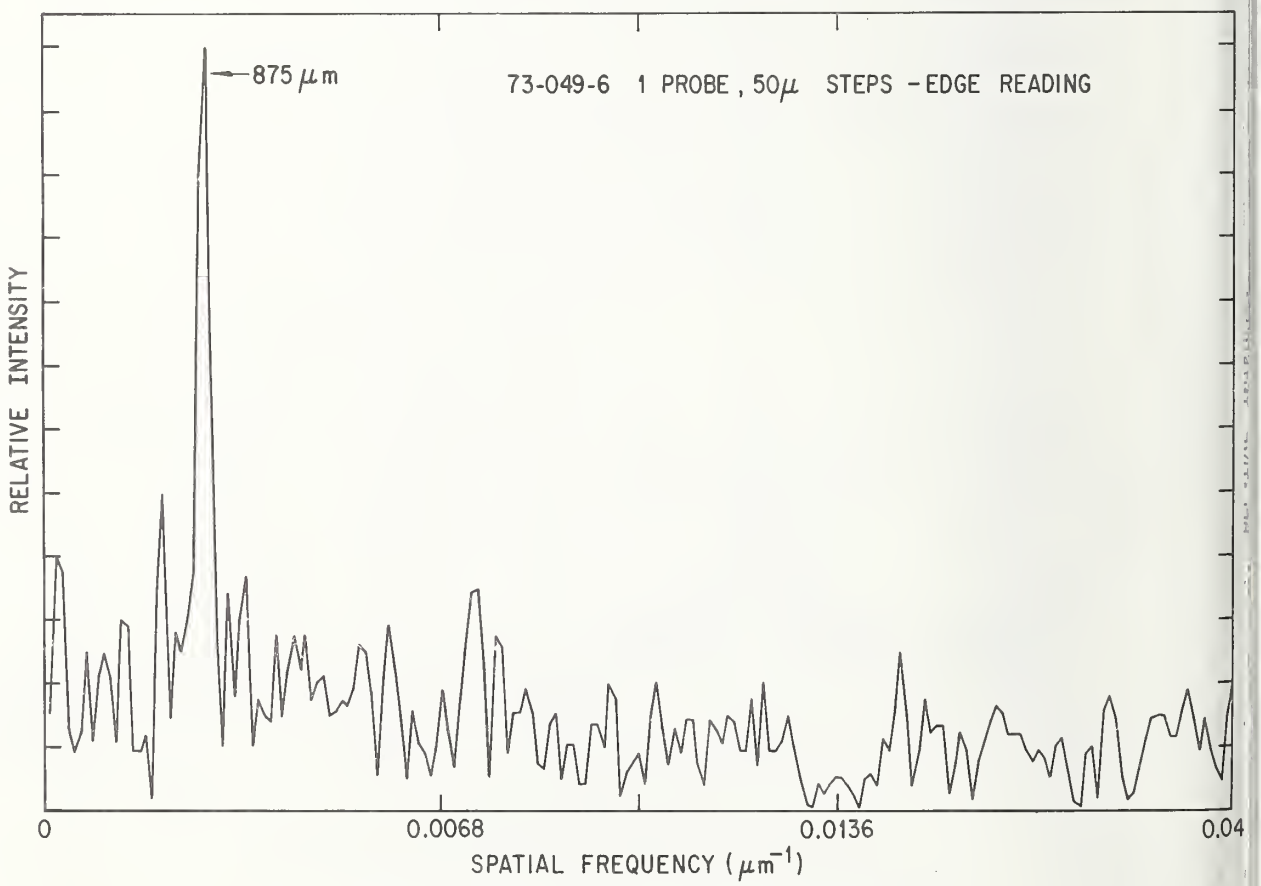

Figure 10. Transform of edge resistivity shown in Figure 9.

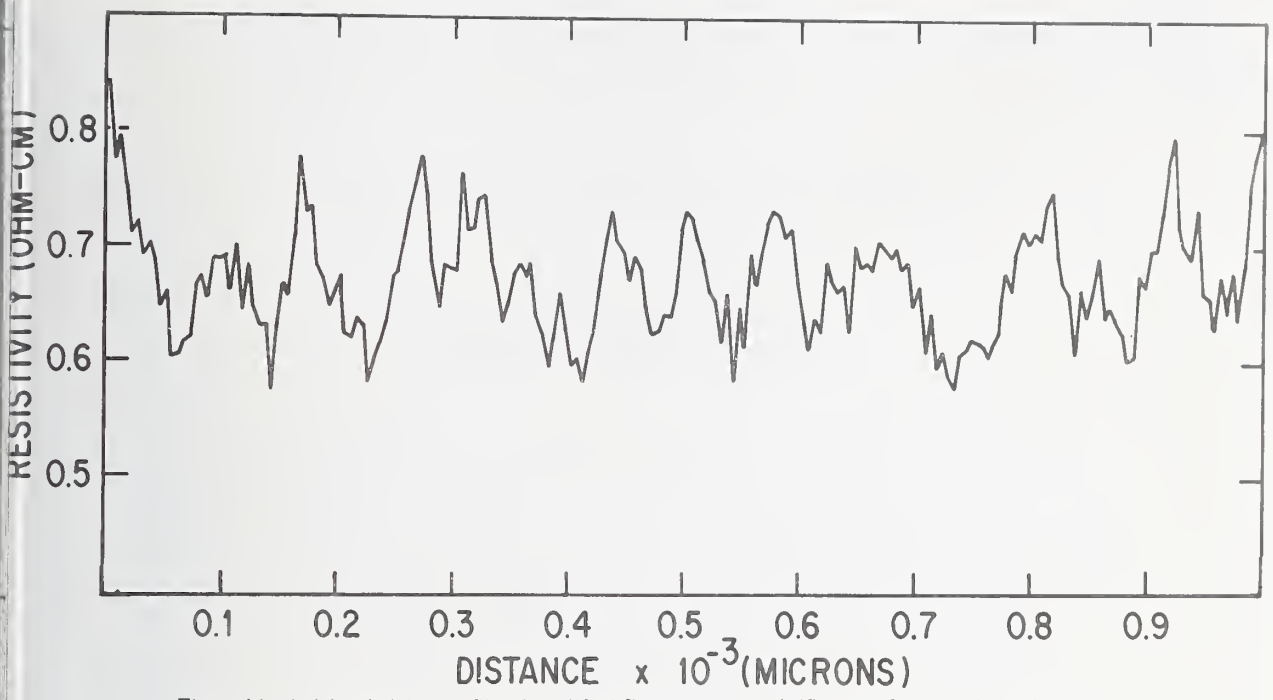

Figure 11. Axial resistivity profile of modified float zone crystal. (See text for growth conditions)

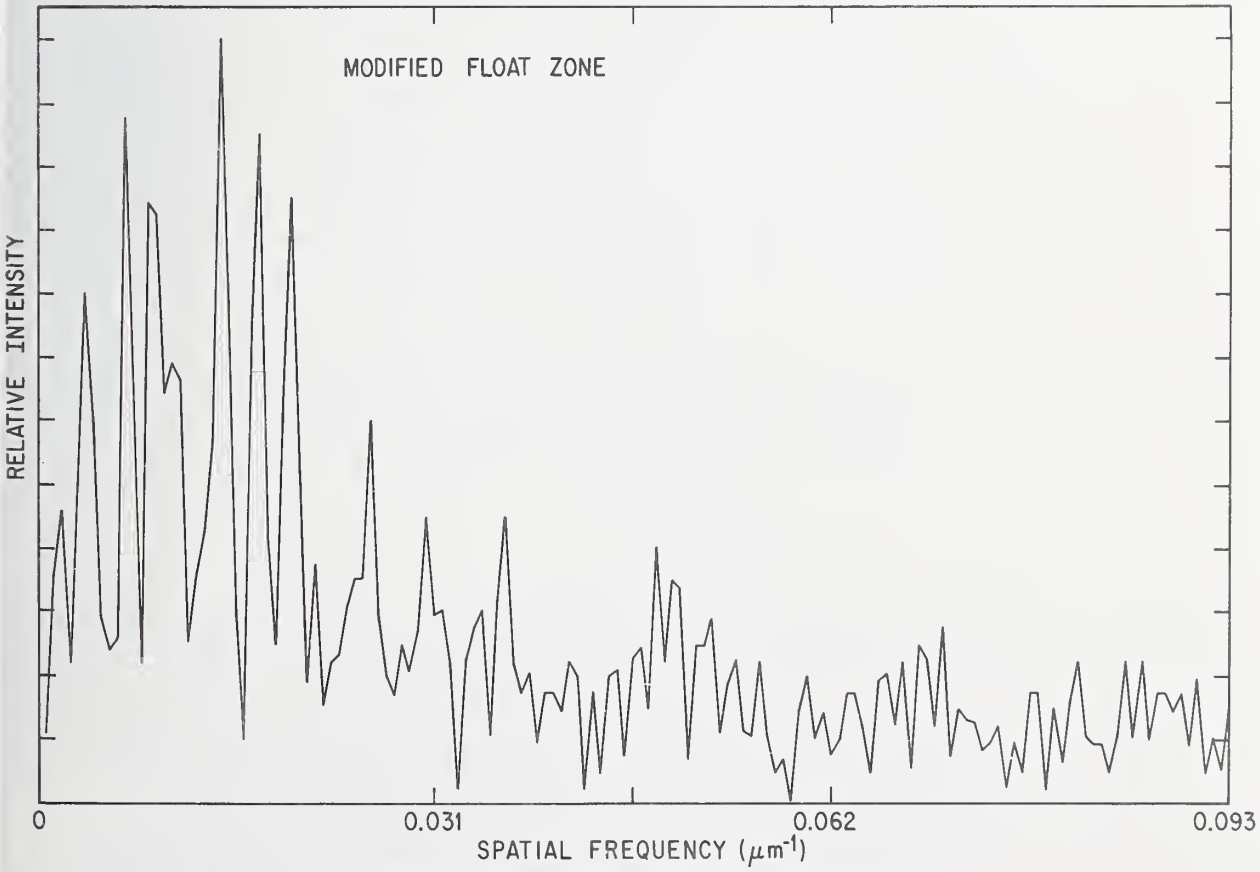

Figure 12. Transform of resistivity of float zone crystal.

565-448 O - 75 - 14

NATIONAL BUREAU OF STANDARDS SPECIAL PUBLICATION 400-10, Spreading Resistance Symposium, Proceedings of a Symposium Held at NBS, Gaithersburg, Md., June 13-14, 1974.

Effects of Oxygen and Gold on Silicon Power Devices

Jacques Assour

RCA Solid State Division
Somerville, New Jersey 08876

Several important features that make the two-probes spreading resistance technique a unique process control tool for designing and manufacturing silicon power devices are elucidated in terms of the effects of electrically active oxygen and gold centers on the characteristics of transistors, thyristors, and rectifiers. The effectiveness of the spreading resistance technique is compared to other commonly practiced techniques for the investigation of diffusion mechanisms of oxygen in homotaxial NPN transistors and of gold in fast switching rectifiers and thyristors.

Key Words: gold in silicon, oxygen in silicon.

1. Introduction

The internal structures of silicon power rectifiers, transistors, and thyristors are haracterized by multiple diffused and/or epitaxially grown junctions ranging in depth from) to 125 microns with doping concentrations varying from 10^{13} to 10^{21} A/cm^3. The control f diffusion and epitaxial processes used in designing and manufacturing these power devices as relied mainly on two commonly practiced techniques. The first is angle lapping and taining(1) to detect the presence and to determine the depth of a single junction or ultiple junctions. The second is the measurement of sheet resistance by the four-probe ethod, which is used in conjunction with the staining technique to determine average esistivities and surface concentrations of diffused and epitaxial layers. The intent is ot to discuss the reliability of each technique in terms of accuracy and reproducibility, ut rather to review their limitations as process control tools in a present day manufacuring environment.

The results of studies based on spreading resistance measurements have shown that the imitations of the staining and sheet resistance techniques reviewed below can be satisactorily resolved by the two-probe spreading resistance (SR) technique. In this paper, he unique features of the SR technique that aided the investigation of the effects of xygen and gold centers on the internal structure and electrical characteristics of power evices are discussed.

2. Limitations of the Staining and Sheet Resistance Techniques

The limitations of angle lapping, staining, and four-probe sheet resistance measurements urrently experienced in a manufacturing environment are noted in Table I. It is no surprise hat angle lapping and staining is operator-dependent, since this technique is considered by any as something of an art, and since it is greatly dependent on the topography of the laped surface, chemical reaction of the staining solution, and relative doping concentrations f the adjacent layers. The factors influencing the accurate delineation of n/n+ and p/p+ iffused layers are complex and little understood. Therefore, the delineation of multiple iffused or epitaxially grown layers in power devices is often fortuitous. The staining echnique is also time consuming in terms of measuring junction depth and recording data or permanent reference.

Figures in brackets indicate the literature references at the end of this paper.

Because of analytical boundary problems, the sheet resistance technique is not readily applicable to multiple layer structures, and consequently, special test samples of controlled geometry are required so that consecutive diffusions or epitaxial growth process can be monitored. This technique also inherently requires samples with areas 10 times larger than the spacings of the probes in order to reduce the influence of geometrical correction factors. Therefore, this technique cannot be used to study manufacturing problems in single, practical power devices. The sheet resistance technique provides average values for a given volume and is incapable of detecting micrononhomogenities. Therefore, it is incompatible with control requirements of current, sophisticated device designs. It is needless to add that the above technique is cost prohibitive for diffusion profile studies in a manufacturing environment.

3. Calibration of the Spreading Resistance Probe

The spreading resistance probe used at RCA as a process control instrument has been purchased commercially from Solid State Measurements. To date, over 400,000 points have been recorded with excellent reproducibility and minimum maintenance. Since the calibration of the SR probe is essential for accurate and reproducible data, the following procedure was adopted to calibrate the instrument. Several n- and p-type silicon wafers ranging in resistivity from 0.001 to 1000 ohm-cm were first profiled in bulk form by the SR probe for homogeneity. The resistivity of each wafer was then measured by the four-probe technique following ASTM Standard F84-72. The homogeneous n-type and p-type calibration samples were then lapped with an alumina abrasive, AO #305, and profiled by the SR probe. Using the SR and resistivity data, a least-square straight line was calculated to fit the data. The resulting calibration curves relating the measured spreading resistance with resistivity data for n-type and p-type samples are shown in Fig. 1. The reproducibility and accuracy of these calibration curves has been found excellent.

Other surface finishing methods based on mechanical and chemical polishing of the calibration samples were also investigated. Although polished surfaces reduced the noise level of the recorded data, these surfaces were found extremely sensitive to ambients and probe pressure, thus resulting in nonreproducible calibration curves.

4. SR Profiles of Multiple Layer Structures

Figs. 2 and 3 show that the limitations of the staining and sheet resistance techniques experienced in a manufacturing environment can be resolved by means of SR profiles. The SR profile of a multiple epitaxial layer structure used in the manufacture of high voltage transistors is shown in Fig. 2. This structure consists of three epitaxial $n/\nu/\pi$ layers grown consecutively on an n^+ substrate. This single profile yields complete and accurate data on the width and resistivity of each epitaxial layer, including the resistivity of the starting n^+ substrate. Clear delineation of the n/n^+ and ν/π interfaces and the non-uniformities in the resistivity of the ν layer can be uniquely achieved with the SR probe. Without the SR technique, angle lapping, staining, and sheet resistance measurements of two p-type control samples would be needed to evaluate the n and ν layers; the same techniques would have to be applied to the epitaxial structure to evaluate the π layer. No information would be available on the uniformity of the grown layers and on out-diffusion and auto-doping effects at the various interfaces. The data available from the SR profiles of epitaxial structures, when properly corrected for p-n junction effects, allow the accurate calculation of the breakdown voltages(2).

The second SR profile shown in Fig. 3, is that of an asymmetrical thyristor structure profiled through the T1 surface. This device consists of four layers diffused into a homogeneous n-type silicon region. It is sufficient to say that a detailed evaluation of the width and doping concentrations of all the active layers would have been a horrendous task by any known characterization technique other than the spreading resistance technique.

The next two discussions on the effects of oxygen and gold centers on power devices can only be investigated with the spreading resistance technique because of its unique ability to detect, reproducibly, micrononhomogeneities in complex diffused structures.

5. Effects of Oxygen on NPN Homotaxial Transistors

A cross section of an NPN homotaxial transistor is shown in Fig. 4. This device is fabricated by simultaneous diffusion of an n-type impurity from each side of a homogeneously doped p-type base. A mesa is etched on one side of the wafer to define the emitter and expose the base region for metal contacts. The starting p-type wafer is Czochralski grown, boron doped silicon crystal. Inherent to their growth process, these crystals contain relatively high concentrations of oxygen atoms, approaching 10^{18} A/cm^3. It has been shown(3) that under certain heat treatment cycles, the oxygen atoms form donor centers which greatly affect the resistivity and lifetime of Czochralski grown n-type and p-type crystals. The influence of oxygen donor centers on the resistivity of one sample from a p-type crystal after heat treatment at 450°C for one hour in an H_2 ambient is shown in Fig. 5. An SR profile in the radial direction of a 2-inch diameter wafer shows an initial resistivity of about 11 ohm-cm. Infrared measurements performed on this wafer revealed a strong peak at 9 micrometers, which is characteristic of oxygen absorption. A concentration of approximately $4x10^{17}$ A/cm^3 oxygen was determined from the absorption peak. After heat treatment, the SR profile in the same radial direction reveals several resistivity peaks with values exceeding 2000 ohm-cm. The resistivity upgrading is the result of oxygen donor formation whose detailed mechanism is not known, but it has been found(3) to be dependent on the parameters of crystal growth, such as heating or cooling rate, rotation rate, gaseous ambient, and crystal diameter. Therefore, as far as wafer processing is concerned, the device manufacturer is completely at the mercy of the impurities that the crystal grower has incorporated into the material. For oxygen, in particular, there is no way to remove what has been grown in. Consequently, unpredictable non-uniform concentrations of oxygen donor centers can form in both the radial and axial directions of p-type wafers. The spatial distribution and magnitude of the high resisitivity peaks shown in Fig. 5 were found by SR profiles to vary in wafers sliced from the same crystal.

The influence of resistivity upgrading on the structure of NPN homotaxial transistors fabricated with Czochralski crystals containing high oxygen concentrations is dramatically illustrated in Figs. 6 and 7. Fig. 6 shows the doping profiles determined from SR profiles of an NPN homotaxial transistor before and after heat treatment at 450°C for one hour. The doping profile measured from the emitter surface clearly delineates the base width and doping concentration, the emitter base, and base collector junctions. After heat treatment, however, the p-base has converted to an n-type region with no apparent junctions. Similarly, in Fig. 7 the doping profile measured from the base contact surface clearly delineates the width of the base region width and the base collector junction. After heat treatment, the p-base has converted to n-type and, consequently, the junction appears displaced at the new p^+/n boundary.

Similar profiles have been measured for several NPN transistor chips located in different areas of a processed wafer. The rate of resistivity upgrading and conversion of the p-base region from p-type to n-type resistivity varied with time and is assumed here to be dependent on the relative concentration of oxygen donor centers across the wafer as shown in Fig. 5. This phenomenon is shown in Fig. 8 for a transistor heated to 450°C. The SR profiles measured from the emitter surface have been superimposed to illustrate the rate of resistivity upgrading and final conversion as a function of time in hours. In this sample, total conversion of the base region from p-type to n-type silicon occurred after seven hours. It has also been reported(3) that these oxygen donor centers can be neutralized by heating the crystal to elevated temperatures. This phenomenon has been confirmed in several bulk wafers and processed devices. In fact, the sample shown in Fig. 8 was heated to 1000°C for 60 hours to obtain the SR profile shown before heat treatment.

Changes in the electrical characteristics of NPN homotaxial transistors with the type of resistivity changes explained above may be summarized as follows; all of these changes lead to yield rejects.

(1) Uniform resistivity upgrading in a device together with narrowing of the base region results in breakdown from premature punchthrough.

(2) Localized resistivity upgrading in the base region results in high leakage currents, I_{ECO}.

(3) Conversion in the base region from p-type and n-type resistivity results in V_{CEO} of zero volts.

(4) In all cases, transistors with high donor center concentrations exhibit very low current gains as a result of poor minority carrier lifetime in the base region. This result is also true in narrow base transistors and has been substantiated for transistors heat treated at 1000°C to neutralize the oxygen donor centers. In other words, oxygen complexes precipitated in the base region can act as effective recombination centers for electrons.

A closing note on this topic is the fact that NPN transistors fabricated with epitaxially grown p-type bases with structures identical to those of the NPN homotaxial transistors exhibit none of the oxygen phenomena discussed above.

6. Effects of Gold Doping in Power Devices

Gold is widely used to control the lifetime of minority carriers during the fabrication of fast switching power devices. Despite extensive studies(4) of the characteristics of gold doped silicon, there remain significant gaps in the understanding of the properties of gold doped silicon. These gaps, or problems, have left the industry without a complete model for gold diffusion into silicon. As a result, in a manufacturing environment, control of gold diffusion is empirical and often elusive. Examples of the unsolved problems are the accumulation of electrically active gold centers near the surfaces of silicon wafers, the diffusion mechanism of gold through heavily doped n and p regions, and the lack of correlation between the total gold concentration and resistivity upgrading of n-type and p-type silicon.

A typical example of gold accumulation near the surfaces of wafers of finite practical thickness is shown in Fig. 9. These are SR profiles of a gold doped n-type wafer for various diffusion times. The wafer has one mechanically polished surface and one lapped surface (12 micrometers alumina). An oxide layer 1 micrometer thick was grown on both surfaces and then removed from the polished surface only. A 50Å gold layer was evaporated on the polished surface. The wafer was divided into several samples which were diffused at 870°C for various times in an argon ambient. The initial and final resistivity values in the bulk are noted in Fig. 9 for reference. The SR profiles show evidence of the accumulation of gold centers near both surfaces even though one surface was masked by a thick oxide layer. The region of accumulation extends about 60 micrometers from each surface after 1 hour diffusion and decreases to about 20 micrometers after 4 hours. Excessive gold accumulation near surfaces has been observed(4), and the degree of accumulation, in homogeneous bulk wafers, has been found to vary slightly with surface and heat treatment of the samples. The diffusion mechanism responsible for the accumulation of gold has been explained(5) theoretically and shown to be related to vacancy generation in the bulk of silicon wafers. The difficulty with applying this model for production processes, however, is that it is nearly impossible to predict the concentration of defects and the accurate generation rate of vacancies in wafers that have undergone various diffusion, oxidation, and cooling treatments.

In practical devices, the degree of gold accumulation near the surfaces is further complicated by the differences in gold solubility in heavily doped layers. Gold appears to be more soluble in phosphorous doped regions as compared to boron doped regions. This property is illustrated in Figs. 10 and 11. Fig. 10 shows the SR profiles of p^+/n and n^+/n junctions fabricated in the same wafer before and after gold doping. The resistivity upgrading in the n region adjacent to the p^+ junction is much higher than that in the neighboring n^+ junction. This result is indicative of a difference in the concentration of electrically active gold centers diffused into the respective n regions. In other words, heavily doped phosphorous regions appear to getter gold atoms more effectively than boron doped regions. It is interesting to note that regardless of the diffusion mechanisms occurring at the p^+/n and n^+/n junctions, gold accumulation near the far surface is evident.

The above phenomenon is also illustrated in Fig. 11 for the case of a gold doped thyristor structure. The SR profile measured from the T1 surface is shown for the structure both before and after gold doping. In this example, gold has been diffused separately from the T1 surface and from the T2 surface. The resistivity upgrading in the n region when gold is diffused from the T2 surface is much higher and more uniform when compared to the T1 surface. The differences in the T1 and T2 SR profiles are interpreted as resulting from differences

n gold solubility and diffusion mechanisms in the n^+ and p^+ layers.

Although gold is used primarily to control the lifetime of minority carriers, its complex diffusion mechanism through heavily doped regions of power devices influences other important electrical parameters. In rectifiers, for example, excessive gold concentration in the n region of $p^+/n/n^+$ structures causes increases in the forward voltage drop at nominal current rating, and extremely short recovery time; the latter causes "ringing" in typical switching circuits. On the other hand, lower gold concentration causes yield depression because of long recovery times. In the case of gold doped thyristors, gold accumulation near surfaces can cause a significant decrease in the lifetime of minority carriers injected from the cathode into the p base; this results in higher gate currents and di/dt power dissipation during turn-on conditions. Secondly, excessive gold concentration in the n region, even if distributed uniformly, causes unpredictable, high resistivity upgrading which leads to premature bulk punchthrough breakdown. Thirdly, the forward voltage drop of thyristors in the on-state is also influenced by gold doping, which greatly decreases the diffusion length of minority in the n region.

7. Summary

The advantages and uniqueness of the two-probe spreading resistance technique as a process control tool for designing and manufacturing silicon power devices have been compared to other commonly practiced methods. The spatial resolving power of the SR method has been used to elucidate the effects of electrically active oxygen and gold centers on the electrical structure and performance of transistors, thyristors, and rectifiers. It is shown that for NPN homotaxial transistors fabricated from Czochralski grown crystals, oxygen donor centers in the base produced by low temperature heat treatment upgrade the resistivity of that region or completely convert the base to n-type. Moreover, the diffusion properties of gold atoms and their selective accumulation near the surfaces of finite, practical structures are illustrated with spreading resistance profiles.

8. References

(1) Research Triangle Institute, Integrated Silicon Device Technology Volume IV.... Diffusion by A. M. Smith, ASD-TDR-63-316, Volume IV, Contract No. AF33(657)-10340, Durham, North Carolina, February (1964).

(2) R. A. Sunshine and J. M. Assour, Avalanche Breakdown Voltage of Multiple Epitaxial pn Junctions, Solid State Electronics, 16, 459-466 (1973).

(3) Fuller, C. S. and Logan, R. A., Effect of Heat Treatment Upon the Electrical Properties of Silicon Crystals, J. Applied Physics 28, 1427 (1957).

(4) An excellent bibliography of the literature on the properties of gold-doped silicon has been published by W. R. Thurber and W. M. Bullis, Resistivity and Carrier Lifetime in Gold-doped Silicon, National Bureau of Standards, Washington, D.C. AFCRL-72-0076 (1971).

(5) F. A. Huntley and A. F. W. Willoughby, The Diffusion of Gold in Thin Silicon Slices, Solid State Electronics, 13, 1231-1240 (1970).

TABLE I

LIMITATIONS OF ANGLE-LAPPING AND STAINING TECHNIQUE

1. OPERATOR DEPENDENT
2. UNRELIABLE FOR n/n+ AND p/p+ DIFFUSED JUNCTIONS
3. TIME CONSUMING

LIMITATIONS OF FOUR-PROBE SHEET RESISTANCE TECHNIQUE

1. UNAPPLICABLE TO MULTIPLE DIFFUSED AND EPITAXIAL STRUCTURES
2. REQUIRES LARGE-AREA SAMPLES
3. PROVIDES AVERAGE VALUES OF A GIVEN VOLUME
4. COST PROHIBITIVE FOR DIFFUSION-PROFILE STUDIES

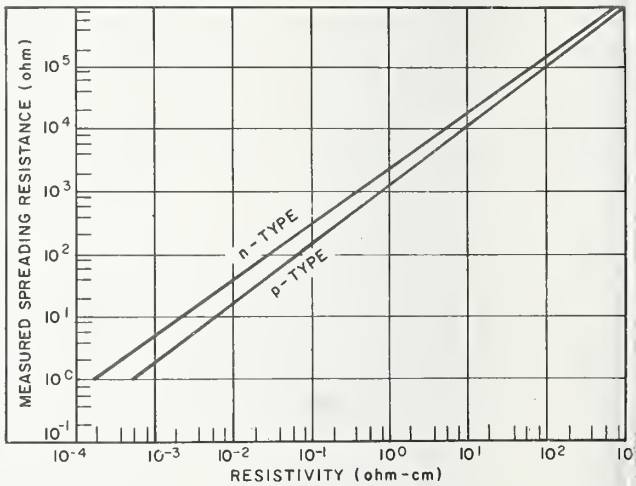

Figure 1. Spreading resistance calibration curves for n-type and p-type silicon.

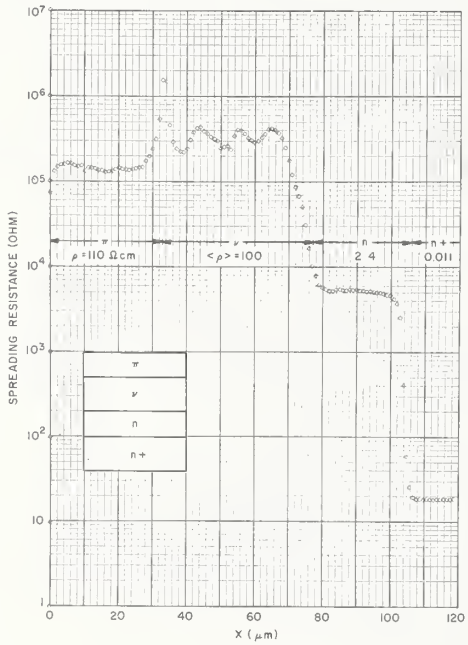

Figure 2. Spreading resistance profile of a multiple epitaxial layer structure.

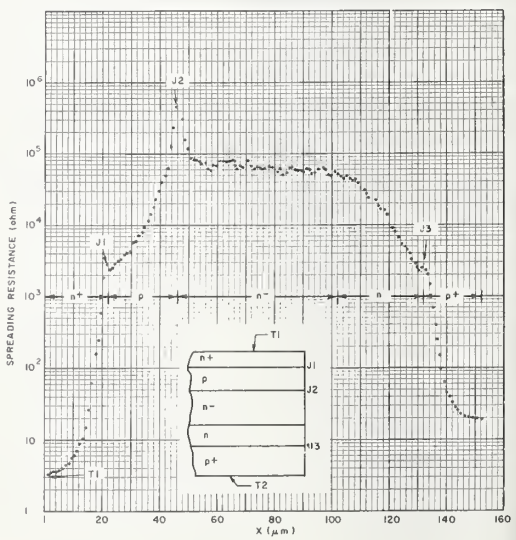

Figure 3. Spreading resistance profile of an asymmetrical thyristor structure.

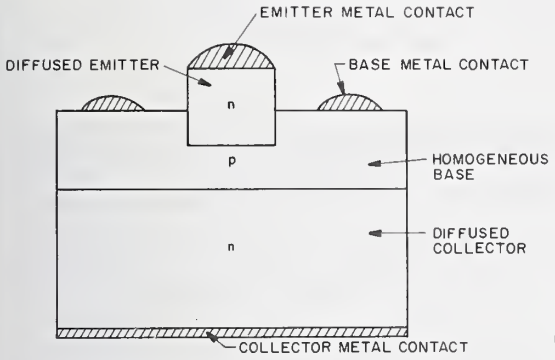

Figure 4. Cross-section of an NPN homotaxial transistor.

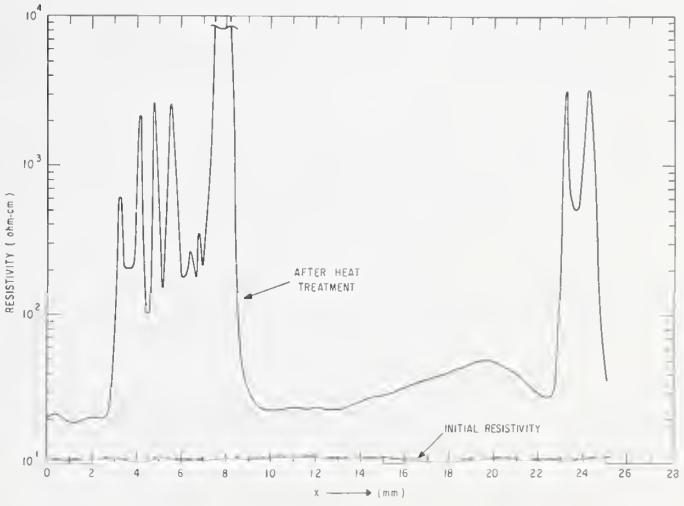

Figure 5. A radial SR profile of a Czochralski grown, boron doped silicon wafer before and after treatment at 450° C for one hour in an H_2 ambient.

Figure 6. Doping profiles of an NPN homotaxial transistor before and after heat treatment at 450°C for one hour. Profiles measured from the emitter contact region.

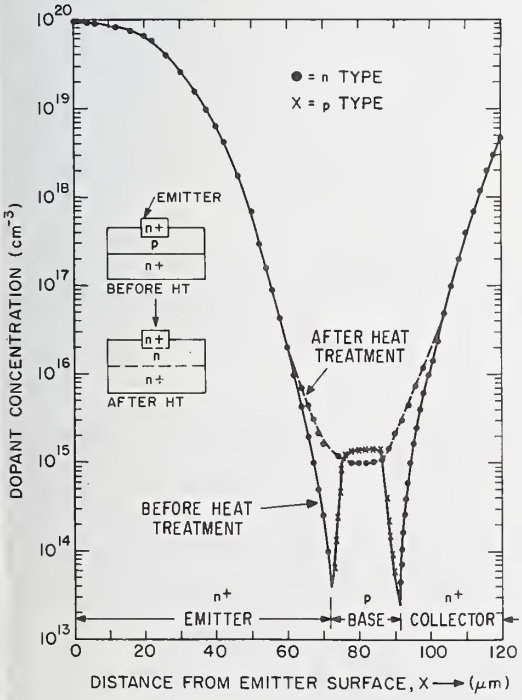

Figure 7. Doping profiles of an NPN homotaxial transistor before and after heat treatment at 450°C for one hour. Profiles measured from the base contact region.

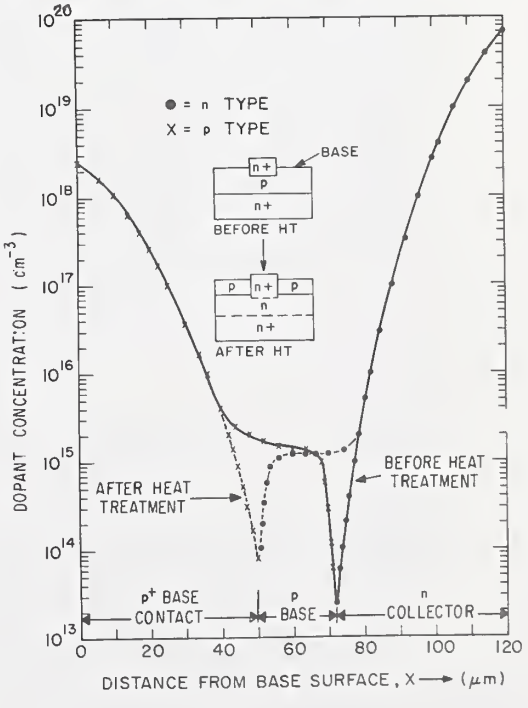

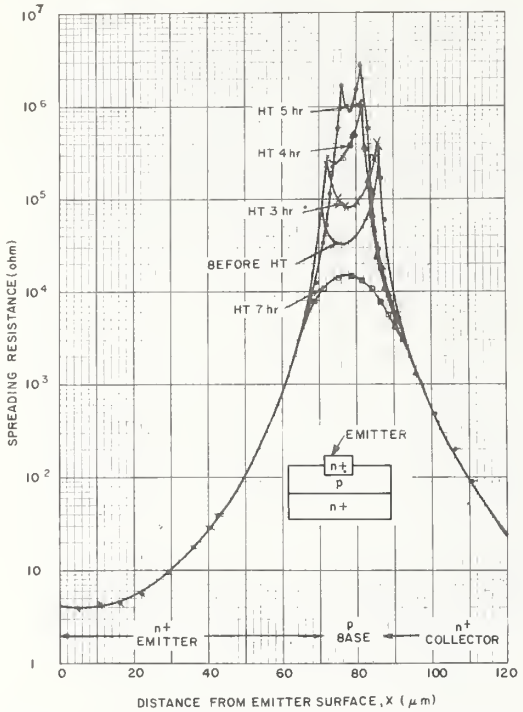

Figure 8. SR profiles of an NPN homotaxial transistor as a function of heat treatment.

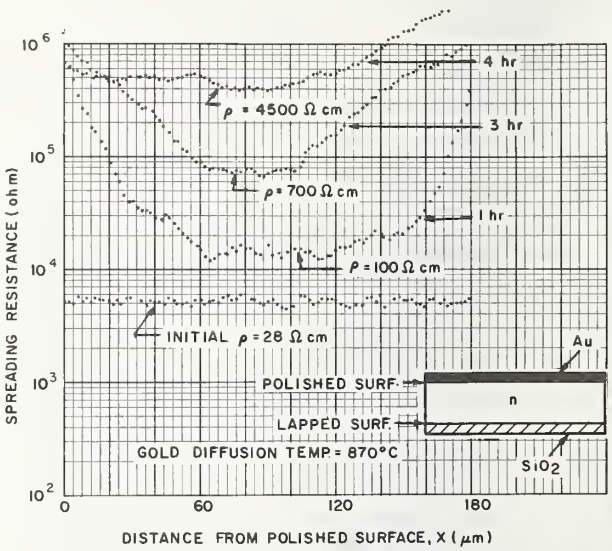

Figure 9. SR profiles of gold doped silicon as a function of gold diffusion time.

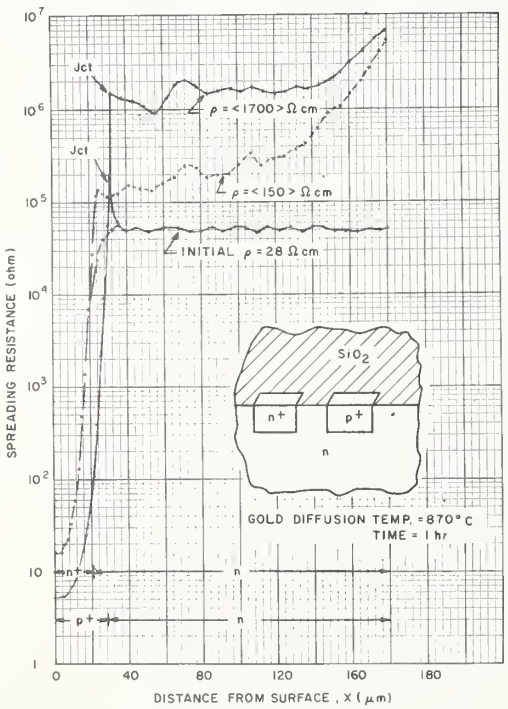

Figure 10. SR profiles of gold doped rectifier structures.

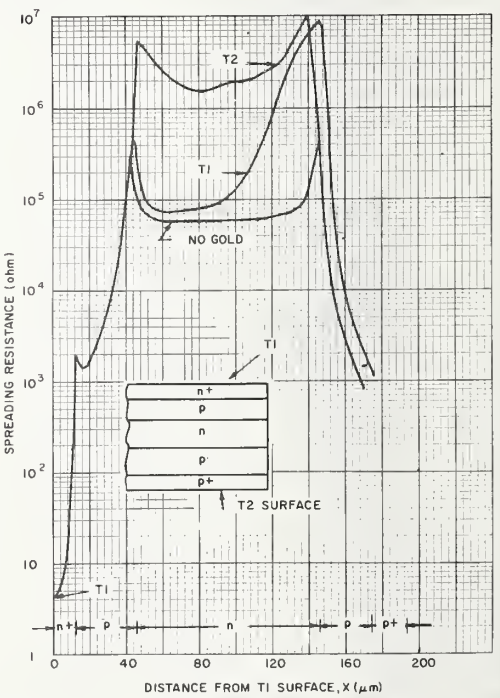

Figure 11. SR profiles of a gold doped thyristor structure.

NATIONAL BUREAU OF STANDARDS SPECIAL PUBLICATION 400-10, Spreading Resistance Symposium, Proceedings of a Symposium Held at NBS, Gaithersburg, Md., June 13-14, 1974.

The Evaluation of Thin Silicon Layers by Spreading Resistance Measurements[1]

Gilbert A. Gruber
Solid State Measurements, Inc., Monroeville, Pennsylvania 15146

and Robert F. Pfeifer
NCR Microelectronics Division, Miamisburg, Ohio 45342

The spreading resistance measurement technique is the only one capable of providing precise thickness measurements and detailed concentration profiles on any type of active device layer or structure formed in silicon on a routine basis. The methods employed in the evaluation of thin layer structures of the type used for microwave devices is discussed and the application of these methods to thin NN^+, P^+NN^+ and P^+N silicon structures formed by combinations of diffusion, epitaxy and ion implantation is illustrated.

Key words: Diffusion; epitaxy; ion implantation; microwave devices; profiling; spreading resistance; thin silicon layers.

1. Introduction

Important criteria for the successful operation of a silicon high frequency device re layer thickness and impurity concentration profile of the device. One of the major roblems of process control in the development and production of this type device is valuation of these two important parameters. Techniques such as infrared interference pectroscopy, angle lap and stain, anodic oxidation with differential four point probe easurements and various capacitance-voltage techniques, however, yield only limited nformation on micrometer and submicrometer thick structures or are extremely time onsuming. Only one method available today can provide precise thickness measurements nd detailed concentration profiles on any type of active device layer or structure ormed in silicon on a routine basis, i.e., the automatic spreading resistance measure-ent.

The purpose of this paper is to illustrate the application of the spreading resis-ance technique to routine evaluation of thin NN^+, P^+NN^+ and P^+N silicon structures ormed by combinations of diffusion, epitaxy and ion implantation.

2. Measurement Procedure

The apparatus used for the measurements of spreading resistance for this study was Model ASR-100 Mazur Automatic Spreading Resistance System (1)[2, 3]. This system is nown schematically in Figure 1 and features a two point probing arrangement with an

---

[1] Work was done at Westinghouse Research Laboratories, Pittsburgh, Pennsylvania 15235

[2] Solid State Measurements, Inc., Monroeville, Pennsylvania 15146

[3] Figures in parenthesis indicate the literature references at the end of this paper

X-Y plotter and a digital acquisition system for computer processing. The "conditioned" probe tips used for this study were each loaded to twenty grams and were spaced one-hundred micrometers apart.

Calibration of the instrument is done by periodic measurement of a specially prepared calibration block made up of a number of individual silicon samples of known resistivities. The calibration samples were initially measured using a four-point probe to determine the average resistivity of each. It was also found desirable to measure these standard samples with the automatic spreading resistance probe in a radial fashion in order to determine their doping uniformity since the accuracy and reliability of the measured sample resistivities is obviously no better than the calibration data to which the sample is compared.

The surfaces of the calibration samples were prepared by chem-mechanically polishing with an alkaline colloidal silica solution on a plastic plate. A typical calibration curve resulting from measurement of standards prepared in this way is shown in Figure 2.

The samples to be measured are prepared by scribing, breaking and then mounting on a bevelled polishing jig. A bevel is then chem-mechanically polished down through the layers to be measured. Surfaces prepared in this way are both smooth with no rounded edges and are damage free. They therefore meet the most important criteria necessary for reliable spreading resistance measurements, i.e. reproducibility.

After polishing, the sample was mounted on the mechanical subsystem of the probe, the bevel edge aligned with the probes and the precise bevel angle measured with the microscope. The measurement cycle was begun and the spreading resistance plotted as a function of position on the bevel edge. This position on the bevel is related to the actual thickness of the layer by:

$$T = NS \sin \alpha$$

where T is the layer thickness in micrometers, N is the number of spreading resistance points in the layer and S is the incremental step size in micrometers. For angles less than approximately 15° then:

$$\sin \alpha \simeq \tan \alpha$$

therefore, since the tangent is measured directly, a convenient working equation is:

$$T = NS \tan \alpha$$

A typical example of a profile of the kind obtained is shown in Figure 3. This is an example of a thin multiple epitaxial structure measured with S = 2.5 micrometers per step and a $\tan \alpha = .020$, therefore, each step across the bevel represents a 500A increment in the thickness of the layer.

Once a sample is measured and a plot is obtained, the real advantage of this technique can be seen. The plot represents a map of the entire electrical structure obtained by the various processing techniques employed. These "raw data" plots of spreading resistance as a function of position on the bevel surface can be used as process monitors without further processing of the data. When necessary, however, these data can be converted to resistivities, by comparison with the calibration curve described above, and impurity concentrations by using the mobility data of Sze and Irvin (2).

3. Corrections for Insulating and Conducting Boundaries

Considerations of the geometric aspects of this measurement require correction to the value of resistivity obtained from measurements taken in close proximity to either of the

wo extreme cases of an insulating or a conducting boundary (3, 4, 5). For this study the correction for the presence of an insulating boundary (a P-N junction) described by Dickey (4) and Mazur (5) was used. In this method the working equation for the correction of resistivity in the proximity of an insulating boundary is:

$$\rho_{corr.} = \frac{4a}{p}\left[\frac{R_m}{k(\rho) - 1 + C}\right]$$

here R_m is the measured spreading resistance, $\rho_{corr.}$ is the corrected resistivity of a ample at a particular point, "a" is the metal-semiconductor contact radius (3×10^{-4} cm.), p" is the number of probes used in the measurement, $k(\rho)$ is a measure of the "zero bias arrier resistance" (4) of the point being measured and "C" is the geometrical correction actor for an insulating boundary. The parameter k is a function of the resistivity and an be determined by solving this equation for $k(\rho)$ using the calibration data and the fact hat C = 1 in the absence of an insulating boundary. To apply this correction, an itera- ive procedure is used. First, the resistivity, ρ, corresponding to the measured resis- ance, R_m (assuming C = 1 and choosing a value for $k(\rho)$ corresponding to that resistivity) s found. Then a value of C is calculated from the equations of Dickey (4) given below:

$$C = 1 + \frac{2a}{\pi t} \ln (D/2t) - 0.116 \qquad (t \geq a)$$

$$\text{or } C = \frac{2a}{\pi t} \ln (2D/a) \qquad (t < a)$$

D" is the lateral spacing between a pair of spreading resistance probes (.01 cm in this ork) and "t" is the thickness of the layer below the spreading resistance probes in centi- eters. From this data a value for $\rho_{corr.}$ is calculated. Then a new value for $k(\rho)$ is etermined for this new value of ρ. A few iterations are usually all that are necessary to ring the corrected resistivity value to within five percent of the previous value in the teration procedure.

This correction is based on geometric considerations of the spreading resistance mea- urement. The following assumptions are made: 1. a perfectly circular contact of radius, a", 2. a perfectly insulating boundary, 3. a relatively uniform layer, 4. no edge effects ue to the pinching of the field as the probe approaches the edges of the sample and 5. an ccurate measure of the thickness at which the junction occurs. These assumptions do not old in all cases and are invalid in the vicinity of a junction. This procedure has the dvantage, however, of being easy to apply and gives results that compare favorably with easurements made by other techniques (6, 7).

The correction used for a conducting boundary is based on the work of Brooks and ttes (8). Since nearly all of the conducting boundary corrections are made to measure- nts of lightly doped silicon layers on a heavily doped layer, e.g., an N-type epitaxial yer on an N^+ ($N \sim 10^{19}/cm.^3$) substrate, the substrate may be assumed to be a perfect con- ctor. A copy of the relevant correction curve is shown in Figure 4. Here the ratio of e corrected spreading resistance value $R_{corr.}$ to the measured spreading resistance R_m is otted as a function of the thickness of the silicon above the conducting layer for a con- ct radius of 3×10^{-4} cm.

4. Results and Discussion

The example in Figure 3 above, is a "raw data" spreading resistance plot of a thin P^+N itaxial structure deposited at a pyrometer temperature of 1050°C. from a silane source on N^+ substrate (9). From this profile it can be seen that the spreading resistance in- eases from the surface (the extreme left hand side of the plot) to the P-N junction (the ximum spreading resistance value). The spreading resistance of the N-type layer appears latively uniform before dropping off to the substrate value. When these data are corrected

for the presence of the P-N junction and for the conducting NN^+ interface, the plot of concentration vs. thickness shown in Figure 6 is obtained. Three rather interesting effects, not apparent in the "raw data" plot, can be seen. First, the impurity concentration of the P^+ region of the curve is uniform from the surface to the P-N junction. Secondly, a dip in the concentration occurs at the N-N^+ interface and third, a steeper N to N^+ transition gradient is seen at the N-N^+ interface. Note again that none of these three effects is apparent from the uncorrected "raw data" plot. The uniform P^+ layer is typical for this type of epitaxial growth and is expected. The "dip" in the impurity concentration at the N-N^+ interface, however, is in contradiction to the normal case where the transition from a heavily doped substrate to lightly doped epitaxial layer occurs in a gradual fashion from one concentration to the other. We believe the cause of this particular phenomenon is that the N-type epitaxial deposition was purposely done in two steps in order to obtain the steeper N to N^+ transition gradient also observed. The first part of the layer was grown with no dopant gas being injected into the reactor and so was doped only by the transported and evaporated dopants from the substrates. After this initial growth which is designed to increase the abruptness of the N^+ to N-type transition, phosphine is injected into the gas stream to dope the remainder of the layer to the proper impurity level. This belief is supported by the series of profiles shown in Figure 6 which are results obtained by varying the length of deposition time for the initial or undoped layer. This study was done using silicon tetrachloride but other experiments indicate that the same relative result is obtained for the silane system. These are raw data plots and as such have not been corrected for the presence of a conducting boundary as in the computer curve above, but the same effect is shown. Curve A shows the effect of a zero time delay between silicon source gas injection and dopant gas injection; and Curves B through D show the effects of delay times of 1, 2 and 5 minutes respectively. As can be seen from the peak in Curve D, a higher resistance layer is formed at the N-N^+ interface the longer the delay time. This peak in the resistance is equivalent to a dip in the impurity concentration. The choice of proper delay time to give the sharpest N^+ to N transition without forming this high resistance layer, which would distort the electric field in this region, depends on the purity level of the silicon source material and the backround purity in the epitaxial reactor.

The profiles shown in Figures 7 and 8 are the raw data plots of spreading resistance and corrected impurity concentration as a function of layer thickness, respectively, for a P^+ layer diffused into an N-type epitaxial layer grown on an N^+ substrate. In Figure 8 the gradual change in the concentration of the P^+ layer and the change in slope at approximately the midpoint of the layer which are not apparent in the "raw data" plot are typical for a boron diffusion done in two steps - a predeposition and a drive-in. Because each of these steps was done under different source conditions, i.e., the predeposition from an infinite source and the drive-in from a limited source, the resulting profile is that of a double diffusion as shown. It is also noteworthy that the impurity concentration in the N region of this structure does not decrease as the N^+N interface is approached and that the N^+ to N resistivity transition occurs over a wider region than seen in the previous example. Both of these effects are probably the result of the higher temperature used throughout the growth of this layer, compared to that of the previous example, and the subsequent diffusion of impurities from the substrate into the epitaxial layer during both the epitaxial deposition and the P-type layer diffusion.

The next example illustrating the use of the spreading resistance technique for profiling thin layers is that of a silicon P-N junction structure prepared by ion implantation followed by an anneal to eliminate damage. This structure is shown in Figures 9 and 10. The ion implantation was done at a B^+ dose of $6 \times 10^{14}/cm.^2$ The most interesting feature to be seen from these profiles is the region of higher impurity concentration between the surface and P-N junction. Although this type of profile is not normal in the case of junctions formed either epitaxially or by diffusion, it is typical of junctions formed by ion implantation (10). The position of the peak of this impurity profile and the shape of the profile depends on the energy of bombardment and the crystallographic orientation of the silicon crystal during bombardment.

5. Conclusion

The automatic spreading resistance probe, by providing detailed evaluation of thickness and impurity concentration in thin layered structures has been shown to be unique in its ability to provide quick, reliable feedback on the effects of semiconductor processing.

General process features such as epitaxial resistivity uniformity and profile reproducibility can be monitored on a routine basis by use of the raw data spreading resistance profiles. In addition, computer processed resistivity or concentration profiles may be obtained from the spreading resistance profiles to be used by the device designer for material evaluation and product improvement.

6. References

(1) R. G. Mazur and D. H. Dickey, J. Electrochem. Soc., 113, 255 (1966).
(2) S. M. Sze and J. C. Irvin, Solid State Electronics, 11, 599 (1968).
(3) E. E. Gardner, P. A. Schumann, Jr. and E. F. Gorey, Measurement Techniques for Thin Films, Bertram Schwartz and Newton Schwartz eds., The Electrochemical Society (1967) p. 258.
(4) D. H. Dickey, "Diffusion Profiles Using a Spreading Resistance Probe", Extended Abs. of the Electronics Div., Electrochem. Soc., Vol. 12, 151 (1963).
(5) R. G. Mazur, "Spreading Resistance Resistivity Measurements on Silicon Containing P-N Junctions", Extended Abs. of the Electronics Div., Electrochem. Soc., Vol. 15, Abs. No. 164, (1966).
(6) R. N. Ghoshtagore, Phys. Rev. B, 3, 389 (1971).
(7) R. N. Ghoshtagore, ibid. 3, 397 (1971).
(8) R. D. Brooks and H. G. Mattes, Bell System Tech. Jour. 50, (1971).
(9) T. L. Chu and G. A. Gruber, J. Electrochem. Soc., 114, 522, (1967).
(10) J. F. Gibbons, Proc. IEEE, 56, 295, (1968).

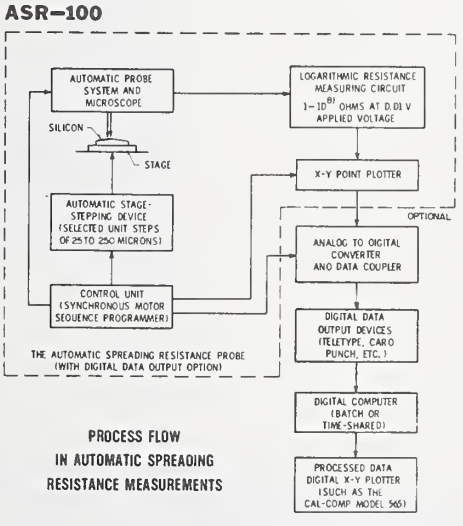

Figure 1. Diagram of ASR-100 Automatic Spreading Resistance System.

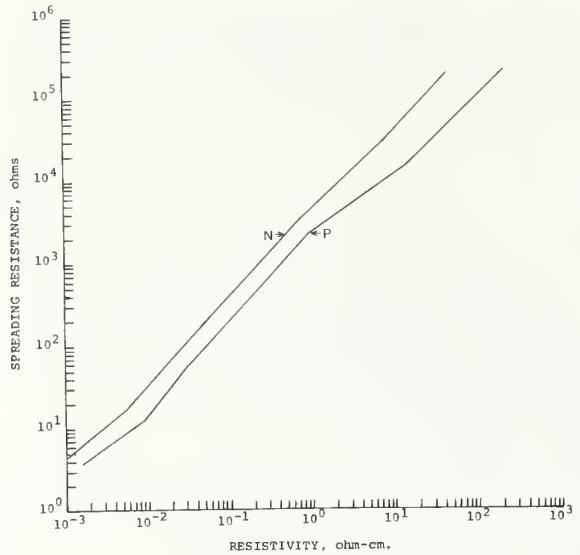

Figure 2. P and N-type Calibration Curves for a Polished Surface, Probe Spacing: 100 Micrometers, Probe Load: 20g.

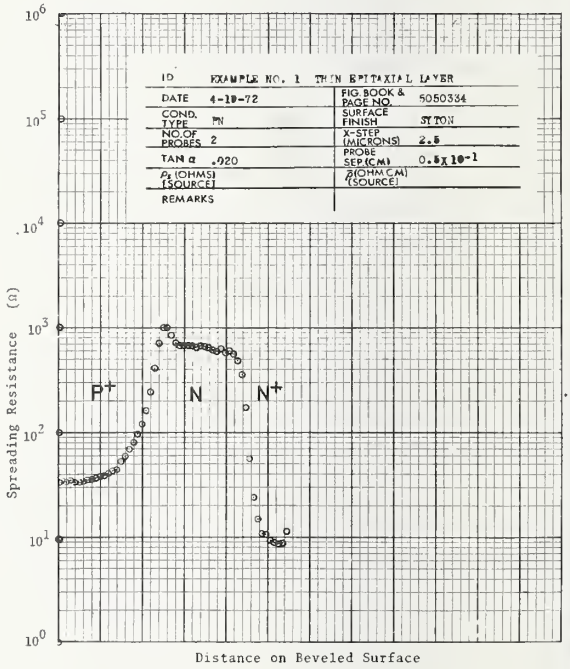

Figure 3. P^+N Double Epitaxial Layer on an N^+ Substrate - Spreading Resistance vs. Position on Bevelled Surface.

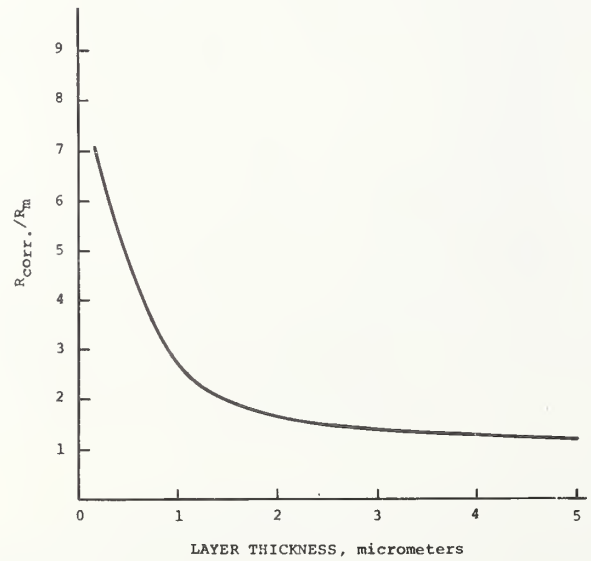

Figure 4. Conducting Boundary Correction Curv Ratio of Corrected Resistance to Measured Resi tance vs. Thickness.

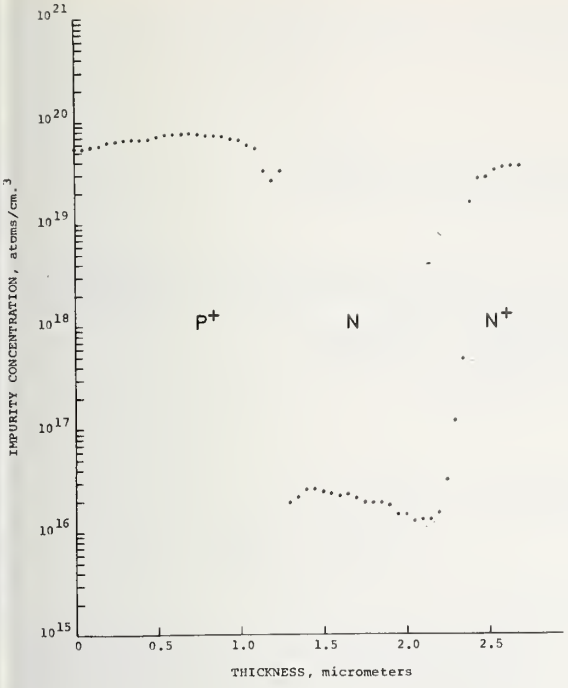

Figure 5. P^+N Double Epitaxial Layer on an N^+ Substrate-Impurity Concentration vs. Thickness.

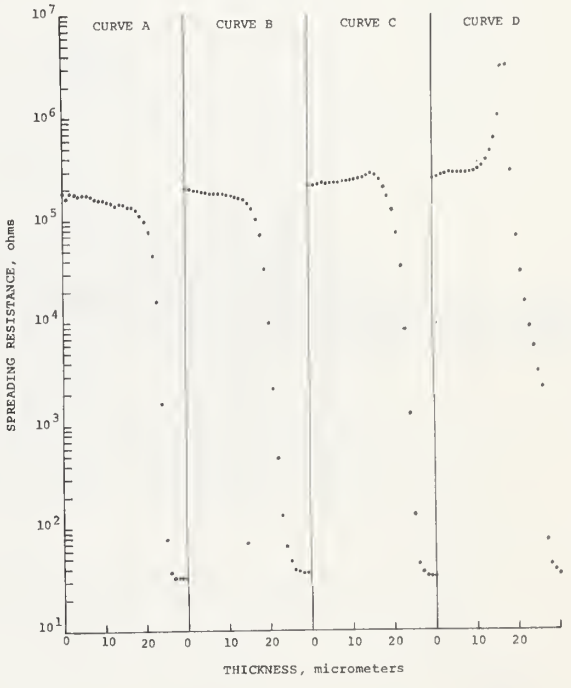

igure 6. Effect of Time Delayed Dopant In-ection on the Interface Between an N^+ Substrate nd an N-type Epitaxial Layer.

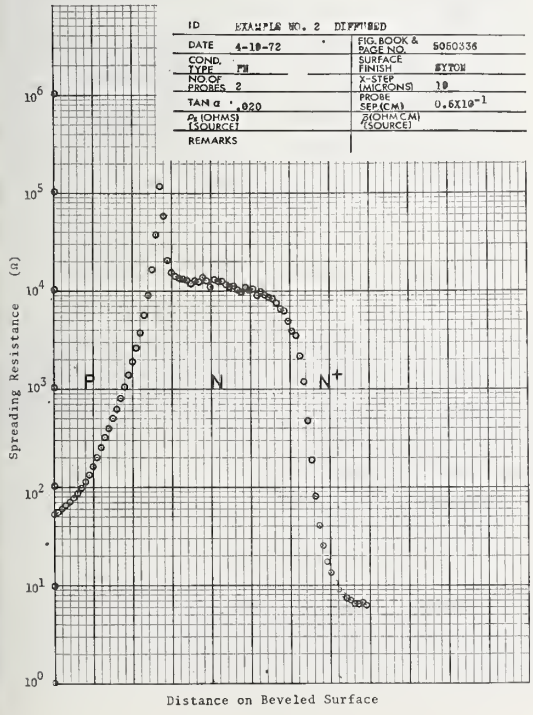

Figure 7. Boron Diffusion into an N-type Epitaxial Layer on an N^+ Substrate-Spreading Resistance vs. Position on Bevelled Surface.

565-448 O - 75 - 15

Figure 8. Boron Diffusion into an N-type Epitaxial Layer on an N^+ Substrate-Impurity concentration vs. Thickness.

Figure 9. Boron Ion Implantation into an N-type Substrate-Spreading Resistance vs. Position on Bevelled Surface.

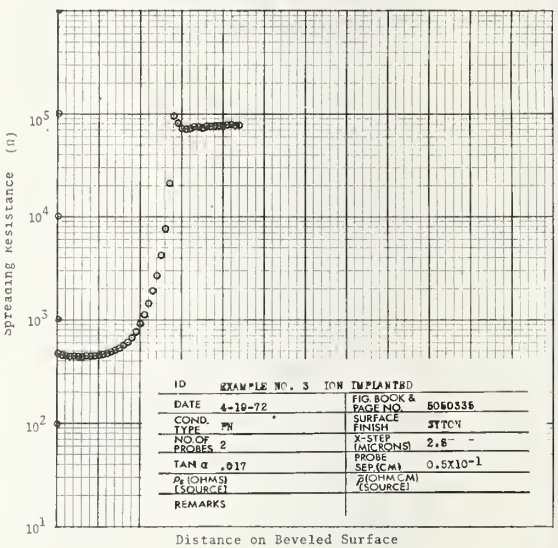

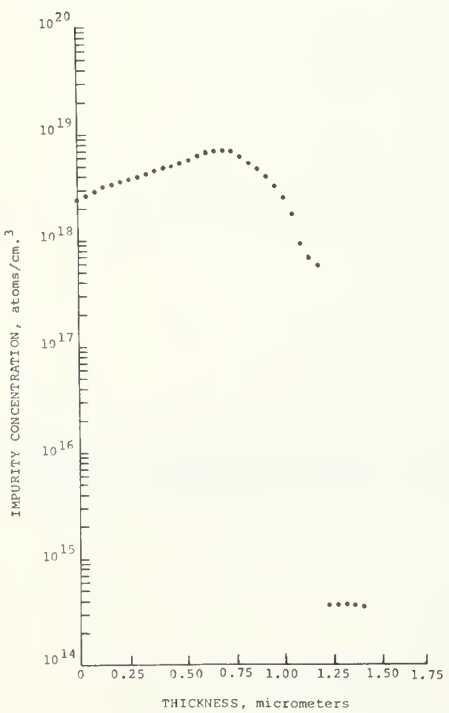

Figure 10. Boron Ion Implantation into an N-type Substrate-Impurity Concentration vs. Thickness.

NATIONAL BUREAU OF STANDARDS SPECIAL PUBLICATION 400-10, Spreading Resistance Symposium, Proceedings of a Symposium Held at NBS, Gaithersburg, Md., June 13-14, 1974.

Evaluation of the Effective Epilayer Thickness by Spreading Resistance Measurement

H. Murrmann and F. Sedlak

Siemens AG, Werk Halbleiter
Munich, Germany

Two types of double layer structure which are dealt with in the multi layer theory have been examined:

1. a top layer is insulated against a bottom layer (i.e. pn-junction, $R(\infty)$).
2. a top layer is shorted by a bottom layer (i.e. n^+-buried layer, $R(0)$).

In both arrangements the Spreading Resistance depends strongly on layer thickness d and on the radius a of contact area. Knowing the effective radius the epilayer thickness can easily be evaluated from Spreading Resistance Measurement and making use of the function $\frac{R(\infty)}{R(0)} = f(\frac{d}{a})$. This method is nondestructive and less time consuming than other common methods. A simple test pattern is proposed for evaluating the thickness on wafers in process. A comparison between this method and an IR-reflexion method (Digilab FTG 12) showed that both are in very good agreement in thickness range of 2.....6/um.

Key words: Epilayer thickness, silicon, spreading resistance, test pattern.

1. Introduction

Exact knowledge of the thickness of epitaxial layers is very important in integrated circuit technology. The methods commonly used to determine thickness are:

angle lapping and HF-staining
stacking fault measurement
IR-reflexion measurement after epitaxial deposition
base breakdown voltage measurement during IC-processing.

Lapping and staining is both destructive and time consuming. Evaluating stacking fault depth is very inaccurate for thin epilayers. The IR-reflexion method requires heavily doped buried layers with concentrations exceeding $5 \cdot 10^{19}$ cm^{-3}. Also using antimony as the buried layer dopant to reduce autodoping and out diffusion effects this concentration limit

may cause problems for successful application of IR-reflexion method. In addition there is often a need to measure the epilayer thickness on wafers being processed in order to optimize and control the deposition process and to characterize the wafers themselves. Based on previous investigations /1/[1] we propose the Spreading Resistance Measurement (SRM) as a means to evaluate epilayer thickness.

2. Method of Evaluation

We have examined two types of double layer structure which are dealt with in the multi-layer-theory /2/:

1. a top layer is insulated against a bottom layer (i.e. pn-junction, $R(\infty)$).
2. a top layer is shorted by a bottom layer (i.e. n^+-buried layer, $R(0)$).

In both arrangements the SR depends strongly on layer thickness and on the radius of contact area. In addition the ratio $R(\infty)/R(0)=k(\infty)/k(0)$ is a unique function of the ratio of the epilayer thickness and contact radius and there is no dependence on resistivity and barrier effects at the probes. In this way we were able to determine the effective radius of the probe by SRM on wafers with known epilayer thickness for different surface orientations and probe loads /1/. Knowing the effective radius, the epilayer thickness can easily be evaluated from SRM of $R(\infty)$ and $R(0)$ and making use of the function $R(\infty)/R(0) = k(\infty)/k(0) = f(d/a)$ in figure 1 and 2.

3. Accuracy of the Method

The graph in figure 2 shows the strong dependence of the function $R(\infty)/R(0) = f(d/a)$ for $d/a < 5$. For larger values the curve will approach 1 asymptotically and the method becomes insensitive. To determine the expected accuracy of the method within the region of interest we made estimations using the error formula

$$\Delta d = \sqrt{\left[\Delta a \cdot \left(\frac{d}{a}\right)\right]^2 + \left[a \cdot \Delta\left(\frac{d}{a}\right)\right]^2},$$

and applying it to figure 2 with

$$a = 2{,}90\,\mu m, \Delta a = 0{,}2\,\mu m, \Delta\left(\frac{R(\infty)}{R(0)}\right) = 5\ \%$$

The result is shown in figure 3. The total error Δd in thickness in the range $d = 2.....4\,\mu m$ was less than $0{,}3\,\mu m$. In this thickness region the method will be a very useful tool for controlling the epilayer deposition process.

It is worth noting that generally the buried layer maximum concentration will not be located at the same point at which the epilayer starts growing. The difference between the two depends on the buried layer and epilayer deposition process. Therefore each evalution is strictly bound to a specific set of process conditions and because of the semi-empiric nature of the evaluation method the SR probe has to be calibrated for each specific process. In addition there should be calibration standard wafers with known epilayer thickness which serve as check routines and as samples for upper and lower tolerance limits.

---

[1] Figures in brackets indicate the literature references at the end of this paper.

4. Experimental Results

In order to test the possibility of applying this SRM method a comparison was made with the IR-reflexion method. P-type wafers with (100) surface orientation were oxidized and from one half of each wafer the oxide was etched off. Then a buried layer diffusion was carried out ($R=25\,\Omega/\square$, $j = 4{,}5\,\mu m$) and all the oxide was etched off. N-epilayers of different thickness were deposited in the range of $d = 2.....10\,\mu m$ /1/. Finally thickness was evaluated by SRM on the wafer halves with and without buried layer using the graph of figure 2 with an effective contact radius of $= 2{,}90\,\mu m$. Thicknesses were also measured using a Digilab FTG 12 IR-equipment. The result of the comparison is shown in figure 4. The data points are very close to a straight line with slope 45^0 passing through zero. Within the thickness range $2.....6\,\mu m$ there is very good agreement between the methods. However at about $10\,\mu m$ the deviation becomes larger as is expected 1).

5. Proposed Test Pattern

The experiment in section 3 was carried out with wafers without patterns. Now the question arises as to a suitable test pattern for the successful evaluation of epilayer thickness on wafers in process. This test pattern should consist of two areas which are separated by a straight boundary. One area should have a buried layer underneath while the other should be isolated by the substrate pn-junction. Test pattern dimensions depend on the lateral influence of the field distortion by the low ohmic buried layer. A theoretical evaluation is difficult but figure 5 shows a practiced SRM made over the boundary between the two areas. A travel of approximately $600\,\mu m$ is required to get out of the field distorted region. Taking this effect into account we propose the test pattern shown in figure 5, with area $1{,}8 \times 1{,}8\ mm^2$ for a 0,6 mm probe spacing.

6. Conclusion

The SRM method proves to be a very useful tool for controlling the epilayer thickness after the deposition process. It is nondestructive and less time consuming than other common methods. Evaluation can be carried out on wafers in process with a simple test pattern consisting of two areas with and without buried layer underneath the epitaxial layer. A comparison between this method and a IR-reflexion method (Digilab FTG 12) showed that both are in very good agreement in thickness range of $2.....6\,\mu m$.

7. References

1/ Murrmann, H. and Sedlak, F., Spreading Resistance Correction Factors for (111) and (100) Surfaces Symposium on Spreading Resistance Measurement, Gaithersburg, Maryland, 1974

/2/ Schumann, P. A. and Gardner, E. E., Application of Multilayer Potential Distribution to Spreading Resistance Correction Factors, J. Electrochem. Soc. 116, 87, (1969)

) The error of the Digilab FTG 12 is $\pm$ 0,05 μm in the film thickness range of $1{,}5.....10\,\mu m$, provided there is a sufficient high concentration in the buried layer.

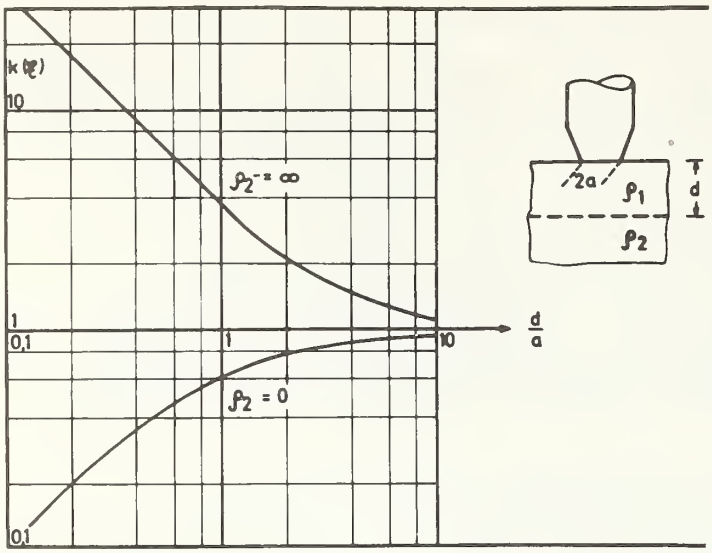

Figure 1. Correction factor due to distortion of the electric field by a two layer configuration.

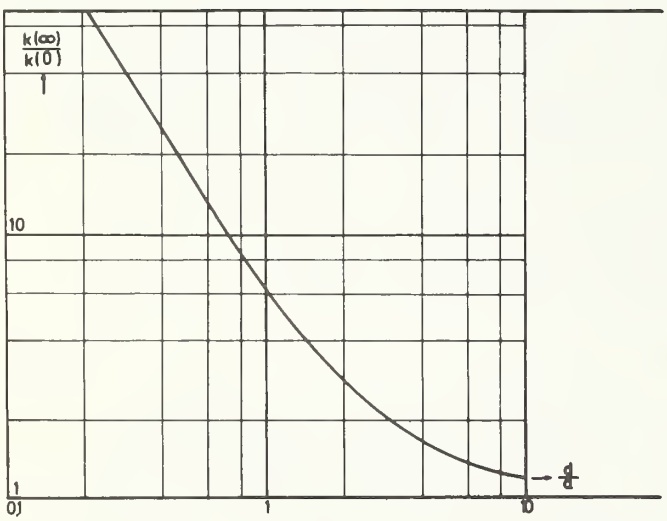

Figure 2. Ratio of the field correction factor for a two layer arrangement with $\rho_2 = \infty$ and $\rho_2 = 0$ respectively (two probes with 0,6 mm spacing).

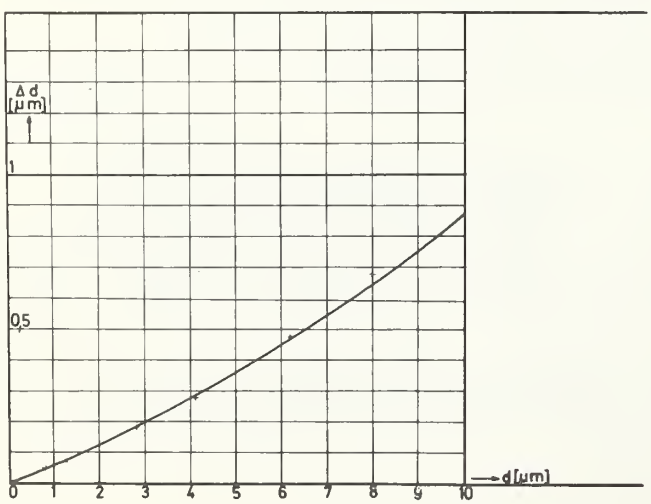

Figure 3. Expected error Δd for evaluation of epilayer thickness by SRM [(a = 2,90 µm, Δa = 0,2 µm, (R(∞)/R(0)) = 5%].

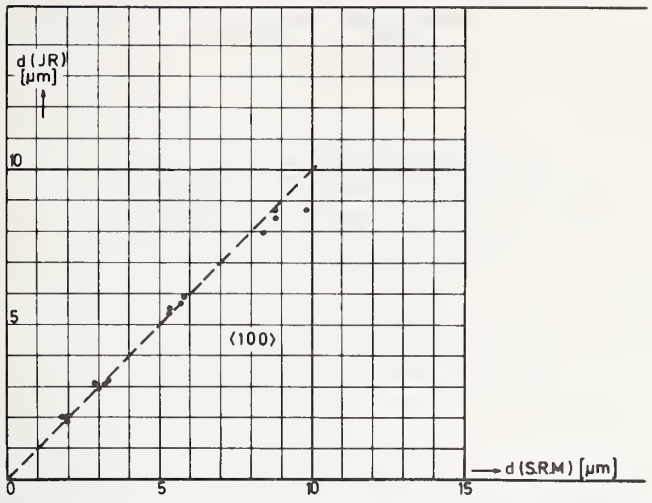

gure 4. Comparison of epilayer thickness measured by IR-reflexion and SRM.

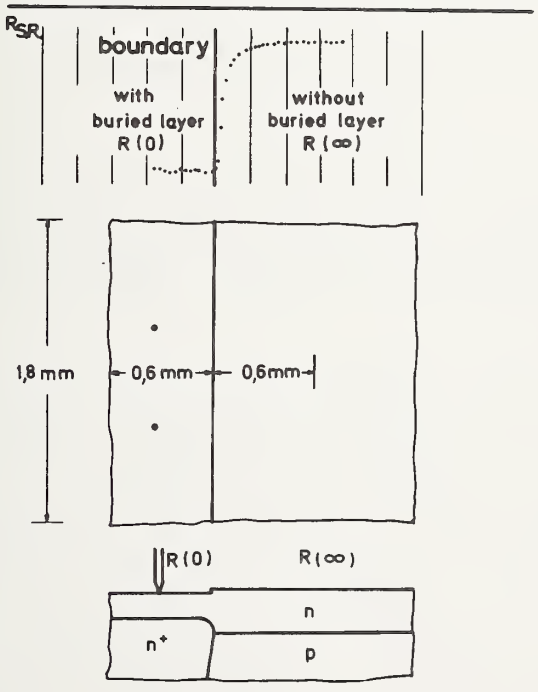

gure 5. SRM across boundary between area of R(0) and R(∞). (above). Dimensions the proposed test pattern (below).

NATIONAL BUREAU OF STANDARDS SPECIAL PUBLICATION 400-10, Spreading Resistance Symposium, Proceedings of a Symposium Held at NBS, Gaithersburg, Md., June 13-14, 1974.

The Experimental Investigation of Two-Point Spreading Resistance Correction Factors for Diffused Layers

N. Goldsmith, R. V. D'Aiello and R. A. Sunshine

RCA Laboratories
Princeton, New Jersey 08540

Spreading resistance measurements have been made on a series of erfc and Gaussian phosphorus diffusions into n and p-type silicon. Conventional four point probe methods were used to obtain values of sheet resistance and surface concentration. Comparison between the two methods shows increasingly large disagreements as the diffusion depth is decreased. The Dickey formula for accounting for the presence of a junction is shown to work well for uniform (non-diffused) samples but to fail to correct fully and properly for diffusions less than 20 μm deep. Empiric curves for estimating errors on lapped surfaces used in this study are given for a wide variety of samples.

Key words: Correction factors; diffused layers; spreading resistance.

I. Introduction

The availability of commercial two-point spreading resistance probes is bringing a new dimension to device fabrication, control, and analysis. With this tool, the internal details of devices having complicated doping profiles are reproducibly and rapidly revealed to the device designer or engineer. However, as with any measurement technique, calibration and correction factors play an important role in the interpretation and usefulness of the data.

In using the two-point probe spreading resistance method for analyzing diffused regions in a semiconductor device, the Dickey [1][1] correction factor due to the junction proximity is generally applied. However, Dickey's original formulation rests upon the assumption that the semiconductor layer beneath the probes is of uniform resistivity. Indeed, the early experimental work of Mazur and Dickey [2] showed this assumption to be quite useful for uniform epitaxial layers and for very deep diffusions. In practice, this assumption is violated in many devices and in particular, for shallow diffused layers where the resistivity can vary by orders of magnitude over a distance of less than one effective probe radius (∿ 4 microns). This can result in serious errors in converting spreading resistance data into a concentration profile, especially for devices having very shallow junctions and narrow or partially "covered" internal layers. Inaccuracies can also result when device parameters such as surface concentration, sheet resistance, and total charge are calculated from measured spreading resistance profiles. A particular case of extreme importance is the base region under the emitter in a bipolar transistor where the sheet resistance and total charge are parameters which must be controlled.

In this paper we present an experimental study of the applicability of the spreading resistance measurements to the case of diffused impurity profiles. We have evaluated a series of diffusions of phosphorus and boron into silicon in which the surface concentration,

[1]Figures in brackets indicate literature references at the end of this paper.

impurity distribution and junction depth were controlled variables. Both junction and non-junction cases were examined for diffusion depths between 5 and 50 microns. Both four-point sheet resistance and concentrations determined from Irvin's [3] curves are compared to the corresponding values determined by an analysis of two-point spreading resistance measurements. The effect of the Dickey correction factor is examined for a uniform sample and for the diffused samples containing a junction. All of the work reported here is for lapped surfaces. A block diagram summarizing our procedure is given in figure 1.

2. Experimental Procedure

2.1. Diffusions

In this section we discuss the methods used to prepare diffused samples having either Gaussian or complementary error function distributions. The majority of the samples were diffused using doped oxides [4] as the source. For samples in which a complementary error function distribution was desired, the doped film was left on the sample for the full diffusion time. For samples where Gaussian distributions were desired, the doped film was completely removed after an initial time at diffusion temperature. The sample was then coated with an undoped film of deposited oxide and the impurities driven in by a second diffusion. The second diffusion time was chosen to be at least 10 times longer than the first so as to approach a Gaussian profile.

Doped oxides were selected since they are a clean and controllable impurity source yielding reproducible surface concentrations below $10^{20} A cm^{-3}$. The surface concentrations in most of our experiments were kept below $\sim 5 \times 10^{19}$ A cm^{-3} to avoid anomalous diffusions which can be caused by crystal damage due to excessively high impurity concentration [5,6]. Thus, with the use of doped oxides, following the procedure outlined above, one can expect to obtain near theoretical complementary error or Gaussian profiles.

Doped oxide source films of one impurity type were deposited simultaneously on p- and n-type wafers to obtain samples with the same surface concentration, both with and without a junction. Although we prepared diffusions from both boron and phosphorus doped oxides, we have restricted the discussion in this paper to the diffusions using phosphorus in order to avoid possible problems associated with outdiffusion of boron at the oxide-silicon interface.

2.2. Measurements and Data Analysis

The diffused samples were measured using a four point probe to determine the sheet resistance (appendix A-1). Sections from each wafer were then prepared for measurement by the spreading resistance probe using the technique given in appendix A-2. The spreading resistance measurements were collected in a manner suitable for analysis using an in-house time-shared computer. By combining the junction depth measurement obtained from the spreading resistance probe with the four point probe sheet resistance, the surface concentration for the junction samples was calculated with the aid of Irvin's curves.

A computer program was written to perform all of the necessary calculations, including those detailed in appendix B. The output of this program was arranged to give both tabular listings of the calculated quantities and a graphic output on a Calcomp plotter.

3. Experimental Results

3.1. Test of Dickey Formulation

The first phase of our investigation was to experimentally verify the validity of the commonly-used Dickey formulation for junction correction. Since this formulation was based upon a uniformly-doped sample with a non-conducting boundary, we fabricated the sample shown in the inset of Figure 2. One micron of oxide was thermally grown upon a uniform, n-type silicon wafer. A poly-silicon "handle" 10 mils thick was grown on the SiO_2, and the sample was flat lapped to reduce its thickness. Four point probe measurements of the sample combined with the thickness obtained from spreading resistance measurements allowed us to calculate the resistivity of the bulk sample. In carrying out the spreading resistance measurements we made careful observations through the microscope to determine as closely as

possible, when the points first contacted the oxide. This position of first contact was assumed to correspond to the location of a p-n junction in the Dickey formulation. The numerical procedure used to apply the Dickey correction is described in appendix B.2.1.

In figure 2 we show the Dickey-corrected and uncorrected impurity profiles for this sample. As can be seen, the Dickey correction is very small at distances greater than several probe radii from the nonconducting plane, but is very accurate for distances as close as 0.3 μm, which corresponds to less than 1/10 of a probe radius. The average resistivity determined from the two-point probe data agreed with that determined using the four-point probe to within 2%.

3.2. Analysis of Diffused Samples

a. Dickey Corrections

Having experimentally verified the validity of the Dickey formula for uniform samples, we attempted to apply it to samples with diffused junctions. Following the procedures outlined in Appendix B, we calculated sheet resistance for the diffused junction samples using the Dickey corrected two point probe data. This calculated sheet resistance was then compared with the value measured using the four point probe method. The results of this comparison are shown graphically in figure 3, where the ratio of the two point sheet resistance to the four point sheet resistance is plotted vs. the junction depth for a variety of samples. This plot shows that the sheet resistance calculated from Dickey corrected spreading resistance measurements begins to deviate from the four point probe values for junction depths less than 25 μm.

If the conversion from spreading resistance to corrected resistivity is properly done, the sheet resistance calculated from two probe measurements should agree with that determined by four probe measurements regardless of the distribution of impurities within the sample. Thus, even if our diffusion techniques failed to yield ideal distributions, the failure to obtain the proper value of sheet resistance indicates that the Dickey procedure does not correct properly for diffused samples.

Since, in a diffused sample, the conductivity is predominantely determined by the carrier density in the top-most portion of the diffusion the disagreement in the sheet resistance for the shallow junction cases implies a large disagreement in the surface concentration. Figures 4a-4d are plots of the Dickey corrected concentration profiles for samples with Gaussian diffusions of increasing junction depth. Superimposed on these curves is a Gaussian distribution calculated using four-point data and Irvin's curves. Figures 5a-d are plots of similar profiles without any correction factors applied. As expected from the values of sheet resistance, there is very poor agreement between the theoretical and measured concentration profiles for shallow junction depths.

Furthermore, as Figure 5 indicates, the spreading resistance procedure underestimates the concentration throughout the profile. The Dickey procedure corrects this data in such a way as to provide the largest correction factor for the points closest to the junction. It is clear from Figure 5a, for example, that the correction factor for a diffused sample should be higher near the surface than the Dickey procedure provides.

b. Non-junction Samples

To determine to what extent the presence of a junction contributes to the errors found in the samples just discussed, we analyzed the junctionless samples in the same manner as described above. Plotted in figure 6a-6d are the impurity profiles determined from the two point probe data for four such samples. These figures also have a superimposed Gaussian distribution. The surface concentration for the Gaussian profile was chosen to be that calculated from a simultaneously prepared junction sample. The departures from the theoretical curve are similar to those found in the junction case. Changing from a Gaussian profile to an error function complement profile introduces comparable errors, as shown in figures 7a and 7b. These results indicate that the discrepancies found are not solely due to the presence of a junction.

c. Comparison of Profiles

In an attempt to determine the range of errors associated with measurement of diffused samples, we have plotted in Figure 8 the ratio of surface concentration calculated from four point data to that calculated from two probe data vs. diffusion depth for a variety of samples. The solid lines arbitrarily enclose the entire range of the data. It is clear that the largest errors in surface concentration occur for the smallest diffusion depths. These large errors are found not only at the surface but also over the whole profile as shown in figures 9-12. No correction factors were applied to the data.

In Figures 9-12, to provide greater clarity, the distance scale has been normalized to the diffusion depth. The results given in figures 9 and 10 are for n^+ into p diffusions while those of Figures 11 and 12 are for n^+ into n-type substrates. The diffusion depth is a parameter in all of these plots and is indicated in the figures. From figures 8-12 it is apparent that the significant parameter in determining the error is the diffusion depth. These graphs can be used to estimate the errors associated with the measurement of diffused layers using a two point spreading resistance probe.

4. Discussion and Conclusions

In this paper we have demonstrated that the direct conversion of two point spreading resistance data into concentration produces a very accurate representation of the impurity profile for very deep diffusions (depths greater than 40 μm). However, when the same procedure is applied to diffusions shallower than 10 μm, very inaccurate results are obtained. The inaccuracies result from the diffusion itself, rather than the presence of a junction, since comparable errors were obtained for n+ diffusions into both n and p material. Although the error is probably associated with the rapid variation of impurity concentration over a depth comparable to a probe radius, we have found that the error is much more strongly correlated with total diffusion depth than local gradient with a profile. The errors grow extremely rapidly for diffusion depths comparable to, and less than, the effective radius of the probe. Although we show that the Dickey correction procedure is quite accurate for "step junctions" having uniform profiles, its application to diffused samples results in a profile of the wrong shape. However, since the Dickey correction factor increases rapidly as the junction depth decreases, its application to very shallow junctions can produce results of the proper order of magnitude.

The data shown in figures 11 and 12 show that the maximum error occurs at a distance roughly equivalent to a probe radius. Since there is no insulating boundary in these samples, this effect can be interpreted as resulting from the presence of the high resistivity substrate below the diffusion. In principle, a multi-layer correction scheme, such as that described by Schuman and Gardner [9] can be used to correct the data. In practice, this procedure requires an inordinate amount of computer time to be used on a routine basis. Similar comments apply to the data shown in Figures 9 and 10, where there is a junction present. As a practical matter, the degree of correction required for various types of diffused samples can be estimated from figures 8-12.

It should be emphasized that the correction factor appears to be sensitive to the manner of surface preparation. Based on a limited number of experiments, we have observed that samples prepared by polishing, rather than by lapping, require less correction at the surface.

5. References

[1] Dickey, D. A., "Diffusion Profile Studies Using a Spreading Resistance Probe," Abs. No. 57, Paper presented at the Pittsburgh Meeting of the Electrochemical Society, April 15-18, 1963; See p. 151, Extended Abstracts of the Electronics Division, Vol. 12, No. 1.

[2] Mazur, R.G. and Mickey, D. A. "A Spreading Resistance Technique for Resistivity Measurements on Silicon," J. Electrochem. Soc., 113 (3), 255 (1966).

[3] Irvin, J.C., "Resistivity of Bulk Silicon and of Diffused Layers in Silicon," Bell System Technical Journal, 56 (2), 388 (1962).

[4] Barry, M. L. "Diffusion from Doped-Oxide Sources," in Silicon Device Processing, N.B.S. Special Publication 337m p. 175 (1970).

[5] Tannenbaum, E., "Detailed Analysis of Thin Phosphorus-Diffused Layers in p-type Silicon," Solid State Electronics 2, 123 (1961).

[6] Nickolas, K. H., "Studies of Anomalous Diffusion of Impurities in Silicon," Solid State Electronics 9, 35 (1966).

[7] Swartzendruber, L. J., "Correction Factor Tables for Four Point Probe Resistivitiy Measurements on Thin Circular Semiconductor Samples," Technical Note 199, NB.TNA, Nt'l Bureau of Standards, April 15, 1964.

[8] Caughey, D. E. and Thomas, R. E., "Carrier Mobilities in Silicon Empirically Related to Doping and Field," Proc. IEEE, p. 2192 December 1967.

[9] Schumann, P. A., Jr., and Gardner, E. E., "Application of Multilayer Potential Distribution to Spreading Resistance Correction Factors," J. Electrochem Soc. 116 (1), 87-91 (1969).

Appendix A - Measurement Procedures

A.1. Four Point Probe Measurements

Four point probe measurements were made using a Fell head. Probe spacing was measured efore the start of these experiments and was found to be 0.030". Voltage was read using a eithley 910B electrometer and current was supplied by a barrier driven source. Five readings ere taken on each sample in a region near the center of the sample, and these were averaged efore applying the appropriate geometric correction factor [7].

A.2. Spreading Resistance Measurements

All spreading resistance measurements were taken using a Model ASR100 manufactured by olid State Measurements Corp. The samples were lapped on an angle block using 6 micron rnet grit as recommended by the probe manufacturer. The angle of the lap was determined the use of the calibrated microscope mounted on the probe stage. Angles used ranged om 1 to 12 degrees depending upon the junction depth. The instrument was calibrated using iform samples of known resistivity. This calibration is periodically checked to ensure obe stability.

Appendix B - Data Acquisition and Analysis

B.1. Data Acquisition

Because of the large number of calculations involved in a study of this type, the out- t of the logarithmic amplifier was digitized using a 0-1.999V panel meter. The digital tput of this meter was transferred, by means of a locally designed and built parallel to rial data decoder, to punched paper tape in a format suitable for use with an in-house me-shared computer. At the start of each run the voltages corresponding to the fixed re- stors built into the equipment were recorded on the tape. A section of the analysis pro- am calculates the curve relating resistance to voltage so that problems of meter linearity d long term electronic drift are eliminated. This program also contains a mathematical presentation of the measured spreading resistance vs. resistivity relationships for n- and type material.

B.2. Numerical Formulation

B.2.1 Dickey correction

The Dickey correction factor for spreading resistance can be combined with the calibra- on data relating spreading resistance to resistivity to produce the following expression r correcting the resistivity of a uniform layer in the presence of a junction.

$$\rho = \frac{R_{sp}}{\frac{R(\rho)}{\rho} + \frac{1}{\pi t}\left[\ell n \frac{D}{2t} - .116\right]} \qquad t \geq a \tag{1}$$

$$\rho = \frac{R_{sp}}{\frac{R(\rho)}{\rho} + \frac{1}{\pi t} \ell n \frac{2D}{a} - \frac{1}{2a}} \qquad t < a \tag{2}$$

where

$R(\rho)$ is the relation between spreading resistance and resistivity

R_{sp} is the measured spreading resistance

a = effective probe radius
D = spacing between the points
t = distance from the junction.

This trancendental equation is solved iteratively using a rapidly converging numerical procedure.

B.2.2 Resistivity to Concentration Procedure

In order to convert from resistivity to concentration the following equations, modifications of those given by Caughy and Thomas [8], were used.

$$\mu_n = \frac{65}{\left(1 + \frac{N_D}{2 \times 10^{20}}\right)^{.53}} + \frac{1265}{\left[1 + \left(\frac{N_D}{8.5 \times 10^{16}}\right)^{.72}\right]} \tag{3}$$

$$\mu_p = 47.7 + \frac{447.3}{\left[1 + \left(\frac{N_A}{6.3 \times 10^{16}}\right)^{.76}\right]} \tag{4}$$

These formulations have been selected to provide agreement with Irvin's curves which were used to analyze impurity profiles. A rapidly converging iteration procedure uses these relationships to calculate a carrier density for a given resistivity. In every case where average properties over a number of data points are required, the concentrations rather than the resistivities are averaged.

B.2.3 Sheet Resistance

Sheet resistance from data point j to sheet resistance data point k (not crossing a junction) is calculated using the formula

$$R_s = \frac{1}{\sum_{i=j}^{k} \frac{1}{\rho(i)} [\sin(\theta)][s]} \tag{5}$$

where $\rho(i)$ is the calculated resistivity at data point i,
θ is the bevel angle
and s is the distance between measured points along the bevel.

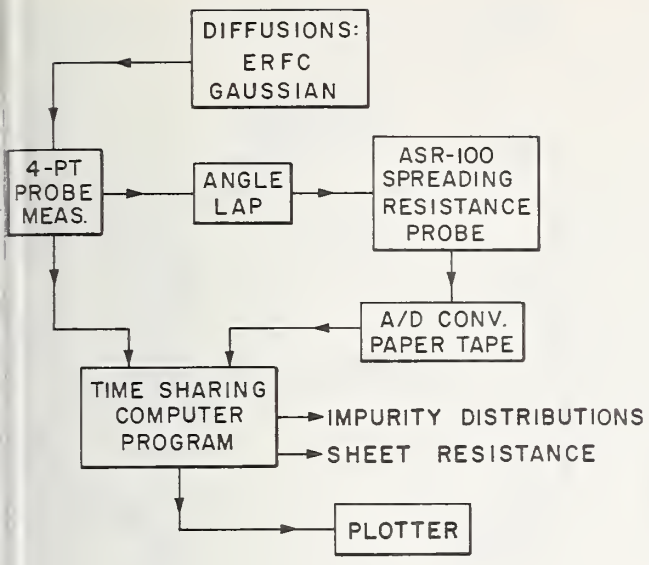

Figure 1: Flow Diagram for Experimental Procedures

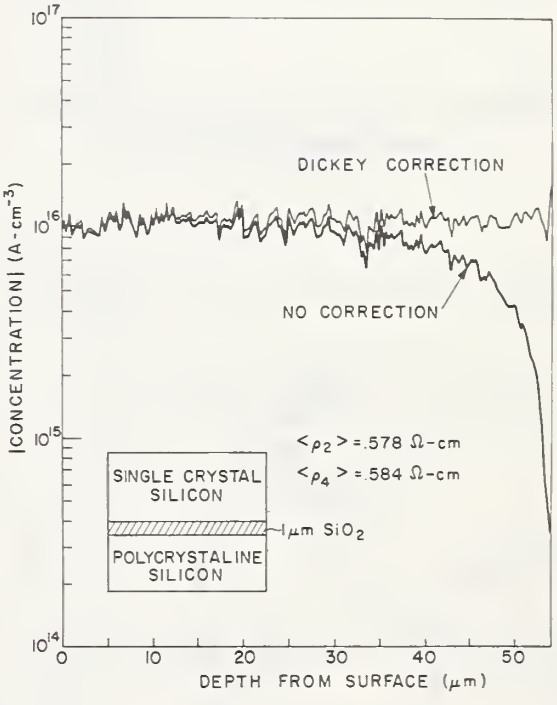

Figure 2: Calculated impurity profile, with and without Dickey correction, for a uniform sample having an insulating boundary.

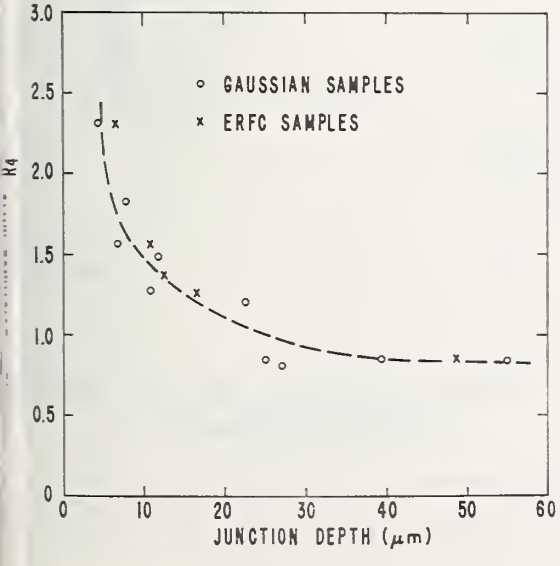

Figure 3: Ratio of sheet resistance calculated from Dickey corrected two point probe data to that measured using four point probe as a function of junction depth.

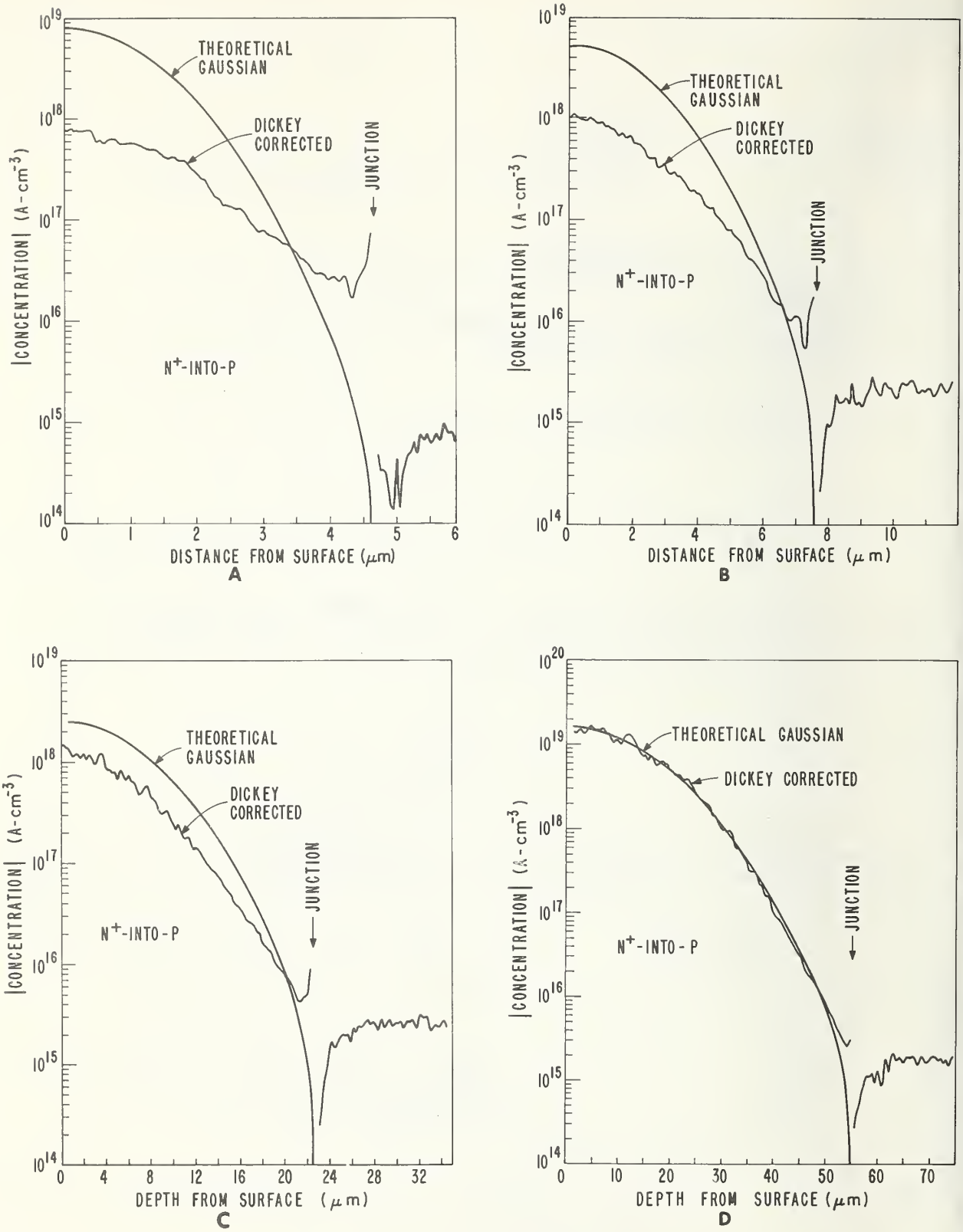

Figure 4: Theoretical and Dickey corrected impurity profiles for Gaussian diffusions of varying depths.

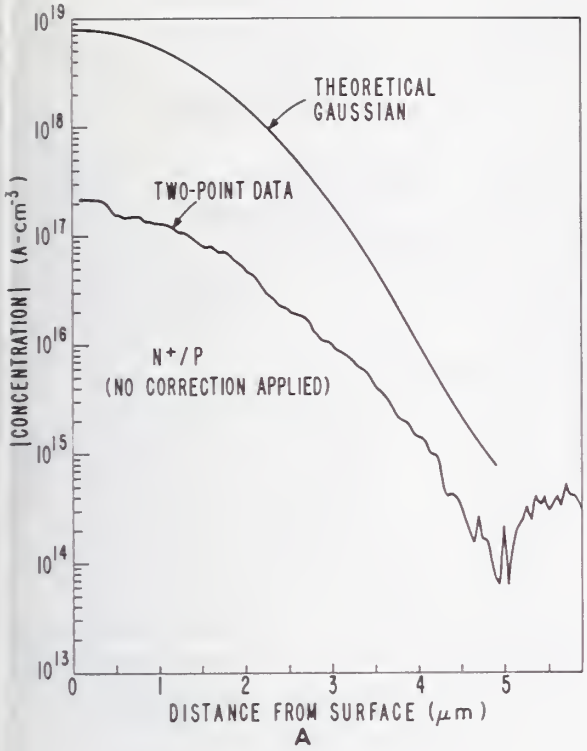

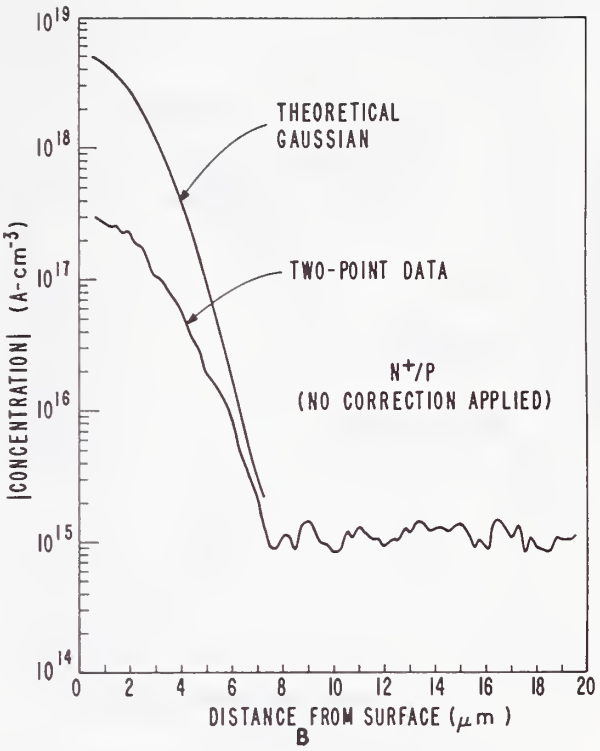

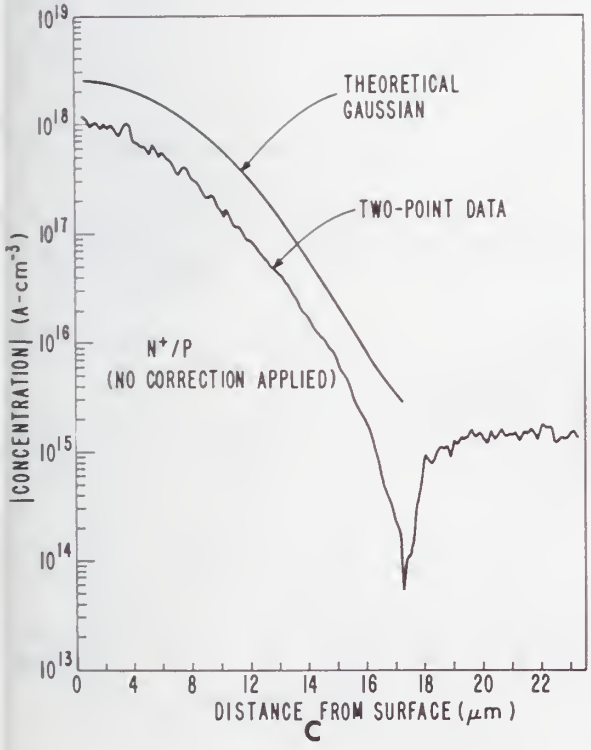

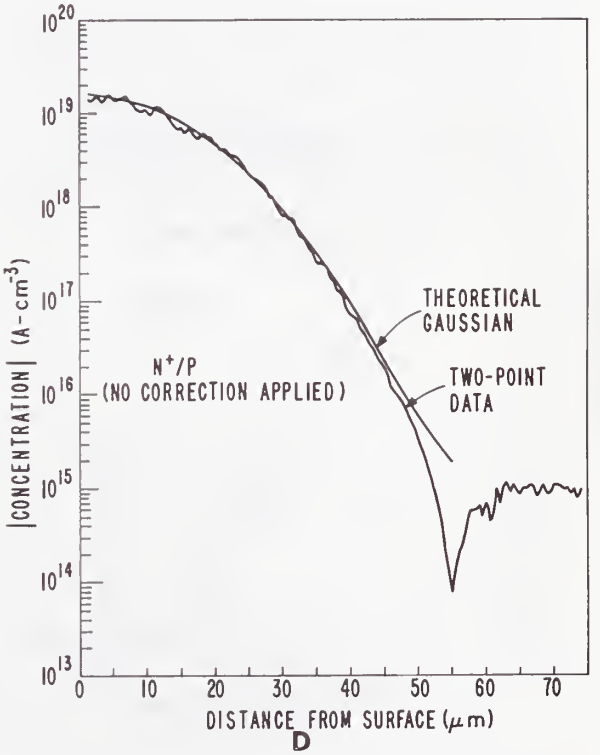

Figure 5: Theoretical and uncorrected impurity profiles for Gaussian diffusions of varying depths.

565-443 O - 75 - 16

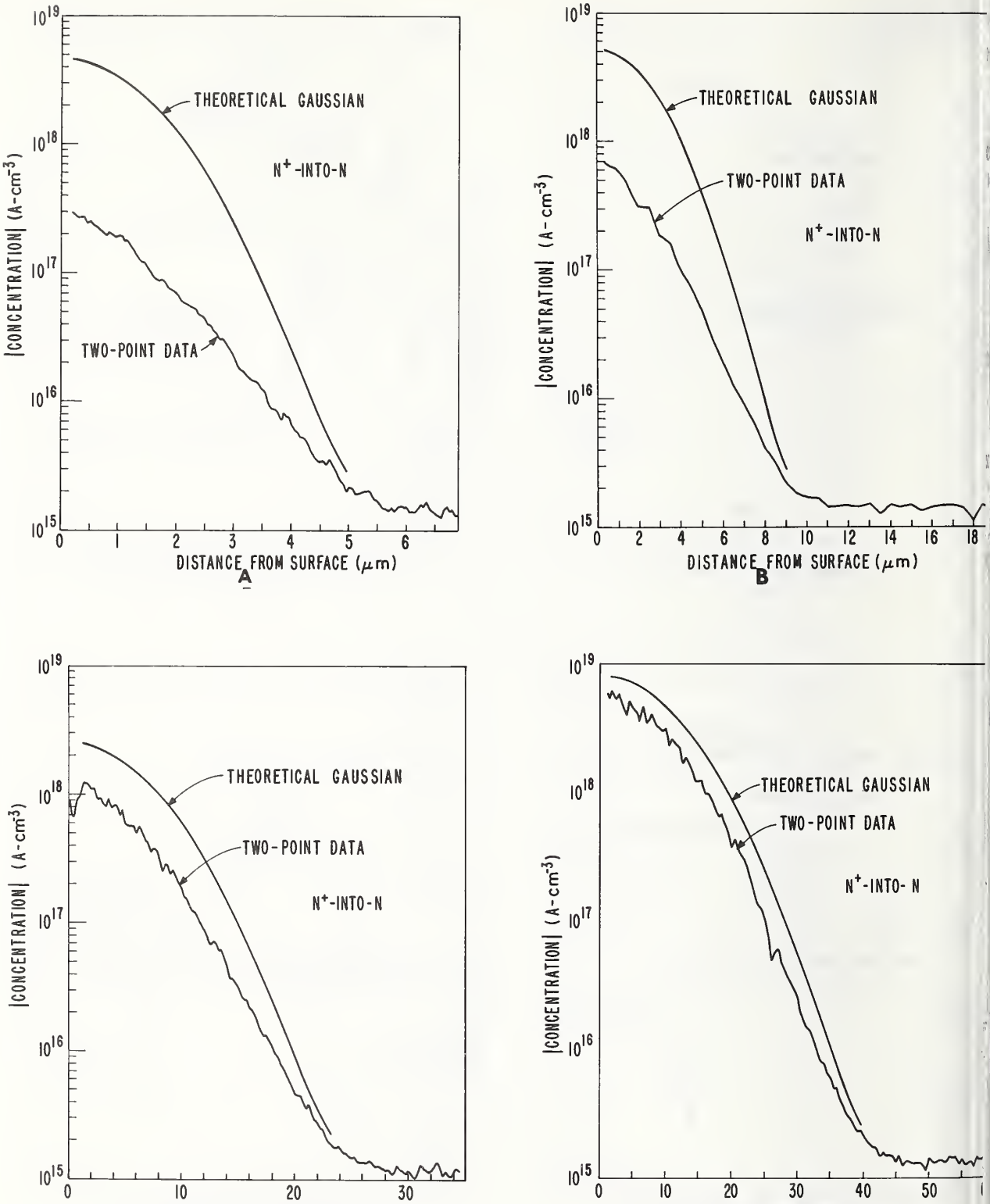

Figure 6: Theoretical and calculated impurity profiles for Gaussian diffusions into bulk wafers of the same conductivity type.

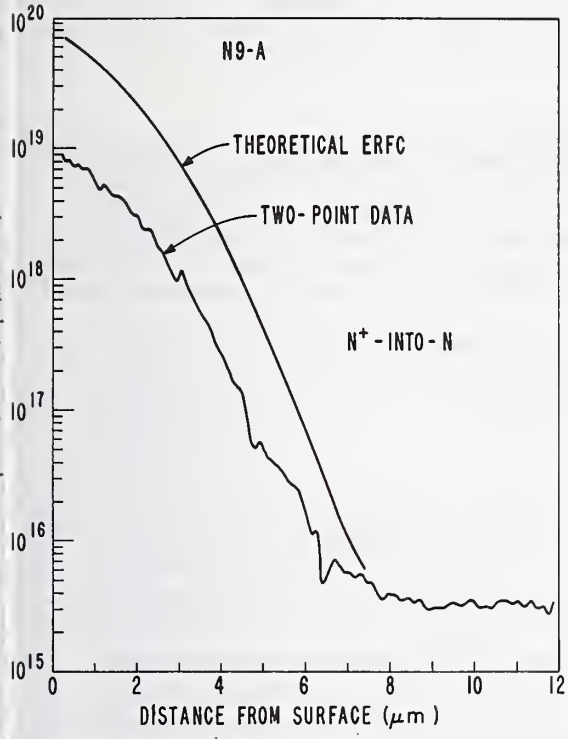

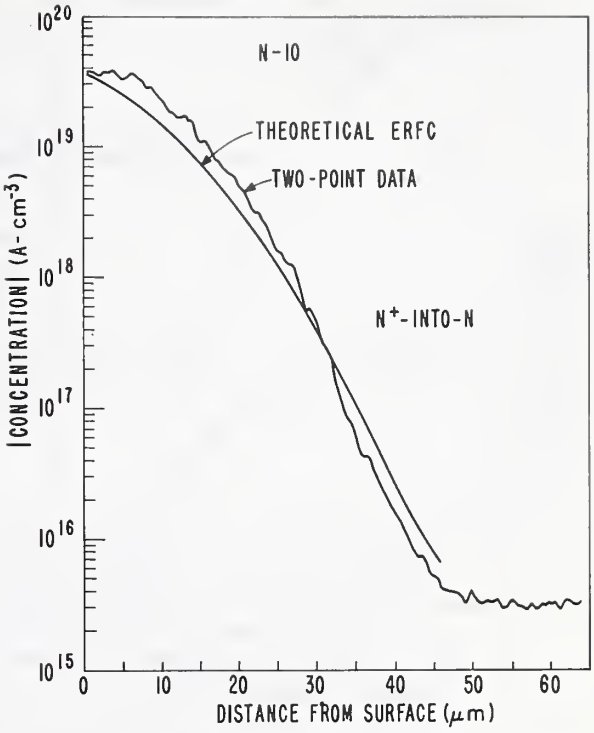

Figure 7: Theoretical and calculated impurity profiles for erfc diffusions into bulk wafers of the same conductivity type.

Fig.8 Ratio of Surface Concentration derived from four point probe measurements as a function of diffusion depth

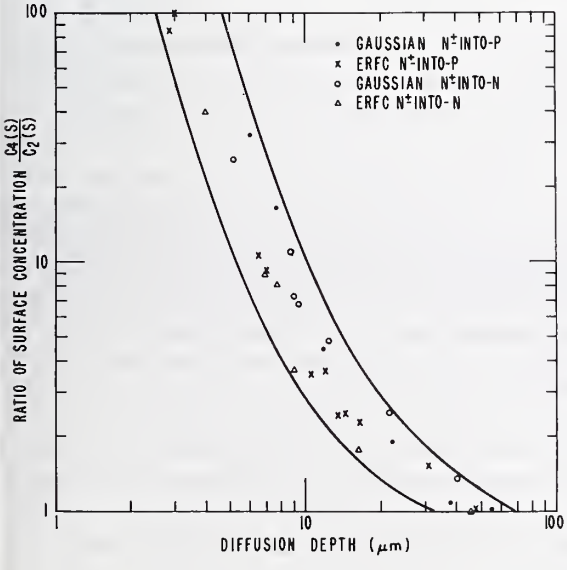

Fig.9 Ratio of local concentration, calculated from four point probe data and Irvin's curves, to that calculated from uncorrected spreading resistance data as a function of distance (normalized to junction depth) for a series of Gaussian diffusions with varying junction depths.

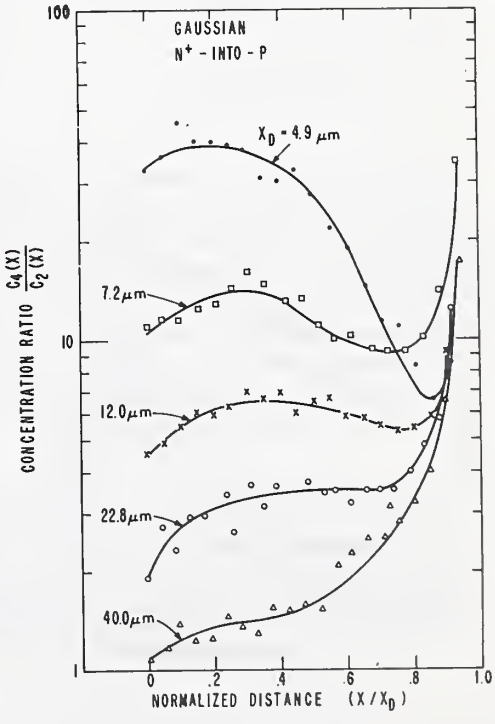

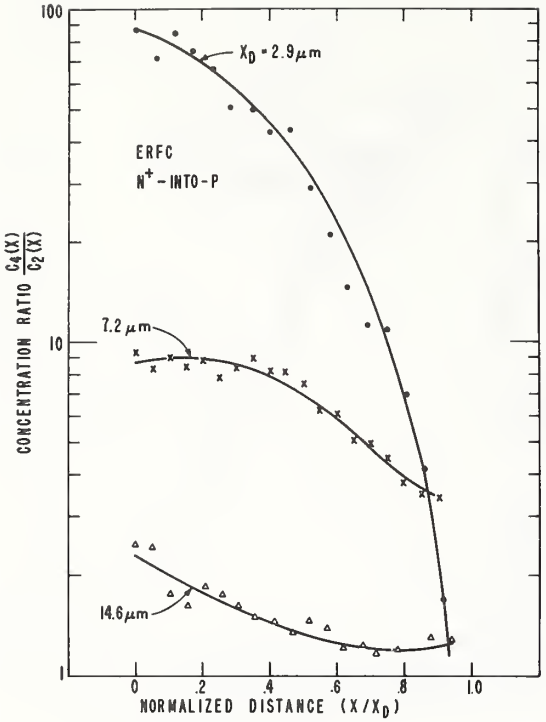

Figure 10. Ratio of local concentration, calculated from four point probe data and Irvin's curves, to that calculated from uncorrected spreading resistance data as a function of distance (normalized to junction depth) for a series of erfc diffusions with varying junction depths.

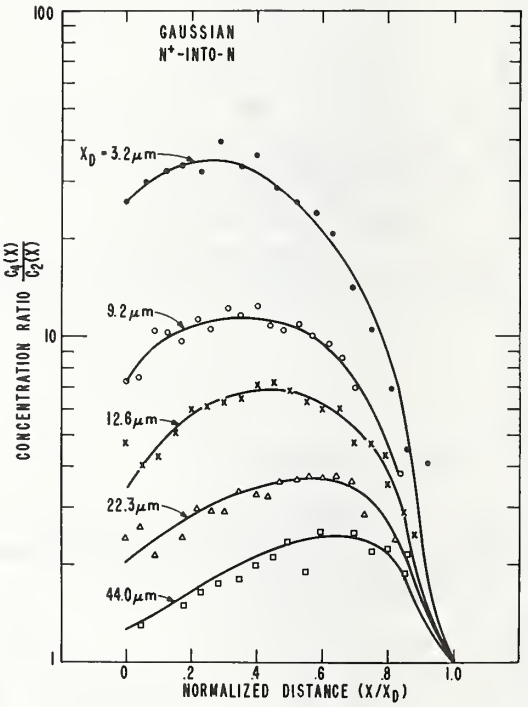

Figure 11. Ratio of local concentration, calculated from four point probe data and Irvin's curves, to that calculated from uncorrected spreading resistance data as a junction of distance (normalized to diffusion depth) for a series of Gaussian diffusions with varying diffusion depths.

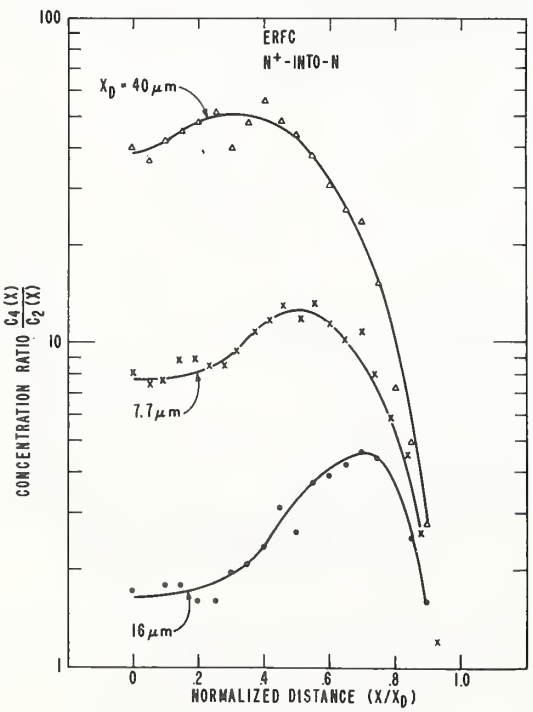

Figure 12. Ratio of local concentration, calculated from four point probe data and Irvin's curves, to that calculated from uncorrected spreading resistance data as a function of distance (normalized to diffusion depth) for a series of erfc diffusions with varying diffusion depths.

ATIONAL BUREAU OF STANDARDS SPECIAL PUBLICATION 400-10, Spreading Resistance Symposium,
roceedings of a Symposium Held at NBS, Gaithersburg, Md., June 13-14, 1974.

Application of the Spreading Resistance Technique to Silicon Characterization for Process and Device Modeling

Walter H. Schroen

Semiconductor Research and Development Laboratories
Texas Instruments Incorporated
Dallas, Texas 75222

In recent years, the interest in modeling of semiconductor processes and silicon device parameters has intensified considerably. Precise knowledge of the doping distribution in the semiconductor emerged as a key requirement for input and starting condition of many of these models and for their verification. It turned out that the spreading resistance technique, after careful probe calibration and multilayer data analysis, is able to supply some of the required data better than any other characterization technique available. This paper discusses these successful applications. On the other hand, this paper points out inherent limitations of the spreading resistance technique with regard to resolution and precision, and how this affects the verification of process and device models. Finally, the paper describes ways to supplement the spreading resistance technique by other material characterization or electrical techniques so that the combination of these methods is capable of generating the required experimental data for the analytical models.

Key words: arsenic; boron; design; device modeling; doping distribution; phosphorus; process control; process modeling; spreading resistance.

1. Introduction

Stimulated by the trend toward increased automation of circuit design and improved process control in silicon ice technology, new approaches and advances in modeling of processes, device and circuit parameters, and device bility have been discussed in the literature [1-9] *. It has been recognized that many device parameters and their bility are controlled by the distribution of the dopants in the semiconductor. The knowledge of details of this tribution, such as variations of the concentration gradient with depth from the surface or with heat treatments ing processing, becomes increasingly important as device structures become smaller and shallower. Since the trend ilicon device development is indeed in this direction – for reasons such as increased circuit speed, enhanced king density, and reduced fabrication cost – the detailed understanding and control of the doping profiles omes mandatory. In addition, analytical expressions or empirical data of the doping distribution form the essary inputs to device models.

This paper emphasizes the outstanding features of the spreading resistance technique as a tool for acquiring cise doping distribution data. This data is needed both for inputs as initial condition of the doping models and for ification of the models. Analytical expressions for describing doping profiles in silicon have been derived for the e of semi-infinite medium, as well as infinite medium. For the semi-infinite medium, the situations of a limited

gures in brackets indicate the literature references at the end of this paper.

source, i.e., the drive-in from an initial condition (ion implantation and diffusion for base and emitter), and of an infinite source, i.e., diffusion from a gaseous source or thick oxide have been treated. For an infinite medium, the limited source situation, i.e., buried layer, is of particular interest. These doping distribution models comprise the category "process modeling" in figure 1.

Process models and device characterization measurements, in turn, serve as inputs to "device models". see figure 1. These models include diode models, intrinsic transistor models (forward active, dc, transient, etc.), and actual transistor models (parasitics and geometry). The spreading resistance probe can supply precise input data directly, or through process models. An example of direct device application for discrete diodes of small and large geometries in epitaxial silicon was recently discussed by Morris [10].

The major part of this paper is devoted to applications of the spreading resistance technique to doping concentration models. The examples are discussed in the sequence in which they appear in silicon device fabrication: First, epitaxial layer growth and buried layer diffusions are described. Then, the formation of base and emitter is illustrated. Finally, complete transistor profiles are presented. The examples demonstrate the capabilities and limitations of the spreading resistance probe for modeling. Supplementary techniques are outlined briefly to indicate ways of compensating for the limitations of the spreading resistance probe.

2. Application to Epitaxial Layers and Deep Diffusions

Models for the doping distribution in epitaxial layers have to account for average doping, surface concentration, and interface doping at substrate or buried layers. These models must therefore include not only doping redistribution during epitaxial growth, but also diffusions during epitaxy of any doped layer generated before epitaxial deposition.

2.1. Epitaxy Models

Calculations for the epitaxial process describe the effects of up-diffusion and autodoping, which have been investigated for a number of years [11-14] and reviewed by Grove [15]. Since some epitaxial layers are thick (2 to 10 μm), the spreading resistance technique is ideal for precise impurity distribution measurements over this wide thickness range. Figure 2 represents an example [16] of an n-type epitaxial layer, 5 μm thick, deposited on a p-type substrate of about equal carrier concentration. This substrate was measured to a depth of 15 μm for detection of concentration irregularities. The data points represent analyzed spreading resistance measurements [17,18].

2.2. Buried-Layer Models

Buried-layer models describe limited-source diffusions in an infinite medium, with the boundary condition of carrier conservation. The model has been established in strength for the case of linear diffusion constants [19,1], such as antimony doping, using Green's functions technique. The distribution, C, as a function of depth, x, is initially

$$C(x,0) = f(x).$$

Its subsequent redistribution at a given temperature, T, follows the differential equation, with time scaled by the diffusivity,

$$\frac{\partial C}{\partial t} = \frac{\partial^2 C}{\partial x^2}$$

The number of impurities has to be conserved, so that

$$\int_{-\infty}^{+\infty} C(x,t) = \text{constant.}$$

The solution is given by the usual superposition expression

$$C(x,t) = \int_{-\infty}^{+\infty} f(x + 2t^{1/2}\,\xi)\,\exp(-\xi^2)\,d\xi$$

which can be calculated using standard numerical techniques.

For non-linear diffusion constants (such as arsenic doping) or field-aided effects different approaches have to replace the linear model.

The spreading resistance probe proved to be the most suitable tool for acquiring the initial condition inputs, for which only insufficient analytical expressions exist, as well as for verifying the buried-layer movements due to diffusion. An example of an antimony buried-layer diffusion is given in figure 3. Although the buried layer had moved only slightly during epitaxial deposition, an additional 45 minutes at the given processing temperature was enough time to diffuse the buried layer all the way through the epitaxial layer. The data points in figure 3 are "as taken" by the spreading resistance probe. Subsequent multilayer analysis will change the absolute values of the concentration, but not the diffusion effect illustrated in figure 3.

The impurity distribution along the epitaxial layer/buried layer/substrate system displays two features perfectly suited for investigations by the spreading resistance probe: deep penetration into the silicon slice, and a wide range of doping concentrations. It seems justified, therefore, to illustrate this system by a few more detailed examples. They will also offer an opportunity to point out some important features of the spreading resistance multilayer analysis, which is indispensable for precise and reliable interpretation of raw spreading resistance data.

2.3. Multilayer Analysis

Figure 4 shows an n-type epitaxial layer of 2 μm thickness on an n-type buried layer almost 7 μm thick, which is diffused into a p-type substrate (beyond total depth of 9 μm). The impurity concentration range covered by the spreading resistance probe is more than four orders of magnitude. The crosses in figure 4 represent data as taken by the spreading resistance probe, while the diamonds indicate the same points after multilayer analysis. The mathematical basis of the multilayer analysis [17] is discussed by Lee in another paper at this symposium [18]. In essence, because each measurement samples a greater depth into the slice than the depth difference between successive measurements, the direct conversion of resistance readings to dopant concentration values (crosses in figure 4) will not yield a correct profile. The direct result of spreading resistance measurements is somewhat like a profile of local averages rather than of discrete point values. The model used to arrive at the "true" doping profile (diamonds in figure 4) starts with the assumption of one circular contact to a laterally infinite medium which is partitioned vertically into layers of homogeneous resistivity, each layer corresponding to one spreading resistance measurement point. The analysis consists of consecutive solutions of Laplace's equation for the potential distribution generated by the circular contact on top of this stack of layers. The solution actually proceeds from the deepest of the stack of layers, with known boundary conditions, back to the top layer. Since the spreading resistance probe consists of two contacts, the two-probe solution is then obtained by superimposing two one-probe potential solutions at a suitable distance. Techniques for the rapid solution of the simultaneous equations have been developed [18] resulting in short enough execution time to allow economical routine use. The cost of the analysis is typically less than the cost of the original measurement.

When input data is not smooth, the multilayer analysis may magnify input irregularities into the output profile. Figure 4 gives an example of this effect at the interface of the epitaxial layer and the slope of the buried layer. The

local concentration dip of the corrected data is an artifact of the analysis and can be disregarded. It occurs when layers beneath layer being corrected make a major contribution to the measured voltage. Under this circumstance, the program decides that minor variations in the measured voltage must be caused by major ones in the single layer under test, since its contribution to the total measured voltage is relatively small. The program thus overcorrects. In figure 4 this is particularly true since the layer at the point where the irregularity begins is underlain by layers having one to three orders of magnitude higher conductivity.

In addition to the question of smooth data, the shape of the potential distribution under the probe is also important for analysis overcorrection. Real probe tips are not single circular contacts of uniform potential, but are composed of a large number of smaller contacts over a generally circular area. Simply reducing the value of the apparent tip radius to a more effective one does indeed remove the profile dip, but generates some side effects. An exact analytical solution for a model of a real probe tip geometry is presently not available due to the complex boundary conditions involved in a tight array of contacts.

The data in figures 2 and 4, and the following figures are analyzed data, thus representing "true" doping profiles. Figure 5 gives another example of the epitaxial layer/buried layer/substrate system. The spreading resistance technique was able to cover a wide range of depths (total of 18 μm) and concentrations (5 orders of magnitude) with both n- and p-type silicon involved. The location of the junction at about 14.25 μm depth can be clearly delineated.

3. Application to Doping of Shallow Layers

Recent advances in very small-angle beveling (< 0.3 degree) with precisely defined slope edges and scratch-free surfaces [20] opened a new field for application of the spreading resistance probe: the shallow, doped regions of emitter and base in bipolar transistors, and source, drain, and gate in MOS transistors. The data acquired by the spreading resistance probe serve, similar to the applications described previously, as inputs to and as verification of the doping distribution models.

3.1. Boron Distribution

Better understanding of the complex diffusion and redistribution processes in silicon and insulating layers has made it evident that final doping distributions in silicon do not follow simple functional relationships. For instance, dopant profiles were long thought of as characterized by a junction depth and sheet resistance. Consider the regime of devices where both measurements are possible and even accurate. Simple functional forms for the profile representation, namely Gaussian or complementary error function, were chosen and a preliminary device analysis constructed accordingly. Figure 6 represents an actual deposition and drive-in for boron and a functional approximation (Gaussian) with the same sheet resistance and junction depth. Sheet resistance of the Gaussian profiles were calculated using accepted mobility-concentration relationships. Experimental values for sheet resistance are accurate to ± 5%. Figure 6 indicates the problems which can arise because of segregation of the boron into the oxide. For a bipolar base this can lead to an error of a factor of 2 in the base sheet under the emitter, and for MOS technology one might find a surface inverted (weakly) when it was expected to be accumulated.

A realistic diffusion model, as the one developed by Prince [21] for ion-implanted boron under oxidizing conditions, starts with an initial condition for the doping concentration, N(x,t)

$$N(x,0) = f(x,0)$$

given either by experimental data (e.g., gained by spreading resistance measurements) or theoretical expressions (LSS range theory [22] for ion implantation). Defining the origin of the coordinate system at the Si-SiO_2 interface, the diffusion of boron atoms is governed by

$$\frac{\partial N}{\partial t} = \frac{\partial (D\, \partial N/\partial x)}{\partial x} + m \frac{dx_o}{dt} \frac{\partial N}{\partial x}$$

where

D = boron diffusion coefficient in silicon

m = thickness of silicon consumed in growing unit thickness of SiO_2 (assumed to be o.44 in this instance)

$x_o(t)$ = SiO_2 thickness

x = depth from Si/SiO_2 interface into the silicon

Boundary conditions are

$$N(\infty,t) = 0, \text{ and}$$

$$\frac{\partial N}{\partial x} \text{ (at } x = 0) = \left[(K - m)/D\right] N(0,t)\, dx_o/dt$$

where

K = segregation coefficient of boron in the $Si\text{-}SiO_2$ system.

The last boundary condition is derived from the requirement of conservation of boron atoms and under the assumption that boron diffusion in the oxide is slow relative to the oxidation rate dx_o/dt, which is true for steam oxidation.

3.2. Arsenic Distribution

Comparing arsenic diffusion data with a Gaussian profile fit using sheet resistance and junction depth in an analogous way to the boron data plotted in figure 6, would result in an even greater discrepancy due to the strongly non-linear diffusion/annealing behavior of arsenic and its incomplete electrical activation at high concentrations. In figure 7, the true arsenic profile is compared with a linear approximation (complementary error function) by normalizing the concentration. The model and data apply to diffused arsenic. As can be seen, the experimental data fall well into the range of a 10% variation of the intrinsic diffusion constant, D_i, for the non-linear model, but not at all into the range of the erfc approximation. The non-linear model [1,23,24] incorporates the effects of an internal electric field and the variation of equilibrium lattice vacancy concentration into the continuity equations. For ion-implanted arsenic, Shah [25] employed field-aided diffusion, concentration enhancement due to enhanced solubility of vacancies in heavily doped silicon, and electrical activation to formulate a realistic relationship for the diffusion coefficient D in the diffusion differential equation.

$$\frac{D}{D_i} = 1 + \frac{1 + (2\, C^+/n_i)}{1 + \beta\, (C^+/n_i)^3}$$

565-448 O - 75 - 17

where

C^+ = concentration of electrically active arsenic

n_i = intrinsic carrier concentration (temperature dependent)

β = fitting parameter for arsenic activation (temperature dependent)

As Shah has also pointed out, β can be chosen so that it fits the diffusion coefficient for boron previously used [1,21] in the form

$$\frac{D}{D_i} = \left[1 + (C^+/n_i)\right]\left\{1 + \left[1 + (2C^+/n_i)\right]^{-1/2}\right\}$$

3.3. Phosphorus Distribution

The third species used for base and emitter formation is phosphorus. Figures 8 and 9 give examples of spreading resistance data acquired in support of phosphorus distribution models. Figure 8 relates to diffused phosphorus, figure 9 to ion-implanted phosphorus. The model of Tsai [26] assumes a moving boundary separating two distinct phases, a constant concentration region and the transition region of the concentration profile. The phase boundary reaction is the rate-limiting process and the phase boundary moves at a nearly constant rate. Subsequently, Schwettmann and Kendall [27,28] have shown that the tail of the phosphorus profile is formed by enhanced diffusion during low temperature heat treatments. The mechanism underlying this effect has been shown to be related to the one forming the kink in the original unannealed layer. However, the detailed processes occurring in the high concentration region are still not fully understood.

Figures 8 and 9 stress the capability of the spresding resistance probe for acquiring a dense array of data points in layers less than 1 μm thick. As mentioned, this capability is based on the recent advances of fabricating very shallow and well-defined angles [20] . It adds a new dimension to the investigation of emitter and base layers, since the spreading resistance probe is applicable to both n- and p-type silicon, and since it can cover a very wide range of doping concentrations, including steep doping gradients. A particularly important feature of the spreading resistance probe is its ability to probe closer to a pn junction than any other characterization technique. Figures 8 and 9 also compare spreading resistance data to measurements obtained by the incremental sheet resistance technique. There is very good agreement after the spreading resistance data have been corrected by the multilayer analysis. This agreement is significant since the incremental sheet resistance technique supplies absolute values by monitoring the difference between data.

A comment may be added concerning the doping distribution in the silicon layer right under the surface. Figures 8 and 9 show a discrepancy between spreading resistance and incremental sheet resistance data; the spreading resistance values suggest a significant decrease in the phosphorus concentration close to the surface. The probable origin of this drop is an effective reduction in carrier concentration caused by the formation of a depletion region under the surface initiated by the deposition of the silicon nitride film; this film is needed for the precise definition of the surface/bevel edge [20] during the small-angle lapping operation. As figure 8 shows, the depletion region is partially reversed and eliminated (square-shaped data points), when the silicon nitride film is removed.

Profiles of implanted boron, arsenic and phosphorus, diffused to depths of 10 μm, have been measured recently [29] using the spreading resistance probe. The data confirmed diffusion calculations, and were in good agreement with results of incremental sheet resistance measurements.

4. Application to Complete Transistor Profiles

An impressive summary of the capabilities of the spreading resistance probe as a tool for supplying doping profile data for device modeling is the monitoring of a complete transistor profile. It demonstrates that the spreading

resistance technique can measure different conductivity types, many orders of magnitude difference in doping concentration, and shallow layers as well as considerable depth into the silicon slice. It also is a means of monitoring junction depths, or profile parts in selected portions of the transistor, when their shifts as a function of continuing time-temperature treatments are to be studied.

Figure 5 described the cross section of a silicon slice with the diffusion of an n-type buried layer up to the point in time of deposition of an n-type epitaxial layer. The examples given in figures 10 through 13 depict and continue a similar case history, namely an npn epitaxial test transistor with an experimental time-temperature sequence of the diffusion processes. The major differences compared to figure 5 is that the remaining epitaxial layer is about 3 μm deep. Using a much finer depth scale than figure 5, figure 10 reproduces the concentration detail of the boron base after completion of all temperature cycles except the emitter diffusion. The surface depletion due to boron redistribution into the grown oxide is clearly visible. The same depth scale is used in figure 11 to measure the diffused phosphorus emitter profile. The shoulder at intermediate concentrations is particularly prominent [27,28]. Figure 12 shows the very narrow boron region of the original base of figure 10 that remains after the emitter of figure 11 has been predeposited and diffused. Figure 12 also emphasizes how close to pn junctions the spreading resistance probe is able to measure.

Finally, figure 13 represents a composite of the measurements of the previous figures, resulting in a complete transistor profile and illustrating the relative doping proportions. To avoid overcrowding only a few of the actual data points have been plotted in figure 13. The connecting line has been added only for clarity and does not represent the result of theoretical calculations. Cross sections like figure 13 are useful verifications of theoretical doping distribution models, and they serve as inputs to device models concerned with the prediction of transistor characteristics [3,30].

5. Conclusions and Recommendations

5.1. Capabilities of the Spreading Resistance Probe for Modeling

This paper has pointed out the capabilities as well as the limitations of the spreading resistance probe for silicon characterization needed for process and device modeling. The most significant capabilities include the doping characterization of complete transistor profiles, covering the whole range from 10^{14} to 10^{21} carriers/cm^3, the measurement of layers from 0.2 μm to greater than 20 μm, and the determination of junctions between n-type and p-type silicon. Consequently, the dopant distributions can be measured as a function of time and temperature processing, and thus supply inputs, starting conditions, and verification of process and device models. Therefore, the spreading resistance probe is an indispensable tool in support of epitaxy models, buried layer, base, and emitter diffusion models, dopant deposition and redistribution models for both ion implantation and diffusion, and device models as much as they are based on doping profile inputs. These capabilities are summarized in figure 14.

5.2. Limitations of the Spreading Resistance Probe for Modeling

The limitations of the spreading resistance probe for its application to process and device modeling are the possibly insufficient density of data points, and the restriction to electrically active dopants. The density (number/depth) of the spreading resistance measurements is limited by the angle of the slice bevel (presently, smallest angle routinely obtainable $\approx$ 0.3 degrees), the probe tip diameter (presently, mechanical radius $\approx$ 25 μm, electrical radius $\approx$ 1μm), and the minimum separation between tip placements (presently, no agreement on definition or minimum). The limited measurement density is particularly aggravating when the doping profiles in extremely shallow layers ($<$ 0.2 μm) or in very rapidly changing doping concentrations ($>$ 3 orders of magnitude in 0.2 μm) are to be determined. High accuracy in these cases is required for some process models (e.g., doping profile shoulders [28]) and device models (e.g., current gain h_{FE}, injection efficiency, and cut-off frequency f_T as a function of heavy doping of the emitter-base profile [31 to 34]).

5.3. Recommendations for Improvements

More precise model predictions can be expected from improved inputs from the spreading resistance probe. Consequently, efforts should be devoted to refine the angle-lap and surface-preparation techniques of the silicon sample, to decrease the effective electrical tip diameter of the probe, and to minimize the distance between tip placings for reproducible measurements. The multilayer correction factors should be extended to represent the experimental situation of numerous micro-contacts forming the actual electrical tip geometry, and to accommodate wider scattering of the data points.

5.4. Recommendations for Supplementary Techniques

In addition to improvements of the spreading resistance technique, it is recommended that the spreading resistance probe be supplemented by the results of other and independent silicon profiling techniques. Most of these techniques are compared to the spreading resistance probe in another paper at this symposium [20]. Figure 14 lists three of these methods: incremental sheet resistance, incremental MOS capacitance/voltage, and Schottky contact.

The incremental sheet resistance technique for determining concentration profiles has been used extensively during the past several years [35], especially for the identification of control problems in the manufacture of shallow devices ($< 1\ \mu m$). The method consists of measuring the sheet resistance after removing thin (≈ 200 Å) layers of silicon by anodic oxidation and stripping in HF. From the resistivity profile, a concentration profile is obtained by using suitable conversion data, such as that of Irvin [36]. The technique is suited for relatively high doping concentrations ($> 10^{18}/cm^3$).

The incremental MOS C-V technique [37] is best suited for low doping concentrations ($< 10^{18}/cm^3$) and very shallow devices. Thin layers of silicon are removed by the growth of an anodic oxide. MOS C-V measurements are made after each oxidation. The oxide is then removed, a new oxide is grown and another MOS C-V measurement is made. The process is repeated a number of times. For each MOS C-V curve the maximum width of the space charge layer, W_m, is determined. An experimental plot is made of W_m versus X_s, the total thickness of silicon removed. The impurity profile is found by calculating the curve $W_m(X_s)$ for a series of theoretical profiles. The profile whose $W_m(X_s)$ curve matches the experimental curve is taken as the correct profile.

The Schottky contact C-V technique [20] is best suited for lightly doped silicon, since it is limited to the breakdown voltage of the Schottky contact. The depth resolution of its application is thus a function of the doping concentration of the sample. This technique supplements the spreading resistance probe mainly for epitaxial silicon; in addition, the low-concentration diffusion tails can be measured after the more highly doped layers have been removed by anodization.

The three techniques described above measure the electrically active part of the dopants. For some models it is desirable to know the sum of the electrically active and neutral dopants. This information can be supplied by techniques such as the ion microprobe, nuclear activation analysis, and optical methods [20]. More detail about these techniques can be found in the literature [1].

Experience has shown that the best way of acquiring the materials characterization needed for precise process and device models is a combination of the spreading resistance probe and the incremental sheet resistance or the ion microprobe techniques. This combination of methods is capable of generating reproducible, precise, and sufficient data for the analytical models. In this context, it can be stated with confidence that the spreading resistance technique will not only retain its place as an indispensable tool to acquire input and verification data for semiconductor process and device models, but will increase its importance and flexibility, as experimental (bevel, sample surface, probe tip) and analytical (multilayer analysis) methods are improved and standardized.

6. Acknowledgements

The author would like to thank Dr. F. W. Voltmer and Mr. R. Byrd for providing the spreading resistance measurements, and Mr. G. A. Lee for supplying the multilayer analysis. The author is also indebted to Drs. P. L. Shah and J. L. Prince for numerous discussions of doping distribution models.

7. References

[1] Schroen, W. H., The impact of process control on parameter stability — A review, Semiconductor Silicon 1973, ed. by H. R. Huff and R. R. Burgess (Electrochem. Soc., Princeton, N. J., 1973), pp. 738-758.

[2] Jenkins, F. S., Lane, E. R., Lattin, W. W., and Richardson, W. S., MOS-Device modeling for computer implementation, IEEE Trans. Circ. Theory, CT-20, 649-658 (1973).

[3] Edwards, J. R. and Marr, G., Depletion-mode IGFET made by deep ion implantation, IEEE Trans. Electron Devices, ED-20, 283-289 (1973).

[4] Sigmon, T. W. and Swanson, R., MOS threshold shifting by ion implantation, Solid-State El., 16, 1217-1232 (1973).

[5] Hachtel, G. D., Joy, R. C., and Cooley, J. W., A new efficient one-dimensional analysis program for junction device modeling, Proc. IEEE, 60, 86-98 (1972).

[6] Kleppinger, D. D. and Lindholm, F. A., Impurity concentration dependent density of states and resulting Fermi level for silicon, Solid-State El., 14, 407-416 (1971).

[7] Poon, H. C., Modeling of bipolar transistor using integral charge-control model with application to third-order distortion studies, IEEE Trans. Electron Devices, ED-19, 719-731 (1972).

[8] Whittier, R. J. and Tremere, D. A., Current gain and cutoff frequency falloff at high currents, IEEE Trans. Electron Devices, ED-16, 39-57 (1969).

[9] Van Overstraeten, R., and Nuyts, W., Comparison of theoretical and experimental values of the capacitance of diffused junctions, J. Appl. Phys., 43, 4040-4050 (1972).

[10] Morris, B., Some device applications of spreading resistance measurements on epitaxial silicon, J. Electrochem. Soc., 121, 422-426 (1974).

[11] Kahng, D., Thomas, C. O., and Manz, R. C., Epitaxial silicon junctions, J. Electrochem. Soc., 110, 394-400 (1963).

[12] Grossman, J. J., A kinetic theory for autodoping for vapor phase epitaxial growth of germanium, J. Electrochem. Soc., 110, 1065-1068 (1963).

[13] Grove, A. S., Roder, A., and Sah, T. C., Impurity distribution in epitaxial growth, J. Appl. Phys., 36, 802-810 (1965).

[14] Langer, P. H. and Goldstein, J. I., Impurity redistribution during silicon epitaxial growth and semiconductor device processing, J. Electrochem. Soc., 121, 563-571 (1974).

[15] Grove, A. S., Physics and Technology of Semiconductor Devices (Wiley, New York, 1967) pp. 43-83.

[16] DeVries, D. B., Lee, G. A., and Watelski, S., Integrated-circuit process control and development, Techn. Report AFAL-TR-73-268 (1973).

[17] Hu, S. M., Calculation of spreading resistance correction factors, Solid-State El., 15, 809-817 (1972).

[18] Lee, G. A., Rapid multilayer correction factors, ASTM/NBS Symp. on Spread. Resist. Meas., Gaithersburg, Md., June 1974.

[19] Hu, S. M., Redistribution of diffused layers during epitaxy and other process steps, J. Appl. Phys., 39, 3844-3849 (1968).

[20] Lee, G. A., Schroen, W. H., and Voltmer, F. W., Comparison of the spreading resistance probe with other silicon characterization techniques, ASTM/NBS Symp. on Spread. Resist. Meas., Gaithersburg, Md., June 1974.

[21] Prince, J. L. andSchwettmann, F. N., Diffusion of boron from ion implanted sources and oxidizing conditions, J. Electrochem. Soc., 121, 705-710 (1974).

[22] Linhard, J., Scharff, M , and Schiott, H. E. Kgl. Danske Videnskap Selskab, Mat.-Fys. Model, 33 14 (1963).

[23] Hu, S. M. and Schmidt, S., Interactions in sequential diffusion processes in semiconductors, J. Appl. Phys, 39, 4272-4283 (1968).

[24] Fair, R. B. and Weber, G. R., Effect of complex formation on diffusion of arsenic in silicon, J. Appl. Phys., 44 273-279 (1973).

[25] Shah, P. L., to be published.

[26] Tsai, J. G., Shallow phosphorus diffusion profiles in silicon, Proc. IEEE, 57, 1499-1506 (1969).

[27] Schwettmann, F. N. and Kendall, D. L., Carrier profile change for phosphorus-diffused layers on low-temperature heat treatment, Appl. Phys. Letters, 19, 218-220 (1971).

[28] Schwettmann, F. N. and Kendall, D. L., On the nature of the kink in the carrier profile for phosphorus diffused layers in silicon, Appl. Phys. Letters, 21, 2-4 (1972).

[29] Douglas, E. C. and Dingwall, A.G.F., Ion implantation for threshold control in COSMOS circuits, IEEE Trans. on El. Dev., ED-**21**, 324-331 (1974).

[30] DeMan, H. J., and Mertens, R., SITCAP — A simulator of bipolar transistors for computer-aided circuit analysis programs, 1973 IEEE Internat. Solid-State Cirucits Conf., Feb. 15, 1973.

[31] Mertens, R. P., DeMan, H. J., and Van Overstraeten, R. J., Calculation of the emitter efficiency of bipolar transistors, IEEE Trans. on El. Dev., ED-**20**, 772-778 (1973).

[32] Van Overstraeten, R. J., DeMan, H. J., and Mertens, R. P., Transport equations in heavy doped silicon, IEEE Trans. on El. Dev., ED-**20**, 290-298 (1973).

[33] Mock, M. S., Transport equations in heavily doped silicon, and the current gain of a bipolar transistor, Solid-State El., **16**, 1251-1259 (1973).

[34] DeMan, H. J., Mertens, R. P., and Van Overstraeten, R. J., Influence of heavy doping effects on the f_T prediction of transistors, Electronic Letters, **10**, (May 1974).

[35] Donovan, R. P. and Evans, R. A., Incremental sheet resistance technique for determining diffusion profiles, Silicon Device Processing, ed. by Ch. P. Marsden (NBS Special Publ. 337, Washington, D.C., 1970), 123-131.

[36] Irvin, J. C., Resistivity of bulk silicon and of diffused layers in silicon, Bell System Tech. J., **41**, 387-410 (1962).

[37] Kronquist, R. L., Soula, J. P., and Brilman, M. E., Diffusion profile measurements in the base of a microwave transistor, Solid-State El., **16**, 1159-1171 (1973).

PROCESS MODELING

EPITAXIAL SILICON
BURIED LAYER DIFFUSION
ION IMPLANTATION AND DIFFUSION

DEVICE MODELING

DIODE MODELS
INTRINSIC TRANSISTOR
ACTUAL TRANSISTOR

Figure 1. Spreading Resistance Technique Applied to Modeling

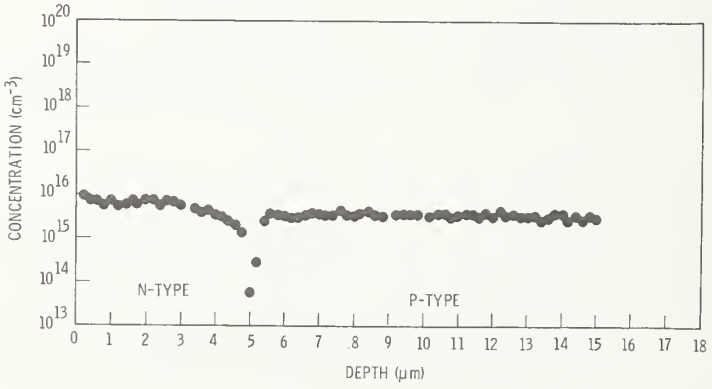

Figure 2. Epitaxy on Substrate

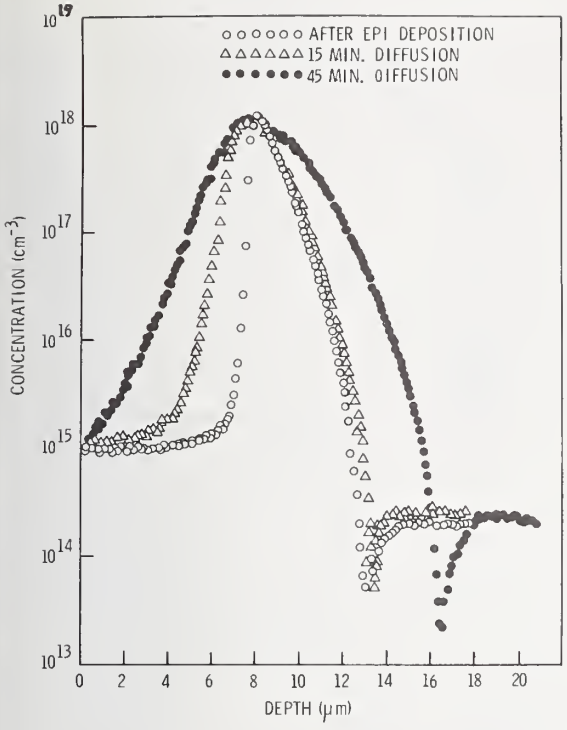

Figure 3. N Buried Layer Diffusion

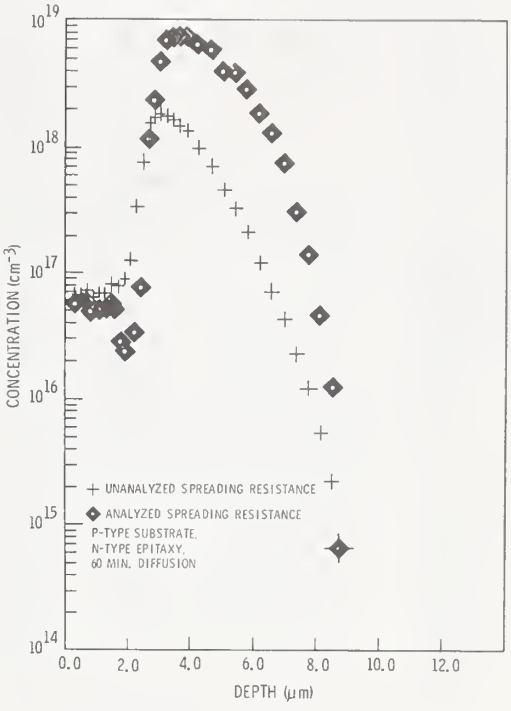

Figure 4. N Buried Layer Diffusion: Spreading Resistance Data with Multilayer Analysis

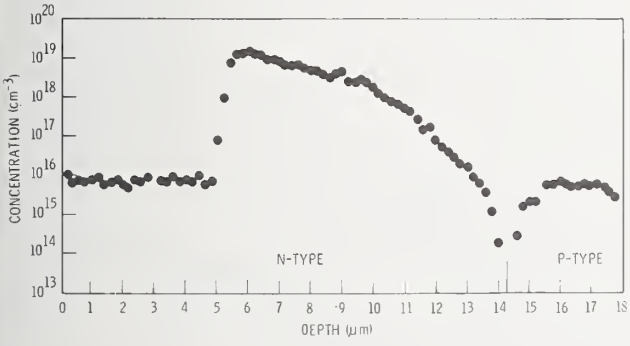

Figure 5. Epitaxy-Buried Layer-Substrate

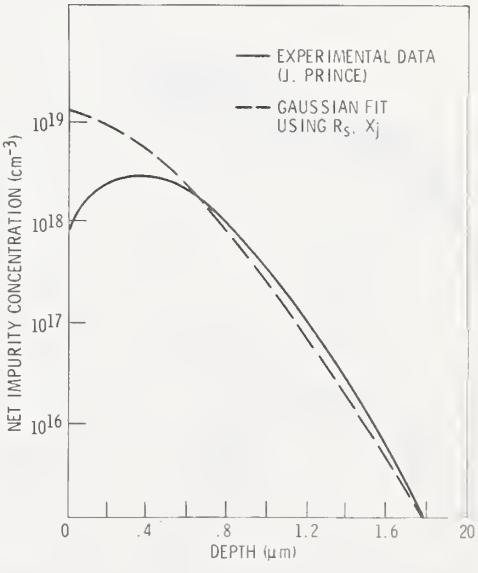

Figure 6. Ion-Implanted Boron: Comparison of Experimental Data [21] with Gaussian Model

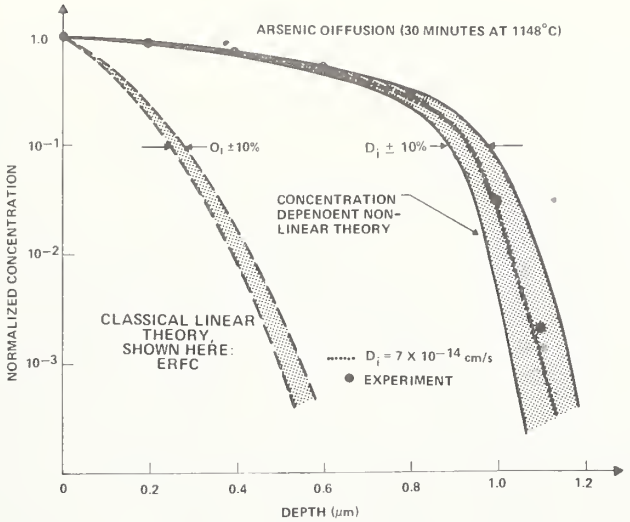

Figure 7. Arsenic Diffusion: Model and Experimental Data

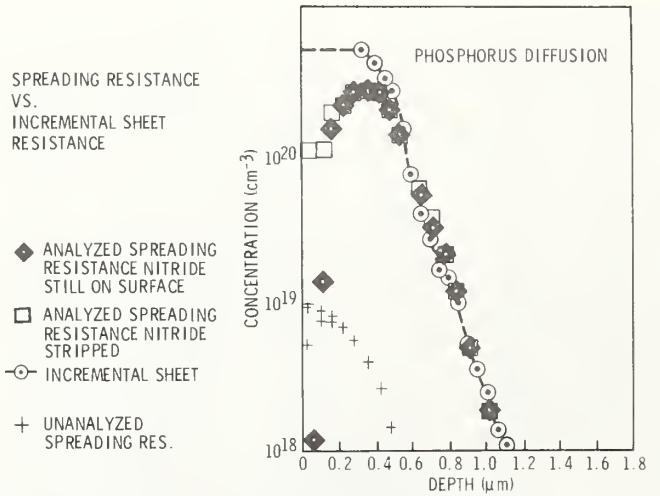

Figure 8. Diffused Phosphorus: Comparison of Spreading Resistance and Incremental Sheet Resistance Data

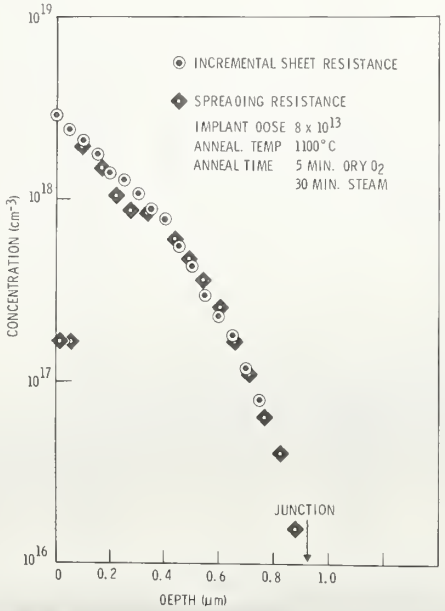

Figure 9. Ion-Implanted Phosphorus: Comparison of Spreading Resistance and Incremental Sheet Resistance Data

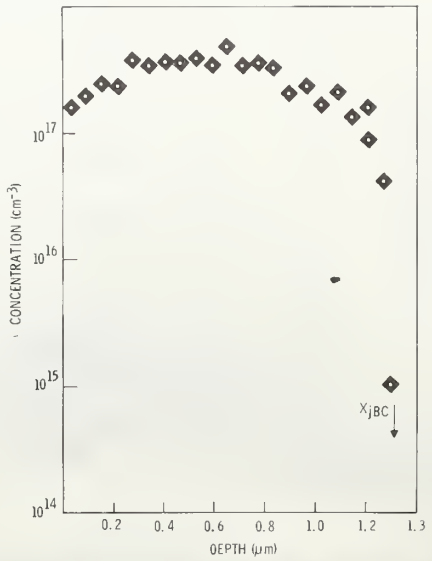

Figure 10. Concentration in Base Layer After All Temperature Cycles Except Emitter Diffusion

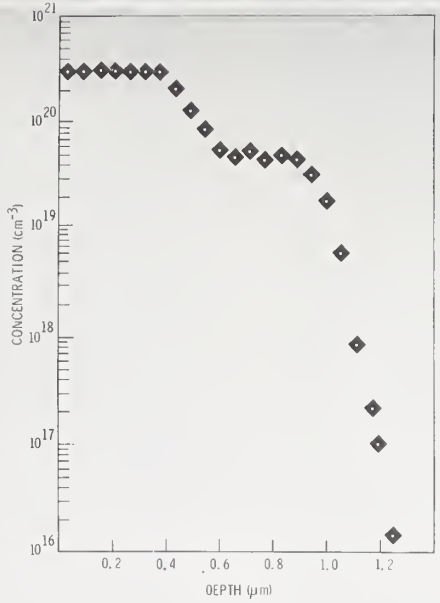

Figure 11. Emitter Profile, Without Base.

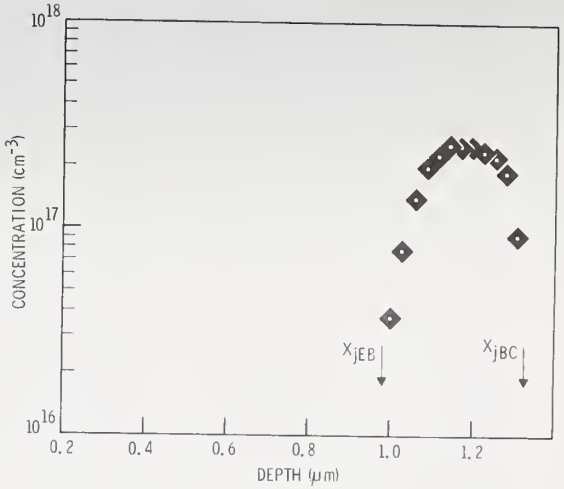

Figure 12. Base Profile After Emitter Diffusion

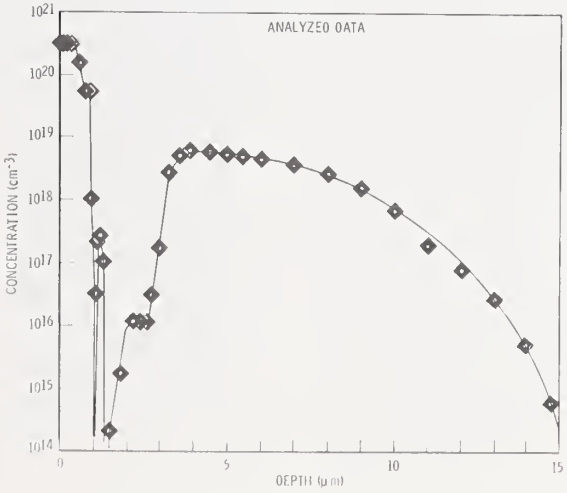

Figure 13. Complete Profile of Test Structure.

CAPABILITIES

- COMPLETE DOPANT DISTRIBUTION
- DEEP LAYERS
- DOPING CONCENTRATION EXTREMES

LIMITATIONS

- SHALLOW LAYERS
- STEEP CONCENTRATION GRADIENTS

SUPPLEMENTAL TECHNIQUES

- INCREMENTAL SHEET RESISTANCE
- INCREMENTAL MOS CAPACITANCE/VOLTAGE
- SCHOTTKY CONTACT

Figure 14. Spreading Resistance Technique Applied to Modeling

NATIONAL BUREAU OF STANDARDS SPECIAL PUBLICATION 400-10, Spreading Resistance Symposium, Proceedings of a Symposium Held at NBS, Gaithersburg, Md., June 13-14, 1974.

Improved Surface Preparation For Spreading Resistance Measurements on *p*-type Silicon

J. R. Ehrstein

Institute for Applied Technology
National Bureau of Standards
Washington, D.C. 20234

The interpretation and the precision of spreading resistance measurements have been seen to be strongly dependent on specimen surface preparation. A bakeout at 150°C for 15 min. following specimen surface preparation with any aqueous polishing solution is considered here. It is shown both to improve the precision of the basic calibration curve for spreading resistance measurements and to significantly improve the correlation between resistivity values derived from spreading resistance measurements on a variety of specimens, and resistivity values derived from other measurement techniques. No bakeout appears to be necessary if specimen surface preparation is done with a non-aqueous polishing process.

Key words: Bevel polishing; *p*-type silicon; resistivity depth profiling; resistivity radial profiling; semiconductors; spreading resistance measurements; surface effects; surface preparation.

1. Introduction

Spreading resistance measurements, despite their high degree of spatial resolution nd versatility for measuring the dopant profile in multilayer semiconductor device tructures, are nevertheless subject to reduced sensitivity and even to misinterpretation f the conditions of measurement are not properly defined and controlled. A recent change n the surface preparation of silicon specimens prior to measurement was necessitated by bservation of apparent changes in the dopant density on the bevel polished surfaces of ulk *p*-type specimens. The change in surface preparation, the addition of a thermal cycle, r bakeout, 150°C for 15 min. was subsequently found to significantly improve measurement esults of three different types. The three measurement areas were 1) the construction of calibration curve from spreading resistance to resistivity for *p*-type silicon specimens,) radial resistivity profiling of silicon slices being inspected for use as four-probe esistivity standards, 3) depth profiling of bevel polished specimens.

2. Observation of a Surface Effect

The existence of a surface related problem in spreading resistance measurements was rimarily noted as a result of an attempt to study redistribution of dopant atoms in ilicon resulting from thermal oxidation. For this study, because of the smallness of ne expected effect, it was necessary to run instrument electronics at nearly maximum gain: ull scale covered only 2 decades of measured spreading resistance as opposed to the decade full scale normally used for profiling of device structures by spreading resistance. ll wafers in this study were approximately 10 Ω·cm boron-doped silicon wafers which had een sectioned by polishing with a silica gel polish at a small bevel angle with respect

to the top surface. The bevel sectioning was done to allow profiling of dopant distribution in depth below the surface, as shown in figure 1. An apparent redistribution of dopant, seen in the form of increased spreading resistance values, and hence of increased resistivity, was observed both for wafers which had undergone thermal oxidation and for control wafers which were merely polished wafers from the same starting batch. The effect was such that even on the nonoxidized wafers the measured spreading resistance was higher on the freshly polished beveled surface than on the original top surface by a factor greater than two.

It is to be noted that the nature of the bevel polishing procedure is such as to remove material only from a section of the silicon chip at a small angle with respect to the top surface. The rest of this original top surface, although it may be in contact with the polishing solution, is not held under any load against the polishing plate, and hence is protected from the effects of the polishing solution by the natural surface oxide of the silicon which remains intact. This surface oxide, generally of the order of 50 Å thickness is readily penetrated by the spreading resistance probes. If the bevel polishing process were completely passive and simply removed silicon layers without leaving electrically active residue or changing the nature the surface states of the silicon, it is expected that the bevel polished and the top surfaces of the nonthermally oxidized chip would have shown differences in spreading resistance of 10% or less. This small change might be expected because of possible changes in contact shape from a slightly different angle of the spreading resistance probe against the silicon surface, small possible changes of resistivity in depth due to the original crystal growth, and possibly a very small effect due to the native oxide on the original top surface.

3. Experimental Results

3.1 Early Surface Treatments

Since the shift in spreading resistance observed in probing across the bevel vertex was much larger than expected as a result of all the component causes that had been considered, it was judged that the polishing process used for beveling was not in fact passive, but changed the electrical nature of the silicon surface. Subsequent similar specimens, without thermal oxide, were bevel polished by the same polishing process and were then variously bathed and swabbed in solutions of hydrofluoric acid, chromic acid, ammonium hydroxide and ammonium hydroxide with hydrogen peroxide. Each of these chemical treatments effected a change of the spreading resistance value of the bevel polished surface from the value measured on the polished only surface, and all but the hydrofluoric acid treatment left unaffected the spreading resistance value on the original top surfaces of the chips which had been protected by the native oxide. However, in no case did one of these chemical treatments bring reasonable agreement between the spreading resistance value on the beveled surface and that on the original top surface. In fact, most of these subsequent surface treatments caused increased measurement scatter as compared with the polished only surfaces. Thermal cycling at 70 to 100°C under partial vacuum for 15 minutes, subsequent to polishing also failed to change the measurement disparity between these two exposed surfaces.

Comparison of these observations with those of members of various other laboratories led to a recommendation[1] for a bakeout at a minimum 150°C for 15 or more minutes subsequent to polishing.

3.2 Bakeout of Bevel Polished Specimens

The recommended bakeout procedure was implemented on a series of bevel polished boron doped silicon chips, each having nominal resistivity value of 10 Ω·cm and having only an ambient oxide layer prior to polishing. The effect of the bakeout procedure is shown in figure 2 for chem-mechanical polishing using two different commercially available silica

[1]Dr. A. Mayer, RCA Laboratories (private communication)

polishing compounds, both in strongly basic aqueous solutions, and the first of which was the polishing compound used when the original surface preparation problem was noted during the study of dopant redistribution. In both cases, the bevel polishing was done against a sheet of methyl methacrylate. The specimens here were sections of a silicon wafer actually measured at 11 Ω·cm by the four-probe method (1)[1] and taken from a lot of wafers for which capacitance-voltage measurements (2) and use of Irvin's curves (3) yielded values of 10 to 12 Ω·cm. The resistivity scales shown in figures 2 to 5 are derived from a calibration curve which was generated from the spreading resistance values near the center of silicon specimens whose resistivity values were carefully measured by the four-probe method and which show a high degree of uniformity of radial resistivity. Spreading resistance data for all parts of this work were taken at the same 2 decade/full scale gain-setting at which the surface preparation problem was originally observed.

It should be noted that there is a shift in apparent resistivity across the bevel vertex from the bevel polished to the original top surface of both unbaked chips. It should also be noted that reasonable agreement with the four-probe and C-V values of resistivity is not obtained on the freshly bevel polished surface, without the addition of the bakeout cycle. This bakeout, however, succeeds in producing resistivity values from spreading resistance which are within 10% of those from both other methods. A limit of about 5% on the resolution of all data is imposed by the analog form in which data were acquired.

In order to investigate whether this shift in spreading resistance was a particular result of silica polishing, further wafer sections were taken and were bevel polished with a zirconium compound in an alkaline solution and with an alumina slurry in water, the latter having a strictly mechanical polishing action. The results are shown in figure 3. Because of the relatively large particle size in both these solutions it was not possible to obtain a sharp bevel vertex. Consequently, polishing actually occurred for a small distance onto the original top surface of the wafer section, which would normally go untouched. This results in an increased value for spreading resistance for a distance on both sides of the bevel vertex as seen in the figure. Again, the point to be noted is that freshly polished surfaces yield spreading resistance, and their corresponding resistivity values which are in marked disagreement with those obtained from the four-probe and C-V methods whereas values obtained on specimens which have undergone the recommended bakeout are in good agreement.

The cases of an etched surface and a surface mechanically polished in the only non-aqueous based solution considered here are both shown in figure 4. Again, effects due to the surface preparation are shown on both sides of the rounded bevel vertex because of the inability to maintain sharp vertices with these processes. A shift in measured spreading resistance due to etching is seen which is also removed by thermal cycling. No measurable shift is seen for the case of non-aqueous surface preparation. The exact mechanism is unknown but the observations are in good agreement with the observations of Mayer and Schwartzmann regarding the effects of aqueous preparations (4).

Two other specimen configurations were also tested for the presence of such an effect. The first, a piece of p-type bulk silicon from the same batch used for previous measurements, had a thermal oxide grown on the top surface before sectioning and bevel polishing. The shape of the spreading resistance data (fig. 5) is of course influenced by the presence of the oxide; however, again, agreement with four-probe resistivity values can only be obtained by the addition of the bakeout subsequent to polishing. The second specimen configuration was a chip with p epitaxy on a $p+$ substrate. The value of the epitaxial resistivity using MOS C-V (5) measurements and Irvin's curves (3) was 12 Ω·cm. This particular epitaxial configuration was chosen since the effect of the high conductivity substrate, for data near the epi-substrate interface, is in the opposite direction from that previously experienced from the polishing process. Again, an artificial increase of measured spreading resistance is seen for the epitaxial layer until the specimen has been baked-out, at which time resistivity values within 10% of that obtained from MOS C-V measurements were achieved.

---

[1] Figures in brackets indicate references at the end of this paper.

3.3 Effect on the Calibration Curve

The second area in which the thermal cycling of specimens was found to be of great benefit was in the construction of the calibration curve itself. As reported elsewhere (6) early calibration data for *p*-type specimens showed scatter of 50 to 80% in spreading resistance values for specimens closely grouped in terms of four-probe resistivity values, lesser scatter being noted for *n*-type specimens. The observed scatter in data for *p*-type silicon was particularly evident in the resistivity range from 1 to 100 Ω·cm. Data from a calibration on chem-mechanically polished *p*-type specimens, which had previously been screened for radial resistivity uniformity of 10% or better, by use of spreading resistance are shown in figure 6. The specimens used were chem-mechanically polished in an aqueous solution against an artificial leather backing.

At first the data scatter seen in this figure may be judged to be insignificant considering the total span and overall linearity of the data. However, our experience indicates such a judgement to be optimistic, at least for high resolution applications, because shifts of measured spreading resistance values, of the type already shown, while strongly linked to the aqueous polishing medium, also appear to be linked to other parameters of polishing such as composition of polishing substrate and rate of material removal. This can be seen in figure 7 where the scatter of the data from figure 6 is expanded by use of a reduced ordinate scale: ratio of measured spreading resistance to four-probe resistivity; (also shown are data taken on the same specimens which had received the bakeout after a fresh chem-mechanical polishing using a silica gel solution). It is to be noted that there are both increases and decreases in measured spreading resistance, rather random as a function of resistivity, resulting from the bakeout. This is particularly to be noted for the three specimens with resistivity in the vicinity of 10 Ω·cm where two of the specimens show an increased spreading resistance after thermal treatment. This is opposed to the strong decrease upon thermal treatment which was seen for all bevel polished specimens, as discussed previously, which were chem-mechanically polished in the same solution but using different loading and a different polishing substrate from the calibration specimens.

It is expected as a result of this variability in response to polishing without subsequent bakeout, that a given specimen may not maintain a specific high or low bias with respect to the line of regression. Therefore, for any highly accurate analysis where the local calibration over a small range of resistivity values becomes important, large scatter in the data about the local regression, particularly if not reproducible point by point, may make interpretation of data erroneous. By contrast, it can be seen from figure 7 that bakeout of the same calibration specimens after a fresh polishing results in highly improved distribution of data about the line of regression.

3.4 Effect on Radial Resistivity Profiling

A third area of improved results due to the bakeout procedure lies in the area of radial resistivity profiling. During the original examination of incoming material for possible use as resistivity standards, now issued by NBS[2] uniformity of radial resistivity was a key acceptance parameter. It was a rather common experience, however, to find that a slice from a crystal, particularly at the 10 Ω·cm level, would yield resistivity profiles radially uniform to within 5% by both four-probe measurements and combined photovoltage/photocurrent measurements (7), while spreading resistance radial profiles showed as much as 100% variation on the same diameter of the slice. Figure 8 shows a typical slice profiled by spreading resistance both with and without a 150°C bakeout after polishing. The sets of probe tracks were approximately along a diameter but were displaced laterally by about 200 μm from each other. The measure of radial variation in the case of the baked-out wafer is in quite good agreement with measurements on the same slice by both the four-probe and photovoltage techniques.

[2]SRM 1520, Silicon Resistivity Standards; Office of Standard Reference Materials, NBS, Washington, D.C. 20234

4. Summary

Although the mechanism for the surface effect is not understood, its inherent association with aqueous based surface treatment is strongly indicated. Such effects may be minimized by other variations in the polishing process such as loading, rate of surface feed during polishing, or the nature of the polishing substrate, but bakeout after polishing has been shown to remove such surface effects almost in their entirety. It must be noted that the strength of the effect may well be related to conductivity type and resistivity level; hence isolated experiments on a limited number of specimens may be inadequate to characterize a particular polishing process for the full spectrum of specimen types which may eventually be considered.

This research was supported by the Advanced Research Projects Agency of the Department of Defense under ARPA Order No. 2397.

5. References

1. Standard Method for Measuring Resistivity of Silicon Slices with a Collinear Four-Probe Array, ASTM Designation F-84, 1973 Annual Book of Standards, part 8, American Society for Testing and Materials, November 1973.

2. Mattis, R. L., and Buehler, M. G., Semiconductor Measurement Technology: A Basic Program for Calculating Dopant Density Profiles from Capacitance-Voltage Data, NBS Special Publication 400-11 (in preparation).

3. Irvin, J. C., Bell System Tech. Journal 41, No. 2, 387-410 (1962).

4. Mayer, A., and Schwartzman, S., this volume, pp. 123-137.

5. Lehovic, K., Solid State Electronics 11, 135-7, (1968).

6. Bullis, W. M., ed., Methods of Measurement for Semiconductor Materials, Process Control, and Devices, Quarterly Report; April to June 1973; NBS Technical Note 806 (November 1973), pp. 9,10.

7. Blackburn, D. L., Schafft, H. A., and Swartzendruber, L. J., Journal of the Electrochemical Society 119, No. 12, 1773-78 (1972).

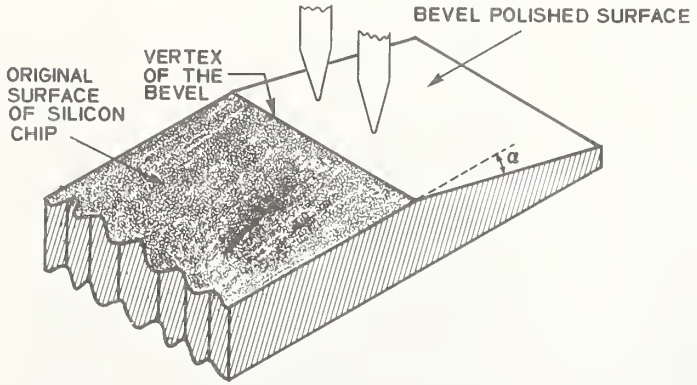

Figure 1. Bevel polished chip being probed parallel to bevel vertex for depth profile.

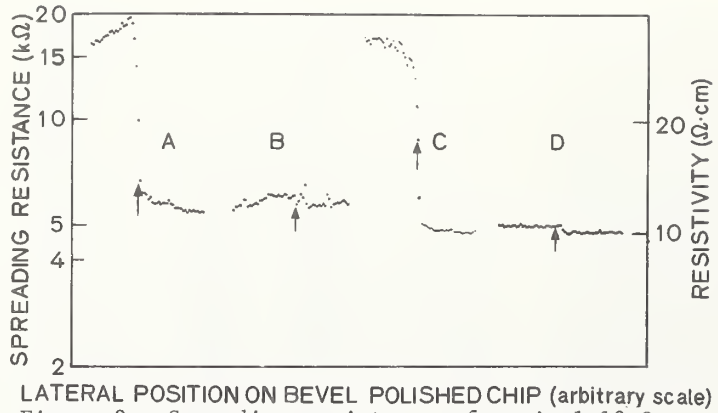

Figure 2. Spreading resistance of nominal 10 Ω-cm p-type beveled specimen for various polishes.

A. Silica gel solution
B. Silica gel solution, followed by bakeout
C. Silica powder in potassium hydroxide solution
D. Silica powder in potassium hydroxide solution, followed by bakeout

Pointer arrow indicates position of bevel vertex

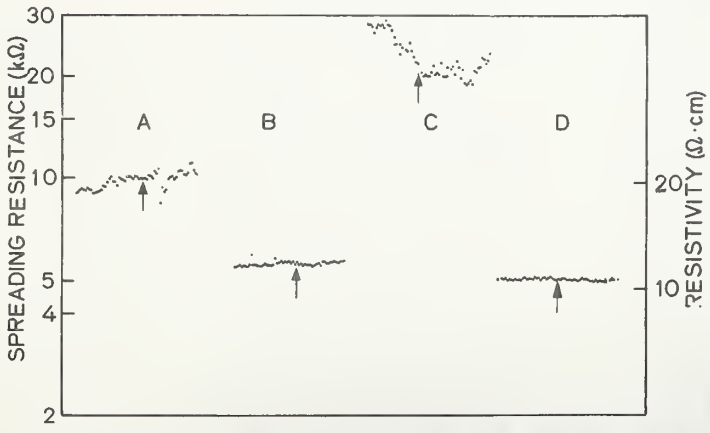

Figure 3. Spreading resistance of nominal 10 Ω-cm p-type beveled specimen for various polishes.

A. Zirconium oxide solution
B. Zirconium oxide, followed by bakeout
C. 0.3 μm alumina in water
D. 0.3 μm alumina in water, followed by bakeout

Pointer arrow indicates position of bevel vertex

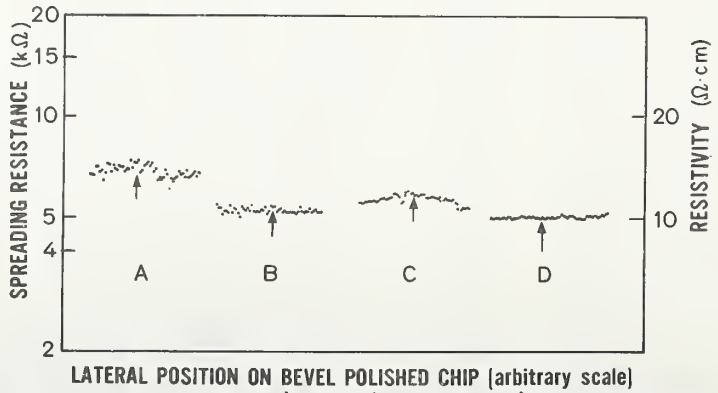

Figure 4. Spreading resistance of nominal 10 Ω-cm p-type beveled specimen for various surface treatments.

A. CP_4 etched
B. CP_4 etched, followed by bakeout
C. Polished with alumina in glycerin and trichloroethylene
D. Polished with alumina in glycerin and trichloroethylene, bakeout

Pointer arrow indicates position of bevel vertex

555-440 O - 75 - 18

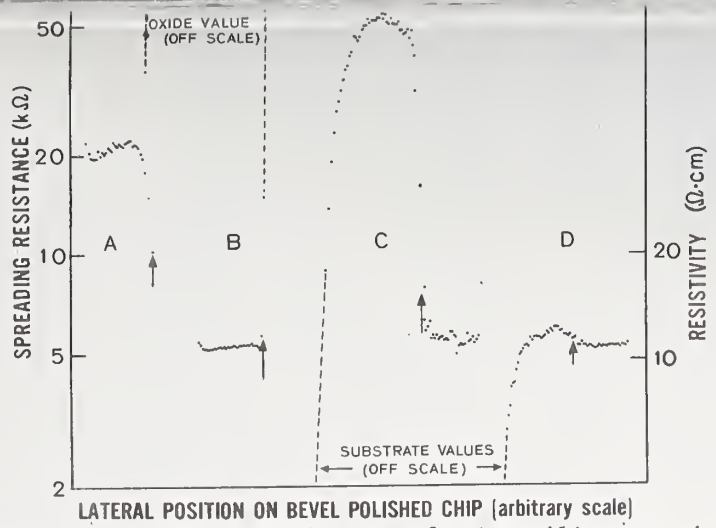

Figure 5. Spreading resistance of other silicon specimens.
A. Thermally oxidized 10 Ω-cm p-type, silica gel polished
B. Same specimen after bakeout
C. Nominal 10 Ω-cm p epitaxy over p^+ substrate, silica gel polished
D. Same specimen after bakeout

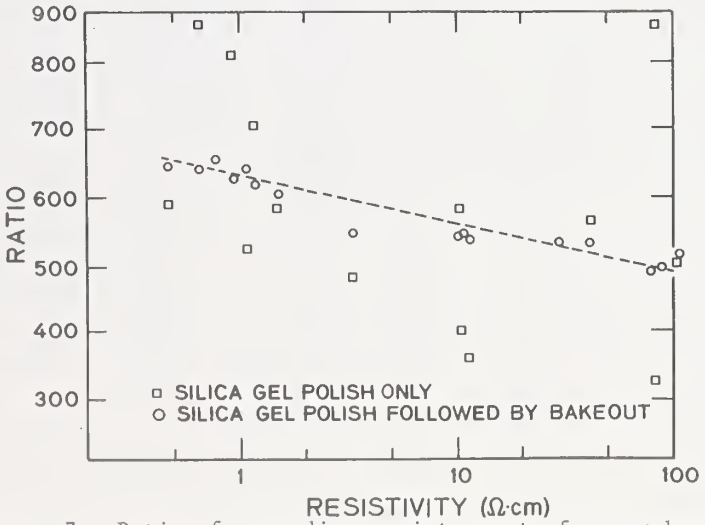

Figure 7. Ratio of spreading resistance to four probe resistivity vs. resistivity for the upper range of the p-type calibration curve.

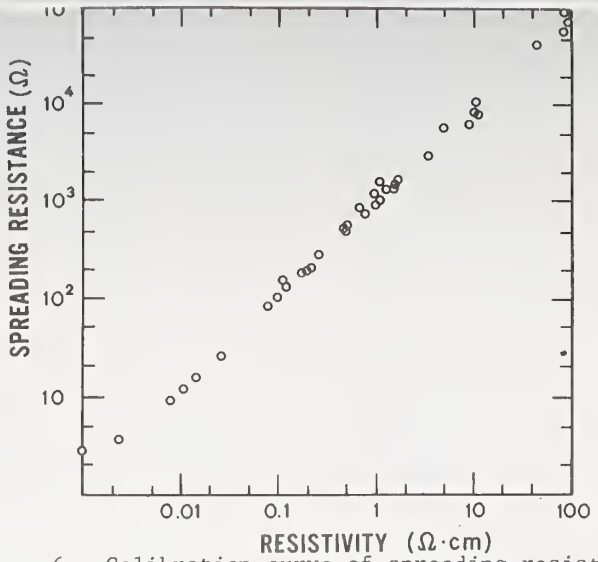

Figure 6. Calibration curve of spreading resistance vs. four probe resistivity for silica gel polished p-type specimens, no bakeout.

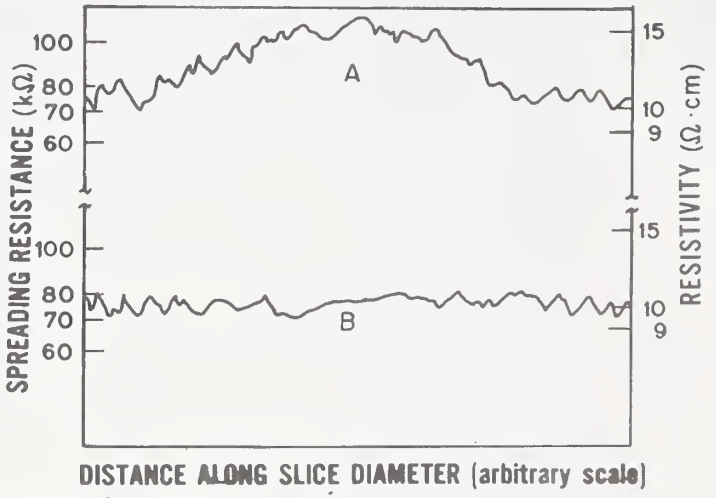

Figure 8. Radial resistivity profile of a 10 Ω-cm p-type slice by spreading resistance.
A. Silica gel polish only
B. Silica gel polish, followed by bakeout

DISCUSSION SESSIONS

The material in this section was taken from tape recordings of discussion periods which were held at the conclusion of the Theory, Practice and Application Sessions with all the speakers in the session forming a panel to respond to questions and comments. Such questions as were asked directly after individual contributed papers, and their answers, are presented in the appropriate discussion section. Since a list of all participants and their affiliations is given at the outset, the respondents are inentified only by name in the discussions. Each respondent was given the opportunity to review his comments prior to publication. Such changes as were made were primarily grammatical or for clarification of intent. The content is substantially unchanged. Editor's notes are also given where it is thought to benefit the discussion.

DISCUSSION SESSION PARTICIPANTS

R. P. Anand
Bell Telephone Laboratory
2525 North 11th Street Box 241
Reading, Pennsylvania 19604

Jacques Assour
RCA SSD
Somerville, New Jersey 08876

Douglas A. Barth
Westinghouse Electric Corporation
Defense and Electronics System Center
P. O. Box 1521 MS 3525
Baltimore, Maryland 21203

Dr. K. E. Benson
Bell Telephone Laboratories
555 Union Boulevard
Allentown, Pennsylvania 18103

David H. Dickey
Bell & Howell
Pasadena, California 91107

John R. Edwards
Bell Telephone Laboratories
555 Union Boulevard
Allentown, Pennsylvania 18103

J. R. Ehrstein
National Bureau of Standards
Washington, D. C. 20234

Stephen J. Fonash
Pennsylvania State University
231 B. Sackett Building
University Park, Pennsylvania 16802

E. E. Gardner
IBM - SPD
P. O. Box A G37/B966
Essex Junction, Vermont 05452

Carl A. Germano
Motorola Semiconductor Products Division
P. O. Box 2953, Mail Drop A-162
Phoenix, Arizona 85036

Gilbert A. Gruber
Solid State Measurements, Inc.
600 Seco Road
Monroeville, Pennsylvania 15146

Norman Goldsmith
RCA Corp. Labs
Route 1
Princeton, New Jersey 08540

Hans Mork Janus
Topsil A/S
Lindervpvej, Frederikssund
Denmark DK-3600

J. Korvemaker
Bell Northern Research
Department 8R81 - P. O. Box 3511 Station C
Ottawa, Ontario, Canada KIY4H7

Dr. J. Krausse
Siemens AG, LLBBGE1
Munich, Frankfurter Ring 152, F. R. Germany

Dr. Paul H. Langer
Bell Telephone Laboratories
555 Union Boulevard
Allentown, Pennsylvania 18103

Alfred Mayer
RCA - Solid State
Route 202
Somerville, New Jersey 08816

Robert G. Mazur
Solid State Measurements, Inc.
600 Seco Road
Monroeville, Pennsylvania 15146

Bernard L. Morris
Bell Telephone Laboratories
555 Union Boulevard
Allentown, Pennsylvania 18103

Dr. Helmuth Murrmann
Siemens AG. WH MB EA 511
Balanst. 73
Muenchen 80 West Germany

Steve Mylroie
Signetics Corporation
811 East Arques 9132
Sunnyvale, California 94986

Pierre Pinchon
RTC La Radiotechnique Complec
Code postale: boite postale 6025 -
14001 - CAEN CEDEX (FRANCE) 14001

Michael Poponiak
IBM - East Fishkill
Department 214, Building 300-94
Hopewell Junction, New York 12533

Simon Prussin
TRW Semiconductors
14520 Aviation Boulevard
Los Angeles, California 90260

A. J. Robinson
IBM
9500 Godwin Drive
Manassas, Virginia 22110

Dr. Walter H. Schroen
Texas Instruments, Inc.
P. O. Box 5012, MS/72
Dallas, Texas 75222

Robert I. Scace
General Electric
Electronics Park, EP7 Box 41
Syracuse, New York 13201

Dr. P. J. Severin
Philips Research Laboratories
Eindhover - Holland

Stanley Shwartzman
RCA Solid State Division
Route #202
Somerville, New Jersey 08876

Fritz G. Vieweg-Gutberlet
Wacker-Chemitronic GMBH
P. O. Box 1140
Burghausen, West Germany D-8263

Fred W. Voltmer
Texas Instruments, Inc.
P. O. Box 5936 MS 144
Dallas, Texas 75222

James C. White, Jr.
Western Electric
555 Union Boulevard
Allentown, Pennsylvania 18103

Don E. Williams
Bell Telephone Laboratories
Reading, Pennsylvania 19604

Douglas Yoder
Delco Electronics, GMC
P. O. Box 1104, Plant 10, Room 328
Kokomo, Indiana 46068

F. MAYER: I think the only speaker who addressed himself on theoretical grounds to the difference between what should be observed on (111) versus (100) material is Steve Fonash. I am interested to know what the other members of the panel expect from theoretical considerations of an orientation dependence.

W. SCHROEN: The multilayer analysis is independent of crystalline orientation. It considers only potential theory. However, I do not exclude that there could well be influences of the crystalline orientation and a complete theory would include crystalline orientation, stress effects, specific contact resistance, and other effects mentioned this morning. The pure potential theory neglects all these.

R. MAZUR: I do not want to leave the question hanging with some of you who are not so familiar with the question of crystallographic orientation but I have gone on record in the past as indicating that I have never seen a significant orientation dependence. Now I get disagreement there from all of IBM combined with all of Bell Labs and a few other places to boot. I may have to retract on this statement in the future; that is possible. I have not had the time to do extensive research with different orientation samples. Bernie Morris did supply me with a couple of wafers about six months ago and I have not had a chance to run them yet believe it or not. But the orientation dependence may, in many practical cases, be so small as to be unobservable from a practical point of view. I see it as a case of the jury still being out.

F. VIEWEG-GUTBERLET: We have had the same experience showing orientation dependence as Bernie Morris, and this is based on over 100 measurements. We got the same curves as shown this morning by Morris. We feel there is a dependence on orientation.

M. POPONIAK: In the last paper today [P-8], I will present some data showing the influence of probe loading on the orientation or I should say the orientation effect due the probe loading. We do see a difference and it is a function of probe loading. The lighter the loading the more sensitive it is to the orientation effect.

F. VIEWEG-GUTBERLET: Does that mean that with constant probe loading you will get another effect of impressions depending on the crystal orientation, i.e., if you set your probe loading with respect to crystal orientation, you should not get a difference for (111) or (100) material.

M. POPONIAK: What I am saying is that due to the atomic structure between (111) and (100) and their mechanical properties, there is a critical level of stress from which we get excessive fracturing, and that seems to be the problem.

K. BENSON: Steve Fonash this morning gave some numbers, about a factor of 10 I think for *p*-type (100) versus (111) and I would like to hear from anybody here that has made a calibration curve, does this number of a factor of 10 seem realistic?

S. FONASH: I forgot to mention [T-1] the fact that the zero bias resistance also in the contacts will depend on stress and I have a reference in my paper on that: Kramer and van Reuyven did some experimental work on this and showed that the zero bias resistance of the contacts does depend on stress also. I think this is rather well known but that is one particular reference. There is another paper in which I made some comments on this which appeared in Journal of Applied Physics in January of 1974. This effect also depends on crystallographic orientation so you have an interplay of those two effects both of which depend on crystallographic orientation. So regarding the factor of 10 which was brought up first there is this interplay of two effects which may change the factor of 10. Secondly, it is based on data that were determined at lower stress levels and I do not think the silicon is behaving elastically underneath these contacts and so I question the use of that data. I am just trying to show the existence of an effect which I think we better take a look at it.

H. MURRMANN: We will present [P-5] in the afternoon experimental data showing a difference between 100 and 111 material. We tried to split the data into mechanical phenomena including the contact radius and other physical phenomena. I would like to reintroduce a ρ dependent correction factor that Bob Mazur dropped some hours ago, [I-3] because I feel there is real physical reason for it.

R. MAZUR: I would like to make a comment here, Dr. Murrmann. I mentioned this to Bernie Morris at the coffee break. I regret mentioning the $K(\rho)$ factor in the way I did because it was misleading. We did not really drop the physical model involved in that $K(\rho)$ function. I was referring to the fact that we had worked out a way to avoid using cumbersome mathematics in making the corrections that get involved in having to plot an extra function: $K(\rho)$. You can treat it through the calibration data but the physical situation is still the same and I would agree with you on that.

J. KORVEMAKER: I would like to know if any of you have any results on other materials than silicon which has been discussed all morning.

R. MAZUR: There is data of course in the literature. I began making measurements on germanium. There is also data in the literature on germanium from T. L. Chu. Not in the scientific literature, but in Solid State Technology; that is a testimonial to the lack of clout of spreading resistance measurements several years ago. Ting Chu was unable to get it accepted by the prestigious journals, but it is good data and it is available in Solid State Technology of several years ago. We at Westinghouse,years ago,did make spreading resistance measurements on silicon carbide. There is a real question about spreading resistance measurements on gallium arsenide. There are ways to do it; whether it is easy or not may depend on a lot of things that would involve more discussion. That is about the size of what I know about it.

K. BENSON: There is also Witt and Gatos' paper looking at inhomogeneities in indium antimonide crystals. I believe spreading resistance was quite easy to use because this material was low resistivity.

B. MORRIS: I would say that probably in general as the band gap gets larger the measurement is going to become more difficult as in the case of gallium arsenide where you have a problem with four point probe measurements. From what I can see there should not be an appreciable problem on materials whose band gaps are similar to silicon or perhaps a little greater. If you can make four point probe measurements you should be able to make spreading resistance measurements.

P. LANGER: I would like to find out what the panel thinks is the lower limit in terms of the thickness to probe radius ratio to which one can extend the correction factor calculations on opposite conductivity type structures.

B. MORRIS: As I mentioned [T-5] we use a minimum value of 0.1 for t/a. This is somewhat arbitrary. I would not say that this minimum value of t/a is all that good. I do not know of any really good independent methods of experimentally verifying it. These methods would be the only ones I would believe. I would not tend to believe any calculations that close to the junction. Unfortunately the differential sheet resistance measurement has a lot of problems that close to the junction. I would be very interested in finding another method which would work in this region. The ion microprobe of course will go right through the junction but then you have first of all the chemical analysis technique and, instead of the net carrier concentration, you would have to subtract, say, the boron from the phosphorus profile and those readings as absolute numbers are not terribly good with the values that you usually get near a p/n junction for most microprobe analysis.

R. MAZUR: Paul should clarify whether he is asking the question of how close you can come to a junction with a good corrected value or whether he is asking the question of how thin a layer you can get a good corrected value on? That is: measurement on a beveled surface, or on top of a thin surface. They are not the same question and it sounds to me that he asked one question and Bernie answered another. On the subject of this layer measurement, Gil Gruber's paper which comes up tomorrow, I believe, will carry good evidence of quite reasonable results on certain sub-fractional micron layers in the range of 3,000 angstroms.

N. GOLDSMITH: I would like to add a comment to that. In my paper [A-7] on the last day of the session I will show an experimental model which you can use to test correction factors very close to an insulating boundary.

E. GARDNER: I heard the Schumann and Gardner paper mentioned quite often this morning so I think I should stand up at least and say hello. When Paul and I wrote the paper about 8 years ago we recognized a number of limitations in the spreading resistance technique and we tried to identify a number of them in our paper. I think many people today are recognizing those same limitations and going beyond our work and that was originally part of the intention of the work, to interest people in developing correction factors for the spreading resistance operation. It seems to me there are still a number of problems that have not really been identified and one is that we, in our analysis, did a finite layer type of structure in which we assumed a finite number of layers whether it was 2 or 40 and if we had been smarter we thought that there should be some way you could do this, not on finite, but on a continuous basis. That is problem #1. The second problem is one that people have alluded to and that is that you do not have a single contact but you have many contacts and how do you develop correction factors for many contacts? The third problem which is related to this, is, how can one explain the spatial resolution that you get whenever you assume that you have a 5 micron contact but you really show curves in which your resolution is 500 angstroms, or as some I saw this past week in which they were getting 50 angstroms resolution. So those are some of the problems I think that still remain with spreading resistance.

B. MORRIS: I have an answer to the last comment on how you can get the resolution that we do get. This is, I believe, due to the fact that instead of having one big flat contact for which one could very nicely calculate a correction factor from theory, we have a large number of small contacts, each of whose diameter is perhaps 1/10 micron, as opposed to 4 or 5 microns for the "flat" radius. Since the theory predicts a depth resolution of the order of magnitude of your radius, this allows us to get this very fine resolution in depth, while the effective radius of four microns is still the value that you get from the calibration as defined by values you measure for ρ and R. Thus, on one hand the micro-contacts add together so you can make real measurements, and on the other hand, you are also fortunate in that, for fine resolution, you may take an average value of the depth, a weighted average is more likely, and while this cannot be calculated it lets us make some very fine resolution measurements. I would say that from measurements with the Mazur probe using 45 gram loading that the physical penetration of the damage is approximately 1/10 of a micron. I cannot measure any better than that and perhaps this is an absolute limit as to how fine you can make the measurement.

J. ASSOUR: I have seen this morning several spreading resistance profiles through thin epitaxial layers and nobody said how these were produced in terms of surface polishing or lapping. I was wondering since we are worrying about correction factors and accuracy, how reproducible are the results in terms of surface finishing?

W. SCHROEN: You will hear data this afternoon [P-6] on this very question of how to prepare the sample surface and the probe tip, how reproducible the data are, and what we need to do to get those very shallow bevels.

P. SEVERIN: May I comment on this question invoking the micro-contacts, which I talked about in the Silicon Device Processing Symposium[1] in 1970. With our steel probe the micro-contact contribution, $\rho/4na$ (where n is the number of contacts which act in parallel to each other) acts in series with the term $\rho/4A$, where A is the total contact diameter. The micro-contacts represent about 5 times as large a resistance in the series combination as the large overall spreading resistance contact. In this case the resolving power of say 0.1 micron is easily explainable. That we have indeed these micro-contacts and that this has nothing to do with contact resistance in the common physical sense is explained by the fact that we find proportionality to ρ over 4 orders of magnitude which is a very unrealistic assumption for a contact resistance. Furthermore, micro-contacts are an extremely interesting subject because there the mechanics and physics enter. Although the term micro-cracking has been used today several times, direct evidence has been given in Russian literature[2, 3, 4] that silicon behaves plastically at room temperature in a very shallow top layer. The thickness of this top layer increases with the applied load. Indirect evidence has been given earlier in various experiments of a different nature,[5, 6, 7, 8]. I think that it is a pity that there are no people in this audience who have more experience on micromechanical properties. On a submicron scale you cannot just talk about the elastic

constant or hardness of silicon.
Ed. Note: In review of his comments, P. Severin supplied the following references.
1. Silicon Device Processing, NBS Spec. Pub. 337 (1970) 224.
2. V.P.Alekhin, O.V. Gusev, et al.-Sov. Phys. Dokl. 14, 894 (1970).
3. V.P. Alekhin, O.V. Gusov, et al. -Sov. Phys. Dokl. 14, 917 (1970).
4. V.J. Nitenko, M.M. Myshlyaev and V.G. Eremenko- Sov. Phys. Sol. St. 9, 2047 (1968).
5. G.R. Booker and R. Stickler-Phil. Mag. 8, 859 (1963).
6. T.R. Wilshaw- J.Phys. D. 4, 1567 (1971).
7. M. Renninger- J. Appl. Cryst. 5, 163 (1972).
8. W. Ridner and J. Braun- J. Appl. Phys. 34, 1958 (1963).

R. MAZUR: I would like to answer - this is also to that last question. We cannot leave it said that way. I mean that I cannot just sit here and leave it in the record that Mazur did not say anything. Regarding the third part of Ed Gardner's comment I need to point out, of course, to be consistent, that the very high spatial resolution can be explained in many cases again because of the work function potential barrier which has a very, very shallow penetration. It is restricted to the immediate surface material. The second part of the question is that using what I call a conditioned probe, which you will remember I defined as one which although made up of multi-contacts, will act as a single contact if you get the little contacts close enough together and distribute them properly. I would refer anybody to a paper by Greenwood (Brit. J. A. P., 1966) which lays this out in great detail. I have pointed out in the past to many people that I think that when the questions come up about spreading resistance resolution, people are often talking about spreading resistance measurements with what I consider unconditioned contacts. If you damage the probes, you will go on and get profiles and you will make measurements and you can even write papers but I do not know that it is going to get anyone anywhere. So you have to be careful about whether the original work and data that went into it was valid or not.

J. KORVEMAKER: I would like to ask Dr. Severin a question. In regard to the plastic behavior, is it similar to the behavior of glasses?

P. SEVERIN: We are talking about monocrystalline structures which are something quite different from a glassy structure. I have given the reference of about 2 years ago about this microplasticity at room temperature of silicon.

D. WILLIAMS: The question that keeps bothering me is that we have talked about accuracy say, comparing spreading resistance to capacitance voltage, but I think in the latest report as published by NBS[1] they also say they have difficulty getting correlation between resistivities that are very close together and spreading resistance. If this is true, since you have calibrated on a set of samples, what are you correcting when you get your profile. Granted a profile may look very consistent but how valid is the calibration back to resistivity?
[1]Ed. Note: W. M. Bullis, Methods of Measurement for Semiconductor Materials, Process Control, and Devices, Quarterly Report; April to June 1973; NBS Technical Note 806 (November 1973), pp. 9, 10.

R. MAZUR: This is a point that should be kept in mind; i.e. that fussing with 2 or 3 or even 5% on the thickness corrections and the other corrections may be senseless if the basic calibration data limits you to ±10 or 15% accuracy. So you have to be practical. It is quite possible still, even at this late date, to get hung up on the micromechanics of that contact and fail to keep your eye on the main thing which is control of silicon processing, if it has to be 100% empirical then that is the way it is going to have to be.

2. PRACTICE

N. GOLDSMITH: Jim White, I noticed in your program you require the orerator to input the thickness. Don't you derive any thickness measurements from the spreading resistance data itself?

J. WHITE: Well, we use the test set for two functions; when making surface measurements, of course, we cannot derive any thickness measurements. For depth dependent measurements we could determine the thickness from the spreading resistance data but we do not use that as an input because we could not correct our first values, we would have to store all the values and correct them later.

N. GOLDSMITH: That was my point.

. VOLTMER: I wondered how you automatically align the probes at the bevel edge?

. WHITE: We have an interference contrast microscope that is mounted a known fixed lateral distance from the wafer stage. We align the bevel edge with the microscope cross air and we move laterally by the known distance to position the probes.

. ASSOUR: I do not know if you said it or if I missed it. How do you measure the depth gain in the case of the groove? By staining technique?

. WHITE: We measure the total width of the groove and from the width of the groove and nowing the diameter of the grooving mandrel you can calculate the total depth and then rom each lateral distance you move you can calculate an incremental depth.

. ASSOUR: I take it that the depth measured by the grooving method was proven by other echniques?

. WHITE: Yes.

. KORVEMAKER: I noticed in all the talk about spreading resistance that you never said nything about the quality of the silicon slice. In our company we have been looking at lices, how much of the slice is really good and how much of the slice is not good. Does his have any effect on the spreading resistance measurements?

. VOLTMER: What do you mean by good?

. KORVEMAKER: We have been doing x-ray analysis of the slice to get an overall view of hat part the slice would be suitable to get good devices from, and there is a fair amount hich is not suitable because there are impurities or strains or stresses. How do these ffect spreading resistance measurements? I think I have also seen this reported in the icroelectronics and Reliability magazine that is from the United Kingdom. There is, I ould say, atleast 30 to 40% of a wafer as such is not useable.

. POPONIAK: I would like to comment. I think in one of the references by D. Gupta of ylvania, he showed that higher dislocation areas of a slice gave him different spreading esistance values if that is what you mean. Well, he has shown it. Jimmy Hu and I have ooked at a microscopic type effect. We looked at copper precipitates using the close pace probing and an infrared microscope so we were able to directly correlate spreading esistance data as affected by a copper precipitate near the silicon surface and that was ublished 2 years ago (*Phys. Stat. Sol.* 18, K5, 1973), so there is a sensitivity to this ype of a defect.

. LANGER: I would like to ask some of the people who discussed other types of equipment nd modifications of the Mazur equipment what they have experienced in terms of precision or two types of specimens. Let's say 1 Ω·cm *n*-type and 1 Ω·cm *p*-type specimens that are niform throughout. Let's go around the table for those people who have automatic probing quipment and consider precision on a long term basis, say several months.

. MURRMANN: As I pointed out, we have done these measurements on our calibration locks for (111) and (100) material. For (111) material we approximately get a reproducbility of ±13%. For the (100) surface the reproducibility of the measurements was rearkably better, approximately 1/2 of this. The reason for that we really do not know. t looks like the (111) surface is more sensitive either to surface contamination or condensation of humidity. In addition, there is some indication that the (111) samples are ore sensitive to the degree of misalignment between the exact (111) orientation and the easured surface plane.

. VOLTMER: Most of our calibration deals with the entire block which is 22 samples and we o not very often compare an individual sample on that block. But from those times we have one so, I feel that our reproducibility on a given sample is something like ±5% over a ong term. That is over a period of weeks. This must be qualified, however, since it pplies to calibration samples which are chosen to be as free as possible from microsegreation.

J. WHITE: We took an ion implanted slice which we had found to be rather uniform by making repetitive probes across the diameter and got a short term reproducibility, say a one day reproducibility, of maybe 10 different measurements, 5 mils apart, of ±1.3%. A long term reproducibility would be around 5%.

P. SEVERIN: We use *N*-type (111) silicon substrate slices for calibration, and since I never have come across a substrate slice which has a resistivity uniformity better than 1 or 2 percent and since you cannot probe the same spot twice I think the reproducibility should be determined as follows. When you measure a track and the next day make a track at 25 μm distance parallel to it, which is the most similar situation you can arrive at, then you find the measured profiles are different by 1 or 2%. The main criterion however, by which I think we should compare performances and quote precision is how much "grass" is to be seen on a smooth spreading resistance curve. In our case this spurious signal amounts to about 1%.

M. POPONIAK: All I have to say is that I agree with Severin. We have done some implanted structures also and by independent measurements across the silicon wafer, say with resistor type structures there were claims of 1% reproducibility or grading across the wafers and what I saw with the probe is less than 2%. It becomes very hard to interpret data less than 2% so I am saying we are nearly at the limit either because of electronics or mechanical stability of the probing system.

J. KORVEMAKER: I noticed that most of the panel speakers are of rather large multinational companies and I wonder if they have any intercompany relations as far as how accurately they can measure, or at different plants how accurately they compare, or is there just one location where all these measurements are done.

F. VOLTMER: Within our plant we have two different probes in different buildings and we are able to get within 10% reliability on those two probes measuring the same samples when they are calibrated by the same procedure. So between two completely different kinds of probes we can get within 10% on a given sample.

J. WHITE: At Western Electric - Allentown we have essentially two measurement systems also, because there is a Mazur set in Bell Laboratories in the same building with us. I do not have a number to compare the two probes but we use the same calibration samples. We are in good agreement that way.

F. MAYER: The question was raised about intercompany comparison. We ran a pilot round robin in Subcommittee 6 of ASTM. We prepared some 50 μm thick epitaxial specimens, and exchanged samples with 5 laboratories. Our first comparison indicated 6.7% difference between the 5 labs which is not bad at all. We tracked across the surface on 2 and 3 decade paper and found less than 10% variation in uniformity across the sample. Each lab used its own method of calibration and surface preparation.

P. PINCHON: I would like to stress one point about the measurement of a thin low resistivity layer deposited on high resistivity material, because in that case the correction factor acts in such a manner that you measure something controlled by sheet resistance. By experiment it is nearly always the case that the spread in measurement is very much lower in the case of low on high resistivity as compared with bulk material or high over low resistivity material. So for the case of calibration, the reported stability of the probe on ion implantation is something optimistic in my point of view.

R. ANAND: My question is concerned with the conditioning of the probes. Bob Mazur pointed out that's one of the most important tricks of the trade, and I was wondering if people who are using other than Mazur type probes, how do they condition their probes and make them stable.

P. SEVERIN: We use steel probes and they are taken from a four-point probe, in general a used one. In order to get a fine microcontact pattern the probe should be broken. Why are the microcontacts there? They are there because there appears to be in steel little, harder particles, therefore called asperities, which upon contact of a flat bottom surface of such a needle with the flat surface of a silicon slice, act as protrusions. Under a scanning electron microscope we found these protrusions to be very small, at most several

enths of a micron. But they are absolutely much harder than the steel and therefore the steel acts as a softer matrix in which these asperities can move more or less elastically. So the system is that you break the steel probe, and in some way that metallurgusts can explain you expose a number of these asperities. Thereafter like a pencil you sharpen it on a sharpening instrument so that the bottom remains untouched. You stop sharpening when the bottom has almost the size which you think will be the final size and then you start using it. At first the steel is too heavily loaded, and is plastically deformed until the contact has expanded and become so wide that it is not anymore plastically deformed. Then it remains just the same for say 10,000 or 20,000 measurements. Upon contact to the silicon these asperities make very small, something like 0.1 or 0.05 micron, impressions which remain constant over the lifetime of the probe. When you use lapped silicon then you find that a rearrangement of the asperity patterns takes place, but the microcontribution determined by (na) remains the same.

. WHITE: We use tungsten-carbide probes and I have found that I am able to use a new probe with no conditioning and get very reproducible results.

. SEVERIN: What is the depth of the damage and do you think the damage does really mean something to the result of the measurement? Tungsten carbide is harder than silicon and the probe I am advocating is softer than silicon with only small protrusions which are harder than silicon. In this way less damage is generated.

. WHITE: I really do not have a number for the depth but when we compare our profiles with profiles done on a Mazur set, they are similar. One thing you have to realize about our system is that we do lower the probes on the surface unloaded. We load them only after they come to rest on the surface so we probably get quite a bit less damage than a probe that would come down on the surface completely loaded.

. LANGER: Let me clarify that. I did work for Western Electric and helped in developing their automatic spreading resistance probe. It is possible with that particular probing arrangement to make indentations or to lower the probes to the surface and raise them under 00 grams apparent load such as to leave no visible marks. By no visible marks:you certainly cannot see them under interference contrast,and even with oblique microscope lighting you cannot find any tracks on the surface,so that this probing arrangement may yield a completely different situation than lowering the probes under full load as is done with the Mazur probe.

. SEVERIN: In order to increase the measurement cycle one could be tempted to increase the landing velocity of the probe. It can be regulated from very small velocities up to about mm/sec with the air escape valve. We have found that above 1 mm/sec the probe shows rebounding on a milisecond scale, actually losing contact and subsequently generating elastic vibrations. It is an interesting observation that the correct spreading resistance value has been reached at the first impact. We have found that a landing velocity of 1 mm/sec, where no rebounds occur, and a measurement cycle of 5 measurements/min. produce most reliable results.

. ROBINSON: I address my question to Mike Poponiak. I noticed you showed a plot of concentration versus depth for the different probe pressures and there was difference in the concentration peaks. Is that attributed to the difference in the probe pressures or is it attributed to something else?

. POPONIAK: Well there were two profiles I showed [P-8] and I think you are talking about the high concentration regions, right? On 40 gram versus 10 gram. What I am saying why there is an apparent difference is due to the inadequacy of the correction factor. They should both be the same C_0. I am saying a 10 gram loading gives us a more accurate representation of the C_0 than a 40 gram loading.

. ROBINSON: Is it determined by the monitor wafers that you use in your subcollector, or in your diffusion? When you say that that is a more accurate representation of the C_0, is that C_0 the determined C_0 that is seen on another monitor wafer and not by spreading resistance?

. POPONIAK: We have done independent correlation with neutron activation or differential sheet conductance measurements. Independent techniques verify that the lower loading works

better with our multilayer correction scheme. Excessive probe penetration at 40 gram loading causes the inaccuracy.

C. GERMANO: I was wondering if any of the participants have noticed the effects of taking small delta X increments where the damage left by the probe marks overlaps the previous steps.

M. POPONIAK: This morning somebody showed data indicating repetitive measurements at the same point and the spreading resistance increased dramatically. Well, in our close space probing where we have done beveling on the probes we are able to achieve a lateral movement of 2 1/2 microns without overlapping. Now a way to test this is to start with something large: 10 micron steps across the surface, reduce it to 5 microns, reduce it to 2 1/2, reduce it to 1. When you see an apparent shift to higher spreading resistance you know you cannot go below that last delta X movement. Someone else said they had a 1/2 mil resolution delta X. I am saying we can go 2 1/2 microns by preparing the probe points properly, without overlapping.

P. SEVERIN: May I ask a question to Mr. Poponiak. One of the key questions that has come here today is the potential distribution around the probe. For then we know whether there is a contact resistance, either a physical contact resistance because of a barrier or a contact resistance because of microcontact. You mentioned 15 microns as the distance between the probes. Could you bring them still closer and then just find out what the key problem is?

M. POPONIAK: It is very difficult, but so far we see no influence.

F. MAYER: In answer to your question we did check on the overlap question, if you have probes that step on each other so to speak. With 2 1/2 micron steps, you see something like a 10% increase in resistivity, with 5 micron steps it is hard to say whether there is an effect: it is no more than 2 or 3%. With 10 micron steps you do not see any effect at all.

I am a little confused about your data, Fred Voltmer, on the interpretation of the contact resistance that you showed. I think you showed a considerably increasing contact resistance after you dipped in HF and as a function of boiling in water. Now on the next slide you showed an oxide growth of up to 700 angstrom. Are you implying that in an hour's boiling you grow 700 angstrom of oxide? Most people consider the maximum oxide growth in boiling water to be about 30 or 40 angstroms. What is your interpretation of that value?

F. VOLTMER: What we did was to take a slice and dipped it in HF to ensure that there was no oxide and when we did that we got a very high spreading resistance. We subsequently grew an oxide in boiling water and measured the oxide thickness and the spreading resistance and what we saw is a dramatic decrease in spreading resistance as the oxide thickness grew to about 100 angstroms. It remained relatively constant then until we grew about 700 angstroms of oxide at which point the spreading resistance got quite large indicating that we were not penetrating the oxide. We grew the oxide for the thin layers of oxide we use boiling water, for the thicker layers they were grown in a furnace tube.

F. VIEWEG-GUTBERLET: I think, Fred, I can now answer for this effect of dipping in HF. We have the same experience measuring p-type polished wafers by four point probe and if you dip the wafer into HF the resistivity increases by about a factor of 10 or more, and if you store the wafer in a temperature of approximately 150° C or you boil the wafer in water, or whatever you do, this increase of resistivity goes down by a time constant of approximately 40 minutes. You can do the same by lapping the wafer and if you lap the wafer partly and you position your probe in the lapped area you can see the decrease of resistivity readings versus time. Our explanation for that is: you have a fluoric layer on the surface, which is strongly n-type, so you bind a part of the holes to that electron layer on the surface, i.e. the negative active layer on the surface. This is related to fluoric ions on the surface.

P. LANGER: Since we have gotten into the area of surface preparation I will just throw in a few remarks and possibly Stan Shwartzman from RCA might want to comment on these. He has the one technique that does not use a aqueous solution in his beveled sample preparation.

What we have found when we went to a lighter loading probes was that you could affect changes anywhere from 100 to 400% in the measured resistance on half ohm cm n-type by heating for about 5 minutes at 180 - 190° C and then cooling the sample back down. These changes have been stable right now up to 3 weeks. We have also found the same effect on Bob Mazur's QTA, we were able to decrease the measured resistance by a factor of 2 by using the same thermal cycle.

S. SHWARTZMANN: All of our samples including Bob Mazur's QTA remain stable after they are swabbed with methylene chloride solution with our probes loaded to 45 grams. When specimens are prepared in the presence of water the same degree of stability can be obtained by baking them at 150° C.

P. LANGER: What I was saying was that since you are the only one that does not get tied up with water during sample preparation you may not see this effect at all. I just wondered if anybody else had seen this type of effect.

J. EHRSTEIN: I have just finished over the last month, following some very helpful suggestions from Fred Mayer, measurements using a modified surface preparation procedure. I hope to have something to say on it tomorrow in the fashion of a late newspaper. I think, in terms of improvement, we have answered at least 3 problems which turned out to be related to surface preparation for the upper ranges of p-type material. I thought they were separate problems, but they all seem to fall into consistent interpretation now, just because of a modified treatment, namely, the bake out procedure; 150° C for 15 minutes or more following an aqueous chem-mechanical polish. Probably this time-temperature cycle could be made hotter and shorter, but we have not tried it. Let me wait until tomorrow to discuss it further.

E. ASSOUR: Since our experience has been concentrated on deep diffusions for power devices, we are not really relating to the thin layers most of you have been talking here. We did look at polishing techniques versus lapping techniques. The lapping technique is what we use constantly, but in terms of the polishing techniques that we tried on the same calibration samples, and that means syton finish, or chemical polish, or other polishing technique, I must say that in these cases although we would reduce the noise level of our spreading resistance readings we have not been able to reproduce our calibration curve in terms of time stability; I mean that we can polish by syton or chemically, measure, and repeat the measurement two or three hours later and get different points due to drifting. In other words, the ambients, dirt in the room, or humidity, or what have you, seem to influence greatly the polished surface. Of course, since we have gone to the lap surfaces for the deep diffusion structures that we are interested in, we really do not see these effects.

E. WILLIAMS: The TI paper that you had on the calibration and performance of the spreading resistance probe, was that (111) material, syton polished?

E. VOLTMER: Yes, it was, it was all (111), but Lustrox polished.

E. WILLIAMS: In our case I used a least square linear regression. The numbers for the slope for both n and p-types are almost the same. I compared the residual sum of squares from the actual data to the fitted line and asked myself whether the slope was unity. With 95% confidence, both slopes included unity. Therefore as far as I can tell from the data the slopes cannot be said to be different from unity. Do you use a slope of unity in your work or do you use the exact value of slope as calculated from your least square regression of the calibration data? I find it interesting that my calculated slope for n-type is slightly larger than unity and for p-type it is slightly less than unity. This of course could have implications for the simple linear model of the spreading resistance measurement.

E. VOLTMER: We use the actual values for slope and intercept from the least squares fit to our calibration data for that particular week. For n-type, it is typically 1.03 and for p-type it is 0.97. As I showed in my paper the long term distribution of the calculated values for these slopes maintain values slightly higher than unity for n-type and lower than unity for p-type. These values are obtained from a linear least squares fit of the data in log-log coordinates, but of course a slope different from unity in these coordinates implies a non-linear relation between spreading resistance and resistivity in the model used.

D. WILLIAMS: Can you then determine resistivity values to better than 10%?

F. VOLTMER: Yes, I have the actual data for any given point in my calibration and the distance between that point and the spreading resistance value of the actual specimen of interest allows me to determine its resistivity to better than 10%.

3. APPLICATIONS SECTION

P. LANGER: Fred Voltmer, you mentioned that you have multiple peaks related in some way to th the sum and difference of the rotation rates. Could you clarify that?

F. VOLTMER: Yes. For the multiple peaks, if you calculate the distance traveled for the various rotation rates, for example, just the crystal spin or just the crucible spin or the sum of crucible spin and the crystal spin, you will get peaks where the periodicity of the fluctuation corresponds to the growth for that time. So that it is not always so simple that there is just one well defined frequency for the microsegregation, but sometimes there are multiple frequencies, and they all can be related to mechanical conditions during the growth of the crystal. It is not always just a single frequency variation.

F. VIEWEG-GUTBERLET: Did you find for the distance between the peaks related to the rotational striations that the equation d = F/W is satisfied where F is the relative pulling rate and W is the rotation rate?

F. VOLTMER: Yes, in fact that was the point. The peaks in the resistivity translate to a spacial frequency in the transform and that spacial frequency, i.e. the dominant frequency is exactly that derived from the pull rate and the rotation frequency.

K. BENSON: Fred, have you been able to correlate the magnitude of the microinhomogeneity in the radial direction versus the magnitude of microinhomogeneity in the longitudinal direction.

F. VOLTMER: Well, they should certainly correlate. We have not quantified it but the same variations occur in both directions.

K. BENSON: Have you been able to correlate the magnitude of one versus the other?

F. VOLTMER: We have not yet done that. We will report on it when it is done.

B. MORRIS: If I am properly interpreting one of the last profiles shown by Dr. Assour, more gold was accumulating in the region of a p^+ diffusion than that of an n^+, is that correct?

J. ASSOUR: No, more gold accumulates in the n region than the p^+. The fact that the p^+ junction seems to have been raised in resistivity is the fact that you have more gold that accumulated right at the junction and in the n region.

F. VIEWEG-GUTBERLET: The explanation you derived from your results in oxygen distribution may lead to the conclusion that oxygen is distributed nonuniformly into the crystal. But I do disagree from our experiments and there may be an explanation that your experiments were done with p-type material. That means that acceptors are distributed in the silicon crystal nonuniformly in the form of striations. If you raise the level of oxygen related donors by the heat treatment at 450° C, you will get compensation at some points and you will increase the compensation rate so the residual resistivity will go up. But this is not due to nonuniform oxygen distribution. It is more due to the nonuniform distribution of acceptors that came out from our experiments when we tried to find out oxygen striations on p-type material but this explanation gave a good agreement of the other measurements on n-type material.

J. ASSOUR: According to your point of view I fail to explain the fact that infrared measurements on wafers before heat treatment do show different oxygen concentrations across the wafer.

F. VIEWEG-GUTBERLET: This may be due to swirls because in crucible pulled material the swirl complexes and distributed very nonuniformly.

K. BENSON: I did have one comment I would like to make to F. Vieweg-Gutberlet. You may have only looked at one oxygen concentration. The problem with all techniques is dependence on the concentration of oxygen in the crystal. If you look at an oxygen concentration of 10^{15} and then at one of 10^{17} you may see completely different reactions. So whether you have seen inhomogeneity or not, I think, depends on what the original oxygen concentration was in the crystal.

F. MAYER: I would suggest that Ken's explanation may be close to the truth. I think the question of time which it takes to develop oxygen donors during the heat treatment comes into it. It takes a long time at 450° C to develop donor dependent resistivity changes associated with striations. I suggest you might try to determine this experimentally.

B. SCACE: The papers were very interesting, both Fritz's paper and the paper that was just given, and we can get into an argument that would last for a week about what is going on inside the silicon but the point is that we have an extremely powerful tool here now for exploring just this kind of thing so let us not get off onto what is happening in the silicon. Let us look at what is happening with the measurement.

R. PRUSSIN: We have been referring to the spreading resistance probe tests as being nondestructive. However, there is no question in the earlier discussion that part of an effective probe measurement is that it leaves a footprint, an area full of little cracks, which act as very nice nucleation sites for dislocation generation if there is any kind of thermal stress. I know that we have tried to remove generation of slip dislocations by the means by which we prepared our wafers. We make sure that we have developed polishing techniques that leave no mechanical damage and so forth and I know that a great many of the studies that have been made in the past have shown a very direct correlation between the presence of mechanical damage and slip associated with thermal shock. I am just wondering has anyone looked into the spread of, or the generation of dislocations or slip from some of these "nondestructive" spreading resistance probe measurements that we have made.

H. MURRMANN: We have not done it until now but we just started experiments and I personally am not afraid of getting dangerous slip damage from that probe tip damaged region especially for (100) material.

F. VIEWEG-GUTBERLET: In answer to the last question, you can see from the slides I showed [A-2] we found spreading resistance traces after heat treatment, and again in the wafer when we etched the wafer after repolishing them. So we have deep damage from the spreading resistance probes and heat treatment at 1100° C.

H. MURRMANN: That is a question of the heat treatment you apply to the wafers, and what you consider to be dangerous damage.

F. VIEWEG-GUTBERLET: May I ask a question of Dr. Murrmann? How does the accuracy of your epi thickness measurement depend on the dopant distribution in your epi layer? Is it true that the assumption is made that the epi layer is uniform in resistivity?

H. MURRMANN: You are right, the method that we have proposed has to be calibrated for *each specific* epitaxial process that you apply. For instance, you would get slight differences between silicon tetrochloride epi and silane epi. In addition, the buried layer diffusion process has some influence on this. But whenever you take a certain buried layer and epitaxial process you can well determine the *effective* epi layer thickness by this method. We have checked it in addition by comparison with breakdown voltage measurements and these values agreed very well too.

H. GOLDSMITH: The only region we have checked for thickness correlation between IR and spreading resistance was a series of samples at around 100 micron epi thickness and here we found that the error was really in point count: you have to choose where you place the interface. For the samples I looked at we agreed to ±1 point count. For the step size and angle we used this was ±1 micron out of 100. The accuracy is also limited by knowing where

you start from which adds to the error of where you place the interface. Our interface position is selected by our computer program which calculates the substrate resistivity and then looks for the point where the substrate resistivity breaks and assigns that as the thickness.

F. MAYER: I would like to add here that the subcommittee 6 of F-1 has just undertaken the evaluation of this method as a standard method and I think Fred Voltmer has volunteered to draft it. Do you want to comment on this, Fred?

F. VOLTMER: Yes, I think that the thickness depends very much on the angle which you are probing and the precision or the range of thicknesses you are looking at. For example, for very shallow angles or very thin epitaxial layers the critical factors are quite often the alignment of the probe and the precision with which you can form a bevel. We feel at TI at least that when we are careful and when we are talking about lapping on 17 minute blocks we can determine the thickness of an epitaxial layer, and that is a defined thickness, let me point out, to about 400 angstroms. We define the thickness as the intercept of the slope in the change in epitaxial resistivity with the extension of the substrate. When one has p/n junctions it becomes quite a bit more difficult because there is quite often a depletion region which makes it difficult to define exactly the point where the junction occurs. For thicker epitaxial layers, it is a matter of how many steps you want to take and how shallow a bevel you want to use for probing. In other words, if you have a thick epitaxial layer and are willing to probe almost forever you can get these same kind of precisions. If you take larger steps the step size becomes a limitation on the precision.

G. GRUBER: Fred and I had a bit of discussion about this same thing at the committee meeting. As he says the thickness measurement is dependent certainly on the ability to measure the ang and also on the ability to determine the position of a p/n junction or what you would call the interface between an n and n^+ region. In most cases, I would say in the majority of cases, the picking of the p/n junction is a matter of extrapolating the two sides of the junction to the point of maximum inflection on the curve and calling this point the p/n junction. If there is a broad high resistance region where the spreading resistance is off scale then you do have a problem in choosing the junction. This however, is not the normal case. For determining the thickness of a layer, such as an n/n^+ or p/p^+, most people do exactly as Fred has said and pick the point where you get maximum inflection in the transitio region from n to n^+. In the normal situation we find that you can determine this thickness to within several percent, or better.

W. SCHROEN: I would like to make a comment on epitaxial layer thickness and concentration. We have seen data this morning which showed that there can be a distinct out diffusion from the substrate at the interface of the substrate and the epi layer. The same sort of out diffusion or autodoping can happen at the interface of the epi layer and the buried layer. From a modeling standpoint this effect has been well explained by researchers at Fairchild such as Grove and Deal and others. Now the question is how do we distinguish between this experimental fact and the multilayer analysis which can pretend such an effect as we have seen yesterday. The answer is that when there is a real out diffusion the original spreading resistance data will show it. The original spreading resistance data can be corroborated by the results of the C-V technique and thus distinguish a true out diffusion effect from the artifact of the multilayer analysis.

S. PRUSSIN: The point was made that by using a very shallow bevels we can increase our precision in measuring shallow diffusions or thin epi layers. By doing that we raise another problem. That is the greater difficulty in determining where to start the probes because the bevel's junction with top surface then becomes less sharp. I think that the end of the layer is one of definition and is not really a problem, but I think there is a major problem with exactly getting your probes to start at the surface-bevel intercept. I was wondering whether there were some suggestions in terms of practical techniques which would enable the operator to start more precisely at this junction.

F. VOLTMER: I would like to address that point. We have established a technique whereby we grow a reactor deposited nitride on the surface of the slice as Walter Schroen pointed out in one of the earlier talks. That nitride is hardness-adjusted to equal that of silicon so that we can get a very distinct intercept between the lapped part and the nitride, so distinct that it is quite apparent in the microscope. The subsequent probing across that

nows then a very drastic change in the spreading resistance when you go off the nitride onto he silicon layer and that then allows you to identify very precisely the position of the eginning of the bevel. The problem is that if you are using, for example, the 17 minute ngle beveling block; a 5 micron error in the position of where you put the bevel will give ou a 500 angstroms error in depth and I feel that doing much better than that with the 5 icron probe point is quite difficult, but we use the nitride to define very precisely the osition at which the bevel occurs. This allows you to see if the bevel is straight, which an be another source of error.

. GRUBER: We have seen the same thing with an oxide layer on the surface. You can use the ame technique.

. SCHROEN: In answer to your question, I feel as Fred Voltmer stated, that the intercept f the bevel and the surface is no longer much of a problem. It is much more of a problem o determine where the junction is with the substrate or with the buried layer, since we may ave to deal with the effects of out diffusion or the artifacts of the multilayer analysis. owever, anyone skilled in the art can extrapolate where the intersection of the epitaxial ayer and the substrate is. This extrapolation is usually precise enough, even for very hin epi layers. I feel confident that we can determine the thickness of the epi layer at he interface with the substrate.

. PRUSSIN: One of the techniques that we have tried was to examine the bevel surface after e completed the spreading resistance analysis and tried to find out where the first foot- rint appeared using interference microscopy. Possibly in this way one can determine very ccurately the relationship of the first footprint with the theoretical bevel-surface inter- ept. What I want to know is whether techniques like this have been tried by anybody.

. GRUBER: I would like to make the comment that we have been talking about very shallow ow angles for measuring very thin layers. We have found in some of the work that we have one that you do not really have to go to as shallow an angle as you might expect to use for very thin layer. If you go to smaller increments, for example, across a less shallow evel, say 1 degree, many people worry about the overlap of the probe imprints and so forth. e have been able to determine experimentally that even down to a 1 micron step increment e have been able to repeat and reproduce the results without any problem due to overlap.

. MORRIS: As to that, I would like to ask what surface preparation technique you use.

. GRUBER: This is a Syton polished surface using a Plexiglas plate.

. MORRIS: I have never found that to be true. I wish it were.

. GRUBER: You have to be sure that when you calibrate, you use the same step increment uring the calibration as is used when running a specimen.

. MORRIS: I still find that with less than 2 1/2 micron steps we have a very large signal o noise degradation and the whole curve shifts. I have one other comment to make as to he surface definition. We do an anodic oxidation, growing about 400 or 500 angstroms which ives you a definite darkening of the surface. This involves no heat so you are not going o change any of the profiles.

. MAZUR: I have a comment on that, I have made this comment to a number of individuals nd perhaps should make it publicly to all, that the business of sample preparation and articularly beveling with small anges is in part a matter of skill. At lunch, I pointed ut the similarity to the situation involved if someone buys a transmission electron micro- cope and just goes in that afternoon and starts to prepare samples. There is a certain mount of skill involved in the preparation of samples! The other point to this is that asically what Gil Gruber has said has merits. What we are suggesting to you is that you onsider the possibility of actually being able to use one micron steps despite what Bernie orris said and thereby achieve greater precision in the measurement of thicknesses on such ayers. Along with that I will make a suggestion that I have made to a number of people hat I have talked to in the past and that is that the contacts we use are 5 - 6 microns iameter and as someone pointed out when you are taking one micron steps and you go back to ook at it afterwards you of course find it hard to see where that first one was because it

565-448 O - 75 - 19

is covered over by subsequent probe marks. I would like to suggest here that at the time you begin the run you set up to center the first contact on the bevel edge and initially set the probe to take a single measurement point. Then when it stops you shift the stage laterally by 5 - 10 microns and continue running. This causes a displacement of the rest of the points in the run from the first point and allows you to go back later with an interference microscope or a scanning electron microscope if you like and locate exactly where that first point was relative to the bevel edge. Perhaps parenthetically, I guess, the point would have to be made that the interference microscope is not going to do you much good beyond about a quarter micron as far as determining where you are in depth.

M. POPONIAK: Just a comment on this overlapping. We have done a considerable amount of study and it is a function of the actual resistivity. What I am saying is that there are ranges of resistivity that you can apparently overlap and that is predominantly the high concentration regions. As you go to lower concentration regions it is very sensitive to this and you cannot overlap.

G. GRUBER: What do you mean by "you cannot overlap"?

M. POPONIAK: You get an increase in apparent spreading resistance, an error due to the overlapping.

G. GRUBER: As I said, it is required that you calibrate using this same step increment as when running the specimen. If you do this you can eliminate any effect of overlap.

M. POPONIAK: All right, that is your comment, but that has to be proven because now you are trying to probe into a mechanical damage area, yet everybody is trying to get a good polish to start with.

G. GRUBER: All I know is that I can use a step increment that results in overlap of successive contacts and if I calibrate with that overlap I can get the same resistivity as for the case where I have used a larger, nonoverlapping step increment for both calibration and sampling.

D. DICKEY: I would like to comment on Goldsmith's paper. The errors that you found in your diffused layers no doubt result from the fact that you do not have uniform resistivity in those layers. The so called Dickey correction assumes that you have uniform resistivity throughout the layer. That assumption is certainly not valid for shallow diffusions. This points up the need for an improved correction scheme and that is the subject of my second comment. The problem of correcting spreading resistance measurements in a layer having depth dependent resistivity is something that needs working on. I indicated on my last slide yesterday that the imaginary superposition of a number of layers of uniform resistivity could be a useful approach. It occurred to be last night that that approach is really just the spreading resistance equivalent of the incremental sheet resistivity experiment that people have used for years with a four point probe. I suggest that you could derive corrected spreading resistance measurements from an incremental approach using the same mathematics that are used with incremental sheet resistivity. The calculations that would be required would be rather trivial and I think it is a very logical thing to try.

N. GOLDSMITH: I will comment on your first point. In the interest of time I did not choose to read our introduction which clearly said that your formula was derived from uniform samples and was hardly expected to provide adequate corrections for a diffused layer.

W. SCHROEN: Let me question you with regard to your suggestion of another approach to correction factors. I did not fully understand your suggestion of using a procedure with overlapping steps in order to get to an analogous situation of the four point probe. Would you please repeat your suggestion?

D. DICKEY: I am just suggesting that you should go through the mathematics of using the superposition principle and find out what the difference between successive spreading resistance measurement should be at slightly different depths. The difference in the measured resistance that you see at two microns down and at 2.1 microns down, for instance, should be characteristic of the resistivity in that (1/10) micron increment just as it is in an incremental sheet resistivity.

. MAYER: Perhaps I could throw another question at you as it seems like an opportune oment. Listening to what we had this morning there has been an excellent correlation etween patterns of resistivity established by other methods and by spreading resistance easurements, which says that the spreading resistance probe has arrived as a tool that is ccepted. Not only is it accepted, by and large the data seem to fit the models we have of roduction processes. Having gotten to this point I think it is pertinent to ask where we o from here. Obviously we are moving into an era where we can begin to standardize preading resistance probe measurements and I think that is underway now. My opinion is hat we have not got the speed yet or the facility to use it as an on-line production control nstrument or even as a routine instrument in a development laboratory situation. It would e interesting to hear what the panel and perhaps what Bob Mazur would have to say on this ubject.

. SCHROEN: Your comment is well taken with regard to the actual probes. In addition, I ould like to suggest that maybe the National Bureau of Standards should start to standardize he multilayer analysis. This standardization should consider what needs to be done analyt- cally, what are reasonable mathematical assumptions, what are reasonable calculation pro- edures, what are the best computer programs and so on to make sure that all users can uni- ormly use spreading resistance data.

. GRUBER: I think it is obvious from this last day and a half that additional work is ecessary in the area of layer corrections, i.e. junction corrections and in technique. I hink also it is becoming obvious that the technique is becoming more accepted in the in- ustry and that applications are being found almost every day, I think in a few years, when e have the next seminar some of those seats that are empty will be filled.

. BENSON: That was a nice leading question to ASTM Subcommittee 6 (of Committee F-1); I ade introductory remarks on it the other day. At present we have 3 documents in Subcommittee on spreading resistance. One is how to make a surface measurement. We have another doc- ment looking at how to make profile measurements and we have another document on using it s a tool to determine thickness. The documents are in various states of preparation and we ave only been on this three or four years and every year we do make progress. If anybody ants to speed this progress up I suggest that you be with us in Scottsdale, Arizona in eptember and by that time we hope to have the first document (on surface measurement) well nderway so that the other two documents can be completed.

. KORVEMAKER: I would like to add a question and remark to what Walter Schroen was saying hat NBS should get us some more idea about the method to follow; so I think what Jim hrstein was doing in the last half hour of the lecture, in stating that there are certain onditions you have to do to prepare to make the measurements more repeatable could be pplicable particularly when you go to a high resistivity area. I wonder if there is not nything there but surface layers of moisture that will give you trouble. I personally lways had great trouble to measure pico-amps without having some trouble with moisture. re the methods that we use for measuring really repeatable and does everyone use the same ethods? I do not think so.

. EHRSTEIN: I do not know exactly how to respond. I can say simply that the work I re- orted on this morning was only a beginning of what we intend to do. The difficulty s that in terms of any of us with the Bureau of Standards or probably with any government gency trying to assess what problem areas need and deserve attention, none of us are really rying to make work. We do need an accurate assessment of what problem areas still remain.

. ASSOUR: Now listening here, I really cannot help to feel my frustrations a few years go when we first were introduced to the spreading resistance probe and the first question hat came to us is how do you calibrate the probe, and everybody said you use the four probe heet resistance method according to the NBS or the ASTM standards; and naively I said, after orking 10 years with silicon, what calibration sample should I use? I have a wafer here and measure 10 Ω·cm on my instrument. How do I know it is 10 Ω·cm material? Well that is when think I called Jim and other people and I asked how do I get my hands on something that I an call 10 Ω·cm material. But then I thought that for the many years I have been dealing ith silicon we have really never concerned ourselves with this problem and everybody had his wn technique for determining his calibration samples. Accordingly, the semiconductor in- ustry has progressed very nicely. If we have 10, 10.2, or 10.5 Ω·cm does it make a

difference? For the past two years a lot of papers have shown that the spreading resistance technique at least can answer many, many questions that frustrated all of us and I hate to see here that we should get hung up on details about the damage or the microcontact or what have you. At the National Bureau of Standards here I would like to see very much not only two samples of known resistivities (SRM 1520) that one can purchase for calibration but a larger number of samples that cover the whole range of resistivity that the semiconductor industry is actively pursuing.

H. JANUS: I would like to ask if anyone has measured bulk resistivity striations letting the probe steps going down towards 0, do the striations peaks head toward infinity or is there an upper limit?

F. VIEWEG-GUTBERLET: We did a lot of measurements especially to build up a spreading resistance topograph of striations and we found that for the rotationals as well as what we call growth striations, which are autofluctuations, we do not see an advantage to lower the step width below 10 micrometers. But for very sharp profiles sometimes it seems to be better to switch from the two point probe mode to the one probe mode.

J. EDWARDS: What we found when we were trying to get very good precision was that as we changed from the 25 micron to the 10 micron step increment, the noise level increased and as we went to the 5 micron step increment the noise level was greater than the resistivity fluctuations which we were trying to measure.

D. YODER: We have on occasion found we do not know what the conductivity type of the top layer is when probing devices or multilayer structures. I wonder if anyone has any idea of how to determine this? Has anyone tried putting a thermal probe in the spreading resistance probe or something of this order?

B. MAZUR: This is in answer to the previous question about conductivity type. Some years ago I did make a thermo-electric probe that went on one of the early prototype spreading resistance probes. You can do that; it works. We do not have anything like that commercially available. Obviously with the ingenuity that has been displayed here in the last day and a half, it really is not going to take a whole heck of a lot for people to wrap little pieces of nichrome wire around one of those probes, and you can do this if you like. I assume that the question was asked in reference to small areas because obviously if you have a large area exposed on the top surface you could check it with a standard thermo-electric probe. I would suggest the use of chemical stains in conjunction with spreading resistance. I would definitely not go home and pitch out your staining stuff. We have been using the stains consistently from the beginning of our measurements as a qualitative indicator of what is going on overall. Remember that the spreading resistance measurement is a very high spatial resolution measurement and if you evaluate a epitaxial layer, you may choose to do so at one point rather than all over the wafer or all across the diameter and so you may get a very detailed picture but it is a very detailed picture of a localized region. It takes only a few seconds after having the sample profiled on the spreading resistance probe to stain it and get an overall view of whether the junction is uniform and so on. You are not then depending on the stain to indicate a p/n junction or anything. You can simply compare it back to the spreading resistance profile and use it as an indicator of that point on the spreading resistance profile where it falls and see whether the layer is uniform and so on. This was found to be quite useful in the power device area for looking at the effect of rough surfaces on diffusions and the like.

F. VIEWEG-GUTBERLET: May I comment to that problem? As you remember the paper presented this morning from RCA with respect to oxygen effects in silicon and silicon striations. There is a great interest to get information if compensation occurs or if the conductivity type changes within the limits of striations so the question is does the system you are suggesting have the resolution to find out these changes in conductivity type or compensation.

M. POPONIAK: Years ago when we had a three point probe which in reality was a one point probe, we reversed the current polarity. If you increase the current sufficiently to get into a non ohmic region you can determine the type down a profile or across the surface by observing the forward and reverse voltages. It is especially sensitive on high resistivity material.

R. MAZUR: I have comments on both those courses. As far as Fritz's problem goes I do not have a quick answer for you on that. You would have to look at the specific situation to see whether anything could be done. We have generally been able to tell a lot about conductivity type from the appearance of the profile in conjunction with other knowledge that is available such as the thermo-electric probe conductivity type of the top surface and perhaps the substrate region (the regions that are accessible) and we have used that in conjunction with the appearance of the profile and with staining techniques to keep track of conductivity type. Your situation may be a way-out case that is hard to do much with. The other suggestion that Mike was talking about I would caution you about doing that with the existing spreading resistance probes that you are using for making measurements. When you start passing large currents through them, you will be heating the material in the region of the probe and I do not know what microcontacts there are there but things could change afterwards. I am not speaking from experience, I have not tried to do that, but just be aware.

M. POPONIAK: Just on a comment to Bob's. In essence, you do not have to go up every high current to look at a very small differential voltage difference between forward and reverse current so we did not burn our probes out and we did not see deterioration in our older type probes. As far as looking at the general profile from a spreading resistance and relating it to a conductivity type if you recall that one slide I showed yesterday where within 10 mils I had three complete different profiles and by no means did the spreading resistance indicate I had a p-type layer all the way up to the top of the epi over my p^+ subcollector. Only the stain showed that up, we did not type it conductivity wise. Right adjacent to that was an epi over p-, adjacent to that was a resistor of the same epi but over an n^+ subcollector. Spreading resistance profiles can be very difficult to interpret as far as conductivity type is concerned.

R. MAZUR: I think Mike has very well made my earlier point about the valuable usage of the stain in conjunction with spreading resistance profiles.

R. MAYER: I have one question that arose out of what Bob said. I would just like to poll the panel quickly. There are two ways of doing this, one is constant current and one is constant voltage. I think the majority of the people here are using constant voltage method. How many of you are using the one millivolt or the 10 millivolt respectively?
R. EHRSTEIN: NBS tends to run the 10 millivolt constant voltage mode;
R. VIEWEG-GUTBERLET: We use the 10 millivolt mode;
R. GRUBER: For higher conductivity material, the opamps in the instrumentation tend to saturate at the 10 millivolt level so we tend to use the one millivolt range;
R. EDWARDS: For the work that I did we used the 10 millivolt range;
R. VOLTMER: We use principally 10 millivolts;
R. GOLDSMITH: All our work was at 10 millivolts;
R. MURRMANN: We too work with 10 millivolts;
R. ASSOUR: 10 millivolts.

R. MAZUR: We are just in the process of modifying our standard equipment to use 5 millivolts. There is a reason for that. The operational amplifiers that are readily available and most readily used have an output current capability of 5 milliamps. When you bias one ohm with a 10 millivolt signal you have to draw 10 milliamps. The older discrete circuit operational amplifiers that we used were very nice in going ahead and doing their bit even far beyond the call of duty. Now those are no longer available and we are using integrated circuit modules that are more tightly designed and will not perform anywhere beyond the specified output current so we are in the process of shifting to a 5 mV bias. The one millivolt arrangement is tricky because drift in the operational amplifiers is such that one or the other of the operational amps may drift in such a direction as to have the offset voltage slightly exceed one millivolt in the wrong direction and if so your log Resistance-ratio unit will malfunction and the output will go off scale up or down. It would then need to have the offset voltages on the operational amplifiers reset which is a relatively complicated procedure. Anyway, we are switching to 5 millivolts. If you need a standard for the future, I would suggest starting there.

R. JANUS: I have one thing that has been worrying me. That is when you talk about the accuracy of the measurements at high resistivities, at 5,000 $\Omega \cdot$cm you have one phosphorous atom in one cubic micron. How can you talk about an accuracy of even 10%?

J. ASSOUR: I guess I should answer this. At least with oxygen and gold you do upgrade the resistivities. I will not even guess what the accuracy of this resistivity is. Usually when we reach these kind of resistivity levels we try very hard to get down as fast as possible or be out of business.

D. BARTH: I want to comment on the closely spaced probes and a question. We have done profiling of thin, one micron and less, epi at one micron stepping distances with a shallow bevel and we have been able to get, with careful surface preparation (a good plate and good polish), good flat curves without a lot of noise. Going down to a half micron and quarter micron steps is very bad. From a noise standpoint, I would consider one micron a lower limit for the time being. Having been involved in ECL and high power microwave transistor work where we have a thousand angstrom emitters and 1,000 to 2,000 angstrom base widths, device performance tells us we are close to that, and we measured that with a spreading resistance probe. I have a question. Have any of you gentlemen done any work on very shallow layers, and I am talking on less than 4,000 angstroms where all the correction factor curves stop, and have you had any success at making those measurements accurately and do you think the spreading resistance technique will be applicable to layers this thin?

G. GRUBER: I have looked at some 0.2 and 0.3 micron layers but they were usually n on n^+ type with no junction involved. We have also looked at thin ion implants but I do not have anything more to say about them.

M. POPONIAK: A comment about Westinghouse's question. We have done very shallow implants and they will be reported on and it looks very feasible.

B. MAZUR: In partial answer to that question and also in line with something that Fred talked about before, obviously, the development of the spreading resistance technique is not finished. I think it is clear always that anything can be improved. We certainly expect to do some additional development work in the future. We also expect to be able to take advantage of some of the genius at IBM and at various other places in order to obtain technique improvements similar to the "bent" probes that we now supply to a lot of people. These are a practical approximation to the IBM closely spaced probes as produced by Ed Gorey. Perhaps in the future we can get closer to the spacing now used at IBM. Certainly I think that you would all agree that there is no fundamental limitation in the use of 25 micron radius probes and certainly no fundamental limitation in the lighter load that we use in normal measurements of 20 grams. Improvements in the mechanical parts, improvements in the probe tips and vibration isolation and so forth may well may allow us to get down to perhaps 1 micron diameter contacts. It should be interesting to see whether something like that can be done and perhaps we could then get to a one-tenth micron capability of doing profiles or something similar for thin layers. One last comment on this and then I will shut up, Fred. This applies to the Westinghouse question; it also applies to the comments that TI has made about the junction position, the lack of information about it and so on. You can of course, use the spreading resistance probe, for instance in the case of samples with base widths of 2 tenths micron or something. Now, if the spreading resistance profiles in those structures are not perfect, what else have you got? Or to put it another way, you can control the production of those base widths and the like with spreading resistance profiles even if you cannot interpret the data to give you absolute impurity concentration profiles. The same thing goes with respect to junction position location. I would be happier to see raw data used more.

D. WILLIAMS: This afternoon I have heard at least two suggestions on where we go from here. The first was that we take a simple empirical approach to the measurement. The other, propose by Dickey, was that we do some more studying of correction factors. It seems to me first of all that spreading resistance is supposed to do something very rapidly, but cheap and dirty to verify something else you have done. NBS, RCA and TI, at least during this meeting, have claimed that there is a linear relationship between resistivity and spreading resistance. I hope this is true because this implies that the measurement data checks with the simple model. Now, if we were not interested in going to doping profiles then all you would have to do is have N samples which you keep the same and as long as you get the same spreading resistance reading then you do not have to worry about the resistivity of the material, you just say that your spreading resistance probe at least on these samples are measuring the same thing. Maybe these are some of the areas that could be investigated. I think that the study of correction factors is very interesting and make a nice mathematical study. What

oes it have to do with actually studying your manufacturing process, if I get a certain preading resistance characteristic and I know I can get good product on that material and I o not if it is some other material, is this the original intention of spreading resistance easurement?

. GOLDSMITH: I would like to add comments to that. There are two aspects to using spreading esistance for production control. In one case you are interested in reproducing something nd in our case, as Jacques Assour showed, we have a high resistivity n layer covered over y a high resistivity p layer and we want to control that high resistivity n layer. Well hen we simply control on the height of the recorder pen. The higher it goes, the higher he resistivity and you can sort by the height of the recorder pen without a calibration raph. That is a practical application; it works and it is in production. However, as alter Schroen pointed out, there are times when you want to go beyond that. You want to redict in advance from the starting material what devices you are going to make. At that oint you have to have quantification of the data and that is when you have to include cor- ection factors. You also have to know what your calibration curve is and it has to be ransferable from laboratory to laboratory.

. ASSOUR: It is true that with production processes you like control. Good or bad. Of ourse, good control makes good devices, and when you have bad control you try to make it etter. On the other hand, there are still a lot of device characteristics that we do not nderstand in solid state devices and there comes a time when you have the structure of the evice you would like to sit down and think about it and try to correlate it with the hysics and in this instance you must have some data that you can rely on in order to devel- p design modeling.

. MYLROIE: I think it was alluded to in some of the other answers that there are really wo areas we are talking about. One is the production control area where the raw data is ood enough for process control and maintaining a process. The other area where we need he calibration and correction factors is that of closing the loop back to the device char- cteristics, in order to work with the circuit designer and the device designer. Then when hey know the devices they want, through models we can develop and characterize the pro- esses needed to generate these devices. For this type of work we need to be able to relate o doping concentrations and the device physics and this area is where we need the accurate orrection factors.

. WILLIAMS: I perfectly agree, I think that the correction factors are an interesting tudy and should be done. That is my point. However, there appears to be many chances for rror in going from spreading resistance to doping profiles. If I have spreading resistance alues I hope by calibration curves to translate to resistivity values. From there I can opefully go to dopant values by using Irvin's curves. Now, many factors, as pointed out by BS and RCA, may cause problems such as surface preparation that gives a high resistivity, r maybe you have a damaged surface, but you are also going through at least two translations nd a correction factor from a spreading resistance to a doping profile before you come up ith any answers. How many other factors there are, I do not know.

. GRUBER: I would like to comment, I think the fact that this is an NBS and ASTM jointly ponsored symposium goes a long way in saying that the real need in the industry is for tandardization of the spreading resistance technique, in fact for standardization of all esistivity measurements. This whole week was interesting for me, it was the first time I ad been to an ASTM meeting and I would recommend it to everyone in the industry. It pointed p to me the need for standards in things that I considered pretty well standardized already, uch as wafer thickness. I also sat in on a discussion of the inaccuracies of mobility mea- urements and the effects on Irvin's curves. Coupled with this I think what we have learned t this Symposium is the fact that the Spreading Resistance technique can be no better than he standards on which it is based.

CONCLUDING REMARKS BY PAUL LANGER

I would like to make a very brief summary. We have heard 22 papers and some last minute remarks in the last couple of days and I think it points up the direction that spreading resistance measurements will probably go in the next few years. There are two areas that will probably get the bulk of the development effort. The first area is probably the development of more reliable correction factors for all types of structures specifically very thin transition regions between either one type or the same type of dopant. I think there is also a need not only to have very complex correction factor models but also a need for fast and simple correction factor models so that one will be able to perform these calculations on a calculator or a mini computer. The second area is that of surface preparation and it is still a big unknown. Most laboratories have standardized more or less on their own type of sample preparation. Under those constraints good intralab precision has been obtained but this high level of precision may degrade in interlab studies due to differences in specimen preparation. So I think surface preparation will get some closer looks over the next few years. On the positive side, it is very nice to see the wide acceptance that spreading resistance has had in all areas of the semiconductor industry. Crystal growers are using it, the people in epi and diffusion are using it, and people modeling devices are using it. Spreading resistance seems to have come of age. It probably does not really have as far to go as one would think from listening to some of the discussions.

I would like to reemphasize the role of ASTM and NBS in the measurements area. The American Society for Testing and Materials is your organization as is the Bureau of Standards. These organizations are here to do the work that people in the semiconductor industry are interested in getting done. The Bureau of Standards does not go off on research projects for the sake of research alone as neither does ASTM. It gets its inputs from the industry and if you have a specific project you think really needs to be pursued or if you would like to help out in pursuing some of the work being done on electrical measurements or other means of characterization I suggest you attend the next meeting in Scottsdale. It is right after Labor Day and I think it will be very beneficial since in obtaining intercompany standardization one really needs to exchange material based on spreading resistance measurements. Finally I would just again like to thank the members of the committee who acted as session chairmen, Ken Benson and Bernie Morris of Bell Labs, Fred Mayer of RCA, Francois Padovani of T. I. and Fritz Vieweg-Gutberlet of Wacker Chemitronic; and also to our arrangements man, Jim Ehrstein from the Bureau of Standards. Thank you all for coming and hope to see you all again soon.

APPENDIX-BIBLIOGRAPHY

The bibliography which follows is intended for the convenience of users of this volume. While not pretending to be an exhaustive list of titles on spreading resistance, it is nevertheless judged to contain all the major references commonly cited by those working on spreading resistance measurements. Entries are listed by year of publication and within each year, by the alphabetic ordering of the primary authors name

1. Kennedy, D. P., Spreading Resistance in Cylindrical Semiconductor Devices, *J. Appl. Phys.* 31 #8, 1490-7 (1960).

2. Dickey, D. H., Diffusion Profiles Using a Spreading Resistance Probe, Extended Abstracts of the Electronics Division, *The Electrochemical Society* 12, No. 1, 151 (April 1963).

3. Mazur, R. G., Dickey, D. H., The Spreading Resistance Probe - A Semiconductor Resistivity Measurement Technique Extended Abstracts of the Electronics Division, *The Electrochemical Society* 12, No. 1, 148 (April 1963).

4. Greenwood, J. A., Constriction Resistance and the Real Area of Contact, *Brit. J. Appl. Phys.* 17, 1621-1632 (1966).

5. Mazur, R. G., Spreading Resistance Resistivity Measurements on Silicon Containing *p-n* Junctions, Extended Abstracts of the Electronics Division, *The Electrochemical Society* 15, No. 1, (1966).

6. Mazur, R. G., Dickey, D. H., A Spreading Resistance Technique for Resistivity Measurements on Silicon, *J. Electrochemical Society* 113, 255-259 (1966).

7. Dickens, L. E., Spreading Resistance As a Function of Frequency, *IEEE Transactions on Microwave Theory and Technique*, MTT-15 No. 2, 101-109 (1967).

8. Greenwood, J. A., The Area of Contact Between Rough Surfaces and Flats, *Trans. ASME*, Ser. F. 89, 81-91 (1967).

9. Holm, R., *Electric Contacts*, 4th ed. Springer-Verlag, New York, (1967).

10. Mazur, R. G., Resistivity Inhomogeneities in Silicon Crystals, *J. Electrochem. Soc.* 114, 255-259 (1967).

11. Adley, J. M., Poponiak, M. R., Schneider, C. P., Schumann, P. J., Tong, A. H., The Design of a Probe for the Measurement of the Spreading Resistance of Semiconductors, *Semiconductor Silicon 1969, The Electrochemical Society*, 721-736 (1969).

12. Keenan, W. A., Schumann, P. A., Tong, A. H., Phillips, R. P., A Model for the Metal-Semiconductor Contact in the Spreading Resistance Probe, Ohmic Contacts to Semiconductors, *The Electrochemical Socity*, 263-276 (1969).

13. Rymaszewski, R., Relationship Between the Correction Factor of the Four-Point Probe Value and the Selection of Potential and Current Electrodes, *J. of Sci. Instr.*, Series 2 Vol. 2, 170-174 (1969).

14. Schumann, P. A., Gardner, E. E., Spreading Resistance Correction Factors, *Solid-State Electronics* 12, 371-375 (1969).

15. Schumann, P. A., Gardner, E. E., Application of Multilayer Potential Distribution to Spreading Resistance Correction Factors, *J. Electrochemical Society* 116, 87-91 (1969).

16. Gorey, E. F., Schneider, C. P., Poponiak, M. R., Preparation and Evaluation of Spreading Resistance Probe Tip, *J. Electrochemical Society* 117, 721-724 (1970).

17. Gupta, D. C., Chan, J. Y, A Semiautomatic Spreading Resistance Probe, *Rev. Sci. Instrum.* 41, 176-179 (1970).

18. Gupta, D. C., Chan, J. Y., Wang, P., Effect of the Surface Quality on the Spreading Resistance Probe Measurements, *Rev. Sci. Instrum.*, 41, 1681-1682 (1970).

19. Hoppenbrouwers, A. M. H., Hooge, F. N., 1/f Noise of Spreading Resistances, *Philips Res. Rep.* 25, 69-80 (1970).

20. Mazur, R. G., Spreading Resistance Measurements on Buried Layers in Silicon Structures, Silicon Device Processing: Gaithersburg, Maryland, NBS Special Publication 337, 240-255 (1970).

21. Yeh, T. H., Khokhani, K. H., Multilayer Theory of Correction Factors for Spreading Resistance Measurements, *J. Electrochemical Society* 116, 1461-1464 (1969).

22. Yeh, T. H, Current Status of the Spreading Resistance Probe and Its Applications, Silicon Device Processing: NBS Special Publication 337, 111-122 (1970).

23. Brooks, R. D., Mattes, H. G., Spreading Resistance Between Constant Potential Surfaces, *Bell System Tech. J.* 50, 775 (1971).

24. Chu, T. L., Ray, R. L., Resistivity Measurements on Germanium Crystals by the Spreading Resistance Technique, *Solid-State Tech.*, 37-40 (September 1971).

25. Ting, Chung-Yu, Chen, C. Y., A Study of the Contacts of a Diffused Resistor, *Solid-State Electronics* 14, 433-38 (1971).

26. Hu, S. M., Calculation of Spreading Resistance Correction Factors, *Solid-State Elec-Electronics* 15, 809-817 (1972).

27. Severin, P. J., Measurement of the Resistivity and Thickness of a Heterotype Epitaxially Grown Silicon Layer with the Spreading Resistance Method, *Philips Res. Rep.* 26, 359-372 (1971).'

28. Severin, P. J., Measurement of the Resistivity of Silicon by the Spreading Resistance Method, *Solid-State Electronics* 14, 247-255 (1971).

29. Tong, A. H., Gorey, E. F., Schneider, C. P., Apparatus for the Measurement of Small Angles, *Rev. Sci. Instrum.* 43, 320-325 (1972).

30. Kraner, P., Van Reuyven, L., The Influence of Temperature on Spreading Resistance Measurement, *Solid-State Electronics* 15, 757-766 (1972).

31. Schumann, P. A., Small Spaced Spreading Resistance Probe, *Solid-State Tech.*, 50-54, (March 1972).

32. Burtscher, J., Krausse, J., Voss, P., Inhomogeneities of the Resistivity in Silicon: Two Diagnostic Techniques, *Semiconductor Silicon 1973, The Electrochemical Society,* 581-589 (1973).

33. Burtscher, J., Dorendorf, H. W., Krausse, J., Electrical Measurement of Resistivity Fluctuations Associated with Striations in Silicon Crystals, *IEEE Trans. on Elec. Dev.* ED-20, No. 8, 702-708 (1973).

34. Hu, S., Poponiak, M. R., Copper Precipitation in Silicon-Observation of Electrical Effect, Phys. Stat. Sol. (a) 18 no. 1, 5-8 (1973).

35. Witt, A. F., Lechtensteiger, M., Gatos, H. C., Experimental Approach to the Quantitative Determination of Dopant Degregat on a Microscale, *J. Electrochemical Society* 120, 1119-1123 (1973).

36. deKock, A. J. R., Severin, P. J., Roksnoer, P. J., On the Relation between Growth Striations and Resistivity Variations in Silicon Crystals, *Phys. Stat. Sol.* 22a, 163-166 (1974).

37. Morris, B. L., Some Device Applications of Spreading Resistance Measurements on Epitaxial Silicon, *J. Electrochemical Society* 121, 422-426 (1974).

NBS-114A (REV. 7-73)

U.S. DEPT. OF COMM. BIBLIOGRAPHIC DATA SHEET	1. PUBLICATION OR REPORT NO. NBS SP-400-10	2. Gov't Accession No.	3. Recipient's Accession No.

4. TITLE AND SUBTITLE

Semiconductor Measurement Technology: SPREADING RESISTANCE SYMPOSIUM
PROCEEDINGS OF A SYMPOSIUM HELD AT NATIONAL BUREAU OF STANDARDS June 13-14, 1974

5. Publication Date: December 1974

6. Performing Organization Code

7. AUTHOR(S): James R. Ehrstein, Editor

8. Performing Organ. Report No.

9. PERFORMING ORGANIZATION NAME AND ADDRESS

NATIONAL BUREAU OF STANDARDS
DEPARTMENT OF COMMERCE
WASHINGTON, D.C. 20234

10. Project/Task/Work Unit No.

11. Contract/Grant No.

12. Sponsoring Organization Name and Complete Address *(Street, City, State, ZIP)*

Committee F-1 of the American Society for Testing and Materials and The National Bureau of Standards

13. Type of Report & Period Covered: Final June 13-14, 1974

14. Sponsoring Agency Code

15. SUPPLEMENTARY NOTES

16. ABSTRACT *(A 200-word or less factual summary of most significant information. If document includes a significant bibliography or literature survey, mention it here.)*

This Proceedings contains the information presented at the Spreading Resistance Symposium held at the National Bureau of Standards on June 13-14, 1974.

This Symposium covered the state of the art of the theory, practice and applications of the electrical spreading resistance measurement technique as applied to characterization of dopant density in semiconductor starting materials and semiconductor device structures. In addition to the presented papers, the transcripts of the discussion sessions which were held directly after the Theory, Practice and Applications sessions are also included. These transcripts, which were reviewed by the respective respondents for clarity, are essentially as presented at the Symposium.

17. KEY WORDS *(six to twelve entries; alphabetical order; capitalize only the first letter of the first key word unless a proper name; separated by semicolons)*

Dopant concentration, dopant profiles, metal-semiconductor contacts, resistivity, semiconductor surface preparation, silicon, spreading resistance.

18. AVAILABILITY

[X] Unlimited

[ ] For Official Distribution. Do Not Release to NTIS

[X] Order From Sup. of Doc., U.S. Government Printing Office Washington, D.C. 20402, SD Cat. No. C13.10:400-10

[ ] Order From National Technical Information Service (NTIS) Springfield, Virginia 22151

19. SECURITY CLASS (THIS REPORT): UNCLASSIFIED

21. NO. OF PAGES: 293

20. SECURITY CLASS (THIS PAGE): UNCLASSIFIED

22. Price: $3.55

USCOMM-DC 29042-P74

U. S. GOVERNMENT PRINTING OFFICE : 1975 O - 565-448

Announcement of New Publications on Semiconductor Measurement Technology

Superintendent of Documents,
Government Printing Office,
Washington, D.C. 20402

Dear Sir:

Please add my name to the announcement list of new publications to be issued in the series: National Bureau of Standards Special Publication 400–.

Name _____

Company _____

Address _____

City _____ State _____ Zip Code _____

(Notification Key N-413)

NBS TECHNICAL PUBLICATIONS

PERIODICALS

JOURNAL OF RESEARCH reports National Bureau of Standards research and development in physics, mathematics, and chemistry. Comprehensive scientific papers give complete details of the work, including laboratory data, experimental procedures, and theoretical and mathematical analyses. Illustrated with photographs, drawings, and charts. Includes listings of other NBS papers as issued.

Published in two sections, available separately:

- **Physics and Chemistry (Section A)**

Papers of interest primarily to scientists working in these fields. This section covers a broad range of physical and chemical research, with major emphasis on standards of physical measurement, fundamental constants, and properties of matter. Issued six times a year. Annual subscription: Domestic, $17.00; Foreign, $21.25.

- **Mathematical Sciences (Section B)**

Studies and compilations designed mainly for the mathematician and theoretical physicist. Topics in mathematical statistics, theory of experiment design, numerical analysis, theoretical physics and chemistry, logical design and programming of computers and computer systems. Short numerical tables. Issued quarterly. Annual subscription: Domestic, $9.00; Foreign, $11.25.

DIMENSIONS/NBS (formerly Technical News Bulletin)—This monthly magazine is published to inform scientists, engineers, businessmen, industry, teachers, students, and consumers of the latest advances in science and technology, with primary emphasis on the work at NBS.

DIMENSIONS/NBS highlights and reviews such issues as energy research, fire protection, building technology, metric conversion, pollution abatement, health and safety, and consumer product performance. In addition, **DIMENSIONS/NBS** reports the results of Bureau programs in measurement standards and techniques, properties of matter and materials, engineering standards and services, instrumentation, and automatic data processing.

NONPERIODICALS

Monographs—Major contributions to the technical literature on various subjects related to the Bureau's scientific and technical activities.

Handbooks—Recommended codes of engineering and industrial practice (including safety codes) developed in cooperation with interested industries, professional organizations, and regulatory bodies.

Special Publications—Include proceedings of high-level national and international conferences sponsored by NBS, precision measurement and calibration volumes, NBS annual reports, and other special publications appropriate to this grouping such as wall charts and bibliographies.

Applied Mathematics Series—Mathematical tables, manuals, and studies of special interest to physicists, engineers, chemists, biologists, mathematicians, computer programmers, and others engaged in scientific and technical work.

National Standard Reference Data Series—Provides quantitative data on the physical and chemical properties of materials, compiled from the world's literature and critically evaluated. Developed under a world-wide program coordinated by NBS. Program under authority of National Standard Data Act (Public Law 90-396).

Building Science Series—Disseminates technical information developed at the Bureau on building materials, components, systems, and whole structures. The series presents research results, test methods, and performance criteria related to the structural and environmental functions and the durability and safety characteristics of building elements and systems.

Technical Notes—Studies or reports which are complete in themselves but restrictive in their treatment of a subject. Analogous to monographs but not so comprehensive in scope or definitive in treatment of the subject area. Often serve as a vehicle for final reports of work performed at NBS under the sponsorship of other government agencies.

Voluntary Product Standards—Developed under procedures published by the Department of Commerce in Part 10, Title 15, of the Code of Federal Regulations. The purpose of the standards is to establish nationally recognized requirements for products, and to provide all concerned interests with a basis for common understanding of the characteristics of the products. The National Bureau of Standards administers the Voluntary Product Standards program as a supplement to the activities of the private sector standardizing organizations.

Federal Information Processing Standards Publications (FIPS PUBS)—Publications in this series collectively constitute the Federal Information Processing Standards Register. The purpose of the Register is to serve as the official source of information in the Federal Government regarding standards issued by NBS pursuant to the Federal Property and Administrative Services Act of 1949 as amended, Public Law 89-306 (79 Stat. 1127), and as implemented by Executive Order 11717 (38 FR 12315, dated May 11, 1973) and Part 6 of Title 15 CFR (Code of Federal Regulations). FIPS PUBS will include approved Federal information processing standards information of general interest, and a complete index of relevant standards publications.

Consumer Information Series—Practical information, based on NBS research and experience, covering areas of interest to the consumer. Easily understandable language and illustrations provide useful background knowledge for shopping in today's technological marketplace.

NBS Interagency Reports—A special series of interim or final reports on work performed by NBS for outside sponsors (both government and non-government). In general, initial distribution is handled by the sponsor; public distribution is by the National Technical Information Service (Springfield, Va. 22151) in paper copy or microfiche form.

Order NBS publications (except Bibliographic Subscription Services) from: Superintendent of Documents, Government Printing Office, Washington, D.C. 20402.

BIBLIOGRAPHIC SUBSCRIPTION SERVICES

The following current-awareness and literature-survey bibliographies are issued periodically by the Bureau:

Cryogenic Data Center Current Awareness Service (Publications and Reports of Interest in Cryogenics). A literature survey issued weekly. Annual subscription: Domestic, $20.00; foreign, $25.00.

Liquefied Natural Gas. A literature survey issued quarterly. Annual subscription: $20.00.

Superconducting Devices and Materials. A literature survey issued quarterly. Annual subscription: $20.00. Send subscription orders and remittances for the preceding bibliographic services to the U.S. Department of Commerce, National Technical Information Service, Springfield, Va. 22151.

Electromagnetic Metrology Current Awareness Service (Abstracts of Selected Articles on Measurement Techniques and Standards of Electromagnetic Quantities from D-C to Millimeter-Wave Frequencies). Issued monthly. Annual subscription: $100.00 (Special rates for multi-subscriptions). Send subscription order and remittance to the Electromagnetic Metrology Information Center, Electromagnetics Division, National Bureau of Standards, Boulder, Colo. 80302.

U.S. DEPARTMENT OF COMMERCE
National Bureau of Standards
Washington, D.C. 20234

OFFICIAL BUSINESS

Penalty for Private Use, $300

POSTAGE AND FEES PAID
U.S. DEPARTMENT OF COMMERCE
COM-215